

DESIGN, SYNTHESIS, AND APPLICATION OF BASE-STABLE CATIONS IN ANION
EXCHANGE MEMBRANES FOR ALKALINE FUEL CELLS

A Dissertation

Presented to the Faculty of the Graduate School
of Cornell University

In Partial Fulfillment of the Requirements for the Degree of
Doctor of Philosophy

by

Kristina Marie Hugar

February 2016

© 2016 Kristina Marie Hugar

DESIGN, SYNTHESIS, AND APPLICATION OF BASE-STABLE CATIONS IN ANION EXCHANGE MEMBRANES FOR ALKALINE FUEL CELLS

Kristina Marie Hugar, Ph. D.

Cornell University 2016

Fuel cells are devices that convert the energy stored in chemical bonds into electrical energy that can be used to do useful work. They are interesting as a source of energy because they possess high energy density, emit few by-products, have high efficiency and are capable of uninterrupted power generation. In particular, alkaline fuel cells (AFCs) are attractive because they enable the use of non-noble metal catalysts, which can significantly reduce production costs. The development of alkaline anion exchange membranes (AAEMs) is necessary for further development of AFCs and polymers that conduct hydroxide efficiently, while maintaining good mechanical strength are needed. Despite significant efforts to achieve viable polymer electrolytes, a standard AAEM has not been realized or successfully commercialized. Many of the polymer backbones and cations that constitute AAEMs have limited stability under the alkaline conditions required for operation. Developing cations that are resistant to degradation with bases and nucleophiles and incorporating them into inert polymer architectures is required for effective AAEMs. Moreover, designing methods that accurately characterize the stability properties and maximize the information acquired from studies will reduce the resources needed to achieve these goals. This dissertation describes the design, synthesis, and characterization of base-stable organic cations and incorporation into polymer electrolytes for AFCs.

We synthesized a tetrakis(dialkylamino)phosphonium functionalized *cis*-cyclooctene (COE) monomer and copolymerized it with COE using Grubbs' second generation catalyst for

ring opening metathesis polymerization (ROMP). After hydrogenation with Crabtree's catalyst, the polymer was essentially composed of polyethylene with phosphonium cations covalently linked to the backbone. The polymer exhibited a room temperature (22 °C) hydroxide conductivity of 22 mS/cm. After storing strips of the polymer membrane in caustic alkaline solutions (1 M KOH @ 80 °C or 15 M KOH @ 22 °C), the conductivity was reanalyzed and remained unchanged for 22 and 138 days, respectively.

A ^1H NMR spectroscopy protocol was developed to quantitatively assess the stability of a wide variety of organic cations under harsh alkaline conditions. We selected methanol- d_3 as the reaction solvent to fully dissolve organic cations and their degradation products. Moreover, the use of methanol that is not fully deuterated prevents a hydrogen/deuterium exchange process that limits the amount of useful information that can be obtained during an experiment. The solutions were stored in flame-sealed NMR tubes to prevent the loss of volatile compounds and heated to 80 °C, a relevant fuel cell temperature. A minimum ratio of 1:10 was used between the cation and hydroxide molarities. A TMS derivative was used as an internal standard to determine the amount of cation remaining in solution over time. Several cations that are of interest to the AAEM community were analyzed over 30 days and compared to the stability of benzyl trimethylammonium (BTMA). When possible, degradation products were identified with ^1H NMR and high resolution mass spectrometry (HRMS).

Finally, we synthesized a series of imidazolium cations with varying substituents on the ring positions and tested their alkaline stability using our protocol. We found that substituents at the C2 position were important and substituted aryl groups were the most effective at preventing degradation. Imidazolium stability was further improved by placing methyl groups at the C4 and C5 positions. Long chain alkyl groups, such as n-butyl groups, at the N1 and N3 positions were the most effective at hindering reactions with hydroxide and methoxide. Ultimately, we achieved imidazolium cations that were completely resistant to degradation for 30 days at 1 M, 2 M, and 5 M KOH concentrations, in methanol- d_3 at 80 °C.

BIOGRAPHICAL SKETCH

Kristina Marie Hugar was born on August 23, 1984 to parents Kim Clark and Chip Hugar. She grew up in Scio, a rural town in western New York with her five brothers: Kevin, Shane, Chip, Shawn, and Rayshawn. Early years were spent helping her Mom bake and clean, insisting that she vacuum even when it was too big for her. She fondly recalls running around outside barefoot, climbing trees and catching crayfish with her brothers. In middle school she was asked to try out for junior varsity soccer and won a spot on the team. This was a life-altering event that helped her grow into a confident young adult, energetically pursuing new challenges. She was involved in several other extracurricular activities throughout high school including, volleyball, softball, choir and band. Yet, she always had a passion for schoolwork and enjoyed Math, Science and English courses the most. As applications for college became imminent her senior year, she applied for a prestigious scholarship from the McKelvey Foundation designed for students that possess an entrepreneurial spirit. She gratefully accepted the award, selecting Ithaca College as the destination for her next scholastic step, and was very excited about moving to a city.

In Fall 2002, Kristina initially majored in Biology at Ithaca College with the intention of pursuing a degree in medicine. However, she was quickly fell in love with Chemistry while taking her first Organic Chemistry lab with Prof. Mike Haaf. In one memorable assignment the students synthesized aspirin and Kristina achieved the highest yield in the class, obtaining beautiful crystals as a product. After this experience she realized, “Hey, this is something that I really enjoy and I might be good at it too!” and she promptly switched to a major in Chemistry. She spent the next two summers doing research under the supervision of Prof. Heinz Koch and appreciated this opportunity to develop her skills as an experimental chemist, realizing in the process that it could be a viable career path.

After graduating in Spring 2006, Kristina took a Scientist position at Wolfe Laboratories, a small contract pharmaceutical company, in Watertown, Massachusetts. While there, she met several amazing individuals who challenged and inspired her, notably Dr. Michael Frid and

Verona Outerbridge. One day, a senior colleague asked about her long term career goals. After explaining that she wanted to pursue something more ambitious, but wasn't completely sure what the best choice was, he gave her the best piece of advice, "Life is not a thought experiment. You can't figure out what you want to do by just thinking about it. You have to go out and start trying things." Immediately, it became crystal clear to Kristina that she needed to try something new and decided to pursue a PhD. It seemed like the most challenging option and she reasoned that if it did not work out she would attempt something easier. Being very conscious of the impact of human habits on the environment, she decided that she wanted to conduct research that would allow her to develop new polymer materials that helped address pollution concerns. With this in mind, she applied to several research universities. Cornell University was not initially on her list because she wanted to move to a city she had never lived in before; however, she was very impressed by the research in the Chemistry Department and applied to Cornell at the last minute. After visiting several of the programs she was accepted into, she knew she had to pursue her degree at Cornell. The collegiate and welcoming atmosphere won her over and never disappointed her from that point forward.

In July 2010, Kristina returned to Ithaca to begin her PhD studies. She had several teaching assignments, including teaching General Chemistry recitations and Organic Chemistry labs. She thoroughly enjoyed her time interacting with students and continued tutoring after her teaching assignments were complete to remain in a teaching capacity. She joined the research group of Geoff Coates in November 2010 and began her project on making base stable cations for anion exchange membranes in fuel cells. She appreciated the dynamic nature of the project and enjoyed collaborating with researchers in other groups and departments. Along the way, she developed friendships with many incredible scientists that made her professional and personal achievements richer. After completing her degree, she will be joining Gabriel Rodriguez-Calero to start a company that is aimed at commercializing the materials that she helped develop at Cornell. Additionally, she looks forward to a chemistry lecture position at her alma mater, Ithaca College.

To my Grandfather, Ernest R. Clark.

ACKNOWLEDGMENTS

I have so many people to thank for my success at Cornell and completing my PhD. It would not have been possible without the encouragement and support of many colleagues, friends, and family members. Each of them contributed in unique ways that reflect our relationships and friendships.

From Ithaca College, I must thank several of my professors that made chemistry engaging and exciting for me, Prof. Michael Haaf, Prof. Scott Ulrich and Prof. Anna Larsen. I sincerely appreciate the offer that Prof. Heinz Koch gave me to work in his research group, as this was my first opportunity to have a job doing scientific research. Dr. Michael Frid, at Wolfe Laboratories, was the first person in my life to push me harder than I pushed myself and for this I will be forever grateful. He challenged to me to reach beyond what I thought was possible and made me rethink my professional goals. To this day, Verona Outerbridge is my greatest female role model. She is an incredibly strong, talented, intelligent and compassionate woman and I am so grateful that our paths crossed when they did. Nicole Krilla and Scott Churchill were my first friends in Boston and they made my transition into a new city and first professional job much easier.

I am endlessly grateful that Prof. Geoff Coates offered me a position in his research group. I appreciate all the energy that he spent training me as a professional scientist. His dedication to excellence and perfection is unparalleled and will continue to have lasting impacts on how we view science. I would also like to thank Prof. William Dichtel and Professor Héctor Abruña for serving on my committee. Professor Abruña's energy and confidence in his students was immensely motivational. I would like to thank Paul Mutolo and Suzanne Aceti Koehl for all the opportunities that they provided me through the Energy Materials Center at Cornell (EMC²). I also must thank Dr. Anne LaPointe for being a great sounding board whenever I had science questions or did not know how to approach a problem.

I learned many of my early skills in lab from Prof. Kevin Noonan and Dr. Henry Kostalik and their training and guidance in the beginning set me up for success. I am grateful for the many

discussions I had with my electrochemistry mentors over the years, Dr. David Finkelstein, Dr. Eric Rus, and Dr. Jimmy John. Any deficiency I have in that subject is not for their lack of efforts and patience. It was a pleasure to work with Dr. Katie Silberstein and Johary Rivera and although our collaborations did not result in immediate gains, they were wonderful to work with. Aside from science and professional reasons, I have to acknowledge several senior group members for the special roles they had in my life. I must thank Taz for mentoring me in the first couple years. He helped me get comfortable in the Coates group and reminded me how important it was to have fun while working hard. I am grateful to Pasquale for being a great IC big brother. I have to thank Angie for teaching me the power of kindness on a whole new level. Her spirit is contagious and it inspired me strive to be a positive role in more people's lives, following her example. I am thankful for my dear friend Rachna for being the voice of reason and always giving genuine advice with kindness. I want to thank "C" for introducing me to Ragnar relay races, a whole new way to enjoy my favorite hobby. We truly were "up all night to go running."

I will always have a place in my life and heart for the four other brave souls that made it through the five years of doing research with me side-by-side: Nate, Ian, Yuki and Tam. I think of Nate as the chemistry "gunslinger," and he has become exceptional chemist. Bickering with Ian was the highlight of my day sometimes and it kept me feeling lively. Weekly runs with Yuki kept me in shape, physically and mentally. I am so excited to see what amazing things happen for all of them in their careers and lives.

I started at Cornell with an absolutely amazing group of students in my class. They are some of the most intelligent, funny and interesting people that I have ever met and my time at Cornell would not have been as memorable without them. I have to thank my sestra, Alli, for always having the best perspective on life. I had so much fun traveling around the area and running with Devin. I have to thank Evan for keeping the group together during busy times by hosting and planning our "no chemistry" dinners (We tried at least!). I have to thank Brandon and Mike for being there with me from day zero, studying until the wee hours of the morning. Their support and encouragement helped me so much. I appreciate my friendships with my other

classmates, Brian, Greg and Dan and I know that they will all be very successful. I am thankful for all of Jenny's efforts towards keeping us all engaged in fun activities and being a sweet and thoughtful person.

I have to thank Kyle for being an incredible lab mate. I am so glad that he joined our research group and ended up sitting right next to me for a couple years. It was a blast to work next to him and he was a great person to chat with about science and life and he always kept me smiling and looking forward to what was up next. I am so happy that I became friends with Carmella in the last year. She is one of the sweetest and most generous people I have ever met. Ryan and Cathy are simply hilarious and I had so much fun planning and making "Shake and Vent" with them. Jessica Lamb is a stellar scientist and I appreciate all of her help organizing ideas and editing papers. I also have to thank James Eagan for all his help with experiments, interpreting data and discussing research. He continues to make a positive impact on the whole research group. I have to thank the undergraduate students that worked with me over the years, Ben and Chinelo. I am certain that I learned more from them than they did from me and they are both exceptional individuals that will do great things.

Finally, I have to thank my family for always believing in me. They were endlessly supportive and motivating throughout the entire process. I thank my Mom and Clay for helping with all the little things and taking every phone call. I thank my brothers for never doubting me. I especially thank Chip and Shawn for listening to all my stories and explanations and always finding a way to make me laugh. I thank my brother Shane for being an inspiration and role model for professionalism and poise. I thank my Dad and Betty for all their help and support. I also appreciate Allison Seamon for pulling me away from my studies to spend time with her and her family, especially sweet little Dexter.

I am so lucky to have such an amazing group of family and friends to share my life with. I look forward to continuing these friendships into the next phase of my life and seeing how they evolve and grow.

TABLE OF CONTENTS

Biographical Sketch	v
Dedication	vii
Acknowledgements	viii
List of Figures	xiii
List of Tables	xxv

CHAPTER ONE – A Brief Review of Anion Exchange Membranes for Alkaline Fuel Cells with an Emphasis on Chemical Stability

1.1.	Introduction	2
1.1.1.	The Role of Fuel Cells in a Sustainable Energy Economy	2
1.1.2.	A Comparison of Fuel Cell Types	4
1.2.	Alkaline Fuel Cells	5
1.2.1.	Advantages of Alkaline Fuel Cells	6
1.2.2.	Remaining Challenges for Alkaline Fuel Cells	7
1.3.	Alkaline Anion Exchange Membranes for Fuel Cells	8
1.3.1.	Advantages of AFCs and Comparison to PEMFCs	8
1.3.2.	AAEM Design Principles	9
1.4.	Types of AAEMs According to Polymer Backbone	11
1.4.1.	Perfluorinated Polymers	11
1.4.2.	Poly(arylenes)	12
1.4.2.1.	Poly(arylene) sulfones	13
1.4.2.2.	Poly(arylene) ketones	14
1.4.2.3.	Poly(arylene)sulfone ketones	15
1.4.2.4.	Polyphenylene Oxides	16
1.4.3.	Aliphatic Hydrocarbon Polymers	17
1.4.3.1.	Via Ring Opening Metathesis Polymerization (ROMP)	17
1.4.3.2.	Via Olefin Polymerization Catalysts	18
1.4.4.	Polystyrenes	19
1.5.	Investigation of AAEM Polymer Stability	20
1.5.1.	Ammonium-based AAEM Stability	22
1.5.2.	Imidazolium-based AAEM Stability	23
1.5.3.	Conclusions	25
1.6.	Alkaline Stability of Cations	25
1.6.1.	Alkaline Stability of Ammonium Cations	26
1.6.1.1.	Ammonium Cations – Computational Studies	26
1.6.1.2.	Ammonium Cations – Experimental Studies	27
1.6.2.	Alkaline Stability of Imidazolium Cations	28
1.6.2.1.	Imidazolium Cations – Computational Studies	28
1.6.2.2.	Imidazolium Cations – Experimental Studies	31
1.7.	Conclusions and Future Outlook	32

REFERENCES	33
------------	----

CHAPTER TWO – Phosphonium Functionalized Polyethylene: A New Class of Base Stable Alkaline Anion Exchange Membranes

2.1	Abstract	38
2.2	Introduction	38
2.3	Results and Discussion	40
2.4	Conclusions	46
2.5	Experimental	47
REFERENCES		85

CHAPTER THREE – A Universal Protocol for the Quantitative Assessment of Pendant Cation Stability in Polymer Electrolytes

3.1	Abstract	91
3.2	Introduction	91
3.3	Results and Discussion	94
3.4	Conclusions	110
3.5	Experimental	112
REFERENCES		216

CHAPTER FOUR – Imidazolium Cations with Exceptional Alkaline Stability: A Systematic Study of Structure-Stability Relationships

4.1	Abstract	225
4.2	Introduction	225
4.3	Results and Discussion	231
4.4	Conclusions	240
4.5	Experimental	242
REFERENCES		364

LIST OF FIGURES

1.1	Schematic of a Fuel Cell.	3
1.2	Chemical Structure and Properties of Nafion 115. [®]	5
1.3	Diagram of an Alkaline Fuel Cell.	6
1.4	Components of an Alkaline Anion Exchange Membrane.	10
1.5	Degradation Pathways of Ammonium Cations.	26
1.6	Ring Opening Degradation of Imidazolium Cations.	28
1.7	Proposed Free Energy Diagram for Ring-Opening Degradation of Imidazolium Cations. (Adapted from Ref. 35)	30
2.1	Stability of [BnNMe ₃] ⁺ and [P(N(Me)Cy) ₄] ⁺ in 1 M NaOD/CD ₃ OD at 80 °C.	40
2.2	Molecular structure of 1 . Hydrogen atoms on the cation have been omitted for clarity. Thermal ellipsoids at 40% probability.	41
2.3	Phosphonium Monomer Synthesis.	43
2.4	Synthesis of Phosphonium Functionalized Polyethylene.	44
2.5	AAEM-17 hydroxide conductivity as a function of time after immersion in 15 M KOH _{aq} at 22 °C. Inset: AAEM-17 hydroxide conductivity as a function of time after immersion in 1 M KOH _{aq} at 80 °C.	45
2.6	¹ H NMR spectra of benzyltrimethylammonium bromide over 20 days dissolved in a mixture of CD ₃ OD, 40 weight percent NaOD/D ₂ O solution (1 M NaOD, [NaOD]/[BTMA] = 10) and, an internal standard (TMS(CH ₂) ₃ SO ₃ Na).	57
2.7	¹ H NMR spectra of tetrakis[cyclohexyl(methyl)amino]phosphonium tetrafluoroborate over 20 days dissolved in a mixture of CD ₃ OD, 40 weight percent NaOD/D ₂ O solution (1 M NaOD, [NaOD]/[P(N(Me)Cy) ₄] = 10) and, an internal standard (TMS(CH ₂) ₃ SO ₃ Na).	59
2.8	³¹ P{ ¹ H} NMR spectra of tetrakis[cyclohexyl(methyl)amino]phosphonium tetrafluoroborate over 20 days dissolved in a mixture of CD ₃ OD, 40 weight percent NaOD/D ₂ O solution (1 M NaOD, [NaOD]/[P(N(Me)Cy) ₄] = 10) and, an internal standard (TMS(CH ₂) ₃ SO ₃ Na). Referenced to 85 % H ₃ PO ₄ .	60
2.9	¹ H NMR Spectrum of 5-mesyl-1-cyclooctene. Signal at 7.24 ppm is residual CHCl ₃ .	63
2.10	¹ H NMR Spectrum of 5-azido-1-cyclooctene. Signal at 7.24 ppm is residual CHCl ₃ .	65

2.11	³¹ P NMR Spectrum of 5-chloroiminophosphorane-1-cyclooctene. Referenced to 85% H ₃ PO ₄ .	67
2.12	¹ H NMR Spectrum of 5-chloroiminophosphorane-1-cyclooctene. Signal at 7.16 ppm is residual C ₆ D ₅ H.	67
2.13	³¹ P{ ¹ H} NMR Spectrum of Tris(cyclohexylamino)-cycloctenylamino-phosphonium tetrafluoroborate. Referenced to 85 % H ₃ PO ₄ .	69
2.14	¹ H NMR Spectrum of Tris(cyclohexylamino)-cycloctenylamino- phosphonium tetrafluoroborate. Signal at 7.24 ppm is residual CHCl ₃ .	69
2.15	³¹ P NMR Spectrum of Tris[cyclohexyl(methyl)amino]-cycloctenyl(methyl)amino-phosphonium tetrafluoroborate in CD ₃ OD.	71
2.16	¹ H NMR Spectrum of Tris[cyclohexyl(methyl)amino]-cycloctenyl(methyl)amino-phosphonium tetrafluoroborate in CD ₃ OD. Signals at 4.52 and 3.31 ppm are due to the NMR solvent.	72
2.17	³¹ P NMR Spectrum of Saturated Copolymer with 17 mol % of Tris[cyclohexyl(methyl)amino]-cycloctenyl(methyl)amino-phosphonium chloride in in CD ₃ OD. Referenced to 85 % H ₃ PO ₄ .	74
2.18	¹ H NMR Spectrum of Saturated Copolymer with 17 mol % of Tris[cyclohexyl(methyl)amino]-cycloctenyl(methyl)amino-phosphonium chloride in DMSO- <i>d</i> ₆ at 135 °C.	75
3.1	Hydrogen/deuterium exchange in model compounds and degradation products.	96
3.2	Summary of protocol for alkaline stability of model compounds.	101
3.3	Model compounds investigated for stability under alkaline conditions.	102
3.4	Degradation of benzyl ammoniums.	104
3.5	Degradation of N,N-ethyl, methyl pyrrolidinium.	105
3.6	Degradation of bicyclic ammoniums.	106
3.7	Degradation of benzyl trimethylphosphonium.	107
3.8	Degradation of benzyl pentamethyl guanadinium.	108
3.9	Degradation of benzyl imidazoliums.	109
3.10	Degradation of 1,3-dimethyl 2-mesityl benzimidazolium.	109
3.11	Stability Model Compounds (0.05 M) in 1 M KOH/CD ₃ OH at 80 °C.	110
3.12	Stability of model compounds (0.05 M) in 2 M KOH/CD ₃ OH at 80 °C.	138
3.13	Comparison of deuterated and non-deuterated stability studies.	138

3.13	Comparison of deuterated and non-deuterated stability studies.	138
3.14	^1H NMR spectra of 1 over 30 days dissolved in a basic CD_3OH solution at 80 °C (1 M KOH, $[\text{KOH}]/[\textbf{1}] = 20$) with an internal standard ($\text{TMS}(\text{CH}_2)_3\text{SO}_3\text{Na}$).	160
3.15	^1H NMR spectra of 2 over 30 days dissolved in a basic CD_3OH solution at 80 °C (1 M KOH, $[\text{KOH}]/[\textbf{2}] = 20$) with an internal standard ($\text{TMS}(\text{CH}_2)_3\text{SO}_3\text{Na}$).	161
3.16	^1H NMR spectra of 3 over 30 days dissolved in a basic CD_3OH solution at 80 °C (1 M KOH, $[\text{KOH}]/[\textbf{3}] = 20$) with an internal standard ($\text{TMS}(\text{CH}_2)_3\text{SO}_3\text{Na}$). Inset is extracted from $t = 5$ d.	162
3.17	^1H NMR spectra of 4 over 10 days dissolved in a basic CD_3OH solution at 80 °C (1 M KOH, $[\text{KOH}]/[\textbf{4}] = 20$) with an internal standard ($\text{TMS}(\text{CH}_2)_3\text{SO}_3\text{Na}$).	163
3.18	^1H NMR spectra of 5 over 30 days dissolved in a basic CD_3OH solution at 80 °C (1 M KOH, $[\text{KOH}]/[\textbf{5}] = 20$) with an internal standard ($\text{TMS}(\text{CH}_2)_3\text{SO}_3\text{Na}$).	164
3.19	^1H NMR spectra of 6 over 30 days dissolved in a basic CD_3OH solution at 80 °C (1 M KOH, $[\text{KOH}]/[\textbf{6}] = 20$) with an internal standard ($\text{TMS}(\text{CH}_2)_3\text{SO}_3\text{Na}$).	165
3.20	^1H NMR spectra of 7 over 30 days dissolved in a basic CD_3OH solution at 80 °C (1 M KOH, $[\text{KOH}]/[\textbf{7}] = 20$) with an internal standard ($\text{TMS}(\text{CH}_2)_3\text{SO}_3\text{Na}$).	166
3.21	^1H NMR spectra of 8 over 30 days dissolved in a basic CD_3OH solution at 80 °C (1 M KOH, $[\text{KOH}]/[\textbf{8}] = 20$ with an internal standard ($\text{TMS}(\text{CH}_2)_3\text{SO}_3\text{Na}$).	167
3.22	^1H NMR spectra of 9 over 30 days dissolved in a basic CD_3OH solution at 80 °C (1 M KOH, $[\text{KOH}]/[\textbf{9}] = 20$) with an internal standard ($\text{TMS}(\text{CH}_2)_3\text{SO}_3\text{Na}$). Inset is extracted from $t = 30$ d.	168
3.23	^1H NMR spectra of 10 over 30 days dissolved in a basic CD_3OH solution at 80 °C (1 M KOH, $[\text{KOH}]/[\textbf{10}] = 20$) with an internal standard ($\text{TMS}(\text{CH}_2)_3\text{SO}_3\text{Na}$).	169
3.24	^1H NMR spectra of 11 over 30 days dissolved in a basic CD_3OH solution at 80 °C (1 M KOH, $[\text{KOH}]/[\textbf{11}] = 20$) with an internal standard ($\text{TMS}(\text{CH}_2)_3\text{SO}_3\text{Na}$). Inset is extracted from $t = 30$ d.	170
3.25	^1H NMR spectra of 12 over 30 days dissolved in a basic CD_3OH solution at 80 °C (1 M KOH, $[\text{KOH}]/[\textbf{12}] = 20$) with an internal standard ($\text{TMS}(\text{CH}_2)_3\text{SO}_3\text{Na}$). Inset is extracted from $t = 30$ d.	171
3.26	^1H NMR spectra of 13 over 30 days dissolved in a basic CD_3OH solution at 80 °C (1 M KOH, $[\text{KOH}]/[\textbf{13}] = 20$) with an internal standard ($\text{TMS}(\text{CH}_2)_3\text{SO}_3\text{Na}$). Inset is extracted from $t = 30$ d. ($\text{TMS}(\text{CH}_2)_3\text{SO}_3\text{Na}$).	172

3.27	¹ H NMR spectra of 14 over 30 days dissolved in a basic CD ₃ OH solution at 80 °C (1 M KOH, [KOH]/[14] = 20) with an internal standard (TMS(CH ₂) ₃ SO ₃ Na).	173
3.28	¹ H NMR spectra of 15 over 30 days dissolved in a basic CD ₃ OH solution at 80 °C (1 M KOH, [KOH]/[15] = 20) with an internal standard (TMS(CH ₂) ₃ SO ₃ Na).	174
3.29	¹ H NMR spectra of 16 over 30 days dissolved in a basic CD ₃ OH solution at 80 °C (1 M KOH, [KOH]/[16] = 20) with an internal standard (TMS(CH ₂) ₃ SO ₃ Na).	175
3.30	¹ H NMR spectra of 1 over 30 days dissolved in a basic CD ₃ OH solution at 80 °C (2 M KOH, [KOH]/[1] = 67) with an internal standard (TMS(CH ₂) ₃ SO ₃ Na).	176
3.31	¹ H NMR spectra of 2 over 30 days dissolved in a basic CD ₃ OH solution at 80 °C (2 M KOH, [KOH]/[2] = 67) with an internal standard (TMS(CH ₂) ₃ SO ₃ Na).	177
3.32	¹ H NMR spectra of 3 over 30 days dissolved in a basic CD ₃ OH solution at 80 °C (2M KOH, [KOH]/[3] = 67) with an internal standard (TMS(CH ₂) ₃ SO ₃ Na).	178
3.33	¹ H NMR spectra of 4 over 5 days dissolved in a basic CD ₃ OH solution at 80 °C (2 M KOH, [KOH]/[4] = 67 with an internal standard (TMS(CH ₂) ₃ SO ₃ Na).	179
3.34	¹ H NMR spectra of 5 over 30 days dissolved in a basic CD ₃ OH solution at 80 °C (2M KOH, [KOH]/[5] = 67) with an internal standard (TMS(CH ₂) ₃ SO ₃ Na).	180
3.35	¹ H NMR spectra of 6 over 30 days dissolved in a basic CD ₃ OH solution at 80 °C (2 M KOH, [KOH]/[6] = 67) with an internal standard (TMS(CH ₂) ₃ SO ₃ Na).	181
3.36	¹ H NMR spectra of 7 over 30 days dissolved in a basic CD ₃ OH solution at 80 °C (2M KOH, [KOH]/[7] = 67) with an internal standard (TMS(CH ₂) ₃ SO ₃ Na).	182
3.37	¹ H NMR spectra of 8 over 30 days dissolved in a basic CD ₃ OH solution at 80 °C (2 M KOH, [KOH]/[8] = 67 with an internal standard (TMS(CH ₂) ₃ SO ₃ Na).	183
3.38	¹ H NMR spectra of 9 over 30 days dissolved in a basic CD ₃ OH solution at 80 °C (2 M KOH, [KOH]/[9] = 67) with an internal standard (TMS(CH ₂) ₃ SO ₃ Na). Inset is extracted from t = 30 d.	184
3.39	¹ H NMR spectra of 10 over 10 days dissolved in a basic CD ₃ OH solution at 80 °C (2 M KOH, [KOH]/[10] = 67) with an internal standard (TMS(CH ₂) ₃ SO ₃ Na).	185
3.40	¹ H NMR spectra of 11 over 30 days dissolved in a basic CD ₃ OH solution at 80 °C (2 M KOH, [KOH]/[11] = 67) with an internal standard (TMS(CH ₂) ₃ SO ₃ Na). Inset is extracted from t = 30 d.	186
3.41	¹ H NMR spectra of 12 over 30 days dissolved in a basic CD ₃ OH solution at 80 °C (2 M KOH, [KOH]/[12] = 67) with an internal standard (TMS(CH ₂) ₃ SO ₃ Na). Inset is extracted from t = 30 d.	187

3.42	^1H NMR spectra of 13 over 30 days dissolved in a basic CD_3OH solution at 80 °C (2 M KOH, $[\text{KOH}]/[\text{13}] = 67$) with an internal standard ($\text{TMS}(\text{CH}_2)_3\text{SO}_3\text{Na}$). Inset is extracted from $t = 30$ d.	188
3.43	^1H NMR spectra of 14 over 30 days dissolved in a basic CD_3OH solution at 80 °C (2 M KOH, $[\text{KOH}]/[\text{14}] = 67$) with an internal standard ($\text{TMS}(\text{CH}_2)_3\text{SO}_3\text{Na}$).	189
3.44	^1H NMR spectra of 15 over 30 days dissolved in a basic CD_3OH solution at 80 °C (2 M KOH, $[\text{KOH}]/[\text{15}] = 67$ with an internal standard ($\text{TMS}(\text{CH}_2)_3\text{SO}_3\text{Na}$).	190
3.45	^1H NMR spectra of 16 over 30 days dissolved in a basic CD_3OH solution at 80 °C (2 M KOH, $[\text{KOH}]/[\text{16}] = 67$) with an internal standard ($\text{TMS}(\text{CH}_2)_3\text{SO}_3\text{Na}$).	191
3.46	^1H NMR spectra of 1 over 5 days dissolved in a basic CH_3OH solution at 80 °C (1 M KOH, $[\text{KOH}]/[\text{1}] = 20$) with an internal standard ($\text{TMS}(\text{CH}_2)_3\text{SO}_3\text{Na}$).	192
3.47	^1H NMR spectra of 2 over 5 days dissolved in a basic CH_3OH solution at 80 °C (1 M KOH, $[\text{KOH}]/[\text{2}] = 20$) with an internal standard ($\text{TMS}(\text{CH}_2)_3\text{SO}_3\text{Na}$).	193
3.48	^1H NMR spectra of 3 over 5 days dissolved in a basic CH_3OH solution at 80 °C (1 M KOH, $[\text{KOH}]/[\text{3}] = 20$) with an internal standard ($\text{TMS}(\text{CH}_2)_3\text{SO}_3\text{Na}$).	194
3.49	^1H NMR spectra of 4 over 5 days dissolved in a basic CH_3OH solution at 80 °C (1 M KOH, $[\text{KOH}]/[\text{4}] = 20$) with an internal standard ($\text{TMS}(\text{CH}_2)_3\text{SO}_3\text{Na}$).	195
3.50	^1H NMR spectra of 5 over 5 days dissolved in a basic CH_3OH solution at 80 °C (1 M KOH, $[\text{KOH}]/[\text{5}] = 20$) with an internal standard ($\text{TMS}(\text{CH}_2)_3\text{SO}_3\text{Na}$). Inset is extracted from $t = 5$ d.	196
3.51	^1H NMR spectra of 6 over 10 days dissolved in a basic CH_3OH solution at 80 °C (1 M KOH, $[\text{KOH}]/[\text{6}] = 20$) with an internal standard ($\text{TMS}(\text{CH}_2)_3\text{SO}_3\text{Na}$). Inset is extracted from $t = 10$ d.	197
3.52	^1H NMR spectra of 7 over 15 days dissolved in a basic CH_3OH solution at 80 °C (1 M KOH, $[\text{KOH}]/[\text{7}] = 20$) with an internal standard ($\text{TMS}(\text{CH}_2)_3\text{SO}_3\text{Na}$). Inset is extracted from $t = 15$ d.	198
3.53	^1H NMR spectra of 8 over 30 days dissolved in a basic CH_3OH solution at 80 °C (1 M KOH, $[\text{KOH}]/[\text{8}] = 20$ with an internal standard ($\text{TMS}(\text{CH}_2)_3\text{SO}_3\text{Na}$).	199
3.54	^1H NMR spectra of 9 over 30 days dissolved in a basic CH_3OH solution at 80 °C (1 M KOH, $[\text{KOH}]/[\text{9}] = 20$) with an internal standard ($\text{TMS}(\text{CH}_2)_3\text{SO}_3\text{Na}$). Inset is extracted from $t = 30$ d.	200

3.55	^1H NMR spectra of 10 over 30 days dissolved in a basic CH_3OH solution at 80°C (1 M KOH, $[\text{KOH}]/[\text{10}] = 20$) with an internal standard ($\text{TMS}(\text{CH}_2)_3\text{SO}_3\text{Na}$). Inset is extracted from $t = 30$ d.	201
3.56	^1H NMR spectra of 11 over 30 days dissolved in a basic CH_3OH solution at 80°C (1 M KOH, $[\text{KOH}]/[\text{11}] = 20$) with an internal standard ($\text{TMS}(\text{CH}_2)_3\text{SO}_3\text{Na}$). Inset is extracted from $t = 30$ d.	202
3.57	^1H NMR spectra of 12 over 30 days dissolved in a basic CH_3OH solution at 80°C (1 M KOH, $[\text{KOH}]/[\text{12}] = 20$) with an internal standard ($\text{TMS}(\text{CH}_2)_3\text{SO}_3\text{Na}$). Inset is extracted from $t = 30$ d.	203
3.58	^1H NMR spectra of 13 over 30 days dissolved in a basic CH_3OH solution at 80°C (1 M KOH, $[\text{KOH}]/[\text{13}] = 20$) with an internal standard ($\text{TMS}(\text{CH}_2)_3\text{SO}_3\text{Na}$). Inset is extracted from $t = 30$ d.	204
3.59	^1H NMR spectra of 14 over 30 days dissolved in a basic CH_3OH solution at 80°C (1 M KOH, $[\text{KOH}]/[\text{14}] = 20$) with an internal standard ($\text{TMS}(\text{CH}_2)_3\text{SO}_3\text{Na}$).	205
3.60	^1H NMR spectra of 15 over 30 days dissolved in a basic CD_3OH solution at 80°C (1 M KOH, $[\text{KOH}]/[\text{15}] = 20$) with an internal standard ($\text{TMS}(\text{CH}_2)_3\text{SO}_3\text{Na}$).	206
3.61	^1H NMR spectra of 16 over 30 days dissolved in a basic CH_3OH solution at 80°C (1 M KOH, $[\text{KOH}]/[\text{16}] = 20$) with an internal standard ($\text{TMS}(\text{CH}_2)_3\text{SO}_3\text{Na}$).	207
3.62	HRMS (DART) of 1 after 5 days dissolved in 1M KOH, CH_3OH solution at 80°C .	208
3.63	HRMS (DART) of 2 after 5 days dissolved in 1M KOH, CH_3OH solution at 80°C .	209
3.64	HRMS (DART) of 3 after 5 days dissolved in 1M KOH, CH_3OH solution at 80°C .	210
3.65	HRMS (DART) of 4 after 5 days dissolved in 1M KOH, CH_3OH solution at 80°C .	211
3.66	HRMS (DART) of 5 after 5 days dissolved in 1M KOH, CH_3OH solution at 80°C .	212
3.67	HRMS (DART) of 6 after 5 days dissolved in 1M KOH, CH_3OH solution at 80°C .	213

3.67	HRMS (DART) of 6 after 5 days dissolved in 1M KOH, CH ₃ OH solution at 80 °C.	213
3.68	HRMS (DART) of 7 after 30 days dissolved in 1M KOH, CH ₃ OH solution at 80 °C.	214
3.69	HRMS (DART) of 7 after 30 days dissolved in 1M KOH, CD ₃ OH solution at 80 °C.	215
3.70	HRMS (DART) of 8 after 20 days dissolved in 1M KOH, CH ₃ OH solution at 80 °C.	216
3.71	HRMS (DART) of 9 after 20 days dissolved in 1M KOH, CH ₃ OH solution at 80 °C.	217
3.72	HRMS (DART) of 9 after 30 days dissolved in 1M KOH, CD ₃ OH solution at 80 °C.	218
3.73	HRMS (DART) of 10 after 20 days dissolved in 1M KOH, CH ₃ OH solution at 80 °C.	219
3.74	HRMS (DART) of 11 after 20 days dissolved in 1M KOH, CH ₃ OH solution at 80 °C.	220
3.75	HRMS (DART) of 11 after 30 days dissolved in 1M KOH, CD ₃ OH solution at 80 °C.	221
3.76	HRMS (DART) of 12 after 20 days dissolved in 1M KOH, CH ₃ OH solution at 80 °C.	222
3.77	HRMS (DART) of 13 after 20 days dissolved in 1M KOH, CH ₃ OH solution at 80 °C.	223
4.1	Selected cations investigated for use in alkaline anion exchange membranes (AAEMs).	227
4.2	Degradation pathways of imidazolium cations under alkaline conditions.	228
4.3	Summary of model compounds investigated, including the synthesis of imidazoliums with varied substitution patterns.	230
4.4	Stability of C4,5 substituted imidazolium cations (0.05 M) in 1 M KOH/CD ₃ OH at 80 °C.	231
4.5	Percent cation remaining after 30 days at 80 °C – Influence of C2 substituents on imidazolium stability. Determined by ¹ H NMR spectroscopy.	233
4.6	Degradation of 4a after 3 months in 1 M KOH/CD ₃ OH at 80 °C.	235
4.7	Percent cation remaining after 30 days at 80 °C – Influence of N1 and N3 substituents on imidazolium stability. Determined by ¹ H NMR spectroscopy.	236

4.8	Percent cation remaining after 30 days at 80 °C – Optimization of base stable imidazoliums. Determined by ^1H NMR spectroscopy.	238
4.9	Analysis of 7a under alkaline conditions using ^1H NMR spectroscopy in CD_3OH . Residual signals between 5.5 – 7.0 ppm are due to solvent; see Section 4.5 for discussion on solvent suppression. ⁴⁴	239
4.10	Comparison of model compound stabilities, percent remaining after 30 days at 80 °C (determined by ^1H NMR spectroscopy relative to an internal standard). ⁴⁴	240
4.11	^1H NMR spectra of 1 over 30 days dissolved in a basic CD_3OH solution at 80 °C (1 M KOH, $[\text{KOH}]/[\textbf{1}] = 20$ with an internal standard ($\text{TMS}(\text{CH}_2)_3\text{SO}_3\text{Na}$).	314
4.12	^1H NMR spectra of 2a over 10 days dissolved in a basic CD_3OH solution at 80 °C (1 M KOH, $[\text{KOH}]/[\textbf{2a}] = 20$) with an internal standard ($\text{TMS}(\text{CH}_2)_3\text{SO}_3\text{Na}$).	315
4.13	Fig ^1H NMR spectra of 2b over 30 days dissolved in a basic CD_3OH solution at 80 °C (1 M KOH, $[\text{KOH}]/[\textbf{2b}] = 20$) with an internal standard ($\text{TMS}(\text{CH}_2)_3\text{SO}_3\text{Na}$).	316
4.14	^1H NMR spectra of 2c over 30 days dissolved in a basic CD_3OH solution at 80 °C (1 M KOH, $[\text{KOH}]/[\textbf{2c}] = 20$) with an internal standard ($\text{TMS}(\text{CH}_2)_3\text{SO}_3\text{Na}$).	317
4.15	^1H NMR spectra of 2d over 30 days dissolved in a basic CD_3OH solution at 80 °C (1 M KOH, $[\text{KOH}]/[\textbf{2d}] = 20$) with an internal standard ($\text{TMS}(\text{CH}_2)_3\text{SO}_3\text{Na}$). Inset is extracted from $t = 30$ d.	318
4.16	^1H NMR spectra of 2e over 30 days dissolved in a basic CD_3OH solution at 80 °C (1 M KOH, $[\text{KOH}]/[\textbf{2e}] = 20$) with an internal standard ($\text{TMS}(\text{CH}_2)_3\text{SO}_3\text{Na}$). Inset is extracted from $t = 30$ d.	319
4.17	^1H NMR spectra of 3a over 30 days dissolved in a basic CD_3OH solution at 80 °C (1 M KOH, $[\text{KOH}]/[\textbf{3a}] = 20$) with an internal standard ($\text{TMS}(\text{CH}_2)_3\text{SO}_3\text{Na}$).	320
4.18	^1H NMR spectra of 3b over 30 days dissolved in a basic CD_3OH solution at 80 °C (1 M KOH, $[\text{KOH}]/[\textbf{3b}] = 20$) with an internal standard ($\text{TMS}(\text{CH}_2)_3\text{SO}_3\text{Na}$).	321
4.19	^1H NMR spectra of 3c over 30 days dissolved in a basic CD_3OH solution at 80 °C (1 M KOH, $[\text{KOH}]/[\textbf{3c}] = 20$) with an internal standard ($\text{TMS}(\text{CH}_2)_3\text{SO}_3\text{Na}$). Inset is extracted from $t = 30$ d.	322
4.20	^1H NMR spectra of 3d over 30 days dissolved in a basic CD_3OH solution at 80 °C (1 M KOH, $[\text{KOH}]/[\textbf{3d}] = 20$) with an internal standard ($\text{TMS}(\text{CH}_2)_3\text{SO}_3\text{Na}$). Inset is extracted from $t = 30$ d.	323

4.21	^1H NMR spectra of 4a over 30 days dissolved in a basic CD_3OH solution at 80 °C (1 M KOH, $[\text{KOH}]/[\mathbf{4a}] = 20$) with an internal standard ($\text{TMS}(\text{CH}_2)_3\text{SO}_3\text{Na}$). Inset is extracted from $t = 30$ d.	324
4.22	^1H NMR spectra of 4b over 30 days dissolved in a basic CD_3OH solution at 80 °C (1 M KOH, $[\text{KOH}]/[\mathbf{4b}] = 20$) with an internal standard ($\text{TMS}(\text{CH}_2)_3\text{SO}_3\text{Na}$). Inset is extracted from $t = 30$ d.	325
4.23	^1H NMR spectra of 4c over 30 days dissolved in a basic CD_3OH solution at 80 °C (1 M KOH, $[\text{KOH}]/[\mathbf{4c}] = 20$) with an internal standard ($\text{TMS}(\text{CH}_2)_3\text{SO}_3\text{Na}$). Inset is extracted from $t = 30$ d.	326
4.24	^1H NMR spectra of 4d over 30 days dissolved in a basic CD_3OH solution at 80 °C (1 M KOH, $[\text{KOH}]/[\mathbf{4d}] = 20$) with an internal standard ($\text{TMS}(\text{CH}_2)_3\text{SO}_3\text{Na}$). Inset is extracted from $t = 30$ d.	327
4.25	^1H NMR spectra of 5a over 30 days dissolved in a basic CD_3OH solution at 80 °C (1 M KOH, $[\text{KOH}]/[\mathbf{5a}] = 20$) with an internal standard ($\text{TMS}(\text{CH}_2)_3\text{SO}_3\text{Na}$). Inset is extracted from $t = 30$ d.	328
4.26	^1H NMR spectra of 5b over 30 days dissolved in a basic CD_3OH solution at 80 °C (1 M KOH, $[\text{KOH}]/[\mathbf{5b}] = 20$) with an internal standard ($\text{TMS}(\text{CH}_2)_3\text{SO}_3\text{Na}$). Inset is extracted from $t = 30$ d.	329
4.27	^1H NMR spectra of 6a over 30 days dissolved in a basic CD_3OH solution at 80 °C (1 M KOH, $[\text{KOH}]/[\mathbf{6a}] = 20$) with an internal standard ($\text{TMS}(\text{CH}_2)_3\text{SO}_3\text{Na}$). Inset is extracted from $t = 30$ d.	330
4.28	^1H NMR spectra of 6b over 30 days dissolved in a basic CD_3OH solution at 80 °C (1 M KOH, $[\text{KOH}]/[\mathbf{6b}] = 20$) with an internal standard ($\text{TMS}(\text{CH}_2)_3\text{SO}_3\text{Na}$). Inset is extracted from $t = 30$ d.	331
4.29	^1H NMR spectra of 7a over 30 days dissolved in a basic CD_3OH solution at 80 °C (1 M KOH, $[\text{KOH}]/[\mathbf{7a}] = 20$) with an internal standard ($\text{TMS}(\text{CH}_2)_3\text{SO}_3\text{Na}$).	332
4.30	^1H NMR spectra of 7b over 30 days dissolved in a basic CD_3OH solution at 80 °C (1 M KOH, $[\text{KOH}]/[\mathbf{7b}] = 20$) with an internal standard ($\text{TMS}(\text{CH}_2)_3\text{SO}_3\text{Na}$).	333
4.31	^1H NMR spectra of 8a over 30 days dissolved in a basic CD_3OH solution at 80 °C (1 M KOH, $[\text{KOH}]/[\mathbf{8a}] = 20$) with an internal standard ($\text{TMS}(\text{CH}_2)_3\text{SO}_3\text{Na}$).	334

4.32	^1H NMR spectra of 8b over 30 days dissolved in a basic CD_3OH solution at 80 °C (1 M KOH, $[\text{KOH}]/[\mathbf{8b}] = 20$) with an internal standard ($\text{TMS}(\text{CH}_2)_3\text{SO}_3\text{Na}$).	335
4.33	^1H NMR spectra of 1 over 30 days dissolved in a basic CD_3OH solution at 80 °C (2 M KOH, $[\text{KOH}]/[\mathbf{1}] = 67$ with an internal standard ($\text{TMS}(\text{CH}_2)_3\text{SO}_3\text{Na}$).	336
4.34	^1H NMR spectra of 2a over 5 days dissolved in a basic CD_3OH solution at 80 °C (2 M KOH, $[\text{KOH}]/[\mathbf{2a}] = 67$ with an internal standard ($\text{TMS}(\text{CH}_2)_3\text{SO}_3\text{Na}$).	337
4.35	^1H NMR spectra of 2b over 10 days dissolved in a basic CD_3OH solution at 80 °C (2 M KOH, $[\text{KOH}]/[\mathbf{2b}] = 67$) with an internal standard ($\text{TMS}(\text{CH}_2)_3\text{SO}_3\text{Na}$).	338
4.36	^1H NMR spectra of 2c over 30 days dissolved in a basic CD_3OH solution at 80 °C (2 M KOH, $[\text{KOH}]/[\mathbf{2c}] = 67$) with an internal standard ($\text{TMS}(\text{CH}_2)_3\text{SO}_3\text{Na}$).	339
4.37	^1H NMR spectra of 2d over 30 days dissolved in a basic CD_3OH solution at 80 °C (2 M KOH, $[\text{KOH}]/[\mathbf{2d}] = 67$) with an internal standard ($\text{TMS}(\text{CH}_2)_3\text{SO}_3\text{Na}$).	340
4.38	^1H NMR spectra of 2e over 30 days dissolved in a basic CD_3OH solution at 80 °C (2 M KOH, $[\text{KOH}]/[\mathbf{2e}] = 67$) with an internal standard ($\text{TMS}(\text{CH}_2)_3\text{SO}_3\text{Na}$).	341
4.39	^1H NMR spectra of 3a over 30 days dissolved in a basic CD_3OH solution at 80 °C (2 M KOH, $[\text{KOH}]/[\mathbf{3a}] = 67$) with an internal standard ($\text{TMS}(\text{CH}_2)_3\text{SO}_3\text{Na}$).	342
4.40	^1H NMR spectra of 3b over 30 days dissolved in a basic CD_3OH solution at 80 °C (2 M KOH, $[\text{KOH}]/[\mathbf{3b}] = 67$) with an internal standard ($\text{TMS}(\text{CH}_2)_3\text{SO}_3\text{Na}$). Inset is extracted from $t = 30$ d.	343
4.41	^1H NMR spectra of 4a over 30 days dissolved in a basic CD_3OH solution at 80 °C (2 M KOH, $[\text{KOH}]/[\mathbf{4a}] = 67$) with an internal standard ($\text{TMS}(\text{CH}_2)_3\text{SO}_3\text{Na}$).	344
4.42	^1H NMR spectra of 4b over 30 days dissolved in a basic CD_3OH solution at 80 °C (2 M KOH, $[\text{KOH}]/[\mathbf{4b}] = 67$) with an internal standard ($\text{TMS}(\text{CH}_2)_3\text{SO}_3\text{Na}$).	345
4.43	^1H NMR spectra of 5a over 30 days dissolved in a basic CD_3OH solution at 80 °C (2 M KOH, $[\text{KOH}]/[\mathbf{5a}] = 67$) with an internal standard ($\text{TMS}(\text{CH}_2)_3\text{SO}_3\text{Na}$).	346
4.44	^1H NMR spectra of 5b over 30 days dissolved in a basic CD_3OH solution at 80 °C (2 M KOH, $[\text{KOH}]/[\mathbf{5b}] = 67$) with an internal standard ($\text{TMS}(\text{CH}_2)_3\text{SO}_3\text{Na}$). Inset is extracted from $t = 30$ d.	347

4.45	¹ H NMR spectra of 6a over 30 days dissolved in a basic CD ₃ OH solution at 80 °C (2 M KOH, [KOH]/[6a] = 67) with an internal standard (TMS(CH ₂) ₃ SO ₃ Na). Inset is extracted from t = 30 d.	348
4.47	¹ H NMR spectra of 7a over 30 days dissolved in a basic CD ₃ OH solution at 80 °C (2 M KOH, [KOH]/[7a] = 67) with an internal standard (TMS(CH ₂) ₃ SO ₃ Na).	350
4.48	¹ H NMR spectra of 7b over 30 days dissolved in a basic CD ₃ OH solution at 80 °C (2 M KOH, [KOH]/[7b] = 67) with an internal standard (TMS(CH ₂) ₃ SO ₃ Na).	351
4.49	¹ H NMR spectra of 8a over 30 days dissolved in a basic CD ₃ OH solution at 80 °C (2 M KOH, [KOH]/[8a] = 67) with an internal standard (TMS(CH ₂) ₃ SO ₃ Na).	352
4.50	¹ H NMR spectra of 8b over 30 days dissolved in a basic CD ₃ OH solution at 80 °C (2 M KOH, [KOH]/[8b] = 67) with an internal standard (TMS(CH ₂) ₃ SO ₃ Na).	353
4.51	¹ H NMR spectra of 1 over 20 days dissolved in a basic CD ₃ OH solution at 80 °C (5 M KOH, [KOH]/[1] = 167) with an internal standard (TMS(CH ₂) ₃ SO ₃ Na).	354
4.52	¹ H NMR spectra of 2a over 5 days dissolved in a basic CD ₃ OH solution at 80 °C (5 M KOH, [KOH]/[2a] = 167) with an internal standard (TMS(CH ₂) ₃ SO ₃ Na).	355
4.53	¹ H NMR spectra of 2b over 1 day dissolved in a basic CD ₃ OH solution at 80 °C (5 M KOH, [KOH]/[2b] = 167) with an internal standard (TMS(CH ₂) ₃ SO ₃ Na).	356
4.54	¹ H NMR spectra of 2c over 2 days dissolved in a basic CD ₃ OH solution at 80 °C (5 M KOH, [KOH]/[2c] = 167) with an internal standard (TMS(CH ₂) ₃ SO ₃ Na).	357
4.55	¹ H NMR spectra of 2d over 5 days dissolved in a basic CD ₃ OH solution at 80 °C (5 M KOH, [KOH]/[2d] = 167) with an internal standard (TMS(CH ₂) ₃ SO ₃ Na).	358
4.56	¹ H NMR spectra of 2e over 3 days dissolved in a basic CD ₃ OH solution at 80 °C (5 M KOH, [KOH]/[2e] = 167) with an internal standard (TMS(CH ₂) ₃ SO ₃ Na).	359
4.57	¹ H NMR spectra of 3a over 30 days dissolved in a basic CD ₃ OH solution at 80 °C (5 M KOH, [KOH]/[3a] = 167) with an internal standard (TMS(CH ₂) ₃ SO ₃ Na).	360

4.58	^1H NMR spectra of 3b over 30 days dissolved in a basic CD_3OH solution at 80 °C (5 M KOH, $[\text{KOH}]/[\text{3b}] = 167$) with an internal standard ($\text{TMS}(\text{CH}_2)_3\text{SO}_3\text{Na}$).	361
4.59	^1H NMR spectra of 4a over 30 days dissolved in a basic CD_3OH solution at 80 °C (5 M KOH, $[\text{KOH}]/[\text{4a}] = 167$) with an internal standard ($\text{TMS}(\text{CH}_2)_3\text{SO}_3\text{Na}$).	362
4.60	Figure 4.60 ^1H NMR spectra of 4b over 5 days dissolved in a basic CD_3OH solution at 80 °C (5 M KOH, $[\text{KOH}]/[\text{4b}] = 167$) with an internal standard ($\text{TMS}(\text{CH}_2)_3\text{SO}_3\text{Na}$).	363
4.61	^1H NMR spectra of 5a over 30 days dissolved in a basic CD_3OH solution at 80 °C (5 M KOH, $[\text{KOH}]/[\text{5a}] = 167$) with an internal standard ($\text{TMS}(\text{CH}_2)_3\text{SO}_3\text{Na}$).	364
4.62	^1H NMR spectra of 5b over 30 days dissolved in a basic CD_3OH solution at 80 °C (5 M KOH, $[\text{KOH}]/[\text{5b}] = 167$) with an internal standard ($\text{TMS}(\text{CH}_2)_3\text{SO}_3\text{Na}$).	365
4.63	^1H NMR spectra of 6a over 30 days dissolved in a basic CD_3OH solution at 80 °C (5 M KOH, $[\text{KOH}]/[\text{6a}] = 167$) with an internal standard ($\text{TMS}(\text{CH}_2)_3\text{SO}_3\text{Na}$).	366
4.64	^1H NMR spectra of 6b over 30 days dissolved in a basic CD_3OH solution at 80 °C (5 M KOH, $[\text{KOH}]/[\text{6b}] = 167$) with an internal standard ($\text{TMS}(\text{CH}_2)_3\text{SO}_3\text{Na}$).	367
4.65	^1H NMR spectra of 7a over 30 days dissolved in a basic CD_3OH solution at 80 °C (5 M KOH, $[\text{KOH}]/[\text{7a}] = 167$) with an internal standard ($\text{TMS}(\text{CH}_2)_3\text{SO}_3\text{Na}$).	368
4.66	^1H NMR spectra of 7b over 30 days dissolved in a basic CD_3OH solution at 80 °C (5 M KOH, $[\text{KOH}]/[\text{7b}] = 167$) with an internal standard ($\text{TMS}(\text{CH}_2)_3\text{SO}_3\text{Na}$). Inset is extracted from $t = 30$ d.	369
4.67	^1H NMR spectra of 8a over 30 days dissolved in a basic CD_3OH solution at 80 °C (5 M KOH, $[\text{KOH}]/[\text{8a}] = 167$) with an internal standard ($\text{TMS}(\text{CH}_2)_3\text{SO}_3\text{Na}$). Inset is extracted from $t = 30$ d.	370
4.68	^1H NMR spectra of 8b over 30 days dissolved in a basic CD_3OH solution at 80 °C (5 M KOH, $[\text{KOH}]/[\text{8b}] = 167$) with an internal standard ($\text{TMS}(\text{CH}_2)_3\text{SO}_3\text{Na}$). Inset is extracted from $t = 30$ d.	371

LIST OF TABLES

1.1	Common Types of Fuel Cells.	4
1.2	AAEMs with Fluorinated Backbones.	12
1.3	AAEMs Comprised of Poly(arylene) ether sulfones.	14
1.4	AAEMs Comprised of Poly(arylene) ether ketones.	15
1.5	AAEMs Comprised of Polyphenylene Oxides.	17
1.6	AAEMs Comprised of Aliphatic Backbones prepared via ROMP.	18
1.7	Aliphatic AAEMs Prepared via Olefin Insertion Polymerization	19
1.8	AAEMs Comprised of Functionalized Polystyrene.	20
1.9	Reported Polymer Stability Studies, by Measurement Technique.	21
2.1	AAEM Characterization Data	55
2.2	AAEM-17 Stability after exposure to 15 M KOH at 22 °C (Data For Figure 2.5)	61
2.3	AAEM-17 Stability after exposure to 1 M KOH at 80 °C (Data For Figure 2.5)	61
2.4	Crystal data and structure refinement for Tetrakis[cyclohexyl(methyl)amino]phosphonium methoxide.	78
2.5	Atomic coordinates ($\times 10^4$) and equivalent isotropic displacement parameters ($\text{\AA}^2 \times 10^3$)	79
2.6	Bond lengths [\AA] and angles [$^\circ$] for Tetrakis[cyclohexyl(methyl)amino]phosphonium methoxide.	81
2.7	Anisotropic displacement parameters ($\text{\AA}^2 \times 10^3$) for Tetrakis[cyclohexyl(methyl)amino]phosphonium methoxide. The anisotropic displacement factor exponent takes the form: $-2p^2[h^2 a^{*2}U^{11} + \dots + 2hka^*b^*U^{12}]$	84
2.8	Hydrogen coordinates ($\times 10^4$) and isotropic displacement parameters ($\text{\AA}^2 \times 10^3$) for Tetrakis[cyclohexyl(methyl)amino]phosphonium methoxide.	86
2.9	Hydrogen bonds for Tetrakis[cyclohexyl(methyl)amino]phosphonium methoxide [\AA and $^\circ$].	89
3.1	Summary of Stability Study Results.	103
3.2	Summary of deuterated stability studies in CD_3OH .	134
3.3	Summary of non-deuterated stability studies in CH_3OH .	136
4.1	Summary of model compound studies.	252
4.2	Model compound studies, selected compounds analyzed at 1-5 days.	254

CHAPTER 1

A Brief Review of Anion Exchange Membranes for Alkaline Fuel Cells with an Emphasis on Chemical Stability

CHAPTER 1

A Brief Review of Anion Exchange Membranes for Alkaline Fuel Cells with an Emphasis on Chemical Stability

1.1 Introduction

Awareness regarding the consequences of our continued reliance on fossil fuels has stimulated an interest in developing a sustainable energy economy.¹ Highly volatile markets and dwindling natural resources have placed a financial burden on established and developing countries alike.^{1d} Moreover, research continues to demonstrate that our primary methods of energy production have negative repercussions on the environment, natural ecosystems and human health.

A variety of approaches to energy storage and conversion have emerged to address these concerns. Some sources, such as geothermal, hydroelectric, wind and solar power tap into an inexhaustible supply of potential energy stored in the earth's natural rhythms. Although these sources are abundant, their intermittency limits their usefulness unless combined with a complementary energy storage technique. Batteries and fuel cells are electrochemical storage and conversion devices that directly convert the energy stored in chemical bonds into electricity to do useful work. However, unlike batteries, which will deplete over time or need to be recharged, fuel cells run continuously with a constant supply of fuel.^{1a} The solution to rising global demands for sustainable energy will likely take the form of a mixture of these practices, drawing on the advantages of each to build a complimentary network.^{1b}

1.1.1 The Role of Fuel Cells in a Sustainable Energy Economy

Fuel cells are generally comprised of an electrolyte medium sandwiched between an anode and a cathode, as shown in Figure 1.1.

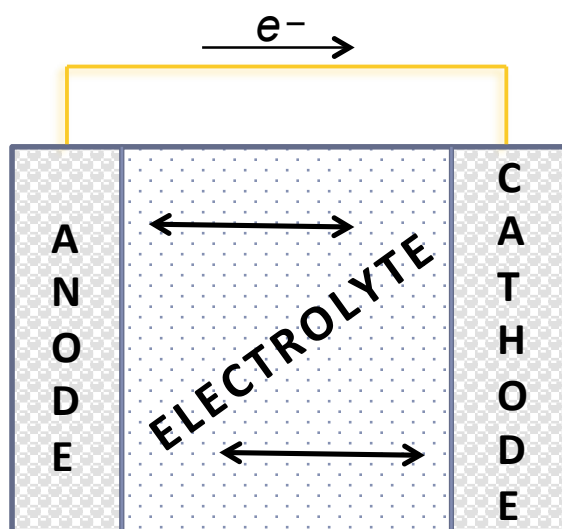


Figure 1.1 Schematic of a Fuel Cell.

Catalysts embedded in the electrode initiate a chemical reaction with the fuel introduced at the anode and the oxidant at the cathode. Ions that are generated pass through the electrolyte layer and electrons flow through an external circuit, producing electricity. The chemical potential in high energy density fuels, such as hydrogen, is transformed with water and heat as the only products. Even when low molecular weight hydrocarbons are employed as fuels, such as methanol, carbon dioxide is the only additional byproduct. This is an advantage over internal combustion engines (ICEs), which release harmful VOCs, carbon monoxide, nitrogen oxides and particulate matter. It is important to note that current commercial supplies of hydrogen derive from methane reforming, which is not a sustainable practice. To reach full potential, fuel cells must be integrated with renewable fuel production and storage methods.² Fuel cells also offer higher theoretical and practical efficiencies compared to ICEs because fewer energy conversions are required to produce electricity and output is not constrained by the Carnot cycle.^{1a} Unlike ICEs, which operate via a dynamic process with moving pistons and gears, fuel cells contain no moving parts and essentially produce no sound or vibrations. Reducing maintenance and noise pollution opens up new application sectors, such as military devices where low acoustic and IR signatures are desired.³

1.1.2 A Comparison of Fuel Cell Types

Fuel cells are unique because they have a flexible configuration that can operate under a range of temperatures using a variety of component materials and fuel types. Some examples are summarized in Table 1.1.^{1a} Depending on the size and type, fuel cells can sustain loads from 1W up to multi-MW power outputs. Conditions of operation and power demands will match a fuel cell to a particular application. SOFCs and MCFCs require very high temperatures to run (>600 °C), but have high electrical efficiencies and can be very useful for stationary applications. In these systems, efficiency is increased when waste heat is repurposed for domestic hot water and space heating or reintroduced in industrial combined heat and power (CHP) applications.

Table 1.1 Common Types of Fuel Cells.

Fuel Cell Type	Typical Fuel	Typical Electrolyte	Typical Anode	Typical Cathode	Operation Temperature
Solid Oxide (SOFC)	Methane	Yttria-stabilized Zirconia (YSZ)	Nickel YSZ-Composite	Strontium-doped Lanthanum Manganite	800–1000 °C
Molten Carbonate (MCFC)	Methane	Lithium Carbonate/Lithium Aluminate	Nickel Chromium	Lithiated Nickel Oxide	600–700 °C
Proton Exchange Membrane (PEMFC)	Hydrogen	Nafion®	Platinum	Platinum/Carbon	60–80 °C
Alkaline Fuel Cell (AFC)	Hydrogen	Potassium Hydroxide	Nickel	Silver/Carbon	0–230 °C

Low temperature fuel cells (<100 °C), such as PEMFCs and AFCs, are suitable for use in consumer electronics and transportation applications, where quick start up times and

responsiveness to power demands are vital. In fact, PEMFCs have been commercialized by a number of companies in the US and worldwide. Unfortunately, these designs are still too expensive to be considered economically feasible for mass production.⁴ Due to the acidic operating pH of PEMFCs, platinum is required for effective catalytic turnover at the electrodes. Research efforts have attempted to reduce the amount of platinum by optimizing the size and morphology of nanoparticles and nanowires, alloying with 3d transition metals or creating Pt-based core-shell structures.^{4a} Yet, platinum is easily poisoned by carbon monoxide and halide impurities, which lowers its activity. Commercial PEMFCs typically contain Nafion,[®] a polymer electrolyte that is composed of a perfluorinated membrane with sulfonate ester functional groups (Figure 1.2).^{4c} The toxicity of Nafion[®] makes it difficult to recycle the platinum from discarded fuel cell stacks. Although, Nafion[®] has high ionic conductivity, the prohibitive manufacturing costs and low durability of the membranes have prompted research into alternative polymers.^{4b} To date, the growth of fuel cells as an efficient and clean source of energy has been stunted by continued reliance on PEMFCs composed of these insufficient materials and systems with improved designs are sought.

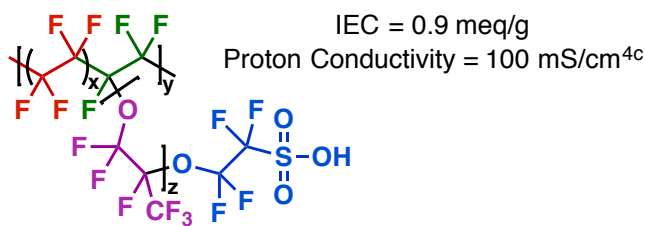


Figure 1.2 Chemical Structure and Properties of Nafion 115.[®]

1.2 Alkaline Fuel Cells

To achieve widespread dissemination of fuel cell technology, the manufacturing costs must be reduced and effective and affordable catalysts must be identified. Designing a device that operates without platinum, a scarce noble metal, is an effective strategy to quickly reduce expenses. This is readily accomplished by running the fuel cell under alkaline conditions. In

fact, alkaline fuel cells were the first type used in a practical application in the 1960s, where they powered NASA spacecraft in the Apollo missions. These fuel cells operated with nickel electrocatalysts and an aqueous potassium hydroxide electrolyte. The steps involved in AFC operation are summarized in Figure 1.3. Oxygen introduced at the cathode reacts with water to produce hydroxide anions that are transported through the electrolyte. At the anode, hydroxide reacts with hydrogen to release electrons, generating water. For several years AFC research was overshadowed by the rapid development of PEMFCs; however, their attributes have stimulated a recent surge of interest.

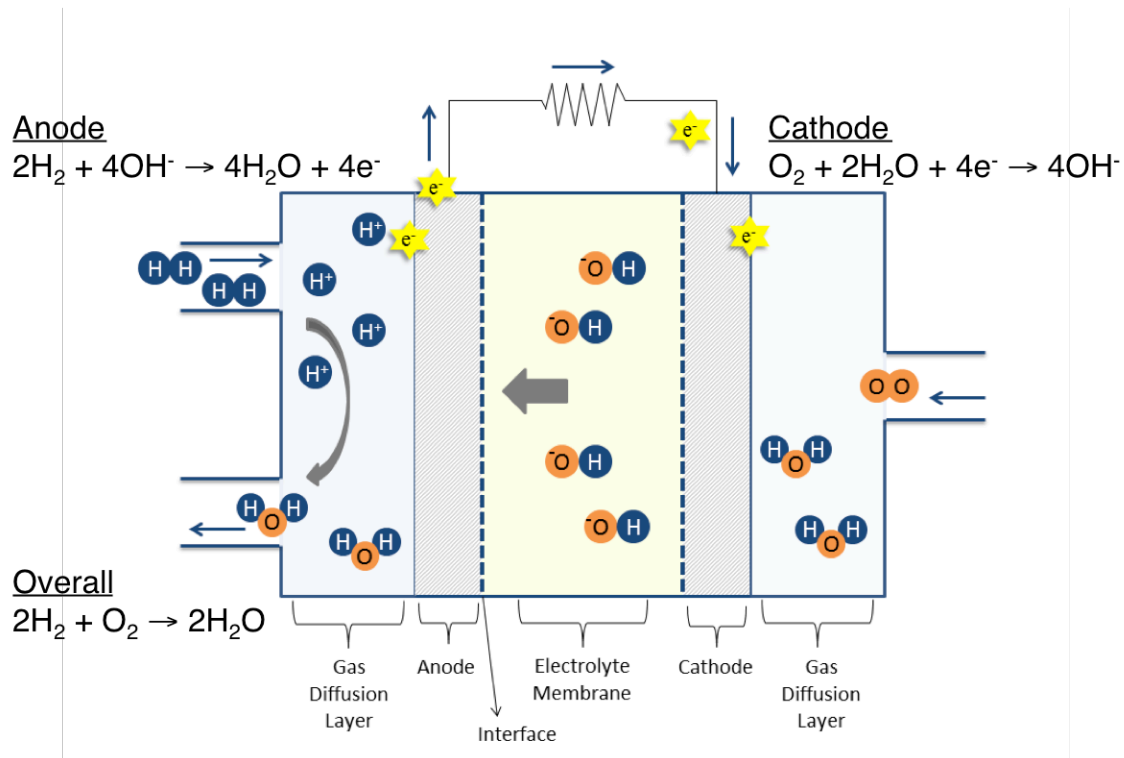


Figure 1.3 Diagram of an Alkaline Fuel Cell.

1.2.1 Advantages of Alkaline Fuel Cells

The acidic nature of a PEMFC requires the use of a noble metal catalyst, but raising the pH permits the use of others metals that do not corrode or dissolve during operation. The oxygen reduction reaction (ORR) is accepted as the kinetically limiting component in fuel cell

electrochemical reactions. The process is highly irreversible and involves several adsorption/desorption steps. Activating ORR as close to reversible conditions as possible improves efficiency. Fortunately, alkaline conditions favor ORR, making the reaction more facile.^{5a} Thus, lower overpotentials are required at high pH. Furthermore, platinum is easily poisoned by carbon monoxide and halide salt impurities that may come into contact with the fuel cell and different metals can offer improved durability of the electrodes.

Crossover of the fuel from the anode to the cathode is a particularly detrimental problem when methanol or ethanol are used as fuels under acidic conditions. In this case, the fuel is not being used efficiently and parasitic side reaction of fuel oxidation occurs at the cathode. Under alkaline conditions the electroosmotic flow is in the opposite direction of PEMCs and directly opposed to the direction that fuel is introduced. Thus, fuel crossover is not an issue in AFCs. There is increasing interest in direct methanol fuel cells (DMFCs) because they circumvent the issue of production and storage of hydrogen. Alkaline conditions promote the advancement of this similar class of fuel cells.

1.2.2 Remaining Challenges for Alkaline Fuel Cells

Although new ORR catalysts have been investigated, only a few reports are available describing the search for efficient hydrogen oxidation reaction (HOR) catalysts. Zhuang, et. al. reported the performance of a fuel cell with a catalyst composed of Ni nanoparticles decorated with Cr, which had a peak power of 50 mW/cm⁻² at 60 ° C.^{5b} Continued improvements in HOR catalysts are important to achieve higher power densities with fully non-Pt based fuel cells.

Ultra-pure oxygen and hydrogen gas streams were used for AFC operation in the space missions. Stringent requirements for the purity of fuel and oxidant gases are cited as the major obstacle for growth of AFCs in terrestrial applications, although this argument is still somewhat debated. The mechanism of failure is attributed to introduction of carbon dioxide to the electrolyte matrix, which reacts with the hydroxide species to form carbonate (Equation 1).^{5c}



Effectively, this reduces the concentration of the highly conductive hydroxide anion in the electrolyte, transforming it into a less conductive charge carrier. In addition to reducing the conductivity, the carbonates combine with potassium cations available in the electrolyte, forming less soluble salts. Precipitation events can block micro-pores in the catalyst or the pathways for the conductive species, increasing electrolyte resistance and reducing catalyst activity. Changes in the electrolyte composition also alter the vapor pressure and electrolyte volume, which complicates water management and system performance. It is proposed that running the fuel cell at high temperatures and current densities will reverse the effects of electrolyte carbonation and regenerate the fuel cell. However, avoiding the formation of carbonate salts altogether is a certain way to overcome this obstacle to developing AFCs.

1.3 Alkaline Anion Exchange Membranes for Fuel Cells⁶

1.3.1 Advantages of AFCs and Comparison to PEMFCs

Taking inspiration from the success with polymers in PEMFCs, polymer electrolytes for AFCs are being developed. AFC membranes would be comprised of polymers with cationic groups appended to the backbone or fused into the backbone structure. Replacing the liquid KOH solutions with a solid polymer eliminates electrolyte seepage and corrosion issues. Using polymers simplifies fabrication of fuel cells, reducing device size and weight.^{6b} Importantly, because the cationic species is covalently linked to the polymer, insoluble carbonate salts will not be generated. Carbonate anions will still form in the presence of carbon dioxide; however, researchers have demonstrated that the carbonate form of the polymer will quickly revert back to the hydroxide form under operating conditions.

As of now, a standard AAEM has not been identified and newly developed AAEMs are typically compared to PEMs, specifically Nafion.[®] This is not always a completely fair comparison because the two operating systems often have substantial differences unrelated to the polymer. For an unbiased assessment, one might presume to keep all components identical between two fuel cells, altering only the polymer electrolyte, to compare the performances. However, the optimal fuel cell components have yet to be identified for alkaline conditions and

comparing the performance to a PEMFC system that has been optimized for decades does not give an accurate representation. Ionic conductivity is inherently lower under alkaline conditions (due to lower ionic mobility of hydroxides compared to protons), but polymer membranes can be optimized to compensate.^{6b} Ultimately for AFC technologies to supersede PEMFCs, they must be competitive with the commercially available system.

Naturally, the initial AAEM architectures were similar to those for PEMFCs, which were actively explored already. Polymers with reactive electrophilic functional groups were prepared via known methods or purchased and treated with amines, such as trimethylamine, generating quaternary ammonium cations. This was effective at producing a variety of polymers quickly as the synthesis was well developed for many of the early examples. Unfortunately, the easy synthesis did not always result in AAEMs with suitable properties and after ~10 years of research there is still a struggle to achieve a membrane with the right characteristics. Relying on synthetic methods for PEMs may be one flaw in the initial approach and materials suitable in acidic conditions do not perform well under the alkaline alternative. Additionally, retrofitting pre-existing polymers to contain cationic groups may not be the best approach. Preparing AAEMs with optimal performance, durability, and cost requires rational design coupled to synthesis to meet these demands.

1.3.2 AAEM Design Principles^{6c-e}

AAEMs are often copolymers prepared by polymerizing two monomers that contribute different characteristics to the final polymer: 1) a functional segment and 2) a structural segment, as shown in Figure 1.4. The functional monomer typically has a cationic moiety already attached or it contains a reactive group that is transformed into a cationic group after polymerization. The functional monomer imparts ionic conductivity and the unfunctionalized structural monomer imparts mechanical strength to the polymer. It is often chemically similar to the functional monomer. Functional and structural segments in a polymer may also be achieved via radiation grafting. Alternatively, the polymer may be a homopolymer that has been functionalized partially to look like a copolymer.

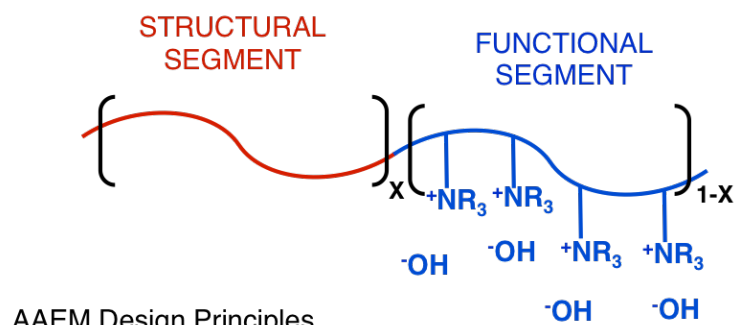


Figure 1.4 Components of an Alkaline Anion Exchange Membrane.

Goals for polymer electrolyte design are improving the hydroxide conductivity, mechanical strength, and chemical stability. In all cases, the polymer composition is optimized to achieve the highest concentration of cation possible without negatively impacting the mechanical strength. Increasing the percent cation in the polymer results in higher ionic conductivities, which increases the current density of the fuel cell. However, introducing too much hydrophilic component into the polymer results in excessive swelling and degrades the mechanical integrity of the film. Sufficient hydration of the cationic domains in the polymer is important for hydroxide anions to move freely through the electrolyte, but too much water will cause flooding, again reducing performance. Thinner membranes are also desirable, as the ohmic resistance is lowered and higher voltages are observed. Often, the range of possible film thicknesses depends on the polymer backbone identity and molecular weight. Finally, the chemical stability of the polymer backbone and the pendant cationic group must be preserved in the presence of hydroxide at elevated temperatures (80–100 °C). Ionic conductivity and mechanical properties of the AAEMs have been optimized sufficiently in recent years; however, chemical stability remains unfulfilled.^{6a} A significant amount of research has been conducted on the alkaline stability of polymers and individual cationic groups, which will be discussed in greater detail in sections 1.5 and 1.6. A summary of the major types of polymers that have been investigated is presented next, organized by polymer backbone. Ammonium-based AAEMs will initially be

examined because they have been the most extensively studied, but other cations will be reviewed along with alkaline stability.

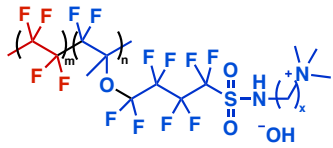
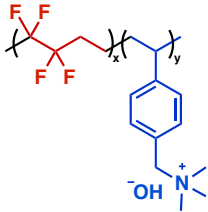
1.4 Types of AAEMs According to Polymer Backbone

The most prominent examples of the major classes of polymers for AAEMs are discussed, although additional types, such as polybenzimidazoles⁷ and composite materials⁸ are actively researched for AAEM electrolytes.

1.4.1 Perfluorinated Polymers⁹

The first viable AAEM that initiated the renewed interest in AFCs is often attributed to the works of Varcoe, Slade and co-workers. They developed a polymer from radiation grafting poly(vinylbenzyl chloride) onto a mixed fluorocarbon/hydrocarbon membrane, followed by amination, that has strong mechanical properties and reasonable hydroxide conductivities (27 mS/cm @ 20 °C).^{9d} Herring *et. al.* reported the modification of a 3M perfluorinated ionomer to include trimethylammonium cations via a sulfonamide linkage.^{9c} Only the chloride conductivity was reported which impedes the meaningful comparison to other membranes (4.8 mS/cm @ 60 °C). Examples of fluorinated AAEMs are presented in Table 1.2.

Table 1.2 AAEMs with Fluorinated Backbones.

Entry	Chemical Structure	Conductivity (Anion) @ Temp	Ref.
1		27 mS/cm (OH ⁻) 20 °C	9c
2		4.8 mS/cm (Cl ⁻) 60 °C	9d

Other attempts by Bosnjakovic and *et. al.* to functionalize 3M ionomers led to unwanted side reactions and AAEMs were not realized.^{9b} Also, Couture *et. al.* described the attempted synthesis of partially fluorinated polymer prepared by radical polymerization of olefins.^{9a} Several options were presented based on this general method and the resulting polymers degraded during functionalization or had undesirable solubility characteristics. Although perfluorinated polymers were successful in PEMFCs, there are severe limitations to applications in AFCs. Aside from modest performance and synthetic roadblocks, these polymers are prepared from expensive and toxic starting materials.

1.4.2 Poly(arylenes)

Polyarylenes, in a multitude of forms, have been the most extensively studied for the synthesis of novel AAEMs. They typically have sulfones, ketones, or a combination of the two functional groups in the backbone. Some of examples of chemical structures and corresponding properties are summarized in Tables 1.3–1.5.

1.4.2.1 Poly(arylene) sulfones¹⁰

Cornelius and co-workers prepared polysulfones via condensation polymerization, followed by chloromethylation and amination of the resulting film.^{10e} Altering the reaction conditions for functionalization resulted in polymer with ion exchange capacities between 0.7–1.9 meq/cm³ and hydroxide conductivities of 3 – 27 mS/cm at 30 °C. Similar polymers prepared by Hickner *et. al.* contained phenyl methyl groups, which were brominated using *N*-bromosuccinamide followed by amination.^{10c} These reaction conditions were less toxic and produced polymers with higher ion exchange capacities (IECs) (1.5–2.4 meq/g), although only bicarbonate conductivities were given (5–27 mS/cm). Zhang and co-workers describe the synthesis and properties of a polysulfone that has a partially fluorinated backbone.^{10d} The IECs ranged from 1.6–3 meq/cm³ and the hydroxide conductivities were between 15–84 mS/cm at 20 °C, reaching some of the highest ambient temperature values observed for AAEMs. Mohanty *et. al.* developed a novel approach to synthesizing polysulfones via C-H Borylation and Suzuki cross-coupling reactions that also avoids chloromethylation.^{10b} The resulting polymers had IECs of 1.3–2.6 meq/cm³ and hydroxide conductivities between 13–56 mS/cm. Finally, a recent example from Liao and co-workers produced a chemically cross-linked membrane with enhanced dimensional stability that had reasonable hydroxide conductivity (22–29 mS/cm, IEC = 1.0–1.2 meq/cm³).^{10a}

Table 1.3 AAEMs Comprised of Poly(arylene) ether sulfones.

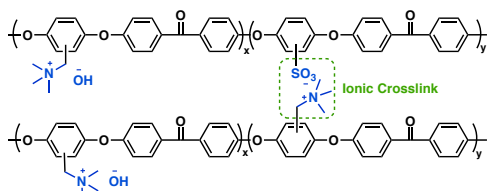
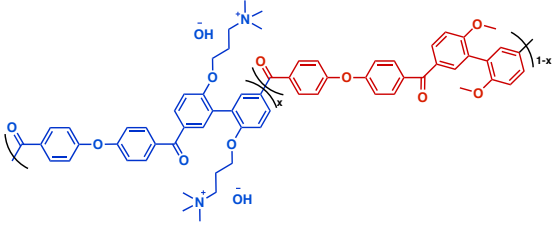
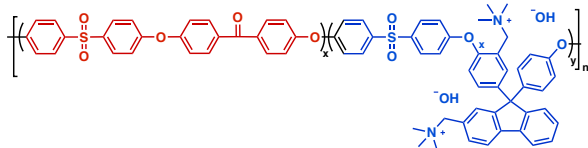
Entry	Chemical Structure	IEC	Conductivity (Anion) @ Temp	Ref.
1		1.2 meq/cm ³	29 mS/cm (OH ⁻) 25 °C	10a
2		2.2 meq/cm ³	43 mS/cm (OH ⁻) 30 °C	10b
3		2.1 meq/g	27 mS/cm (HCO ₃ ⁻) 30 °C	10c
4		2.8 meq/g	65 mS/cm (OH ⁻) 20 °C	10d
5		1.9 meq/cm ³	27 mS/cm (OH ⁻) 30 °C	10e

1.4.2.2 Poly(arylene) ketones¹¹

Zhuang *et. al.* synthesized a unique poly(arylene) ketone with mixed ammonium cations and sulfonate anions.^{11a} The combination of charged species on the polymer resulted in an ionically cross-linked network with an IEC of 1.1 mmol/g and hydroxide conductivity of 25

mS/cm at 20 °C. Xu and co-workers prepared a poly(arylene) ketone that and ammonium groups appended to the backbone with long alkoxy spacers.^{11b} Increasing distance between the cation and backbone is proposed to improve conductivity and stability. One polymer based on this motif had and IEC of 1.9 mmol/g and hydroxide conductivity of 91 mS/cm at 60 °C (30 mS/cm @ 25 °C).

Table 1.4 AAEMs Comprised of Poly(arylene) ether ketones.

Entry	Chemical Structure	IEC	Conductivity (mS/cm) @ Temp.	Ref.
1		1.1 mmol/g	25 mS/cm (OH ⁻) 30 °C	11a
2		1.9 mmol/g	91 mS/cm (OH ⁻) 60 °C	11b
3		1.5 meq/g	93 mS/cm (OH ⁻) 60 °C	12

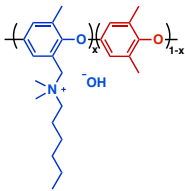
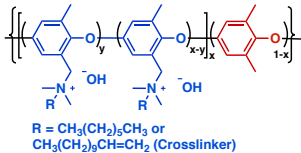
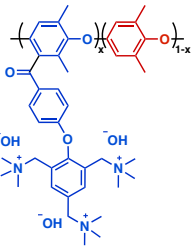
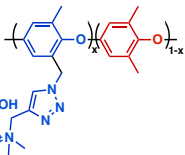
1.4.2.3 Poly(arylene)sulfone ketones¹²

Perhaps the highest hydroxide conductivity for aromatic polymers was observed by Watanabe and co-workers, who prepared a block polymer containing poly(arylene ether) sulfones and ketones.¹² They prepared a series of polymers with various block sizes and degrees of functionalization to tune the IEC and conductivity. For example, a polymer with an IEC of 1.5 meq/g had a conductivity of 93 mS/cm and a polymer with an IEC of 1.9 meq/g obtained 126 mS/cm. The block copolymers had better performance compared to random copolymers of similar composition (i.e. IEC = 1.23, σ = 9.0 mS/cm; IEC = 1.88, σ = 35 mS/cm).

1.4.2.4 Polyphenylene Oxides¹³

Li *et. al.* describe ammonium functionalized polyphenylene oxide that has a long alkyl chain dangling from the cation, producing a comb-shaped architecture.^{13a} A sample with an IEC of 2.1 meq/g had hydroxide conductivity of 28 mS/cm. When the IEC was increased to 2.8 meq/g, the conductivity increased to 43 mS/cm; however, the polymer swelled to 200% its original size. The same group published a subsequent report, which incorporated an aliphatic cross linker into the same architecture.^{13b} This had the anticipated effect of reducing the swelling, while maintaining the conductivity (IEC = 3.20 meq/g, σ = 40 mS/cm, 8% swelling ratio). Bai and co-workers synthesized a PPO with trifunctional cationic moieties attached to the backbone.^{13c} The polymer with the best performance had an IEC of 1.5 meq/g and hydroxide conductivity of 72 mS/cm at 60 °C. Binder and co-workers prepared an azide functionalized PPO, to which ammoniums were incorporated through the azide-alkene “click” reaction.^{13d} IEC values of 1.8 meq/g were realized with hydroxide conductivities of 62 mS/cm at 20 °C.

Table 1.5 AAEMs Comprised of Polyphenylene Oxides.

Entry	Chemical Structure	IEC	Conductivity (mS/cm) @ Temp.	Ref.
1		2.1 meq/g	28 mS/cm (OH ⁻) 20 °C	13a
2	 R = CH ₃ (CH ₂) ₅ CH ₃ or CH ₃ (CH ₂) ₉ CH=CH ₂ (Crosslinker)	3.2 meq/g	40 mS/cm (OH ⁻) 20 °C	13b
3		1.5 meq/g	72 mS/cm (OH ⁻) 60 °C	13c
4		1.8 meq/g	62 mS/cm (OH ⁻) 20 °C	13d

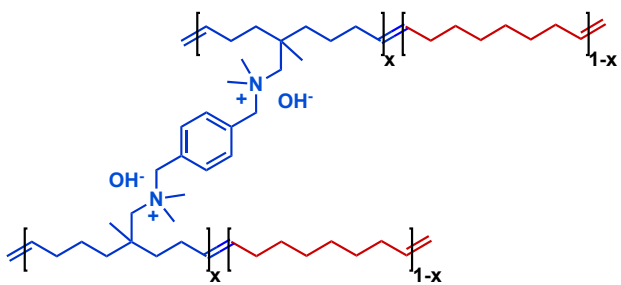
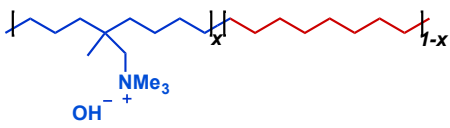
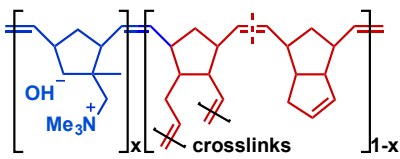
1.4.3 Aliphatic Hydrocarbon Polymers

1.4.3.1 Via Ring Opening Metathesis Polymerization (ROMP)¹⁴

Our research group has led the way in the area of AAEM synthesis via ROMP, summarized in Table 1.6. Clark *et. al.* described the properties of an AAEM prepared from the copolymerization of neopentyl ammonium functionalized norbornene and dicyclopentadiene.^{14c} The resulting cross-linked network had IEC values of 1.0 or 1.4 mmol/g and σ_{OH} of 14 or 18 mS/cm, respectively. Robertson *et. al.* reported a polymer prepared from cis-cyclooctene (COE) and a bifunctional benzyl diammonium cross-linker that had hydroxide conductivity on par with Nafion[®], 69 mS/cm @ 22 °C and 111 mS/cm @ 50 °C.^{14a} Kostalik *et. al.* described the copolymerization of COE with a neopentyl ammonium COE, followed by hydrogenation to

achieve a polymer that was essentially high molecular weight polyethylene with cationic groups appended to it.^{14b} The resulting polymer had an IEC of 1.5 mmol/g and hydroxide conductivity of 65 mS/cm at 50 °C (48 mS/cm @ 20 °C). Importantly, this polymer was readily soluble in volatile, low boiling point solvents, which made it an ideal ionomer for MEA fabrication.

Table 1.6 AAEMs Comprised of Aliphatic Backbones prepared via ROMP.

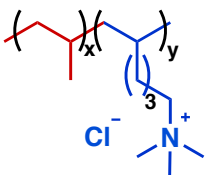
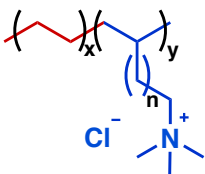
Entry	Chemical Structure	IEC	Conductivity (mS/cm) @ Temp.	Ref.
1		--	111 mS/cm (OH ⁻) 50 °C	14a
2		1.5 mmol/g	65 mS/cm (OH ⁻) 50 °C	14b
3		1.0 mmol/g	14 mS/cm (OH ⁻) 20 °C	14c

1.4.3.2 Via Olefin Polymerization Catalysts¹⁵

Recent reports have demonstrated the feasibility of preparing AAEMs with olefin insertion transition metal polymerization catalysts, shown in Table 1.7. Chung and co-workers describe the synthesis and optimization of polyolefin AAEMs prepared via a metallocene/MAO catalyst system.^{15b} Ethylene was copolymerized with an α -olefin containing a TMS-protected amine and the amine was deprotected and converted to an ammonium post-polymerization. High IECs were observed; however, the conductivities were determined using a method that did not allow direct comparison to other reported. Chung and co-workers also reported the synthesis of

functionalized isotactic polypropylene using a similar strategy.^{15a} Propylene and an α -olefin containing a TMS-protected amine were copolymerized using a titanium-based Ziegler-Natta catalyst system. After polymerization, the TMS groups were removed to produce primary amines that were then converted to imides, which demonstrated that additional functionalization was possible. The resulting polymers were not characterized for IEC or conductivity.

Table 1.7 Aliphatic AAEMs Prepared via Olefin Insertion Polymerization.

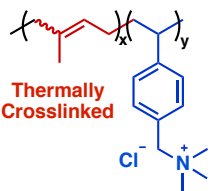
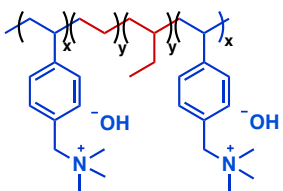
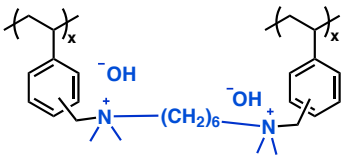
Entry	Chemical Structure	Ref.
1		15a
2		15b

1.4.4 Polystyrenes¹⁶

Polystyrenes are another important class of polymers that have shown promise, especially when copolymerized with olefins, as shown in Table 1.8. Varcoe *et. al.* first described the use of cross-linked polystyrene as a method to prepare AAEMs. Although the electrochemical performance of these membranes was tested, IEC and conductivity by impedance spectroscopy was not reported. Tu and co-workers functionalized a commercial polystyrene-block-poly(ethylene-ran-butylene)-block-polystyrene via chloromethylation and amination. The resulting polymers had very low hydroxide conductivity (<2.5 mS/cm @ 30 °C), which is due to low degree of functionalization. Coughlin and co-workers described the synthesis of a random copolymer of isoprene and chloromethylstyrene via nitroxide mediated radical polymerization. The functional groups were converted to ammoniums after polymerization and membranes were

cast from the soluble ionomers. Notably, the resulting films were thermally cross-linked, which improved the mechanical properties. Chloride conductivities (9–17 mS/cm @ 60 °C) were reported for a series of polymers with IECs between 1.3–2.3 mmol/g.

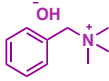
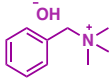
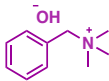
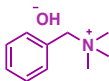
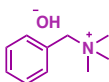
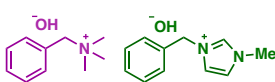
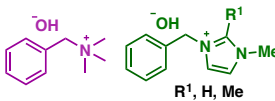
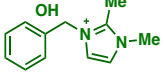
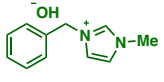
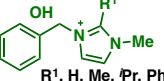
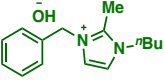
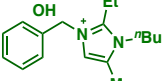
Table 1.8 AAEMs Comprised of Functionalized Polystyrene.

Entry	Chemical Structure	IEC	Conductivity (mS/cm) @ Temp.	Ref.
1		1.5 mmol/g	17 mS/cm (Cl ⁻) 60 °C	16a
2		0.3 meq/g	2.5 mS/cm (OH ⁻) 30 °C	16b
3		--	--	16c

1.5 Investigation of AAEM Polymer Stability

The variations in polymer architecture and composition have made it possible to achieve a wide range of hydroxide conductivities and new strategies for improving the mechanical integrity of the resulting membranes. However, developing polymers with higher resistance to degradation under the operating conditions of an AFC remains an issue. Reports indicate that many of the commonly used polymer backbones degrade under alkaline conditions. Furthermore, the ammonium cations that are the easiest to access synthetically, do not typically have suitable alkaline stability. Degradation of ammonium cations will be addressed in section 1.6. Several methods have surfaced to understand the nature of polymer stability and decomposition and the examples shown in Table 1.9 will be reviewed.

Table 1.9 Reported Polymer Stability Studies, by Measurement Technique.

Entry	Polymer ^{Ref}	Cationic Moieties	Primary Techniques	Secondary Techniques	Results
1	PAES ¹⁷		—	IEC $\sigma(\text{OH}^-)$	Stable
2	PAES ¹⁸		2D NMR	—	Backbone Degrades
3	F-PAE, PAES, PP ¹⁹		FTIR	$\sigma(\text{OH}^-)$	Backbone And Cation Degrade
4	PS, PAES, PPO ²⁰		¹ H NMR	—	Cation Degrades
5	PAE, PP ²¹		FTIR	¹ H NMR	Backbone And Cation Degrade
6	PAESK ²²		¹ H NMR	IEC Viscosity	Backbone And Cation Degrade
7	ETFE-PS ²³		Raman ¹⁵ N, ¹³ C NMR	IEC $\sigma(\text{HCO}_3^-)$	Cation Degrades
8	PPO ²⁴		FTIR	IEC	Cation Degrades
9	PP ²⁵		¹ H NMR	—	Cation Degrades
10	PS ²⁶		¹ H NMR	$\sigma(\text{OH}^-)$	Stable
11	PS/PAES ²⁷		FTIR ¹ H NMR	$\sigma(\text{OH}^-)$	Stable
12	PAES ²⁸		—	$\sigma(\text{OH}^-)$	Stable

1.5.1 Ammonium-based AAEM Stability

Early studies indicated that ammonium-based AAEMs were stable under alkaline conditions. For example, Zhang and co-workers tested the alkaline stability of PAES polymers that contained benzyl trimethylammonium (BTMA) groups by submerging them in 4 M NaOH solution at 20 °C for 48 hours.¹⁷ The polymer integrity and appearance did not change and neither did the reported IECs or hydroxide conductivities.

However, several other reports suggest that AAEMs with pendant ammonium groups are not stable under all conditions. In some of these studies, the polymer backbone is not innocent and plays a role in degradation mechanism. Ramani and co-workers subjected PAES membranes functionalized with BTMA to 1M and 6M KOH solutions at 60 °C for 30 days.¹⁸ The 2D NMR studies (COSY and HMQC) conducted on the resulting samples conclusively determined that degradation was occurring at the backbone of the polymer and not at the BTMA cations. The authors state that relying on ¹H NMR alone would not have provided sufficient evidence for this event. Control studies conducted with non-cationic PAESs did not result in degradation, indicating that cation incorporation weakens the polymer backbone stability. The theory is that hydrophilic cations swell the polymer with solvent and bring the nucleophilic hydroxide anions closer to the backbone to participate in reactions.

Degradation of the PAES backbone was observed in another study conducted by Fujimoto *et. al.*, in which partially fluorinated F-PAE, PAES and polyphenylene membranes were prepared containing BTMA groups.¹⁹ Samples were treated with 0.5 M NaOH at 80 °C for up to an hour and analyzed by FTIR and hydroxide conductivity. Notably, phenolic –OH stretches were observed in the IR for both PAES samples after base treatment, but not for polyphenylene. However, decreases in the ammonium C-N stretches were observed for F-PAE and polyphenylene, but not for PAES. This suggested that there was backbone and cation degradation in F-PAE, backbone degradation and PAES and cation degradation in polyphenylene. The authors also noticed that conductivity did not always predict degradation accurately. Clearly, the fragmentation of polymer chains would not necessarily reduce

conductivity if ammonium cations persevered, but AAEM performance would still suffer.

Hickner and Nuñez used ^1H NMR to follow the stability of PAES membrane functionalized with BTMA.²⁰ The polymer was dissolved in a 3:1 $\text{CD}_3\text{OD}:\text{D}_2\text{O}$ mixture containing 0.6 M KOD and heated to 80 °C. Rapid degradation of the cationic group was observed over 12 hours, producing the known degradation products benzylmethyl ether and benzyl dimethylamine. Similar polymer samples prepared from polystyrene or PPO did not degrade as rapidly, although some loss was observed. This supports that the polymer backbone plays a role in the stability of the appended cation.

Kim and co-workers studied the stability of F-PAE and polyphenylene membranes with BTMA groups by treating the samples with 0.5 M NaOH at 80 °C for 2 hours.²¹ The changes in FTIR suggested that F-PAE degraded at the backbone and BTMA, whereas polyphenylene degraded only at cationic site. Computational studies support these observations by showing that the energy barrier for degradation at the BTMA benzylic position is similar to the barrier for the backbone ether in PAES. Comparatively, the energy barrier for backbone degradation of polyphenylene is more than twice the barrier for BTMA.

1.5.2 Imidazolium-based AAEM Stability

The degradation of BTMA has prompted investigation into alternative cations for AAEMs and imidazoliums were selected as a promising choice due to their resonance stabilization. However, a few studies comparing the stability of ammonium-based AAEMs to imidazolium-based AAEMs indicated that imidazolium cations were less stable. Hickner and Chen investigated the stability of PAES with BTMA and imidazolium cations appended via a fluorenyl group.²² The polymers were stored in 1 M NaOH at either 60 °C or 80 °C over 48 hours and then monitored by IEC and intrinsic viscosity. A similar decrease in IEC was observed at 60 °C for both polymers, yet the imidazolium AAEM experienced a larger decrease at 80 °C. Substantial losses in viscosity were observed for the ammonium polymer at both temperatures and the imidazolium polymer became insoluble and could not be tested, which indicates backbone degradation in addition to loss of cation.

Varcoe and co-workers directly compared the stability of ETFE-PS polymers containing BTMA and two different imidazolium cations, which differed in substitution at the C2 position.²³ The imidazolium numbering scheme is described in Figure 1.6. The samples were stored in 1 M KOH at 60 °C over 15 days and analyzed by IEC, bicarbonate conductivity, Raman and NMR (¹⁵N and ¹³C). The BTMA polymer was stable by IEC and conductivity and the unsubstituted imidazolium decreased rapidly within one day. The imidazolium with a C2-methyl group also degraded, but the rate was much slower. Changes were also observed by spectroscopy, although the indicated techniques did not provide quantitative results.

Further investigations into imidazolium-based AAEMs indicated that they were unstable under alkaline operating conditions. Xu and co-workers examined the stability of PPO functionalized with an imidazolium with a C2-methyl group.²⁴ The polymer was stored in 2 M KOH at 25 or 60 °C and analyzed by IEC and FTIR over nine days. The polymer was stable at room temperature, but the IEC decreased steadily and fewer imidazolium cation stretches were observed by FTIR.

Elabd and co-workers investigated the alkaline stability of an acrylate homopolymer that was functionalized with unsubstituted imidazolium cations.²⁵ It was concluded that the stability of the polymer depended on a combination of the base concentration, temperature and relative humidity. At KOH concentrations greater than 1 M the polymer was unstable, even at room temperature. Moreover, the dry membrane was observed to decomposed when heated to 80 °C. Amide signals were observed for the degraded samples analyzed by ¹H NMR, suggesting that the imidazolium degraded via a ring-opening pathway, discussed in section 1.6.

Although these reports suggest that imidazoliums are not suitable for AAEMs due to poor alkaline stability, research has surfaced that indicates imidazolium cations can be stable with the right substitution patterns. Yan and co-workers investigated polystyrene AAEMs that had pendant imidazoliums containing various C2 substituents (C2 = hydrogen, methyl, isopropyl, or phenyl).²⁶ The polymers were dissolved in solutions of 1 or 2 M KOH in D₂O and stored at 80 °C. Over 60 hours, precipitate was observed for all the samples, indicating degradation of the

polymer, except the C2-Me substituted imidazolium. Further analysis by ^1H NMR confirmed this assessment. A cross-linked polystyrene network was prepared containing the C2-Me imidazolium and the alkaline stability was monitored by hydroxide conductivity for up to three days. Degradation of this polymer was not observed, which supports that imidazoliums with the right substitution patterns can be suitable for AAEMs.

Yan and co-workers also prepared a polystyrene matrix functionalized with imidazolium cations that had PAES side chains.²⁷ Based on previous studies, they selected C2-methyl and N-butyl substituents for the imidazolium ring. The authors declared the polymer stable after 20 days in 1 M KOH at 60 °C and supported this claim with FTIR, ^1H NMR and hydroxide conductivity. Zhang and co-workers describe the stability of an imidazolium functionalized PAES membrane, with C2-ethyl, C4-methyl and N-butyl substituents.²⁸ The ionic conductivity was assessed after 2.4 days in 1 M KOH at 60 °C and 80% of the initial hydroxide conductivity was conserved. These studies did not comment on the alkaline stability of the PAES backbone, which was observed to be unstable under similar conditions in previously discussed reports.

1.5.3 Conclusions

The bulk of literature investigations on AAEM stability are unclear as to whether ammonium cations are more or less stable than imidazolium cations. The studies appear to be highly dependent on the measurement technique, as well as exact structure of the cations. To complicate matters more the polymer backbones are involved in degradation of AAEMs and it is difficult to ascertain how much of the decomposition is due to the cation or backbone. In many of these examples, only two simple cations were compared. To investigate a larger number of cations concomitantly and rank alkaline stability a more effective technique must be employed.

1.6 Alkaline Stability of Cations

Model compound studies, wherein small molecule cations are synthesized and studied under a variety of alkaline conditions, have been informative to describe the stability and degradation of cations in AAEMs. This method allows for a quick examination of many types of cations, without the added concern of polymer synthesis and stability. A number of theoretical

and experimental studies have evolved to investigate cation stability. Unfortunately, the inconsistencies between studies make it difficult for direct comparisons. However, some trends have emerged that have been validated by different methods and researchers. The goal is to understand the relative stability of cations so cations with improved design can be incorporated into polymers. Polymer stability under alkaline conditions, including *in situ* fuel cells testing, is the ultimate parameter to measure; however this requires significant effort. Model compound studies have the power to reduce the time, energy and resources needed to develop AAEMs with exceptional stability. Ammonium and imidazolium cations have been the most extensively researched and will be summarized.

1.6.1 Alkaline Stability of Ammonium Cations

1.6.1.1 Ammonium Cations – Computational Studies

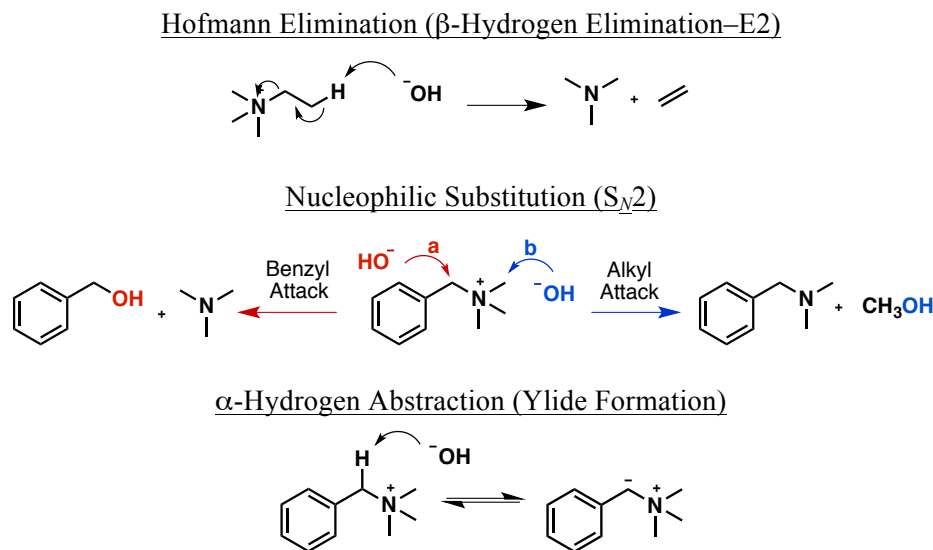


Figure 1.5 Degradation Pathways of Ammonium Cations.

The reactions of ammonium cations with bases and nucleophiles are well known and include Hofmann elimination, nucleophilic substitution and α -hydrogen abstraction (ylide formation), summarized in Figure 1.5.

In series of accounts, Pivovar and co-workers investigated the stability of various tetraalkylammonium cations in the presence of hydroxide.²⁹ Typically, DFT B3LYP was used in

Gaussian (G09) with a 6-311++G(2d,p) basis set and a polarizable continuum solvation model (PCM). Their computations suggested that cation stability was highly dependent on solvation of the cation and the description of solvation in their model was very important. The energy barrier for Hofmann elimination (E2) is lower than the S_N2 reaction barriers for ethyltrimethylammonium hydroxide; therefore, elimination is preferred when β -hydrogens are present. The barrier for elimination increased with longer alkyl chain lengths up to a certain extent. They observed that the ylide species formed during deprotonation of BTMA and other cations was a very reversible and typically did not degrade the cation. There did not appear to be a significant difference between S_N2 reactions at methyl and benzylic positions in BTMA. In a recent study, Pivovar and Long assessed the change in activation energy for S_N2 reactions of hydroxide with BTMA that occurred with different substituents on the aromatic ring.³⁰ Electron-donating substituents increased the barrier for S_N2 attack to a limited extent; yet, electron withdrawing groups noticeably decreased the barrier. The authors state that they do not believe aromatic substitutions will improve BTMA cation stability to any appreciable extent.

1.6.1.2 Ammonium Cations – Experimental Studies

To compliment their computational studies on substituted trimethylammonium cations, Pivovar *et. al.* synthesized discrete complexes of cations in the deuteroxide form.³¹ The salts were heated controllably by TGA and the evolved gases were analyzed by MS. The effect of alkyl chain length and steric bulk was examined with ethyl, n-propyl, iso-butyl and neo-pentyl substituents. It was proposed that as the number of β -hydrogens decreased and steric bulk increased with these groups, the imidazoliums would be less reactive with bases and nucleophiles. The experimental results confirmed that as the number of hydrogens available for elimination decreased, the occurrence of nucleophilic degradation increased. S_N2 attack occurred more prevalently at the methyl position, due to the increase in steric bulk at the longer alkyl substituents.

Sturgeon *et. al.* have proposed a method for determining the alkaline stability of model compounds to mimic cation degradation in AAEMs and applied it to BTMA.³² They examined

many experimental conditions, altering concentrations of reagents and reaction temperature. Ultimately, they arrived at a set of conditions that they believe accurately describes the alkaline stability of BTMA. Solutions were prepared to contain high KOH concentration (1 M) and low cation concentration (< 0.1 M) in non-deuterated solvents and were stored in Teflon-lined Parr reactors. With this method they achieve reproducible degradation rates under accelerated conditions. Notably, the authors suggest that BTMA is more stable than previous reports have suggested, making it an option again as an AAEM cation.

Mohanty and Bae investigated the alkaline stability of ammonium cations other than BTMA.³³ Discrete complexes of the ammonium hydroxide salts were synthesized and the stability was determined in hot water. They proposed this alternative method to mimic fuel cells conditions more closely. The study showed that switching the benzyl ammonium substituents from methyl groups to n-propyl or cyclohexyl groups resulted in cations with greater stability. Moreover, the best stability was observed for a trimethylammonium where the cationic nitrogen was far removed from the aromatic group. This effective strategy of eliminating the reactive benzylic position has been observed in accounts on polymer stability.

1.6.2 Alkaline Stability of Imidazolium Cations

1.6.2.1 Imidazolium Cations – Computational Studies

There is an interest in replacing ammonium cations in AAEMs with imidazoliums because cations that are stabilized by charge delocalization are hypothesized to be more resistant to alkaline degradation. The most reported mode of degradation for imidazolium cations results from nucleophilic addition of hydroxide to the C2 position and subsequent ring opening, as shown in Figure 1.6. Researchers have investigated the energy barriers to various reaction pathways associated with interactions of hydroxide and imidazolium cations.

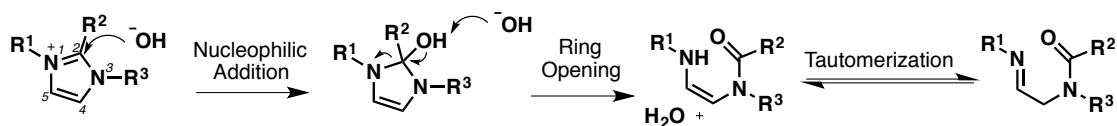


Figure 1.6 Ring Opening Degradation of Imidazolium Cations.

Li and co-workers calculated the LUMO energies for a variety of imidazolium cations with different substitution patterns to discern the influence of substitution on the reactivity.³⁴ DFT calculations were performed using the DMol3 program in Materials Studio (version 6.0). A conductor-like screening model (COSMO) was used to model solvent effects. They suggest that LUMO energies will correlate well with reactivity such that imidazoliums relatively higher LUMOs will be more stable than those with lower LUMOs. This is based on the assumption that nucleophilic addition of hydroxide to the imidazolium cation is a major factor in the reaction rate, which may not always be the case. They found that LUMO energies changed based on the electron donating characteristics and hyperconjugation capacity of the substituents. They noticed that electron-withdrawing groups at the C2 position lowered the LUMO, whereas electron-donating alkyl groups were most effective at raising the LUMO of the imidazolium. Perhaps more importantly, hyperconjugation effects of various alkyl substituents at the C2 and N3 positions impacted LUMO energies. They observed that α -CH hydrogens raised the energy of the unoccupied π orbitals of the adjacent ring system. For example, phenyl groups (with zero α -H's) had lower LUMO energies compared to alkyl groups. Alkyl groups with α -branching at the C2 position (i.e. isopropyl or tert-butyl) disrupted the hyperconjugation between the substituent and the ring and secondary hyperconjugation between substituents. Methyl groups (with 3 CH's) appear to be the most effective at increasing the LUMO energy. Higher LUMO energies are observed for N3 alkyl groups with carbon lengths between C3-C6; however, a drop was observed for longer chains. The authors hypothesize that very long chains aggregate, distorting the structure and disrupting the hyperconjugation effect.

Based on DFT calculations (similar to Section 1.6.6.1), Pivovar and Long modeled the degradation pathway of imidazolium cations.³⁵ They proposed a mechanism that proceeds via two transitions states, as shown in Figure 1.7. A number of imidazolium cations with varying C2 and C4,C5 groups were studied and the rate determining step changed based on the substituent patterns.

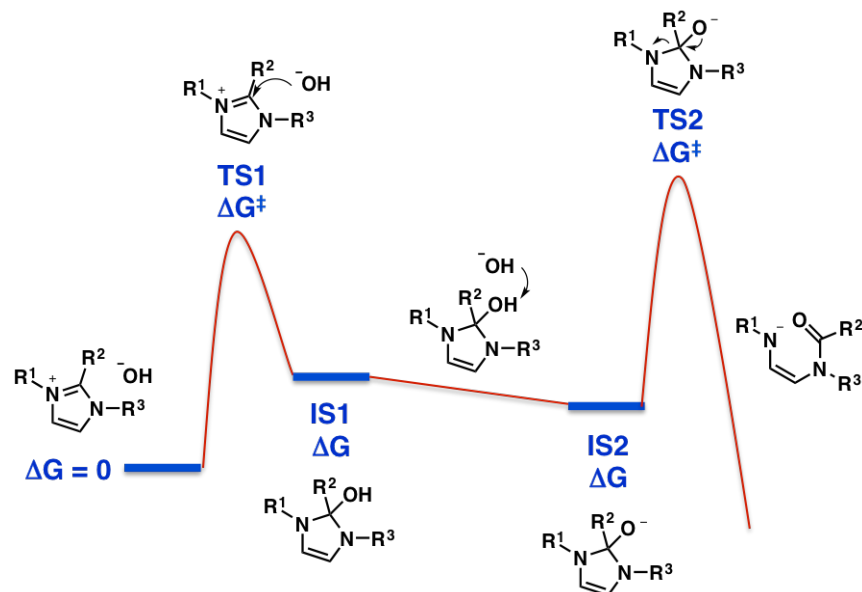


Figure 1. 7 Proposed Free Energy Diagram for Ring-Opening Degradation of Imidazolium Cations. (Adapted from Ref. 35)

Changing the R-groups will alter the activation barriers, thereby making degradation more or less favorable. Specifically, any substitution at the C2 position raises the energy barrier and makes the cation more stable. Importantly, the substituents not only have an impact on the addition of hydroxide to the C2 position (TS1), but they also influence the ring-opening event (TS2). The steric effects proceed either by directly blocking the preferred trajectory of a nucleophile or by reducing the rotational freedom within the cation. Methyl groups at the 2' and 6' position of the C2-phenyl groups increase the energy barrier relative to the unsubstituted phenyl group because the additional substituents increase the dihedral angle between the two ring systems, reducing favorable orbital overlap and physically blocking addition to the C2 position. Finally, the calculations suggested that C4,C5 methyl groups improve stability over hydrogens and not just by eliminating the deprotonation reaction. The activation barrier for TS1 is actually lower for the substituted version because steric interference within the ring raises the ground state energy. However, steric interference creates a very large TS2 barrier, which changes the RDS and raises the activation energy. This work provides a complementary theoretical explanation for many trends observed experimentally.

Ramani and co-workers also conducted DFT calculations that support many earlier claims. Of interest, they also describe the Schiff base tautomers that result from ring opening of the imidazolium ring and propose that they are most energetically favorable. Moreover, they did not observe a significant difference in which side the imidazolium ring opened in the final step of degradation for the asymmetric cations investigated.³⁶

1.6.2.2 Imidazolium Cations – Experimental Studies

In a series of reports, Yan and co-workers conducted alkaline stability studies on a number of small molecule imidazolium cations, as models for the cations incorporated into polymers.³⁷ It is important to note that there were differences in the exact nature of the stability procedures during the separate investigations. Caution should be taken when comparing exact values, although the overall trends may be useful. Cations with N1-ethyl, N3-methyl substituents with varied C2-groups (H, Me, ⁱPr and Ph) were investigated. Imidazolium stability improved in the following order: Me > ⁱPr > Ph > H. Although the reported BTMA stability was determined under different conditions, the authors concluded that these imidazolium cations with C2 substitution were more stable than BTMA. Next, the stability of imidazolium cations with 1,2 dimethyl substituents and varied N3 groups were investigated. The stability of N-methyl, isopropyl and n-butyl groups were compared and the results were ⁱPr > ⁿBu > Me. The experimental results corroborate their calculations (1.6.2.1). In a subsequent investigation, they revisited C2 substitution with imidazolium cations that contained N1-methyl and N3-butyl groups. Specifically, they looked at the length of the alkyl chain by comparing C2-methyl, ethyl and n-butyl groups. They reported that the ethyl group was less stable compared to methyl; however, the n-butyl group was the most stable substituent.

Zhang and co-workers used model compound studies to compare the alkaline stability of similar imidazolium cations with C4-hydrogen or methyl substituents.³⁸ Although the degradation was not followed quantitatively, the authors observed new signals related to decomposition in the ¹H NMR of the compound with C4-hydrogen. Under the conditions examined, degradation was not observed for the compound with C4-methyl, which

experimentally supports theoretical studies.

Benzimidazolium cations are a unique class of imidazolium cations that are also interesting for AAEMs. Of note, Holdcroft and co-workers discovered the benefit of using mesityl aryl groups at the C2-position to prevent nucleophilic addition and ring-opening degradation reactions.³⁹ This work inspired many of the subsequent studies involving C2 substitution of imidazolium cations.

1.7 Conclusions and Future Outlook

A variety of polymer architectures, containing pendant cations, have been explored as potential candidates for use as AAEMs in AFCs. Selection of polymer backbone and modifications like crosslinking have made it possible to achieve high incorporation of cations into the polymers, resulting in high IEC and conductivity, without sacrificing the mechanical properties. To develop AAEMs that can compete with commercially available PEMs, the alkaline stability of the polymer backbones and cations must be improved. As new structures are proposed, the methods of assessing polymer stability must be unified and comprehensive to predict which polymers will perform best. Model compound studies are effective at isolating the contribution that the cationic moiety has on the overall stability and allow rapid selection of the most stable cation. New synthetic approaches to preparing polymers for AAEMs are required because many of the established polymer backbones have been shown to degrade under alkaline conditions. Modifications to the current backbones to make them more stable or development of alternative polymerization techniques are required to meet this goal. Adapting the morphology of the polymer by synthesizing block copolymers or grafted polymers may be an interesting avenue to increasing hydroxide conductivity and stability. Finally, incorporating the polymers into MEAs and devices and assessing the performance *in situ* is necessary to validate the effectiveness of the AAEMs as components in fuel cells.

REFERENCES

- (1) (a) Sharaf, O. Z.; Orhan, M. F. *Renewable Sustainable Energy Rev.* **2014**, *32*, 810–853. (b) Ehteshami, S. M. M.; Chan, S. H. *Energy Policy* **2014**, *73*, 103–109. (c) Rao, M. C. *Int. J. Mod. Phys.: Conf. Ser.* **2013**, *22*, 385–390. (d) Dunn, S. *Int. J. Hydrogen Energy* **2002**, *27* (3), 235–264.
- (2) (a) Ehret, O.; Bonhoff, K. *Int. J. Hydrogen Energy* **2015**, *40* (15), 5526–5533. (b) Bocci, E.; Di Carlo, A.; McPhail, S. J.; Gallucci, K.; Foscolo, P. U.; Moneti, M.; Villarini, M.; Carlini, M. *Int. J. Hydrogen Energy* **2014**, *39* (36), 21876–21895.
- (3) Patil, A. S.; Dubois, T. G.; Sifer, N.; Bostic, E.; Gardner, K.; Quah, M.; Bolton, C. J. *Power Sources* **2004**, *136* (2), 220–225.
- (4) (a) Scofield, M. E.; Liu, H.; Wong, S. S. *Chem. Soc. Rev.* **2015**. (b) Kraytsberg, A.; Ein-Eli, Y. *Energy Fuels* **2014**, *28* (12), 7303–7330. (c) Zawodzinski Jr, T. A.; Neeman, M.; Sillerud, L. O.; Gottesfeld, S. *J. Phys. Chem.* **1991**, *95* (15), 6040–6044.
- (5) (a) Ge, X.; Sumboja, A.; Wu, D.; An, T.; Li, B.; Goh, F. W. T.; Hor, T. S. A.; Zong, Y.; Liu, Z. *ACS Catal.* **2015**, *5*, 4643–4667. (b) Lu, S.; Pan, J.; Huang, A.; Zhuang, L.; Lu, J. *Proc. Natl. Acad. Sci.* **2008**, *105* (52), 20611–20614. (c) McLean, G. *Int. J. Hydrogen Energy* **2002**, *27* (5), 507–526.
- (6) (a) Varcoe, J. R.; Atanassov, P.; Dekel, D. R.; Herring, A. M.; Hickner, M. A.; Kohl, P. A.; Kucernak, A. R.; Mustain, W. E.; Nijmeijer, K.; Scott, K.; Xu, T.; Zhuang, L. *Energy Environ. Sci.* **2014**, *7* (10), 3135–3191. (b) Wang, Y.-J.; Qiao, J.; Baker, R.; Zhang, J. *Chem. Soc. Rev.* **2013**, *42* (13), 5768. (c) Merle, G.; Wessling, M.; Nijmeijer, K. *J. Membr. Sci.* **2011**, *377* (1-2), 1–35. (d) Couture, G.; Alaaeddine, A.; Boschet, F.; Ameduri, B. *Prog. Poly. Sci.* **2011**, *36* (11), 1521–1557. (e) Poynton, S. D.; Kizewski, J. P.; Slade, R. C. T.; Varcoe, J. R. *Solid State Ionics* **2010**, *181* (3-4), 219–222.
- (7) (a) Thomas, O. D.; Soo, K. J. W. Y.; Peckham, T. J.; Kulkarni, M. P.; Holdcroft, S. *J. Am. Chem. Soc.* **2012**, *134* (26), 10753–10756. (b) Henkensmeier, D.; Cho, H.-R.; Kim, H.-J.; Nunes Kirchner, C.; Leppin, J.; Dyck, A.; Jang, J. H.; Cho, E.; Nam, S.-W.; Lim, T.-H. *Polym. Degrad. Stab.* **2012**, *97* (3), 264–272.
- (8) (a) Song, F.; Fu, Y.; Gao, Y.; Li, J.; Qiao, J.; Zhou, X.-D.; Liu, Y. *Electrochim. Acta* **2015**. (b) Liu, L.; Tong, C.; He, Y.; Zhao, Y.; Hu, B.; Lü, C. *RSC Adv.* **2015**, *5* (54), 43381–43390. (c) García-Cruz, L.; Casado-Coterillo, C.; Iniesta, J.; Montiel, V.; Irabien, Á. *J. Appl. Polym. Sci.* **2015**, *132* (29), DOI:10.1002/APP.42240. (d) Li, X.;

Yu, Y.; Meng, Y. *ACS Appl. Mater. Interfaces* **2013**, *5* (4), 1414–1422.

- (9) (a) Couture, G.; Ladmiral, V.; Améduri, B. *RSC Adv.* **2015**, *5* (14), 10243–10253. (b) Bosnjakovic, A.; Danilczuk, M.; Schlick, S.; Xiong, P. N.; Haugen, G. M.; Hamrock, S. J. *J. Membr. Sci.* **2014**, *467*, 136–141. (c) Vandiver, M. A.; Horan, J. L.; Yang, Y.; Tansey, E. T.; Seifert, S.; Liberatore, M. W.; Herring, A. M. *J. Polym. Sci. Part B: Polym. Phys.* **2013**, *51* (24), 1761–1769. (d) Varcoe, J. R.; Slade, R. C. T.; Lam How Yee, E.; Poynton, S. D.; Driscoll, D. J.; Apperley, D. C. *Chem. Mater.* **2007**, *19* (10), 2686–2693.
- (10) (a) Nie, G.; Li, X.; Tao, J.; Wu, W.; Liao, S. *J. Membr. Sci.* **2015**, *474*, 187–195. (b) Mohanty, A. D.; Lee, Y.-B.; Zhu, L.; Hickner, M. A.; Bae, C. *Macromolecules* **2014**, *47* (6), 1973–1980. (c) Yan, J.; Hickner, M. A. *Macromolecules* **2010**, *43* (5), 2349–2356. (d) Wang, J.; Zhao, Z.; Gong, F.; Li, S.; Zhang, S. *Macromolecules* **2009**, *42* (22), 8711–8717. (e) Hibbs, M. R.; Hickner, M. A.; Alam, T. M.; McIntyre, S. K.; Fujimoto, C. H.; Cornelius, C. J. *Chem. Mater.* **2008**, *20* (7), 2566–2573.
- (11) (a) Zhang, Z.; Wu, L.; Varcoe, J.; Li, C.; Ong, A. L.; Poynton, S.; Xu, T. *J. Mater. Chem. A* **2013**, *1* (7), 2595. (b) Han, J.; Peng, H.; Pan, J.; Wei, L.; Li, G.; Chen, C.; Xiao, L.; Lu, J.; Zhuang, L. *ACS Appl. Mater. Interfaces* **2013**, *5* (24), 13405–13411.
- (12) Tanaka, M.; Fukasawa, K.; Nishino, E.; Yamaguchi, S.; Yamada, K.; Tanaka, H.; Bae, B.; Miyatake, K.; Watanabe, M. *J. Am. Chem. Soc.* **2011**, *133* (27), 10646–10654.
- (13) (a) Li, N.; Leng, Y.; Hickner, M. A.; Wang, C.-Y. *J. Am. Chem. Soc.* **2013**, *135* (27), 10124–10133. (b) Li, N.; Wang, L.; Hickner, M. *Chem. Commun.* **2014**, *50* (31), 4092. (c) Li, Q.; Liu, L.; Miao, Q.; Jin, B.; Bai, R. *Chem. Commun.* **2014**, *50* (21), 2791. (d) Li, N.; Guiver, M. D.; Binder, W. H. *ChemSusChem* **2013**, *6* (8), 1376–1383.
- (14) (a) Robertson, N. J.; Kostalik, H. A.; Clark, T. J.; Mutolo, P. F.; Abruña, H. D.; Coates, G. W. *J. Am. Chem. Soc.* **2010**, *132* (10), 3400–3404. (b) Kostalik, H. A.; Clark, T. J.; Robertson, N. J.; Mutolo, P. F.; Longo, J. M.; Abruña, H. D.; Coates, G. W. *Macromolecules* **2010**, *43* (17), 7147–7150. (c) Clark, T. J.; Robertson, N. J.; Kostalik IV, H. A.; Lobkovsky, E. B.; Mutolo, P. F.; Abruña, H. D.; Coates, G. W. *J. Am. Chem. Soc.* **2009**, *131* (36), 12888–12889.
- (15) (a) Zhang, M.; Yuan, X.; Wang, L.; Chung, T. C. M.; Huang, T.; deGroot, W. *Macromolecules* **2014**, *47* (2), 571–581. (b) Zhang, M.; Kim, H. K.; Chalkova, E.; Mark, F.; Lvov, S. N.; Chung, T. C. M. *Macromolecules* **2011**, *44* (15), 5937–5946.

- (16) (a) Tsai, T.-H.; Ertem, S. P.; Maes, A. M.; Seifert, S.; Herring, A. M.; Coughlin, E. B. *Macromolecules* **2015**, *48*, 655–662. (b) Zeng, Q. H.; Liu, Q. L.; Broadwell, I.; Zhu, A. M.; Xiong, Y.; Tu, X. P. *J. Membr. Sci.* **2010**, *349* (1-2), 237–243. (c) Varcoe, J. R.; Slade, R. C. T.; Lam How Yee, E. *Chem. Commun.* **2006**, No. 13, 1428.
- (17) Wang, J.; Wang, J.; Li, S.; Zhang, S. *J. Membr. Sci.* **2011**, *368* (1-2), 246–253.
- (18) Arges, C. G.; Ramani, V. *Proc. Natl. Acad. Sci.* **2013**, *110* (7), 2490–2495.
- (19) Fujimoto, C.; Kim, D.-S.; Hibbs, M.; Wroblewski, D.; Kim, Y. S. *J. Membr. Sci.* **2012**, *423-424*, 438–449.
- (20) Nuñez, S. A.; Hickner, M. A. *ACS Macro Lett.* **2013**, *2* (1), 49–52.
- (21) Choe, Y.-K.; Fujimoto, C.; Lee, K.-S.; Dalton, L. T.; Ayers, K.; Henson, N. J.; Kim, Y. S. *Chem. Mater.* **2014**, *26* (19), 5675–5682.
- (22) Chen, D.; Hickner, M. A. *ACS Appl. Mater. Interfaces* **2012**, *4* (11), 5775–5781.
- (23) Page, O. M. M.; Poynton, S. D.; Murphy, S.; Lien Ong, A.; Hillman, D. M.; Hancock, C. A.; Hale, M. G.; Apperley, D. C.; Varcoe, J. R. *RSC Adv.* **2013**, *3* (2), 579–587.
- (24) Lin, X.; Varcoe, J. R.; Poynton, S. D.; Liang, X.; Ong, A. L.; Ran, J.; Li, Y.; Xu, T. *J. Mater. Chem. A* **2013**, *1* (24), 7262.
- (25) Ye, Y.; Elabd, Y. A. *Macromolecules* **2011**, *44* (21), 8494–8503.
- (26) Lin, B.; Dong, H.; Li, Y.; Si, Z.; Gu, F.; Yan, F. *Chem. Mater.* **2013**, *25* (9), 1858–1867.
- (27) Si, Z.; Sun, Z.; Gu, F.; Qiu, L.; Yan, F. *J. Mater. Chem. A* **2014**, *2* (12), 4413.
- (28) Yang, Y.; Wang, J.; Zheng, J.; Li, S.; Zhang, S. *J. Membr. Sci.* **2014**, *467*, 48–55.
- (29) (a) Long, H.; Kim, K.; Pivovar, B. S. *J. Phys. Chem. C* **2012**, *116* (17), 9419–9426. (b) Chempath, S.; Boncella, J. M.; Pratt, L. R.; Henson, N.; Pivovar, B. S. *J. Phys. Chem. C* **2010**, *114* (27), 11977–11983. (c) Chempath, S.; Einsla, B. R.; Pratt, L. R.;

- Macomber, C. S.; Boncella, J. M.; Rau, J. A.; Pivovar, B. S. *J. Phys. Chem. C* **2008**, *112* (9), 3179–3182.
- (30) Long, H.; Pivovar, B. S. *EChem Lett.* **2015**, *116* (17), 9419–9426.
- (31) Edson, J. B.; Macomber, C. S.; Pivovar, B. S.; Boncella, J. M. *J. Membr. Sci.* **2012**, *399-400*, 49–59.
- (32) Sturgeon, M. R.; Macomber, C. S.; Engtrakul, C.; Long, H.; Pivovar, B. S. *J. Electrochem. Soc.* **2015**, *162* (4), F366–F372.
- (33) Mohanty, A. D.; Bae, C. *J. Mater. Chem. A* **2014**, *2* (41), 17314–17320.
- (34) Dong, H.; Gu, F.; Li, M.; Lin, B.; Si, Z.; Hou, T.; Yan, F.; Lee, S.-T.; Li, Y. *ChemPhysChem* **2014**, *15* (14), 3006–3014.
- (35) Long, H.; Pivovar, B. *J. Phys. Chem. C* **2014**, *118* (19), 9880–9888.
- (36) Wang, W.; Wang, S.; Xie, X.; Lv, Y.; Ramani, V. *Int. J. Hydrogen Energy* **2014**, *39* (26), 14355–14361.
- (37) (a) Si, Z.; Sun, Z.; Gu, F.; Qiu, L.; Yan, F. *J. Mater. Chem. A* **2014**, *2* (12), 4413. (b) Si, Z.; Qiu, L.; Dong, H.; Gu, F.; Li, Y.; Yan, F. *ACS Appl. Mater. Interfaces* **2014**, *6* (6), 4346–4355. (c) Gu, F.; Dong, H.; Li, Y.; Si, Z.; Yan, F. *Macromolecules* **2014**, *47* (1), 208–216. (d) Lin, B.; Dong, H.; Li, Y.; Si, Z.; Gu, F.; Yan, F. *Chem. Mater.* **2013**, *25* (9), 1858–1867.
- (38) Yang, Y.; Wang, J.; Zheng, J.; Li, S.; Zhang, S. *J. Membr. Sci.* **2014**, *467*, 48–55.
- (39) Thomas, O. D.; Soo, K. J. W. Y.; Peckham, T. J.; Kulkarni, M. P.; Holdcroft, S. *J. Am. Chem. Soc.* **2012**, *134* (26), 10753–10756.

CHAPTER 2

Phosphonium Functionalized Polyethylene: A New Class of Base Stable Alkaline Anion Exchange Membranes

Reprinted with Permission from

Journal of the American Chemical Society **2012**, *134*, 18161—18164

Copyright © 2012 by the American Chemical Society

CHAPTER 2

Phosphonium Functionalized Polyethylene: A New Class of Base Stable Alkaline Anion Exchange Membranes

2.1 Abstract

A tetra(dialkylamino)phosphonium cation was evaluated as a functional group for alkaline anion exchange membranes (AAEMs). The base stability of $[P(N(Me)Cy)_4]^+$ was directly compared to that of $[BnNMe_3]^+$ in 1 M NaOD/CD₃OD. The high base stability of $[P(N(Me)Cy)_4]^+$, relative to $[BnNMe_3]^+$, motivated the preparation of AAEM materials composed of phosphonium units attached to polyethylene. The AAEMs (OH^- $s_{22} = 22 \pm 1$ mS cm^{-1}) were prepared using ring opening metathesis polymerization (ROMP) and their stability was evaluated in 15 M KOH at 22 °C and in 1 M KOH at 80 °C.

2.2 Introduction

Fuel cell devices are currently being investigated for a variety of applications as they efficiently convert the chemical energy stored in a fuel (e.g. H₂ or CH₃OH) directly into electrical energy.¹ One type of fuel cell that has been investigated extensively is the so-called proton exchange membrane fuel cell (PEMFC). These cells operate at relatively low temperatures (50 to 100 °C) with high efficiencies and consist of an ionically conducting polymeric material pressed between the cathode and anode to provide ion conduction and electrical insulation. Fuel cells operated under acidic conditions commonly employ Nafion, a perfluorinated polymer with pendant sulfonic acid groups that facilitate the flow of protons.² Unfortunately, the oxygen reduction reaction is rate limiting for acidic fuel cells, and the most commonly employed cathode materials are based on platinum and its alloys.² Since platinum is an expensive noble metal, investigation into fuel cells operated under alkaline conditions is drawing interest since the kinetics of oxygen reduction are more facile in alkaline media enabling the use of less expensive metals as the cathode catalyst.³ Consequently, researchers have attempted to prepare alkaline anion exchange membranes (AAEMs) with similar stability and conductivity to Nafion.⁴

Ideal AAEMs would be mechanically and chemically robust, exhibit good hydroxide ion conductivity and display limited swelling. Various polymer backbones have been investigated to date including hydrocarbon polymers prepared via ROMP,⁵ fluoropolymers,⁶ polysulfones,⁷ polyarylenes⁸ and poly(ether-imide)s.⁹ These polymeric supports contain pendant ammonium cations to facilitate hydroxide ion conduction from the cathode to the anode. However, the degradation pathways for ammonium cations in alkaline conditions have been well documented,¹⁰ and the long-term stability of the ammonium cation under fuel cell operating conditions remains a concern.¹¹ This has sparked investigation of other cationic species appended to polymeric supports for use in alkaline membrane fuel cells (AMFCs), including delocalized guanidinium¹² and imidazolium¹³ cations. Holdcroft and co-workers have recently reported a sterically crowded benzimidazolium polymer that exhibits excellent base stability when heated to 60 °C in 2 M KOH over a 13 day period.¹⁴ Tetraalkylphosphonium cations represent another exciting class of functional groups for AAEMs as the synthesis of phosphonium ionomers has already been established.¹⁵ Both the benzyltrimethylphosphonium¹⁶ and benzyltris(2,4,6-trimethoxyphenyl) phosphonium¹⁷ cations are being evaluated in AAEM materials. While the tetraalkylphosphonium cation ($[PR_4]^+$) is attracting attention in AAEMs, the tetra(dialkylamino)phosphonium cation ($[P(NR_2)_4]^+$) is also of interest.¹⁸ Recent reports have shown the exceptional stability of $[P(NR_2)_4]OR'$ ($R' = H, \text{alkyl}$) compounds and their application in phase transfer,¹⁹ transesterification,²⁰ and polymerization²¹ reactions have been demonstrated. Herein, we report a new class of hydroxide ion exchange membranes that consist of a tetra(dialkylamino)phosphonium cation appended to polyethylene. These materials exhibit excellent stability in strongly basic solution.

2.3 Results and Discussion

The benzyltrimethylammonium ($[\text{BnNMe}_3]^+$) cation is commonly employed in AAEMs. As a result, we chose to compare its base stability to that of the bulky $[\text{P}(\text{N}(\text{Me})\text{Cy})_4]^+$ cation. Since $[\text{BnNMe}_3]\text{OH}$ exhibits negligible degradation in 1 M NaOH at 80 °C over 29 days in water,^{10f} stability in methanol was explored since (a) it accelerates cation degradation, (b) it often dissolves polyatomic cations better than water, and (c) is applicable to direct methanol fuel cells.²²

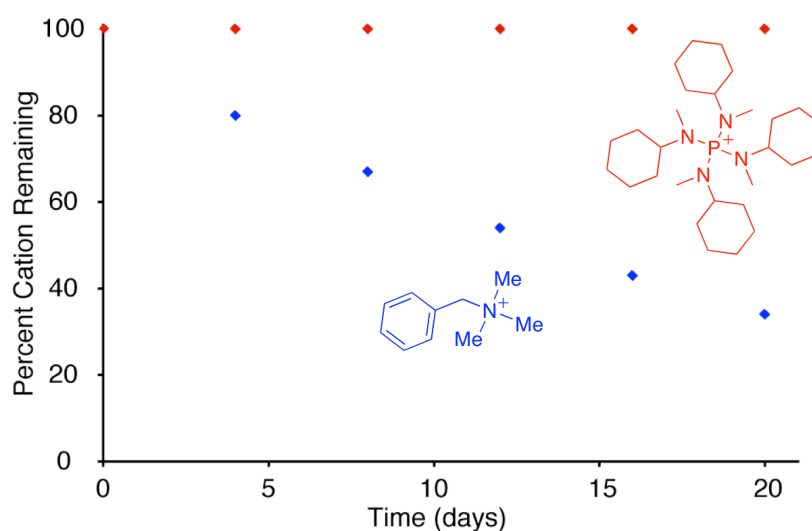


Figure 2.1 Stability of $[\text{BnNMe}_3]^+$ and $[\text{P}(\text{N}(\text{Me})\text{Cy})_4]^+$ in 1 M NaOD/ CD_3OD at 80 °C.

The combination of $[\text{BnNMe}_3]\text{Br}$ and NaOD (1 M NaOD, 0.1 M $[\text{BnNMe}_3]\text{Br}$) in CD_3OD at 80 °C resulted in 66% degradation of the BnNMe_3 cation after 20 days (Figure 2.1).²² In solution, $[\text{BnNMe}_3]^+$ degrades primarily by nucleophilic attack at either the benzylic or methyl positions (confirmed by ^1H NMR and GC-MS). In stark contrast, when $[\text{P}(\text{N}(\text{Me})\text{Cy})_4]\text{BF}_4$ and NaOD are dissolved in CD_3OD (1 M NaOD, 0.1 M $[\text{P}(\text{N}(\text{Me})\text{Cy})_4]\text{BF}_4$), no degradation of $[\text{P}(\text{N}(\text{Me})\text{Cy})_4]^+$ was observed over a 20 day period at 80 °C (as measured by ^1H and ^{31}P NMR spectroscopy). This stability under basic conditions in methanol is noteworthy and suggests that

the tetra(dialkylamino)phosphonium cation may be a promising functional group choice for AAEM fuel cells, especially when methanol is being used as the fuel (i.e. in “direct methanol” fuel cells).

To further investigate the stability of the dialkylamino phosphonium cation, we sought to synthesize and characterize a discrete alkoxide species. $[\text{P}(\text{N}(\text{Me})\text{Cy})_4]\text{BF}_4$ was combined with KOH in methanol; precipitation and filtration of KBF_4 followed by removal of the solvent resulted in crystals suitable for X-ray diffraction. The solid state molecular structure of $[\text{P}(\text{N}(\text{Me})\text{Cy})_4][\text{OMe}] \cdot 3\text{MeOH}$ (**1**) is displayed in Figure 2.2. This crystal structure further documents the unique stability of the phosphonium cation since very few other organic cations are known to be stable enough to crystallize with a methoxide anion. Two other reports describe organic cations with a methoxide. Love and co-workers reported a tetraprotonated polypyrrole macrocycle crystallized with three tosylate counterions and one methoxide counterion,²³ and Ou and co-workers described an ion pair where a hydrogen bond exists between an NH_3 moiety and the anionic methoxide.²⁴

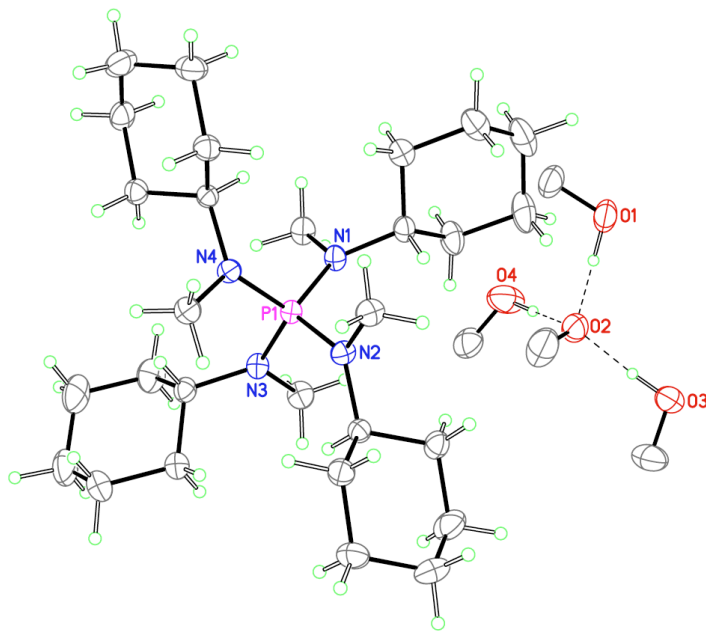


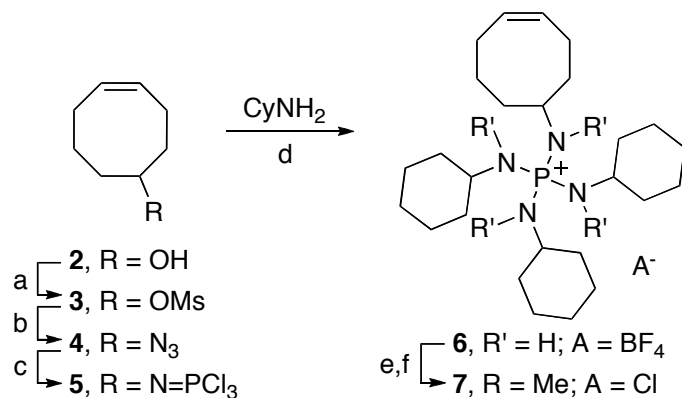
Figure 2.2 Molecular structure of **1**. Hydrogen atoms on the cation have been omitted for clarity. Thermal ellipsoids at 40% probability.

The P-N bond lengths of **1** are quite similar (1.638(1)-1.655(1) Å) to the P-N bond lengths reported for [P(N(Me)Cy)₄]PF₆ (1.636(1) Å).¹⁹ The anionic methoxide is hydrogen bonded to three methanol molecules.²⁵ The short O-O separations (2.576-2.636 Å) between the neighboring methanol molecules and the methoxide anion of **1** suggest relatively strong hydrogen bonding; typical O-O distances for a hydrogen bonded system are 2.75 Å. These strong O-H contacts provide significant energetic stabilization to the reactive methoxide anion.²⁶

The stability of [P(N(Me)Cy)₄]BF₄ in 1 M NaOD/CD₃OD and the preparation of crystalline **1** suggested that these delocalized phosphonium cations might be suitable for AAEM applications. Although there have been previous reports describing polymers with appended dialkylamino phosphoniums,^{18,27} none have been examined under fuel cell relevant conditions. This prompted us to target a polyethylene based phosphonium ionomer.

Our group has previously reported two separate cross-linked polymer networks bearing pendant ammonium groups as potential AAEMs.^{5c,d} The ammonium groups were appended to norbornyl and cyclooctenyl derivatives and the functionalized monomers were polymerized via ROMP. The commercially available Grubbs 2nd generation catalyst (Ru-cat) was employed since it is tolerant of quaternary ammonium halides.^{5,28} The synthesis of non-crosslinked AAEMs has also been achieved using ROMP.^{5b} A cyclooctenyl trimethylammonium monomer was copolymerized with cyclooctene in the presence of Ru-cat to afford an unsaturated copolymer. Hydrogenation of this material yielded a solution processable and mechanically strong ammonium-functionalized polyethylene (OH⁻ σ_{50} = 65 mS cm⁻¹). Using a similar strategy, a tetra(dialkylamino)phosphonium functionalized cyclooctene was targeted and prepared in six steps from 5-hydroxy-1-cyclooctene (Figure 2.3).²⁹ Mesylation of 5-hydroxy-1-cyclooctene (**2**) followed by reaction with NaN₃ afforded 5-azido-1-cyclooctene (**4**). A Staudinger reaction was employed to yield iminophosphorane **5** and immediate reaction with cyclohexylamine produced phosphonium salt **6**. Methylation was conducted using standard phase transfer protocols yielding the tetra(dialkylamino)phosphonium cation **7** (Figure 2.3).

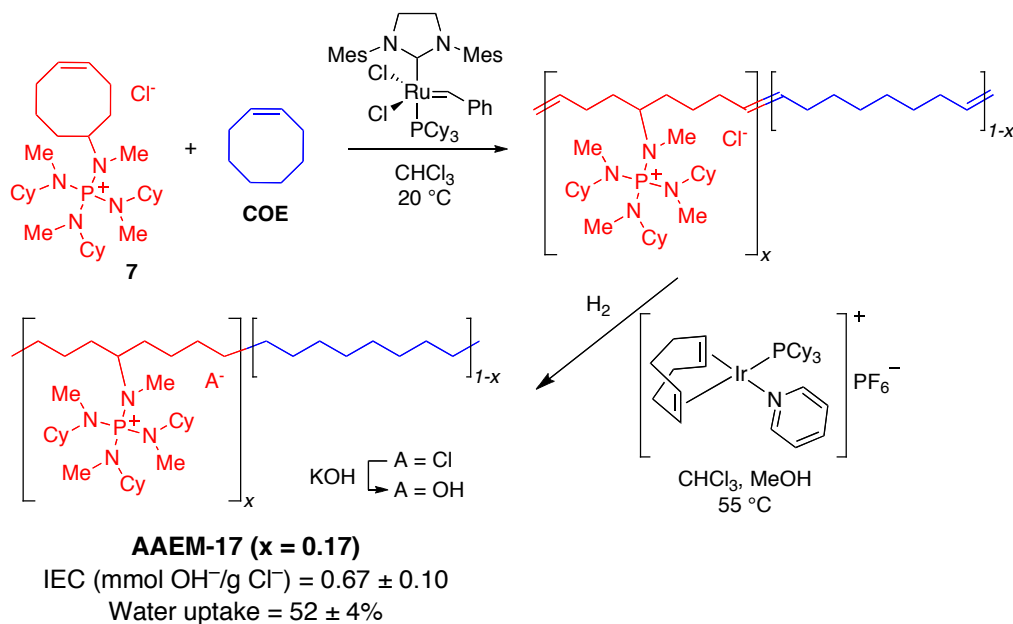
Figure 2.3 Phosphonium Monomer Synthesis.^a



^a Reagents and Conditions: (a) 1.2 eq. MsCl , pyridine, 0 °C; (b) 1.5 eq. NaN_3 , DMSO, 50 °C; (c) 5 eq. PCl_3 , toluene, 70 °C; (d) CH_2Cl_2 , 0 °C, followed by workup with 1 M NaBF_4 ; (e) 5 eq. Me_2SO_4 , 40 eq. NaOH , H_2O , chlorobenzene, 70 °C; (f) chloride anion exchange resin.

Monomer **7** was copolymerized with cyclooctene (COE) in the presence of Ru-cat in chloroform for 18 h (Figure 2.4). ^1H NMR spectroscopy of the reaction mixture indicated that COE was incorporated into the growing polymer chain more readily than **5**. Thus, this polymerization strategy could potentially be modified to yield block copolymer architectures, an area currently drawing interest with respect to AAEMs.^{7a,30} We are currently investigating the synthesis of random and block copolymers bearing these phosphonium moieties.

Figure 2.4 Synthesis of Phosphonium Functionalized Polyethylene.



The unsaturated ROMP polymer was hydrogenated ([Ir(COD)(py)(PCy₃)]PF₆; CHCl₃/MeOH; 600 psig H₂; 17 h) and ¹H NMR spectroscopy revealed near quantitative hydrogenation. The reduced copolymers (chloride form) were dissolved in a 1,2-dichloroethane/ethanol cosolvent mixture (1:1) and cast onto a glass dish preheated to 45 °C from which the volatiles were slowly evaporated to yield a film. The polymers were converted into their hydroxide form by soaking the films in 1 M KOH for 2 h and washing with deionized water for 1 h. Samples containing a range of comonomer ratios were tested but polymers with higher percentages of **5** exhibited excessive swelling at higher temperature. An optimized AAEM used for conductivity and base stability studies had 17 mol % of monomer **5** (**AAEM-17**). Conductivity, ion exchange capacity and water uptakes for **AAEM-17** are presented in Figure 2.4.³¹

To investigate the stability of the phosphonium membrane materials under highly alkaline conditions, we exposed **AAEM-17** (OH⁻ s₂₂ = 22 ± 1 mS cm⁻¹) to a solution of 15 M KOH in water. The hydrogenated copolymer, in the chloride form, was immersed in 1 M KOH_{aq}

following the standard exchange procedure³¹ yielding **AAEM-17** which was immediately exposed to 15 M KOH_{aq} at 22 °C. Over a 138-day period, **AAEM-17** was periodically removed from the 15 M solution and soaked in deionized water for 18 h to ensure complete rehydration. The membrane was re-exchanged with 1 M KOH_{aq}, washed with water to remove any residual base and the in-plane hydroxide conductivity was measured at 22 °C. The data obtained are presented in Figure 2.5. Interestingly, no significant loss of conductivity was observed for **AAEM-17** after exposure to 15 M KOH_{aq} over the 20-week period. To investigate the stability of the membrane at elevated temperatures **AAEM-17** was exposed to 1 M KOH_{aq} in water at 80 °C. A small initial loss of conductivity (from 22 mS cm⁻¹ to 18 mS cm⁻¹) was observed after 3 days but no further loss in conductivity was evident up to 22 days. The alkaline stability of the phosphonium AAEM in 1 M KOH_{aq} at 80 °C suggests these may be excellent candidates for higher temperature AFC devices.

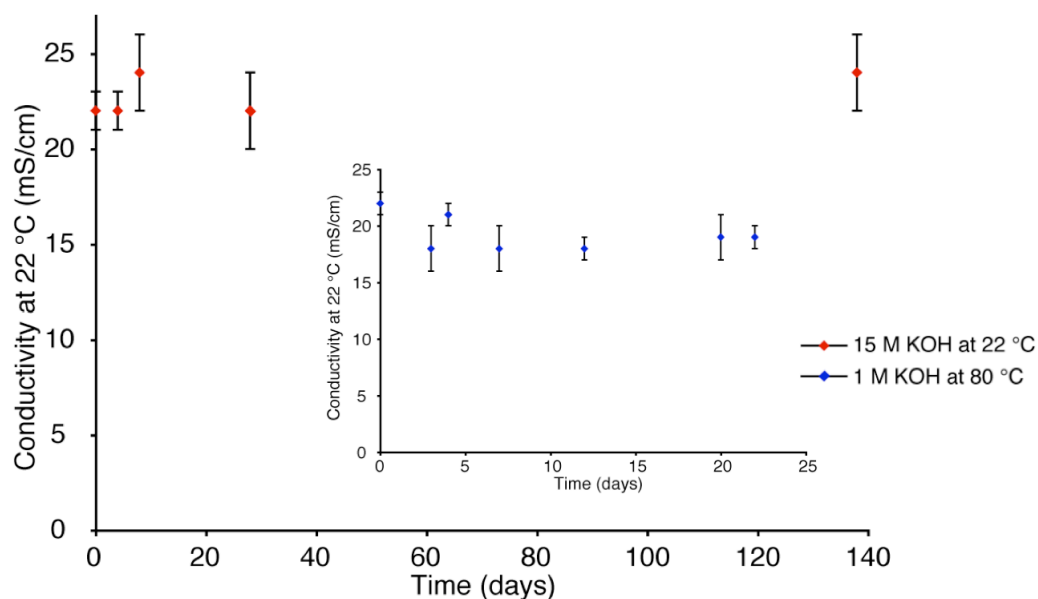


Figure 2.5 **AAEM-17** hydroxide conductivity as a function of time after immersion in 15 M KOH_{aq} at 22 °C. Inset: **AAEM-17** hydroxide conductivity as a function of time after immersion in 1 M KOH_{aq} at 80 °C.

2.4 Conclusion

In conclusion, the alkaline stability of a tetra(dialkylamino)phosphonium cation was evaluated and directly compared to a benzyltrimethylammonium cation. In model compound investigations, the $\text{P}(\text{N}(\text{Me})\text{Cy})_4$ cation outperformed the BnNMe_3 cation. Consequently, a new methodology for appending these delocalized phosphonium cations to polyethylene was developed. The membrane stability of **AAEM-17** in 15 M KOH at 22 °C and 1 M KOH at 80 °C confirm that tetra(dialkylamino)phosphonium materials are promising candidates for testing in AMFCs. Our future work will focus on controlling polymer morphology in an effort to increase the conductivity of these materials while

2.5 Experimental

2.5.1 General Considerations

All reactions and manipulations of air or water sensitive compounds were carried out under dry nitrogen using a Braun UniLab drybox or standard Schlenk techniques unless otherwise specified. HBr 33% in acetic acid, methanesulfonyl chloride, pyridine, sodium azide, 1,5-cyclooctadiene, *meta*-Chloroperoxybenzoic acid, lithium aluminum hydride, phosphorus trichloride, Grubbs 2nd Generation catalyst ($\text{Cl}_2\text{Ru}(\text{iMes})(\text{PCy}_3)\text{CHPh}$), Crabtree's catalyst $[(\text{COD})\text{Ir}(\text{py})(\text{PCy}_3)]\text{PF}_6$, dimethyl sulfate, sodium tetrafluoroborate (98%), sodium thiosulfate, CaH_2 , P_2O_5 , 4Å sieves, sodium deuterioxide (40 wt % in D_2O), and 3-(Trimethylsilyl)-1-propanesulfonic acid sodium salt were purchased from Aldrich and used as received. Cis-cyclooctene (95%) was purchased from Aldrich and distilled from 4Å sieves prior to use. Benzyltrimethylammonium bromide was prepared from benzyl bromide and a 4.2M solution of NMe_3 in ethanol (both were purchased from Aldrich). Cyclohexylamine was purchased from Aldrich, stirred over CaH_2 for 24 hours and vacuum transferred to a Schlenk bomb where it was stored under N_2 prior to use. Sodium hydroxide, sodium bicarbonate, sodium chloride and potassium hydroxide were purchased from Mallinckrodt and used as received. All solvents (toluene, methylene chloride, diethyl ether, tetrahydrofuran, hexanes, dimethyl sulfoxide) were purchased from Sigma-Aldrich or Mallinckrodt. Anhydrous chlorobenzene was purchased from Aldrich and used as received. Methylene chloride and tetrahydrofuran were purified over an alumina column and degassed by three freeze-pump-thaw cycles before use. Chloroform was dried over P_2O_5 and distilled prior to use. Chloride form ion exchange resin (Amberlite-IRA 400(Cl) form) was purchased from Aldrich and washed with methanol prior to use. Hydrogen (99.99%) was purchased from Airgas. NMR solvents (CDCl_3 , CD_3OD , $\text{DMSO}-d_6$) were purchased from Cambridge Isotope Laboratories (CIL) and used as received. C_6D_6 (CIL) was dried over 4Å sieves prior to use.

5-Bromo-1-cyclooctene was prepared according to a literature procedure³² but it was typically contaminated with 4-bromo-1-cyclooctene³³ (~10 %) and was therefore not used to

prepare the desired 5-azido-1-cyclooctene. 5-Hydroxy-1-cyclooctene (**2**) was prepared from a literature procedure.²⁹ Tetrakis[cyclohexyl(methyl)amino]phosphonium tetrafluoroborate was prepared according to a literature procedure.¹⁹ Standardized hydrochloric acid (0.1014 M) and potassium hydroxide (0.1000 ± 0.0001 M) solutions were purchased from Sigma-Aldrich and Riedel-de Haën, respectively.

2.5.2 Small Molecule Characterization

¹H and ¹³C NMR spectra were collected in deuterated solvents on a Varian INOVA 400, Bruker Avance 500 (¹³C, 125 MHz), Varian 500 (¹³C, 125 MHz) or a Varian INOVA 600 (¹³C, 150 MHz). The spectra were referenced internally to residual protio-solvents (¹H) or to deuterio-solvent signals (¹³C) and are reported relative to tetramethylsilane ($\delta = 0$ ppm). Stability investigations were referenced to the TMS signal of TMS(CH₂)₃SO₃Na at 0.00 ppm. ³¹P NMR spectra were recorded on a Bruker ARX 300 (³¹P, 121 MHz), Varian INOVA 400 (³¹P, 161 MHz) or a Bruker Avance 500 (³¹P, 202 MHz) spectrometer and referenced to an external standard (85% H₃PO₄).

ESI mass spectra were collected at The University of Illinois Urbana-Champaign Mass Spectrometry Facility. Elemental analyses were performed by Robertson Microlit Laboratories, Inc. Madison, New Jersey.

2.5.3 AAEM Characterization

Ion exchange capacities (IECs) were determined using standard back titration methods. The thin film as synthesized (in the chloride form) was dried under full vacuum at 90 °C in order to completely dehydrate it and then weighed. Conversion to the hydroxide form was achieved by immersing the film in a stirring 60 mL portion of 1 M potassium hydroxide for a minimum of 2 hours with the 1 M KOH solution being replaced twice with fresh 1 M KOH during that time. Residual potassium hydroxide was washed away by immersing the membrane in 3×125 mL portions of deionized water for 20 minutes each. The AAEM was then stirred in 25 mL

standardized 0.1 M $\text{HCl}_{(\text{aq})}$ solution for 48 hours followed by titration with standardized 0.1 M $\text{KOH}_{(\text{aq})}$ to determine the equivalence point. Control acid samples (with no AAEM present) were also titrated with standardized 0.1 M $\text{KOH}_{(\text{aq})}$, and the difference between the volume required to titrate the control and the sample was used to calculate the amount of hydroxide ions in the membrane. This was divided by the dried mass of the membrane (*vide supra*) to give an IEC value with the units mmol $\text{OH}^-/\text{g Cl}^-$.

The in-plane hydroxide conductivity of the AAEM sample was measured by four-probe electrochemical impedance spectroscopy (EIS) using a Solartron 1280B electrochemical workstation along with ZPlot and ZView software. The conductivity cell was purchased from BektEck LLC (Loveland, CO), and a helpful schematic and description of a similar experimental setup has been reported.³⁴ A strip of the thin film in chloride form (ca. 4 cm long x 0.5 cm wide) was converted to the hydroxide form by immersing it in a stirring 30 mL portion of 1 M potassium hydroxide for a minimum of 2 h and the 1 M KOH solution was replaced twice with fresh solution during that time. Residual potassium hydroxide was washed away by immersing the membrane in 3×60 mL portions of deionized water for 20 minutes each. The AAEM was then clamped into the cell using a Proto 6104 torque screwdriver set to 1 inch ounce and completely immersed in deionized water at either 22 °C or 50 °C, during the measurement time. EIS was performed by imposing a small sinusoidal (AC signal) voltage, 10 mV, across the membrane sample at frequencies between 20,000 Hz and 0.1 Hz (scanning from high to low frequencies) and measuring the resultant current response. A Bode plot was used to assess the frequency range over which the impedance approached a constant and the phase angle approached zero. In a Nyquist plot of the data, the high frequency intercept on the real impedance axis was taken to be the resistance of the membrane. This was then used to calculate the hydroxide conductivity by employing the following formula: $\sigma = L / Z' \cdot A$ where L is the length between sense electrodes (0.425 cm), Z' is the real impedance response at high frequency, and A is the membrane area available for hydroxide conduction (width·thickness). The dimensional measurements were performed using a digital micrometer (± 0.001 mm) purchased

from Marathon Watch Company Ltd. (Richmond Hill, ON).

The hydroxide conductivity was measured for a minimum of four separate AAEMs (per composition) and the precision of these measurements was evaluated. All errors are determined from sample standard deviations. Confidence intervals are at the 95 % confidence level based on the sample deviations and using the relevant student-*t* distribution (*N*-1 degrees of freedom, *N* is the number of samples tested for each membrane).

Water uptake was measured by the mass change between the fully hydrated and dried AAEMs. The thin film as synthesized (in the chloride form) was dried under full vacuum at 90 °C in order to completely dehydrate it and then weighed. Conversion to the hydroxide form was achieved by immersing the film in a stirring 60 mL portion of 1 M potassium hydroxide for a minimum of 2 hours with the 1 M KOH solution being replaced twice with fresh solution during that time. Residual potassium hydroxide was washed away by immersing the membrane in 3 × 125 mL portions of deionized water for 20 minutes each. Immediately following hydroxide ion exchange, a sample was dried with a paper towel and weighed on the balance with a piece a weighing paper. The water uptake percentage value was calculated by: $WU = [(Mass_{final} - Mass_{initial}) / Mass_{initial}] * 100$.

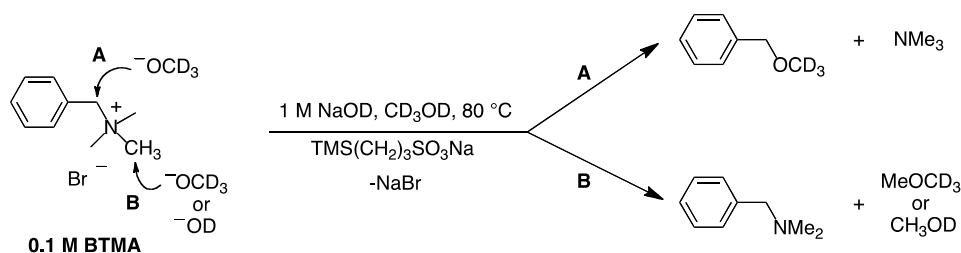
Table 2.1 AAEM Characterization Data

measurement	AAEM-17
IEC (mmol OH ⁻ /g Cl ⁻) ^a	0.67 ± 0.10
Water uptake ^b	52 ± 4
OH ⁻ σ ₂₂ (mS cm ⁻¹) ^c	22 ± 1
OH ⁻ σ ₅₀ (mS cm ⁻¹) ^c	32 ± 2

^aIon exchange capacity determined by back-titration, average of three trials. ^bGravimetric Analysis of the fully hydrated membranes, average of 4 trials. ^cHydroxide conductivities of the AAEMs fully immersed in degassed water at 22 and 50 °C, average of four trials.

2.5.4 Investigation of Benzyltrimethylammonium (BTMA) Cation Stability

BTMA-Br (0.230 g, 1.00 mmol), sodium deuteroxide (40 wt% in D₂O, 1.03 g, 10.0 mmol), 3-(trimethylsilyl)-1-propanesulfonic acid sodium salt (0.107 g, 0.490 mmol) and CD₃OD (10 ml) were placed in a fluoropolymer lined vessel and heated at 80 °C for 1 h. After 1 h an aliquot was removed and analyzed by ¹H NMR spectroscopy. The integration of the aromatic region of BTMA relative to 3-(trimethylsilyl)-1-propanesulfonic acid sodium salt provided the initial quantity of BTMA. Aliquots of the reaction were removed every 4 days and analyzed by ¹H NMR spectroscopy in order to determine the quantity of BTMA remaining and degradation products (a stack plot of the ¹H NMR spectra is provided in Figure S1). The aliquot taken on the 16th day was analyzed using GC-MS. The primary degradation products were confirmed as benzyl deuteriomethyl ether (PhCH₂OCD₃) and *N,N*-dimethylbenzylamine (PhCH₂N(CH₃)₂).³⁵ Since NaOD is in equilibrium with NaOCD₃ there are two nucleophiles present in the mixture. Moreover, as both the deuterio methoxide and deuterio hydroxide are basic as well as nucleophilic, H/D exchange occurs at both the benzylic and methyl positions. The mass spectra of the decomposition products confirmed deuteration had occurred, as signals corresponding to several different isotopologues were observed with the benzyl deuteriomethyl ether and *N,N*-dimethylbenzylamine. The primary modes of decomposition in basic media appear to be nucleophilic attack at the benzylic (pathway **A**) or methyl positions (pathway **B**) of the BTMA cation.³⁵



Scheme 1 Degradation pathways of BTMA.

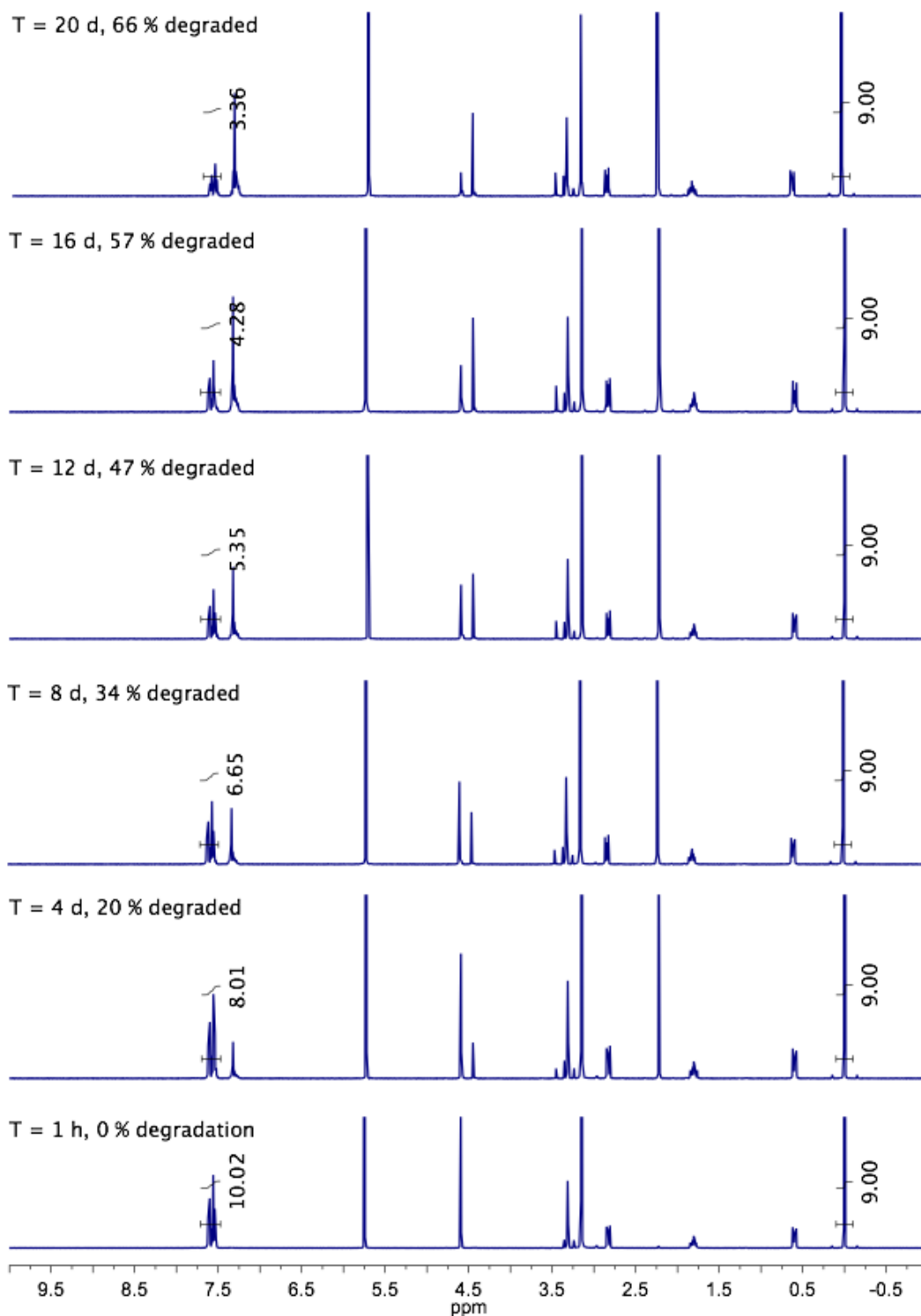


Figure 2.6 ^1H NMR spectra of benzyltrimethylammonium bromide over 20 days dissolved in a mixture of CD_3OD , 40 weight percent $\text{NaOD}/\text{D}_2\text{O}$ solution (1 M NaOD , $[\text{NaOD}]/[\text{BTMA}] = 10$) and, an internal standard ($\text{TMS}(\text{CH}_2)_3\text{SO}_3\text{Na}$).

2.5.5 Investigation of $[\text{P}(\text{N}(\text{Me})\text{Cy})_4]^+$ Cation Stability

Tetrakis[cyclohexyl(methyl)amino]phosphonium tetrafluoroborate (0.568 g, 1.00 mmol), sodium deuterioxide (40 wt% in D_2O , 1.03 g, 10.0 mmol), 3-(trimethylsilyl)-1-propanesulfonic acid sodium salt (0.109 g, 0.499 mmol) and CD_3OD (10 mL) were placed in a fluoropolymer lined vessel and heated at 80 °C for 1 h. After 1 h an aliquot was removed and analyzed by ^1H NMR and ^{31}P NMR spectroscopy. The integration of the N-methyl relative to 3-(trimethylsilyl)-1-propanesulfonic acid sodium salt provided the initial quantity of tetrakis[cyclohexyl(methyl)amino]phosphonium. Aliquots of the reaction were removed every 4 days (a series of the spectra over time are shown in Figure S2 and Figure S3) and analyzed by ^1H NMR spectroscopy and ^{31}P NMR spectroscopy. No degradation products were observed in either the ^1H and ^{31}P NMR spectra over a 20-day period.

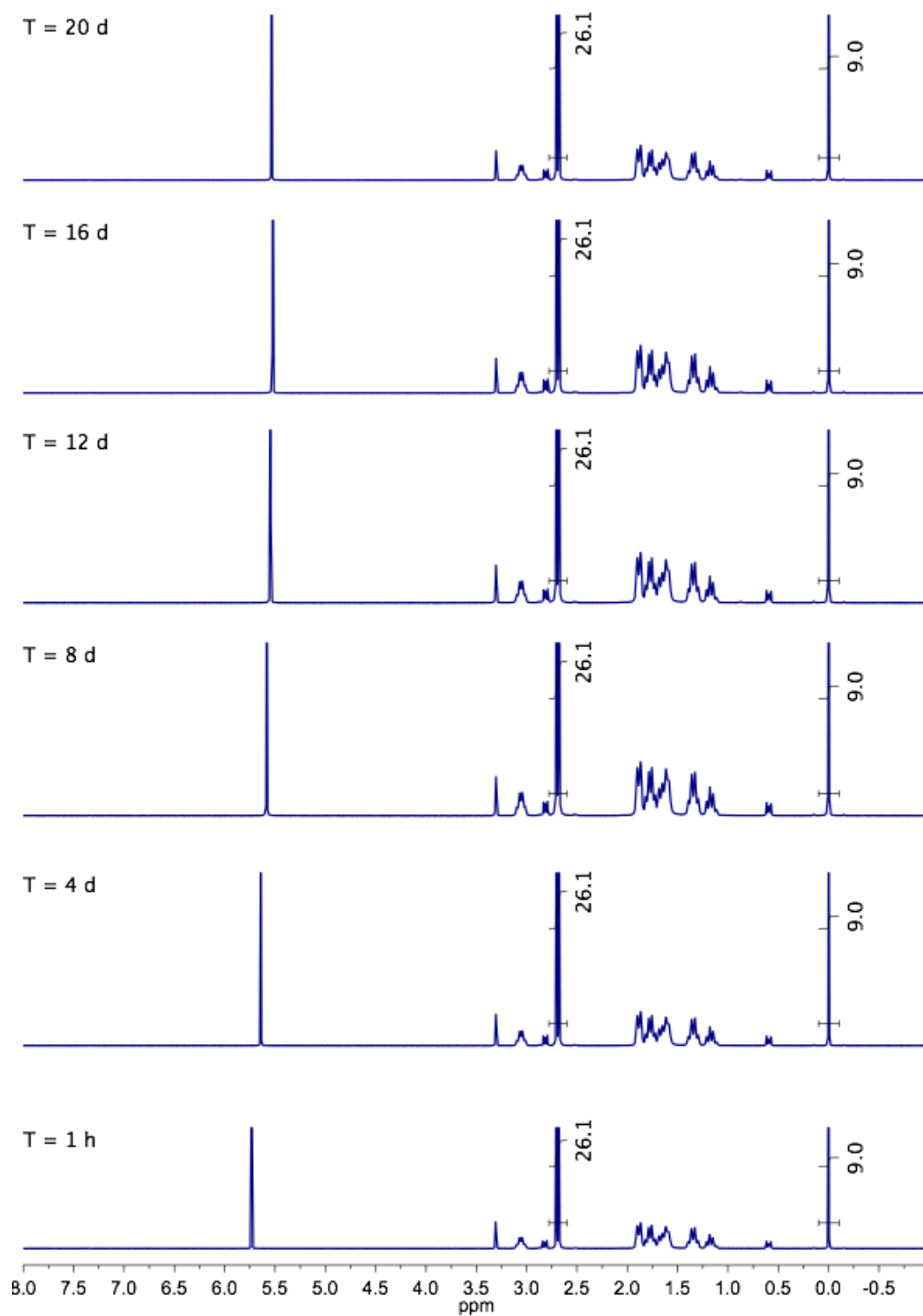


Figure 2.7 ^1H NMR spectra of tetrakis[cyclohexyl(methyl)amino]phosphonium tetrafluoroborate over 20 days dissolved in a mixture of CD_3OD , 40 weight percent $\text{NaOD}/\text{D}_2\text{O}$ solution (1 M NaOD , $[\text{NaOD}]/[\text{P}(\text{N}(\text{Me})\text{Cy})_4] = 10$) and, an internal standard ($\text{TMS}(\text{CH}_2)_3\text{SO}_3\text{Na}$).

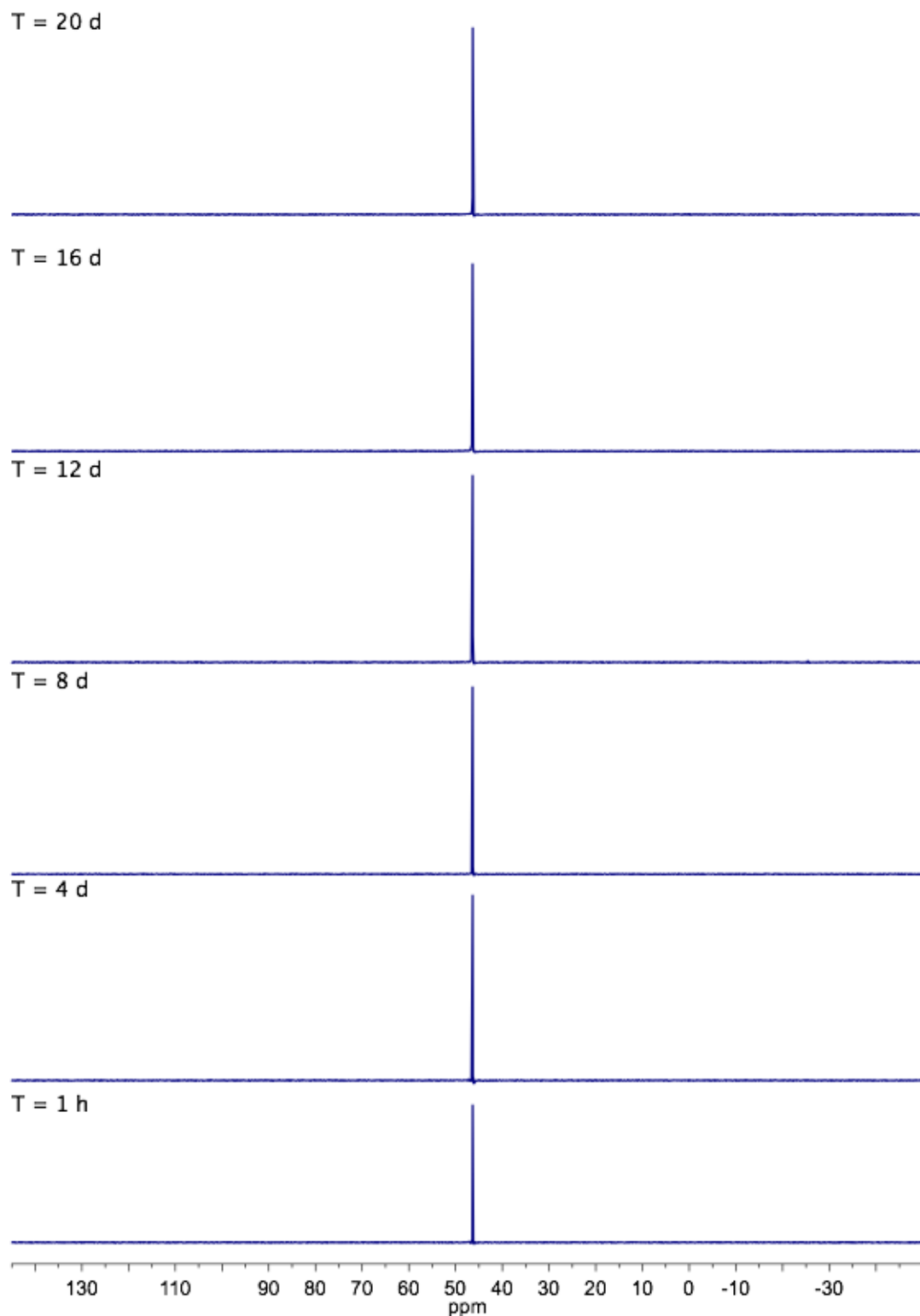


Figure 2.8 $^{31}\text{P}\{^1\text{H}\}$ NMR spectra of tetrakis[cyclohexyl(methyl)amino]phosphonium tetrafluoroborate over 20 days dissolved in a mixture of CD_3OD , 40 weight percent $\text{NaOD}/\text{D}_2\text{O}$ solution (1 M NaOD , $[\text{NaOD}]/[\text{P}(\text{N}(\text{Me})\text{Cy})_4] = 10$) and, an internal standard ($\text{TMS}(\text{CH}_2)_3\text{SO}_3\text{Na}$). Referenced to 85 % H_3PO_4 .

2.5.6 Stability Investigation of AAEM -17

A strip of the thin film in the hydroxide form (ca. 4 cm long \times 0.5 cm wide) was removed from 1 M KOH following the typical exchange procedure and immediately placed in a plastic bottle containing 15 M KOH at 22 °C. At specified time intervals, membrane strips were removed and soaked in deionized water for 18 h to ensure complete hydration, re-exchanged with 1 M KOH (typical procedure with a 2 h exchange), washed with water to remove any residual base and the in-plane hydroxide conductivity measured at 22 °C.

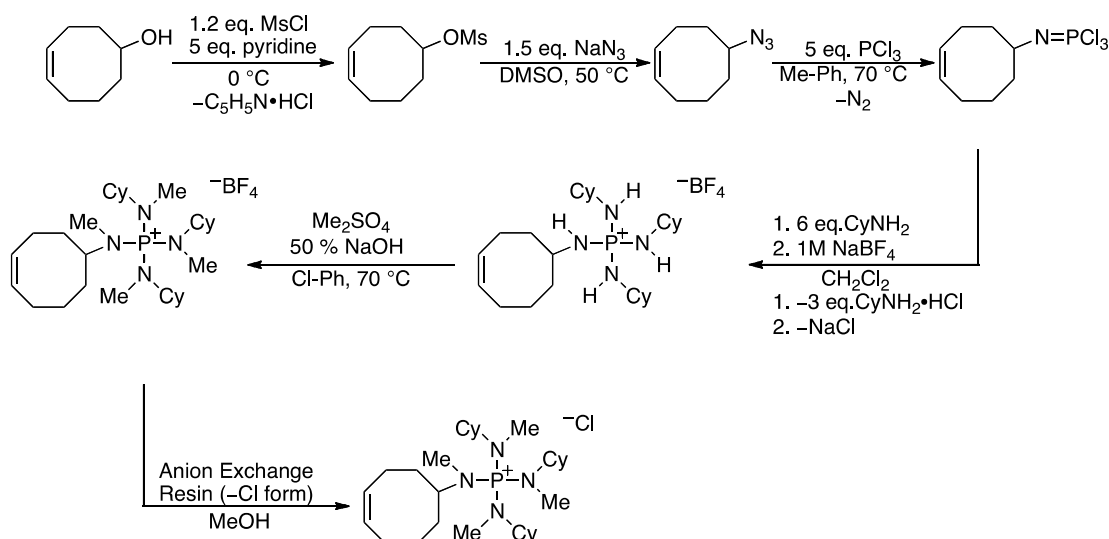
Table 2.2 AAEM-17 Stability after exposure to 15 M KOH at 22 °C (Data For Figure 2.5)

Entry	Time (days)	Conductivity (mS cm ⁻¹)	Error (mS cm ⁻¹)
1	0	22	1
2	4	22	1
3	8	24	2
4	28	22	2
5	138	24	2

Table 2.3 AAEM-17 Stability after exposure to 1 M KOH at 80 °C (Data For Figure 2.5)

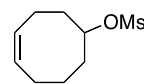
Entry	Time (days)	Conductivity (mS cm ⁻¹)	Error (mS cm ⁻¹)
1	0	22	1
2	3	18	2
3	4	21	1
4	7	18	2
5	12	18	1
6	20	19	2
7	22	19	1

2.5.7 Synthesis of Phosphonium Monomer



Scheme 2. General Scheme for the Synthesis of the Phosphonium Monomer.

Preparation of 5-mesyloxy-1-cyclooctene (3). In a 100 mL round-bottom flask, 5-Hydroxy-1-cyclooctene³ (5.50 g, 43.6 mmol) was combined with pyridine (17.5 mL, 217 mmol). The round-bottom flask was cooled to 0 °C using an ice bath and methanesulfonyl chloride (4.1 mL, 53.0 mmol) was added to the reaction mixture by syringe over a period of one minute. Upon addition of the methanesulfonyl chloride, the yellow reaction mixture was stirred for 30 min at 0 °C. The ice bath was then removed and the reaction mixture was warmed to room temperature and the C₅H₅N•HCl precipitated from the solution. The reaction mixture was poured into 100 mL of water and the aqueous fraction was extracted three times with diethyl ether (1 × 100 mL and 2 × 75 mL portions). The organic layers were combined and washed with 100 mL of water. Finally, the organic layer was dried with Na₂SO₄ and removal of the solvent by rotary evaporation afforded the crude product. The crude compound was dried *in vacuo* to remove residual pyridine furnishing a yellow oil (8.35 g, 94%). This compound was used without further purification. ¹H NMR (400 MHz, CDCl₃) δ 5.70-5.59 (2H, br m), 4.81-4.73 (1H, br m), 2.96 (3H, s), 2.44-2.31 (1H, br m), 2.24-1.91 (6H, br m), 1.87-



1.75 (1H, br m), 1.75-1.65 (1H, br m), 1.60-1.45 (1H, br m). ^{13}C NMR (100 MHz, CDCl_3) δ 130.2, 129.3, 84.8, 38.7, 35.1, 34.5, 25.7, 24.8, 22.3.

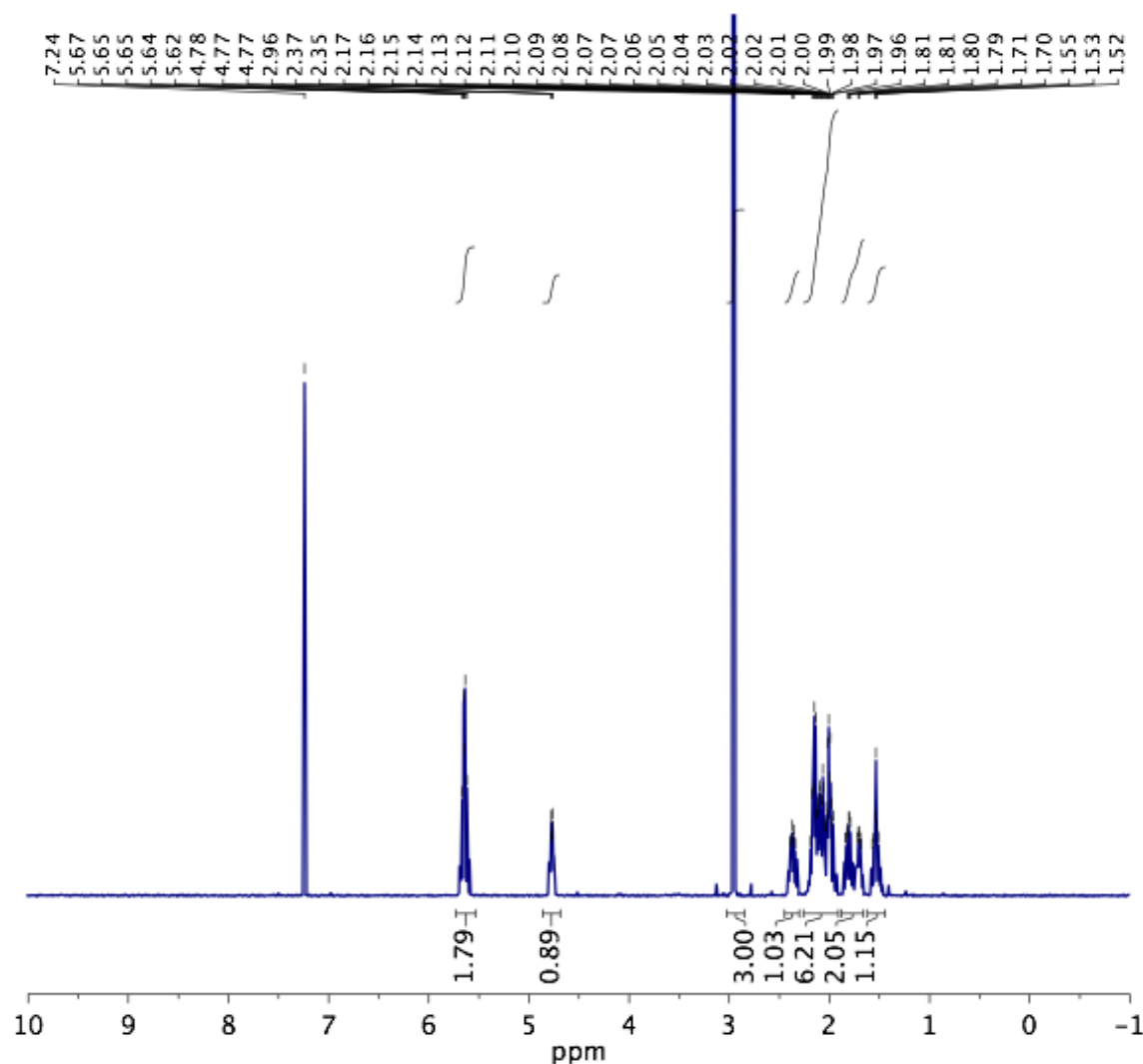
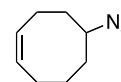


Figure 2.9 ^1H NMR Spectrum of 5-mesyl-1-cyclooctene. Signal at 7.24 ppm is residual CHCl_3 .

Preparation of 5-azido-1-cyclooctene (4). This compound has been prepared previously³⁶ but a modified alternate procedure was employed.³⁷ **Caution:** NaN_3 must be handled carefully to avoid exposure. Organic azides can be explosive, however in our laboratory the small amount of this compound did not detonate when heated to 100 °C behind a safety shield. Solid NaN_3 (3.82 g, 58.8 mmol) was carefully added to a solution of 5-Mesyl-1-cyclooctene (8.00 g, 39.2 mmol) in 30 mL of dimethyl sulfoxide at room



temperature. The 250 mL reaction vessel was fitted with a glass stopper and heated to 50 °C using an oil bath. The reaction mixture was stirred for 2 days at which point it was slowly quenched with 100 mL of water. Once the mixture had cooled to room temperature, it was extracted with diethyl ether (3 × 100 mL). The combined ether extracts were washed with water (1 × 100 mL). The organic layer was subsequently dried with Na₂SO₄ and the solvent was removed by rotary evaporation. The product was chromatographed on a short path of silica using hexanes/ethyl acetate, 19/1 (TLC analysis: R_f product = 0.4, R_f starting material = 0.1) to afford the desired azide as a colorless oil (4.57 g, 74 %). ¹H NMR (400 MHz, CDCl₃) δ 5.68-5.57 (2H, br m), 3.50-3.42 (1H, br m), 2.41-2.29 (1H, br m), 2.21-2.03 (3H, br m), 1.96-1.87 (1H, br m), 1.86-1.66 (3H, br m), 1.65-1.52 (1H, br m), 1.51-1.38 (1H, br m). ¹³C NMR (100 MHz, CDCl₃) δ 130.1, 129.6, 62.4, 34.0, 33.0, 26.1, 25.8, 23.2.

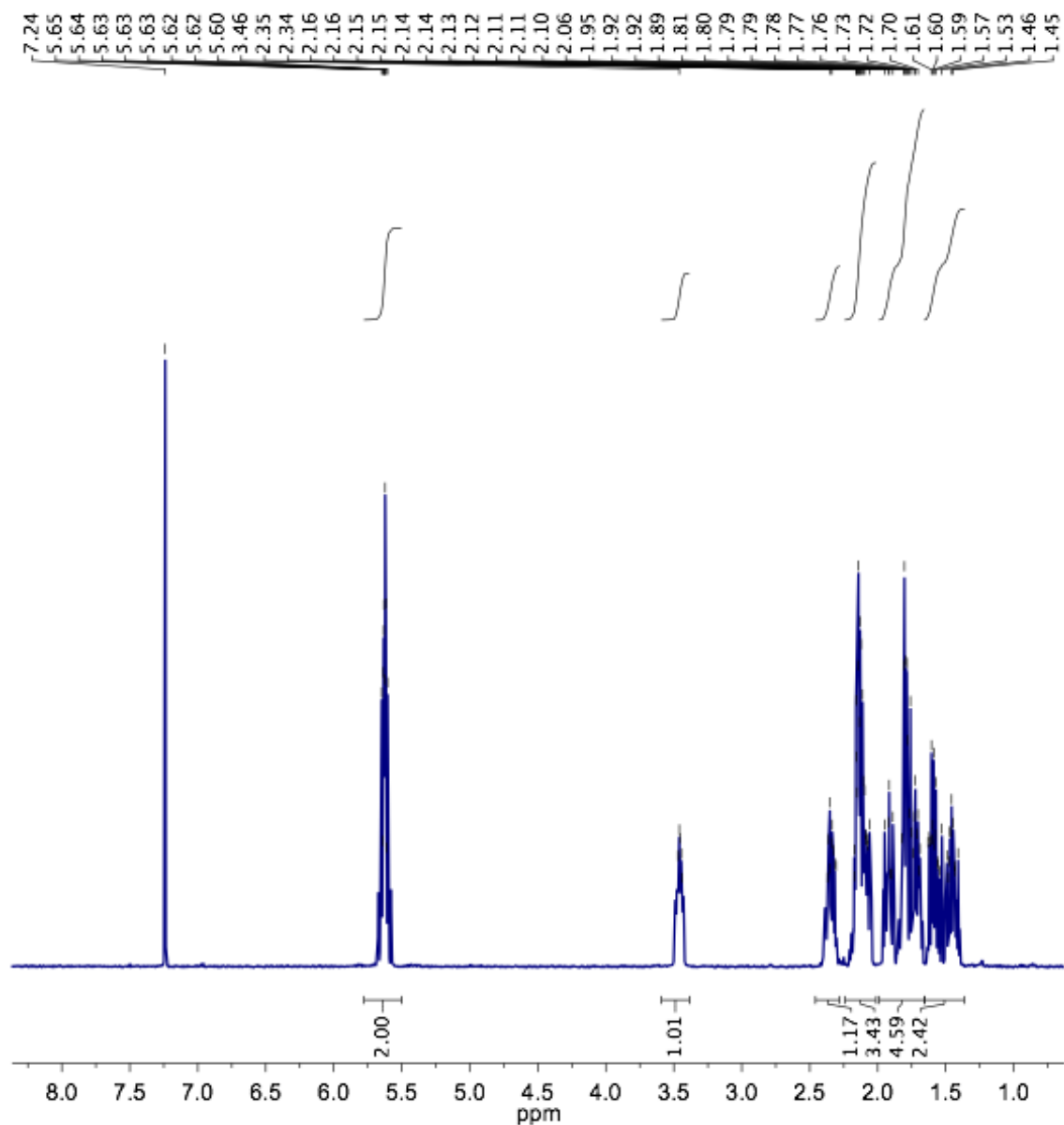
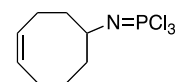


Figure 2.10 ^1H NMR Spectrum of 5-azido-1-cyclooctene. Signal at 7.24 ppm is residual CHCl_3 .

Preparation of 5-chloroiminophosphorane-1-cyclooctene (5). 5-Azido-1-cyclooctene (4.00 g, 26.5 mmol) was combined with 10 mL of dry toluene in a flame dried schlenk tube equipped with a magnetic stir bar. To this mixture, PCl_3 (11.5 mL, 132 mmol) was added by syringe with vigorous stirring. The reaction mixture was then heated to 70°C for approximately 48 h. The reaction mixture was quantitatively transferred to a 50 mL round-bottom flask in the glovebox and capped with a glass stopper. The flask was removed



from the glovebox and connected to a flame-dried distillation apparatus. Toluene and PCl_3 were removed *in vacuo*. Fractional distillation of the mixture afforded some crude 5-azido-1-cyclooctene (oil bath at 90 °C and stillhead temperature between 60-65 °C) and the desired product as a colorless oil (oil bath at 110 °C and stillhead temperature between 85-90 °C) in 43 % yield (2.94 g). This compound was used immediately for subsequent reactions as it dimerizes upon standing at 22 °C. Small amounts of (<5 %) 5-azido-1-cyclooctene does not seem to affect the subsequent reaction. ^{31}P NMR (121 MHz, C_6D_6) -72.9 (1P, d, $J_{\text{PH}} = 42.4$ Hz). ^1H NMR (400 MHz, C_6D_6) δ 5.67-5.45 (2H, br m), 3.73 (1H, d m, $J_{\text{PH}} = 43.0$ Hz), 2.31-2.17 (1H, br m), 2.17-2.02 (1H, br m), 2.01-1.65 (6H, br m), 1.65-1.50 (1H, br m), 1.41-1.26 (1H, br m). ^{13}C NMR (100 MHz, C_6D_6) δ 130.6, 129.8, 59.4 ($J_{\text{PC}} = 11.3$ Hz), 38.7 ($J_{\text{PC}} = 16.3$ Hz), 36.4 ($J_{\text{PC}} = 17.3$ Hz), 26.4, 26.2, 24.3.

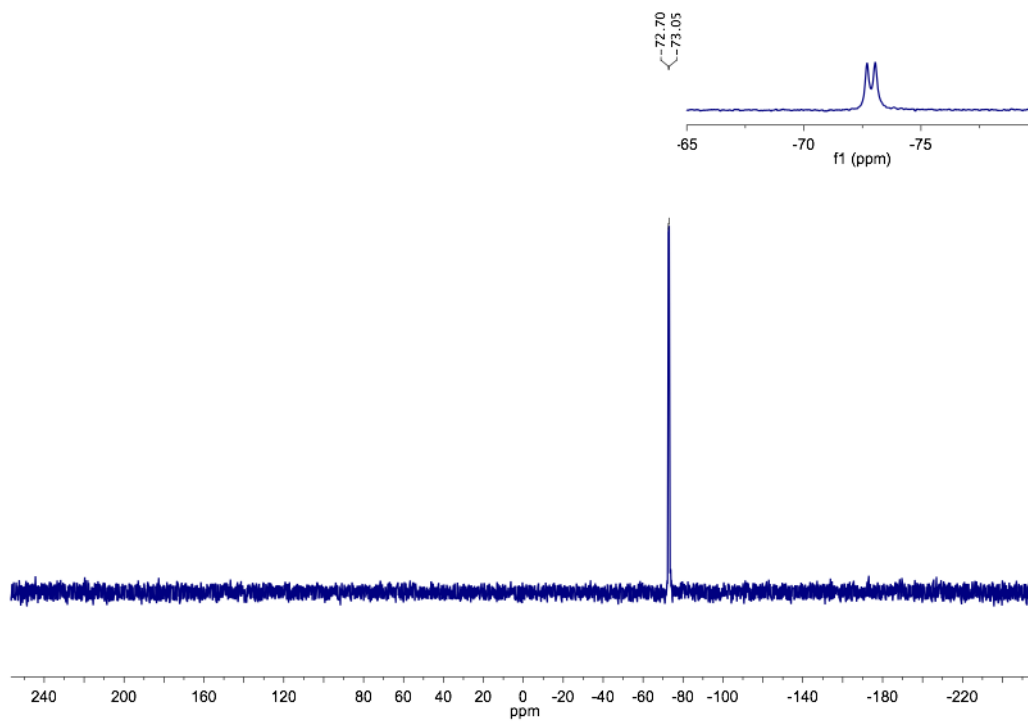


Figure 2.11 ^{31}P NMR Spectrum of 5-chloroiminophosphorane-1-cyclooctene. Referenced to 85% H_3PO_4 .

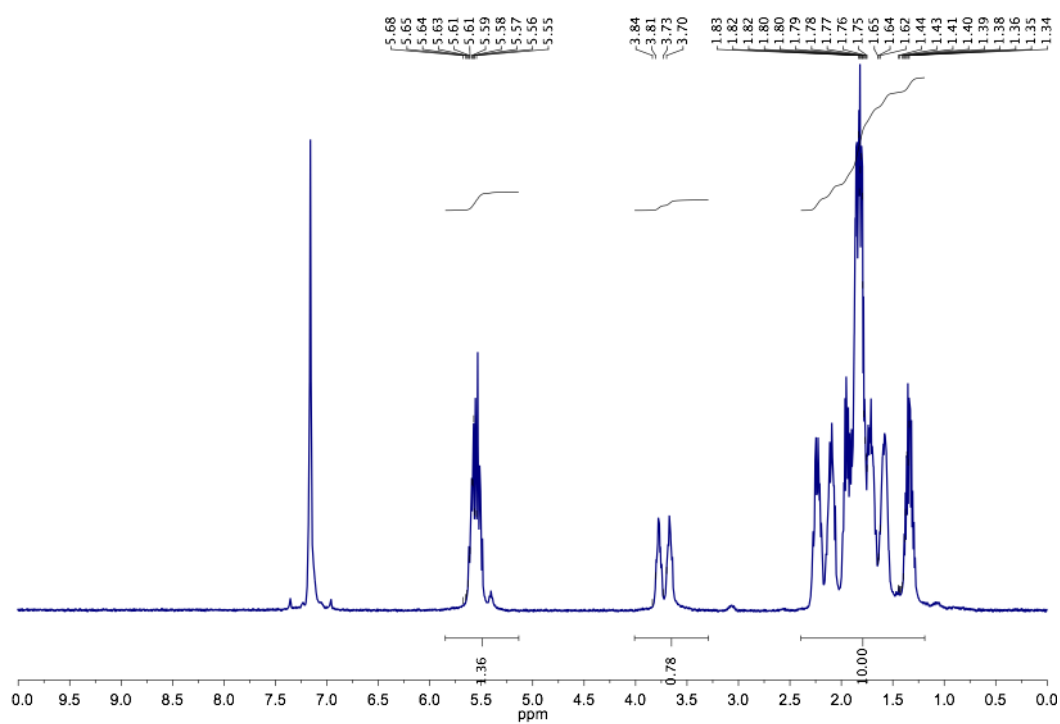
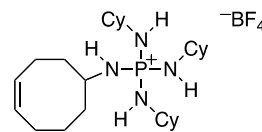


Figure 2.12 ^1H NMR Spectrum of 5-chloroiminophosphorane-1-cyclooctene. Signal at 7.16 ppm is residual $\text{C}_6\text{D}_5\text{H}$.

Preparation of Tris(cyclohexylamino)-cycloctenylamino-phosphonium tetrafluoroborate (6). This compound was



prepared according to a modified literature procedure.³⁸ Crude 5-

chloroiminophosphorane-1-cyclooctene (2.94 g, 11.3 mmol) was combined with dry CH₂Cl₂ (75 mL) in a 250 mL round bottom Schlenk flask equipped with a magnetic stir bar under an atmosphere of N₂. The solution was stirred magnetically and placed in an ice bath at 0 °C. Six equivalents of cyclohexylamine (7.75 mL, 67.7 mmol) were added to the solution using a syringe and the evolution of HCl gas was observed. Upon complete addition of the amine, the reaction mixture was kept at 0 °C for approximately 30 min at which point the ice bath was removed and the mixture was warmed to room temperature and stirred for two days. Analysis of the reaction mixture using ³¹P NMR spectroscopy confirmed the formation of tris(cyclohexylamino)-cycloctenylamino-phosphonium tetrafluoroborate ($\delta^{31}\text{P} = 20.5$). Approximately 50 mL of wet CH₂Cl₂ and 100 mL of water were added to the reaction mixture. The aqueous and organic layers were separated and the organic layer was washed with a further 100 mL of water. The CH₂Cl₂ solution was then washed with (3 × 50 mL) of a 1 M NaBF₄ aqueous solution and a subsequent 100 mL of water. The organic layer was then dried with Na₂SO₄ and the solvent was removed by rotary evaporation. Residual solvents were removed from the crude product upon heating to 75 °C *in vacuo* for 17 hours and a white solid was obtained (5.22 g, 86 %). This compound was typically used without further purification. ³¹P{¹H} NMR (121 MHz, CDCl₃) 20.5 (1P, s). ¹H NMR (400 MHz, CDCl₃) δ 5.71-5.54 (2H, m), 3.60 (1H, dd, *J* = 14.6 Hz, 10.5 Hz), 3.42 (3H, dd, *J* = 13.4 Hz, 9.9 Hz), 3.23-3.10 (1H, br m), 2.97-2.81 (3H, br m), 2.40-2.26 (1H, br m), 2.21-1.97 (3H, br m), 1.94-1.50 (20H, br m), 1.48-1.36 (1H, br m), 1.35-1.03 (15H, br m). ¹³C NMR (125 MHz, CD₃OD) δ 131.4, 130.5, 52.7, 52.2, 38.7 (d, *J*_{PC} = 5.4 Hz), 38.5 (d, *J*_{PC} = 4.7 Hz), 37.0 (app dd, *J* = 7.1, 5.0 Hz), 27.4, 27.3, 26.8, 26.5, 24.6. HRMS (ESI) *m/z* calculated for C₂₆H₅₀N₄P⁺ (M⁺) 449.3770, found 449.3773.

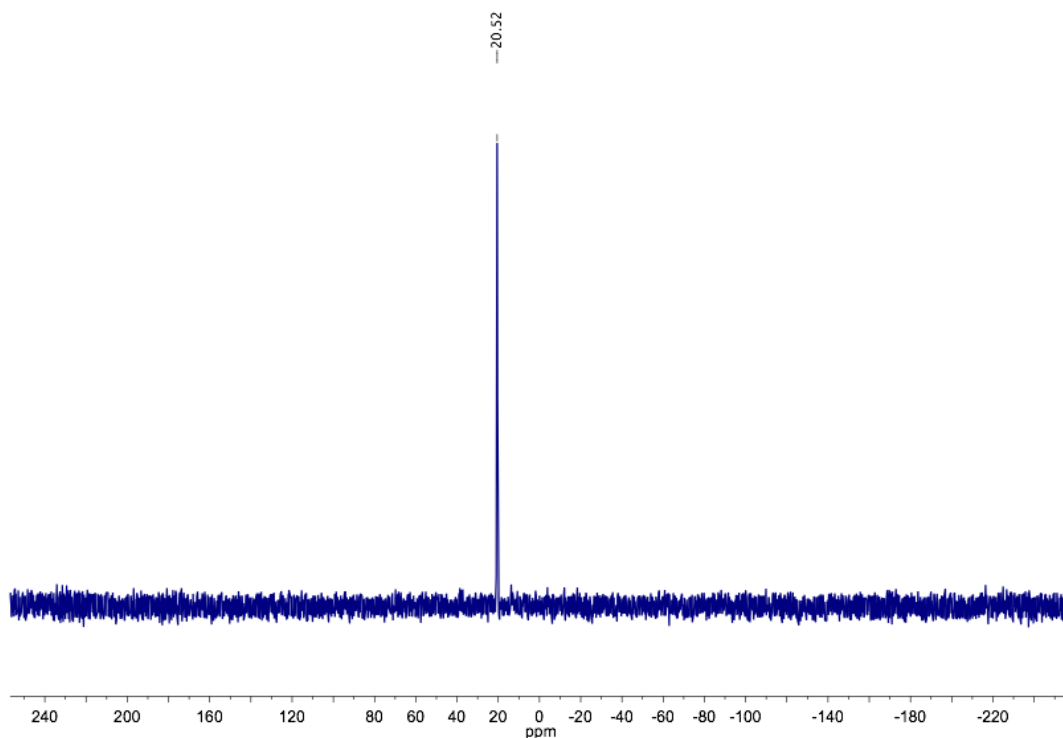


Figure 2.13 $^{31}\text{P}\{^1\text{H}\}$ NMR Spectrum of Tris(cyclohexylamino)-cycloctenylamino- phosphonium tetrafluoroborate. Referenced to 85 % H_3PO_4 .

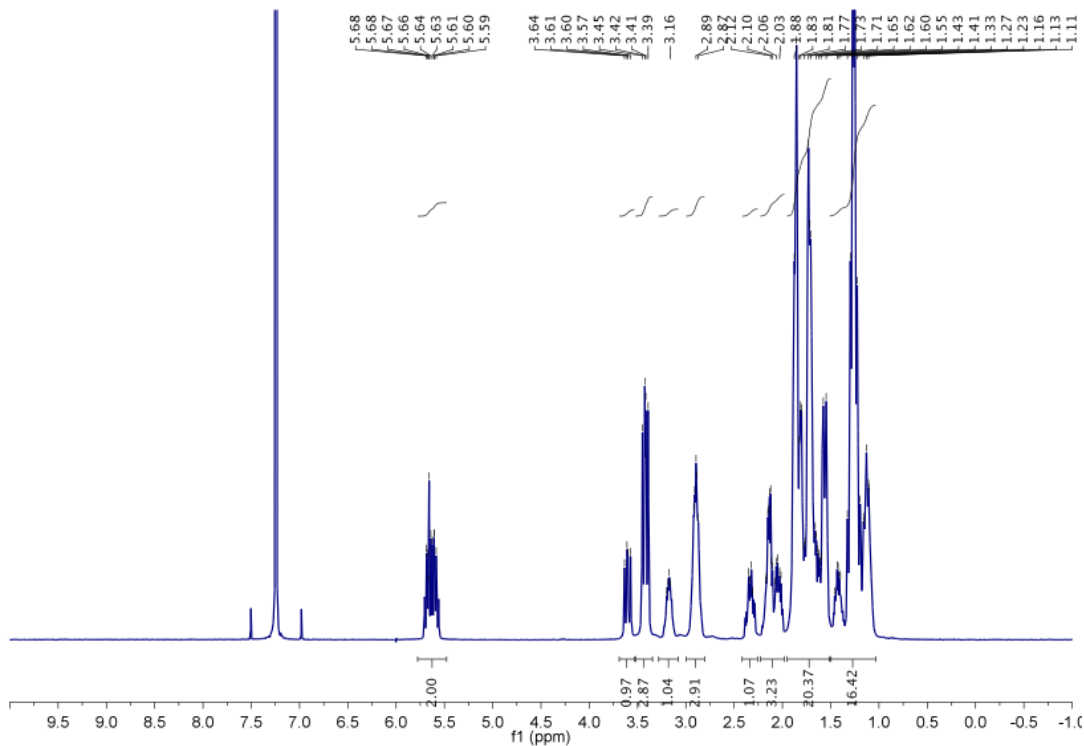
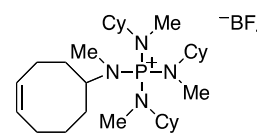


Figure 2.14 ^1H NMR Spectrum of Tris(cyclohexylamino)-cycloctenylamino- phosphonium tetrafluoroborate. Signal at 7.24 ppm is residual CHCl_3 .

Preparation of Tris[cyclohexyl(methyl)amino]-cycloctenyl(methyl)amino-phosphonium tetrafluoroborate.



This compound was prepared according to a modified literature procedure.⁴ In

a 100 mL round bottom flask equipped with a magnetic stir bar, tris(cyclohexylamino)-cycloctenylamino-phosphonium tetrafluoroborate (3.00 g, 5.59 mmol) was combined with chlorobenzene (20 mL) and 17.9 g of a 50 % NaOH solution (by weight). Dimethyl sulfate (2.65 mL, 27.9 mmol) was added in a cautious manner by syringe as the reaction is somewhat exothermic. After the addition of dimethyl sulfate the temperature of the reaction flask was monitored until it returned to ambient temperature at which time the reaction flask is placed in an oil bath at 70 °C for 8 h. Upon cooling the mixture to room temperature, 150 mL of water was added. The reaction mixture was extracted using wet CH₂Cl₂ (2 × 100 mL) and the combined organic extracts were washed with water (100 mL), dried with Na₂SO₄ and the CH₂Cl₂ was removed by rotary evaporation. The resultant oil was precipitated into 300 mL of diethyl ether. The white solid was collected on a Buchner funnel and residual solvent was removed at 80 °C *in vacuo*. The crude product was redissolved in CH₂Cl₂ (100 mL) and washed with aqueous 1 M NaBF₄ (2 × 50 mL) and precipitated into 300 mL of diethyl ether. The crude solid was collected on a Buchner funnel, dried *in vacuo*, dissolved in a minimal amount of CHCl₃ and dried *in vacuo* at 80-90 °C to remove residual solvents. The white solid was obtained in 82 % yield (2.7 g). ³¹P{¹H} NMR (202 MHz, CD₃OD, 60 °C) 45.0 (1P, br s). ¹H NMR (500 MHz, CD₃OD, 60 °C) δ 5.79 (1H, ddd, *J* = 10.2 Hz, 7.5 Hz, 7.5 Hz), 5.66 (1H, dddd, *J* = 10.4 Hz, 10.4 Hz, 6.8 Hz, 1.3 Hz), 3.48-3.39 (1H, br m), 3.14-3.03 (3H, br m), 2.69 (3H, d, *J* = 9.9 Hz), 2.68 (9H, d, *J* = 9.9 Hz), 2.50-2.40 (1H, m), 2.31-2.02 (4H, br m), 1.98-1.86 (7H, br m), 1.85-1.72 (8H, br m), 1.71-1.65 (3H, br m), 1.65-1.59 (6H, br m), 1.58-1.43 (2H, br m), 1.42-1.28 (6H, br m), 1.25-1.11 (3H, m). ¹³C NMR (125 MHz, CD₃OD, 60 °C) δ 132.1, 130.2, 57.2 (d, *J*_{PC} = 5.0 Hz), 56.2 (d, *J*_{PC} = 4.8 Hz), 34.5 (d, *J*_{PC} = 2.9 Hz), 33.7 (d, *J*_{PC} = 2.6 Hz), 31.9 (d, *J*_{PC} = 2.8 Hz), 30.9 (d, *J*_{PC} = 3.3 Hz), 30.6 (d, *J*_{PC} = 4.1 Hz), 27.4, 27.3, 27.16 and 27.12 (Two discernible signals seem to arise very close together which were not attributed to phosphorus carbon coupling. We suspect that

two carbon atoms of the cyclohexyl ring are inequivalent due to a steric constraint and produce independent signals), 26.3, 24.0. HRMS (ESI) m/z calculated for $C_{30}H_{58}N_4P^+$ (M^+) 505.4402, found 505.4399. Anal. Calc. for $C_{30}H_{58}B_1F_4N_4P_1$: C, 60.80; H, 9.87; N, 9.45. Found C, 60.78; H, 9.99; N, 9.49.

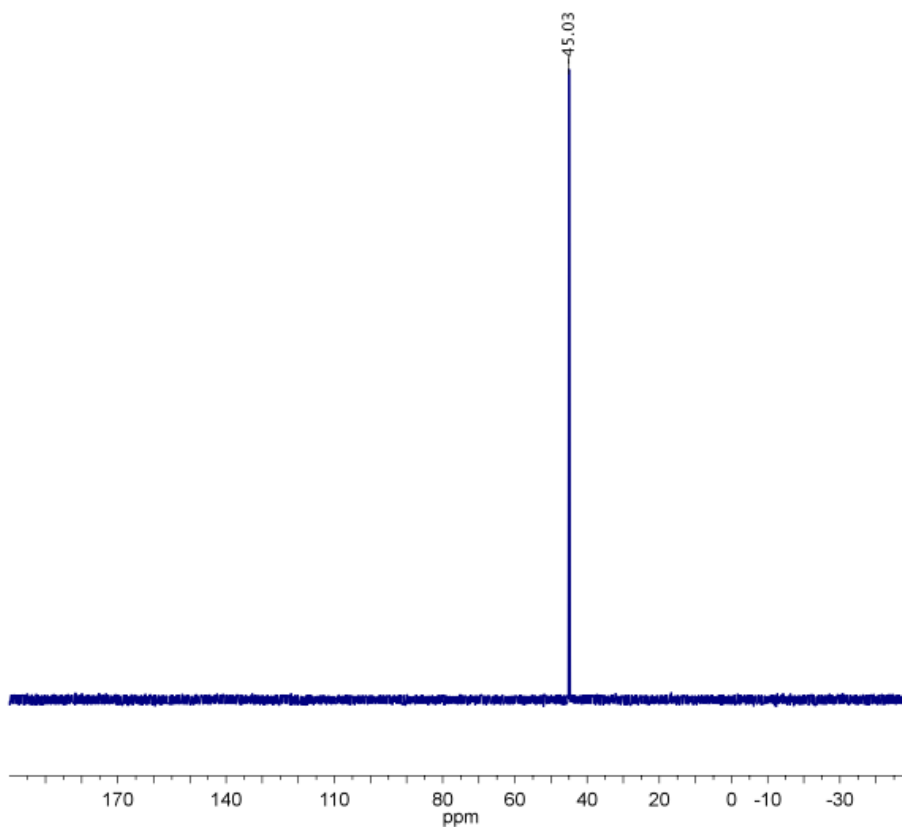


Figure 2.15 ^{31}P NMR Spectrum of Tris[cyclohexyl(methyl)amino]-cyclooctenyl(methyl)amino-phosphonium tetrafluoroborate in CD_3OD .

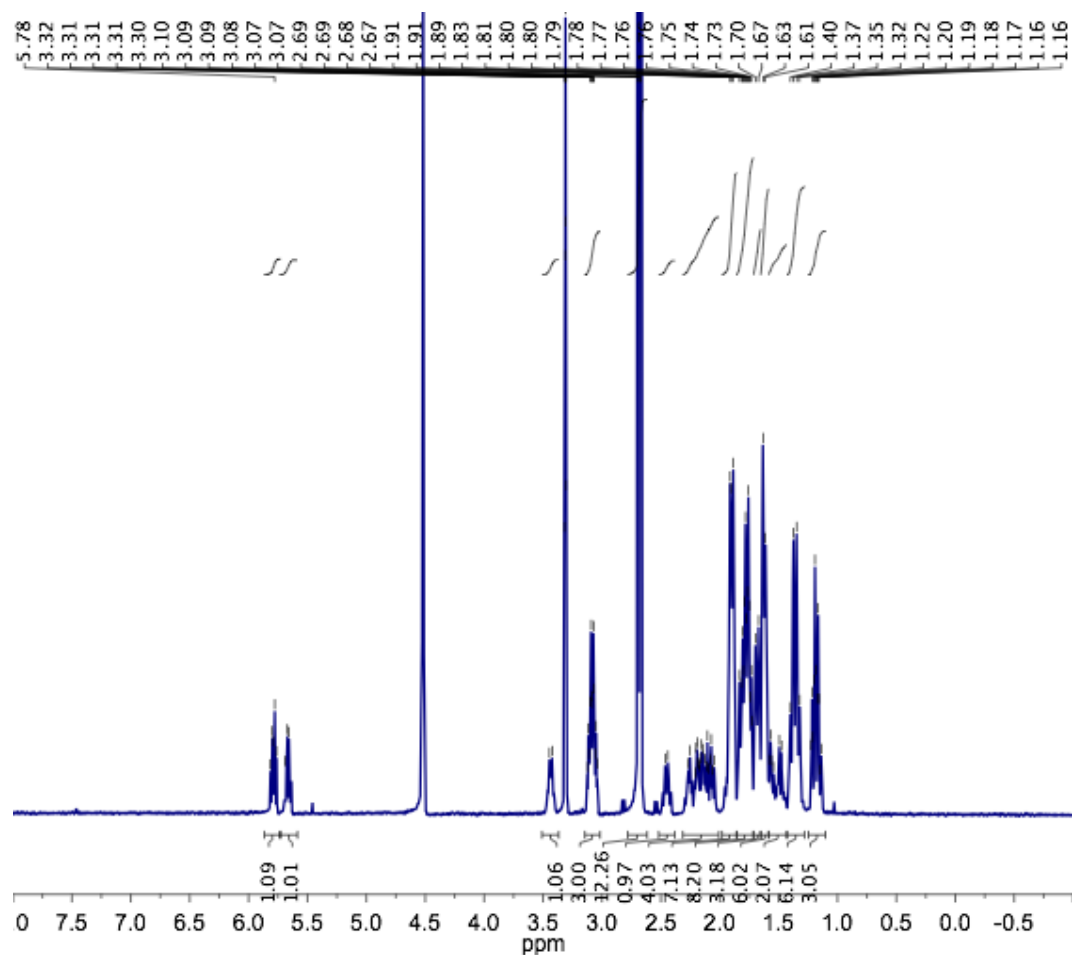
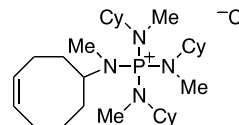


Figure 2.16 ^1H NMR Spectrum of Tris[cyclohexyl(methyl)amino]-cycloctenyl(methyl)amino-phosphonium tetrafluoroborate in CD_3OD . Signals at 4.52 and 3.31 ppm are due to the NMR solvent.

Preparation of Tris[cyclohexyl(methyl)amino]-cycloctenyl(methyl)amino-phosphonium chloride (7). This compound



was obtained by dissolving Tris[cyclohexyl(methyl)amino]-cycloctenyl(methyl)amino-phosphonium tetrafluoroborate (2.804 g, 4.732 mmol) in methanol and treating it with 30 g of ion exchange resin (Amberlite-IRA 400(Cl) form). The resin was filtered off and washed with methanol. The filtrate was rotary evaporated and immediately dissolved in CH₂Cl₂. The solution was washed twice with water, rotary evaporated and subsequently dried *in vacuo* at 80 °C affording a white solid in 88% yield (2.25 g). ¹H and ³¹P NMR spectra are the same as tris[cyclohexyl(methyl)amino]-cycloctenyl(methyl)amino-phosphonium tetrafluoroborate.

2.5.8 Synthesis of Phosphonium Polymer

Preparation of the Saturated Copolymer with 17 mol % of Tris[cyclohexyl(methyl)amino]-cycloctenyl(methyl)amino-phosphonium chloride: Under a nitrogen atmosphere Tris[cyclohexyl(methyl)amino]-cycloctenyl(methyl)amino-phosphonium chloride (0.4 g, 0.74 mmol) and COE (0.4 g, 3.63 mmol) were combined and dissolved in chloroform (2.0 mL). To the reaction mixture, Grubbs' 2nd Generation catalyst (3.8 mg, 0.0045 mmol) dissolved in 1.0 mL of chloroform was added and the solution was stirred vigorously. The reaction mixture became a swollen gel in a matter of minutes. The reaction was conducted for a minimum of 17 hours. The unsaturated copolymer was then dissolved in a 1:1 chloroform/methanol cosolvent (20 mL) forming a yellow solution. The polymer solution and Crabtree's catalyst (14.3 mg, 0.0178 mmol) were combined in a Parr reactor and sealed. It was pressurized to 600 psig hydrogen and then vented down to 50 psig. This process was repeated twice more to purge the reactor of air, then pressurized to 600 psig and heated to 55 °C with stirring. After 17 hours, it was cooled, vented and the swollen polymer gel dried under vacuum at 90 °C, washed with chloroform and dried again under vacuum at 90 °C furnishing a yellow solid (0.739 g, 92 %). The ¹H NMR spectrum suggests greater than 99% of the alkene units have been hydrogenated. ³¹P{¹H} NMR (161 MHz,

CDCl₃ and CD₃OD) 49.6 (1P, br s) ¹H NMR (500 MHz, DMSO-d₆, 135 °C) δ Note: integrations are not perfect match to expected polymer spectrum 3.17-3.01 (3H, br m), 3.01-2.82 (1H, br s), 2.74-2.55 (12H, br dd), 1.92-1.80 (8H, br d), 1.80-1.67 (11H, br m), 1.67-1.54 (12H, br m), 1.53-1.43 (4H, br), 1.42-1.21 (84H, br m) 1.21-1.09 (5H, br m).

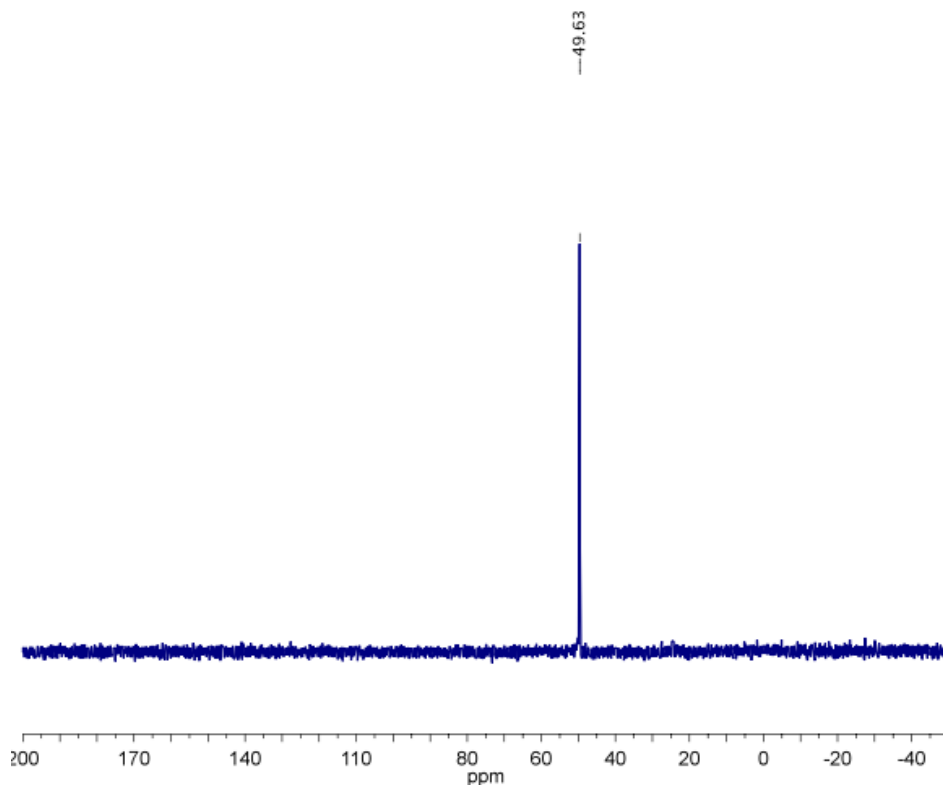


Figure 2.17 ³¹P NMR Spectrum of Saturated Copolymer with 17 mol % of Tris[cyclohexyl(methyl)amino]-cycloctenyl(methyl)amino-phosphonium chloride in in CD₃OD. Referenced to 85 % H₃PO₄.

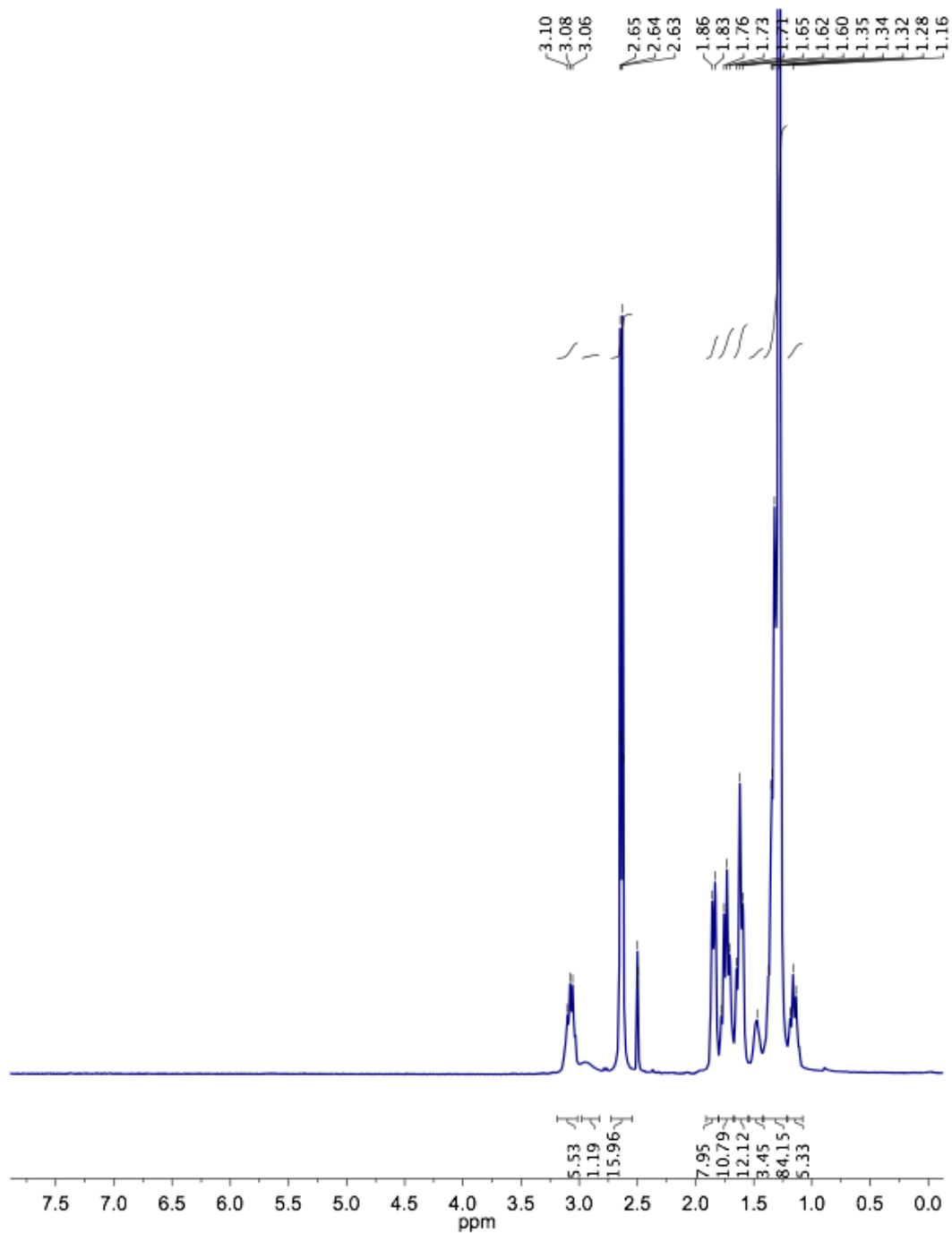


Figure 2.18 ^1H NMR Spectrum of Saturated Copolymer with 17 mol % of Tris[cyclohexyl(methyl)amino]-cyclooctenyl(methyl)amino-phosphonium chloride in $\text{DMSO-}d_6$ at 135 °C.

Preparation of AAEM-17: The saturated copolymer with 17 mol percent of Tris[cyclohexyl(methyl)amino]-cyclooctenyl(methyl)amino-phosphonium chloride was dissolved in a 1,2-dichloroethane/ethanol cosolvent mixture (8 mL) forming a light yellow solution and then transferred to a preheated (45 °C) glass dish (diameter of 5.25 cm and depth of 3.0 cm) on top of a hot plate covered with a metal plate to ensure uniform heating. The dish was covered with a round glass cover with a diameter of 7 cm and volume of 550 mL bearing one Kontes glass valve on top to control the rate of solvent evaporation. After a minimum of 4 hours the cover was removed and the temperature was increased to 80 °C for another hour. Following this, water was added and the translucent film was removed from the dish. The AAEM was generated by immersing the film in a 1 M KOH solution as described above.

2.5.8 Preparation of Tetrakis[cyclohexyl(methyl)amino]phosphonium Methoxide (1):

Tetrakis[cyclohexyl(methyl)amino]phosphonium tetrafluoroborate (1.134 g, 2.002 mmol) was dissolved in 8 mL of MeOH in a 20 mL scintillation vial with a teflon cap and heated to completely dissolve the salt. Potassium hydroxide (0.150 g, 2.67 mmol) was dissolved in 0.2 mL of deionized water and added to the scintillation vial containing the phosphonium salt. Potassium tetrafluoroborate immediately precipitated from solution and the reaction was stirred for approximately 30 min. The reaction mixture was cooled in an ice bath for several minutes prior to filtration. The mixture was filtered thru a PTFE membrane to remove the potassium tetrafluoroborate and as the solvent was removed *in vacuo* crystals suitable for x ray diffraction were obtained. The crystalline structure is illustrated below for $[P(N(Me)Cy)_4][OMe] \cdot 3MeOH$ (**1**).

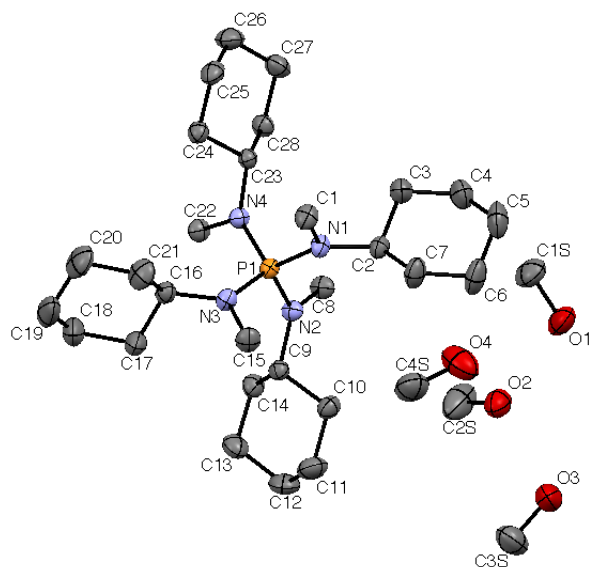
Single-crystal X-ray Crystallography: a suitable single crystal was chosen and mounted on a Bruker X8 APEX II diffractometer (MoK α radiation) and cooled to -100°C. Data collection and reduction were done using Bruker APEX2³⁹ and SAINT⁴⁰ software packages. An empirical absorption correction was applied with SADABS.⁴¹ Structure was solved

by direct methods and refined on F^2 by full matrix least-squares techniques using SHELXTL⁴² software package. All non-hydrogen atoms were refined anisotropically.

The sample size was 0.60 x 0.25 x 0.10 mm³. Overall 42306 reflections were collected, 9528 of which were symmetry independent ($R_{\text{int}} = 0.0312$); with 7152 ‘strong’ reflections (with $F_o > 4\sigma(F_o)$). Final $R_1 = 4.70\%$.

2.5.9 Crystallographic Data

Crystallographic data is also available from the Cambridge Structural Database. Structure requests can be made at <http://www.ccdc.cam.ac.uk/>. Deposition Number: CCDC 889152.



Scheme 3 Crystal Structure of Compound **1**.

Table 2.4 Crystal data and structure refinement for
Tetrakis[cyclohexyl(methyl)amino]phosphonium methoxide.

Identification code	kn11	
Empirical formula	C ₃₂ H ₇₁ N ₄ O ₄ P	
Formula weight	606.90	
Temperature	173(2) K	
Wavelength	0.71073 Å	
Crystal system	Monoclinic	
Space group	P2(1)/n	
Unit cell dimensions	a = 11.967(2) Å	a = 90°.
	b = 14.415(2) Å	b = 92.789(7)°.
	c = 22.293(4) Å	g = 90°.
Volume	3841.0(11) Å ³	
Z	4	
Density (calculated)	1.049 Mg/m ³	
Absorption coefficient	0.107 mm ⁻¹	
F(000)	1352	
Crystal size	0.60 x 0.25 x 0.10 mm ³	
Theta range for data collection	1.68 to 28.28°.	
Index ranges	-15 ≤ h ≤ 15, -19 ≤ k ≤ 13, -29 ≤ l ≤ 29	
Reflections collected	38576	
Independent reflections	9528 [R(int) = 0.0312]	
Completeness to theta = 28.28°	100.0 %	
Absorption correction	Semi-empirical from equivalents	
Max. and min. transmission	0.9893 and 0.9384	
Refinement method	Full-matrix least-squares on F ²	
Data / restraints / parameters	9528 / 0 / 599	
Goodness-of-fit on F ²	1.030	
Final R indices [I > 2σ(I)]	R1 = 0.0470, wR2 = 0.1290	
R indices (all data)	R1 = 0.0683, wR2 = 0.1451	
Largest diff. peak and hole	0.620 and -0.294 e.Å ⁻³	

Table 2.5 Atomic coordinates ($\times 10^4$) and equivalent isotropic displacement parameters ($\text{\AA}^2 \times 10^3$)

for Tetrakis[cyclohexyl(methyl)amino]phosphonium methoxide. $U(\text{eq})$ is defined as one third of the trace of the orthogonalized U^{ij} tensor.

P(1)	5329(1)	8216(1)	1377(1)	23(1)
O(1)	6639(1)	2158(1)	1058(1)	61(1)
O(2)	4685(1)	2294(1)	1487(1)	56(1)
O(3)	3172(1)	1308(1)	885(1)	75(1)
O(4)	5426(1)	1934(2)	2595(1)	81(1)
N(1)	6165(1)	7310(1)	1397(1)	27(1)
N(2)	4561(1)	8244(1)	746(1)	26(1)
N(3)	4547(1)	8099(1)	1964(1)	27(1)
N(4)	6040(1)	9187(1)	1413(1)	25(1)
C(1)	6753(2)	7050(1)	1977(1)	34(1)
C(1S)	7374(2)	2715(2)	1405(1)	60(1)
C(2)	6485(1)	6780(1)	853(1)	30(1)
C(2S)	4379(3)	3222(2)	1402(2)	91(1)
C(3)	7672(2)	7005(1)	664(1)	44(1)
C(3S)	2140(2)	1426(2)	1128(1)	70(1)
C(4)	7951(2)	6470(2)	92(1)	55(1)
C(4S)	4677(2)	2240(2)	2988(1)	70(1)
C(5)	7779(2)	5425(2)	169(1)	63(1)
C(6)	6586(2)	5217(1)	348(1)	59(1)
C(7)	6321(2)	5732(1)	936(1)	46(1)
C(8)	5095(1)	8534(1)	185(1)	32(1)
C(9)	3319(1)	8123(1)	705(1)	26(1)
C(10)	2956(1)	7210(1)	395(1)	35(1)
C(11)	1671(2)	7110(2)	379(1)	51(1)
C(12)	1073(2)	7951(2)	90(1)	52(1)
C(13)	1462(2)	8850(1)	400(1)	44(1)
C(14)	2742(1)	8954(1)	389(1)	34(1)
C(15)	3999(2)	7198(1)	2079(1)	36(1)
C(16)	4291(1)	8882(1)	2376(1)	30(1)
C(17)	3076(2)	9213(2)	2306(1)	50(1)

C(18)	2894(2)	10069(2)	2706(1)	64(1)
C(19)	3239(2)	9877(2)	3365(1)	68(1)
C(20)	4443(2)	9523(2)	3430(1)	60(1)
C(21)	4610(2)	8655(2)	3037(1)	49(1)
C(22)	5452(1)	10083(1)	1293(1)	31(1)
C(23)	7264(1)	9248(1)	1573(1)	24(1)
C(24)	7519(1)	9649(1)	2208(1)	31(1)
C(25)	8792(1)	9610(1)	2354(1)	39(1)
C(26)	9447(2)	10128(1)	1882(1)	47(1)
C(27)	9154(1)	9766(1)	1246(1)	41(1)
C(28)	7882(1)	9803(1)	1101(1)	32(1)

Table 2.6 Bond lengths [Å] and angles [°] for Tetrakis[cyclohexyl(methyl)amino]phosphonium methoxide.

P(1)-N(4)	1.6386(12)
P(1)-N(2)	1.6441(12)
P(1)-N(1)	1.6448(12)
P(1)-N(3)	1.6553(13)
O(1)-C(1S)	1.397(2)
O(2)-C(2S)	1.397(3)
O(3)-C(3S)	1.384(3)
O(4)-C(4S)	1.358(3)
N(1)-C(1)	1.4911(18)
N(1)-C(2)	1.4977(19)
N(2)-C(8)	1.4916(19)
N(2)-C(9)	1.4946(18)
N(3)-C(15)	1.4826(19)
N(3)-C(16)	1.4966(19)
N(4)-C(22)	1.4888(18)
N(4)-C(23)	1.4931(17)
C(2)-C(3)	1.536(2)
C(2)-C(7)	1.536(2)
C(3)-C(4)	1.540(3)
C(4)-C(5)	1.531(3)
C(5)-C(6)	1.530(4)
C(6)-C(7)	1.552(3)
C(9)-C(14)	1.535(2)
C(9)-C(10)	1.540(2)
C(10)-C(11)	1.543(3)
C(11)-C(12)	1.533(3)
C(12)-C(13)	1.530(3)
C(13)-C(14)	1.540(2)
C(16)-C(17)	1.532(2)
C(16)-C(21)	1.537(2)
C(17)-C(18)	1.543(3)
C(18)-C(19)	1.532(4)
C(19)-C(20)	1.529(4)

C(20)-C(21)	1.547(3)
C(23)-C(28)	1.540(2)
C(23)-C(24)	1.544(2)
C(24)-C(25)	1.543(2)
C(25)-C(26)	1.537(3)
C(26)-C(27)	1.535(3)
C(27)-C(28)	1.543(2)

N(4)-P(1)-N(2)	106.74(6)
N(4)-P(1)-N(1)	111.34(6)
N(2)-P(1)-N(1)	110.88(6)
N(4)-P(1)-N(3)	111.18(6)
N(2)-P(1)-N(3)	111.42(6)
N(1)-P(1)-N(3)	105.37(6)
C(1)-N(1)-C(2)	116.51(12)
C(1)-N(1)-P(1)	118.90(10)
C(2)-N(1)-P(1)	124.22(9)
C(8)-N(2)-C(9)	116.59(11)
C(8)-N(2)-P(1)	118.68(10)
C(9)-N(2)-P(1)	124.19(9)
C(15)-N(3)-C(16)	116.72(12)
C(15)-N(3)-P(1)	119.86(10)
C(16)-N(3)-P(1)	123.31(10)
C(22)-N(4)-C(23)	116.25(11)
C(22)-N(4)-P(1)	119.51(10)
C(23)-N(4)-P(1)	124.22(9)
N(1)-C(2)-C(3)	112.98(12)
N(1)-C(2)-C(7)	111.39(13)
C(3)-C(2)-C(7)	111.51(15)
C(2)-C(3)-C(4)	111.18(15)
C(5)-C(4)-C(3)	111.35(19)
C(4)-C(5)-C(6)	110.75(18)
C(5)-C(6)-C(7)	110.99(18)
C(2)-C(7)-C(6)	109.63(16)
N(2)-C(9)-C(14)	111.12(12)
N(2)-C(9)-C(10)	112.62(12)

C(14)-C(9)-C(10)	110.46(12)
C(9)-C(10)-C(11)	110.42(14)
C(12)-C(11)-C(10)	112.31(16)
C(13)-C(12)-C(11)	110.74(16)
C(12)-C(13)-C(14)	110.90(15)
C(9)-C(14)-C(13)	110.03(14)
N(3)-C(16)-C(17)	113.13(12)
N(3)-C(16)-C(21)	112.23(13)
C(17)-C(16)-C(21)	110.80(16)
C(16)-C(17)-C(18)	110.44(15)
C(19)-C(18)-C(17)	111.8(2)
C(20)-C(19)-C(18)	111.15(18)
C(19)-C(20)-C(21)	111.25(18)
C(16)-C(21)-C(20)	109.74(17)
N(4)-C(23)-C(28)	111.31(11)
N(4)-C(23)-C(24)	112.91(11)
C(28)-C(23)-C(24)	110.64(12)
C(25)-C(24)-C(23)	109.25(13)
C(26)-C(25)-C(24)	111.61(14)
C(27)-C(26)-C(25)	111.49(15)
C(26)-C(27)-C(28)	111.16(15)
C(23)-C(28)-C(27)	109.84(13)

Table 2.7 Anisotropic displacement parameters ($\text{\AA}^2 \times 10^3$) for Tetrakis[cyclohexyl(methyl)amino]phosphonium methoxide. The anisotropic displacement factor exponent takes the form: $-2p^2 [h^2 a^{*2} U^{11} + \dots + 2 h k a^* b^* U^{12}]$

	U11	U22	U33	U23	U13	U12
P(1)	26(1)	21(1)	21(1)	2(1)	-1(1)	0(1)
O(1)	68(1)	66(1)	48(1)	-21(1)	8(1)	-23(1)
O(2)	52(1)	50(1)	65(1)	-13(1)	-10(1)	9(1)
O(3)	47(1)	75(1)	103(1)	-39(1)	14(1)	-3(1)
O(4)	56(1)	121(2)	66(1)	7(1)	3(1)	18(1)
N(1)	33(1)	23(1)	24(1)	0(1)	-3(1)	4(1)
N(2)	26(1)	30(1)	22(1)	3(1)	-1(1)	-1(1)
N(3)	33(1)	24(1)	24(1)	1(1)	2(1)	-3(1)
N(4)	25(1)	20(1)	29(1)	3(1)	-1(1)	1(1)
C(1)	41(1)	29(1)	31(1)	3(1)	-7(1)	6(1)
C(1S)	64(1)	70(1)	46(1)	-13(1)	-8(1)	-13(1)
C(2)	34(1)	25(1)	30(1)	-4(1)	-1(1)	2(1)
C(2S)	87(2)	60(2)	120(2)	-25(2)	-48(2)	26(1)
C(3)	39(1)	44(1)	49(1)	-13(1)	7(1)	-2(1)
C(3S)	49(1)	65(1)	100(2)	0(1)	21(1)	2(1)
C(4)	54(1)	59(1)	53(1)	-17(1)	17(1)	0(1)
C(4S)	65(1)	74(2)	72(2)	-9(1)	12(1)	-26(1)
C(5)	78(2)	54(1)	57(1)	-20(1)	11(1)	20(1)
C(6)	92(2)	32(1)	55(1)	-15(1)	12(1)	-3(1)
C(7)	65(1)	26(1)	47(1)	-7(1)	11(1)	-3(1)
C(8)	33(1)	41(1)	24(1)	5(1)	1(1)	-2(1)
C(9)	26(1)	26(1)	25(1)	-1(1)	0(1)	1(1)
C(10)	37(1)	28(1)	39(1)	-3(1)	-4(1)	-1(1)
C(11)	40(1)	47(1)	64(1)	-3(1)	-4(1)	-14(1)
C(12)	28(1)	65(1)	63(1)	-4(1)	-9(1)	-3(1)
C(13)	32(1)	52(1)	49(1)	-2(1)	-2(1)	11(1)
C(14)	34(1)	30(1)	36(1)	-1(1)	-4(1)	6(1)
C(15)	42(1)	29(1)	37(1)	6(1)	8(1)	-5(1)
C(16)	33(1)	33(1)	25(1)	-3(1)	3(1)	-4(1)
C(17)	37(1)	55(1)	57(1)	-26(1)	-3(1)	4(1)

C(18)	49(1)	67(1)	76(2)	-40(1)	3(1)	8(1)
C(19)	71(2)	72(2)	63(1)	-37(1)	32(1)	-25(1)
C(20)	80(2)	72(1)	29(1)	-15(1)	3(1)	-15(1)
C(21)	64(1)	57(1)	25(1)	-1(1)	1(1)	-4(1)
C(22)	32(1)	23(1)	37(1)	4(1)	-2(1)	3(1)
C(23)	24(1)	22(1)	26(1)	-1(1)	1(1)	1(1)
C(24)	32(1)	32(1)	28(1)	-3(1)	-1(1)	2(1)
C(25)	37(1)	39(1)	40(1)	-8(1)	-12(1)	5(1)
C(26)	30(1)	47(1)	62(1)	-4(1)	-6(1)	-5(1)
C(27)	31(1)	44(1)	50(1)	2(1)	10(1)	-1(1)
C(28)	32(1)	33(1)	30(1)	1(1)	5(1)	-1(1)

Table 2.8 Hydrogen coordinates ($\times 10^4$) and isotropic displacement parameters ($\text{\AA}^2 \times 10^{-3}$) for Tetrakis[cyclohexyl(methyl)amino]phosphonium methoxide.

	x	y	z	U(eq)
H(1O)	5870(30)	2210(20)	1226(13)	100
H(3O)	3727	1665	1140	100
H(4O)	5118	2068	2156	100
H(1C)	7561(17)	7039(13)	1956(8)	41(5)
H(1B)	6514(17)	6451(15)	2118(9)	47(5)
H(1A)	6606(16)	7491(14)	2307(9)	45(5)
H(1S1)	7439	3323	1213	91
H(1S2)	8112	2419	1439	91
H(1S3)	7088	2794	1807	91
H(2)	5948(15)	6955(12)	537(8)	32(4)
H(2S1)	4250	3508	1790	137
H(2S2)	3699	3258	1142	137
H(2S3)	4987	3554	1211	137
H(3B)	8162(19)	6817(15)	968(10)	53(6)
H(3A)	7706(17)	7696(16)	588(9)	52(6)
H(3S1)	2247	1546	1560	106
H(3S2)	1693	862	1065	106
H(3S3)	1754	1953	934	106
H(4B)	7430(20)	6685(16)	-261(11)	63(7)
H(4A)	8690(20)	6621(18)	-59(12)	79(8)
H(4S1)	4763	1883	3362	105
H(4S2)	3917	2159	2813	105
H(4S3)	4812	2898	3074	105
H(5B)	8360(20)	5209(16)	501(11)	68(7)
H(5A)	7940(20)	5105(18)	-231(12)	79(8)
H(6A)	6045(19)	5434(15)	-10(10)	57(6)
H(6B)	6480(20)	4570(20)	414(13)	91(9)
H(7B)	6842(19)	5500(15)	1274(10)	58(6)
H(7A)	5560(20)	5619(15)	1080(10)	58(6)
H(8C)	5887(16)	8488(13)	238(8)	38(5)
H(8B)	4850(17)	8133(14)	-145(9)	46(5)

H(8A)	4907(17)	9180(15)	84(9)	49(5)
H(9)	3083(14)	8102(11)	1126(8)	29(4)
H(10B)	3232(16)	7219(13)	-13(9)	40(5)
H(10A)	3319(15)	6677(13)	606(8)	37(5)
H(11B)	1422(19)	7039(16)	758(11)	58(7)
H(11A)	1440(20)	6540(18)	141(11)	72(7)
H(12B)	250(20)	7875(16)	118(10)	62(6)
H(12A)	1309(18)	8011(15)	-374(11)	57(6)
H(13B)	1057(16)	9394(14)	199(9)	44(5)
H(13A)	1233(18)	8848(15)	824(10)	57(6)
H(14B)	2949(15)	8988(12)	-28(9)	36(5)
H(14A)	3005(15)	9553(14)	584(8)	41(5)
H(15C)	4174(18)	6764(14)	1781(10)	51(6)
H(15B)	4286(17)	6947(14)	2457(10)	46(5)
H(15A)	3186(18)	7249(14)	2071(9)	45(5)
H(16)	4767(14)	9396(12)	2274(7)	28(4)
H(17B)	2900(20)	9363(17)	1886(12)	67(7)
H(17A)	2599(19)	8737(16)	2403(10)	53(6)
H(18A)	3400(20)	10596(19)	2574(11)	78(8)
H(18B)	2070(20)	10206(19)	2707(12)	87(8)
H(19A)	2770(20)	9376(18)	3535(11)	69(7)
H(19B)	3170(20)	10448(18)	3622(11)	75(7)
H(20B)	5010(20)	10049(19)	3312(11)	74(7)
H(20A)	4610(20)	9348(19)	3844(13)	86(8)
H(21B)	5390(20)	8426(16)	3073(10)	60(6)
H(21A)	4110(20)	8125(16)	3166(10)	64(7)
H(22C)	4635(16)	9990(12)	1225(8)	37(5)
H(22B)	5767(16)	10392(13)	946(9)	42(5)
H(22A)	5535(16)	10486(14)	1637(9)	43(5)
H(23)	7558(13)	8610(12)	1575(7)	23(4)
H(24B)	7232(15)	10285(13)	2228(8)	36(5)
H(24A)	7090(15)	9293(12)	2505(8)	34(4)
H(25A)	9037(15)	8964(13)	2367(8)	33(4)
H(25A)	8952(16)	9868(14)	2783(9)	50(5)
H(26B)	9282(17)	10795(16)	1887(9)	50(6)
H(26A)	10240(20)	10062(16)	1983(10)	62(6)

H(27B)	9523(17)	10125(14)	941(9)	50(6)
H(27A)	9425(17)	9108(15)	1220(9)	51(6)
H(28B)	7633(14)	10441(13)	1094(8)	33(4)
H(28A)	7681(14)	9525(12)	691(8)	35(4)

Table 2.9 Hydrogen bonds for Tetrakis[cyclohexyl(methyl)amino]phosphonium methoxide [\AA and $^\circ$].

D-H...A	d(D-H)	d(H...A)	d(D...A)	$\angle(\text{DHA})$
O(1)-H(1O)...O(2)	1.02(3)	1.56(3)	2.576(2)	180(3)
O(3)-H(3O)...O(2)	0.9959(16)	1.6274(14)	2.619(2)	173.59(13)
O(4)-H(4O)...O(2)	1.0463(18)	1.5896(15)	2.635(2)	178.10(13)

REFERENCES

- (1) O'Hayre, R. P. *Fuel Cell Fundamentals*; John Wiley and Sons: Hoboken, NY, 2006.
- (2) Bocarsly, A.; Mingos, D. A. P. *Fuel Cells and Hydrogen Storage*; Springer: New York, 2011.
- (3) (a) Poynton, S. D.; Kizewski, J. P.; Slade, R. C. T.; Varcoe, J. R. *Solid State Ionics* **2010**, *181*, 219-222. (b) Sleightholme, A. E. S.; Varcoe, J. R.; Kucernak, A. R. *Electrochem. Commun.* **2008**, *10*, 151-155. (c) Wagner, N.; Schulze, M.; Gulzow, E. *J. Power Sources* **2004**, *127*, 264-272.
- (4) (a) Couture, G.; Alaaeddine, A.; Boschet, F.; Ameduri, B. *Prog. Polym. Sci.* **2011**, *36*, 1521-1557. (b) Merle, G.; Wessling, M.; Nijmeijer, K. *J. Membr. Sci.* **2011**, *377*, 1-35. (c) Varcoe, J. R.; Slade, R. C. T. *Fuel Cells* **2005**, *5*, 187-200.
- (5) (a) Zha, Y. P.; Disabb-Miller, M. L.; Johnson, Z. D.; Hickner, M. A.; Tew, G. N. *J. Am. Chem. Soc.* **2012**, *134*, 4493-4496. (b) Kostalik, H. A.; Clark, T. J.; Robertson, N. J.; Mutolo, P. F.; Longo, J. M.; Abruña, H. D.; Coates, G. W. *Macromolecules* **2010**, *43*, 7147-7150. (c) Robertson, N. J.; Kostalik, H. A.; Clark, T. J.; Mutolo, P. F.; Abruña, H. D.; Coates, G. W. *J. Am. Chem. Soc.* **2010**, *132*, 3400-3404. (d) Clark, T. J.; Robertson, N. J.; Kostalik, H. A.; Lobkovsky, E. B.; Mutolo, P. F.; Abruña, H. D.; Coates, G. W. *J. Am. Chem. Soc.* **2009**, *131*, 12888-12889.
- (6) (a) Guo, T. Y.; Zeng, Q. H.; Zhao, C. H.; Liu, Q. L.; Zhu, A. M.; Broadwell, I. *J. Membr. Sci.* **2011**, *371*, 268-275. (b) Zhang, F. X.; Zhang, H. M.; Ren, J. X.; Qu, C. *J. Mater. Chem.* **2010**, *20*, 8139-8146. (c) Varcoe, J. R.; Slade, R. C. T.; Yee, E. L. H.; Poynton, S. D.; Driscoll, D. J.; Apperley, D. C. *Chem. Mater.* **2007**, *19*, 2686-2693. (d) Varcoe, J. R.; Slade, R. C. T.; Lam How Yee, E. *Chem. Commun.* **2006**, 1428-1429. (e) Varcoe, J. R.; Slade, R. C. T. *Electrochem. Commun.* **2006**, *8*, 839-843.
- (7) (a) Zhao, Z.; Wang, J. H.; Li, S. H.; Zhang, S. B. *J. Power Sources* **2011**, *196*, 4445-4450. (b) Wang, J. H.; Wang, J.; Li, S. H.; Zhang, S. B. *J. Membr. Sci.* **2011**, *368*, 246-253. (c) Ni, J.; Zhao, C. J.; Zhang, G.; Zhang, Y.; Wang, J.; Ma, W. J.; Liu, Z. G.; Na, H. *Chem. Commun.* **2011**, *47*, 8943-8945. (d) Zhang, Q. A.; Zhang, Q. F.; Wang, J. H.; Zhang, S. B.; Li, S. H. *Polymer* **2010**, *51*, 5407-5416. (e) Wang, J. H.; Zhao, Z.; Gong, F. X.; Li, S. H.; Zhang, S. B. *Macromolecules* **2009**, *42*, 8711-8717. (f) Wang, G. G.; Weng, Y. M.; Chu, D.; Chen, R. R.; Xie, D. *J. Membr. Sci.* **2009**, *332*, 63-68. (g) Hibbs, M. R.; Hickner, M. A.; Alam, T. M.; McIntyre, S. K.; Fujimoto, C. H.; Cornelius, C. J. *Chem. Mater.* **2008**, *20*, 2566-2573.

- (8) Hibbs, M. R.; Fujimoto, C. H.; Cornelius, C. J. *Macromolecules* **2009**, *42*, 8316-8321.
- (9) (a) Wang, G. G.; Weng, Y. M.; Zhao, J.; Chu, D.; Xie, D.; Chen, R. R. *Polym. Adv. Technol.* **2010**, *21*, 554-560. (b) Wang, G. G.; Weng, Y. M.; Chu, D.; Xie, D.; Chen, R. R. *J. Membr. Sci.* **2009**, *326*, 4-8.
- (10) (a) Long, H.; Kim, K.; Pivovar, B. S. *J. Phys. Chem. C* **2012**, *116*, 9419-9426. (b) Edson, J. B.; Macomber, C. S.; Pivovar, B. S.; Boncella, J. M. *J. Membr. Sci.* **2012**, *399*, 49-59. (c) Chempath, S.; Boncella, J. M.; Pratt, L. R.; Henson, N.; Pivovar, B. S. *J. Phys. Chem. C* **2010**, *114*, 11977-11983. (d) Chempath, S.; Einsla, B. R.; Pratt, L. R.; Macomber, C. S.; Boncella, J. M.; Rau, J. A.; Pivovar, B. S. *J. Phys. Chem. C* **2008**, *112*, 3179-3182. (e) Macomber, C. S.; Boncella, J. M.; Pivovar, B. S.; Rau, J. A. *J. Therm. Anal. Calorim.* **2008**, *93*, 225-229. (f) Einsla, B. R.; Chempath, S.; Pratt, L. R.; Boncella, J. M.; Rau, J.; Macomber, C. S.; Pivovar, B. S. *ECS Trans.* **2007**, *11*, 1173-1180.
- (11) Vega, J. A.; Chartier, C.; Mustain, W. E. *J. Power Sources* **2010**, *195*, 7176-7180.
- (12) (a) Kim, D. S.; Labouriau, A.; Guiver, M. D.; Kim, Y. S. *Chem. Mater.* **2011**, *23*, 3795-3797. (b) Zhang, Q. A.; Li, S. H.; Zhang, S. B. *Chem. Commun.* **2010**, *46*, 7495-7497. (c) Wang, J. H.; Li, S. H.; Zhang, S. B. *Macromolecules* **2010**, *43*, 3890-3896.
- (13) (a) Zhang, F. X.; Zhang, H. M.; Qu, C. *J. Mater. Chem.* **2011**, *21*, 12744-12752. (b) Thomas, O. D.; Soo, K. J. W. Y.; Peckham, T. J.; Kulkarni, M. P.; Holdcroft, S. *Polym. Chem.* **2011**, *2*, 1641-1643. (c) Li, W.; Fang, J.; Lv, M.; Chen, C. X.; Chi, X. J.; Yang, Y. X.; Zhang, Y. M. *J. Mater. Chem.* **2011**, *21*, 11340-11346. (d) Ye, Y. S.; Elabd, Y. A. *Macromolecules* **2011**, *44*, 8494-8503. (e) Deavin, O. I.; Murphy, S.; Ong, A. L.; Poynton, S. D.; Zeng, R.; Herman, H.; Varcoe, J. R. *Energy Environ. Sci.* **2012**. DOI: 10.1039/c2ee22466f.
- (14) Thomas, O. D.; Soo, K. J.; Peckham, T. J.; Kulkarni, M. P.; Holdcroft, S. *J. Am. Chem. Soc.* **2012**, *134*, 10753-10756.
- (15) For examples of phosphonium ionomer synthesis see: (a) Laschewsky, A. *Curr. Opin. Colloid Interface Sci.* **2012**, *17*, 56-63. (b) Cheng, S. J.; Beyer, F. L.; Mather, B. D.; Moore, R. B.; Long, T. E. *Macromolecules* **2011**, *44*, 6509-6517. (c) Parent, J. S.; Penciu, A.; Guillen-Castellanos, S. A.; Liskova, A.; Whitney, R. A. *Macromolecules* **2004**, *37*, 7477-7483. (d) Ghassemi, H.; Riley, D. J.; Curtis, M.; Bonaplata, E.; McGrath, J. E. *Appl. Organomet. Chem.* **1998**, *12*, 781-785.

- (16) (a) Arges, C. G.; Parrondo, J.; Johnson, G.; Nadhan, A.; Ramani, V. *J. Mater. Chem.* **2012**, *22*, 3733-3744. (b) Arges, C. G.; Jung, M. S.; Johnson, G.; Parrondo, J.; Ramani, V. *ECS Trans.* **2011**, *41*, 1795-1816. (c) Stokes, K. K.; Orlicki, J. A.; Beyer, F. L. *Polym. Chem.* **2011**, *2*, 80-82. (d) Arges, C. G.; Kulkarni, S.; Baranek, A.; Pan, K. J.; Jung, M. S.; Patton, D.; Mauritz, K. A.; Ramani, V. *ECS Trans.* **2010**, *33*, 1903-1913.
- (17) (a) Gu, S.; Cai, R.; Yan, Y. S. *Chem. Commun.* **2011**, *47*, 2856-2858. (b) Gu, S.; Cai, R.; Luo, T.; Jensen, K.; Contreras, C.; Yan, Y. S. *ChemSusChem* **2010**, *3*, 555-558. (c) Gu, S.; Cai, R.; Luo, T.; Chen, Z. W.; Sun, M. W.; Liu, Y.; He, G. H.; Yan, Y. S. *Angew. Chem. Int. Ed.* **2009**, *48*, 6499-6502.
- (18) (a) Kong, X.; Wadhwa, K.; Verkade, J. G.; Schmidt-Rohr, K. *Macromolecules* **2009**, *42*, 1659-1664. (b) Pivovar, B. S.; Thorn, D. L. Anion-conducting Polymer Composition, and Membrane. US2006/0217526, Sept 28, 2006.
- (19) Schwesinger, R.; Link, R.; Wenzl, P.; Kossek, S.; Keller, M. *Chem. Eur. J.* **2006**, *12*, 429-437.
- (20) (a) Kim, M. J.; Kim, M. Y.; Kwon, O. Z.; Seo, G. *Fuel Process. Technol.* **2011**, *92*, 126-131. (b) Kim, M. Y.; Seo, G.; Kwon, O. Z.; Chang, D. R. *Chem. Commun.* **2009**, 3110-3112.
- (21) (a) Rexin, O.; Mülhaupt, R. *Macromol. Chem. Phys.* **2003**, *204*, 1102-1109. (b) Rexin, O.; Mülhaupt, R. *J. Polym. Sci., Part A: Polym. Chem.* **2002**, *40*, 864-873.
- (22) Kostalik, H. A. Dissertation, Cornell University, 2011.
- (23) Givaja, G.; Blake, A. J.; Wilson, C.; Schroder, M.; Love, J. B. *Chem. Commun.* **2003**, 2508-2509.
- (24) Sun, R.; Wang, K.; Wu, D. D.; Huang, W.; Ou, Y. B. *Acta Crystallogr., Sect. E: Struct. Rep. Online* **2012**, *68*, o824.
- (25) One other report of interest describes a methoxide anion found in the crystal of a chromium complex. The methoxide is hydrogen bonded to three water molecules. Bino, A. *J. Am. Chem. Soc.* **1987**, *109*, 275-276.

- (26) Shokri, A.; Schmidt, J.; Wang, X. B.; Kass, S. R. *J. Am. Chem. Soc.* **2012**, *134*, 2094-2099.
- (27) (a) Gorbunova, M. N. *Russ. J. Appl. Chem.* **2011**, *84*, 867-872. (b) Ohta, M.; Ono, T.; Sada, K. *Chem. Lett.* **2011**, *40*, 648-650. (c) Gorbunova, M. N.; Batueva, T. D. *Russ. J. Appl. Chem.* **2010**, *83*, 2016-2019. (d) Vorob'eva, A. I.; Gorbunova, M. N.; Sataeva, F. A.; Muslukhov, R. R.; Kolesov, S. V.; Tolstikov, A. G.; Monakov, Y. B. *Russ. J. Appl. Chem.* **2008**, *81*, 840-844. (e) Wehmeyer, R. M. Method For Preparing And Using Supported Phosphazanium Catalysts. US2002/0022714, Feb 21, 2002.
- (28) For some examples of PEM membrane materials made using ROMP see: (a) Santiago, A. A.; Vargas, J.; Tlenkopatchev, M. A.; Lopez-Gonzalez, M.; Rianded, E. *J. Membr. Sci.* **2012**, *403*, 121-128. (b) Chen, L.; Hallinan, D. T.; Elabd, Y. A.; Hillmyer, M. A. *Macromolecules* **2009**, *42*, 6075-6085. (c) Fei, S. T.; Wood, R. M.; Lee, D. K.; Stone, D. A.; Chang, H. L.; Allcock, H. R. *J. Membr. Sci.* **2008**, *320*, 206-214.
- (29) Clark, P. G.; Guidry, E. N.; Chan, W. Y.; Steinmetz, W. E.; Grubbs, R. H. *J. Am. Chem. Soc.* **2010**, *132*, 3405-3412.
- (30) (a) Tanaka, M.; Fukasawa, K.; Nishino, E.; Yamaguchi, S.; Yamada, K.; Tanaka, H.; Bae, B.; Miyatake, K.; Watanabe, M. *J. Am. Chem. Soc.* **2011**, *133*, 10646-10654. (b) Bae, B.; Miyatake, K.; Uchida, M.; Uchida, H.; Sakiyama, Y.; Okanishi, T.; Watanabe, M. *ACS Appl. Mater. Interfaces* **2011**, *3*, 2786-2793. (c) Faraj, M.; Elia, E.; Boccia, M.; Filpi, A.; Pucci, A.; Ciardelli, F. *J. Polym. Sci., Part A: Polym. Chem.* **2011**, *49*, 3437-3447. (d) Elabd, Y. A.; Hickner, M. A. *Macromolecules* **2011**, *44*, 1-11. (e) Zeng, Q. H.; Liu, Q. L.; Broadwell, I.; Zhu, A. M.; Xiong, Y.; Tu, X. P. *J. Membr. Sci.* **2010**, *349*, 237-243.
- (31) Section 2.5 – Experimental.
- (32) Ashby, E. C.; Coleman, D. J. *Org. Chem.* **1987**, *52*, 4554.
- (33) Fresnet, P.; Dubois, J. E. *Tetrahedron Lett.* **1979**, 2137.
- (34) Fujimoto, C. H.; Hickner, M. A.; Cornelius, C. J.; Loy, D. A. *Macromolecules* **2005**, *38*, 5010.
- (35) Kostalik, H. A. Dissertation, Cornell University, 2011.

- (36) Demonceau, A.; Stumpf, A. W.; Saive, E.; Noels, A. F. *Macromolecules* **1997**, *30*, 3127.
- (37) Alvarez, S. G.; Alvarez, M. T. *Synthesis* **1997**, 413.
- (38) Schwesinger, R.; Willaredt, J.; Schlemper, H.; Keller, M.; Schmitt, D.; Fritz, H. *Chem. Ber.* **1994**, *127*, 2435.
- (39) APEX2 v.1.0-22 User Manual, Bruker AXS Inc., Madison WI 53719, 2004
- (40) SAINT+ v.6.02 User Manual, Bruker AXS Inc., Madison WI 53719, 1999
- (41) G.M.Scheldrick, SADABS, Program for Empirical Absorption Correction of Area Detector Data, University of Göttingen, 1996
- (42) G.M.Scheldrick, SHELXTL v. 5.10 Bruker AXS Inc., Madison WI 53719, 1999

CHAPTER 3

A Universal Protocol for the Quantitative Assessment of Pendant Cation Stability in Polymer Electrolytes

CHAPTER 3

A Universal Protocol for the Quantitative Assessment of Pendant Cation Stability in Polymer Electrolytes

3.1 Abstract

Synthesizing polymer electrolytes that are resistant to degradation under alkaline conditions and at high temperatures is the prominent remaining challenge to developing viable anion exchange membranes for alkaline fuel cells. Polymer stability studies are ineffective at evaluating the intrinsic stability of a series of cations due to the extensive resources needed. Furthermore, degradation of the polymer backbone complicates the stability results, making it hard to discern how different classes of cations contribute to polymer decomposition. Using model compounds studies to assess the alkaline stability of small molecule organic cations is an efficient strategy to avoid the challenges with polymer studies and quickly rank cations based on their stabilities. Herein, we outline the important criteria for a quantitative and robust model compound protocol and rationalize our selection of each parameter. Finally, we assessed the alkaline stability of a several ammonium, imidazolium and phosphonium cations using our protocol, highlighting the insights into cation decomposition that we discovered with our method.

3.2 Introduction

Polymers with cationic moieties appended to the backbone have been employed in a diverse range of applications and can be broadly categorized into two groups: 1) membranes that sequester ions or small molecules (i.e. water purification¹ and gas separation²) and 2) membranes that facilitate ion conduction (i.e. electrolysis,³ redox-flow batteries,⁴ and fuel cells⁵). A net energy analysis was conducted by Pellow et. al., which highlighted the high efficiency energy storage with a regenerative hydrogen fuel cell (RHFC).⁶ Designing efficient and durable polymer membranes is critical to developing high-performance materials for these applications.⁷

Alkaline fuel cells (AFCs) are investigated as alternatives to commercially available proton exchange membrane fuel cells (PEMFCs)⁸ because they enable the use of non-noble metal catalysts,⁹ including metal-free catalysts or the oxygen reduction reaction (ORR).¹⁰

Running a fuel cell at high pH improves the electrochemical reaction kinetics for ORR and mitigates electrode degradation,¹¹ yet significant improvement is still needed for the alkaline anion exchange membranes (AAEM).¹² Ideal AAEMs are mechanically strong, chemically robust in the presence of hydroxide at elevated temperatures (1 M [OH⁻], ≥ 80 °C) and approach the desired lifetime of 5,000 hours.¹³

Many types of polymers have been used to prepare AAEMs, including perfluorinated membranes,¹⁴ aromatic polysulfones,¹⁵ poly(arylene ethers),¹⁶ poly(arylene ether ketones),¹⁷ polyphenylenes,¹⁸ polystyrenes,¹⁹ and various aliphatic backbones.²⁰ New classes of polymer composite materials are also being investigated that are comprised of silica,²¹ cellulose,²² chitosan²³ or graphene.²⁴ Polymers synthesized for AAEMs are often optimized to increase conductivity, while maintaining robust mechanical properties. This leads to an enormous diversity in molecular weight and percentage of cations incorporated into the polymers, in addition to the multitude of architectures explored.

Tetraalkylammonium groups, particularly benzyl trimethylammonium (BTMA), have been the most widely utilized organic cations due to their synthetic accessibility, however several studies indicate that their alkaline stability is too low for practical devices.²⁵⁻²⁸ This has encouraged researchers to investigate other cations such as cyclic,²⁹ spiro-³⁰ and bicyclic ammonium,³¹ pyridinium,³² guanadinium,³³ phosphonium,³⁴ imidazolium³⁵⁻³⁷ and benzimidazolium³⁸ groups for stability in AAEMs.

For complete durability, the polymer backbone and the pendant cationic group must be resistant to chemical degradation. Polymer stability is commonly reported as a function of conductivity or ion exchange capacity (IEC).³⁹ Unfortunately, these secondary measurements do not describe the chemical transformations that are occurring and important information regarding the nature of the polymer decomposition is obfuscated. In many cases, it is unclear whether the loss of material performance is due to reactions occurring on the polymer backbone, at the pendant cations or a combination of both.⁴⁰ Spectroscopic techniques such as FTIR and Raman have been used to monitor polymer stability by probing changes in chemical bonds, yet these

methods are not quantitative.⁴¹ Primary measurements, such as nuclear magnetic resonance spectroscopy (NMR), are necessary to accurately and quantitatively describe the chemical stability of polymer electrolytes.^{25,40a-b,42} Ramani et. al. successfully employed 2D NMR techniques to characterize the change in polymer composition when exposed to alkaline conditions⁴³ and the report emphasizes the contribution of polymer backbones to the overall degradation. Direct comparison of polymers containing various cationic moieties is complicated by degradation of the polymer backbone in AAEMs and the diversity of polymers hinders meaningful comparisons.

Due to the complications of studying cation stability when attached to polymers, we believe model compound studies are necessary to decouple the intrinsic stability of cations from polymer decomposition. Investigating small molecules allows us to quantitatively evaluate the alkaline stability of the core cationic moieties and predict which groups will resist decomposition in polymers. Once a suitable cation is selected it must be incorporated into a polymer that resembles the model compound and the polymer stability assessed. These simple, early phase analytical methods reduce the time and resources needed to reach the ultimate goal of polymer stability in a membrane electrode assembly (MEA) or an operating fuel cell.

Model compound studies, wherein small molecules are subjected to various alkaline degradation conditions, have been effective at assessing the chemical stability of organic cations before embarking on extensive polymer stability studies.^{27,28,44-46} A well-designed model compound will have nearly identical features to the cation in the anticipated polymer. For example, BTMA is an appropriate analog for trimethylammonium cations appended to the benzylic position of an aromatic polymer. Unfortunately, it is difficult to compare the stability results among many literature accounts because there are a number of inconsistencies in the procedures. Since reaction rates change with modifications in solvent, temperature, and reactant concentrations, without a unified set of conditions among protocols, it is impossible to directly compare the outcomes. To develop a universal protocol for assessing and comparing the alkaline stability of various cations we outlined the pivotal criteria for a robust method, incorporating

some of the best features from reported procedures. Our protocol is designed to quickly provide the maximum amount of information necessary to rank the stability of cations, while providing insights on how to improve the chemical stability.⁴⁷ To demonstrate the applicability of our method, we characterized the stability of a variety of cations interesting to the AAEM community. Ultimately, after identifying the optimal cations from these preliminary screens, they must be incorporated into polymers and re-evaluated.

3.3 Results and Discussion

3.3.1 Protocol Design

Proton nuclear magnetic resonance spectroscopy, ¹H NMR, is often employed to study the course of reactions because it is very sensitive to changes in composition and highly quantitative. The loss of signal for the initial reactants is readily detected and it permits the structural identification of emerging species. Proposed degradation products can be confirmed using a high-resolution mass spectrometry technique (HRMS). This diagnostic capability helps determine the degradation mechanisms and guides the design of cations with improved stability. To accurately describe cation stability in a timely manner we considered the following criteria:

- A. Solvent
- B. Hydrogen/Deuterium Exchange
- C. Internal Standard
- D. Base Concentration
- E. Cation Concentration (Ratio of Reactants)
- F. Temperature
- G. Reaction Vessel
- H. Comparison to Standard Cation
- I. Data Acquisition and Display

A. Solvent

Several solvent systems have been employed to investigate the stability of organic cations under alkaline conditions. Because AFCs operate under aqueous conditions, D₂O is an obvious

choice to follow the reactions by NMR spectroscopy. Indeed, this selection works well for simple ammonium cations, such as BTMA, and experiments have been conducted at concentrations of up to 1 M BTMA.⁴⁶ Unfortunately, other solvents such as dimethyl sulfoxide and methanol must be added to adequately dissolve other AAEM candidates, such as phosphonium,^{34d} imidazolium^{39c,44b} and benzimidazolium^{38e-f} cations. Complete dissolution of the organic salt is required to have accurate and reproducible comparisons among studies. As such, we selected methanol as our reaction medium. Similar to water, methanol is a polar, protic solvent and it completely dissolves all the organic compounds we tested. Additionally, methanol is a potential fuel in AFCs, which makes it more relevant than other organic solvents. Furthermore, basic methanol solutions are expected to accelerate the degradation rate of organic cations compared to the analogous aqueous solutions. A solution of alkali metal hydroxide dissolved in methanol will be comprised of methoxide and hydroxide anions in equilibrium with each other. Methoxide is a stronger base than hydroxide and has a smaller sphere of hydration due to reduced hydrogen-bonding capability, resulting in more aggressive reaction conditions. As new cations are identified with higher resistance to reaction with bases and nucleophiles, this alternative is becoming more essential to delineate stability trends in a meaningful timeframe.

B. Hydrogen/Deuterium Exchange

The complications of conducting NMR spectroscopy studies in basic solutions with fully deuterated protic solvents have been highlighted by several researchers.^{44d,46} In a non-destructive chemical process, protons on the model compound are removed by a basic species and replaced with deuteriums available in the solvent molecule. Eventually hydrogen/deuterium (H/D) exchange reduces the proton signal for the cation although no degradation has occurred. The rate of H/D exchange depends on the acidity of the initial proton in the parent compound and can vary within a single molecule, as well as between compounds, as shown in Figure 3.1a.

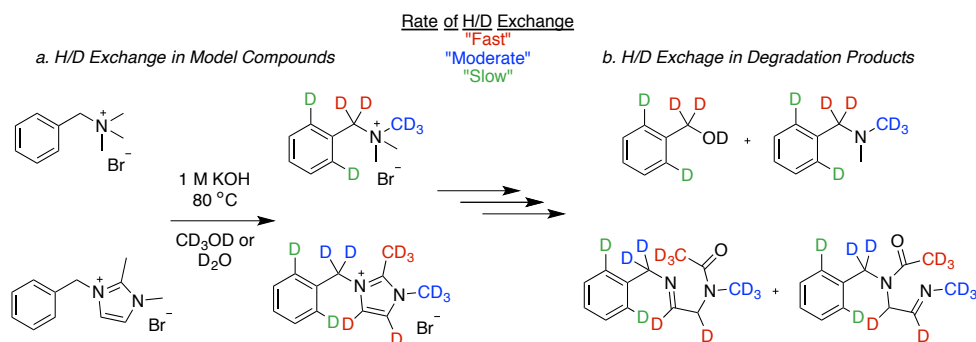


Figure 3.1 Hydrogen/deuterium exchange in model compounds and degradation products.

Certain sites, such as benzylic positions, exchange very rapidly, while others like neighboring alkyl groups exchange at a slower rate. Over time, even relatively unreactive protons, such as those on phenyl rings, can undergo H/D exchange. Therefore, it is difficult to obtain a reliable value for the amount of cation in solution when fully deuterated protic solvents are employed in alkaline stability studies. Furthermore, H/D exchange lowers the number of signals present in the degradation products that are forming, as shown in Figure 3.1b. This obscures the mechanistic insights and decreases the overall impact of the model compound study. Fortunately, our choice of methanol as a solvent allows us to use CD_3OH , which contains the appropriate deuterium locking signals for NMR spectroscopy ($\text{CD}_3\text{-OH}$), but does not contain deuterium in the exchangeable position ($\text{CD}_3\text{-OH}$). This eliminates the H/D exchange process altogether and provides the maximum information for reactants and products. With this solvent choice, the loss of proton signal can be solely attributed to chemical degradation of model compound and important information about the identity of the new species is revealed. We applied a standard solvent suppression bias during typical ^1H NMR spectroscopy acquisition, which reduced the (-OH) signal and simplified data processing.⁴⁷ Additional processing in MesReNova provides NMR spectra with very high signal/noise response and clear interpretation of the data. Relying on signals too close to the solvent can result in inconsistent integrations and we recommend analyzing signals at least 0.5 ppm removed from suppression frequency.

C. Internal Standard

The use of an internal standard in NMR spectroscopy studies ensures accurate quantification of analytes in solution. As such, researchers have referenced cation signals to dioxane or crown ether in model compound studies.^{28,37c,38c} A suitable internal standard should be soluble, stable under alkaline conditions and not interfere with the reaction progress, and the proton signals should not interfere with signals in the model compound. To circumvent some of these issues, Pivovar and coworkers used a special NMR tube insert containing their deuterated solvent for locking and referencing.⁴⁶ In our stability protocol, we include 3-(Trimethylsilyl)-1-propanesulfonic acid sodium salt, which is soluble and stable in methanol, non-volatile, and has several unique reference signals, which avoids interference with the signals of various model compounds. By integrating relative to the internal standard, we can detect changes in cation concentration that would not be apparent if the degradation products were insoluble or too volatile.

D. Base Concentration

In an operating fuel cell, the concentration of hydroxide in the electrolyte is dependent on the concentration of cations in the polymer and maintaining charge neutrality is favorable. To mimic these conditions, Mohanty and Bae²⁸ synthesized discrete hydroxide complexes of several interesting ammonium cations and investigated their stability in water. For this approach to work successfully, the reaction atmosphere must be rigorously purged of carbon dioxide to prevent the formation of carbonate anions, CO_3^{2-} , which readily form from the reaction of hydroxide with CO_2 . Carbonate is non-nucleophilic and a much weaker base than hydroxide, so the presence of carbonate will make the cations appear more resistant to degradation and not accurately describe the alkaline stability. Moreover, species in strongly basic solutions may react with certain glass containers, causing etching of the glass, which reduces the concentration of hydroxide in solution.^{44c,46} For these reasons, we suggest that an excess of base is necessary to obtain meaningful information about the reactivity of the model compounds. Our studies were conducted in 1 M potassium hydroxide (KOH), which is a common concentration used in

reported procedures. Higher concentrations, 2 – 5 M, may be applied to accelerate the reaction rates further. These preliminary tests are designed to rank the relative stability of cations. While, these conditions may not be entirely representative of AFC operating conditions, the protocol will help prioritize which cations are worth pursuing in subsequent polymer investigations.

E. Cation Concentration (Ratio of Reactants)

Similarly to base concentration, the molarity of the model compound controls the reaction rate, yet it is often not reported in protocols. The concentration of cation should be sufficient to achieve high signal/noise resolution in the NMR spectroscopy experiment, while maintaining an excess of base. A molar ratio of at least 1:10 between cation and base simplifies the kinetics by making the reaction a pseudo first order decay process for the model compound under these conditions. At a minimum, to effectively compare reaction rates for model compounds the cation concentration must be clearly reported. We conducted our 1 M KOH studies with a 1:20 ratio between species (0.05 M in model compound) and 2 M KOH studies, included in the supporting information, had a 1:67 ratio between species (model compound concentration reduced to 0.03 M for solubility reasons). Increasing the initial concentration of hydroxide accelerated the overall rate of the reaction, although 1 M KOH studies were sufficient to observe trends over 30 days.

F. Temperature

A typical AFC will operate in the range of 60 – 100 °C. Model compound stability protocols should be conducted in this range because temperature has a substantial impact on the reaction kinetics. Additionally, many cations that have reasonable room temperature stability have been shown to degrade under more relevant operating temperatures. Thus, stability studies conducted below 60 °C will not likely reveal exciting cation candidates for AAEMs. At higher temperatures, the reaction rates are accelerated and the amount of time needed to delineate cation stability is reduced. We conducted our stability studies at an intermediate temperature, 80 °C to accelerate reactions and reveal degradation processes in shorter time frames. The boiling point of neat methanol is 65 °C at standard pressure and upon heating our solvent reaches an equilibrium

between the gas and liquid phases, which is typical of any solvent that could be used. For efficient and consistent heat transfer, our samples were partially submerged in an oil bath. This heating method is widely available in standard laboratories, which makes our protocol easily transferrable. We recommend taking precautions when using flammable liquids above their boiling points and suggest not using an oven to heat samples.

G. Reaction Vessel

It is a common practice to conduct model compound studies in glass vials. Many researchers have converted to using containers with fluorinated coatings to avoid interactions between the bases in solution and functional groups on the surface of the glass.^{28,34d,46} Typically, the solutions are stored and heated in glass vials and portions of the samples are removed for analysis after designated periods of time. However, important signals in the sample can be diminished or lost during the sample transfer step, especially when degradation products are volatile. Stability studies conducted directly in NMR tubes are the simplest analytical procedure and prevent the loss of sample information. Due to the transparency of the tubes, visual observations such as changes in color or precipitation of degradation products are evident. The amount of materials required for each experiment and ultimately the cost is reduced using this method.

In our protocol, mixtures composed of CD₃OH, KOH, internal standard and the model compound are prepared and stored in flame-sealed NMR tubes. The tubes are sealed using a simple procedure that can be done in any laboratory and does not require special capital equipment. Solvent and volatile byproducts are contained within the sealed vessel for the duration of the experiment. Unlike Yan,^{44c} we did not observe etching of the glass NMR tubes, which may indicate that methanol mitigates potential reactions between basic species in solution and the glass. Another possibility is that the NMR tubes are composed of a higher quality borosilicate glass that is more resistant to corrosion; whereas, typical lab vials are often made from lower quality soda-lime glass, which contain trace impurities that could initiate unwanted reactions.⁴⁸ Nevertheless, we believe our procedure provides a quick and facile approach to

monitor the progress of model compound degradation and provide a full picture of the reactions occurring in our studies.

H. Comparison to Standard Cation

Researchers in the field have noticed that the reactions followed in these studies are sensitive to small changes in the concentrations of reactants and deviations of the amount of water present in the sample. One approach to resolving this is to conduct the studies under very strict anhydrous conditions. Alternatively, conducting the studies alongside a standard cation is proposed to compensate for small deviations. Generally, the absolute values derived from model compound studies are less important than the trends in stability. BTMA is the obvious choice because 1) it is the most widely investigated cationic moiety in AAEMs and 2) a significant amount of information has already been established regarding its alkaline stability.^{27,28} Evaluating the stability of BTMA and new cations under identical conditions allows for easier comparison to the rest of the literature.

I. Data Acquisition and Display

Finally, establishing a uniform method for collecting and reporting the stability data was required. In addition to reporting a single value for percent cation remaining after a certain amount of time, it is informative to describe the change in percent cation remaining over the course of the reaction. Samples should be analyzed at regular time intervals over the course of the degradation period. Initial rates can vary drastically for reactions that ultimately have the same final concentration of cation remaining and the overall kinetics must be shown to glean meaningful information about the relative stability. For example, we report the percent cation remaining every five days over a period of 30 days for all our model compounds.

After careful considerations of all the parameters in the protocol design, we arrived at a set of conditions that we believe will fully characterize the stability of a variety of organic cations, with an easily transferrable procedure that minimizes the amount of time and resources. A summary of our protocol is represented in Figure 3.2.

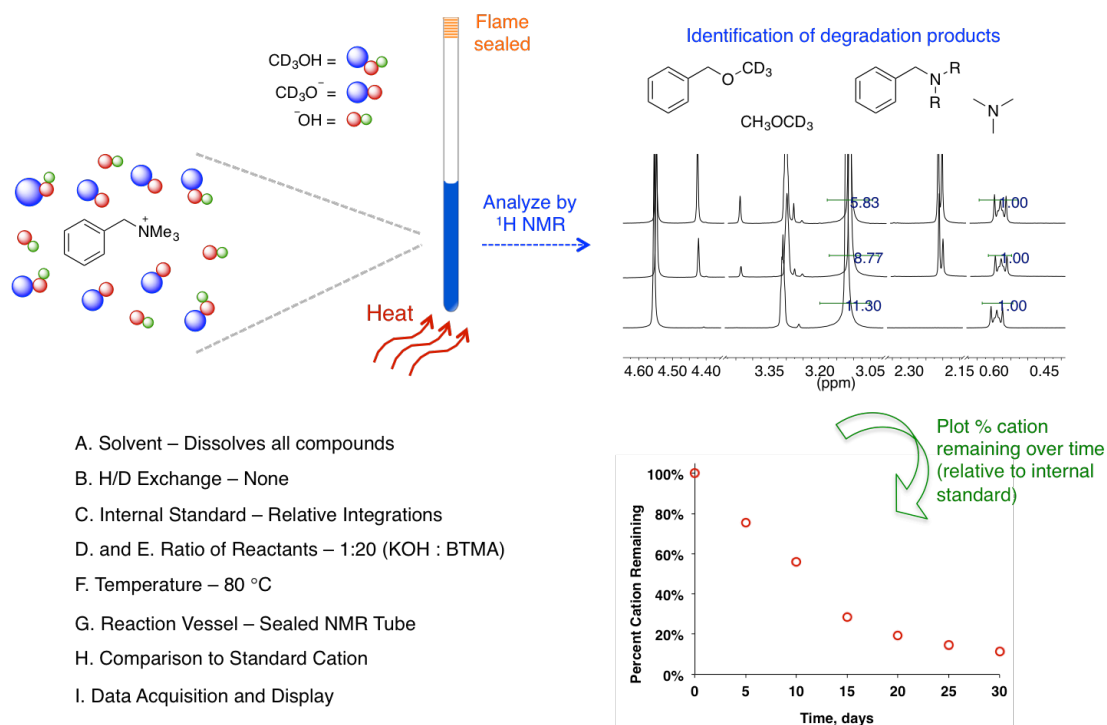


Figure 3.2 Summary of protocol for alkaline stability of model compounds.

3.3.2 Model Compound Studies

A variety of cations that have been investigated for use in AAEMs were evaluated using our protocol for alkaline stability. The model compounds synthesized are summarized in Figure 3.3. Samples for stability studies were prepared by dissolving the model compounds (0.05 M) in CD_3OH containing 1 M KOH and 3-(Trimethylsilyl)-1-propanesulfonic acid sodium salt (0.025 M), as an internal standard. The resulting solutions were transferred to NMR tubes, flame-sealed and partially submerged in an oil bath equilibrated to 80 °C. Over the course of 30 days, the samples were removed, cooled to room temperature and analyzed by ^1H NMR spectroscopy. The percent cation remaining in solution was determined by integrating a signal in the model compound relative to a signal in the internal standard, the results of which are briefly summarized in Table 3.1. The cations were grouped into classes based on similar degradation mechanisms, also indicated in Table 3.1, and discussed further in Figures 3.4 – 3.10. ^1H NMR

spectroscopy and HRMS were used to identify degradation products, supporting the proposed reaction mechanisms.

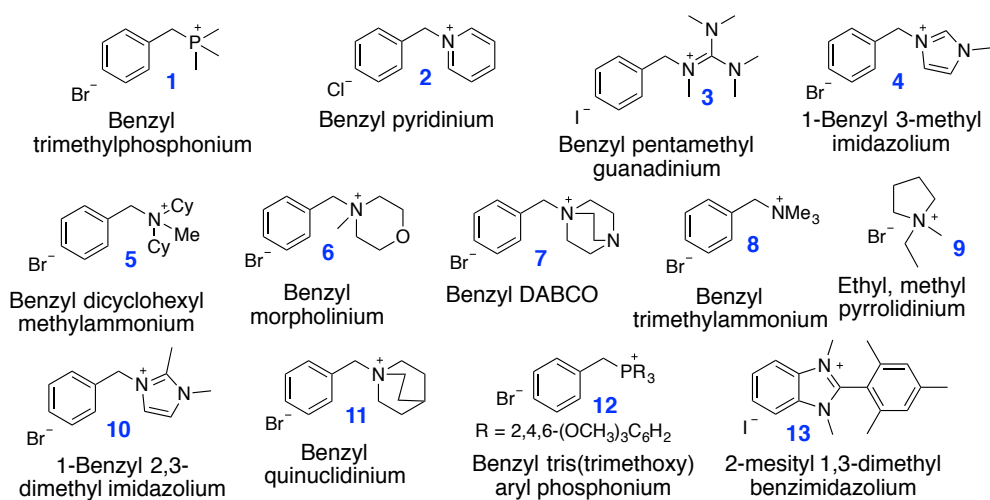


Figure 3.3 Model compounds investigated for stability under alkaline

Table 3.1 Summary of Stability Study Results.

Model Compounds 1-13		1 M KOH CD ₃ OH 80 °C <i>time varies</i>	Analyzed by: * ¹ H NMR Spectroscopy * HRMS (DART) Determined: * % Cation Remaining * Modes of Degradation
Model Cmpd.	Time (days)	Cation Remaining	Degradation Analysis – Cation Class
1	5	< 1%	Figure 3.7 – phosphoniums
2	5	< 1%	<i>Inconclusive</i> – pyridinium
3	5	< 1%	Figure 3.8 – guanadinium
4	5	< 1%	Figure 3.9 – imidazoliums
5	5	< 1%	Figure 3.4 – benzyl ammoniums
6	15	< 1%	Figure 3.4 – benzyl ammoniums
7	30	5%	Figure 3.6 – bicyclic ammoniums
8	30	11%	Figure 3.4 – benzyl ammoniums
9	30	33%	Figure 3.5 – pyrrolidinium
10	30	36%	Figure 3.9 – imidazoliums
11	30	65%	Figure 3.6 – bicyclic ammoniums
12	30	66%	Figure 3.7 – phosphoniums
13	30	87%	Figure 3.10 – benzimidazolium

As previously reported, BTMA (**8**) degraded over 30 days via S_N2 substitution at the benzylic (Figure 3.4a) or methyl positions (Figure 3.4b), producing ether and tertiary amine products.

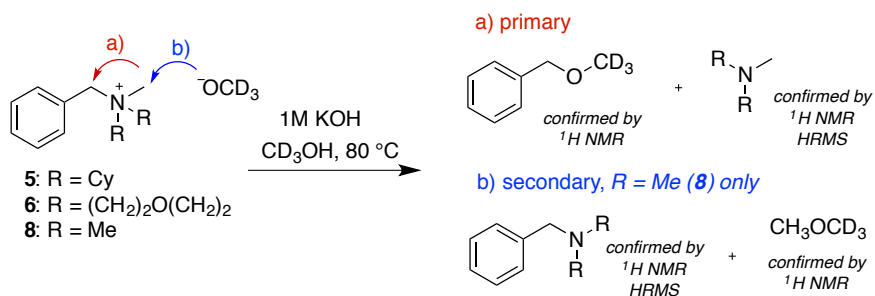


Figure 3.4 Degradation of benzyl ammoniums.

When two of the methyl groups in BTMA were replaced with cyclohexyl groups producing benzyl dicyclohexyl methylammonium (**5**), a rapid loss of cation was observed (<1 % remaining after five days). This trend contrasts with results obtained by Mohanty and Bae,²⁸ where the stability of the ammonium cation increased with cyclohexyl substituents.¹ Under our conditions the only products observed by ¹H NMR spectroscopy were benzyl methyl ether and dicyclohexyl methylamine (Figure 3.a), indicating that reaction at the benzylic position was preferred.

Cations containing hydrophilic functional groups are hypothesized to increase conductivity and alkaline stability by expanding the hydration sphere surrounding organic cations.⁴⁹ As such, benzyl morpholinium (**6**), which contains an ether functional group, is an interesting cation to compare to alkyl ammoniums. Over 15 days, **6** degraded completely, which was an improvement in stability over compound **5**, but not BTMA. Nucleophilic attack at the benzylic position (Figure 3.4a), producing N-methyl morpholine and benzyl methyl ether, was the only degradation pathway observed. For ammonium model compounds **5**, **6**, and **8**, the identity of amine products were confirmed by comparison to the ¹H NMR of the commercially available amine and by analyzing the reaction mixture with HRMS.

Similar to the ammonium cations, degradation at the benzylic position (Figure 3.4a) was predicted for benzyl pyridinium (**2**). However, the ¹H NMR spectrum for **2**, which degraded

¹ Discrete hydroxide complexes of **5** and **8** were synthesized and the stability was assessed in water at 100 °C.

completely within five days (< 1% remaining), did not contain identifiable signals. Mohanty and Bae suggested a degradation pathway leading to the formation of a pyridinone species,²⁸ but we were unable to confirm this by ¹H NMR or HRMS and investigation into the degradation products under our conditions was inconclusive.

Polydiallyldimethylammonium chloride (polyDADMAC) has been studied as an AAEM material, but membranes with suitable solubility and mechanical properties have not been identified. Nevertheless, it is possible to append pyrrolidinium, the cationic moiety present in polyDADMAC, to a monomer and copolymerize with an unfunctionalized monomer, resulting in a polymer with tunable properties. Yan et. al.^{29b} reported the alkaline stability of several such cyclic ammonium model compounds and we selected ethyl methyl pyrrolidinium (**9**) to compare to the other cations in our series. Notably, the degradation rate of **9** was slower than BTMA, leaving 33% cation remaining after 30 days. We identified the resonances for several compounds in the ¹H NMR spectrum, which suggested multiple degradation routes. Although N-methyl pyrrolidine was formed by nucleophilic attack at the N-ethyl position (Figure 3.5b), S_N2 reaction was not observed at the N-methyl position. We propose another degradation pathway via nucleophilic addition of methoxide to the α-carbon in the ring (Figure 3.5a). The proposed ring-opened product is supported by HRMS, where addition of **OCD₃** is observed. To further support this proposed structure we analyzed a solution of **9** that was tested in non-deuterated solvent (1 M KOH, CH₃OH). Indeed, the exact mass of ring-opened product containing the **-OCH₃** adduct was observed by HRMS (Figure 3.5c). A modest preference was observed for nucleophilic addition over substitution, with a ratio of 1.3:1.

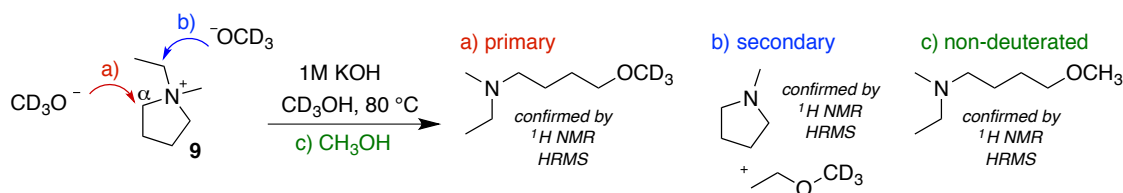


Figure 3.5 Degradation of N,N-ethyl, methyl pyrrolidinium.

Bicyclic ammonium compounds have been proposed to be more resistant to nucleophilic degradation reactions due to steric effects from the bridging carbons. In fact, the DABCO functional group has been incorporated into many AAEM polymer architectures, where it exhibited comparable hydroxide conductivity to other ammonium cations.^{31c-d} Under our alkaline conditions, benzyl DABCO (**7**) degraded over 30 days leaving 5% cation remaining. The complex ¹H NMR spectrum suggested two concomitant degradation pathways. As expected, nucleophilic attack at the benzylic position produced benzyl methyl ether and DABCO (Figure 3.6b). However, these were minor degradation products. The major degradation reaction occurred via nucleophilic attack of methoxide at the carbon α to the cationic nitrogen, resulting in a ring-opened degradation product (Figure 3.6a). The ring-opened product was favored approximately 2:1 over S_N2 attack at the benzylic position.

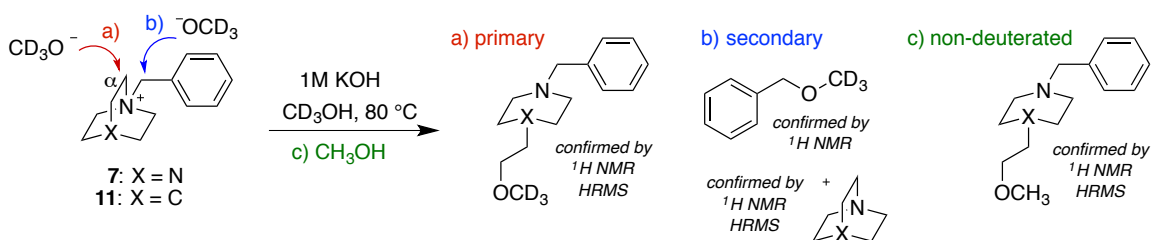


Figure 3.6 Degradation of bicyclic ammoniums.

The proposed ring-opened product is consistent with the signals observed in the ¹H NMR spectrum and is further confirmed by HRMS, in which isotopically labeled -OCD₃ (from CD₃OH) is apparent. The ring-opened product containing the -OCH₃ adduct (from CH₃OH) was observed by HRMS (Figure 3.6c) when **7** was treated with 1 M KOH in CH₃OH.

Benzyl quinuclidinium (**11**), another bicyclic ammonium cation that has been investigated for AAEMs,^{40b} differs from benzyl DABCO by having carbon at one of the bridgehead carbons, instead of nitrogen. This substitution resulted in a significant improvement in the alkaline stability of the cation, which degraded to only 65% cation remaining after 30

days. Importantly, **11** was more stable than all the other ammonium cations investigated. Similar to **7**, the degradation pathways produced benzyl methyl ether, quinuclidine (Figure 3.6b) and the ring-opened product (Figure 3.6a). A small preference was observed for the ring opening reaction (1.2:1) and both isotopes of the product (**OCD₃** and **OCH₃**) were observed by HRMS depending on the solvent choice.

Tetraalkylphosphonium cations are another class of functional groups that have attracted interest for use in AAEMs. Degradation of benzyl trimethylphosphonium (**1**) began immediately following preparation at room temperature, resulting in < 1% cation remaining after five days. Nucleophilic addition of hydroxide to phosphorous produced toluene and trimethyl phosphonium oxide as the only observed products (Figure 3.7a). It is known that installing sterically bulky substituents on the phosphonium cation can prevent this addition reaction. As such, a substantial improvement in stability was observed by switching from methyl groups to the aryl groups in benzyl tris(trimethoxy) arylphosphonium (**12**), which degraded to 66% cation remaining over 30 days. The triarylphosphine was observed in the reaction mixture by ¹H NMR and HRMS (Figure 3.7b), but NMR resonances related to other degradation products were also present. We propose reactions involving the methoxy substituents, but further work is needed to confirm the degradation routes.

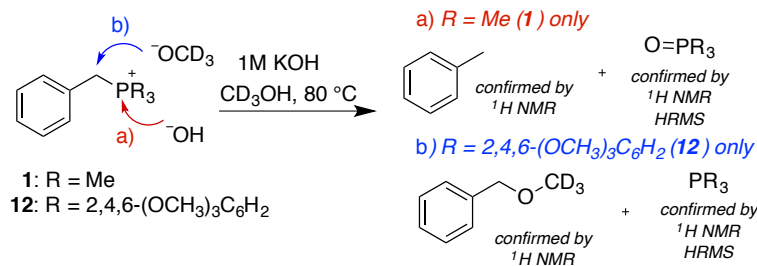


Figure 3.7 Degradation of benzyl trimethylphosphonium.

Organic cations with delocalized charge are hypothesized to have greater alkaline stability due to resonance stabilization. We investigated benzyl pentamethylguanadinium (**3**), a

moiety that has been incorporated into AAEMs, under our protocol conditions. The model compound degraded quickly (< 1% remaining in five days) by nucleophilic attack of hydroxide at the central α -carbon, producing an amide and dimethyl amine (Figure 3.8). The products were confirmed by ^1H NMR and HRMS. We suggest that using substituents larger than methyl groups around the guanadinium core will help improve the stability by preventing nucleophilic attack.

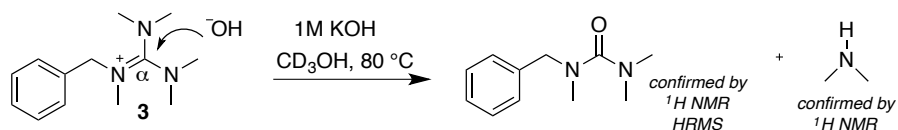


Figure 3.8 Degradation of benzyl pentamethyl guanadinium.

Imidazoliums, another class of resonance-stabilized cations, have received a great deal of attention recently. The ability to easily modify the substituents and incorporate bulky groups to block degradation pathways make them attractive targets as AAEM materials. We reported several possible degradation routes for imidazolium cations and hypothesized that the initial degradation products were often unstable under our aggressive reaction conditions.⁴⁵ The reaction solutions of 1-Benzyl 3-methyl imidazolium cations with hydrogen or methyl groups at the C2 position (**4** and **10**, respectively) were further assessed. 1-benzyl 2,3-dimethyl imidazolium (**10**) degraded to 36% cation remaining over 30 days. We conducted 2D NMR experiments (HSQC and HMBC) to identify the products, but the product structures remained elusive. Fortunately, we were able to identify formate (in **4**) and acetate (in **10**) in the reaction mixtures. Thus, we propose that the imidazolium cations degraded by nucleophilic attack at the C2 carbon, followed by ring-opening to amides (Figure 3.9a). The initial amide products were rapidly hydrolyzed, which released the observed formate and acetate (Figure 3.9b). Currently, we are unclear about the fate of the remainder of the molecule and additional 2D NMR experiments did not provide any further insights.

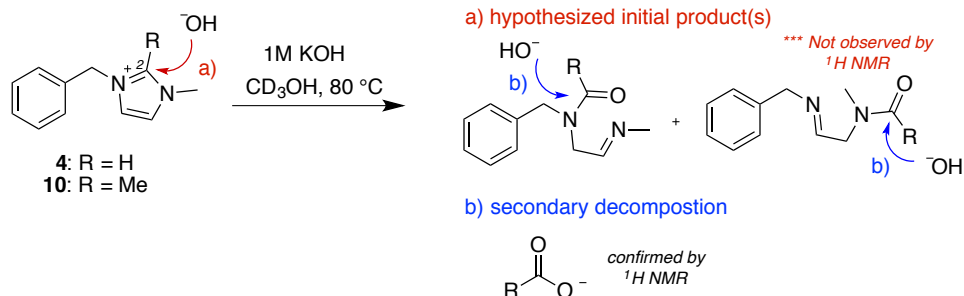


Figure 3.9 Degradation of benzyl imidazoliums.

The benzimidazolium cation identified by Holdcroft^{38e} demonstrates promise as a component in AAEMs. Indeed, the mesityl benzimidazolium cation (**13**) degraded slower than the other model compounds we tested under our conditions, with 87% cation remaining after 30 days. The major degradation product observed is the result of nucleophilic addition of hydroxide to the C2 position followed by ring-opening (Figure 3.10a). Identification of the product was facilitated by ¹H NMR, HRMS and 2D NMR experiments (HSQC and HMBC). Nucleophilic attack at the N-methyl position to produce the neutral benzimidazole is another suggested pathway, which was supported by ¹H NMR and HRMS.

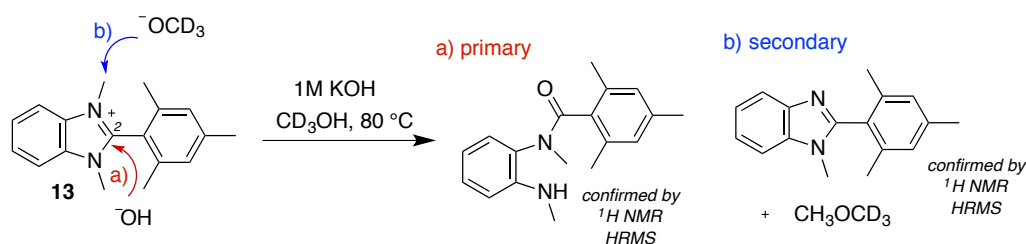


Figure 3.10 Degradation of 1,3-dimethyl 2-mesityl benzimidazolium.

Finally, we wanted to compare the alkaline stability of model compounds **1** – **13** to imidazolium and phosphonium cations that our group has developed (Figure 3.11b). The percent cation remaining is plotted as a function of time to reveal the relative rates of degradation (Figure 3.11a). Reaction conditions were not suitable to observe degradation of compounds **14** – **16** and

we are continuing to search for appropriate degradation conditions to experimentally confirm their degradation pathways.

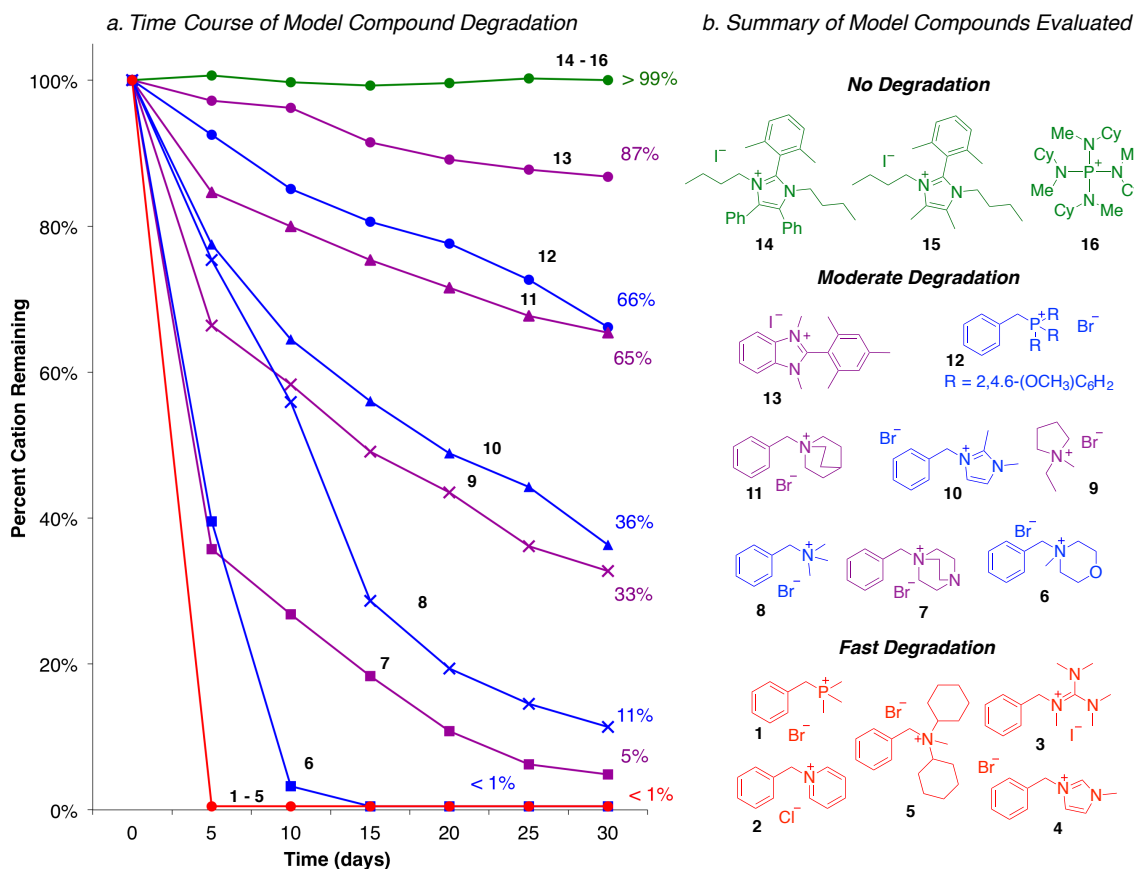


Figure 3.11 Stability Model Compounds (0.05 M) in 1 M KOH/CD₃OH at 80 °C.

3.4 Conclusions

An efficient and transferrable protocol was developed for characterizing the alkaline stability of a multitude of organic cations. The reactivity of small molecules with anions in solution is followed by ¹H NMR spectroscopy. Methanol was selected as a solvent because it readily dissolves organic cations and it is a relevant solvent for fuel cells. Fortunately, basic methanol solutions provide more aggressive reaction conditions, which is more important as organic cations are developed with increasing resistance to bases and nucleophiles. *d*3-methanol was used instead of *d*4-methanol to prevent the hydrogen/deuterium exchange process from

limiting the amount of information gathered from the stability study. Sufficiently high concentrations of KOH were used in the studies to avoid carbonation issues and ensure that the stability of the cation in the presence of hydroxide/methoxide was the measured parameter. The concentration of the cation was also reported (i.e. ratio of cation to base), which is important for directly comparing the degradation rates of different cations. Flame-sealed NMR tubes were heated to 80 °C to mimic fuel cell operating conditions, while preventing the loss of solvent and volatile degradation products. The loss of cation was monitored relative to an internal standard and reported every five days over a 30 day time period.

We used our protocol to assess the stability of a variety of model compounds, including ammonium, phosphonium, imidazolium and benzimidazolium cations. The rates of degradation were reported and modes of degradation were proposed based on the data obtained from NMR analysis (^1H , HSQC, HMBC) and supported by HRMS (DART). Future work will focus on appending base-stable cations to highly stable polymer architectures and characterizing the membranes for hydroxide conductivity and alkaline stability.

3.5 Experimental

3.5.1 General Considerations

Methods and Instruments

^1H and ^{13}C NMR spectra were recorded on a Varian INOVA 500 or 600 MHz instrument at 22 °C with shifts reported relative to the residual solvent peak (CD_3OD or CD_3OH); 3.31 ppm (^1H) and 49.00 ppm (^{13}C). High resolution mass spectrometry (DART-HRMS) analyses were performed on a Thermo Scientific Exactive Orbitrap MS system equipped with an Ion Sense DART ion source.

Solvent Suppression Procedure⁵⁰

Quantitative ^1H NMR spectra for model compound stability studies were acquired in CD_3OH to 1) prevent unwanted hydrogen/deuterium exchange in model compounds and degradation products and 2) improve the solubility of model compounds and degradation products. The $-\text{OH}$ signal in CD_3OH was suppressed by prestauration with a 2 second presaturation delay and continuous wave irradiation with decoupler field strength (gB1) of 113 Hz (equivalent to a presaturation power of 9). Spectra were acquired over a spectral width of -1 to 14 ppm with 60 second relaxation delay and nominal 90° excitation pulse. 16 scans were averaged for each analysis. NMR spectra were processed using MestReNova Version 9.0.1-13254 (Mestrelab Research S.L). Residual $-\text{OH}$ signal was further suppressed with the signal suppression feature in the software. Spectra were zero-filled to 256k complex points and an exponential window function of 0.2 Hz was applied prior to manual phase correction. Whittaker smoother baseline correction was applied and linear correction was used for all integrals. Note: Residual signals between 5.5 – 6.5 ppm often derive from solvent suppression and shift depending on sample pH.

Chemicals

Benzyl bromide, benzyl chloride, 2-bromoethane, 1-methylpyrrolidine, pyridine, trimethylphosphine, tris(2,4,6-trimethoxyphenyl)phosphine, quinuclidine, 1-methylmorpholine, *N*-methyl-dicyclohexylamine, 1,1,3,3-tetramethylguanidine, 2,4,6-trimethylbenzoic acid, polyphosphoric acid, cyclohexylamine, phosphorus pentachloride, dimethyl sulfide, sodium hydride, dimethylformamide, 1-methyl imidazole and 1,2-dimethyl imidazole were purchased from Aldrich and used as received. 1,2-phenylenediamine was purchased from Aldrich and recrystallized in toluene prior to use. Chloride ion exchange resin (Amberlite-IRA 400 (Cl) form) was purchased from Aldrich and washed with methanol prior to use. Methyl iodide was purchased from Alfa Aesar and used as received. Chlorobenzene, dichloromethane, ethyl acetate and chloroform were purchased from Fischer and used as received. 3-(Trimethylsilyl)-1-propanesulfonic acid sodium salt was purchased from TCI Chemicals and used as received. 1,4-Diazabicyclo[2.2.2]octane and methanol-*d*3 were purchased from Acros and used as received. Methanol-*d*4 was purchased from Cambridge Isotope Laboratories and used as received. Sodium hydroxide, sodium bicarbonate, sodium sulfate, methanol, acetone, and acetonitrile were purchased from Macron and used as received. Tetrahydrofuran and diethyl ether were purchased from J.T. Baker and used as received. Potassium hydroxide was purchased from Mallinckrodt and used as received.

The following compounds were prepared previously according to literature procedures: 2-Benzyl-1,1,3,3-tetramethylguanidine (**3a**);^{33b} 2-Mesitylbenzimidazole (**14a**);^{38e} 1-*n*-Butyl-2-(2,6-dimethylphenyl)-4,5-diphenyl-1*H*-imidazole (**15a**);⁵¹ 1-*n*-Butyl-2-(2,6-dimethylphenyl)-4,5-dimethyl-1*H*-imidazole (**16a**);⁵¹ Tetrakis(cyclohexylamino)phosphonium tetrafluoroborate (**17a**);⁵² Benzyltrimethylphosphonium bromide (**1**);⁵³ 1-Benzylpyridin-1-ium chloride (**2**);⁵⁴ *N*-[Bis(dimethylamino)methylene]-*N*-methyl-1-phenylmethanaminium iodide (**3**);^{33b} 1-Benzyl-3-methylimidazolium bromide (**4**); *N*-Benzyl-*N*-cyclohexyl-*N*-methylcyclohexanaminium bromide (**5**);²⁸ 1-Benzyl-1,4-diazabicyclo[2.2.2]octan-1-ium bromide (**7**);²⁸ Benzyltrimethylammonium

bromide (**8**);^{34d} 1-Ethyl-1-methylpyrrolidin-1-ium bromide (**9**);^{29b} 1-Benzyl-2,3-dimethylimidazolium bromide (**10**);^{35d} 1-Benzylquinuclidin-1-ium bromide (**11**);⁵⁵ Benzyl-tris(2,4,6-trimethoxyphenyl)phosphonium bromide (**12**);⁵⁶ 1,3-Dimethyl-2-mesityl-1*H*-benzimidazolium iodide (**13**);^{38e} 1,3-Di-*n*-butyl-2-(2,6-dimethylphenyl)-4,5-diphenylimidazolium iodide (**14**);⁵¹ 1,3-Di-*n*-butyl-2-(2,6-dimethylphenyl)-4,5-dimethylimidazolium iodide (**15**);⁵¹ Tetrakis[cyclohexyl(methyl)amino]phosphonium chloride (**16**).⁵²

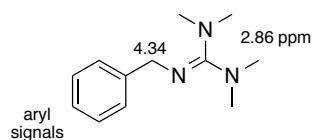
3.5.2 Synthetic Procedures

General Procedure A – Quaternization of Model Compounds

The appropriate model compound precursor was dissolved in a specified solvent and halide reagent was added while stirring. The mixture was stirred at a specified temperature for a specified length of time. The residue was purified via wash ether or ethyl acetate, precipitation into ether or ethyl acetate (unless otherwise specified). Precipitation was repeated to obtain pristine products. Note: To obtain salts without residual solvent, the powders were mixed with a small portion of dichloromethane and solvent was removed under reduced pressure.

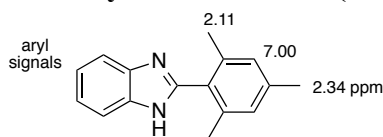
Synthesis of model compound precursors

2-Benzyl-1,1,3,3-tetramethylguanidine (**3a**)



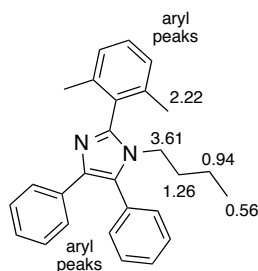
1,1,3,3-tetramethylguanidine (33 ml, 260 mmol) was treated with benzyl chloride (3.0 ml, 26 mmol) under neat conditions and stirred for 17 hours at room temperature. The residue was dissolved in diethyl ether, washed with water (3 x 5 ml) and the organic layer was dried with sodium sulfate. The solvent was removed *in vacuo* to give **3a** (0.961 g, 18 %) as a pale brown oil. ¹H NMR (500 MHz, CD₃OD): δ 7.43 – 7.14 (m, 5H), 4.34 (s, 2H), 2.86 (s, 12H). ¹³C NMR (126 MHz, CD₃OD): δ 163.90, 143.32, 129.31, 128.47, 127.55, 53.33, 40.04, 39.26. HRMS (DART) *m/z* calculated for C₁₂H₂₀N₃⁺ (M + H⁺) 206.16517, found 206.16509.

2-Mesitylbenzimidazole (13a)



1,2-phenylenediamine (3.00 g, 18.3 mmol) was dissolved in polyphosphoric acid (55 g) at 120 °C, treated with 2,4,6-trimethylbenzoic acid (2.17 g, 20.1 mmol) and stirred for 12 hours at 150 °C. The crude mixture was carefully poured into 1M sodium bicarbonate (1L). The solid was collected by filtration to give **13a** (2.82 g, 65 %) as a pale tan powder. **¹H NMR** (500 MHz, CD₃OD): δ 7.59 (m, 2H), 7.27 (m, 2H), 7.00 (s, 2H), 2.34 (s, 3H), 2.11 (s, 6H). **¹³C NMR** (126 MHz, CD₃OD): δ 153.44, 140.68, 138.89, 129.34, 129.18, 123.51, 21.33, 20.00. **HRMS** (DART) *m/z* calculated for C₁₆H₁₇N₂⁺ (M + H⁺) 237.13862, found 237.13856.

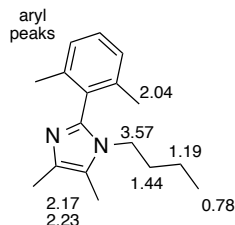
1-*n*-Butyl-2-(2,6-dimethylphenyl)-4,5-diphenyl-1*H*-imidazole (14a)



2,6-dimethylbenzaldehyde (2.00 g, 14.9 mmol), diphenylethanedione (3.13 g, 14.9 mmol), *n*-butylamine (1.5 ml, 15 mmol) and ammonium acetate (1.15 g, 14.9 mmol) were combined with L-proline (0.257 g, 2.26 mmol) in methanol (60 ml). The mixture was stirred at 60 °C for 24 hours. Upon cooling, the residue was purified via flash column chromatography (10% ethyl acetate/hexanes). The product was recrystallized in acetonitrile to give **14a** (0.975 g, 17 %) as a white powder. **¹H NMR** (600 MHz, CD₃OD): δ 7.55 – 7.46 (m, 3H), 7.44 – 7.41 (dm, *J* = 7.4 Hz, 2H), 7.40 – 7.38 (dm, *J* = 7.9 Hz, 2H), 7.34 (t, *J* = 7.7 Hz, 1H), 7.22 (d, *J* = 7.7 Hz, 2H), 7.19 – 7.15 (tm, *J* = 7.6 Hz, 2H), 7.15 – 7.11 (tm, *J* = 7.3 Hz, 1H), 3.63 – 3.59 (m, 2H), 2.22 (s, 6H), 1.26 (p, *J* = 7.4 Hz, 2H), 0.94 (sextet, *J* = 7.4 Hz, 2H), 0.56 (t, *J* = 7.4 Hz, 3H). **¹³C NMR** (126 MHz, CD₃OD): δ 147.49, 139.87, 138.34, 135.44, 132.30, 132.21, 131.38, 130.90, 130.26,

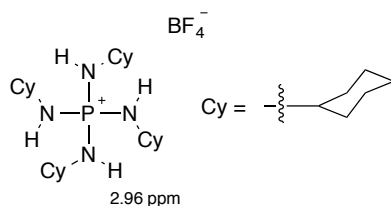
130.06, 129.94, 129.10, 128.73, 128.08, 127.52, 45.10, 33.14, 20.48, 20.31, 13.52. **HRMS** (DART) m/z calculated for $C_{27}H_{29}N_2^+$ ($M + H^+$) 381.23253, found 381.23138.

1-*n*-Butyl-2-(2,6-dimethylphenyl)-4,5-dimethyl-1*H*-imidazole (15a)



2,6-dimethylbenzaldehyde (2.00 g, 14.9 mmol), 2,3-butanedione (1.3 ml, 15 mmol), *n*-butylamine (1.5 ml, 15 mmol) and ammonium acetate (1.15 g, 14.9 mmol) were combined with L-proline (0.251 g, 2.24 mmol) in methanol (60 ml). The mixture was stirred at 60 °C for 24 hours. The crude mixture was initially purified via flash column chromatography (5% methanol/dichloromethane to 50% methanol/dichloromethane) to afford a brown oil. The residue was further purified via flash column chromatography (5% ethyl acetate/hexanes to 100% ethyl acetate) to give **15a** (0.554 g, 15 %) as a pale brown oil. ¹H NMR (600 MHz, CD₃OD): δ 7.27 (t, $J = 7.6$ Hz, 1H), 7.14 (d, $J = 7.6$ Hz, 2H), 3.63 – 3.48 (m, 2H), 2.23 (s, 3H), 2.17 (s, 3H), 2.04 (s, 6H), 1.49 – 1.40 (p, $J = 7.4$ Hz, 2H), 1.19 (sext, $J = 7.4$ Hz, 2H), 0.78 (t, $J = 7.4$ Hz, 3H). ¹³C NMR (126 MHz, CD₃OD): δ 145.11, 139.87, 132.93, 131.97, 130.51, 128.50, 123.49, 44.78, 33.50, 20.78, 20.05, 13.79, 12.29, 8.95. **HRMS** (DART) m/z calculated for $C_{17}H_{25}N_2^+$ ($M + H^+$) 257.201.23, found 257.20141.

Tetrakis(cyclohexylamino)phosphonium tetrafluoroborate (16a)

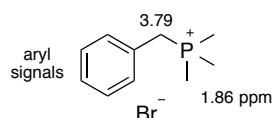


Freshly distilled cyclohexylamine was (2.9 ml, 25 mmol) was dissolved in dichloromethane (6 ml) in a flame-dried schlenk flask under an atmosphere of nitrogen. The solution was cooled to 0 °C. Phosphorus pentachloride (0.520 g, 2.52 mmol) was added to the stirring solution over a

period of 5 minutes. The mixture was equilibrated to room temperature slowly overnight. The residue was washed with 1M sodium tetrafluoroborate (3 x 50 ml) and the organic layer was dried with sodium sulfate. The solvent was removed *in vacuo* yielding **16a** (0.903 g, 63%) as a white powder. ^{31}P NMR (162 MHz, C_6D_6) 20.83 (1P, s). ^{19}F NMR (376 MHz, CD_3OD): δ -154.66 (4F, s). ^1H NMR (500 MHz, CD_3OD): δ 2.96 (s, 4H), 2.14 – 1.48 (m, 22H), 1.45 – 0.96 (m, 22H). ^{13}C NMR (126 MHz, CD_3OD): δ 52.03, 36.77, 36.73, 26.62, 26.37. HRMS (DART) m/z calculated for $\text{C}_{24}\text{H}_{48}\text{N}_4\text{P}^+$ (M^+) 423.36111, found 423.36103.

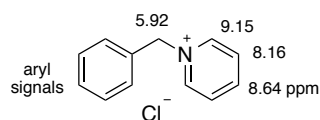
Synthesis of model compounds

Benzyltrimethylphosphonium bromide (**1**)



Following General Procedure A, trimethylphosphine (12.6 ml, 12.6 mmol), 1M in THF, was treated with benzyl bromide (0.50 ml, 4.2 mmol) in diethyl ether (200 ml) and stirred for 17 hours at room temperature under an atmosphere of nitrogen. The white precipitate was filtered, and washed with diethyl ether to give **1** (0.695 g, 67 %) as a white powder. ^{31}P NMR (162 MHz, CD_3OD) 26.88 (1P, s). ^1H NMR (600 MHz, CD_3OD): δ 7.50 – 7.30 (m, 5H), 3.79 (d, J_{HP} = 16.2 Hz, 2H), 1.86 (d, J_{HP} = 14.4 Hz, 9H). ^{13}C NMR (126 MHz, CD_3OD): δ 130.93, 130.24, 129.77 (d, J_{CP} = 9.0 Hz), 129.26, 30.98 (d, J_{CP} = 49.5 Hz), 7.70 (d, J_{CP} = 55.1 Hz). HRMS (DART) m/z calculated for $\text{C}_{10}\text{H}_{16}\text{P}^+$ (M^+) 167.09841, found 167.09894.

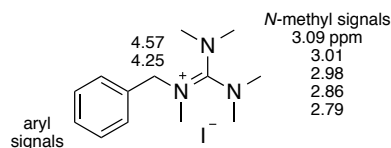
1-Benzylpyridin-1-ium chloride (**2**)



Following General Procedure A, pyridine (0.51 ml, 1.0 mmol) was treated with benzyl chloride (0.74 ml, 1.0 mmol) in acetonitrile (5 ml) and stirred for 12 hours at 80 °C. The residue was dissolved in chloroform, purified via precipitation into ether to give **2** (1.30 g, 98 %) as an off-

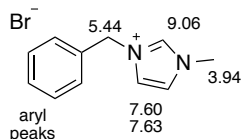
white powder. **¹H NMR** (600 MHz, CD₃OD): δ 9.15 (m, 2H), 8.64 (m, 1H), 8.16 (m, 2H), 7.59 – 7.54 (m, 2H), 7.53 – 7.42 (m, 3H), 5.92 (s, 2H). **¹³C NMR** (151 MHz, CD₃OD): δ 147.02, 145.72, 134.45, 130.71, 130.41, 129.92, 129.46, 65.40. **HRMS** (DART) *m/z* calculated for C₁₂H₁₂N⁺ (M⁺) 170.09643, found 170.09694.

***N*-[Bis(dimethylamino)methylene]-*N*-methyl-1-phenylmethanaminium iodide (3)**



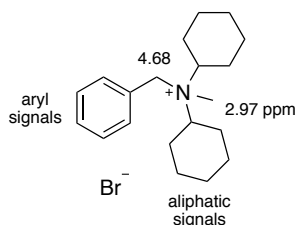
Following General Procedure A, **3a** (0.961 g, 4.68 mmol) was treated with iodomethane (0.87 ml, 14 mmol) in dichloromethane (5 ml) and stirred for 5 hours at room temperature. The residue was washed with water (3 x 5 ml) and the organic layer was dried with sodium sulfate. The dichloromethane solution was added drop-wise to diethyl ether and the precipitate was collected to give **3** (1.08 g, 66 %) as a white powder. **¹H NMR** (500 MHz, CD₃OD): δ 7.49 – 7.32 (m, 5H), 4.57 (m, 1H), 4.25 (m, 1H), 3.09 (s, 3H), 2.99 (m, 6H), 2.86 (s, 3H), 2.79 (s, 3H). **¹³C NMR** (126 MHz, CD₃OD): δ 164.31, 136.03, 129.93, 129.76, 129.46, 57.16, 40.54, 40.37, 39.94, 38.15. **HRMS** (DART) *m/z* calculated for C₁₃H₂₂N₃⁺ (M⁺) 220.18082, found 220.18040.

1-Benzyl-3-methylimidazolium bromide (4)



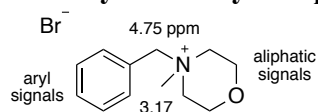
Following general procedure A, 1-methylimidazole (1.0 ml, 12 mmol) was treated with benzyl bromide (1.5 ml, 12 mmol) in acetonitrile (10 ml). The residue was dissolved in chloroform and purified via precipitation into ether to give **4** (3.03 g, 98 %) as a brown oil. **¹H NMR** (600 MHz, CD₃OD): δ 9.06 (s, 1H), 7.64 – 7.62 (m, 1H), 7.61 – 7.58 (m, 1H), 7.47 – 7.40 (m, 4H), 5.44 (s, 2H), 3.94 (s, 3H). **¹³C NMR** (151 MHz, CD₃OD): δ 137.97, 135.25, 130.39, 130.33, 129.71, 125.26, 123.66, 54.11, 36.69. **HRMS** (DART) *m/z* calculated for C₁₁H₁₃N₂⁺ (M⁺) 173.10732, found 173.10709.

***N*-Benzyl-*N*-cyclohexyl-*N*-methylocyclohexanaminium bromide (5)**



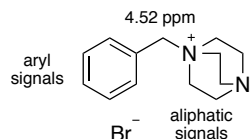
Following General Procedure A, *N*-methyl-dicyclohexylamine (1.0 ml, 4.7 mmol) was treated with benzyl bromide (0.60 ml, 5.1 mmol) in acetonitrile (5 ml) and stirred for 17 hours at 80 °C. The white precipitate was filtered and washed with diethyl ether to give **5** (1.52 g, 89 %) as a white powder. **¹H NMR** (600 MHz, CD₃OD): δ 7.60 (m, 2H), 7.57 – 7.49 (m, 3H), 4.68 (s, 2H), 3.65 – 3.51 (m, 2H), 2.97 (s, 3H), 2.37 (m, 2H), 2.21 (m, 2H), 2.04 – 1.97 (m, 2H), 1.92 (m, 2H), 1.76 (m, 2H), 1.71 – 1.64 (m, 4H), 1.50 – 1.32 (m, 4H), 1.26 (m, 2H). **¹³C NMR** (151 MHz, CD₃OD): δ 133.62, 131.29, 130.38, 130.10, 73.00, 72.93, 62.78, 49.03, 43.56, 28.91, 28.66, 26.82, 26.74, 25.82. **HRMS** (DART) *m/z* calculated for C₂₀H₃₂N⁺ (M⁺) 286.25293, found 286.25364.

4-Benzyl-4-methylmorpholin-4-ium bromide (6)



Following General Procedure A, 1-methylmorpholine (1.0 ml, 9.6 mmol) was treated with benzyl bromide (1.26 ml, 10.6 mmol) in acetonitrile (10 ml) and stirred for 12 hours at 80 °C. The residue was dissolved in chloroform and purified via precipitation into ethyl acetate to give **6** (2.08 g, 79 %) as an off-white powder. **¹H NMR** (500 MHz, CD₃OD): δ 7.69 – 7.48 (m, 5H), 4.75 (s, 2H), 4.05 (m, 4H), 3.66 (m, 2H), 3.41 (m, 2H), 3.17 (s, 3H). **¹³C NMR** (126 MHz, CD₃OD): δ 134.21, 131.75, 130.10, 127.69, 70.13, 61.38, 60.30, 46.17. **HRMS** (DART) *m/z* calculated for C₁₂H₁₈NO⁺ (M⁺) 192.13829, found 192.138437.

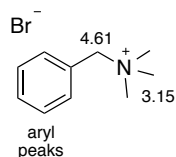
1-Benzyl-1,4-diazabicyclo[2.2.2]octan-1-ium bromide (7)



Following General Procedure A, 1,4-diazabicyclo[2.2.2]octane (0.943 g, 8.41 mmol) was treated with benzyl bromide (1.0 ml, 8.4 mmol) in ethyl acetate (6 ml) and stirred for 48 hours at room temperature. The residue was dissolved in chloroform and filtered through a pad of celite into ethyl acetate. The solid was further purified via recrystallization in acetone to give **7** (0.636 g, 27 %) as a white powder. **¹H NMR** (500 MHz, CD₃OD): δ 7.54 (m, 5H), 4.52 (s, 2H), 3.48 – 3.35 (m, 6H), 3.24 – 3.11 (m, 6H). **¹³C NMR** (126 MHz, CD₃OD): δ 134.12, 131.57, 130.15, 127.62, 68.94, 53.23, 45.91. **HRMS** (DART) *m/z* calculated for C₁₃H₁₉N₂⁺ (M⁺) 203.15428, found 203.15481.

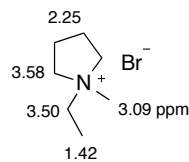
Benzyltrimethylammonium bromide (**8**)

Following General Procedure A, trimethylamine, 30% in ethanol, (0.76 ml, 3.1 mmol) was treated with benzyl bromide (0.40 ml, 3.4 mmol) in acetonitrile (5 ml). The residue was dissolved in chloroform and purified via precipitation into ether to give **8** (0.693 g, 90 %) as a



white powder. **¹H NMR** (600 MHz, CD₃OD): δ 7.63 – 7.60 (m, 2H), 7.59 – 7.52 (m, 3H), 4.61 (s, 2H), 3.15 (s, 9H). **¹³C NMR** (126 MHz, CD₃OD): δ 134.10, 131.87, 130.26, 129.19, 70.15, 53.19, 53.16, 53.13. **HRMS** (DART) *m/z* calculated for C₁₀H₁₆N⁺ (M⁺) 150.12773, found 150.12750.

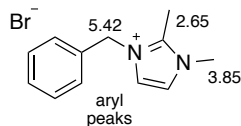
1-Ethyl-1-methylpyrrolidin-1-ium bromide (**9**)



Following General Procedure A, 1-methylpyrrolidine (1.0 ml, 10 mmol) was treated with 2-bromoethane (0.75 ml, 10 mmol) under neat conditions and stirred for 48 hours at room temperature. The residue was dissolved in chloroform, purified via precipitation into ether to give **9** (1.49 g, 76 %) as a pale yellow powder. **¹H NMR** (600 MHz, CD₃OD): δ 3.59 (m, 4H),

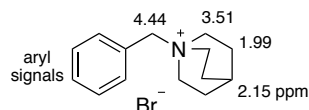
3.53 (m, 2H), 3.09 (s, 3H), 2.25 (m, 4H), 1.42 (m, 3H). ^{13}C NMR (126 MHz, CD_3OD): δ 64.77, 60.44, 48.40, 22.48, 9.58. HRMS (DART) m/z calculated for $\text{C}_7\text{H}_{16}\text{N}^+$ (M^+) 114.12773, found 114.12817.

1-Benzyl-2,3-dimethylimidazolium bromide (10)



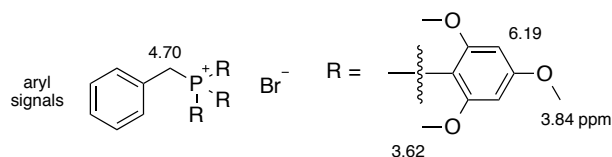
Following general procedure A, 1,2-dimethyl imidazole (2.00 g, 20.8 mmol) was treated with benzyl bromide (3.0 ml, 25 mmol) in acetonitrile (100 ml). The product was recrystallized from chloroform to give **10** (3.05 g, 55 %) as a white powder. ^1H NMR (600 MHz, CD_3OD): δ 7.53 (m, 2H), 7.45 – 7.41 (m, 2H), 7.41 – 7.37 (m, 1H), 7.36 – 7.33 (m, 2H), 5.42 (s, 2H), 3.85 (s, 3H), 2.65 (s, 3H). ^{13}C NMR (126 MHz, CD_3OD): δ 146.06, 135.18, 130.25, 129.84, 129.11, 123.77, 122.43, 52.66, 35.96, 10.58. HRMS (DART) m/z calculated for $\text{C}_{12}\text{H}_{15}\text{N}_2^+$ (M^+) 187.12298, found 187.12293.

1-Benzylquinuclidin-1-ium bromide (11)



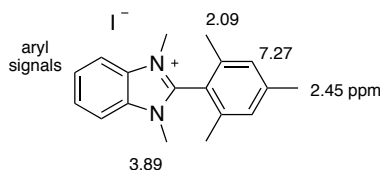
Following General Procedure A, quinuclidine (0.200 g, 1.80 mmol) was treated with benzyl bromide (0.26 ml, 2.2 mmol) in ethyl acetate:tetrahydrofuran (2:1 ml) and stirred for 12 hours at room temperature. The white precipitate was filtered and washed with ethyl acetate to give **11** (0.498 g, 98 %) as a white powder. ^1H NMR (600 MHz, CD_3OD): δ 7.60 – 7.45 (m, 5H), 4.44 (s, 2H), 3.57 – 3.45 (m, 6H), 2.15 (m, 1H), 1.99 (m, 6H). ^{13}C NMR (126 MHz, CD_3OD): δ 133.96, 131.39, 130.03, 128.33, 68.60, 55.47, 24.66, 21.13. HRMS (DART) m/z calculated for $\text{C}_{14}\text{H}_{20}\text{N}^+$ (M^+) 202.15903, found 202.15969.

Benzyl-tris(2,4,6-trimethoxyphenyl)phosphonium bromide (12)



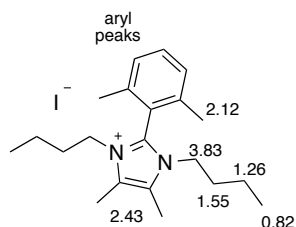
Following General Procedure A, tris(2,4,6-trimethoxyphenyl)phosphine (0.500 g, 0.939 mmol) was treated with benzyl bromide (0.11 ml, 0.94 mmol) in acetonitrile (2.5 ml) and stirred for 17 hours at 80 °C. The residue was dissolved in chloroform and purified via precipitation into ether to give **12** (0.416 g, 63 %) as a white powder. ^{31}P NMR (162 MHz, CD_3OD) 5.73 (1P, s). ^1H NMR (500 MHz, CD_3OD): δ 7.14 – 7.00 (m, 5H), 6.19 (d, J = 4.7 Hz, 6H), 4.70 (d, J = 17.3 Hz, 2H), 3.84 (s, 9H), 3.62 (s, 18H). ^{13}C NMR (126 MHz, CD_3OD): δ 167.01 (d, J_{CP} = 1.6 Hz), 164.73 (d, J_{CP} = 1.2 Hz), 134.70 (d, J_{CP} = 6.7 Hz), 130.44 (d, J_{CP} = 8.9 Hz), 128.58 (d, J_{CP} = 2.0 Hz), 127.49 (d, J_{CP} = 3.1 Hz), 93.78 (d, J_{CP} = 105.8 Hz), 91.70 (d, J_{CP} = 7.2 Hz), 56.06, 55.93, 36.73 (d, J_{CP} = 56.9 Hz). HRMS (DART) m/z calculated for $\text{C}_{34}\text{H}_{40}\text{O}_9\text{P}^+$ (M^+) 623.24045, found 623.24096.

1,3-Dimethyl-2-mesityl-1*H*-benzimidazolium iodide (**13**)



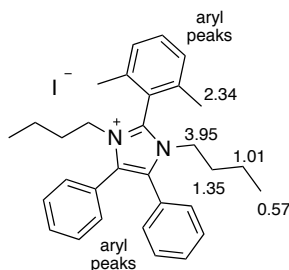
14a (1.29 g, 5.46 mmol) was dissolved in dimethylformamide (30 ml), cooled to 0 °C and treated with sodium hydride (262 mg, 10.9 mmol). After 30 minutes iodomethane (1.7 ml, 27 mmol) was added to the mixture, which was allowed to slowly warm to room temperature overnight. The crude mixture was poured into 1M sodium bicarbonate (100 ml) and extracted with ether (2 x 50 ml). The aqueous layer was collected and the water was removed *in vacuo* to give **13** (1.29 g, 68 %) as a tan powder. ^1H NMR (500 MHz, CD_3OD): δ 8.05 (m, 2H), 7.81 (m, 2H), 7.27 (s, 2H), 3.89 (s, 6H), 2.45 (s, 3H), 2.09 (s, 6H). ^{13}C NMR (126 MHz, CD_3OD): δ 151.98, 145.32, 139.97, 133.17, 130.53, 128.39, 118.28, 114.67, 33.14, 21.55, 19.63. HRMS (DART) m/z calculated for $\text{C}_{18}\text{H}_{21}\text{N}_2^+$ (M^+) 265.16993, found 265.16964.

1,3-Di-*n*-butyl-2-(2,6-dimethylphenyl)-4,5-diphenylimidazolium iodide (**14**)



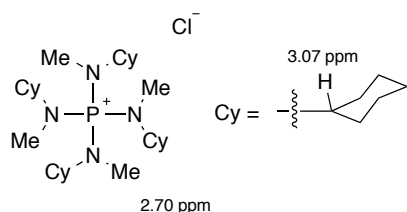
Following general procedure A, **14a** (1.86 g, 4.89 mmol) was treated with *n*-butyl iodide (0.61 ml, 5.4 mmol) in acetonitrile (5 ml). The product was dissolved in chloroform and purified via precipitation into ether to give **14** (1.27 g, 46 %) as a pale beige powder. **¹H NMR** (600 MHz, CD₃OD): δ 7.63 (t, *J* = 7.7 Hz, 1H), 7.57 – 7.54 (m, 4H), 7.54 – 7.44 (m, 8H), 3.99 – 3.89 (m, 4H), 2.34 (s, 6H), 1.40 – 1.29 (p, *J* = 7.4 Hz, 4H), 1.01 (sext, *J* = 7.4 Hz, 4H), 0.57 (t, *J* = 7.4 Hz, 6H). **¹³C NMR** (126 MHz, CD₃OD): δ 144.95, 140.54, 134.31, 134.06, 132.26, 131.61, 130.29, 130.23, 126.76, 122.42, 47.65, 32.22, 20.39, 20.32, 13.24. **HRMS** (DART) *m/z* calculated for C₃₁H₃₇N₂⁺ (*M*⁺) 437.29513, found 437.29517.

1,3-Di-*n*-butyl-2-(2,6-dimethylphenyl)-4,5-dimethylimidazolium iodide (**15**)



Following general procedure A, **15a** (0.240 g, 0.937 mmol) was treated with *n*-butyl iodide (0.13 ml, 1.1 mmol) in acetonitrile (1.5 ml). The product was dissolved in chloroform and purified via precipitation into ether to give **15** (0.366 g, 89 %) as a light beige powder. **¹H NMR** (600 MHz, CD₃OD): δ 7.57 (t, *J* = 7.7 Hz, 1H), 7.39 (d, *J* = 7.7 Hz, 2H), 3.89 – 3.75 (m, 4H), 2.43 (s, 6H), 2.12 (s, 6H), 1.59 – 1.52 (p, *J* = 7.4 Hz, 4H), 1.26 (sext, *J* = 7.4 Hz, 4H), 0.82 (t, *J* = 7.4 Hz, 6H). **¹³C NMR** (126 MHz, CD₃OD): δ 143.30, 140.40, 133.97, 130.02, 128.66, 122.75, 46.91, 32.43, 20.61, 20.09, 13.57, 9.06. **HRMS** (DART) *m/z* calculated for C₂₁H₃₃N₂⁺ (*M*⁺) 313.26383, found 313.26388.

Tetrakis[cyclohexyl(methyl)amino]phosphonium chloride (**16**)



A solution of **16a** (0.844 g, 1.49 mmol) in chlorobenzene (5 ml) was treated with 50% sodium hydroxide (5 ml). With continuous stirring dimethylsulfide (0.55 ml, 7.5 mmol) was added. The mixture was stirred at 50 °C for 17 hours. After cooling to room temperature, water was added (40 ml) and the mixture was extracted with dichloromethane (2 x 50 ml). The organic layer was dried with sodium sulfate and the solvent was removed *in vacuo*. The resulting pale yellow oil was dissolved in methanol (10 ml) and treated with 20 g chloride ion exchange resin (Amberlite-IRA 400(Cl) form) for 4 hours. The resin was filtered off and washed with methanol. The residue was purified via precipitation into ether to give **16** (0.450 g, 59%) as a white powder. ³¹P NMR (162 MHz, CD₃OD) 45.27 (1P, s). ¹H NMR (500 MHz, CD₃OD): δ 3.07 (m, 4H), 2.70 (d, *J* = 9.9 Hz, 12H), 1.95 – 1.57 (m, 28H), 1.37 (m, 8H), 1.18 (m, 4H). ¹³C NMR (126 MHz, CD₃OD): δ 56.81 (d, *J*_{CP} = 5.2 Hz), 31.42 (d, *J*_{CP} = 2.9 Hz), 30.52 (d, *J*_{CP} = 3.6 Hz), 27.00, 26.21. HRMS (DART) *m/z* calculated for C₂₈H₅₆N₄P⁺ (M⁺) 479.42371, found 479.42320.

3.5.3 Model Compound Study Procedures

General Procedure B – Deuterated Stability Study Procedure

Stock solutions of basic methanol were prepared by dissolving KOH (1 M or 2 M) and 3-(Trimethylsilyl)-1-propanesulfonic acid sodium salt (0.025M) in CD₃OH. For example, a 1 M solution was prepared by dissolving KOH (141 mg, 2.51 mmol) and internal standard (14 mg, 0.063 mmol) in 2.5 mL of CD₃OH. The model compound (0.05 M for 1 M KOH and 0.03 M for 2 M KOH) was dissolved in the methanol solution (0.5 mL) and passed through a glass wool plug into an NMR tube. For example, **6** (6.8 mg, 0.025 mmol) was dissolved in 0.5 mL methanol solution. The NMR tube was flame sealed and analyzed by ¹H NMR spectroscopy for the initial

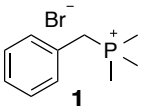
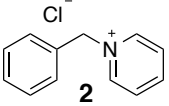
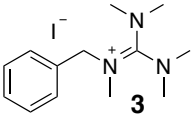
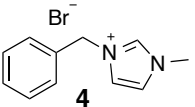
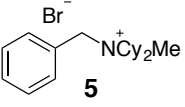
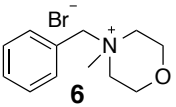
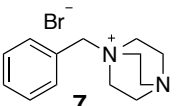
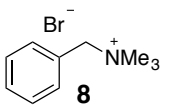
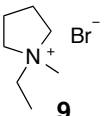
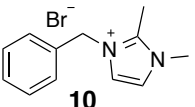
time point. Integration of a selected signal in the model compound relative to a signal related to 3-(Trimethylsilyl)-1-propanesulfonic acid sodium salt provided the initial quantity of model compound. The tube was heated in an oil bath at 80 °C. At specified time points, every 5 days, the tubes were removed, cooled to room temperature and analyzed by ^1H NMR spectroscopy to determine the quantity of model compound remaining (^1H NMR spectra are provided in Figures 3.14-3.77).

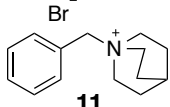
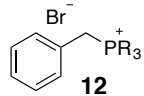
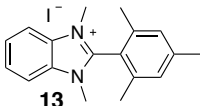
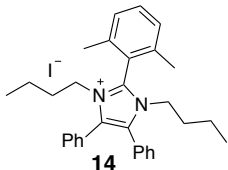
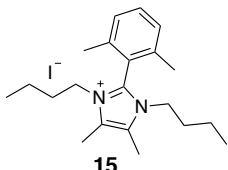
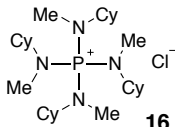
General procedure C – Non-deuterated Stability Study Procedure

A stock solution of basic methanol was prepared by dissolving 1M KOH (3.46 g, 61.7 mmol) in 60 mL of CH_3OH . The model compounds (0.05M) were dissolved in the methanol solution (5.0 mL) and sealed in glass vials with Teflon-coated caps. The vials were heated in reactor block that was equilibrated to 80 °C. At specified time points, every 5 days, the vials were removed, cooled to room temperature and 0.500 g was transferred to a separate vial. A 1 M HCl stock solution was prepared by dissolving 5.0 mL HCl in 55 mL of CH_3OH . Excess KOH in the stability study solution was quenched by adding 0.500 g of 1M HCl solution. The solvent was removed under vacuum. A 0.025 M internal standard solution was prepared by dissolving 3-(Trimethylsilyl)-1-propanesulfonic acid sodium salt (222 mg, 1.02 mmol) in 40 mL of CD_3OD . A single batch of internal standard solution was used for all time points to ensure consistency across the study. The stability study sample was dissolved in 0.500 g of internal standard solution, passed through a glass wool plug into an NMR tube and analyzed by ^1H NMR spectroscopy. Integration of a selected signal in the model compound relative to a signal related to 3-(Trimethylsilyl)-1-propanesulfonic acid sodium salt provided the initial quantity of model compound. (^1H NMR spectra are provided in Figures 3.14-3.77).

Expanded Data Tables

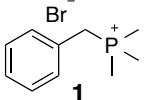
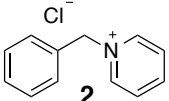
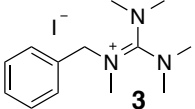
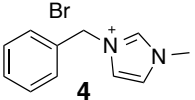
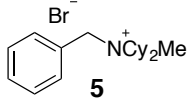
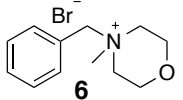
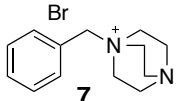
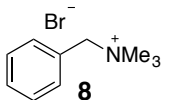
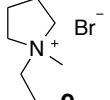
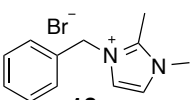
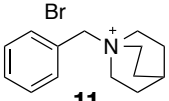
Table 3.2 Summary of deuterated stability studies in CD₃OH.^a

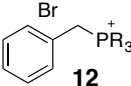
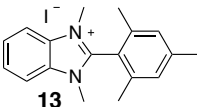
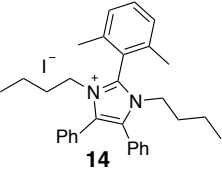
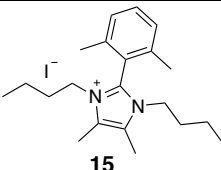
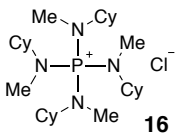
Model Compound	[KOH]	Cation remaining (%) ^b					
		5d	10d	15d	20d	25d	30d
 1	1M	<1	n.d. ^d	n.d.	n.d.	n.d.	n.d.
	2M ^c	<1	n.d.	n.d.	n.d.	n.d.	n.d.
 2	1M	<1	n.d.	n.d.	n.d.	n.d.	n.d.
	2M ^c	<1	n.d.	n.d.	n.d.	n.d.	n.d.
 3	1M	<1	n.d.	n.d.	n.d.	n.d.	n.d.
	2M ^c	<1	n.d.	n.d.	n.d.	n.d.	n.d.
 4	1M	<1	n.d.	n.d.	n.d.	n.d.	n.d.
	2M ^c	<1	n.d.	n.d.	n.d.	n.d.	n.d.
 5	1M	<1	n.d.	n.d.	n.d.	n.d.	n.d.
	2M ^c	<1	n.d.	n.d.	n.d.	n.d.	n.d.
 6	1M	40	3	<1	n.d.	n.d.	n.d.
	2M ^c	<1	n.d.	n.d.	n.d.	n.d.	n.d.
 7	1M	36	27	18	11	6	5
	2M ^c	22	6	2	1	n.d.	n.d.
 8	1M	75	56	29	19	15	11
	2M ^c	67	42	27	14	7	5
 9	1M	66	58	49	44	36	33
	2M ^c	38	31	22	19	14	12
 10	1M	77	64	56	49	44	36
	2M ^c	44	11	3	n.d.	1	n.d.

Model Compound	[KOH]	Cation remaining (%) ^b					
		5d	10d	15d	20d	25d	30d
 11	1M	85	80	75	72	68	65
	2M ^c	72	62	56	48	41	38
 12 R = 2,4,6-(OCH ₃) ₃ C ₆ H ₂	1M	93	85	81	78	73	66
	2M ^c	90	79	69	56	46	38
 13	1M	97	96	92	89	88	87
	2M ^c	93	81	76	74	72	70
 14	1M	>99	>99	>99	>99	>99	>99
	2M ^c	>99	>99	>99	>99	>99	>99
 15	1M	>99	>99	>99	>99	>99	>99
	2M ^c	>99	>99	98	>99	>99	>99
 16	1M	>99	>99	>99	>99	>99	>99
	2M ^c	>99	>99	>99	>99	>99	>99

^aReaction Conditions: [Cation]:[KOH] = 1:20 or 1:67 for 1M or 2M KOH experiments, respectively and at 80 °C. ^bPercent of cation remaining, determined by ¹H NMR spectroscopy relative to an internal standard, 3-(trimethylsilyl)-1-propanesulfonic acid sodium salt. ^cThe cation concentration was reduced from 0.05M to 0.03M at higher base concentrations due to reduced solubility of the organic salt. ^dNot determined.

Table 3.3 Summary of non-deuterated stability studies in CH₃OH.^a

Model Compound	Cation remaining (%) ^b					
	5d	10d	15d	20d	25d	30d
 1	<1	n.d. ^c	n.d.	n.d.	n.d.	n.d.
 2	<1	n.d.	n.d.	n.d.	n.d.	n.d.
 3	<1	n.d.	n.d.	n.d.	n.d.	n.d.
 4	<1	n.d.	n.d.	n.d.	n.d.	n.d.
 5	<1	n.d.	n.d.	n.d.	n.d.	n.d.
 6	7	<1	n.d.	n.d.	n.d.	n.d.
 7	14	6	2	n.d.	n.d.	n.d.
 8	71	50	37	25	17	12
 9	89	77	68	56	46	40
 10	65	47	36	29	21	13
 11	97	93	88	83	77	72

Model Compound	Cation remaining (%) ^b					
	5d	10d	15d	20d	25d	30d
 12 R = 2,4,6-(OCH ₃) ₃ C ₆ H ₂	94	85	80	74	70	63
 13	99	96	93	92	90	86
 14	99	98	97	>99	>99	>99
 15	>99	>99	>99	>99	>99	>99
 16	>99	>99	>99	>99	>99	>99

^aReaction Conditions: [Cation]:[KOH] = 1:20 and 1M KOH in non-deuterated methanol (CH₃OH) and at 80 °C. ^bPercent of cation remaining, determined by ¹H NMR spectroscopy relative to an internal standard, 3-(trimethylsilyl)-1-propanesulfonic acid sodium salt. ^cNot determined.

Figure 3.12 Stability of model compounds (0.05 M) in 2 M KOH/CD₃OH at 80 °C.

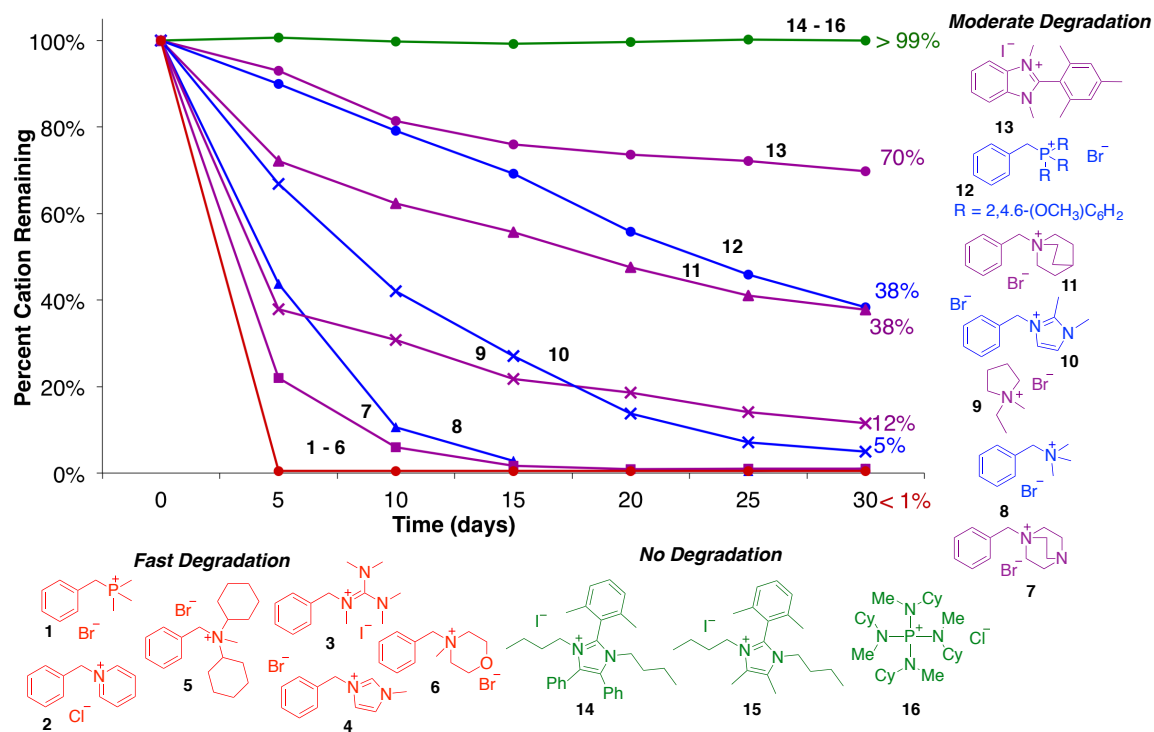
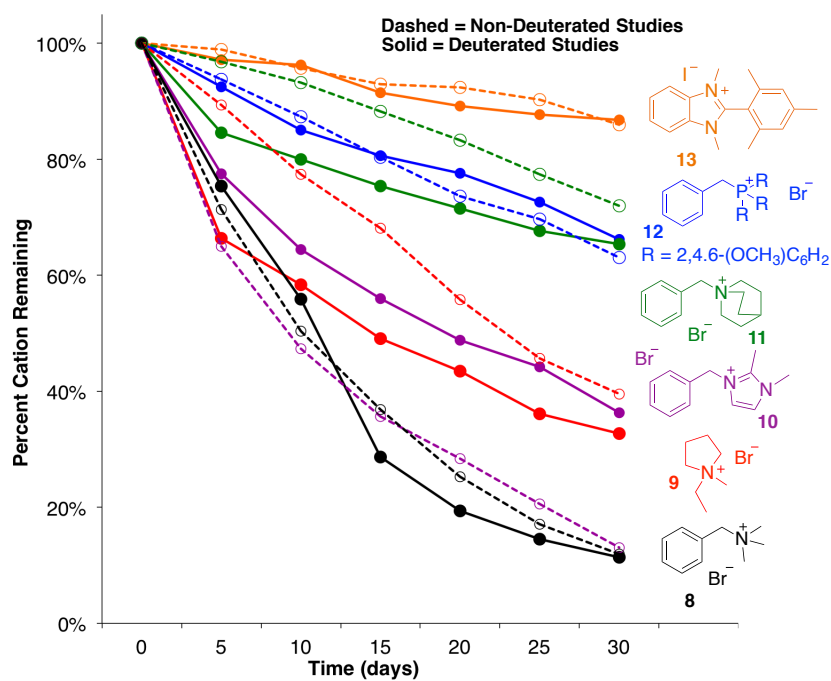


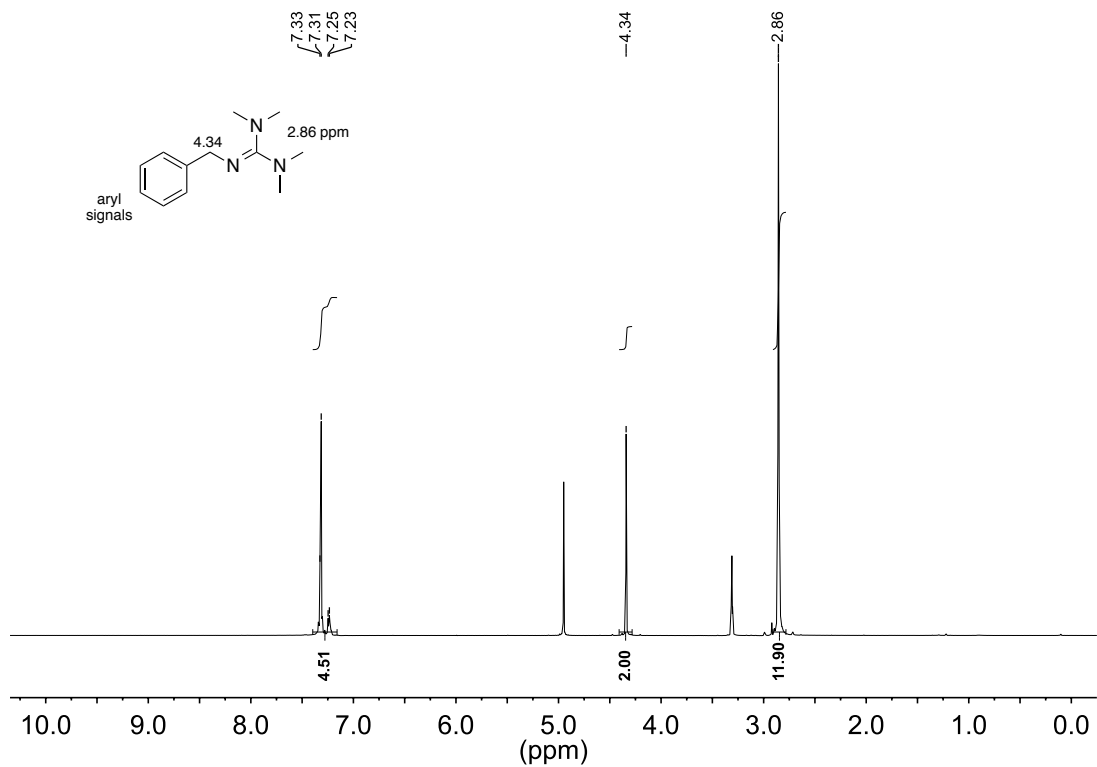
Figure 3.13 Comparison of deuterated and non-deuterated stability studies.



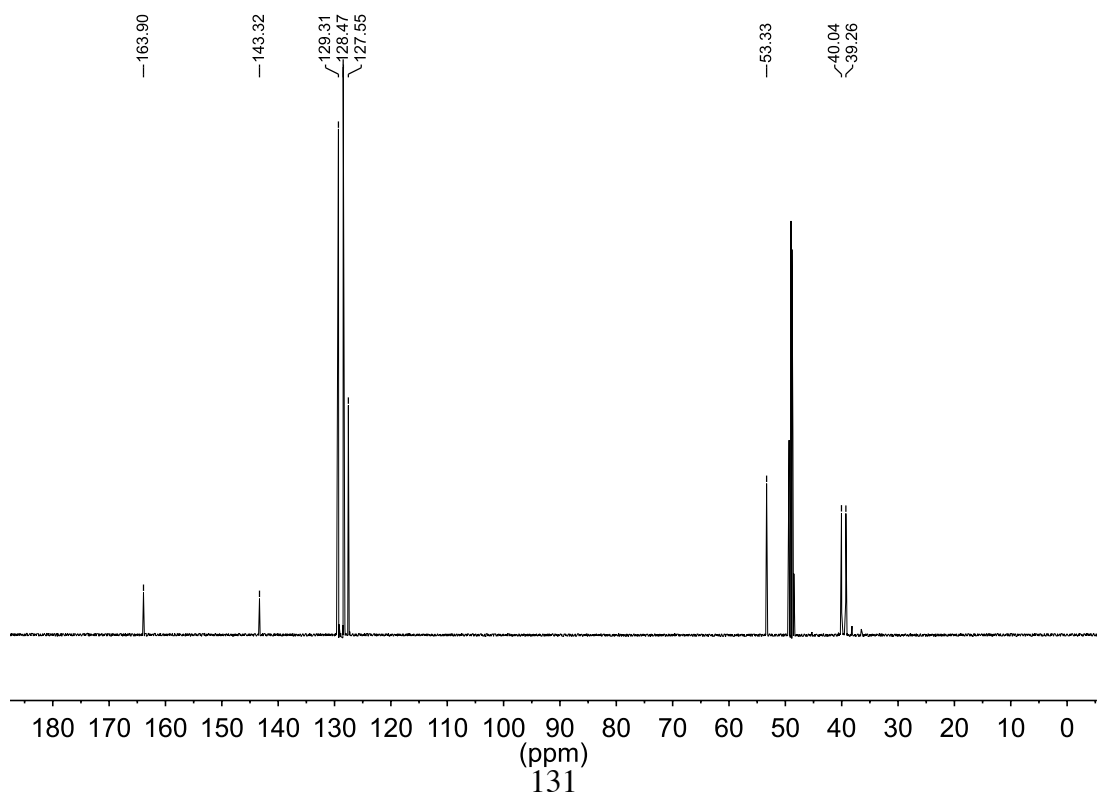
3.5.4 Copies of ^1H and ^{13}C NMR Spectra

2-benzyl-1,1,3,3-tetramethylguanidine (3a)

^1H NMR spectrum (500 MHz, CD_3OD)

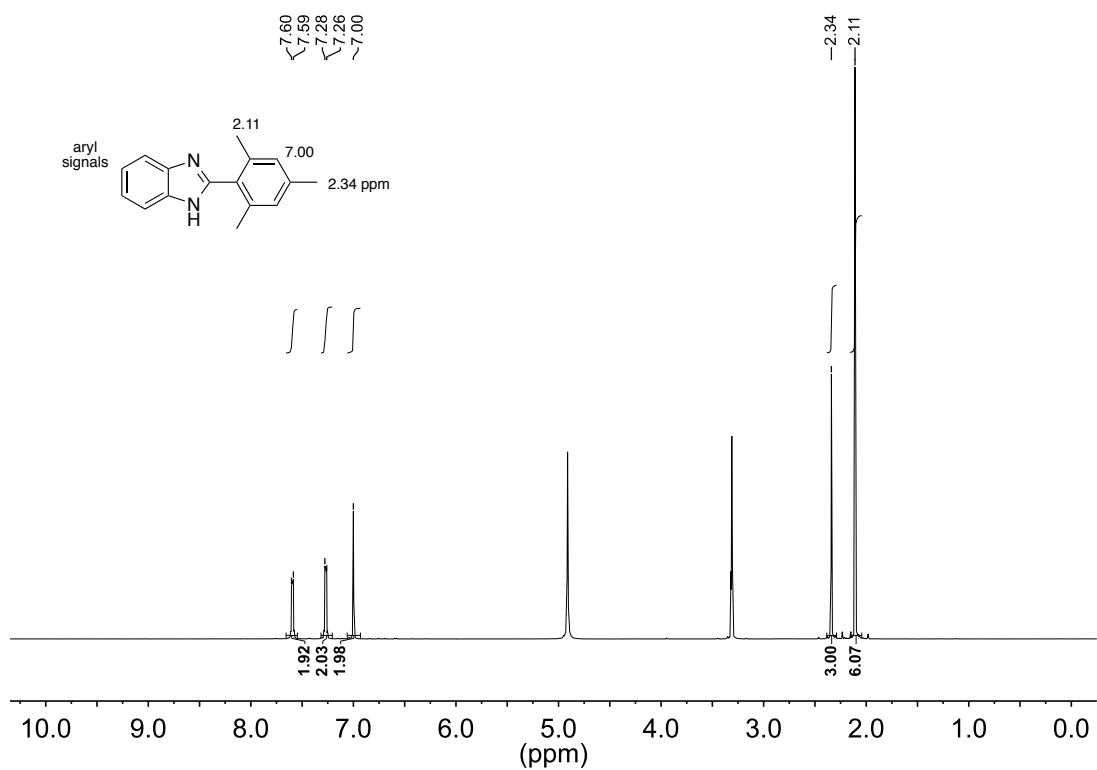


^{13}C NMR spectrum (126 MHz, CD_3OD)

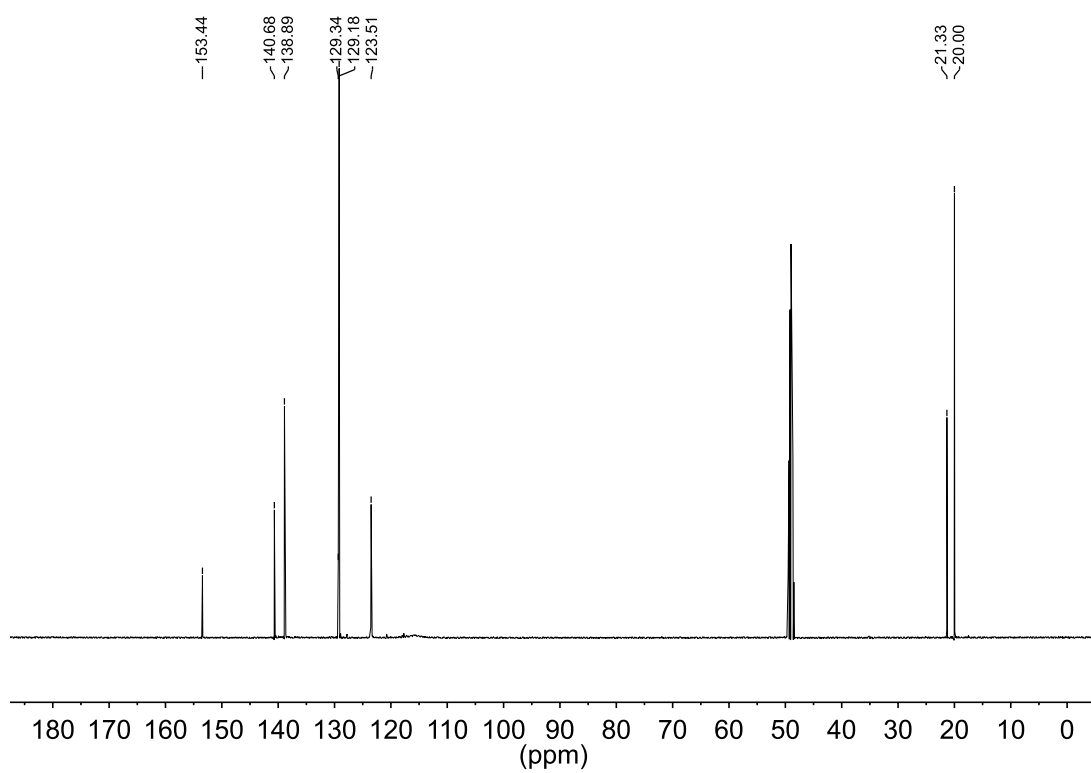


2-Mesitylbenzimidazole (13a)

^1H NMR spectrum (500 MHz, CD_3OD)

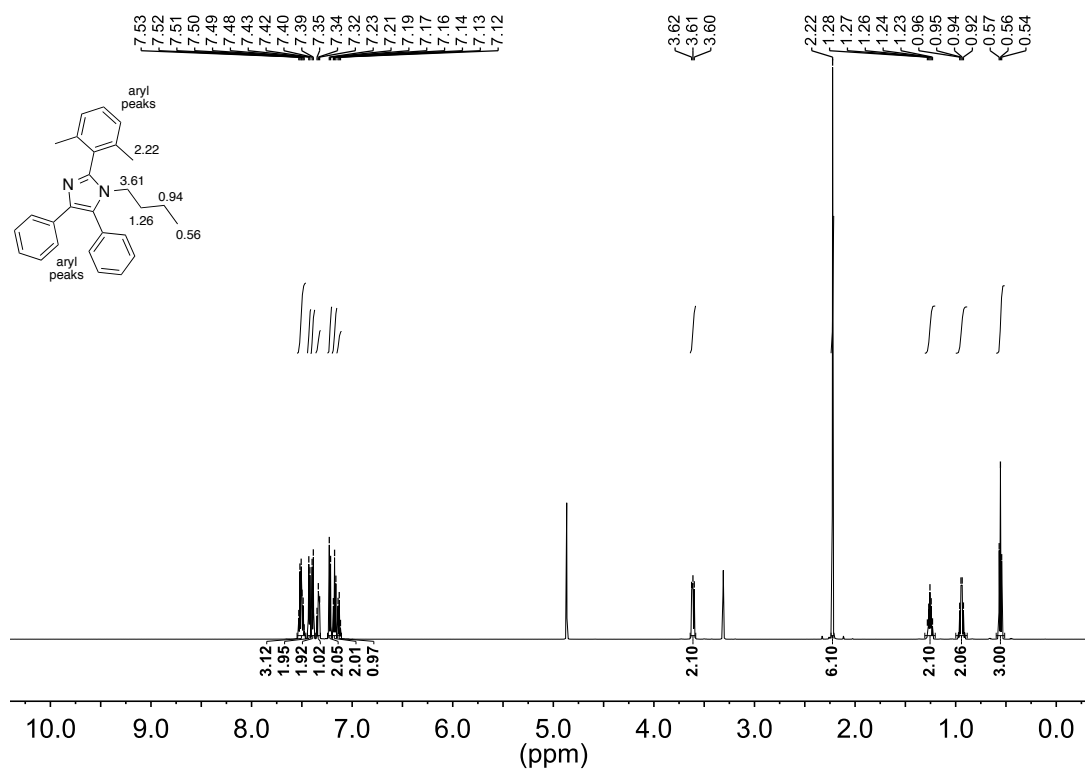


^{13}C NMR spectrum (126 MHz, CD_3OD)

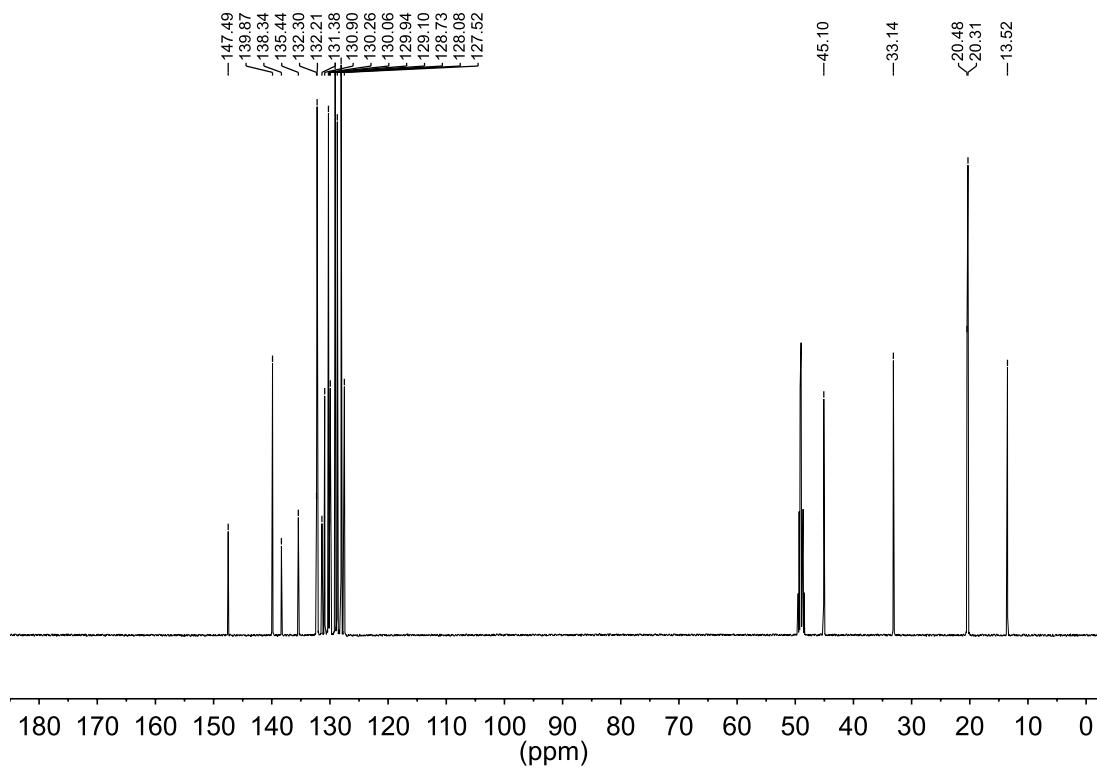


1-*n*-Butyl-2-(2,6-dimethylphenyl)-4,5-diphenyl-1*H*-imidazole (14a)

¹H NMR spectrum (600 MHz, CD₃OD)

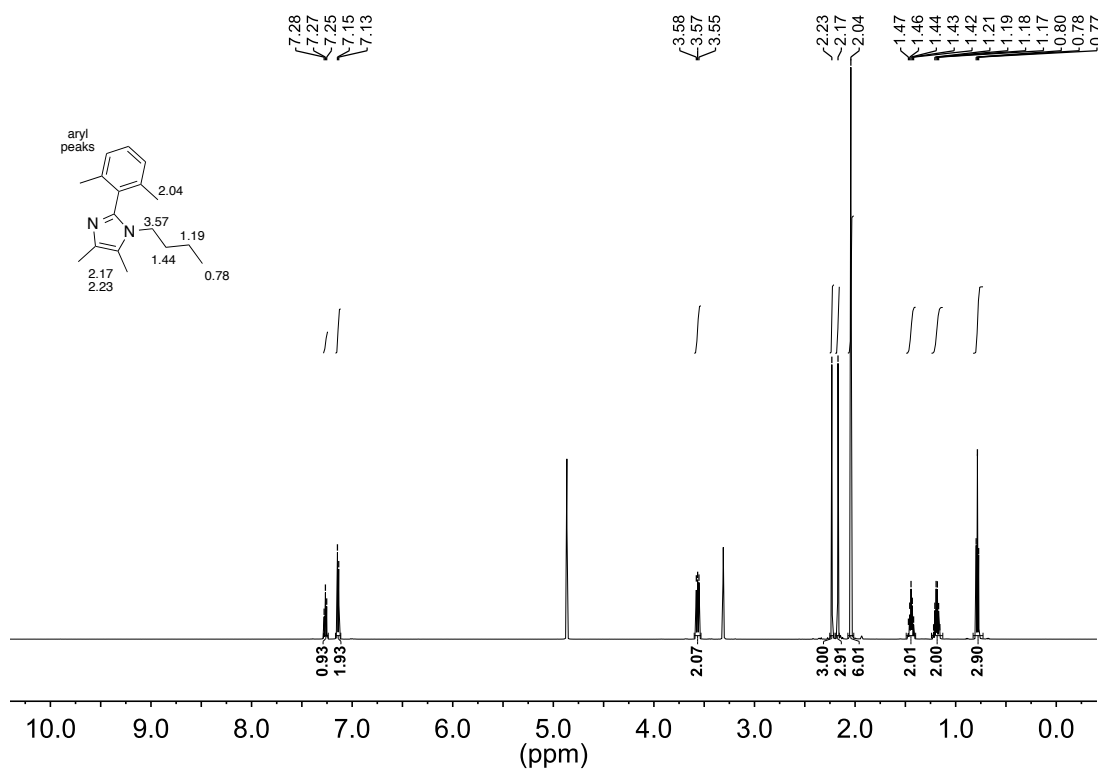


¹³C NMR spectrum (126 MHz, CD₃OD)

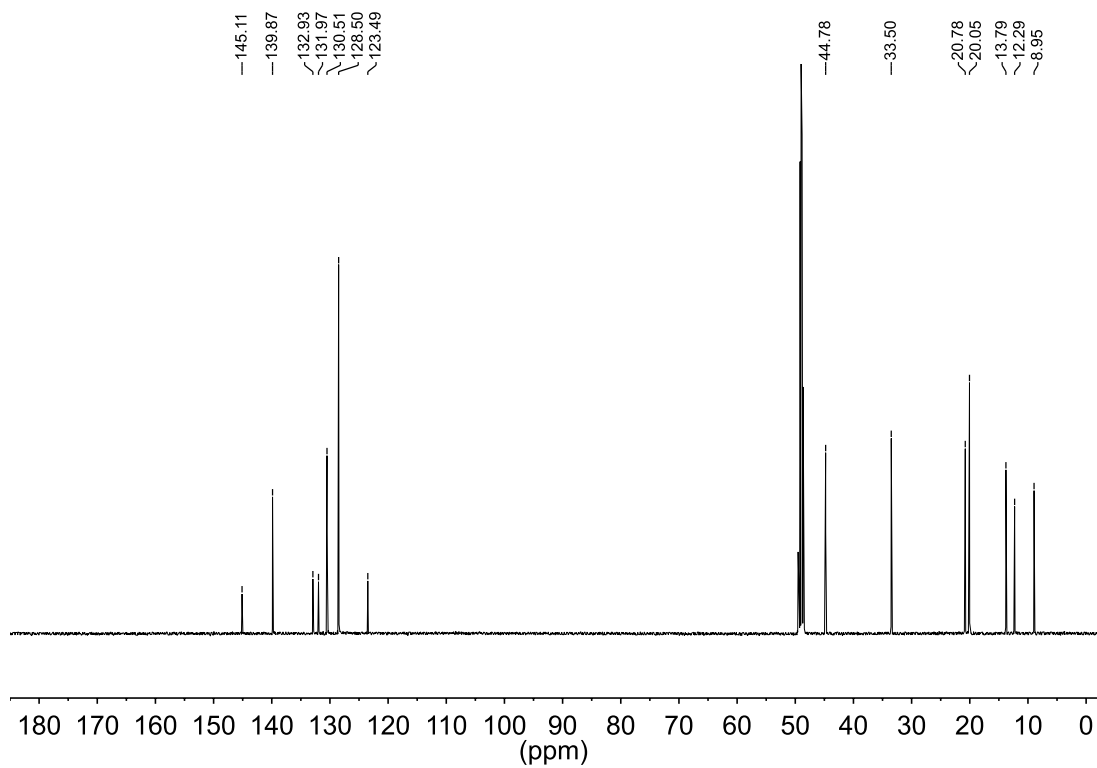


1-*n*-Butyl-2-(2,6-dimethylphenyl)-4,5-dimethyl-1*H*-imidazole (15a)

¹H NMR spectrum (600 MHz, CD₃OD)

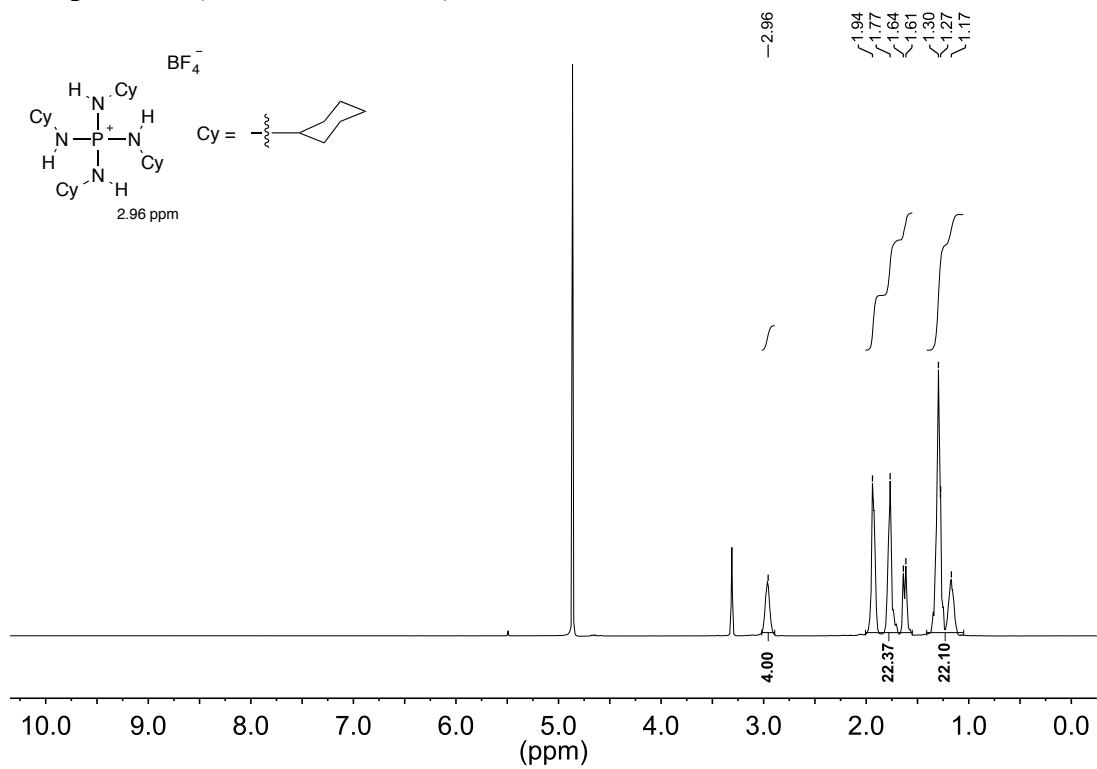


¹³C NMR spectrum (126 MHz, CD₃OD)

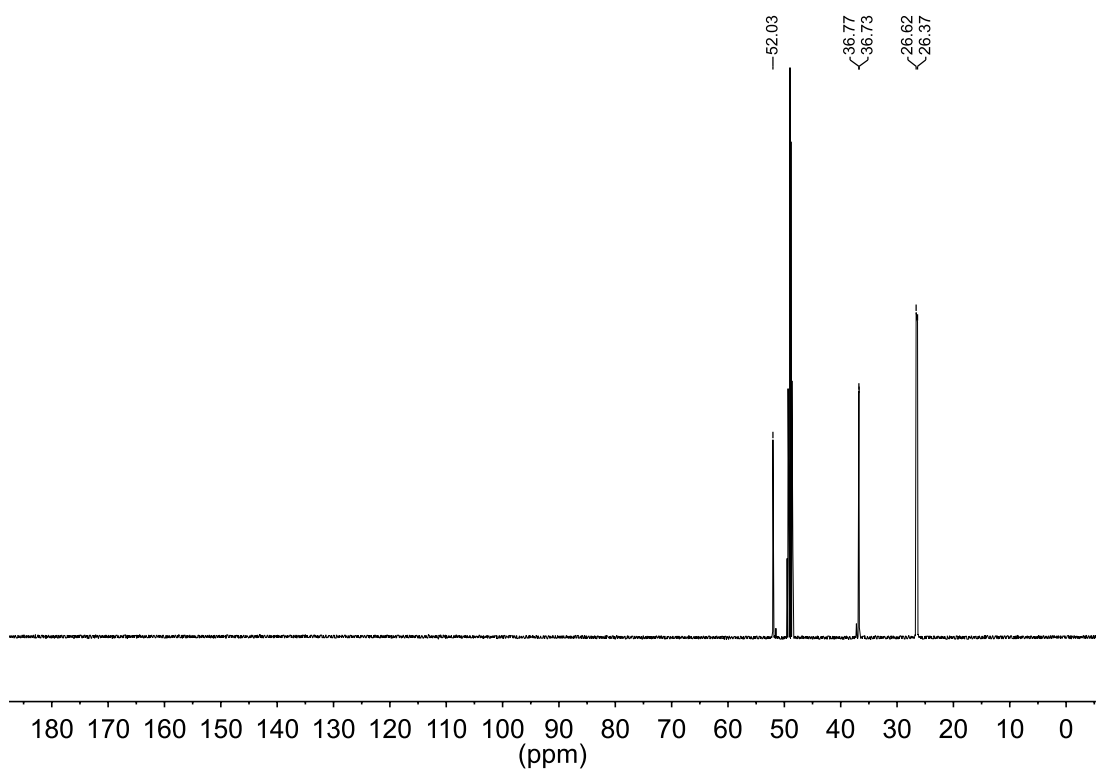


Tetrakis(cyclohexylamino)phosphonium tetrafluoroborate (16a)

^1H NMR spectrum (500 MHz, CD_3OD)

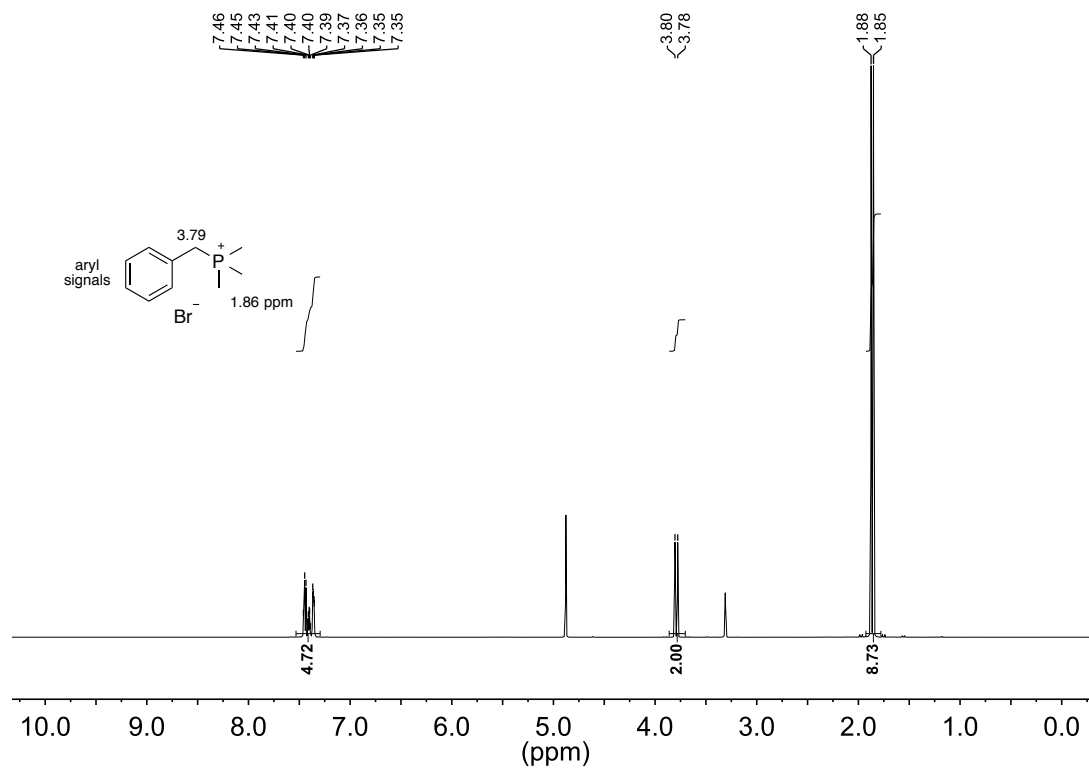


^{13}C NMR spectrum (126 MHz, CD_3OD)

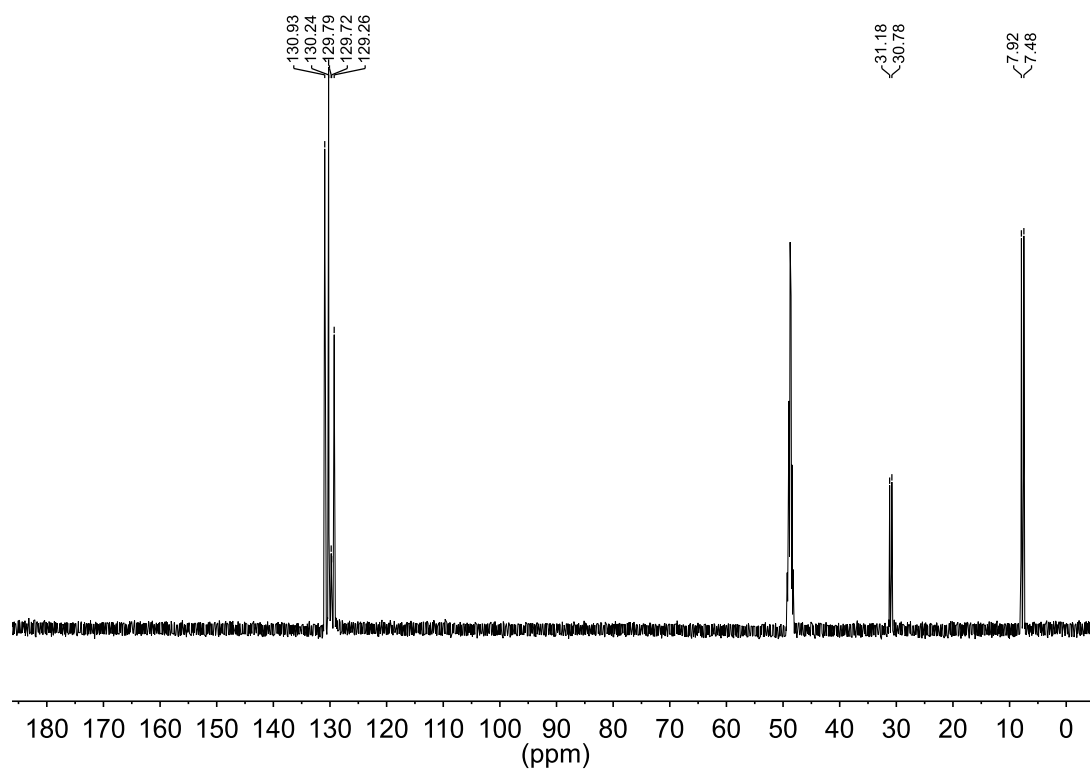


Benzyltrimethylphosphonium bromide (1)

^1H NMR spectrum (600 MHz, CD_3OD)

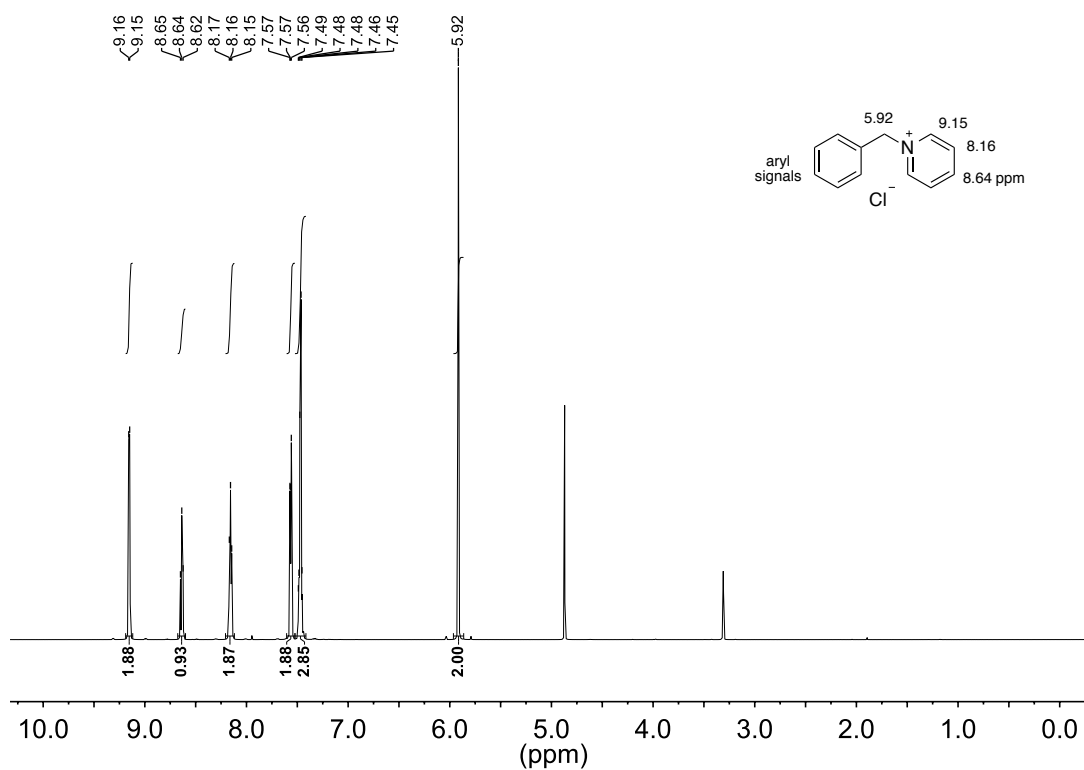


^{13}C NMR spectrum (126 MHz, CD_3OD)

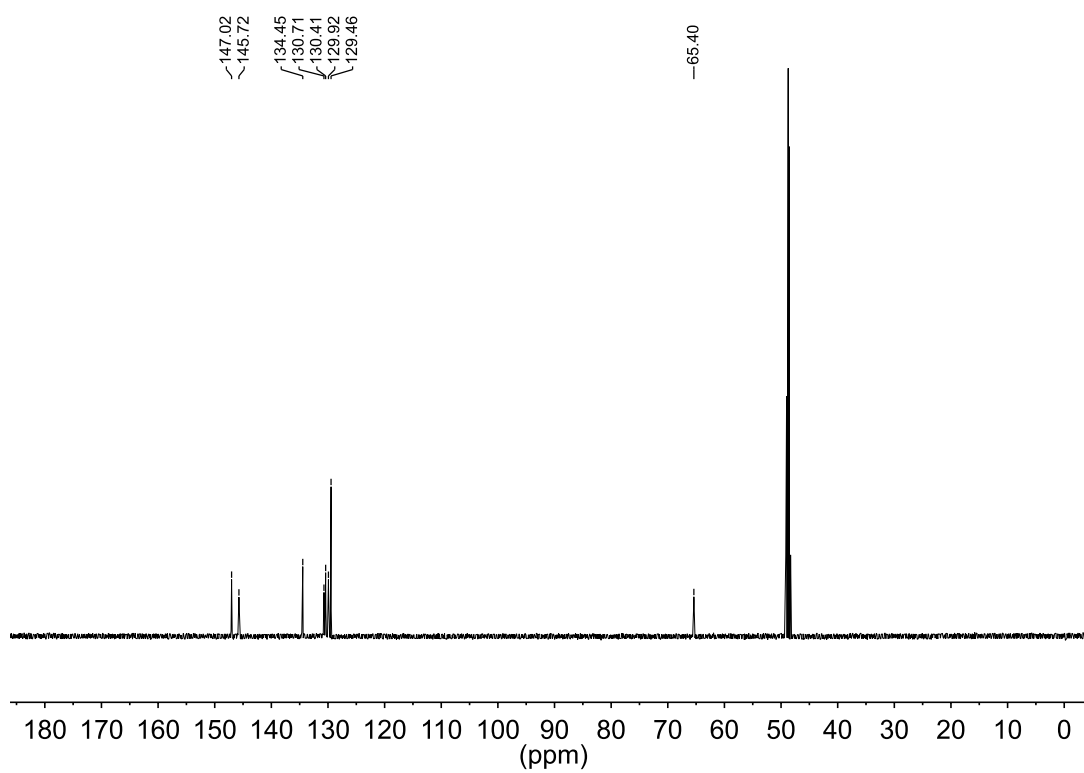


1-Benzylpyridin-1-ium chloride (2)

^1H NMR spectrum (600 MHz, CD_3OD)

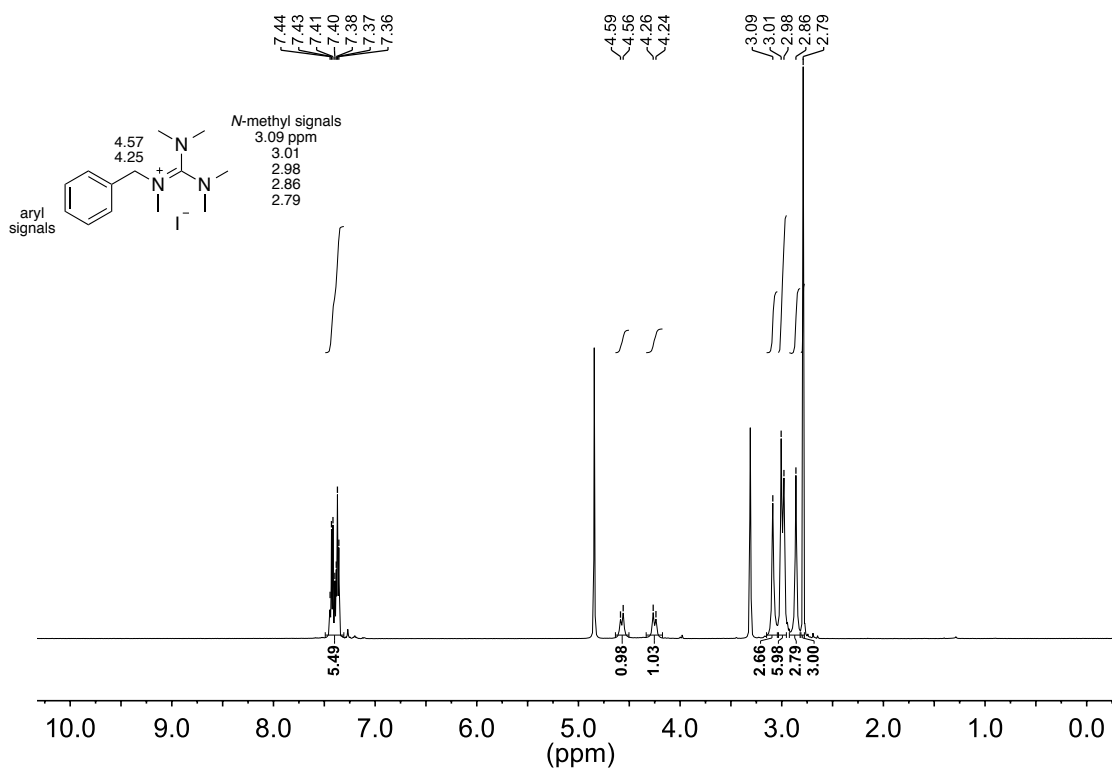


^{13}C NMR spectrum (151 MHz, CD_3OD)

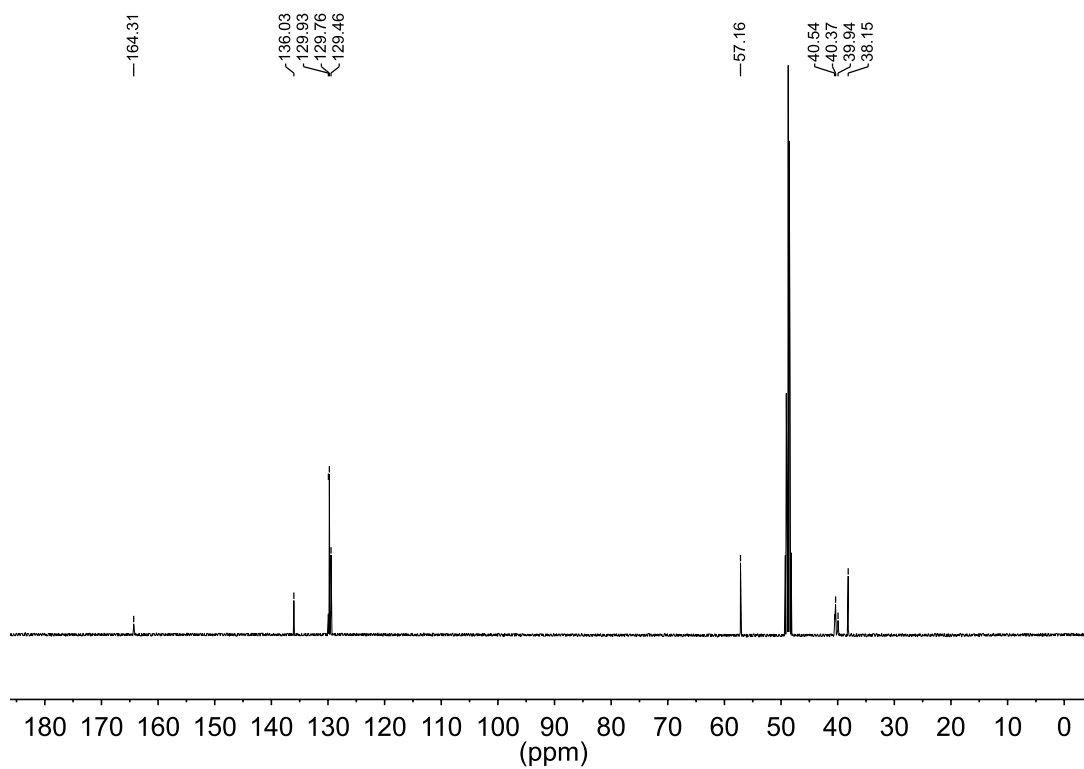


***N*-(Bis(dimethylamino)methylene)-*N*-methyl-1-phenylmethanaminium iodide (3)**

¹H NMR spectrum (500 MHz, CD₃OD)

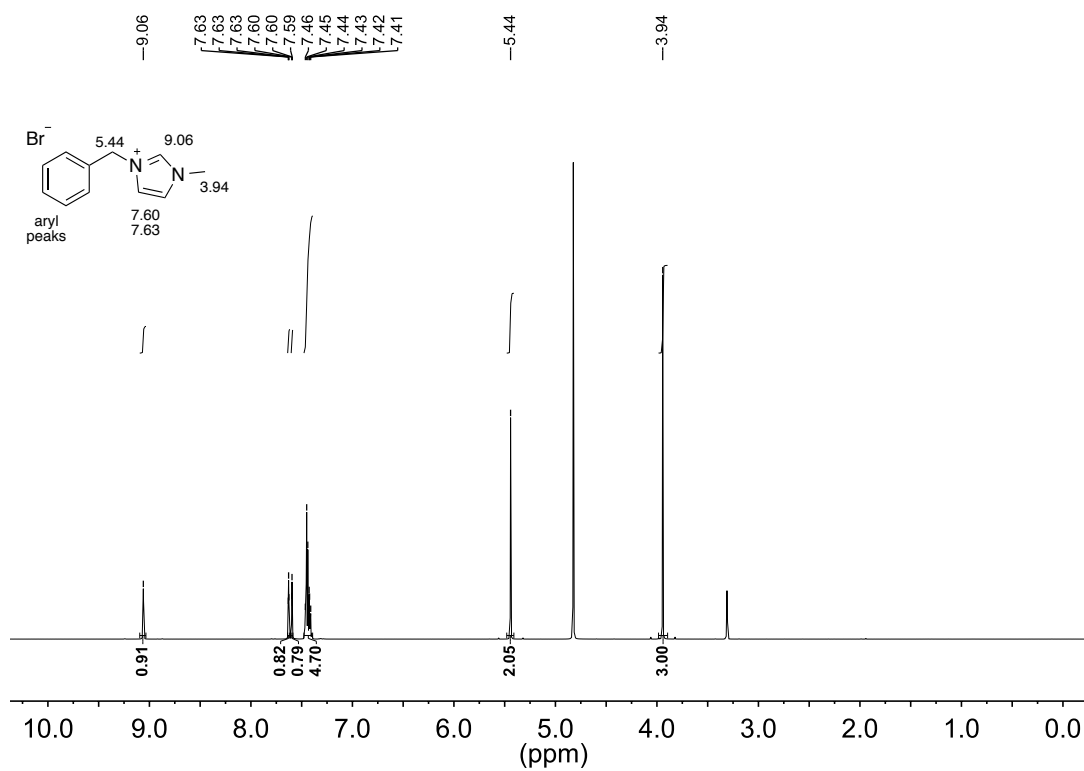


¹³C NMR spectrum (126 MHz, CD₃OD)

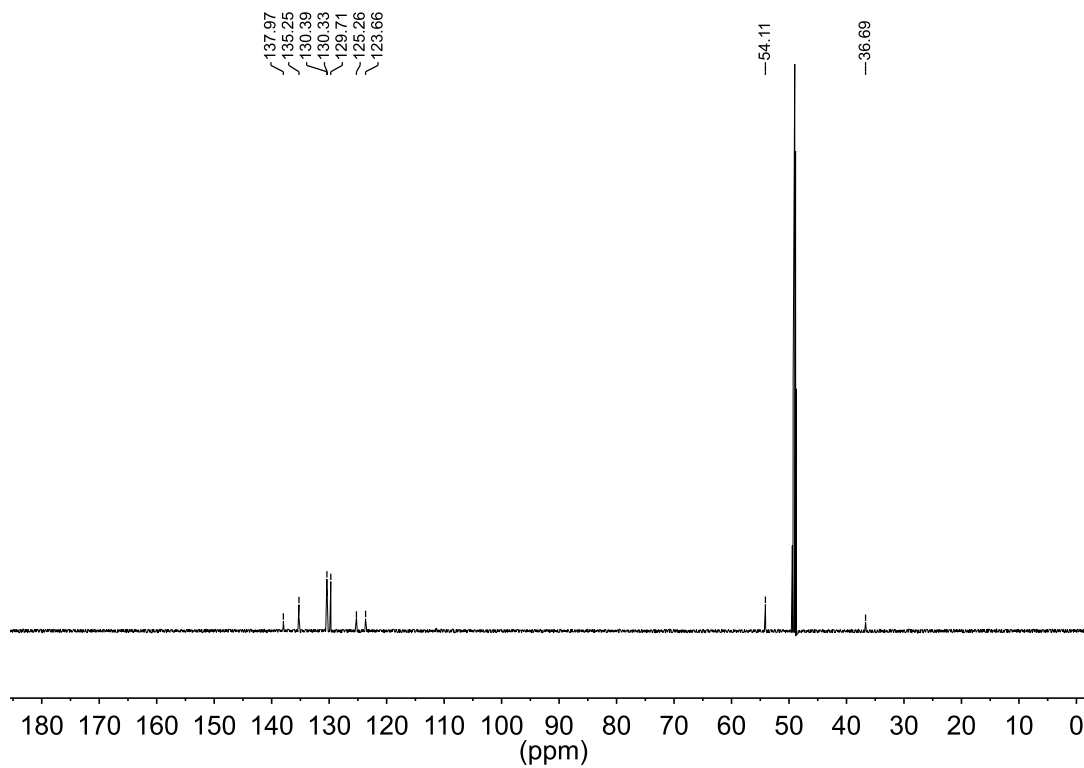


1-Benzyl-3-methylimidazolium bromide (4)

^1H NMR spectrum (600 MHz, CD_3OD)

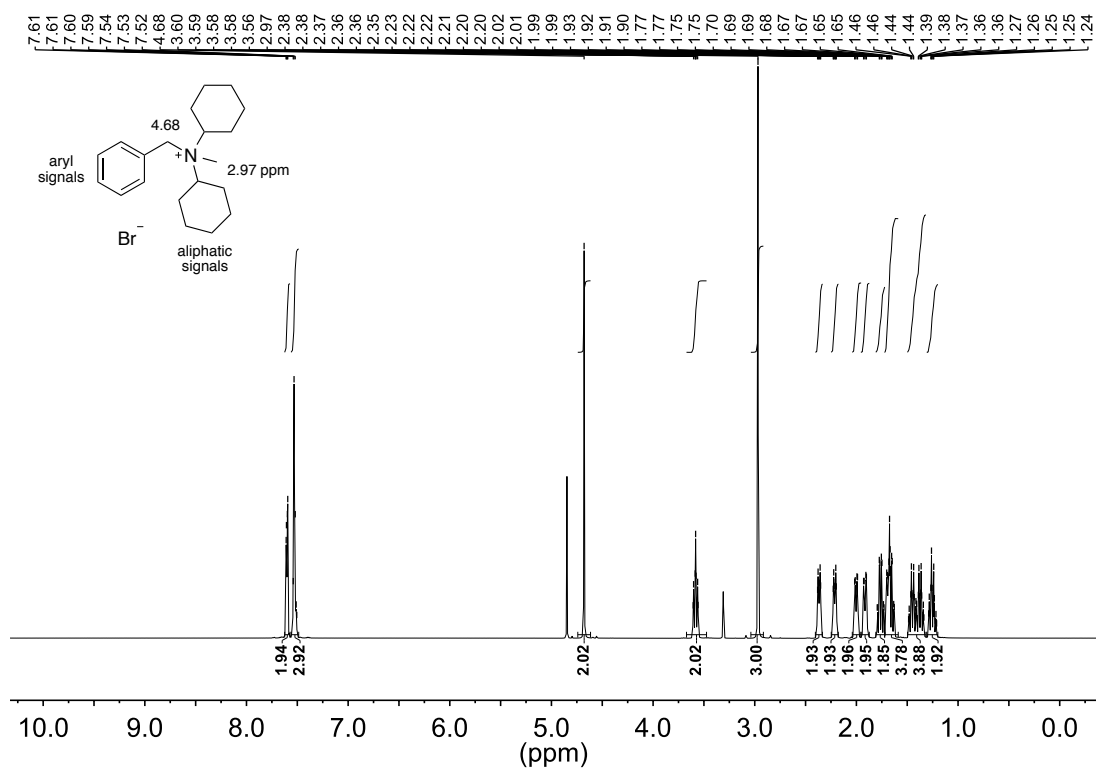


^{13}C NMR spectrum (151 MHz, CD_3OD)

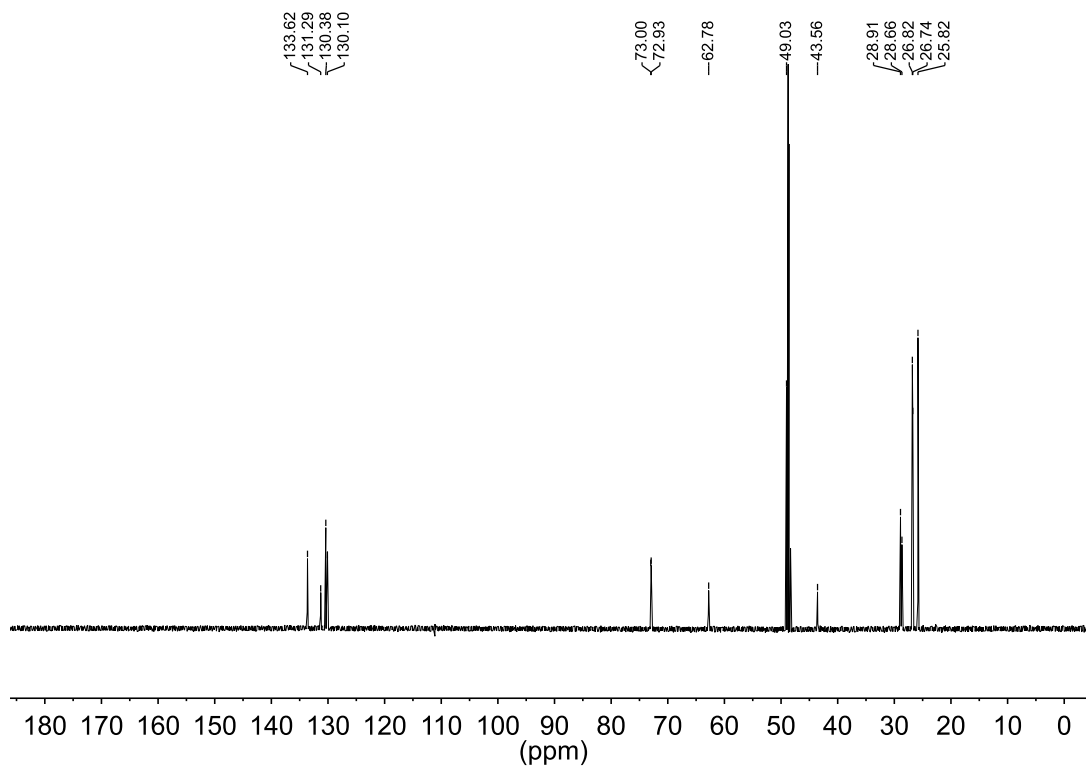


***N*-Benzyl-*N*-cyclohexyl-*N*-methylcyclohexanaminium bromide (5)**

¹H NMR spectrum (600 MHz, CD₃OD)

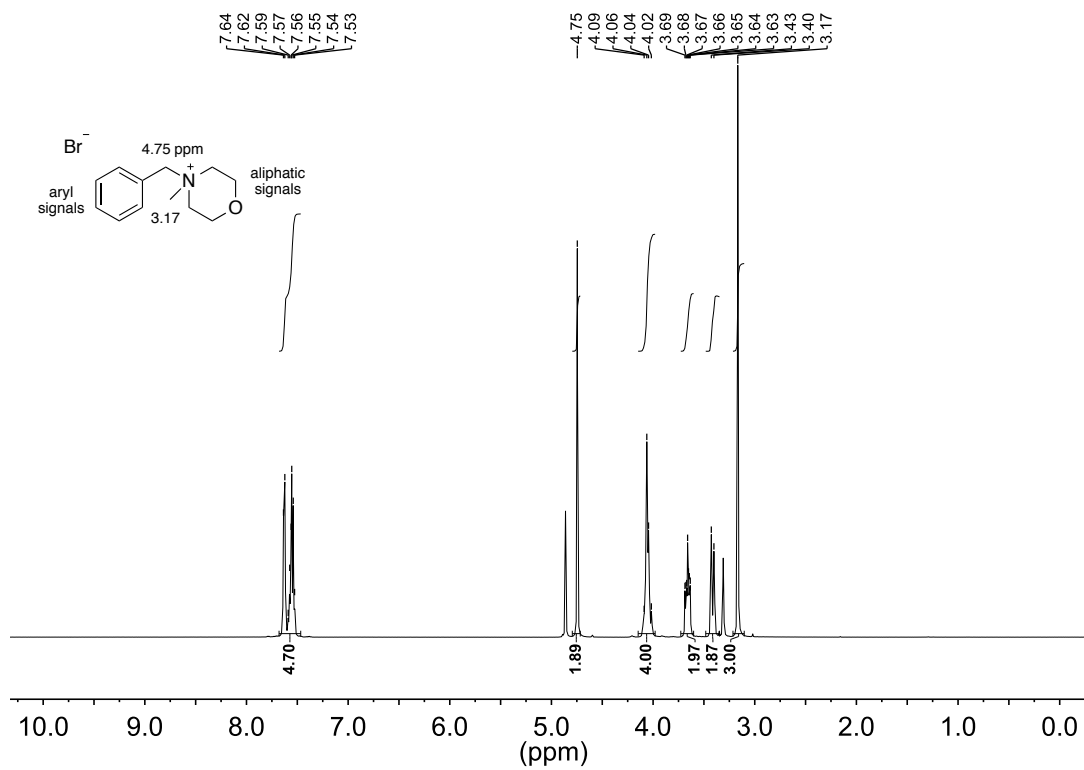


¹³C NMR spectrum (151 MHz, CD₃OD)

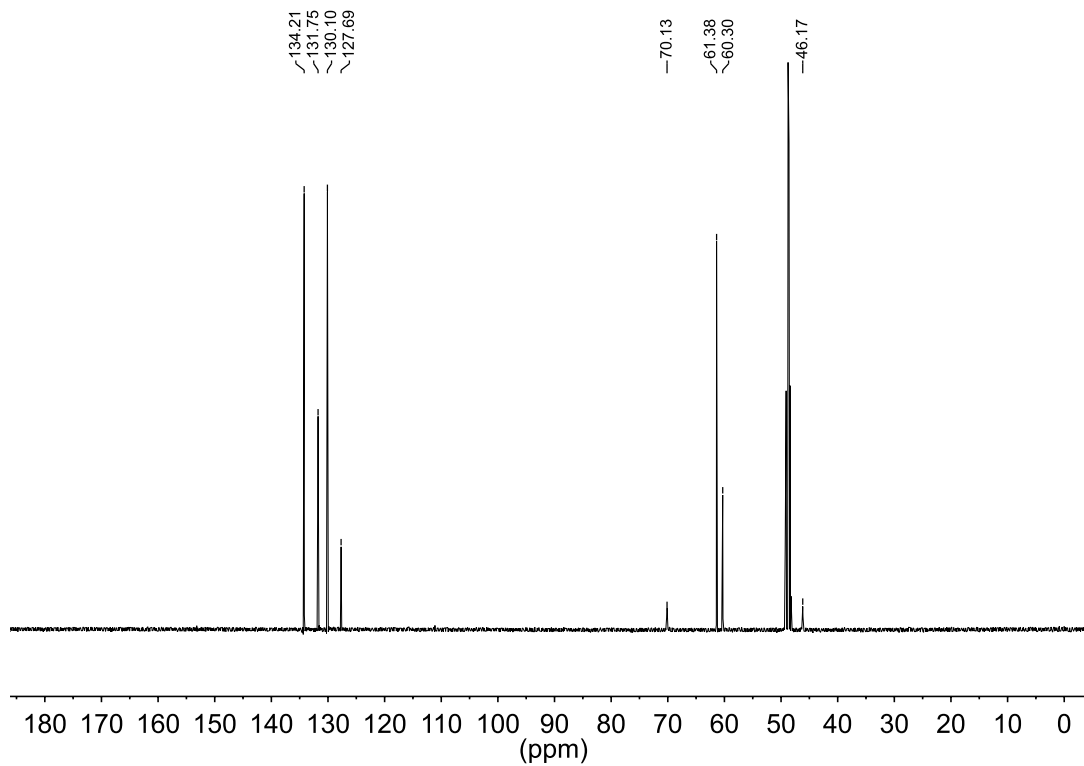


4-Benzyl-4-methylmorpholin-4-ium bromide (6)

^1H NMR spectrum (500 MHz, CD_3OD)

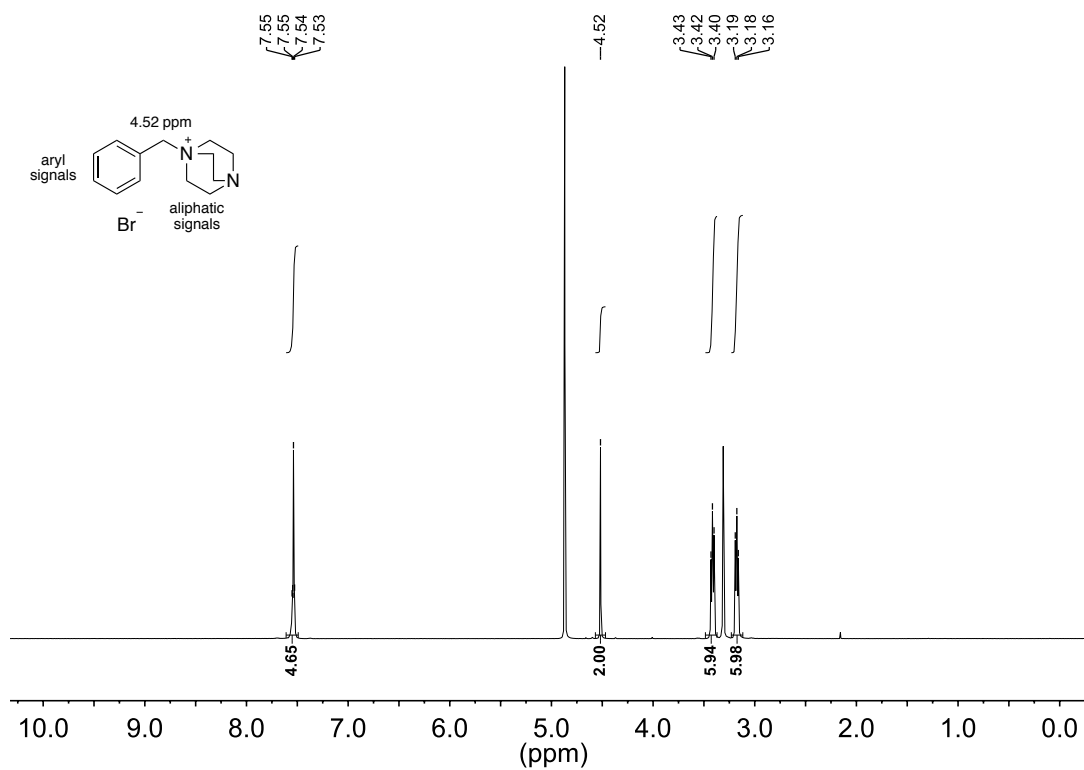


^{13}C NMR spectrum (126 MHz, CD_3OD)

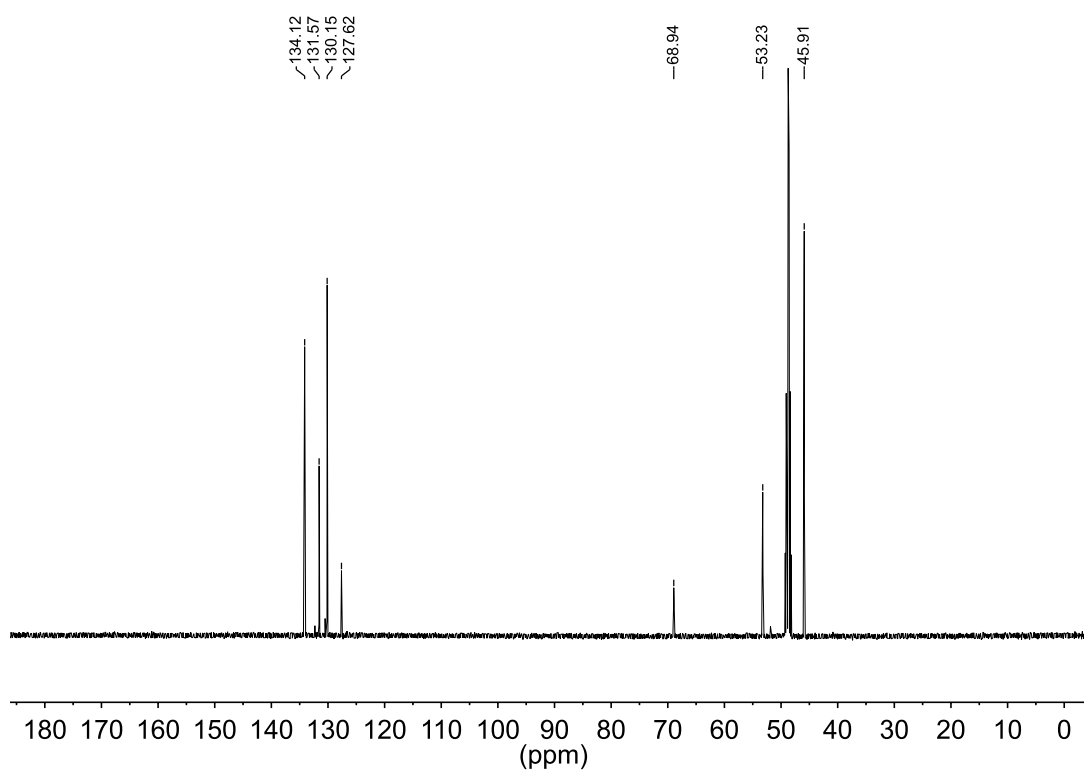


1-Benzyl-1,4-diazabicyclo[2.2.2]octan-1-ium bromide (7)

^1H NMR spectrum (500 MHz, CD_3OD)

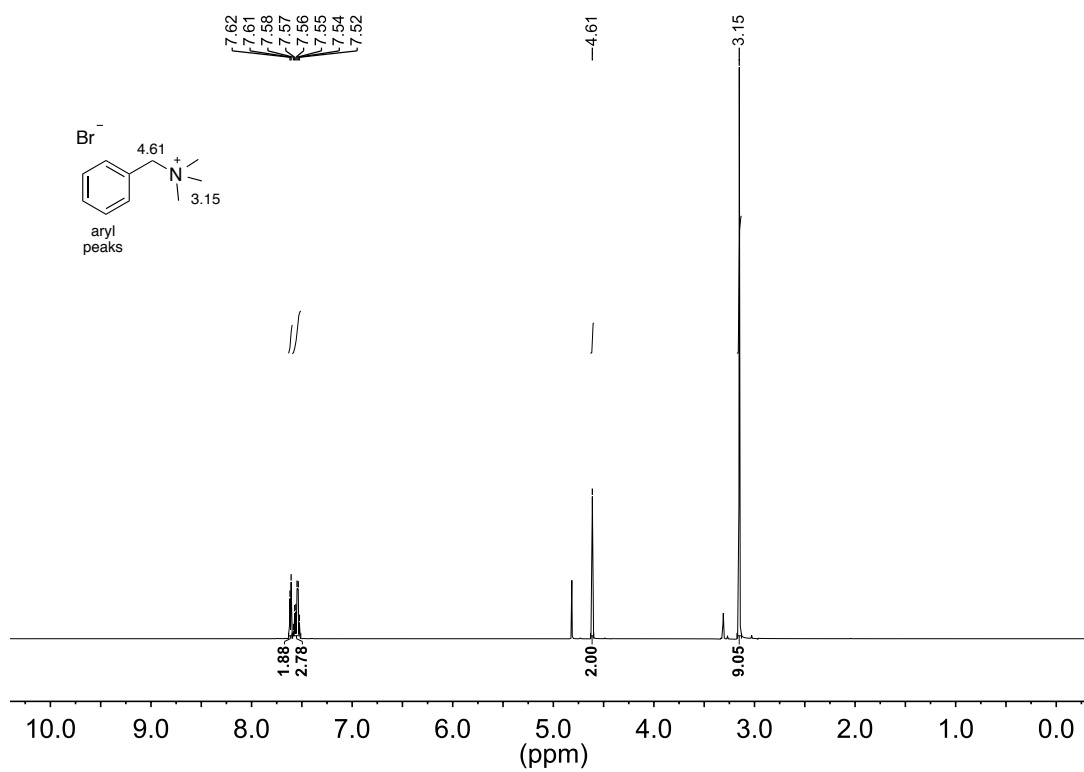


^{13}C NMR spectrum (126 MHz, CD_3OD)

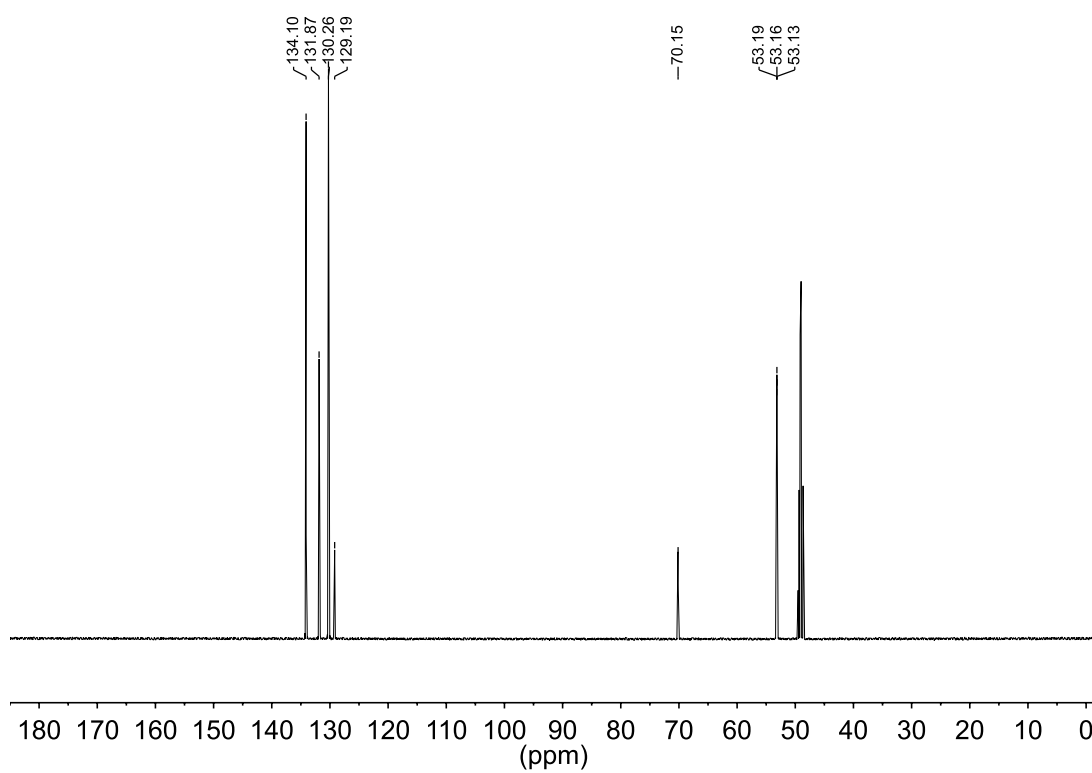


Benzyltrimethylammonium bromide (8)

^1H NMR spectrum (600 MHz, CD_3OD)

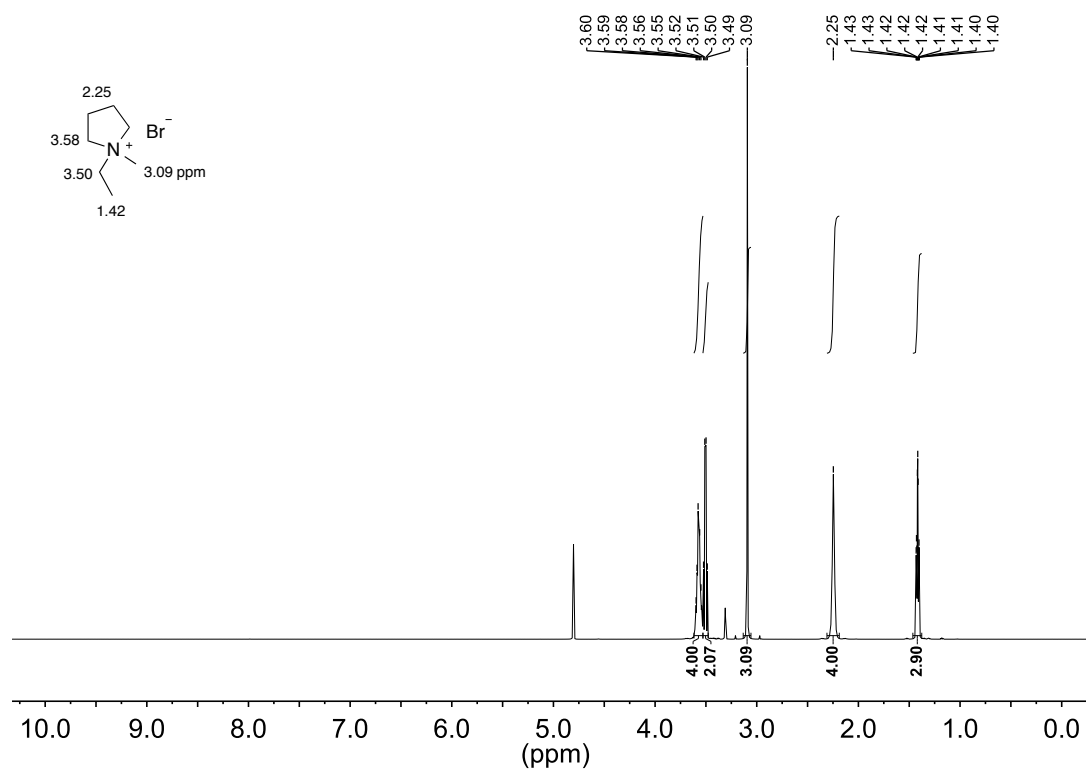


^{13}C NMR spectrum (126 MHz, CD_3OD)

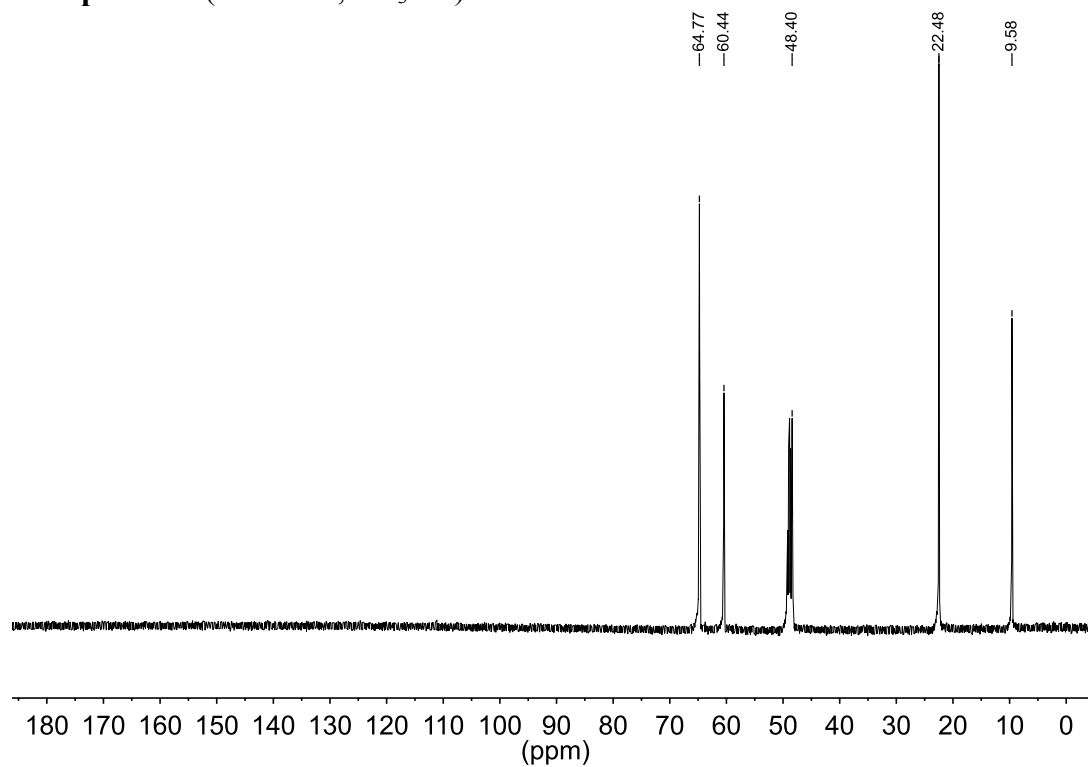


1-Ethyl-1-methylpyrrolidin-1-ium bromide (9)

^1H NMR spectrum (600 MHz, CD_3OD)

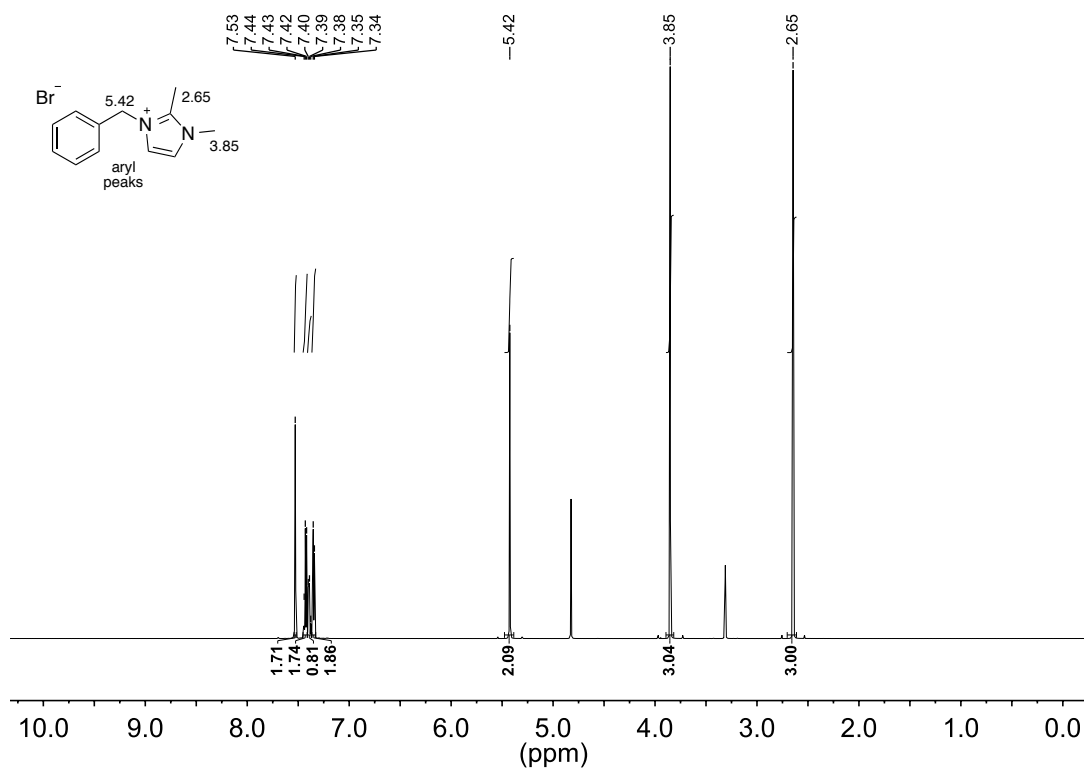


^{13}C NMR spectrum (126 MHz, CD_3OD)

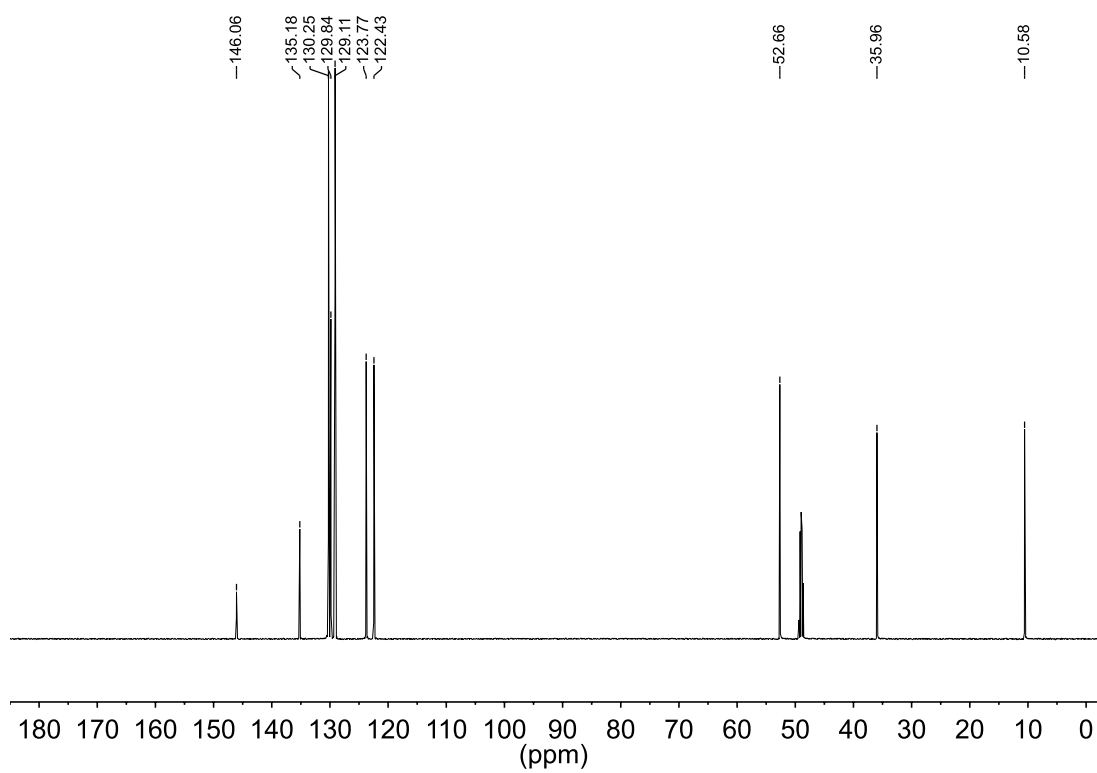


1-Benzyl-2,3-dimethylimidazolium bromide (10)

^1H NMR spectrum (600 MHz, CD_3OD)

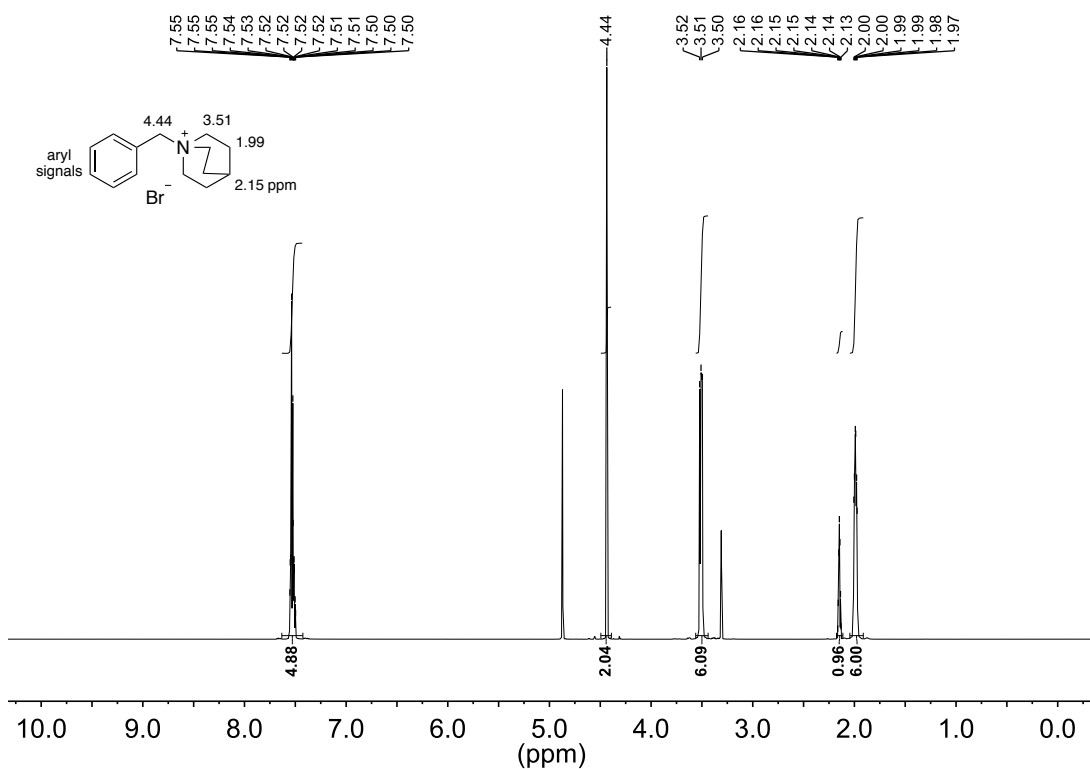


^{13}C NMR spectrum (126 MHz, CD_3OD)

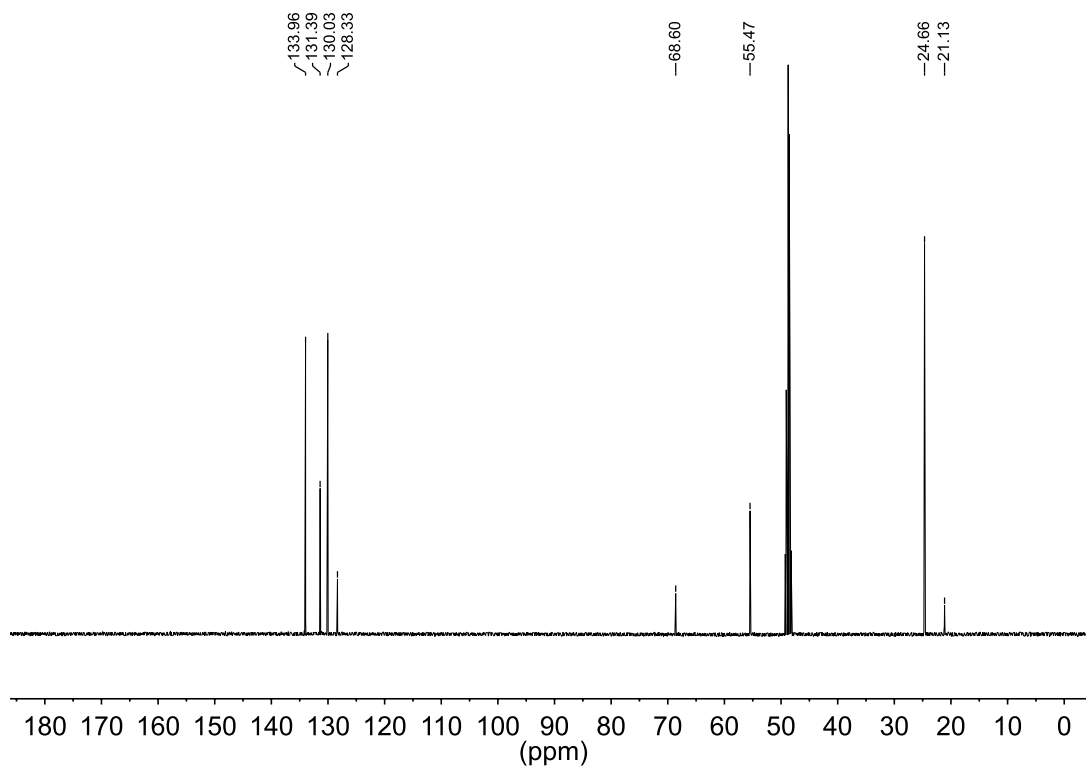


1-Benzylquinuclidin-1-ium bromide (11)

^1H NMR spectrum (600 MHz, CD_3OD)

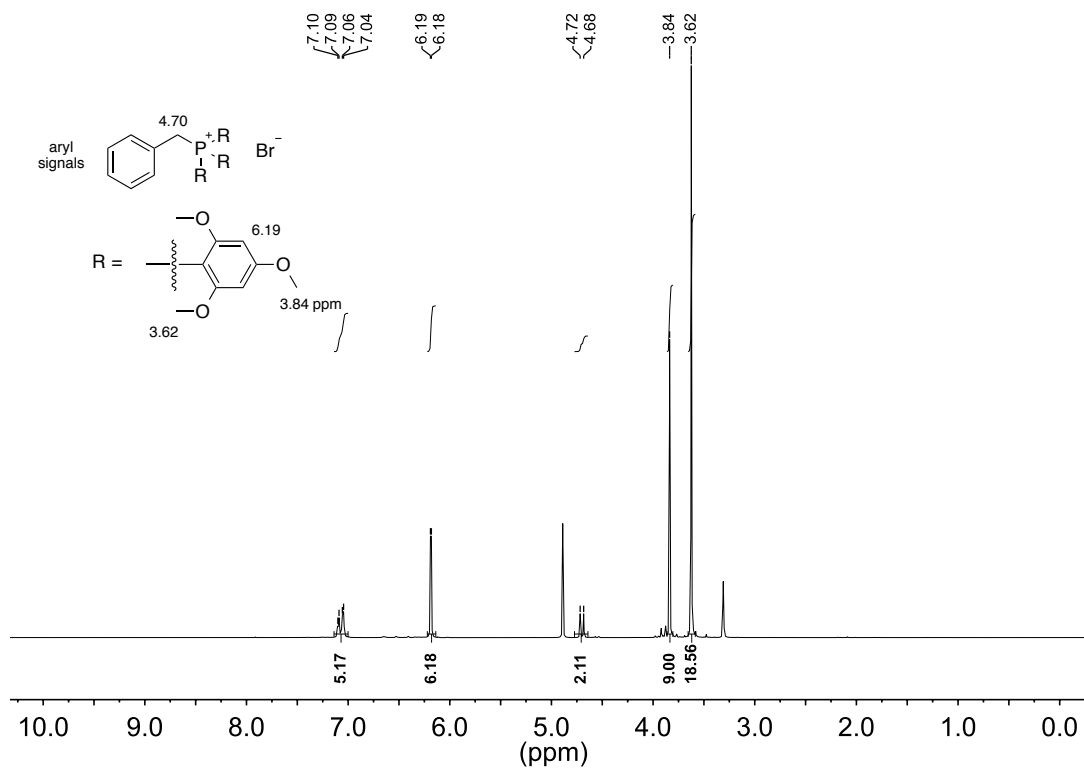


^{13}C NMR spectrum (126 MHz, CD_3OD)

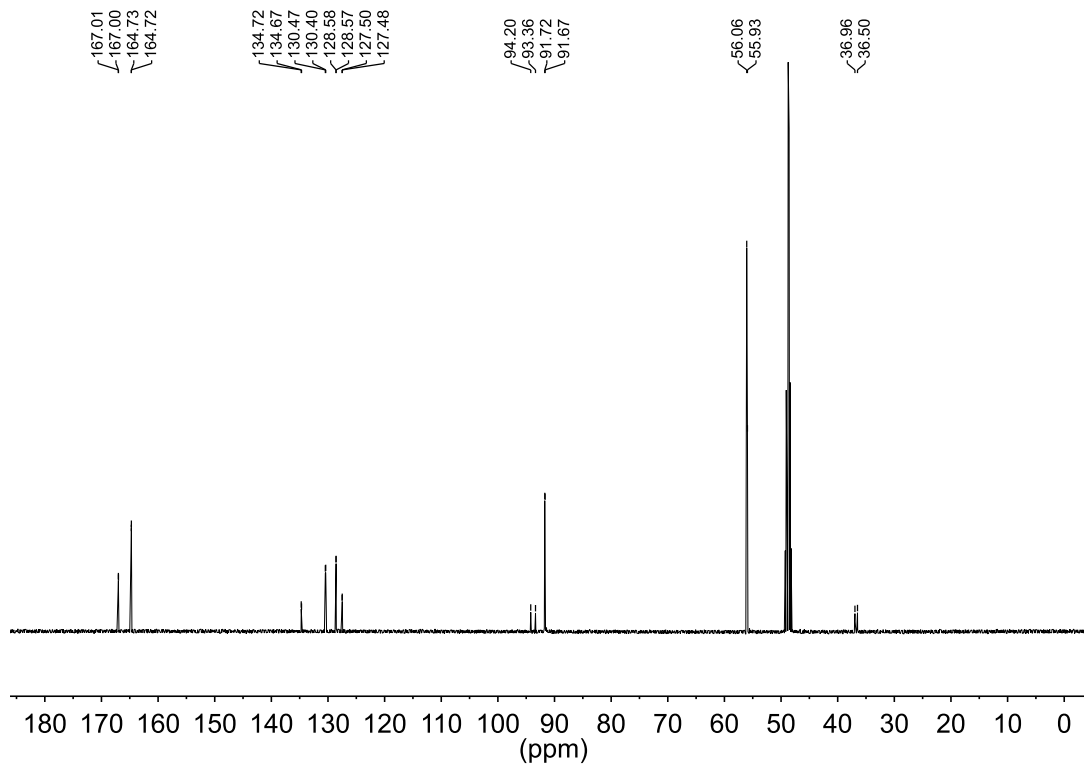


Benzyl-tris(2,4,6-trimethoxyphenyl)phosphonium bromide (12)

¹H NMR spectrum (500 MHz, CD₃OD)

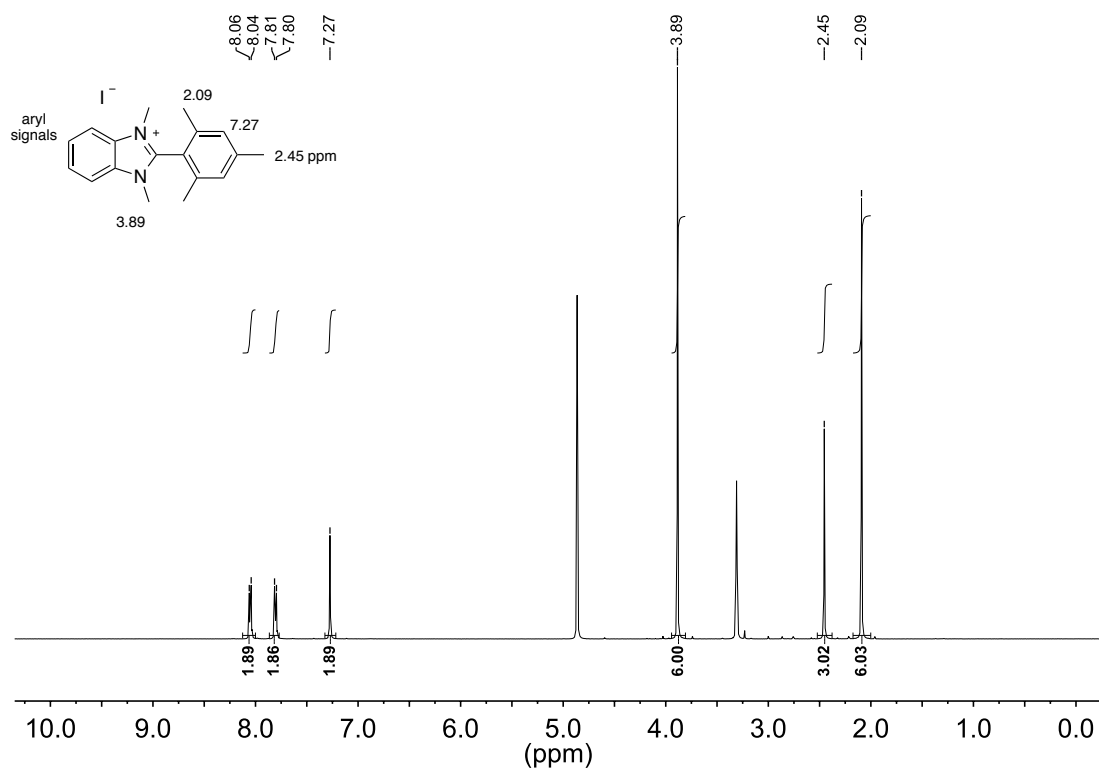


¹³C NMR spectrum (126 MHz, CD₃OD)

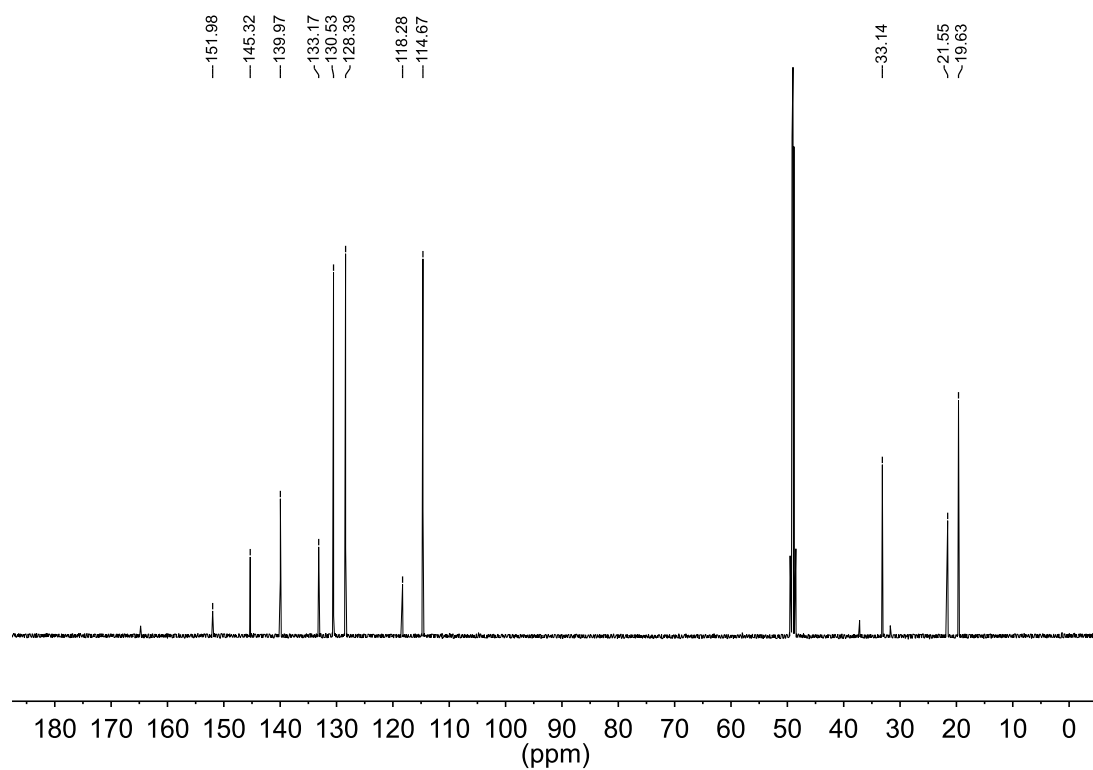


1,3-Dimethyl-2-mesityl-1*H*-benzimidazolium iodide (13)

^1H NMR spectrum (500 MHz, CD_3OD)

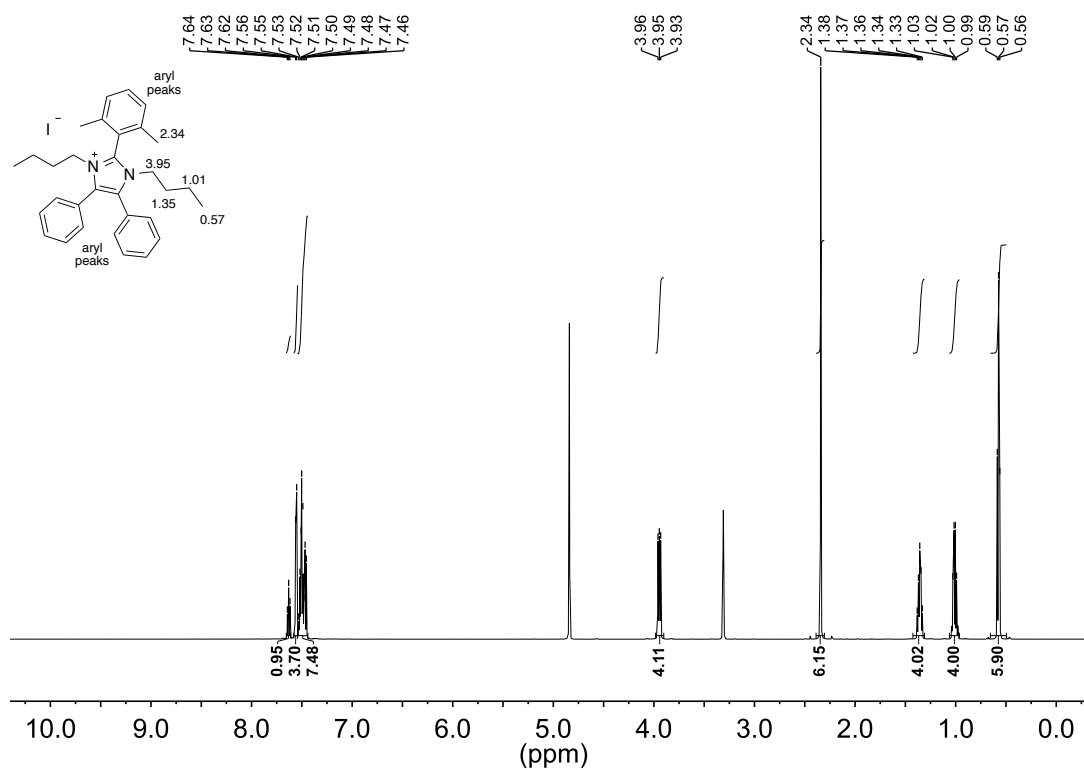


^{13}C NMR spectrum (126 MHz, CD_3OD)

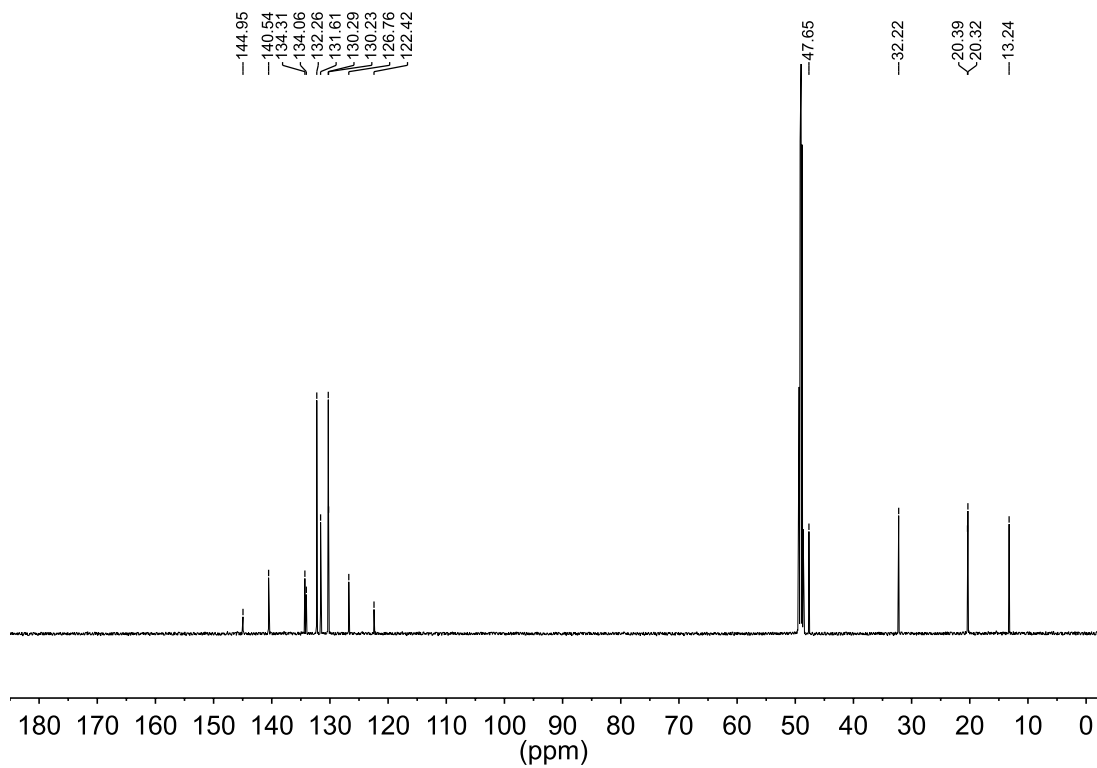


1,3-Di-*n*-butyl-2-(2,6-dimethylphenyl)-4,5-diphenylimidazolium iodide (14)

¹H NMR spectrum (600 MHz, CD₃OD)

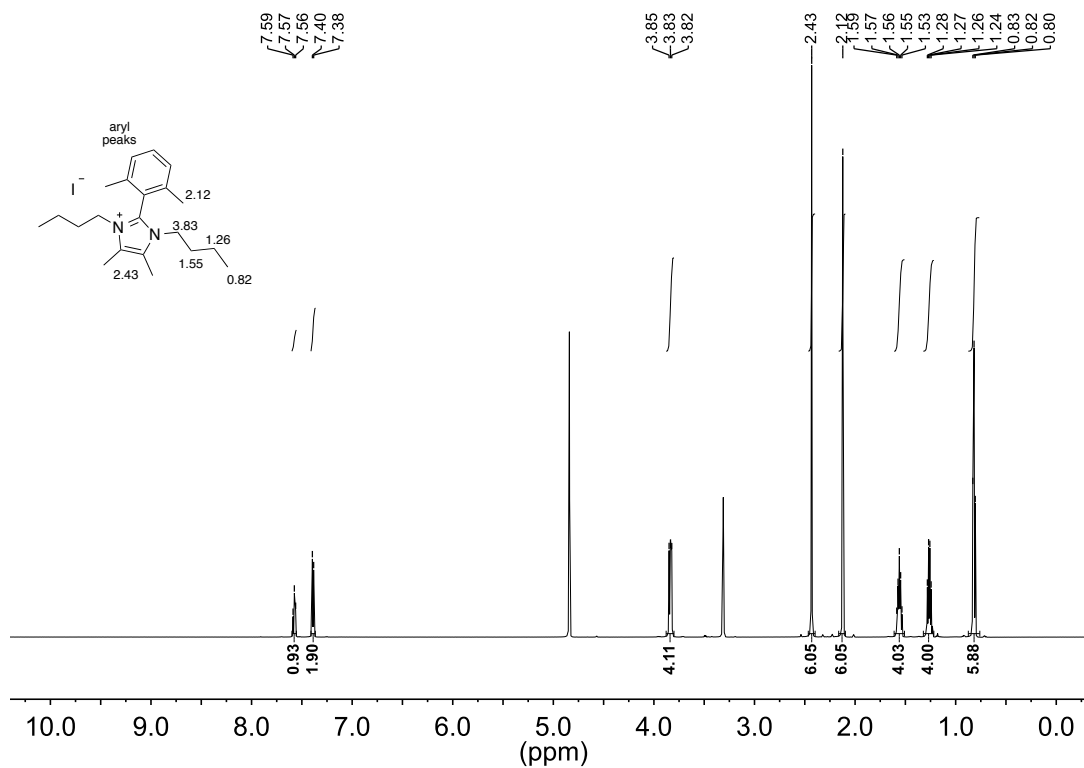


¹³C NMR spectrum (126 MHz, CD₃OD)

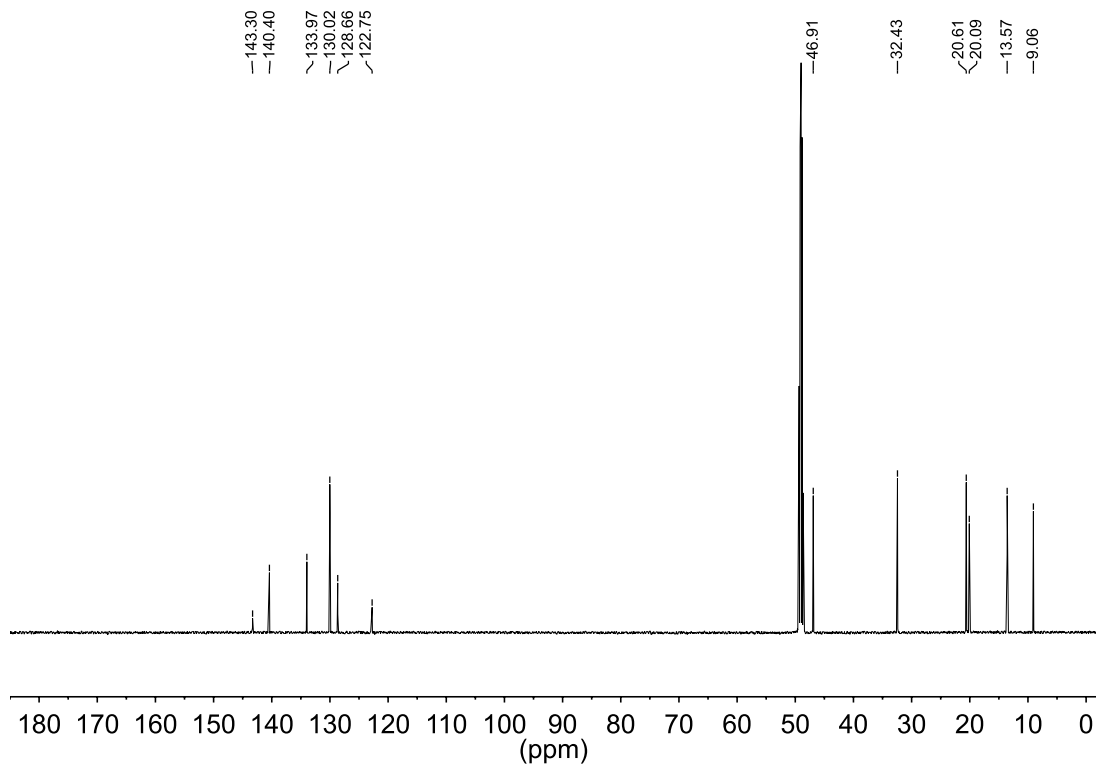


1,3-Di-*n*-butyl-2-(2,6-dimethylphenyl)-4,5-dimethylimidazolium iodide (15)

^1H NMR spectrum (600 MHz, CD_3OD)

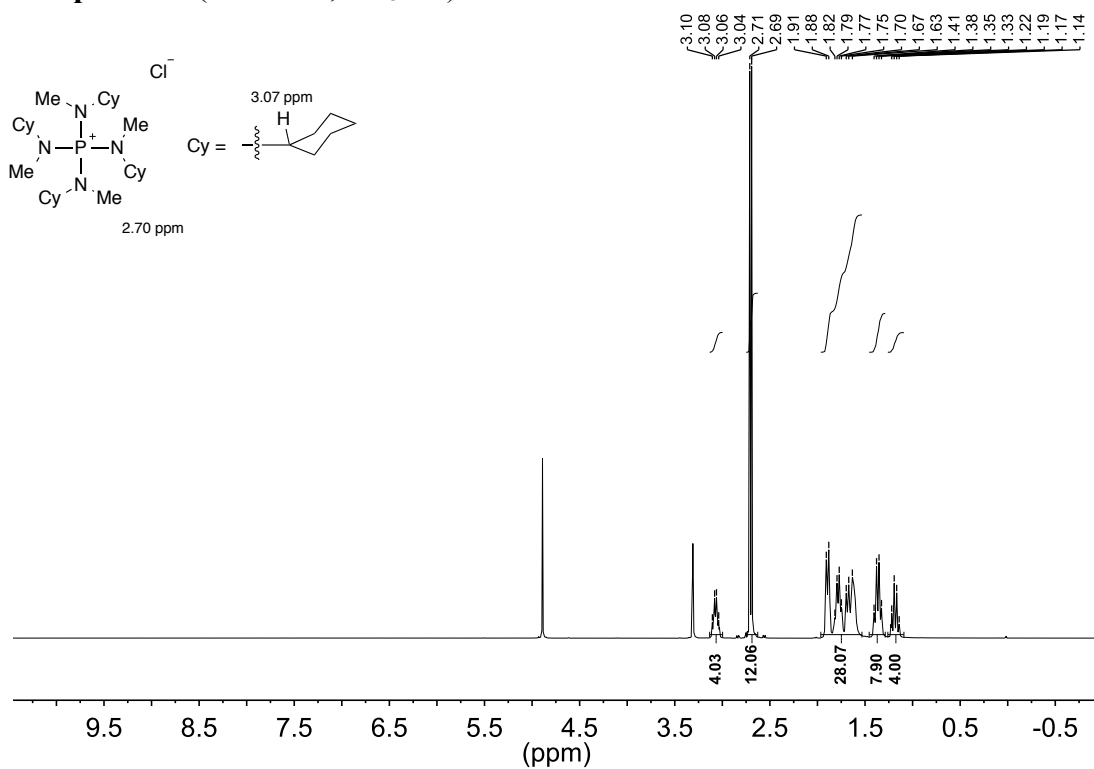


^{13}C NMR spectrum (126 MHz, CD_3OD)

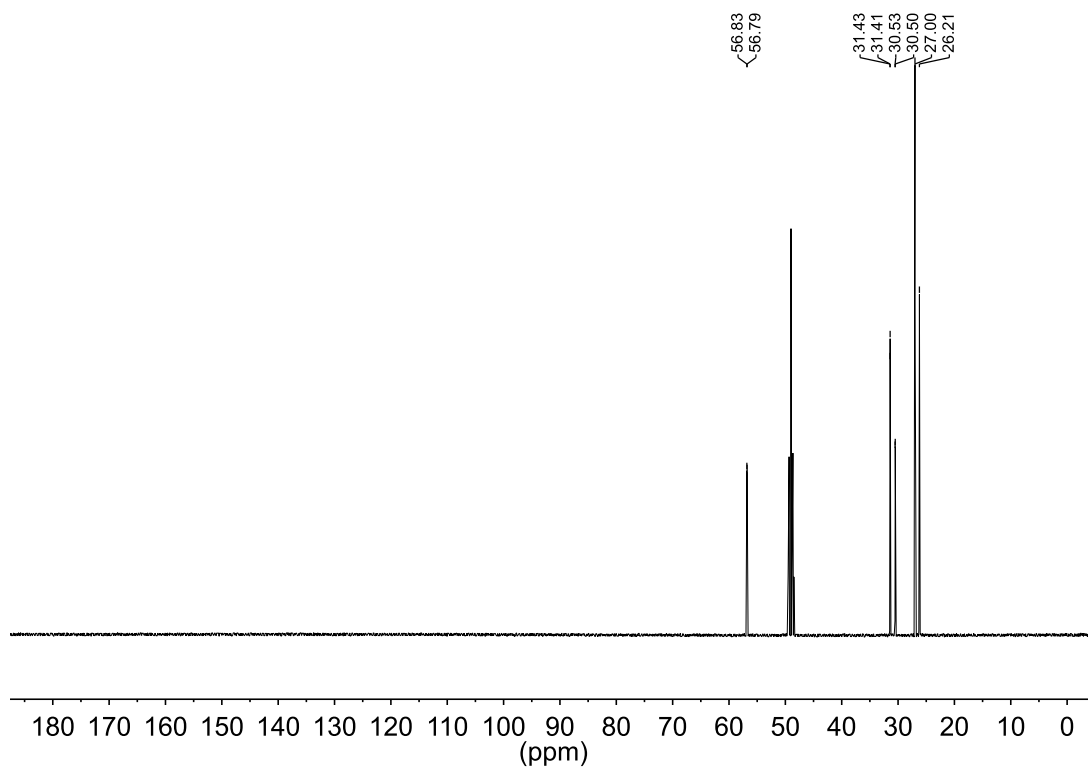


Tetrakis[cyclohexyl(methyl)amino]phosphonium chloride (16)

¹H NMR spectrum (500 MHz, CD₃OD)



¹³C NMR spectrum (126 MHz, CD₃OD)



3.5.5 Copies of ^1H NMR Spectra for Model Compound Studies, 1M KOH

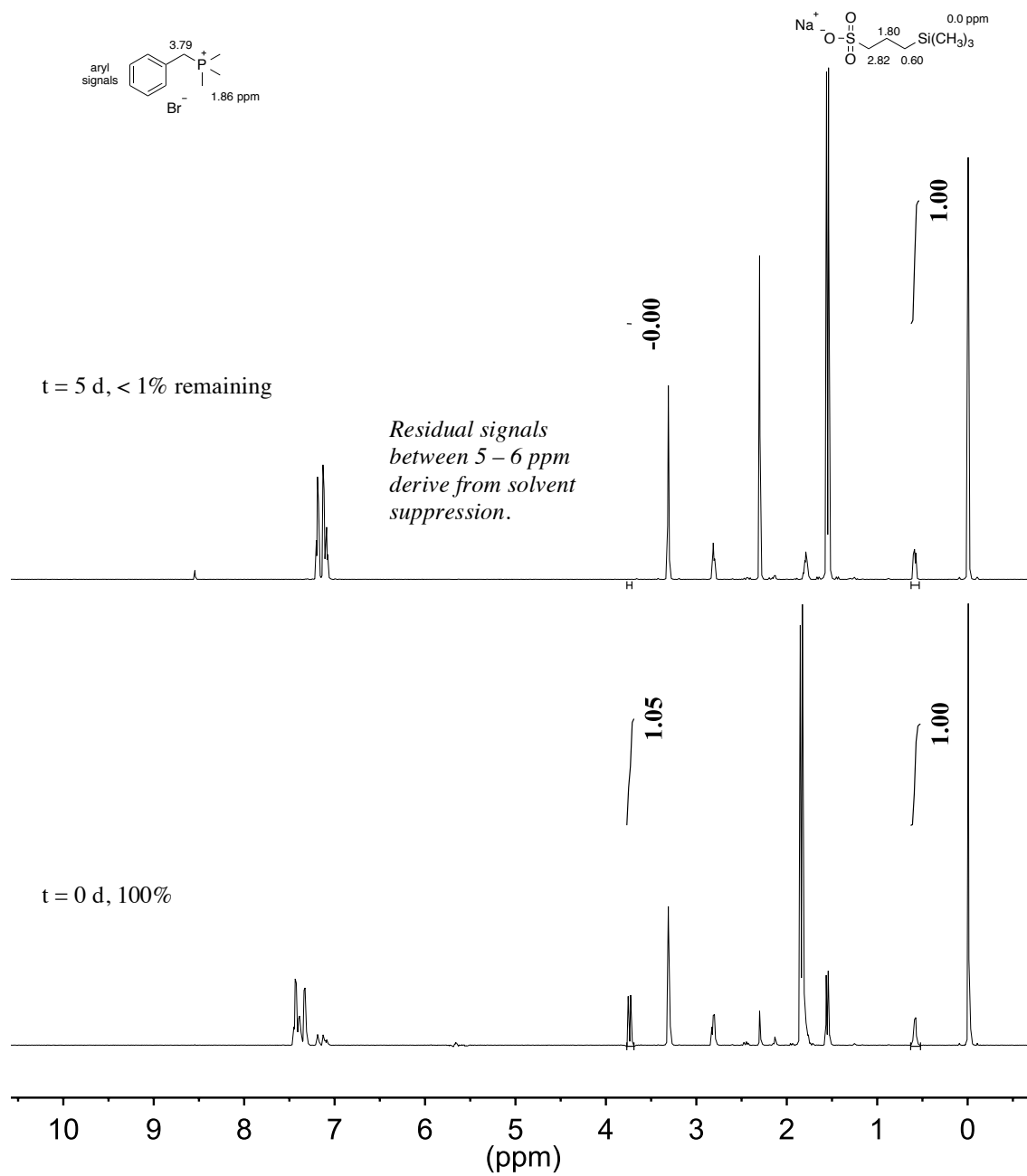


Figure 3.14 ^1H NMR spectra of **1** over 30 days dissolved in a basic CD_3OH solution at $80\text{ }^\circ\text{C}$ (1 M KOH, $[\text{KOH}]/[\textbf{1}] = 20$) with an internal standard ($\text{TMS}(\text{CH}_2)_3\text{SO}_3\text{Na}$).

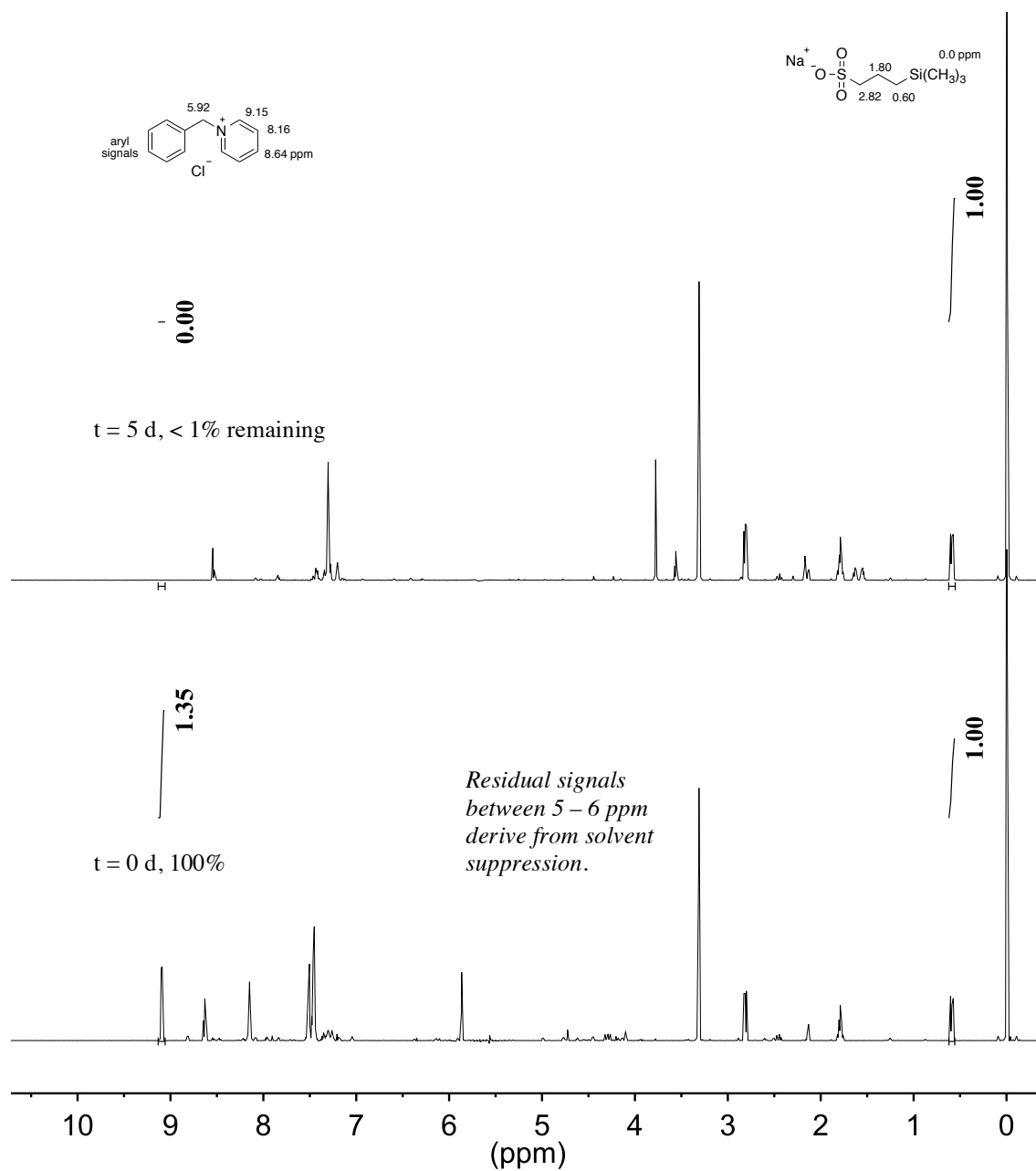


Figure 3.15 ¹H NMR spectra of **2** over 30 days dissolved in a basic CD₃OH solution at 80 °C (1 M KOH, [KOH]/[**2**] = 20) with an internal standard (TMS(CH₂)₃SO₃Na).

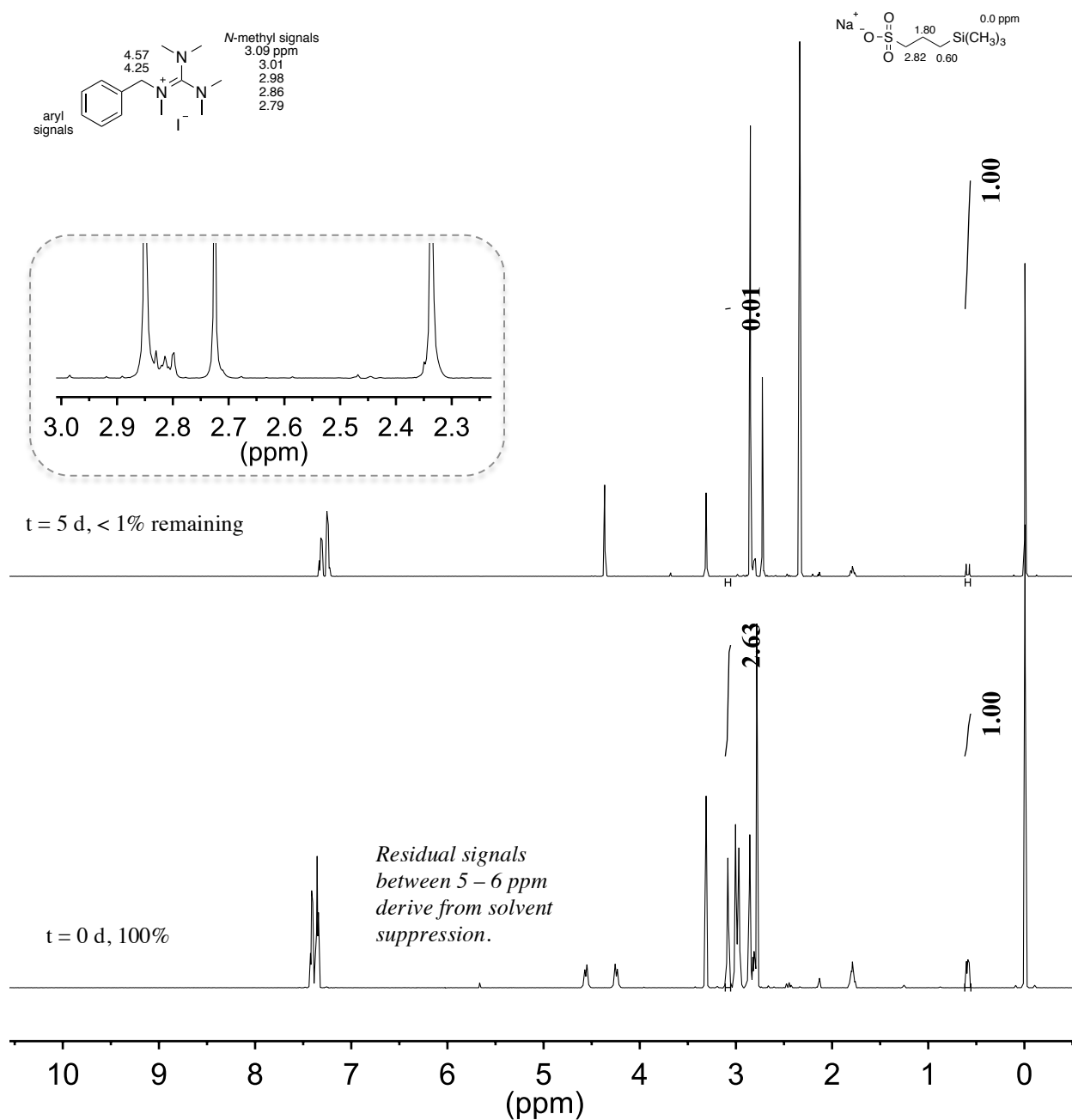


Figure 3.16 ^1H NMR spectra of **3** over 30 days dissolved in a basic CD_3OH solution at 80°C (1 M KOH, $[\text{KOH}]/[\mathbf{3}] = 20$) with an internal standard ($\text{TMS}(\text{CH}_2)_3\text{SO}_3\text{Na}$). Inset is extracted from $t = 5$ d.

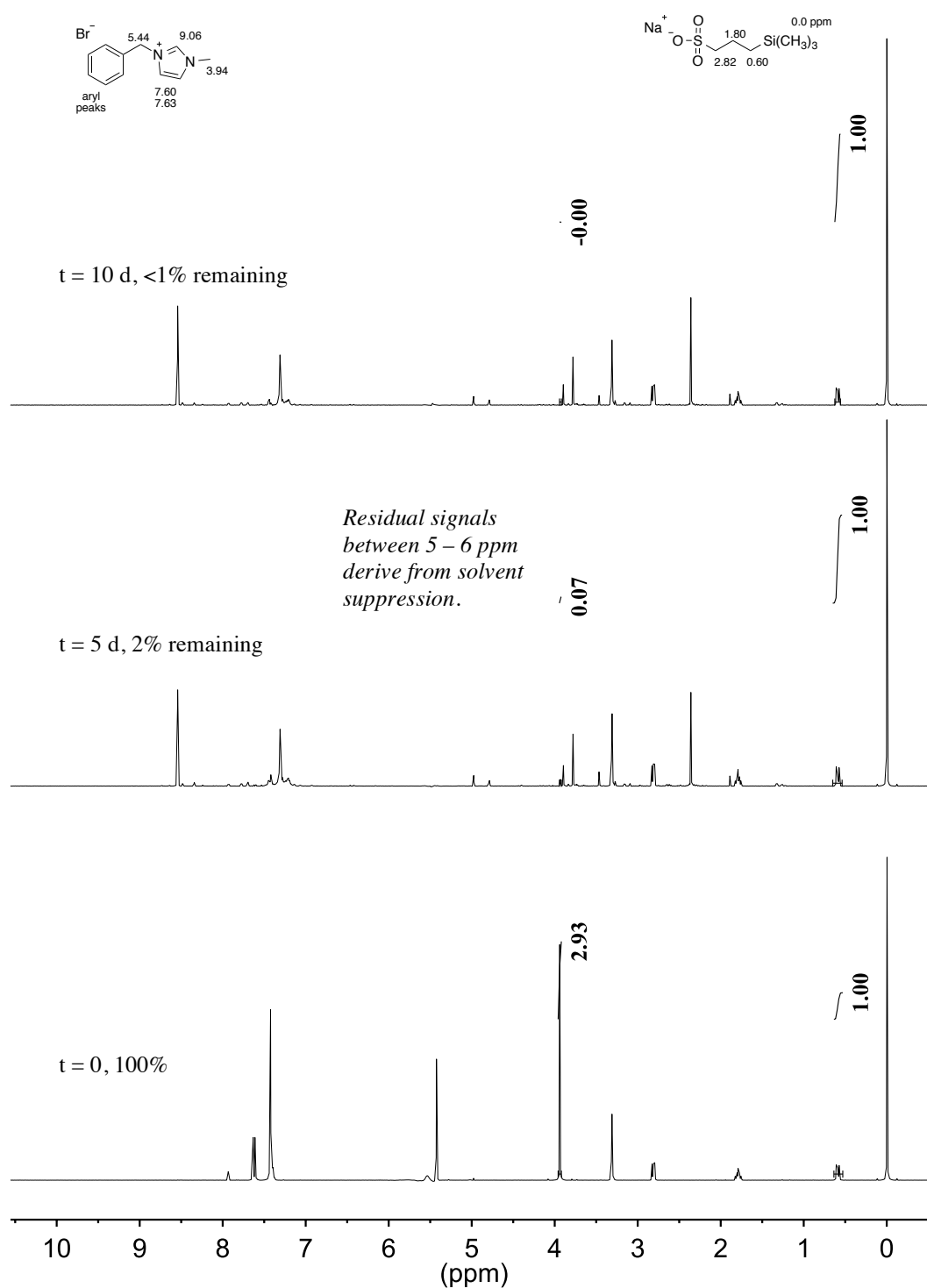


Figure 3.17 ^1H NMR spectra of **4** over 10 days dissolved in a basic CD_3OH solution at $80\text{ }^\circ\text{C}$ (1 M KOH, $[\text{KOH}]/[\textbf{4}] = 20$) with an internal standard ($\text{TMS}(\text{CH}_2)_3\text{SO}_3\text{Na}$).

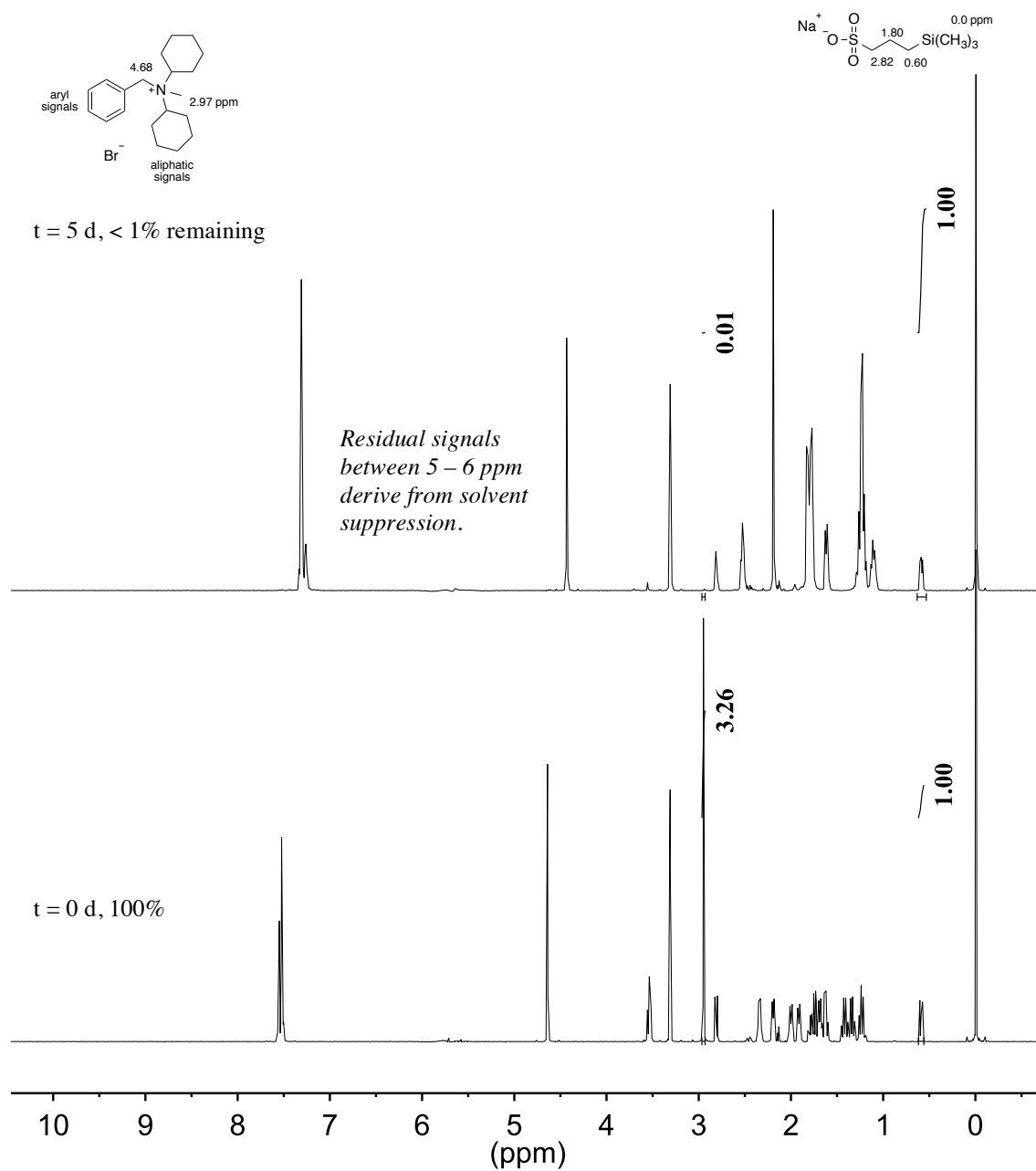


Figure 3.18 ^1H NMR spectra of **5** over 30 days dissolved in a basic CD_3OH solution at 80°C (1 M KOH, $[\text{KOH}]/[\mathbf{5}] = 20$) with an internal standard ($\text{TMS}(\text{CH}_2)_3\text{SO}_3\text{Na}$).

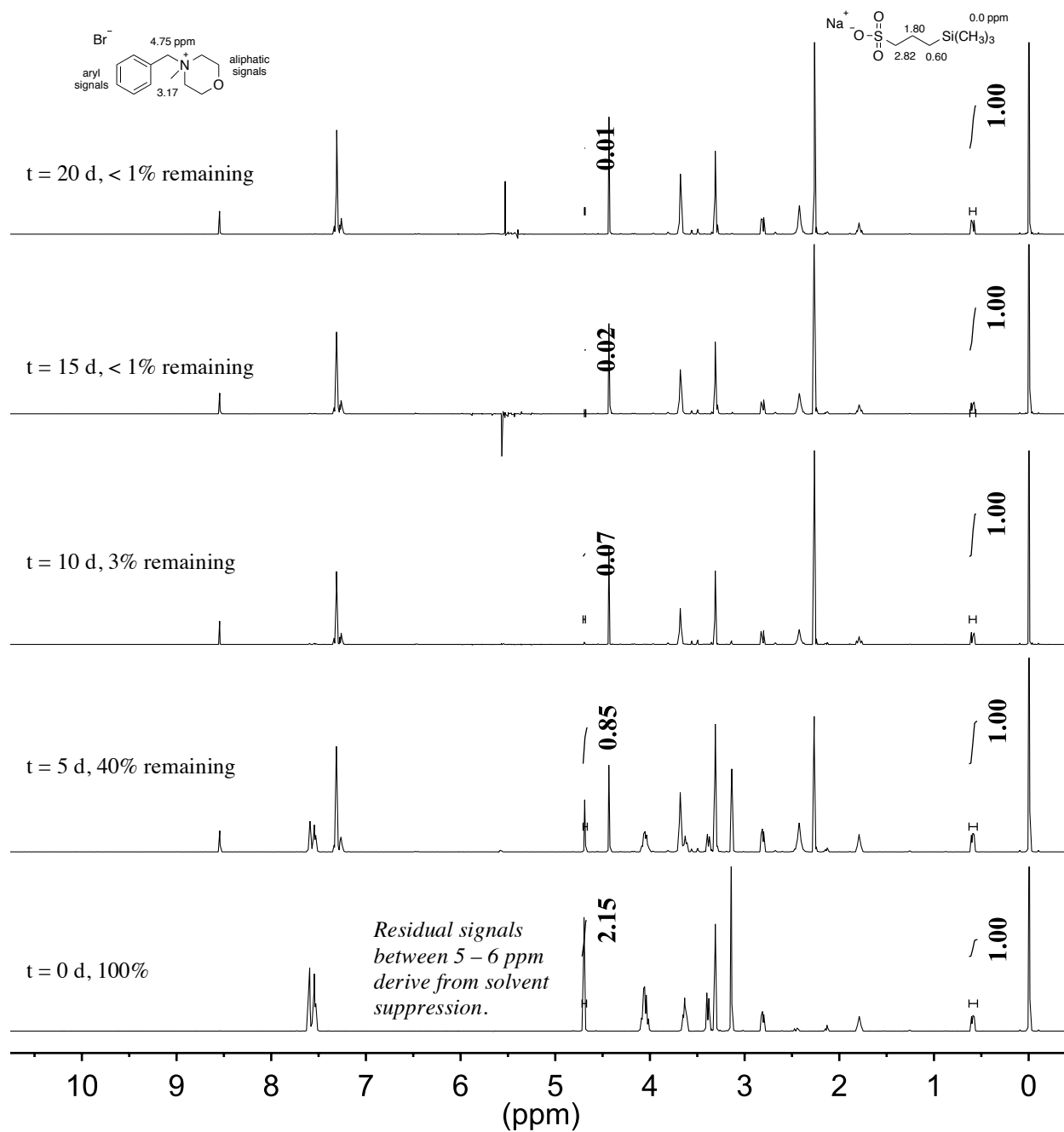


Figure 3.19. ^1H NMR spectra of **6** over 30 days dissolved in a basic CD_3OH solution at 80°C (1 M KOH, $[\text{KOH}]/[\mathbf{6}] = 20$) with an internal standard ($\text{TMS}(\text{CH}_2)_3\text{SO}_3\text{Na}$).

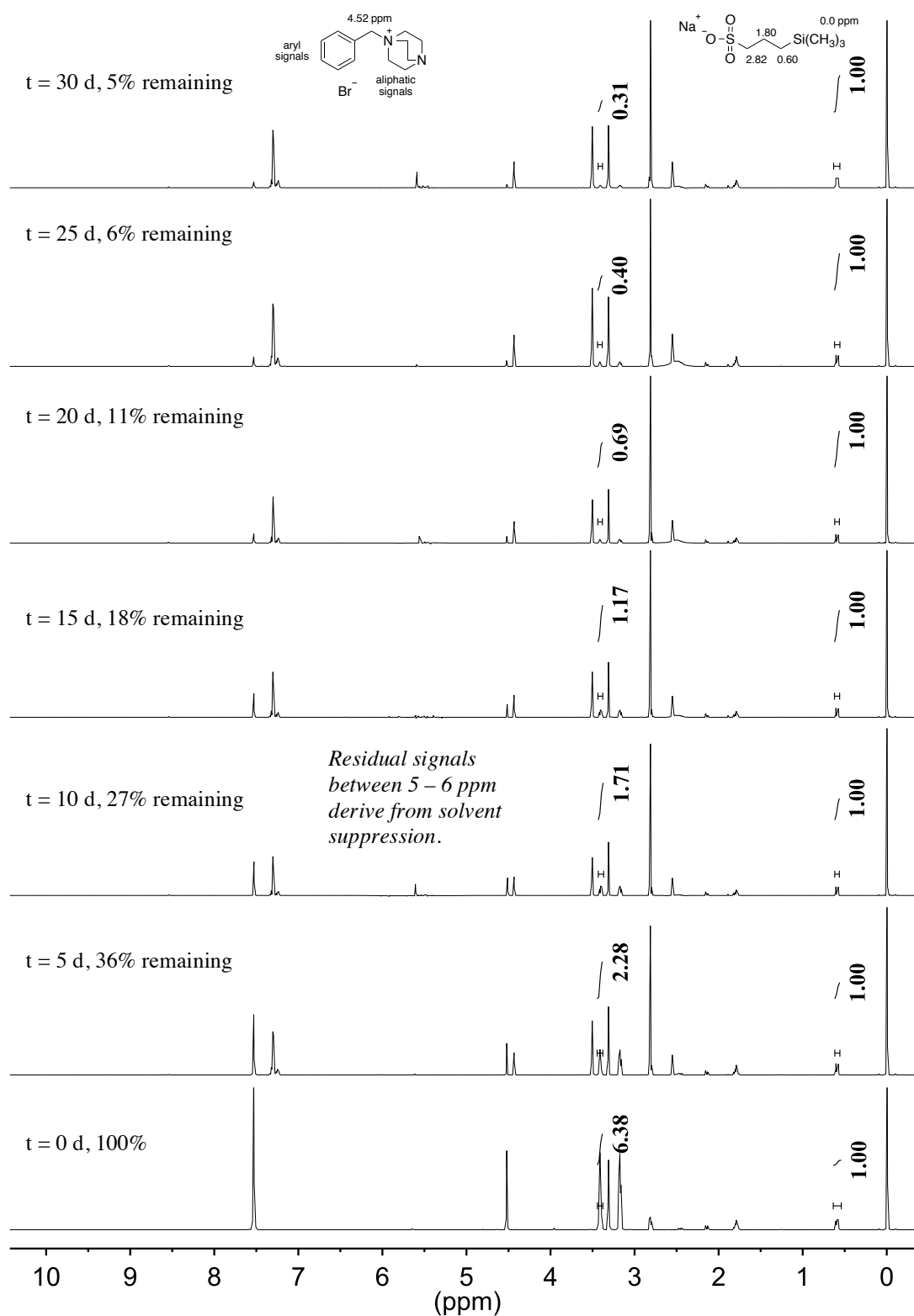


Figure 3.20 ¹H NMR spectra of **7** over 30 days dissolved in a basic CD₃OH solution at 80 °C (1 M KOH, [KOH]/[**7**] = 20) with an internal standard (TMS(CH₂)₃SO₃Na).

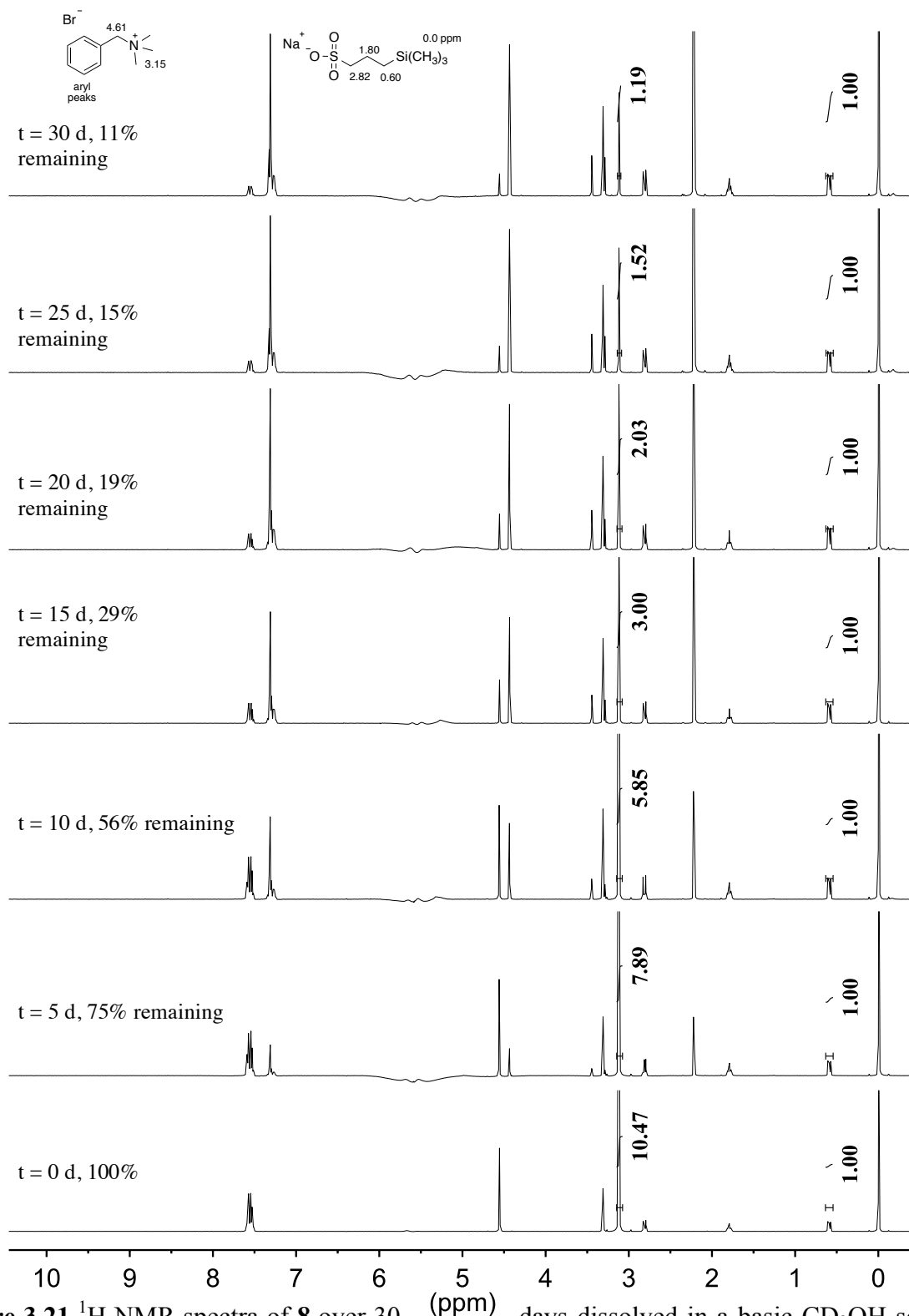


Figure 3.21 ^1H NMR spectra of **8** over 30 days dissolved in a basic CD_3OH solution at 80°C (1 M KOH, $[\text{KOH}]/[\mathbf{8}] = 20$ with an internal standard $\text{TMS}(\text{CH}_2)_3\text{SO}_3\text{Na}$).

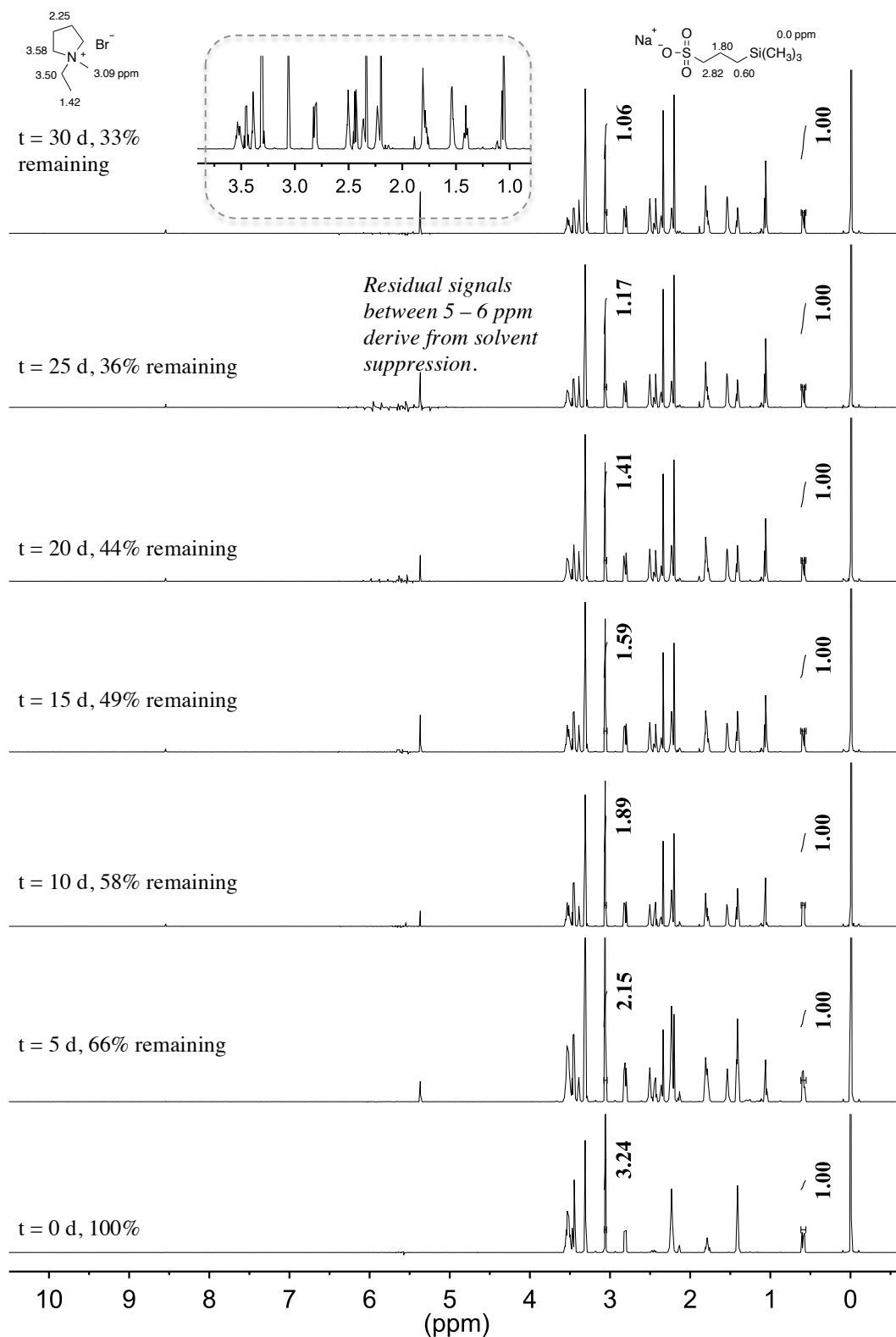


Figure 3.22 ¹H NMR spectra of **9** over 30 days dissolved in a basic CD₃OH solution at 80 °C (1 M KOH, [KOH]/[**9**] = 20) with an internal standard (TMS(CH₂)₃SO₃Na). Inset is extracted from t = 30 d.

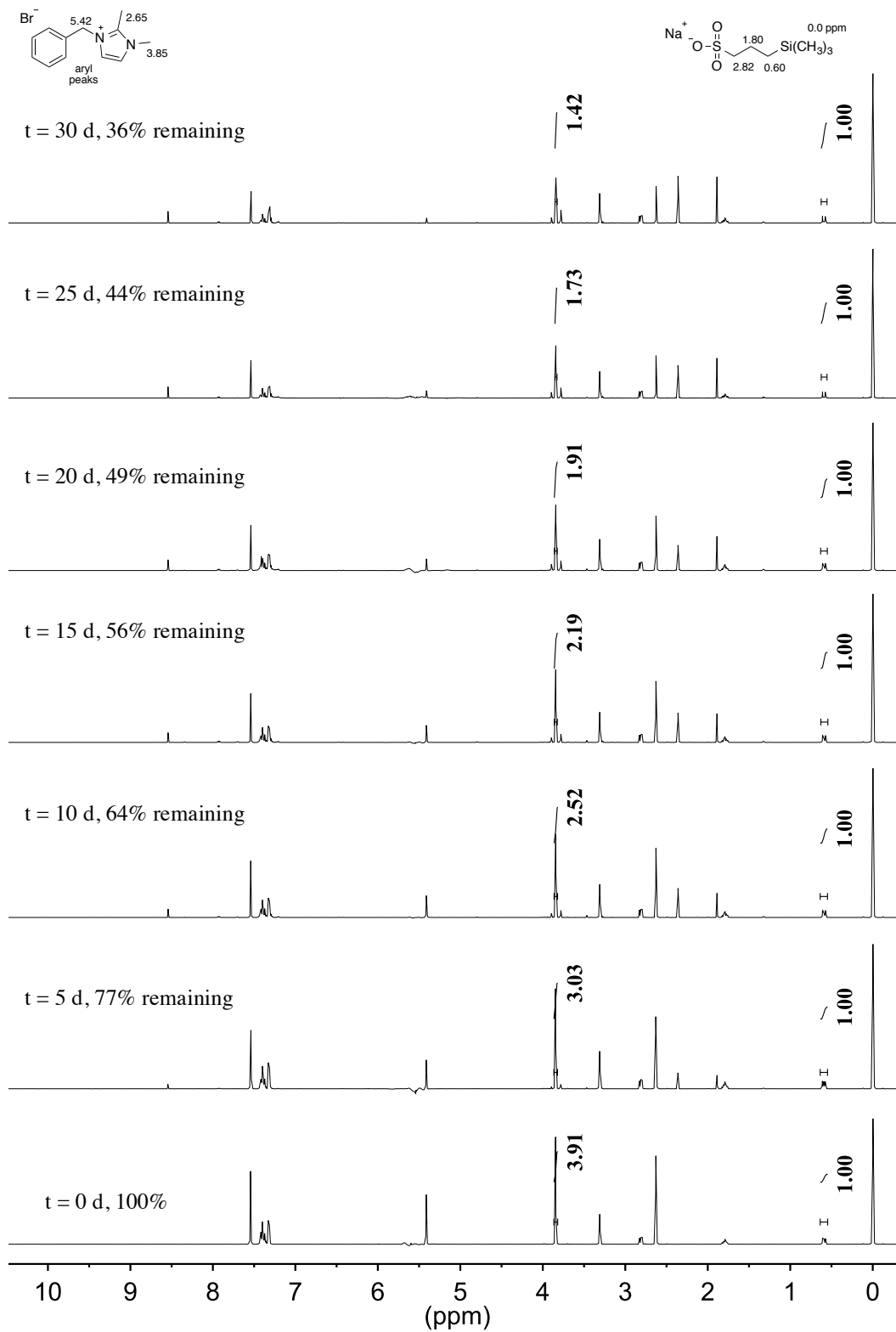


Figure 3.23 ^1H NMR spectra of **10** over 30 days dissolved in a basic CD_3OH solution at $80\text{ }^\circ\text{C}$ (1 M KOH , $[\text{KOH}]/[\text{10}] = 20$) with an internal standard ($\text{TMS}(\text{CH}_2)_3\text{SO}_3\text{Na}$).

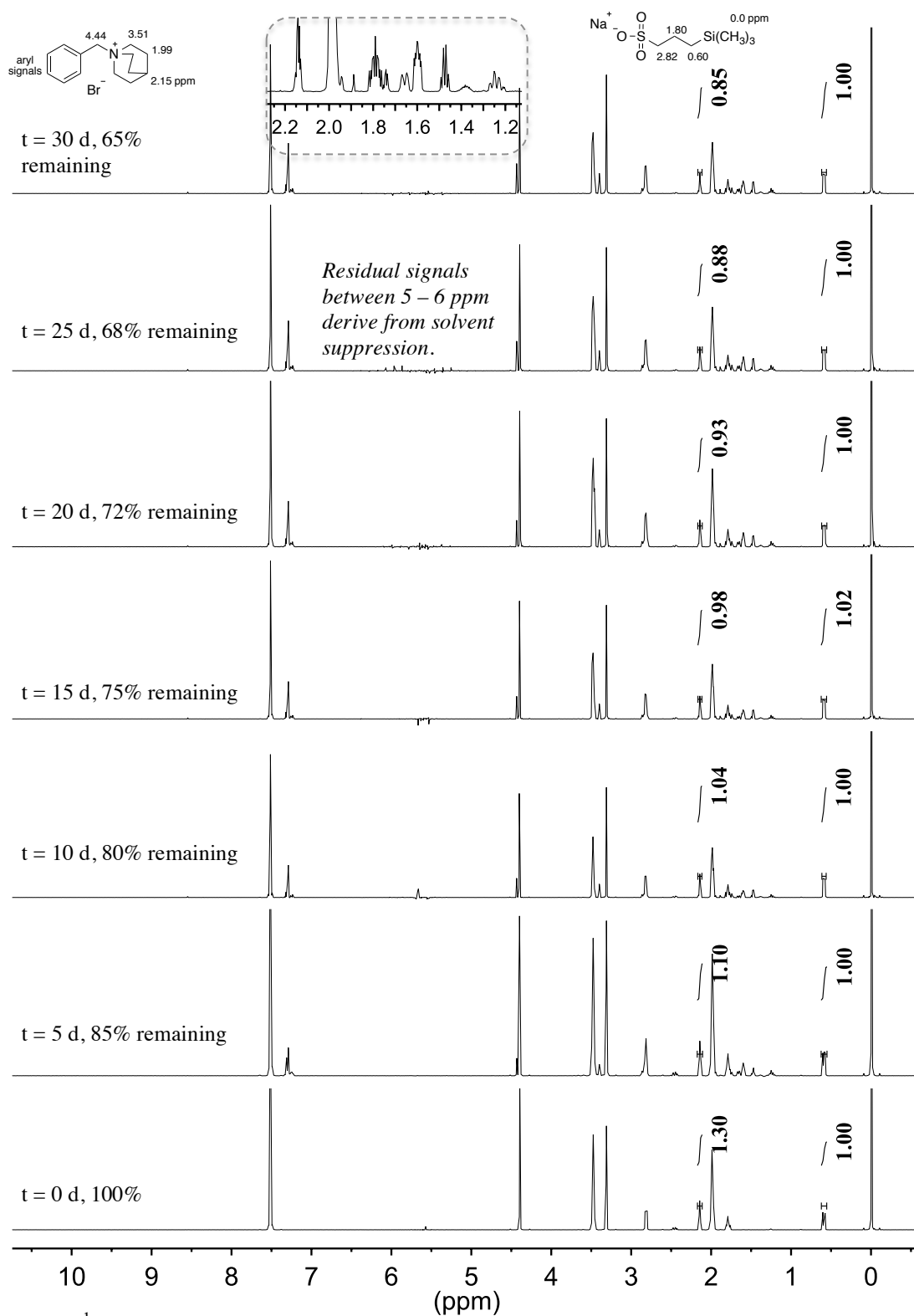


Figure 3.24 ¹H NMR spectra of **11** over 30 days dissolved in a basic CD₃OH solution at 80 °C (1 M KOH, [KOH]/[**11**] = 20) with an internal standard (TMS(CH₂)₃SO₃Na). Inset is extracted from t = 30 d.

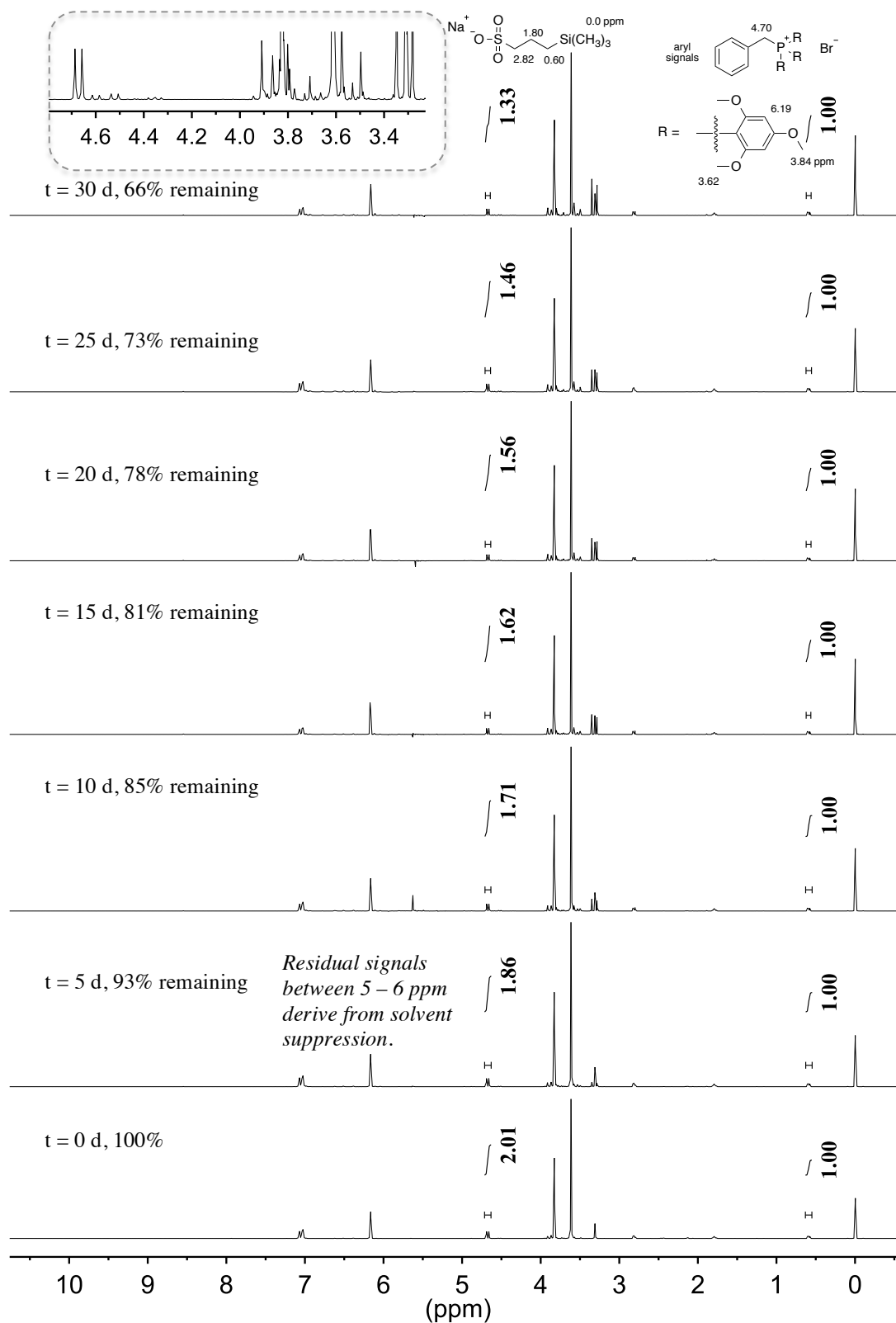


Figure 3.25 ^1H NMR spectra of **12** over 30 days dissolved in a basic CD_3OH solution at 80°C (1 M KOH, $[\text{KOH}]/[\text{12}] = 20$) with an internal standard ($\text{TMS}(\text{CH}_2)_3\text{SO}_3\text{Na}$). Inset is extracted from $t = 30$ d.

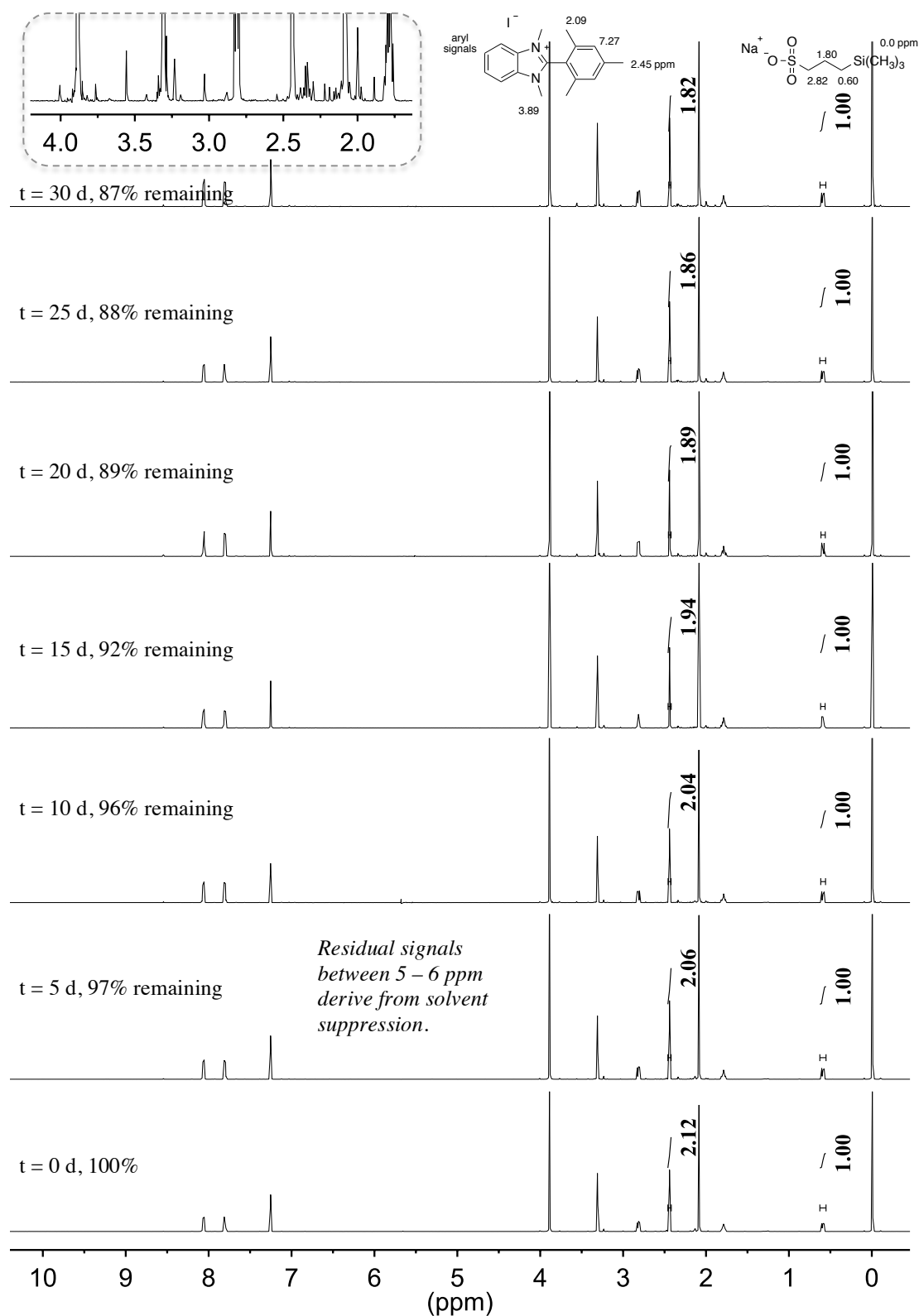


Figure 3.26 ^1H NMR spectra of **13** over 30 days dissolved in a basic CD_3OH solution at 80°C (1 M KOH, $[\text{KOH}]/[\textbf{13}] = 20$) with an internal standard ($\text{TMS}(\text{CH}_2)_3\text{SO}_3\text{Na}$). Inset is extracted from $t = 30$ d. ($\text{TMS}(\text{CH}_2)_3\text{SO}_3\text{Na}$).

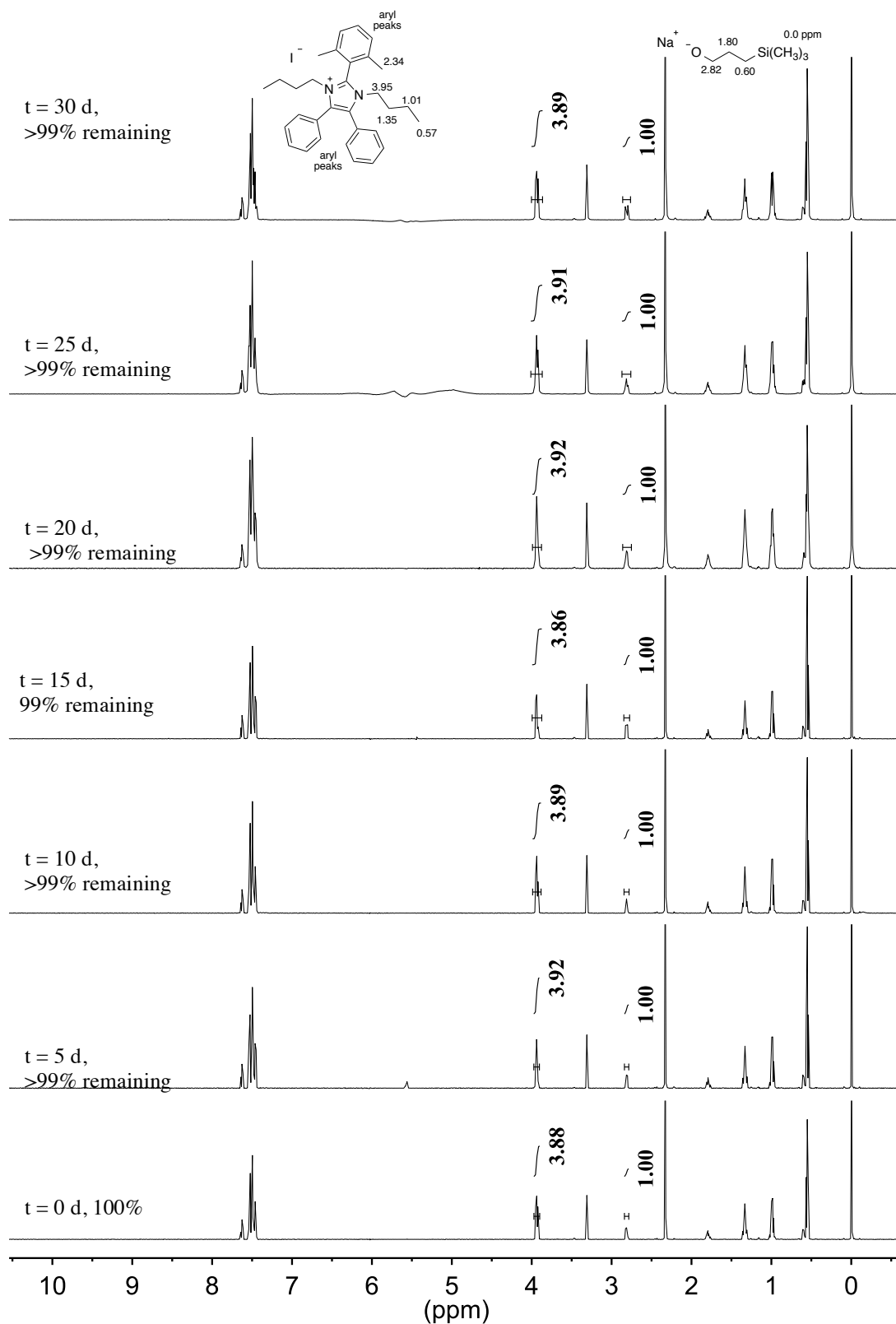


Figure 3.27 ¹H NMR spectra of **14** over 30 days dissolved in a basic CD₃OH solution at 80 °C (1 M KOH, [KOH]/[**14**] = 20) with an internal standard (TMS(CH₂)₃SO₃Na).

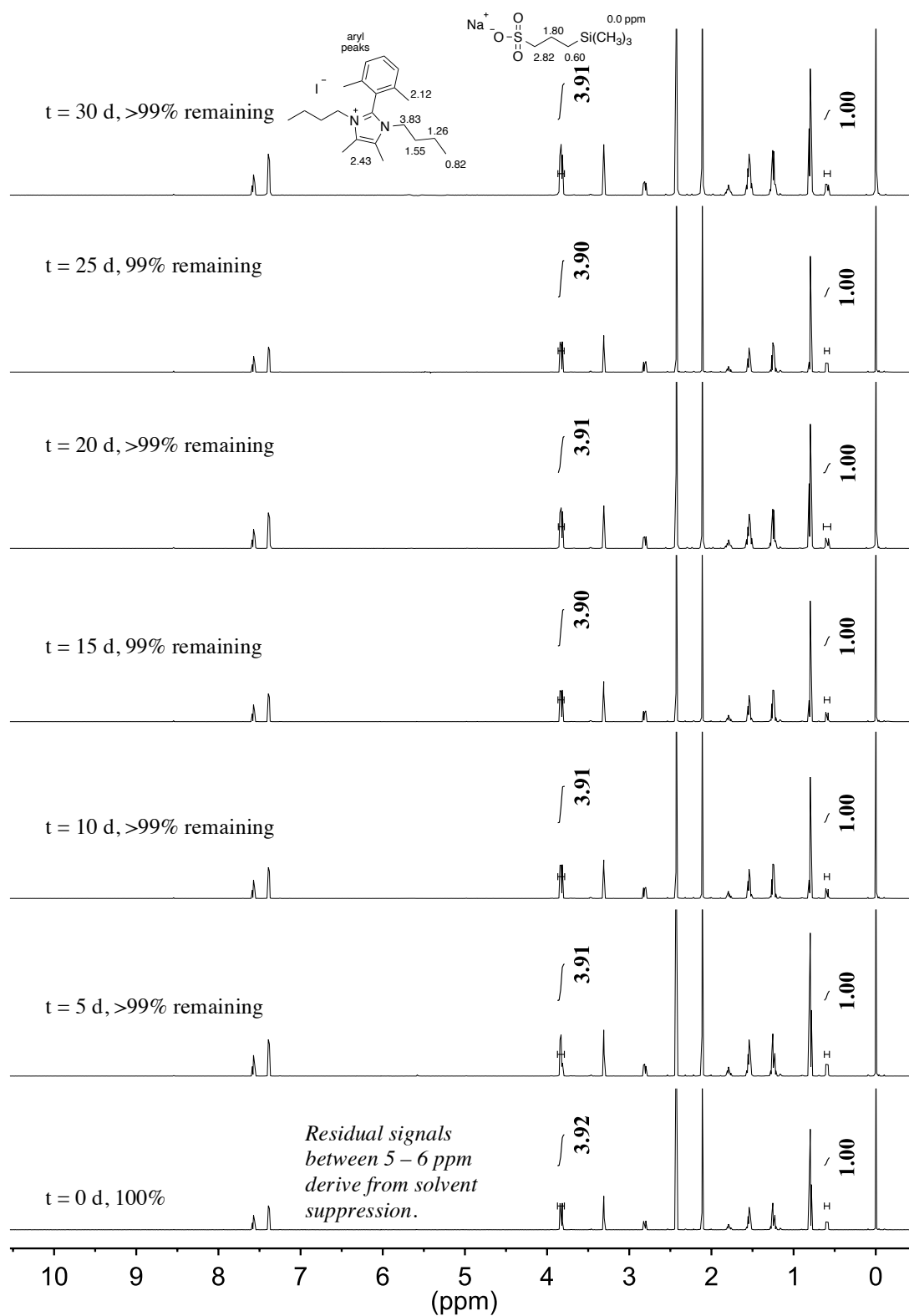


Figure 3.28 ^1H NMR spectra of **15** over 30 days dissolved in a basic CD_3OH solution at 80°C (1 M KOH, $[\text{KOH}]/[\text{15}] = 20$) with an internal standard ($\text{TMS}(\text{CH}_2)_3\text{SO}_3\text{Na}$).

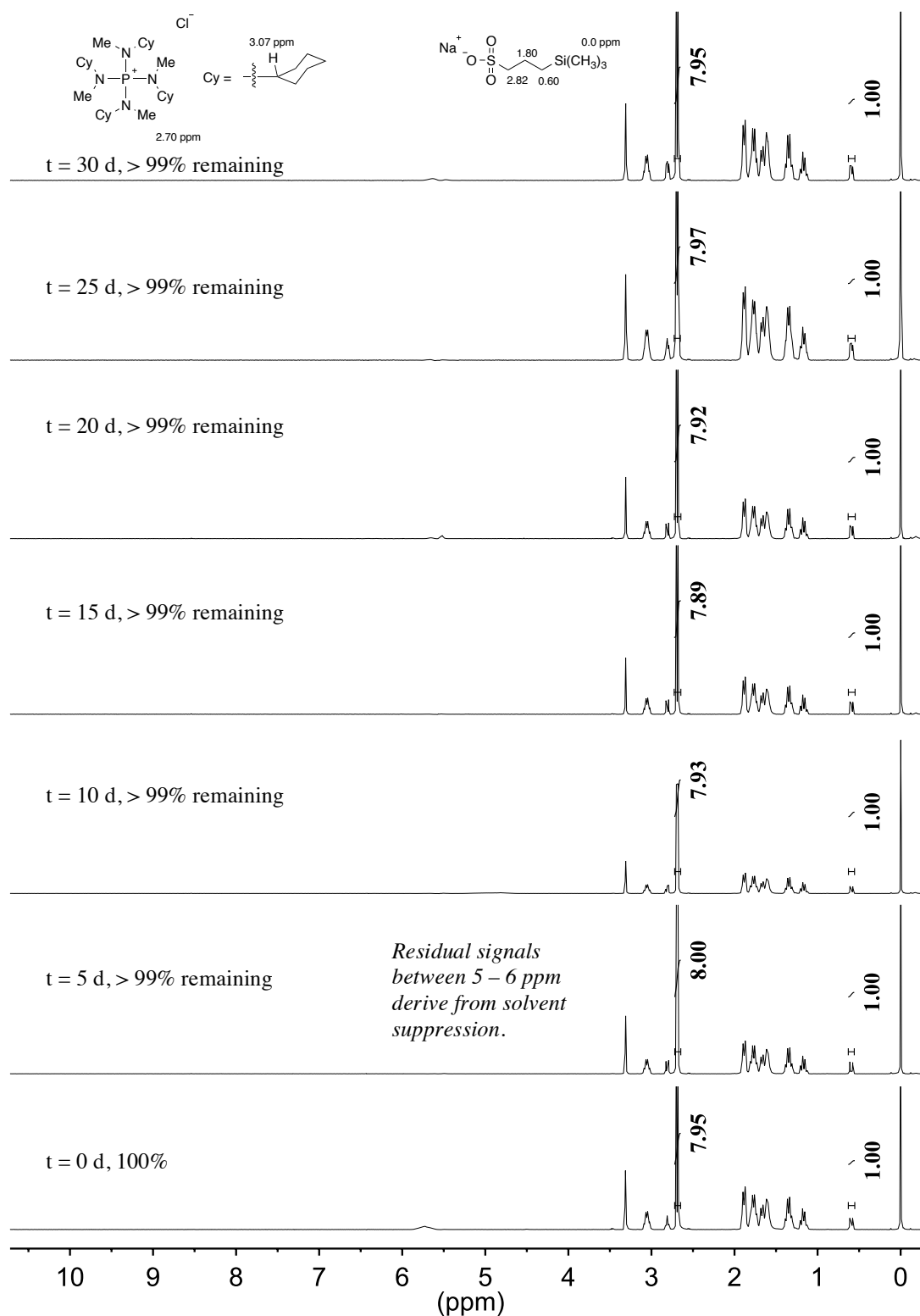


Figure 3.29 ^1H NMR spectra of **16** over 30 days dissolved in a basic CD_3OH solution at 80°C (1 M KOH, $[\text{KOH}]/[\text{16}] = 20$) with an internal standard ($\text{TMS}(\text{CH}_2)_3\text{SO}_3\text{Na}$).

3.5.6 Copies of ^1H NMR Spectra for Model Compound Studies, 2M KOH

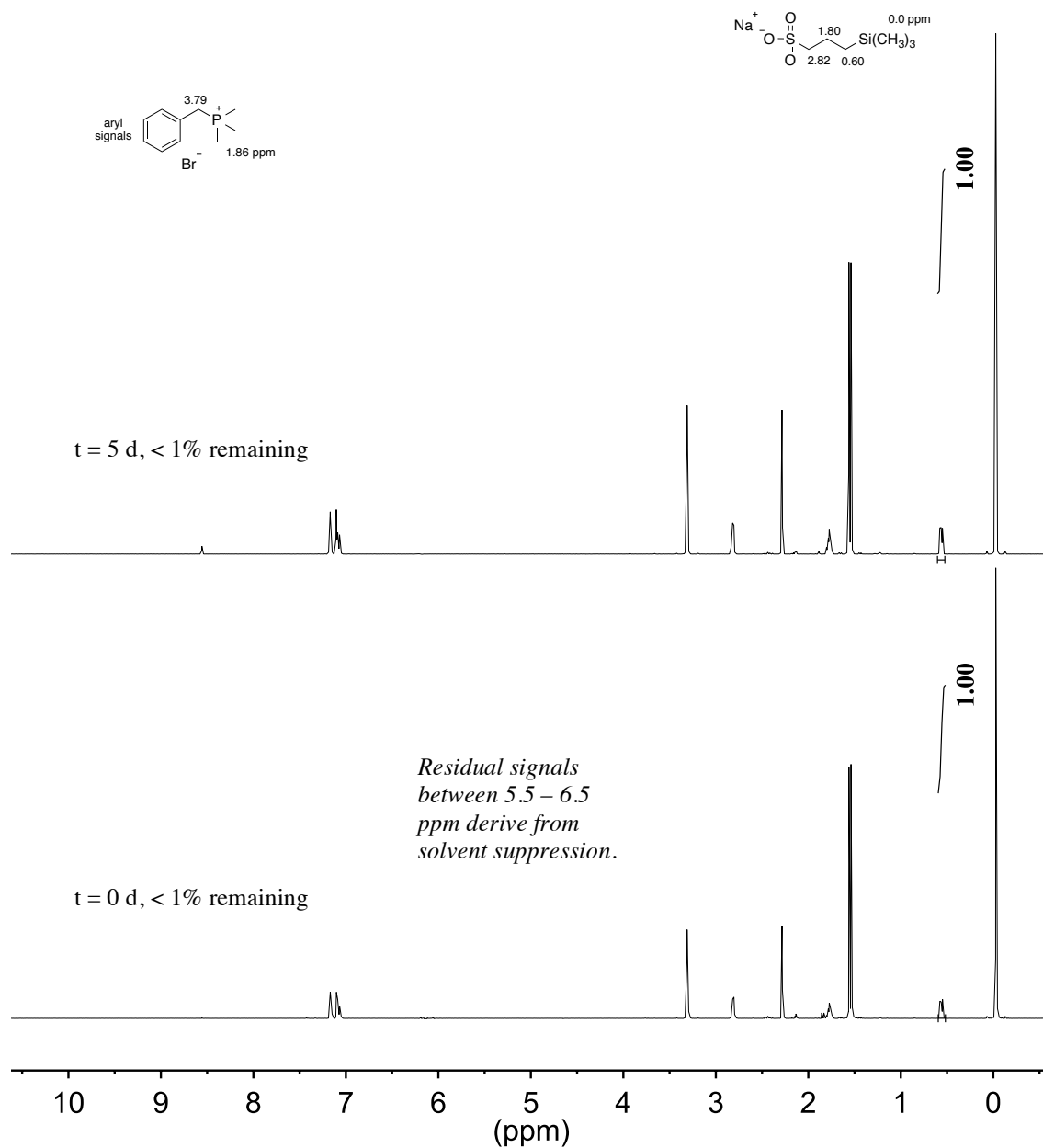


Figure 3.30 ^1H NMR spectra of **1** over 30 days dissolved in a basic CD_3OH solution at 80°C (2 M KOH, $[\text{KOH}]/[\text{1}] = 67$) with an internal standard ($\text{TMS}(\text{CH}_2)_3\text{SO}_3\text{Na}$).

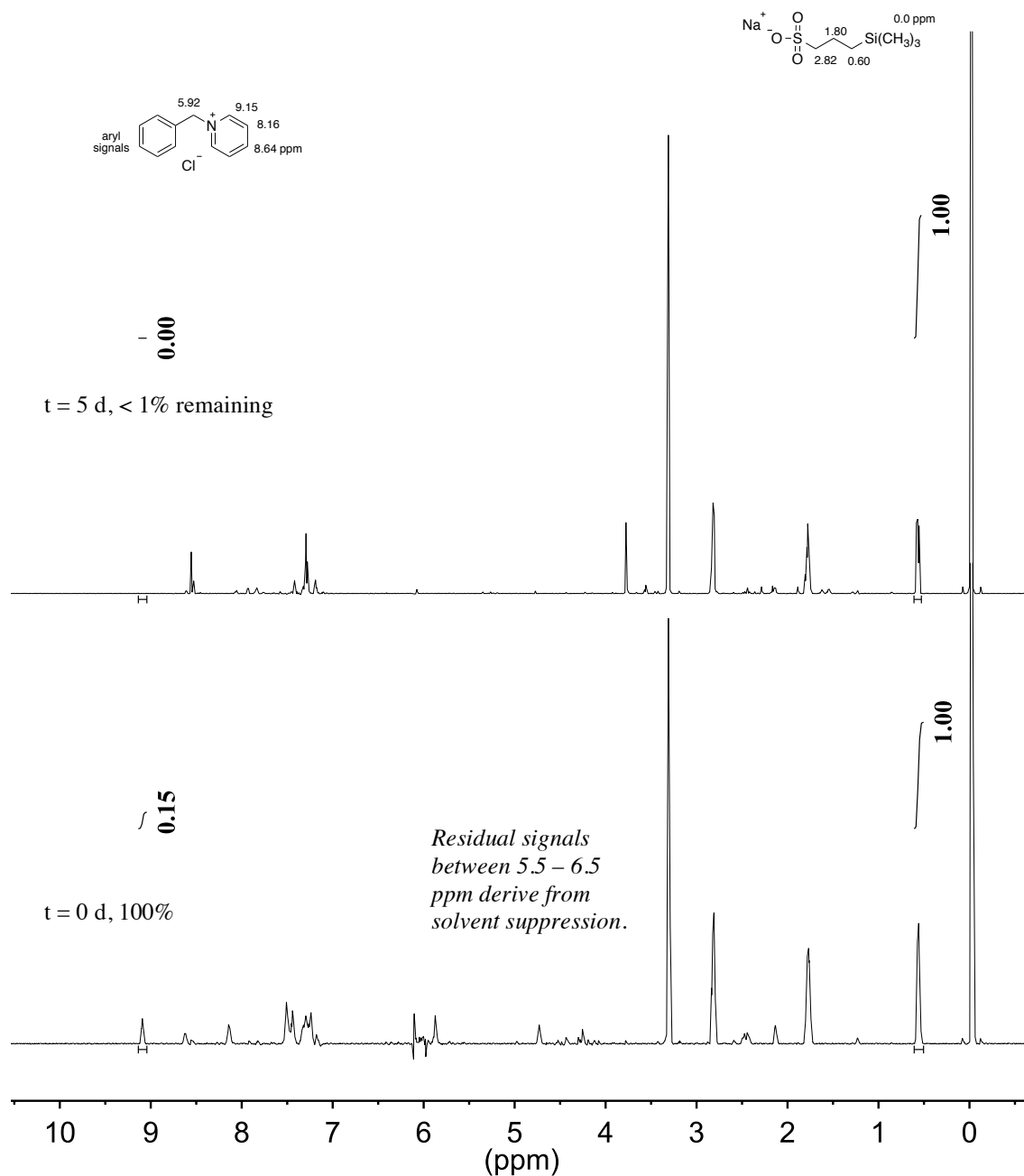


Figure 3.31 ¹H NMR spectra of **2** over 30 days dissolved in a basic CD₃OH solution at 80 °C (2 M KOH, [KOH]/[**2**] = 67) with an internal standard (TMS(CH₂)₃SO₃Na).

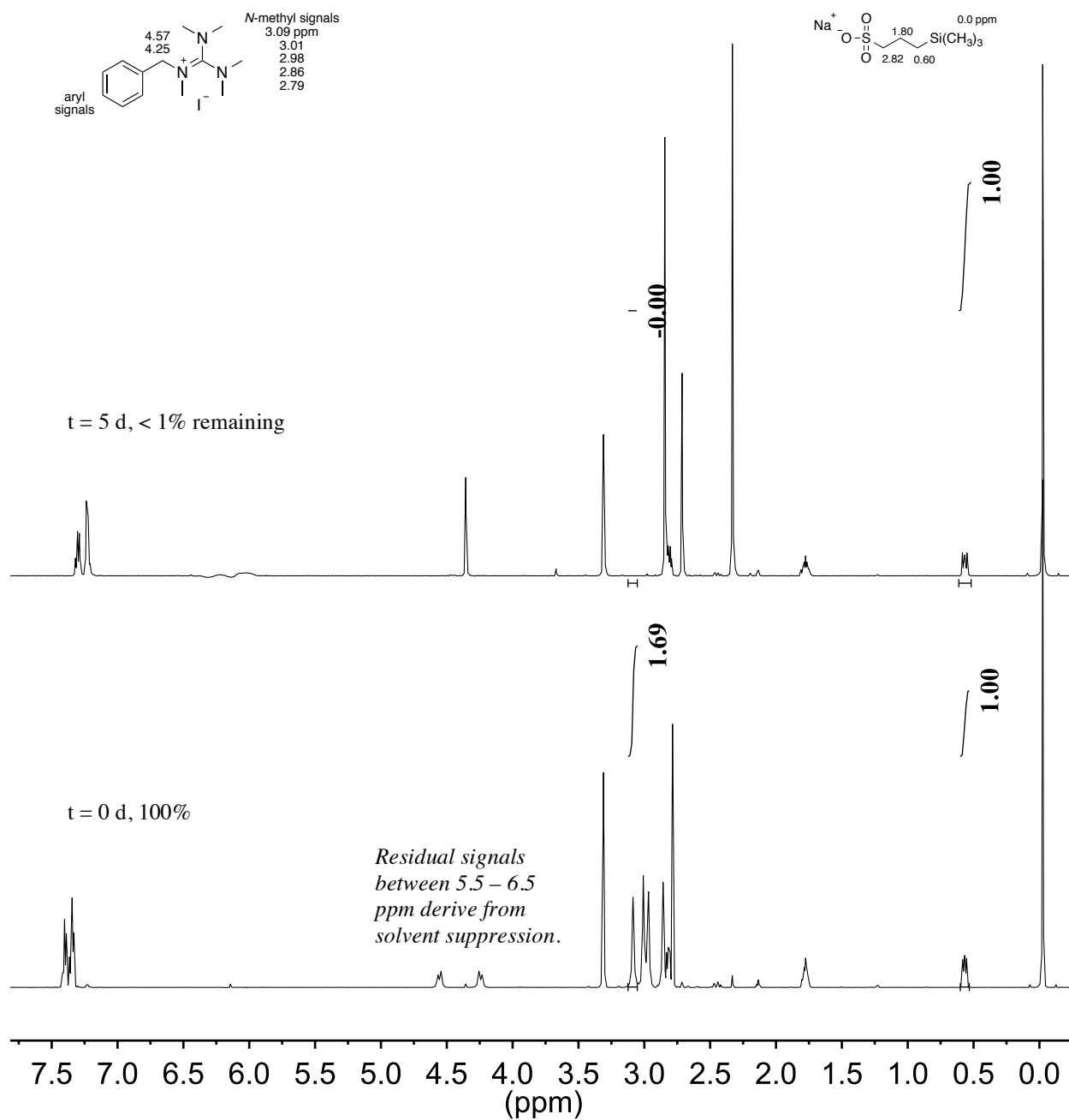


Figure 3.32 ^1H NMR spectra of **3** over 30 days dissolved in a basic CD_3OH solution at 80°C (2M KOH, $[\text{KOH}]/[\mathbf{3}] = 67$) with an internal standard ($\text{TMS}(\text{CH}_2)_3\text{SO}_3\text{Na}$).

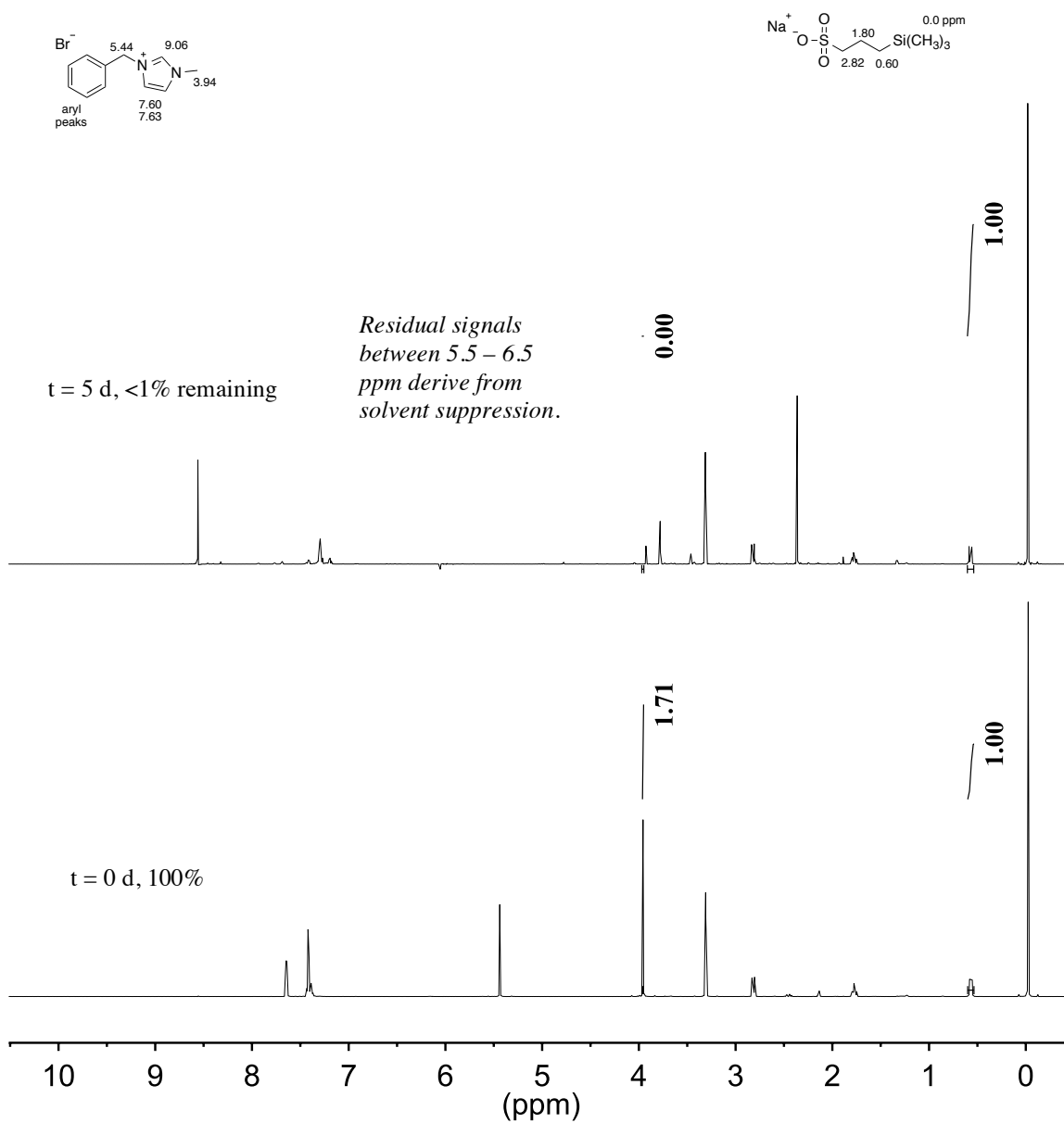


Figure 3.33 ^1H NMR spectra of **4** over 5 days dissolved in a basic CD_3OH solution at $80\text{ }^\circ\text{C}$ (2 M KOH, $[\text{KOH}]/[\text{4}] = 67$ with an internal standard ($\text{TMS}(\text{CH}_2)_3\text{SO}_3\text{Na}$).

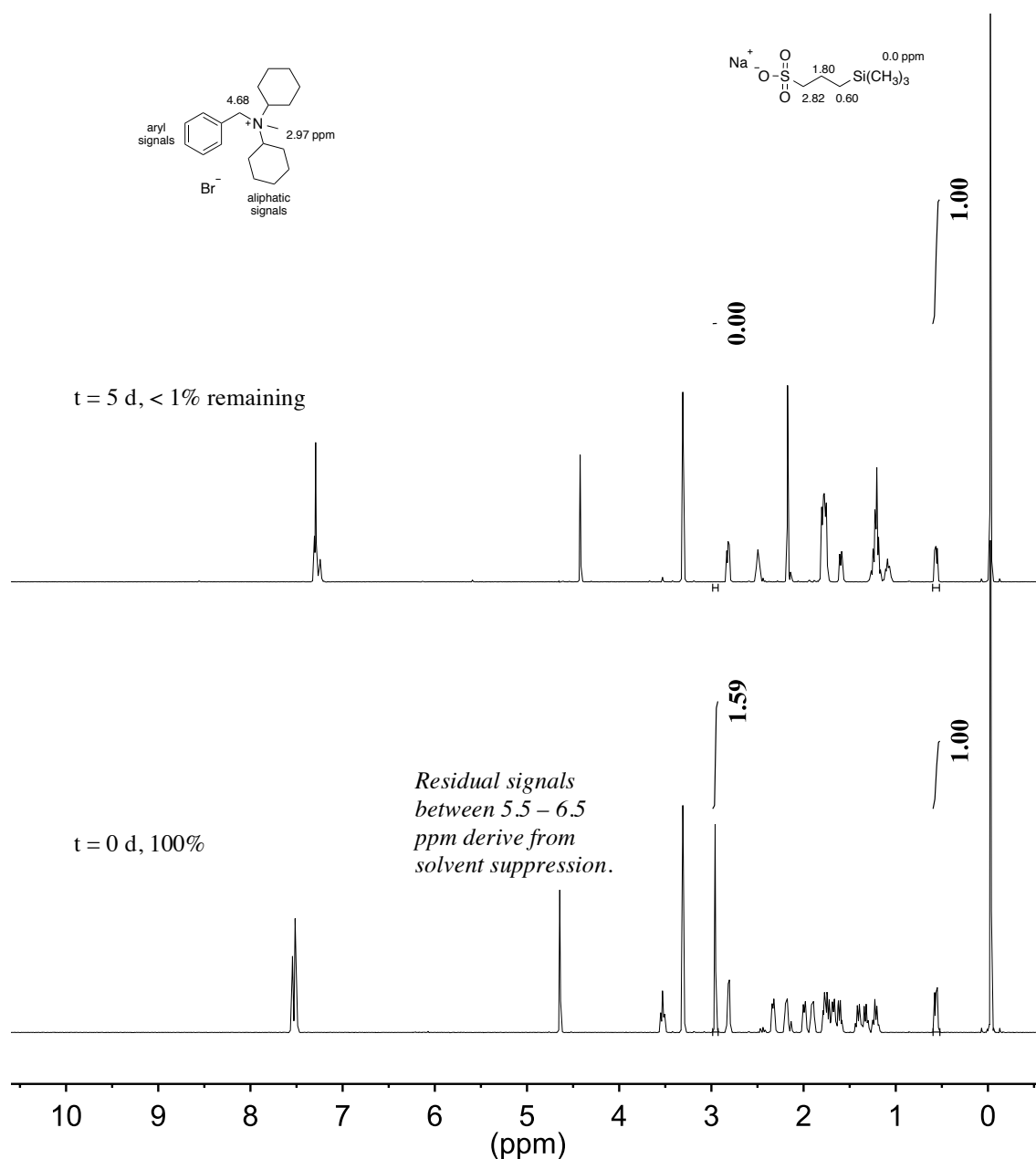


Figure 3.34 ^1H NMR spectra of **5** over 30 days dissolved in a basic CD_3OH solution at 80°C (2M KOH, $[\text{KOH}]/[\mathbf{5}] = 67$) with an internal standard ($\text{TMS}(\text{CH}_2)_3\text{SO}_3\text{Na}$).

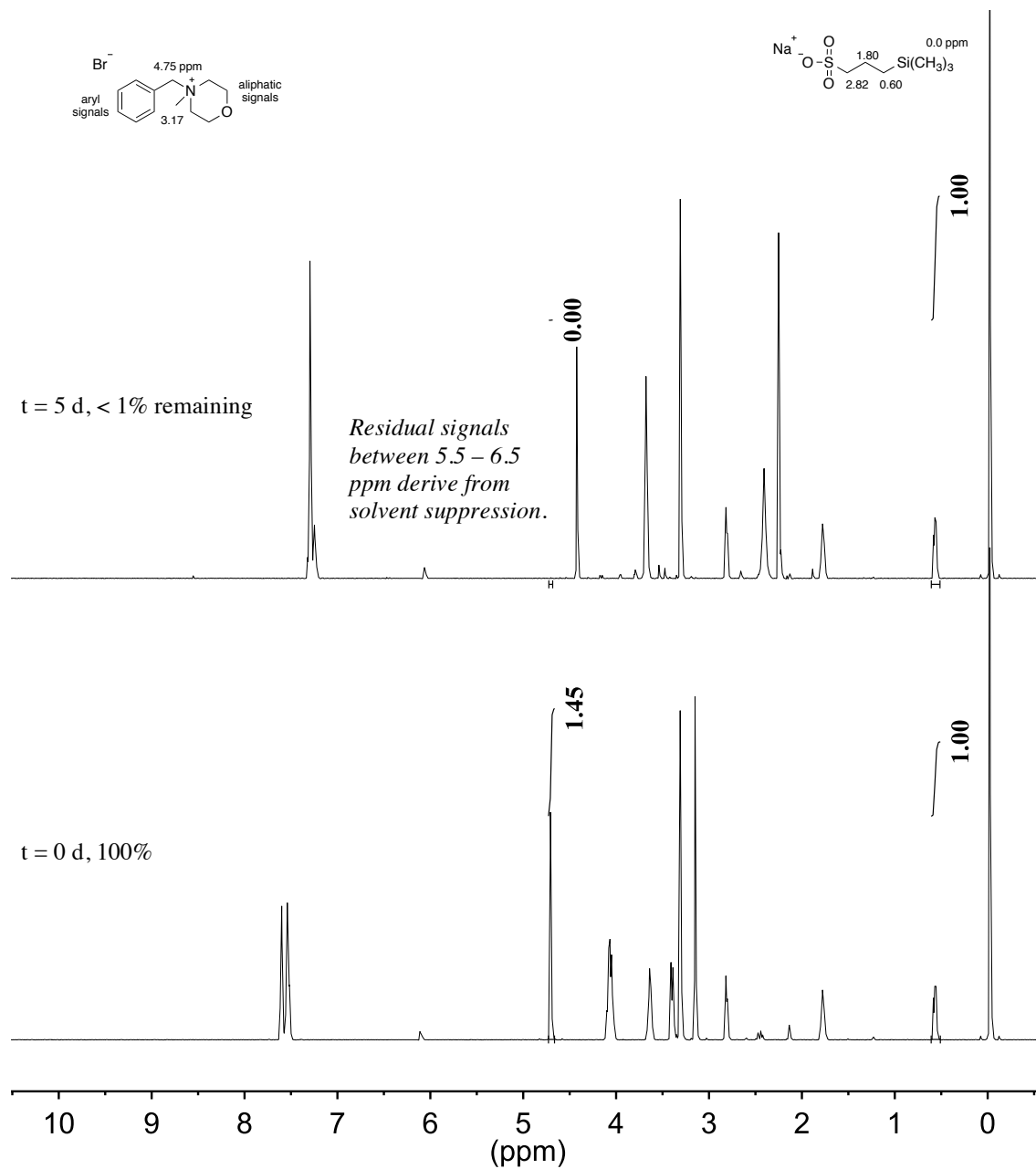


Figure 3.35 ^1H NMR spectra of **6** over 30 days dissolved in a basic CD_3OH solution at 80°C (2 M KOH, $[\text{KOH}]/[\mathbf{6}] = 67$) with an internal standard ($\text{TMS}(\text{CH}_2)_3\text{SO}_3\text{Na}$).

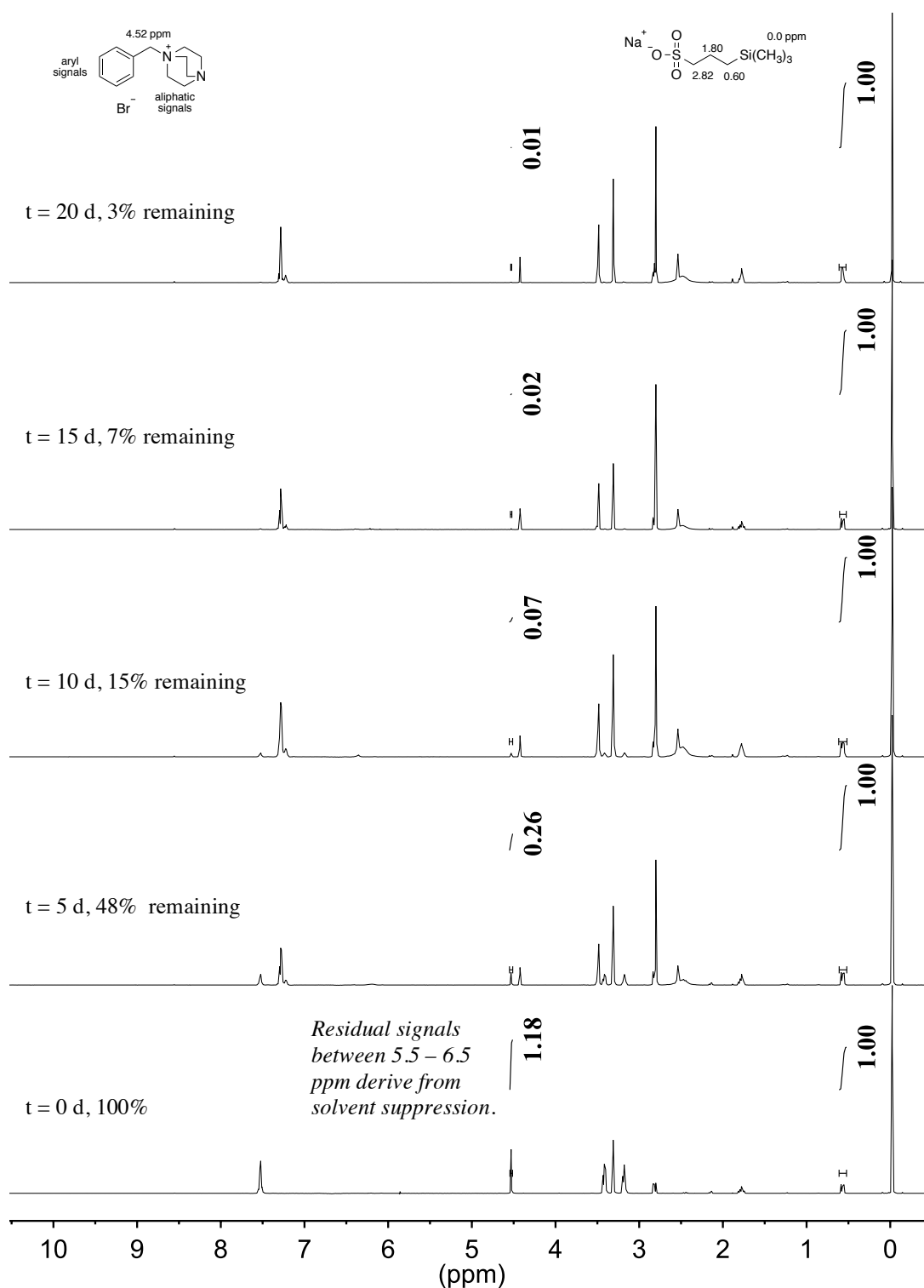


Figure 3.36 ^1H NMR spectra of **7** over 30 days dissolved in a basic CD_3OH solution at $80\text{ }^\circ\text{C}$ (2M KOH , $[\text{KOH}]/[\text{7}] = 67$) with an internal standard ($\text{TMS}(\text{CH}_2)_3\text{SO}_3\text{Na}$).

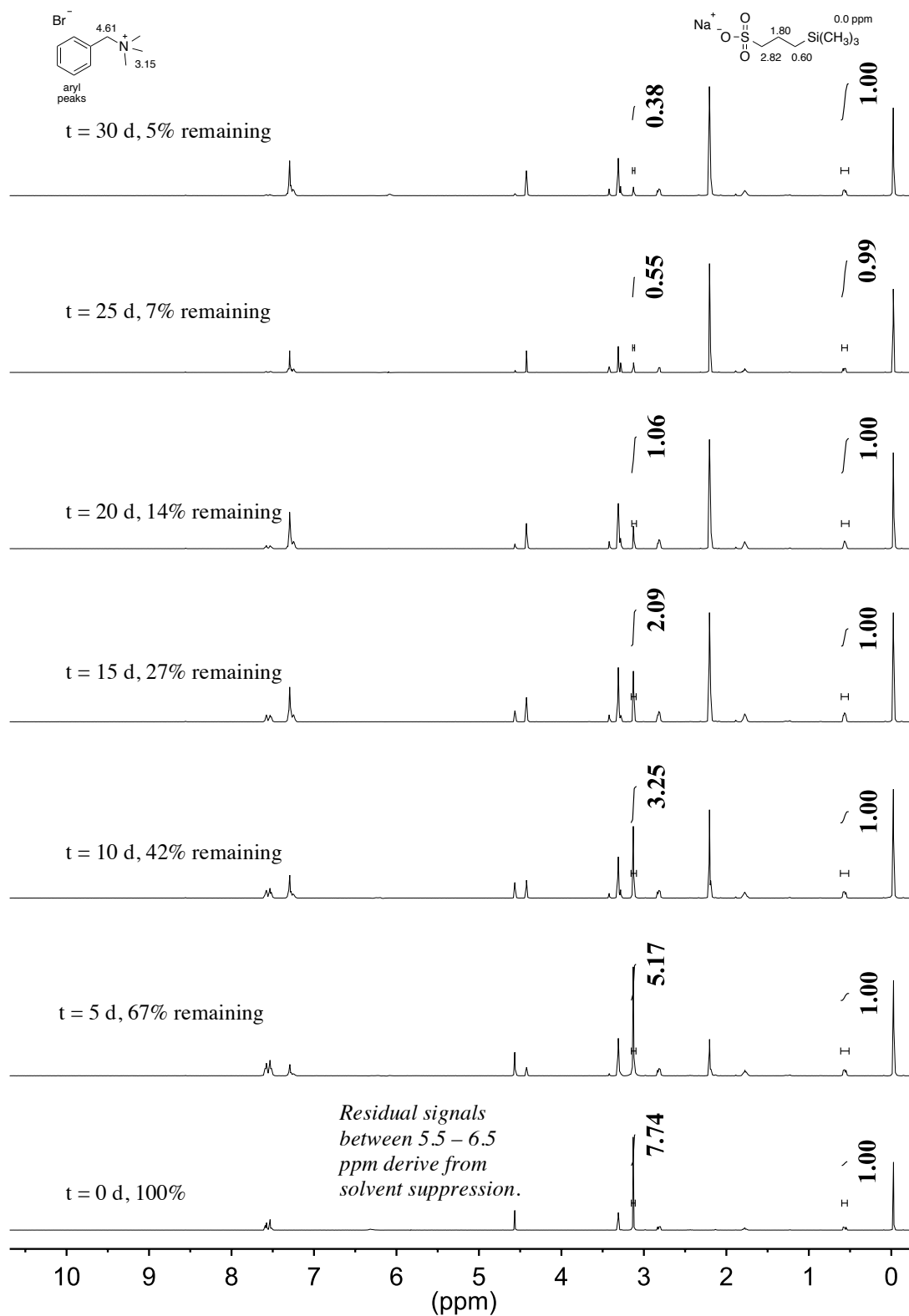


Figure 3.37 ^1H NMR spectra of **8** over 30 days dissolved in a basic CD_3OH solution at $80\text{ }^\circ\text{C}$ (2 M KOH, $[\text{KOH}]/[\textbf{8}] = 67$ with an internal standard ($\text{TMS}(\text{CH}_2)_3\text{SO}_3\text{Na}$).

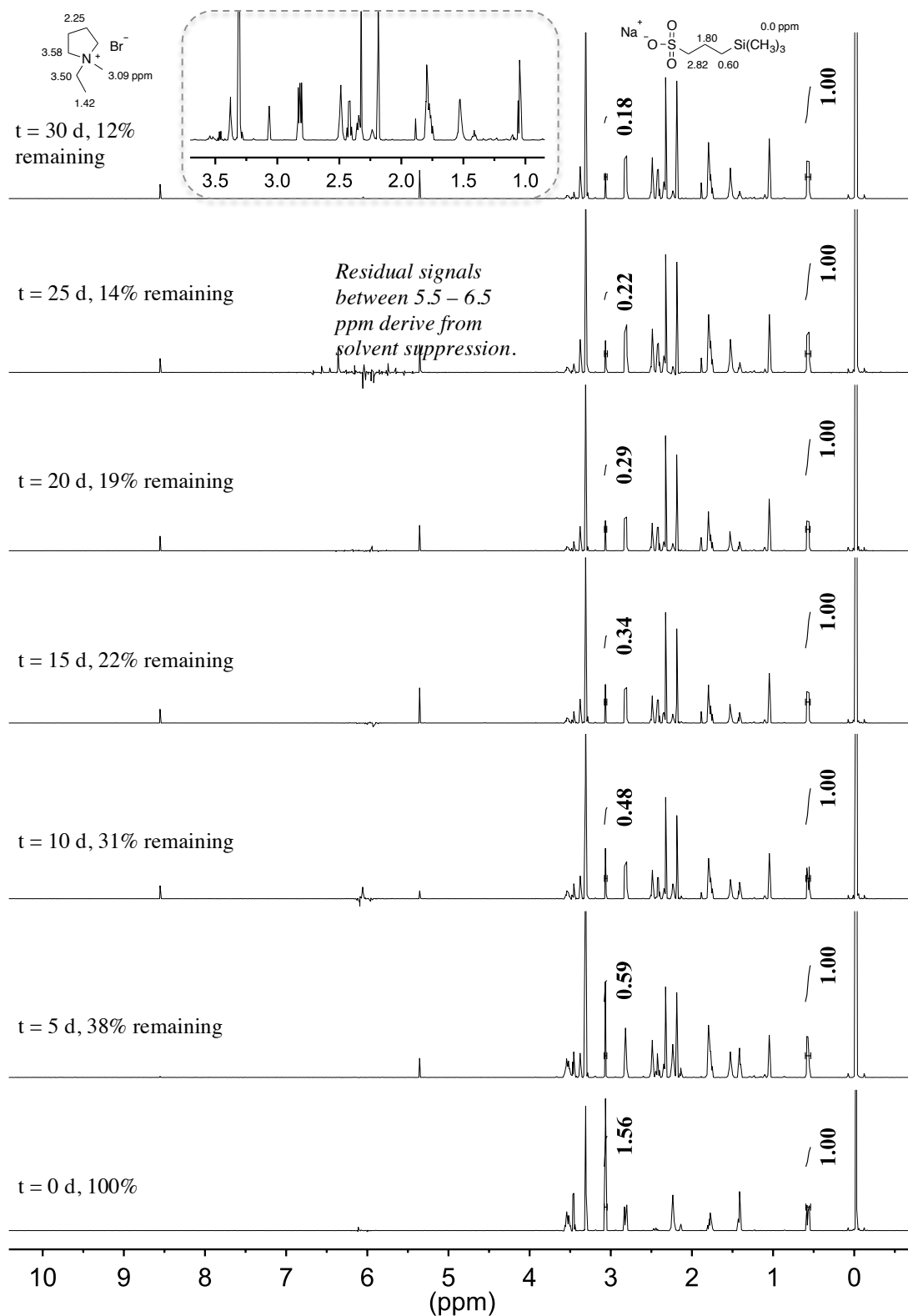


Figure 3.38 ^1H NMR spectra of **9** over 30 days dissolved in a basic CD_3OH solution at 80°C (2 M KOH, $[\text{KOH}]/[\mathbf{9}] = 67$) with an internal standard ($\text{TMS}(\text{CH}_2)_3\text{SO}_3\text{Na}$). Inset is extracted from t = 30 d.

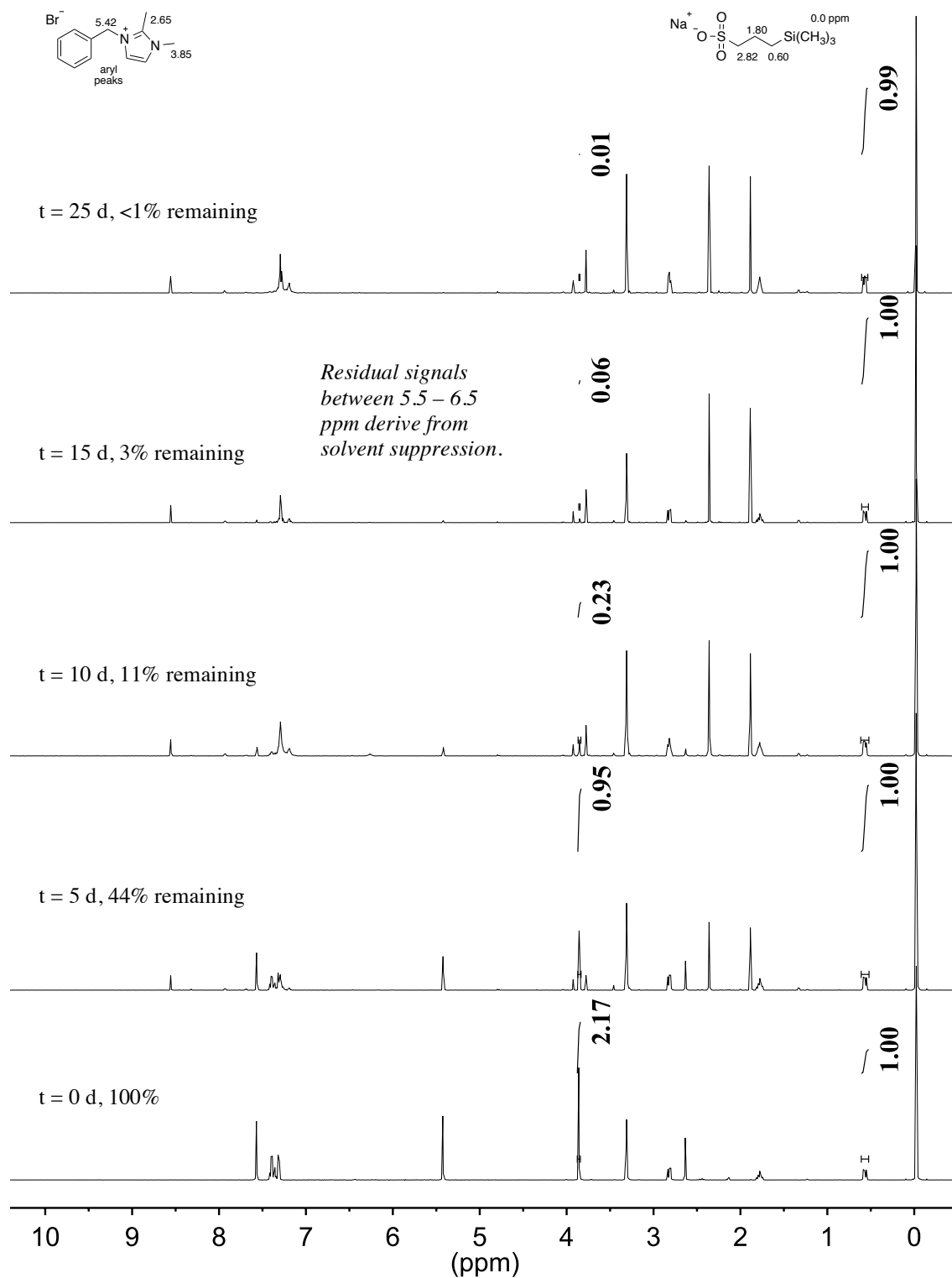


Figure 3.39 ¹H NMR spectra of **10** over 10 days dissolved in a basic CD₃OH solution at 80 °C (2 M KOH, [KOH]/[**10**] = 67) with an internal standard (TMS(CH₂)₃SO₃Na).

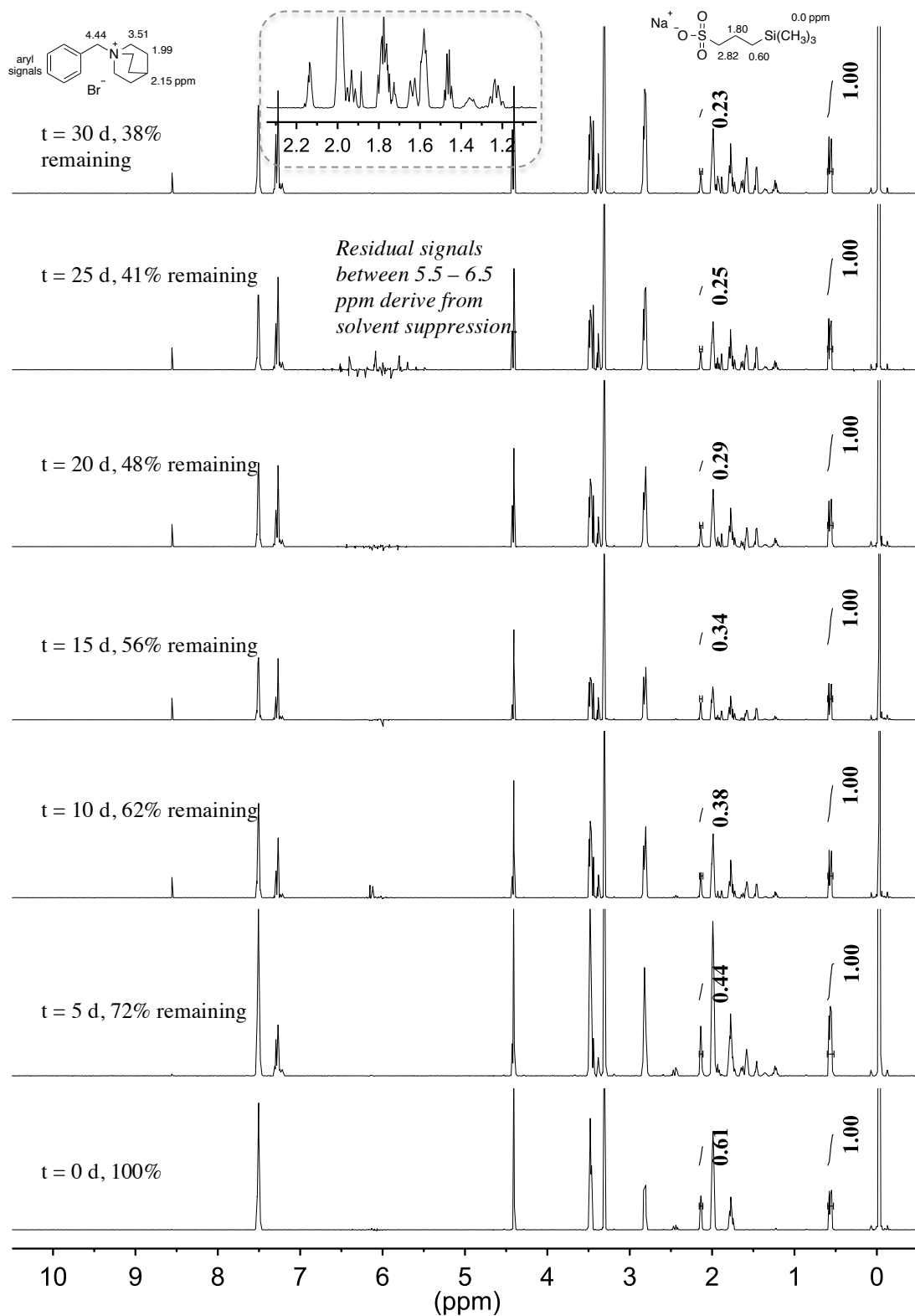


Figure 3.40 ¹H NMR spectra of **11** over 30 days dissolved in a basic CD₃OH solution at 80 °C (2 M KOH, [KOH]/[**11**] = 67) with an internal standard (TMS(CH₂)₃SO₃Na). Inset is extracted from t = 30 d.

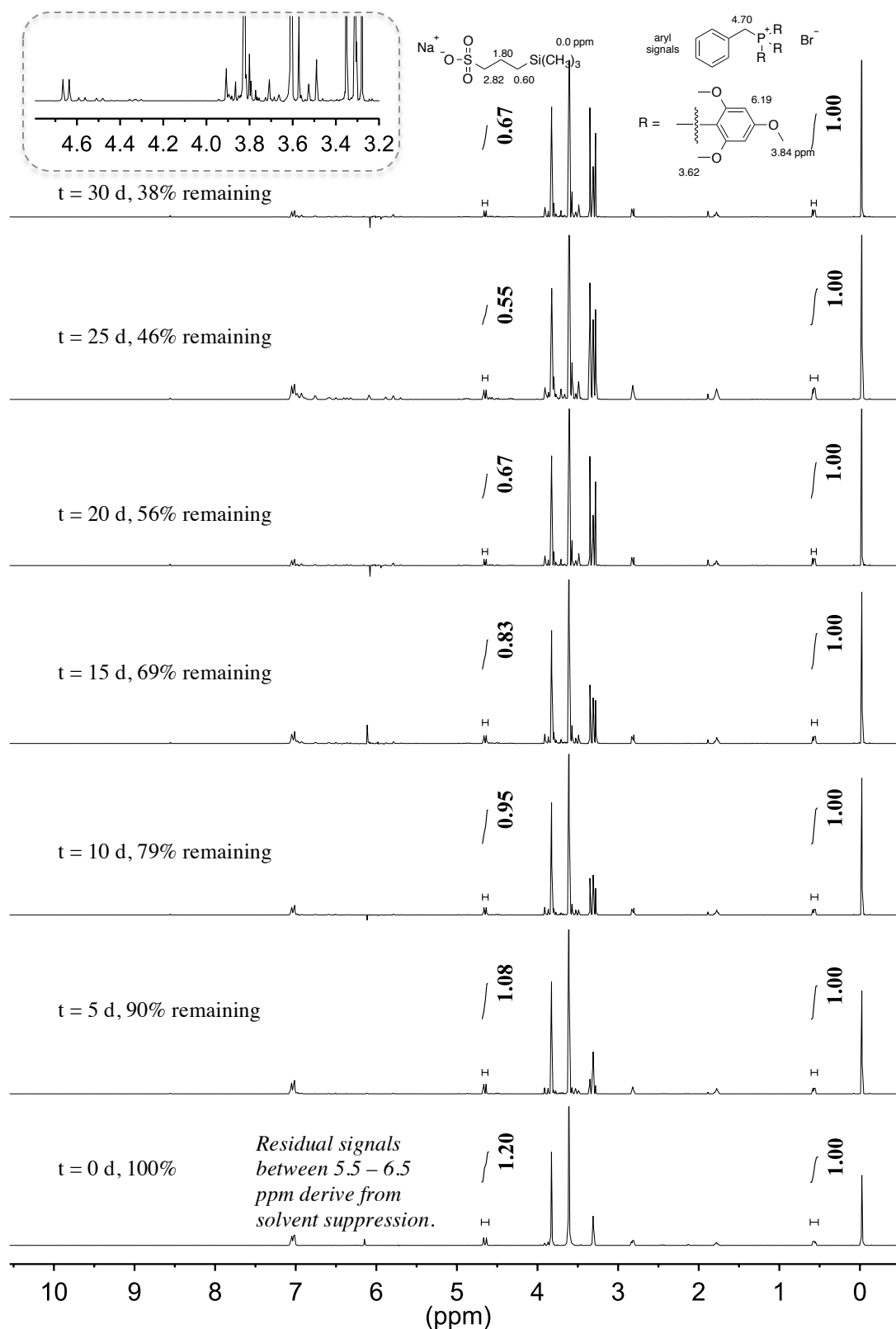


Figure 3.41 ^1H NMR spectra of **12** over 30 days dissolved in a basic CD_3OH solution at 80°C (2 M KOH, $[\text{KOH}]/[\text{12}] = 67$) with an internal standard (TMS(CH_2) $_3$ SO $_3$ Na). Inset is extracted from $t = 30$ d.

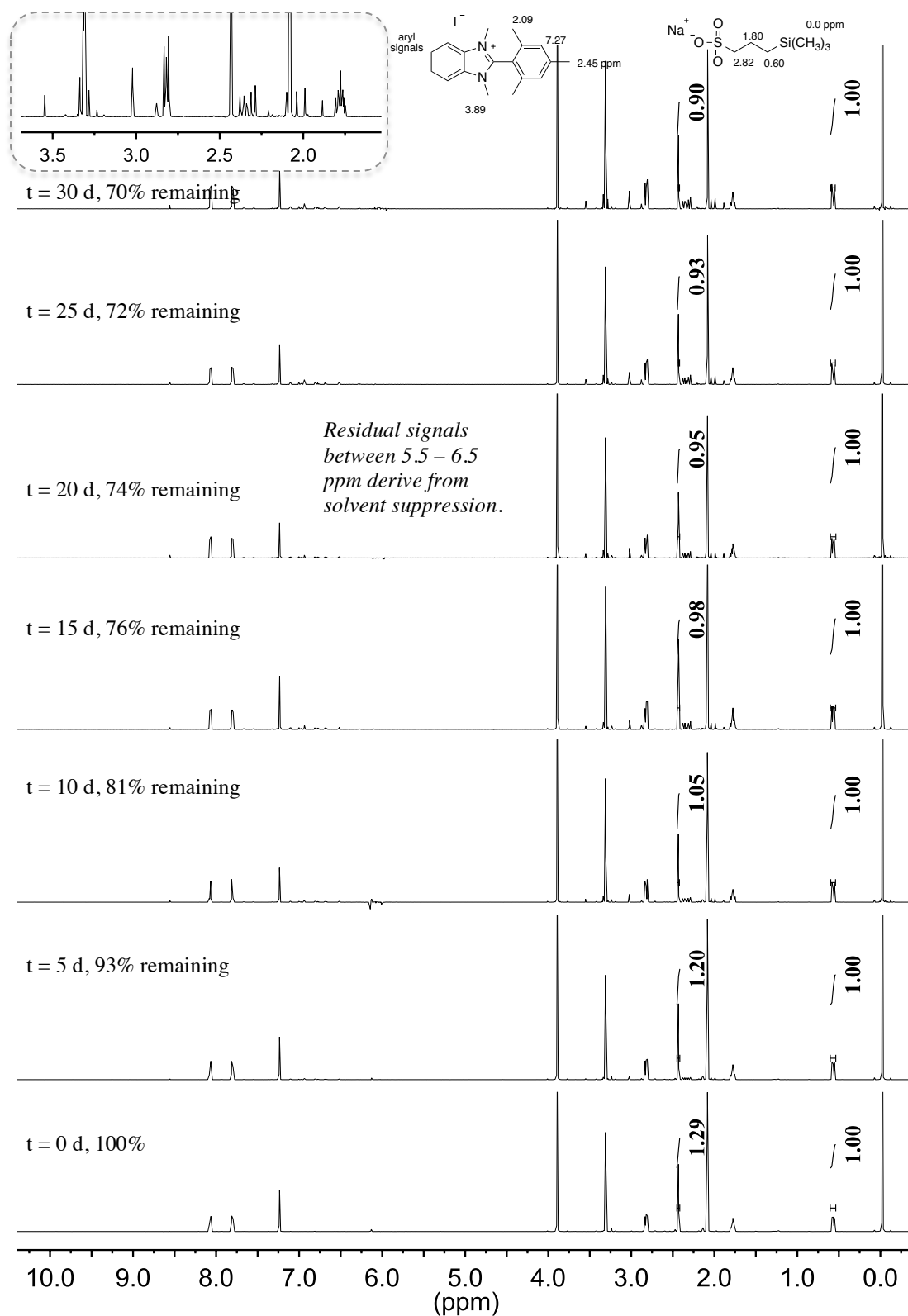


Figure 3.42 ¹H NMR spectra of **13** over 30 days dissolved in a basic CD₃OH solution at 80 °C (2 M KOH, [KOH]/[**13**] = 67) with an internal standard (TMS(CH₂)₃SO₃Na). Inset is extracted from t = 30 d.

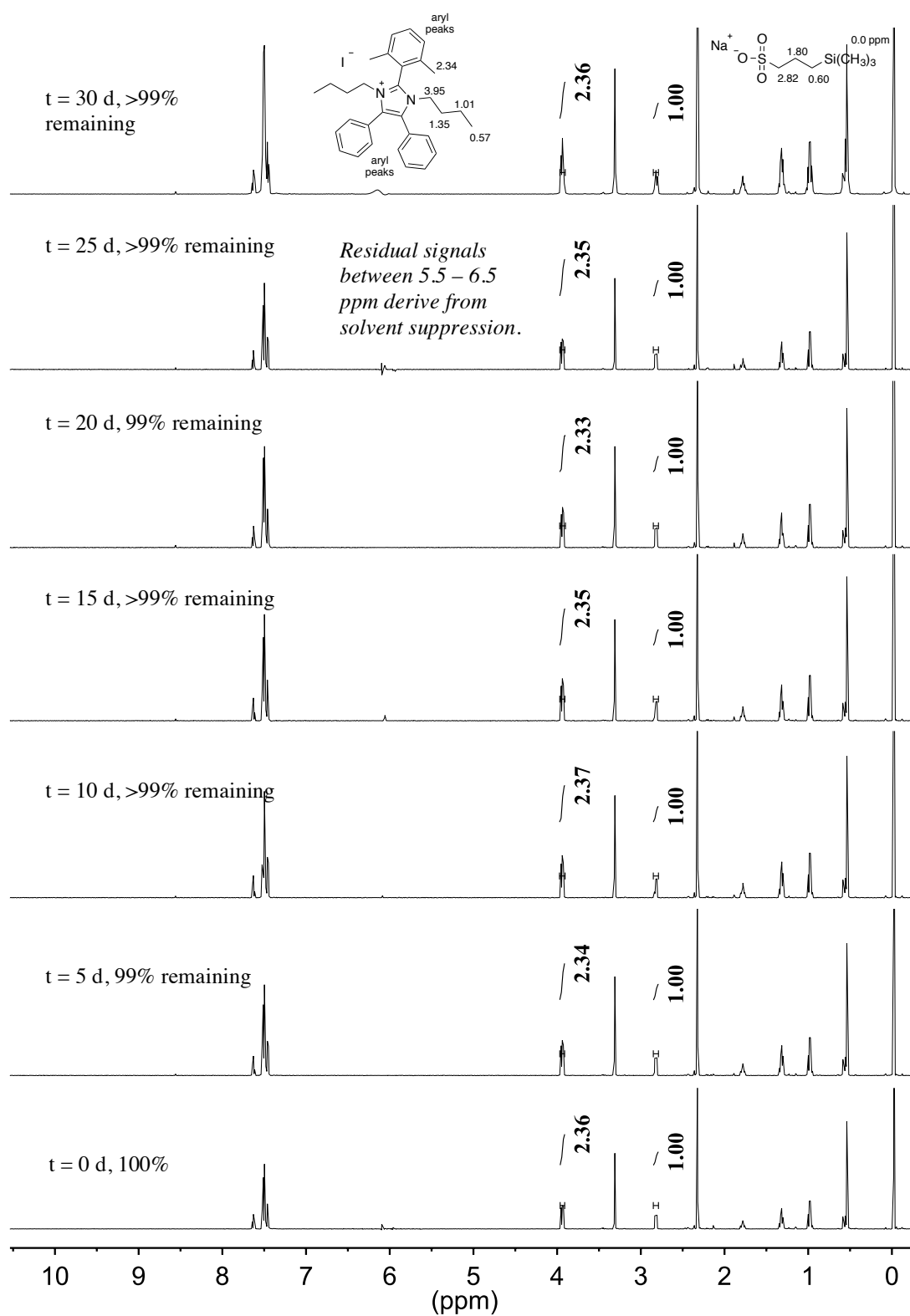


Figure 3.43 ¹H NMR spectra of **14** over 30 days dissolved in a basic CD₃OH solution at 80 °C (2 M KOH, [KOH]/[**14**] = 67) with an internal standard (TMS(CH₂)₃SO₃Na).

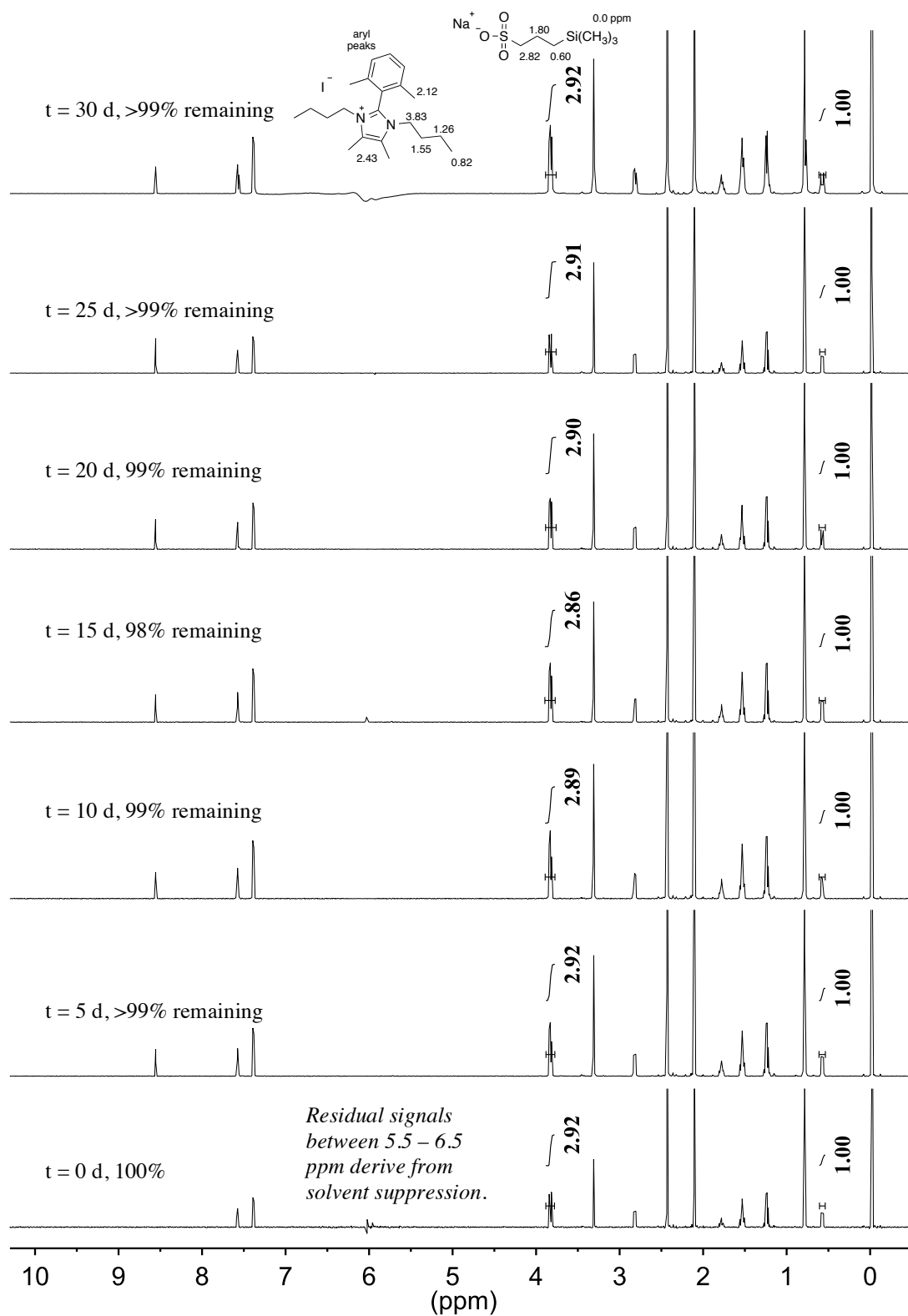


Figure 3.44 ¹H NMR spectra of **15** over 30 days dissolved in a basic CD₃OH solution at 80 °C (2 M KOH, [KOH]/[**15**] = 67 with an internal standard (TMS(CH₂)₃SO₃Na).

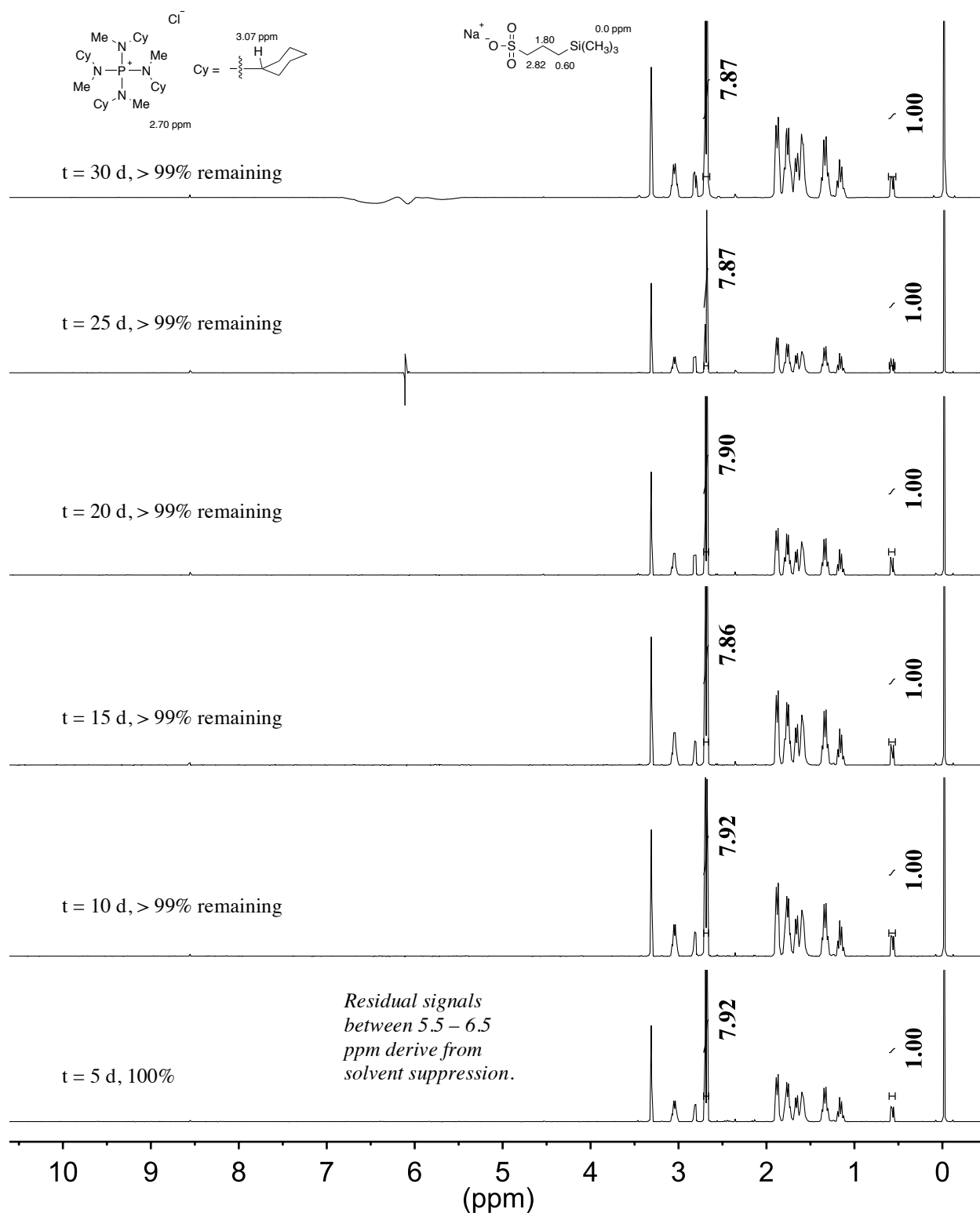


Figure 3.45 ^1H NMR spectra of **16** over 30 days dissolved in a basic CD_3OH solution at $80\text{ }^\circ\text{C}$ (2 M KOH, $[\text{KOH}]/[\textbf{16}] = 67$) with an internal standard ($\text{TMS}(\text{CH}_2)_3\text{SO}_3\text{Na}$).

3.5.7 Copies of ^1H NMR Spectra for Non-deuterated Stability Studies

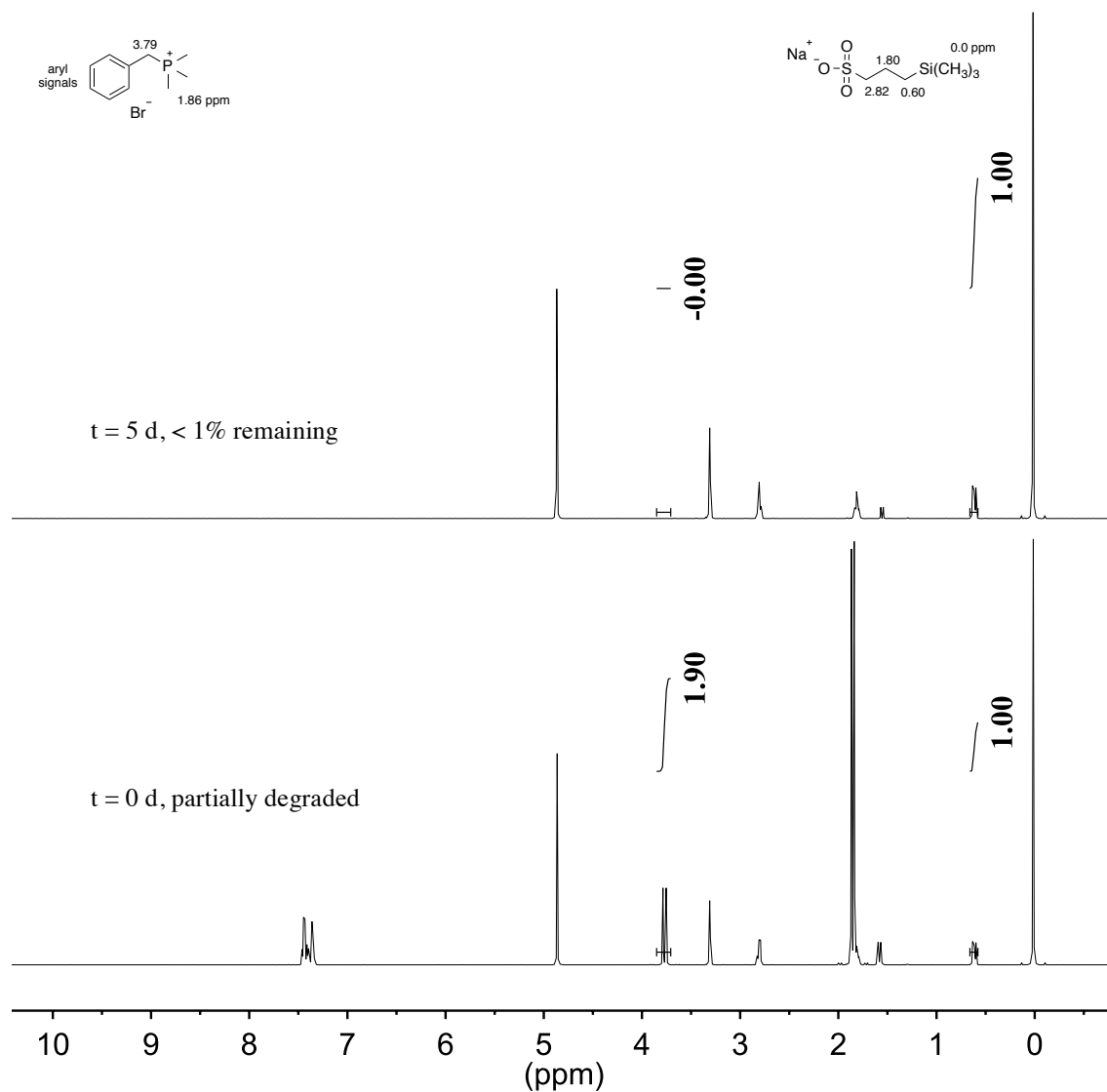


Figure 3.46 ^1H NMR spectra of **1** over 5 days dissolved in a basic CH_3OH solution at $80\text{ }^\circ\text{C}$ (1 M KOH, $[\text{KOH}]/[\mathbf{1}] = 20$) with an internal standard ($\text{TMS}(\text{CH}_2)_3\text{SO}_3\text{Na}$).

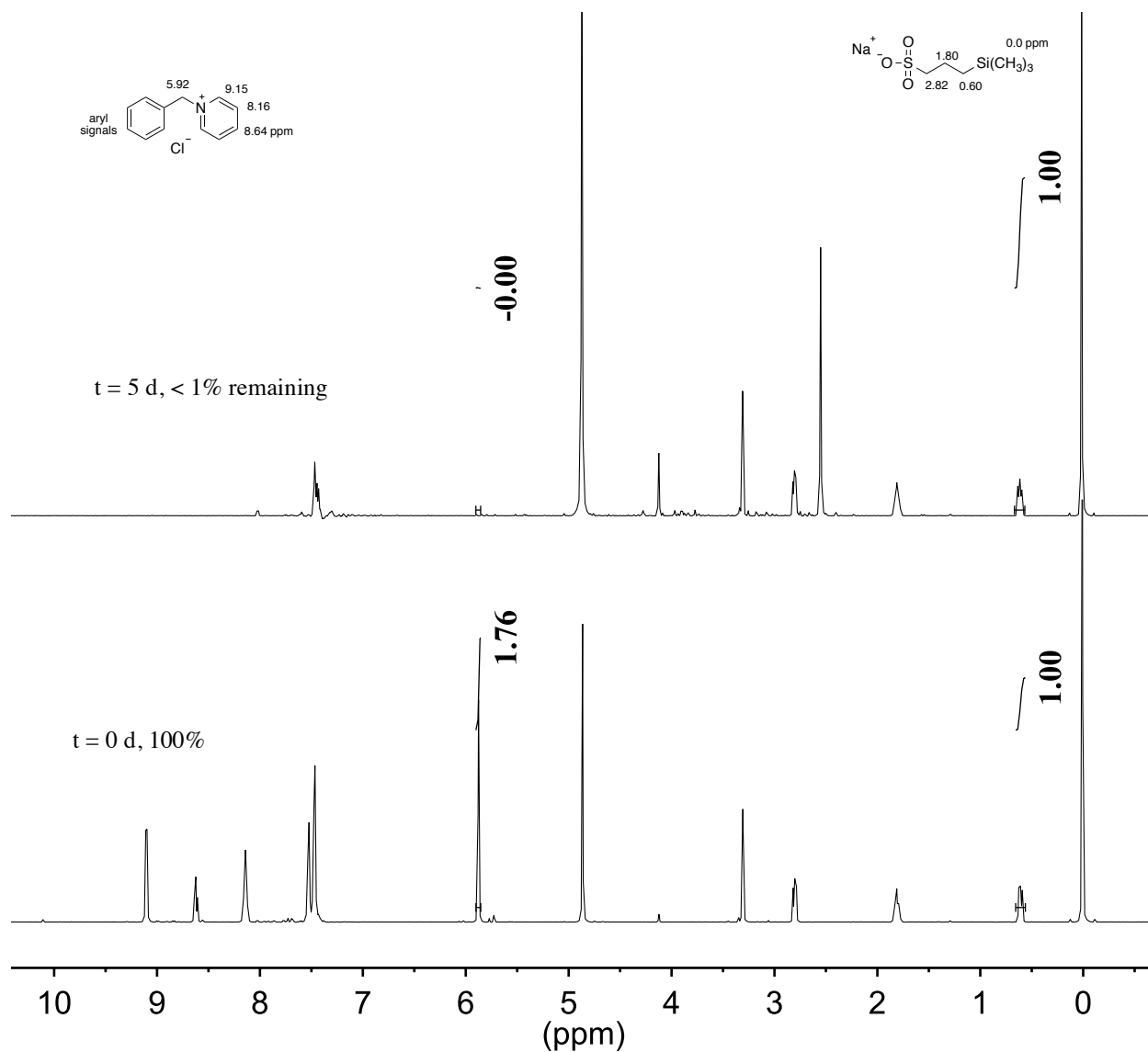


Figure 3.47 ^1H NMR spectra of **2** over 5 days dissolved in a basic CH_3OH solution at 80°C (1 M KOH, $[\text{KOH}]/[\text{2}] = 20$) with an internal standard ($\text{TMS}(\text{CH}_2)_3\text{SO}_3\text{Na}$).

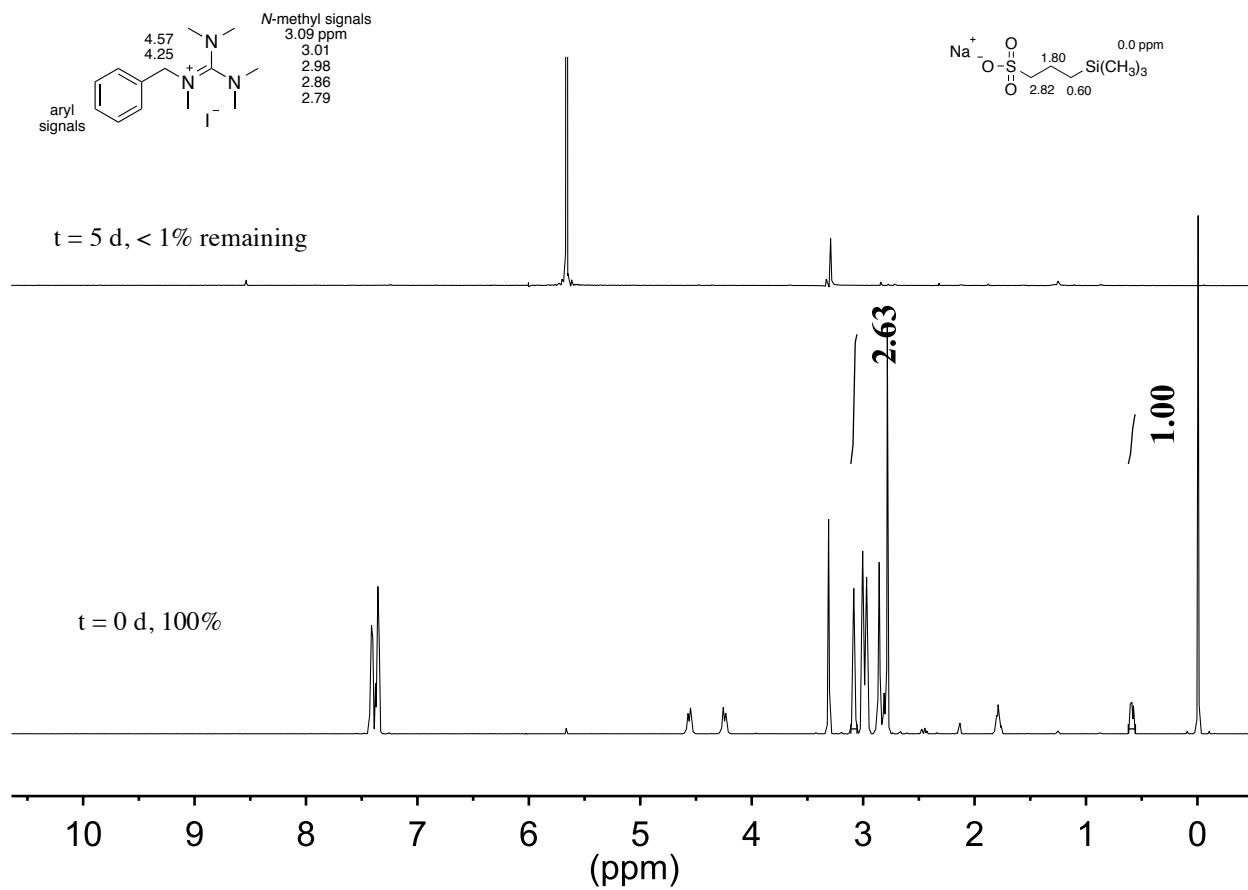


Figure 3.48 ^1H NMR spectra of **3** over 5 days dissolved in a basic CH_3OH solution at 80°C (1 M KOH, $[\text{KOH}]/[\mathbf{3}] = 20$) with an internal standard ($\text{TMS}(\text{CH}_2)_3\text{SO}_3\text{Na}$).

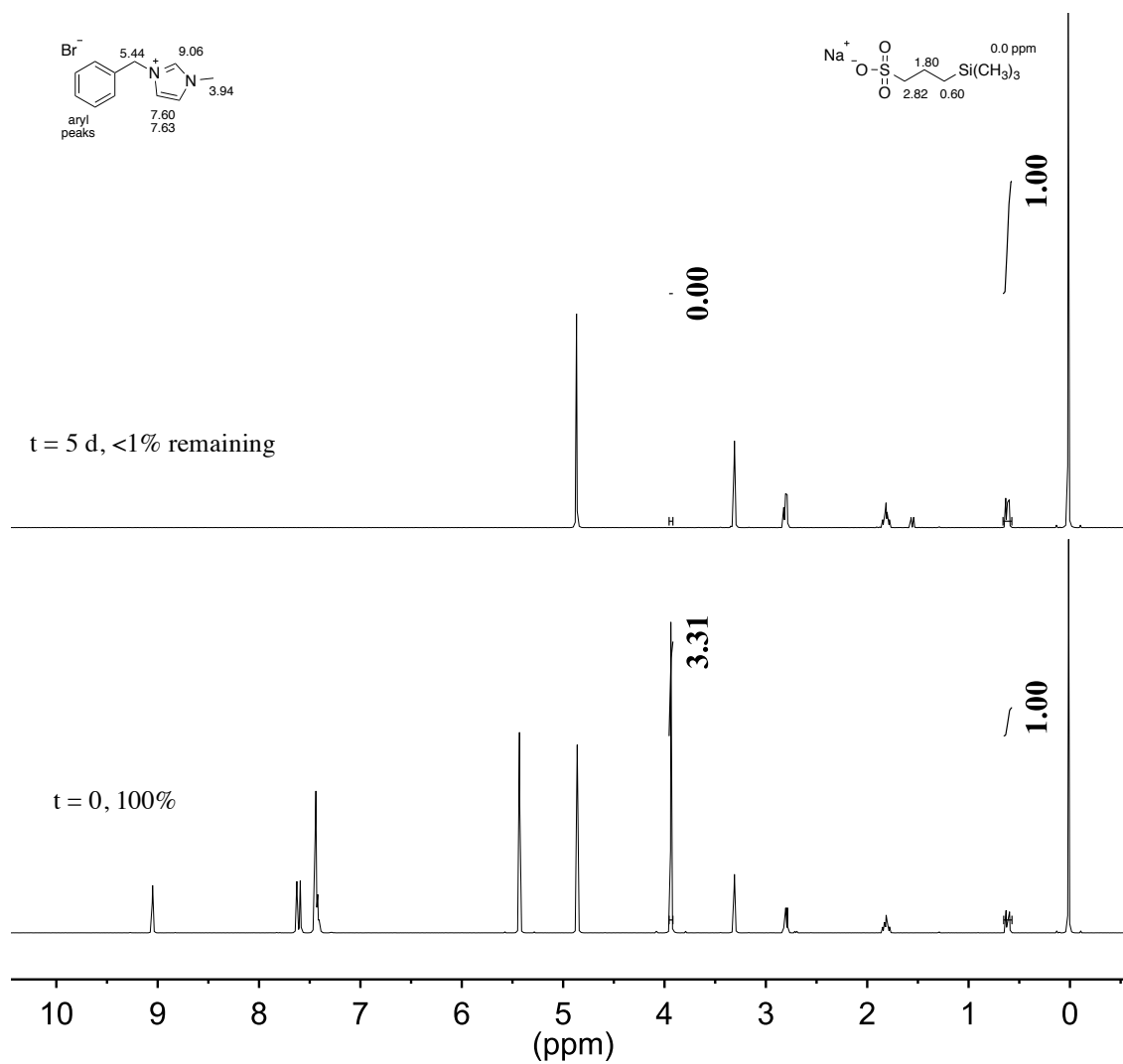


Figure 3.49 ^1H NMR spectra of **4** over 5 days dissolved in a basic CH_3OH solution at $80\text{ }^\circ\text{C}$ (1 M KOH, $[\text{KOH}]/[\mathbf{4}] = 20$) with an internal standard ($\text{TMS}(\text{CH}_2)_3\text{SO}_3\text{Na}$).

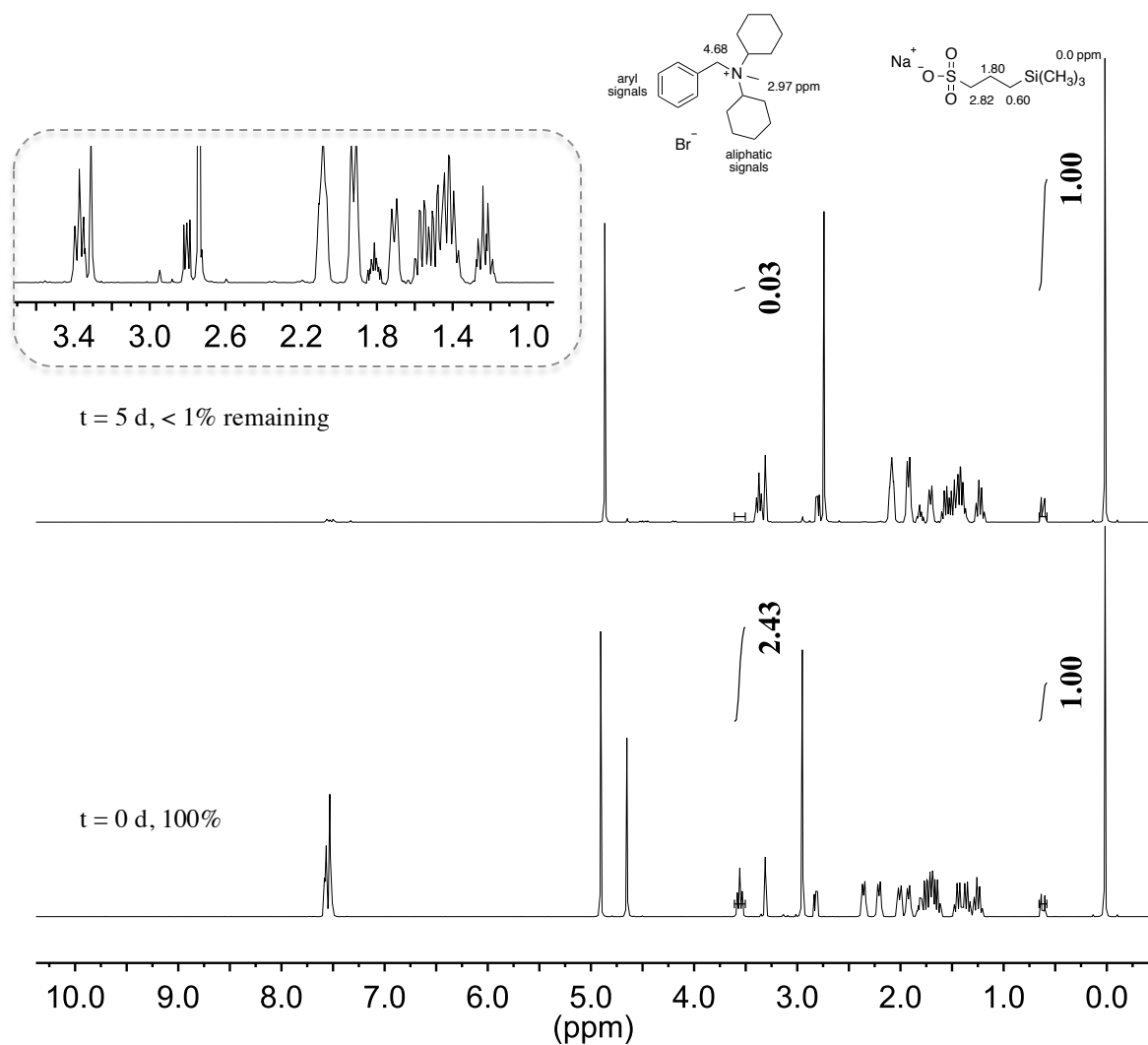


Figure 3.50 ^1H NMR spectra of **5** over 5 days dissolved in a basic CH_3OH solution at $80\text{ }^\circ\text{C}$ (1 M KOH, $[\text{KOH}]/[\mathbf{5}] = 20$) with an internal standard ($\text{TMS}(\text{CH}_2)_3\text{SO}_3\text{Na}$). Inset is extracted from $t = 5\text{ d}$.

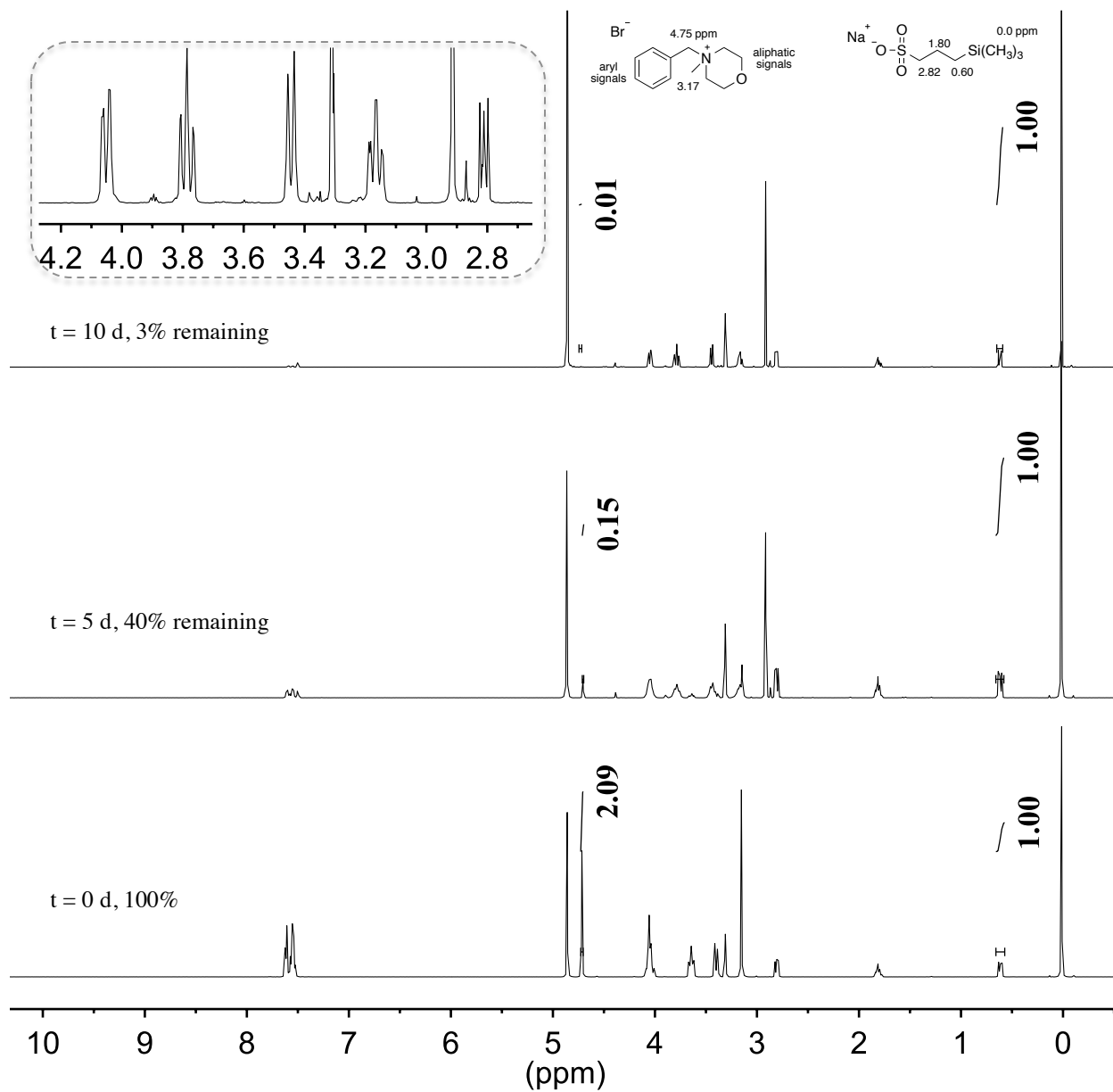


Figure 3.51 ^1H NMR spectra of **6** over 10 days dissolved in a basic CH_3OH solution at 80°C (1 M KOH, $[\text{KOH}]/[\text{6}] = 20$) with an internal standard ($\text{TMS}(\text{CH}_2)_3\text{SO}_3\text{Na}$). Inset is extracted from t = 10 d.

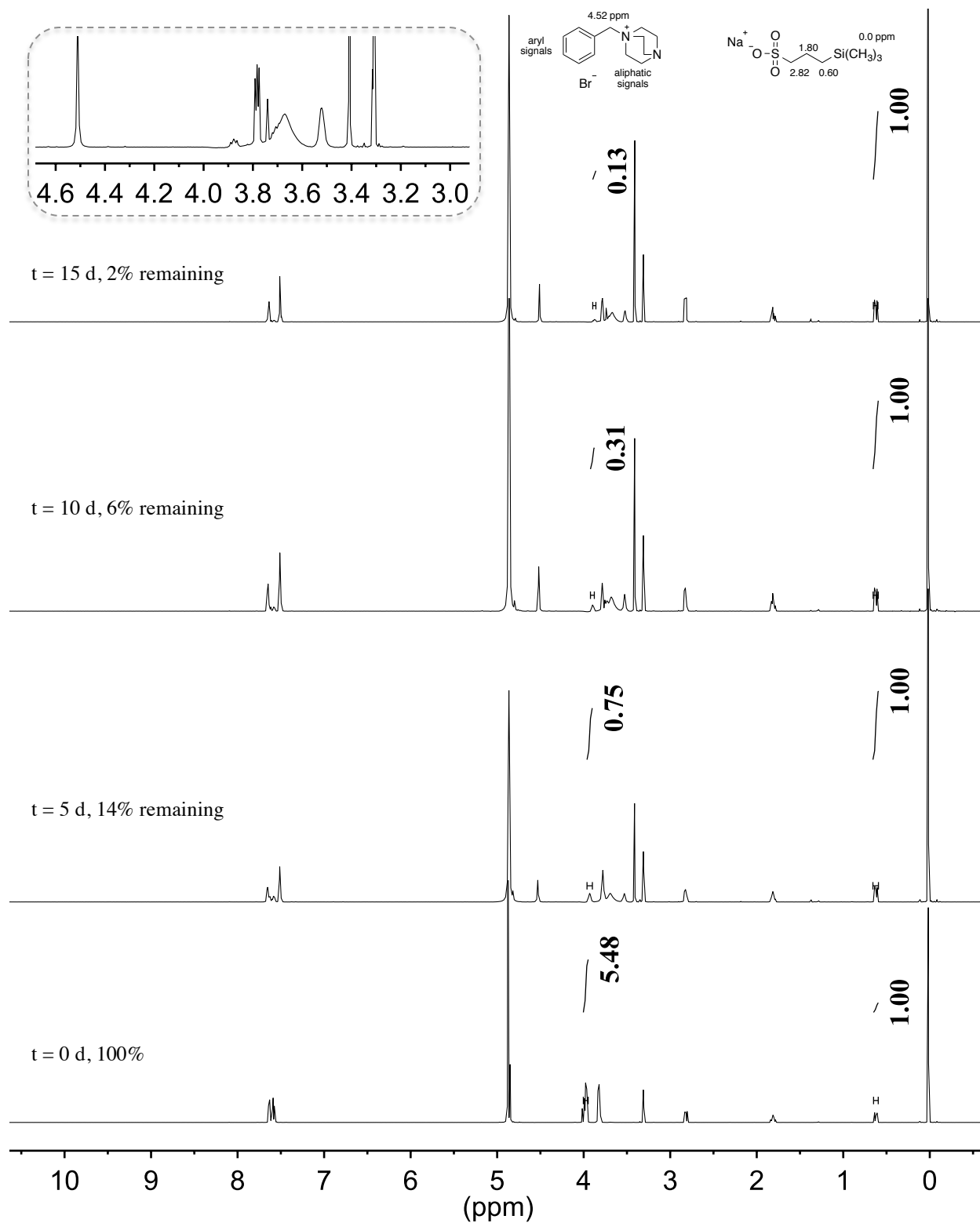


Figure 3.52 ^1H NMR spectra of **7** over 15 days dissolved in a basic CH_3OH solution at 80°C (1 M KOH, $[\text{KOH}]/[\textbf{7}] = 20$) with an internal standard ($\text{TMS}(\text{CH}_2)_3\text{SO}_3\text{Na}$). Inset is extracted from $t = 15$ d.

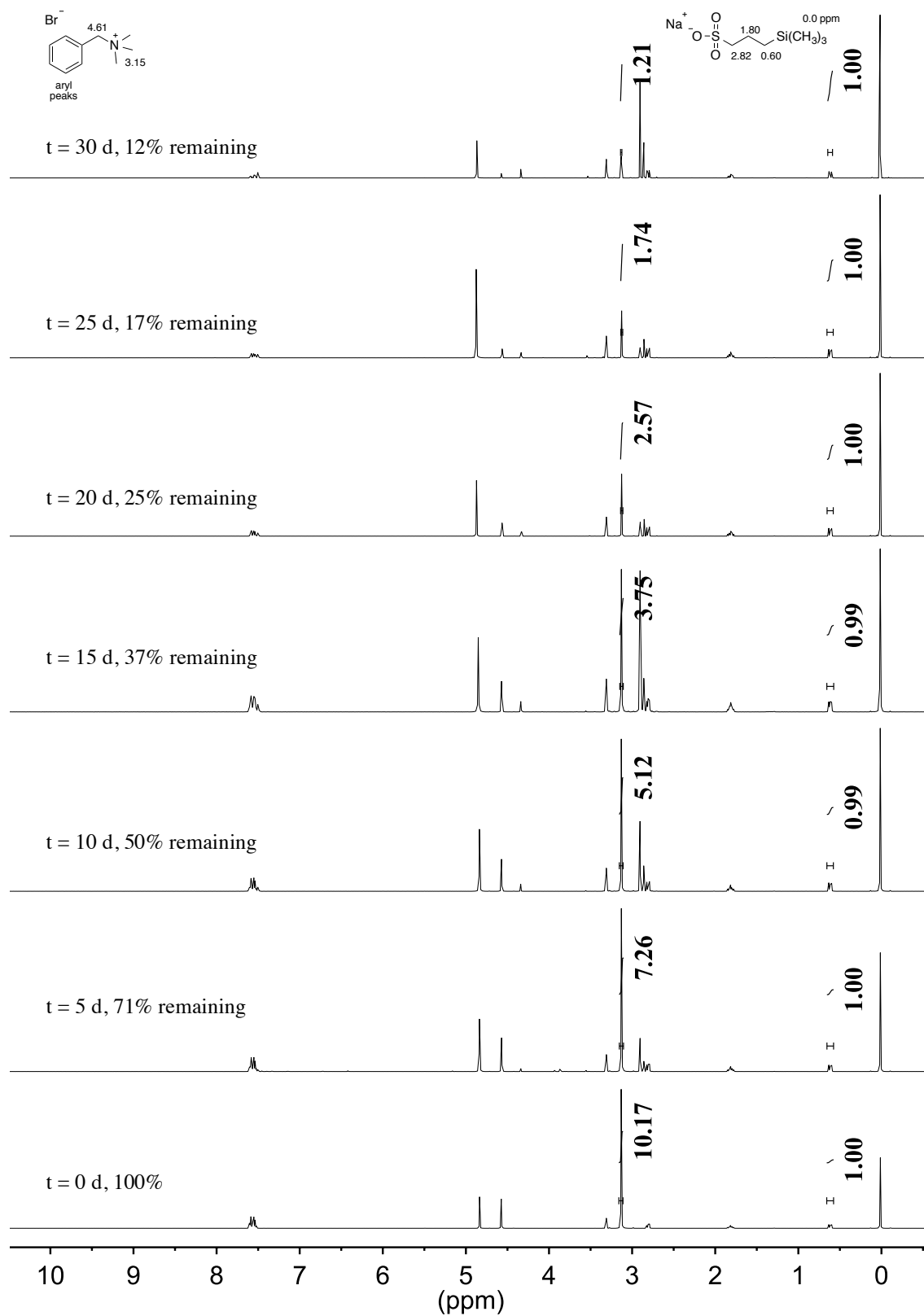


Figure 3.53 ^1H NMR spectra of **8** over 30 days dissolved in a basic CH_3OH solution at 80°C (1 M KOH, $[\text{KOH}]/[\mathbf{8}] = 20$ with an internal standard ($\text{TMS}(\text{CH}_2)_3\text{SO}_3\text{Na}$).

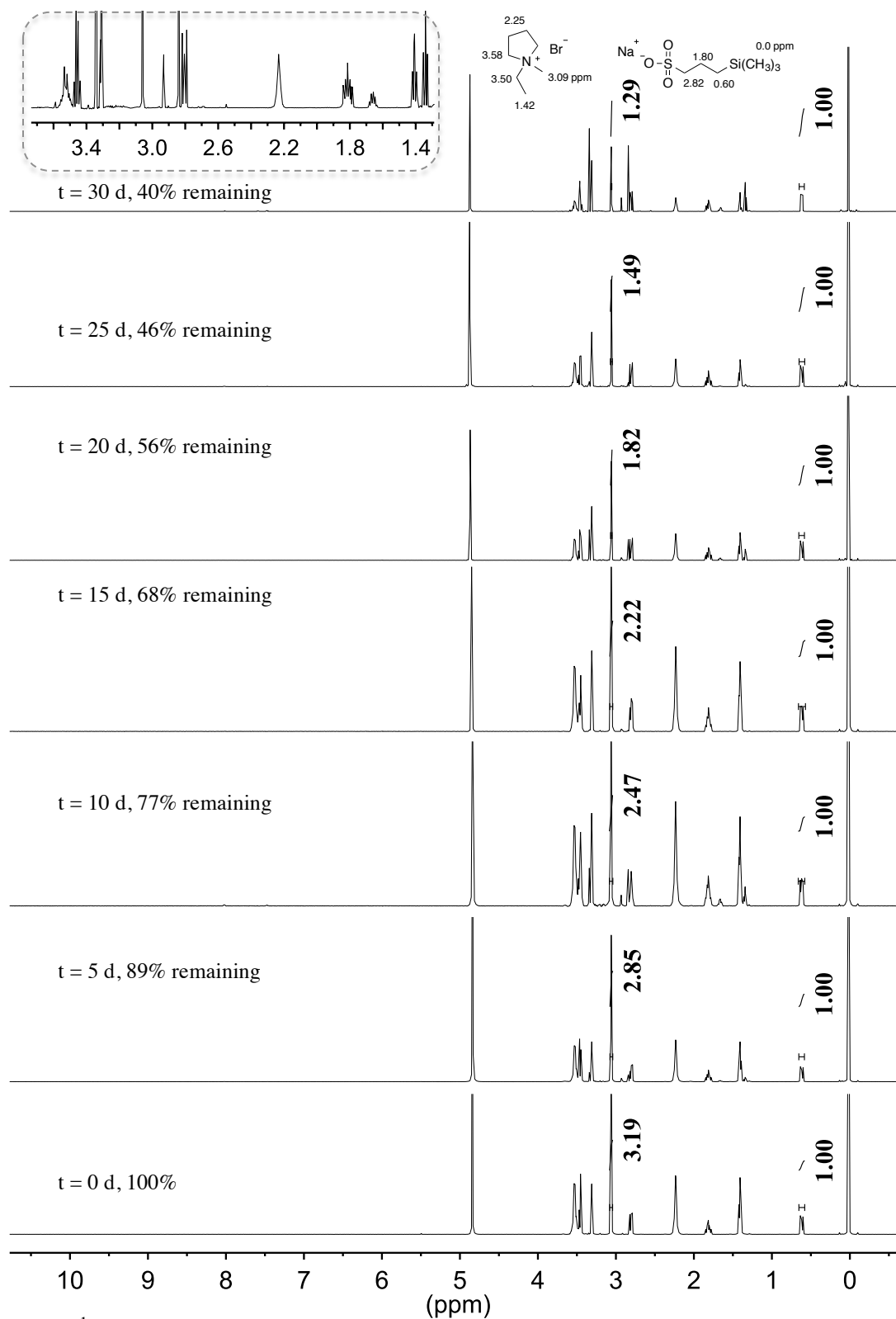


Figure 3.54 ^1H NMR spectra of **9** over 30 days dissolved in a basic CH_3OH solution at 80°C (1 M KOH, $[\text{KOH}]/[\mathbf{9}] = 20$) with an internal standard ($\text{TMS}(\text{CH}_2)_3\text{SO}_3\text{Na}$). Inset is extracted from $t = 30$ d.

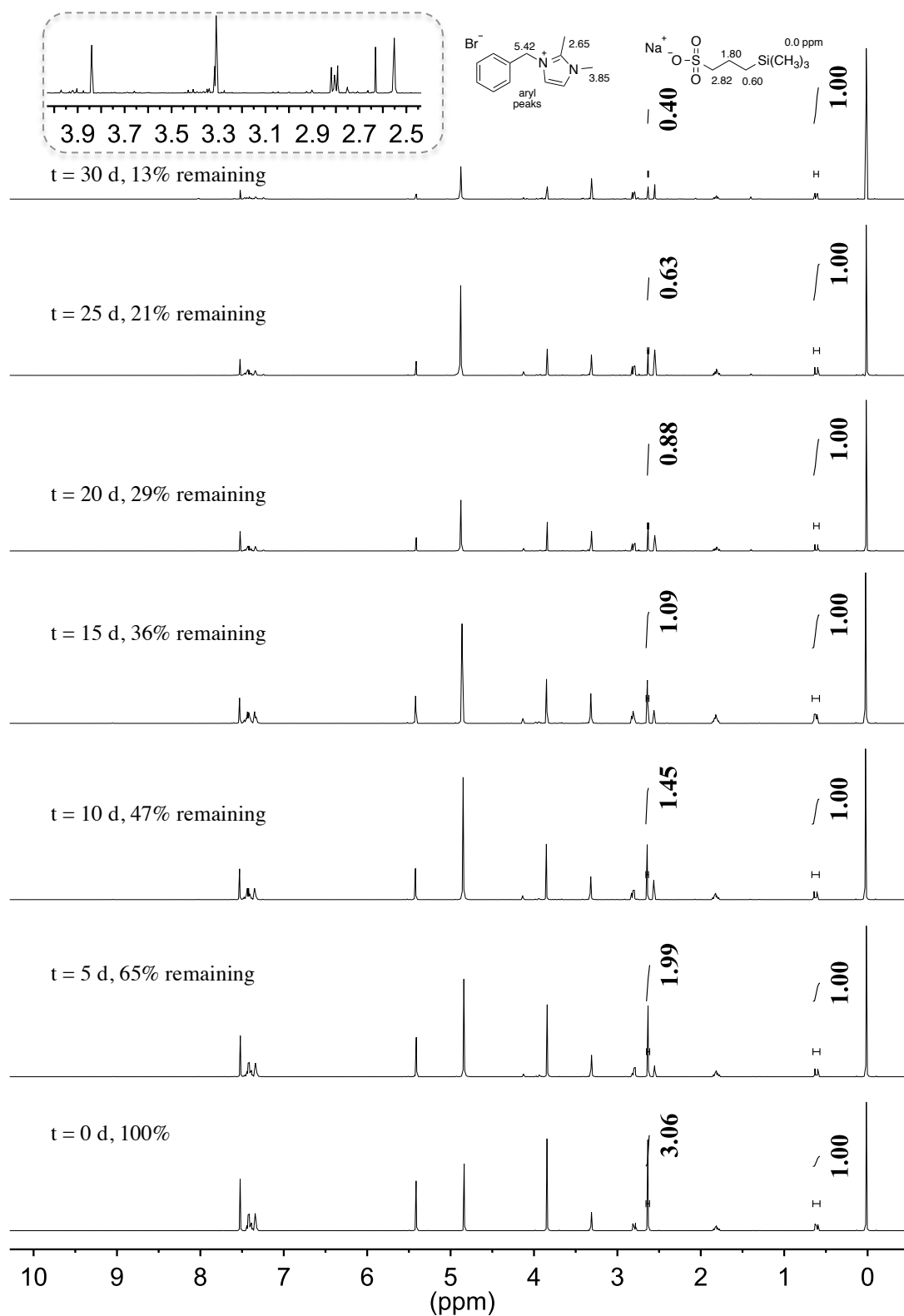


Figure 3.55 ^1H NMR spectra of **10** over 30 days dissolved in a basic CH_3OH solution at 80°C (1 M KOH, $[\text{KOH}]/[\text{10}] = 20$) with an internal standard (TMS(CH_2) $_3$ SO $_3$ Na). Inset is extracted from t = 30 d.

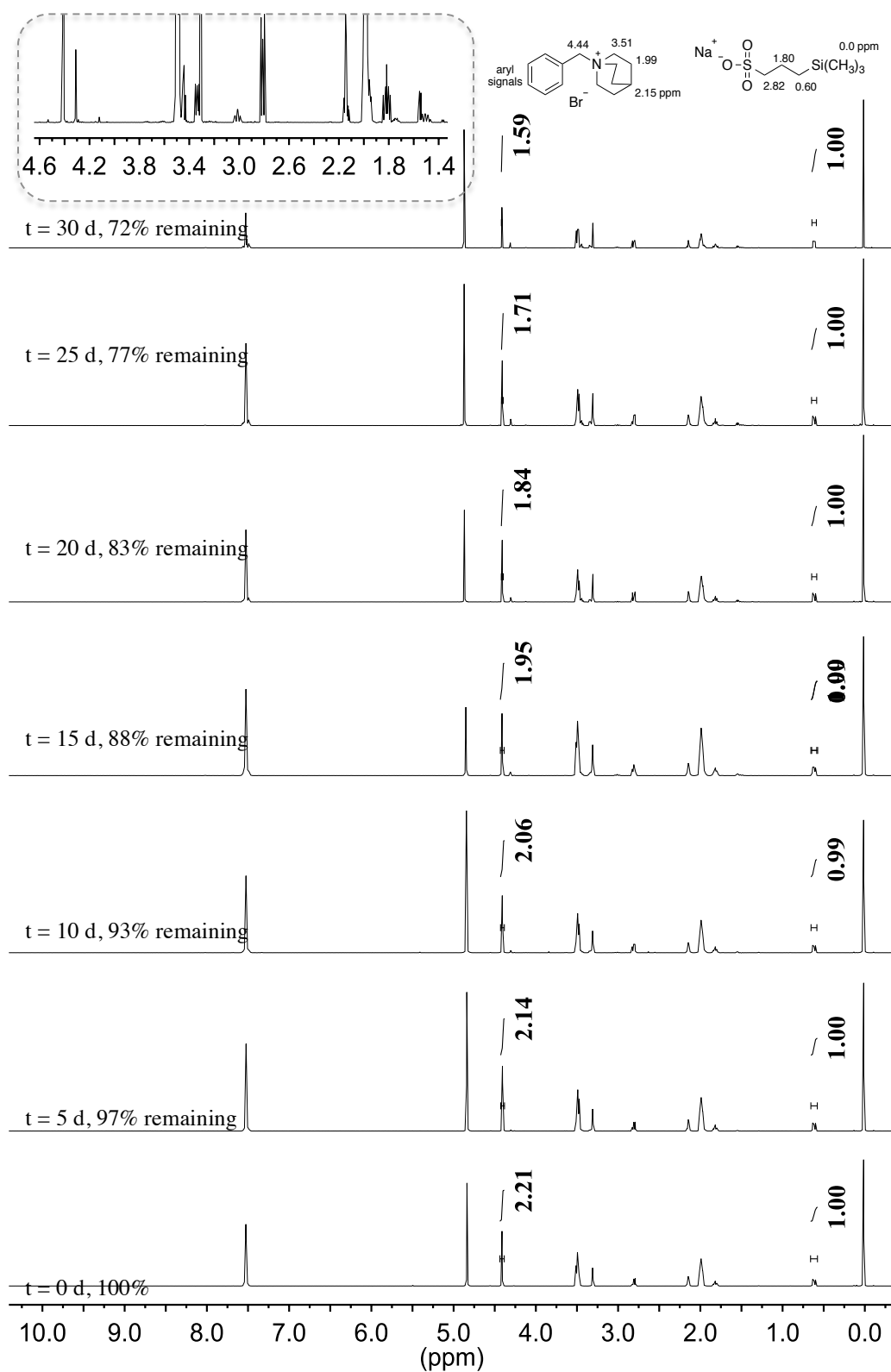


Figure 3.56 ^1H NMR spectra of **11** over 30 days dissolved in a basic CH_3OH solution at 80°C (1 M KOH, $[\text{KOH}]/[\textbf{11}] = 20$) with an internal standard (TMS(CH_2) $_3\text{SO}_3\text{Na}$). Inset is extracted from $t = 30$ d.

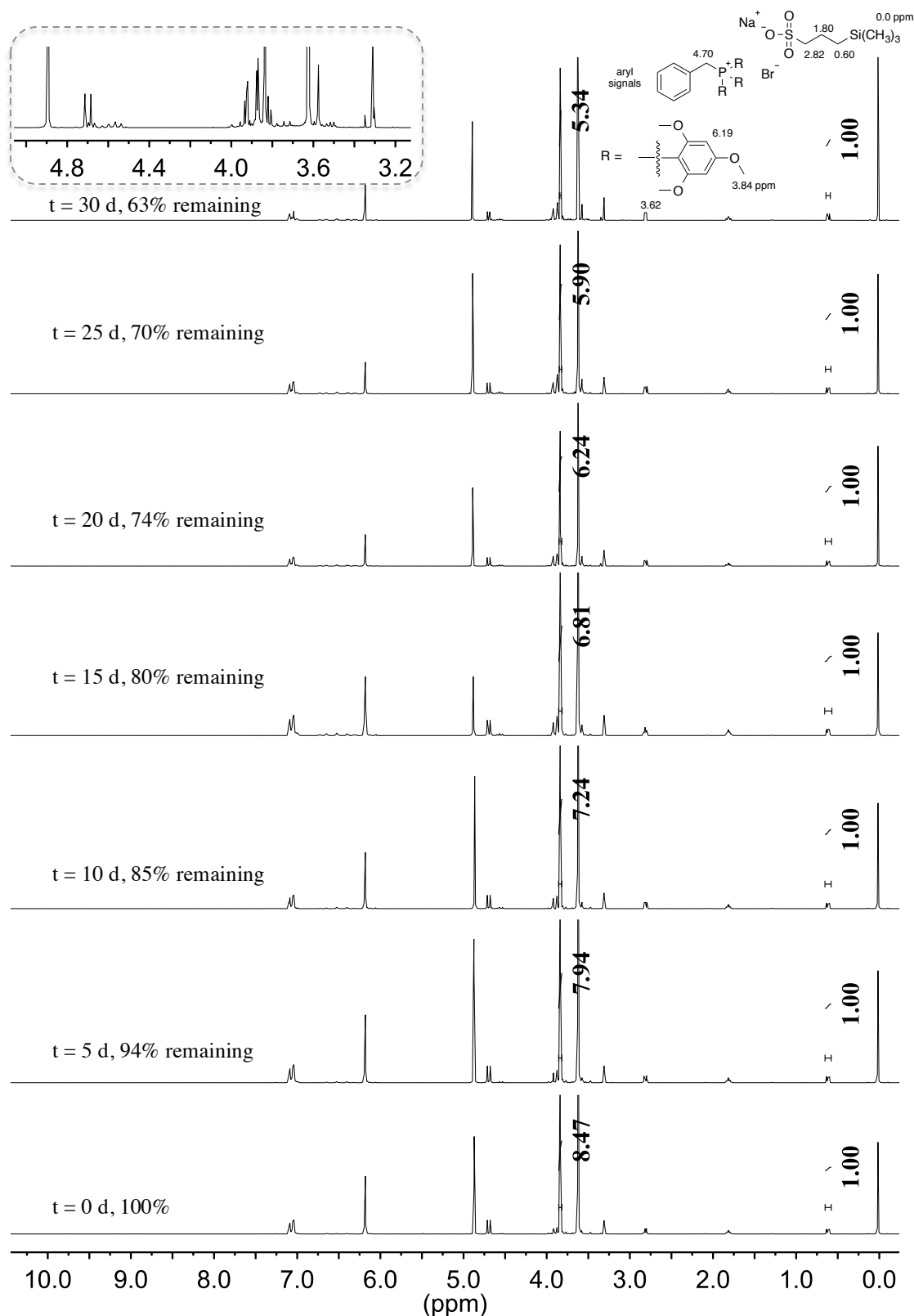


Figure 3.57 ^1H NMR spectra of **12** over 30 days dissolved in a basic CH_3OH solution at 80°C (1 M KOH, $[\text{KOH}]/[\text{12}] = 20$) with an internal standard ($\text{TMS}(\text{CH}_2)_3\text{SO}_3\text{Na}$). Inset is extracted from $t = 30$ d.

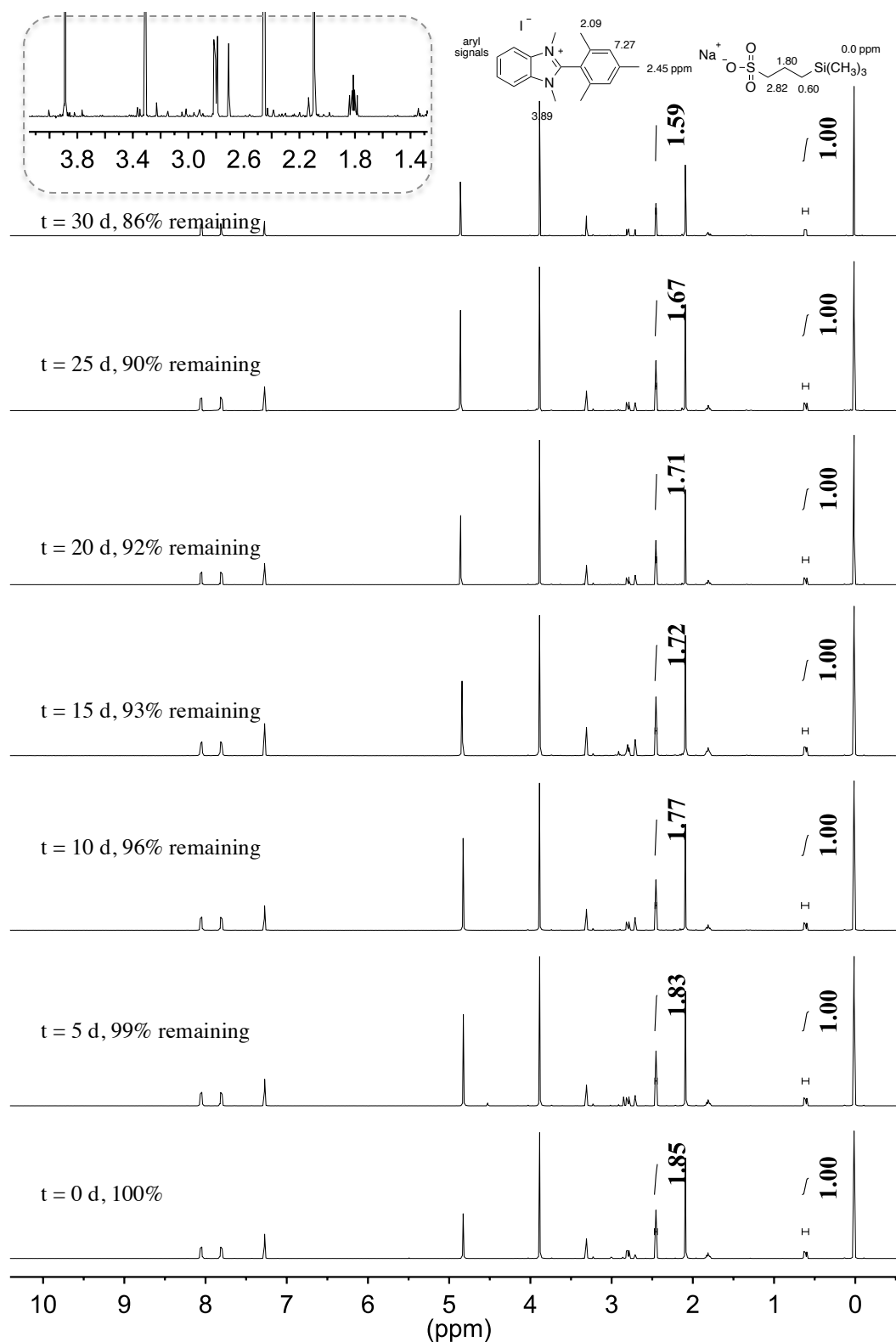


Figure 3.58 ^1H NMR spectra of **13** over 30 days dissolved in a basic CH_3OH solution at 80°C (1 M KOH, $[\text{KOH}]/[\textbf{13}] = 20$) with an internal standard (TMS(CH_2) $_3$ SO $_3$ Na). Inset is extracted from t = 30 d.

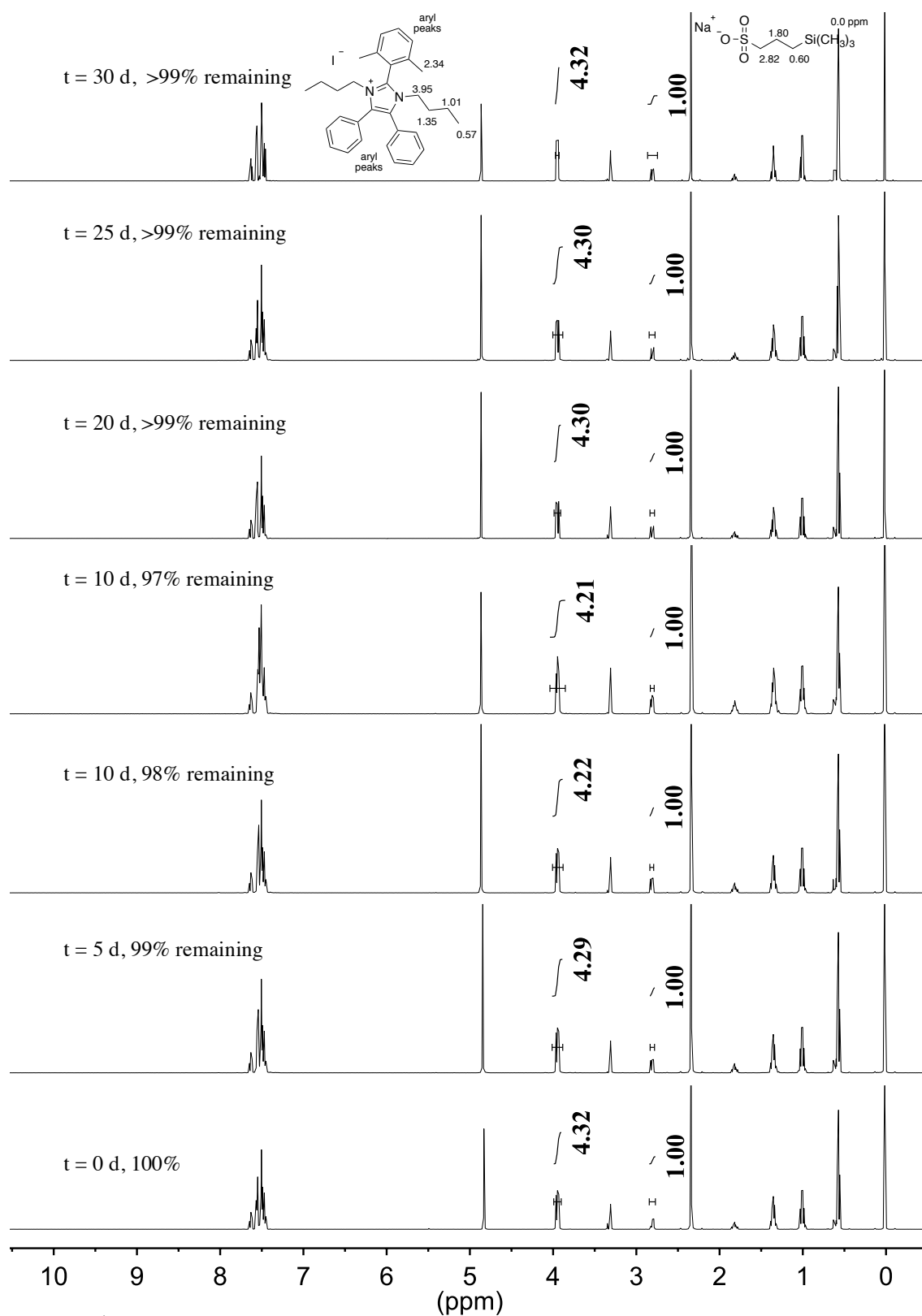


Figure 3.59 ¹H NMR spectra of **14** over 30 days dissolved in a basic CH₃OH solution at 80 °C (1 M KOH, [KOH]/[**14**] = 20) with an internal standard (TMS(CH₂)₃SO₃Na).

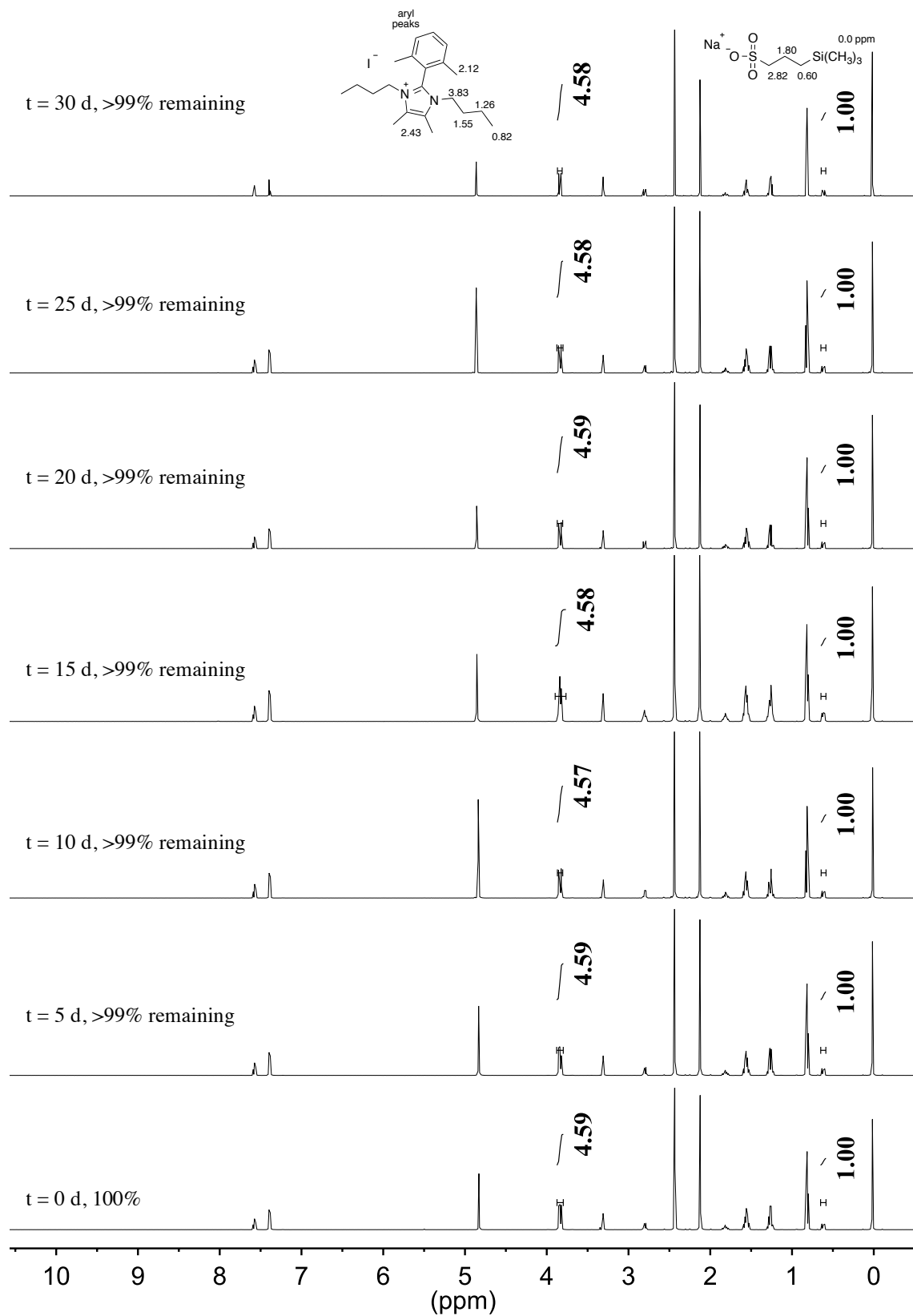


Figure 3.60 ^1H NMR spectra of **15** over 30 days dissolved in a basic CD_3OH solution at 80°C (1 M KOH, $[\text{KOH}]/[\text{15}] = 20$) with an internal standard ($\text{TMS}(\text{CH}_2)_3\text{SO}_3\text{Na}$).

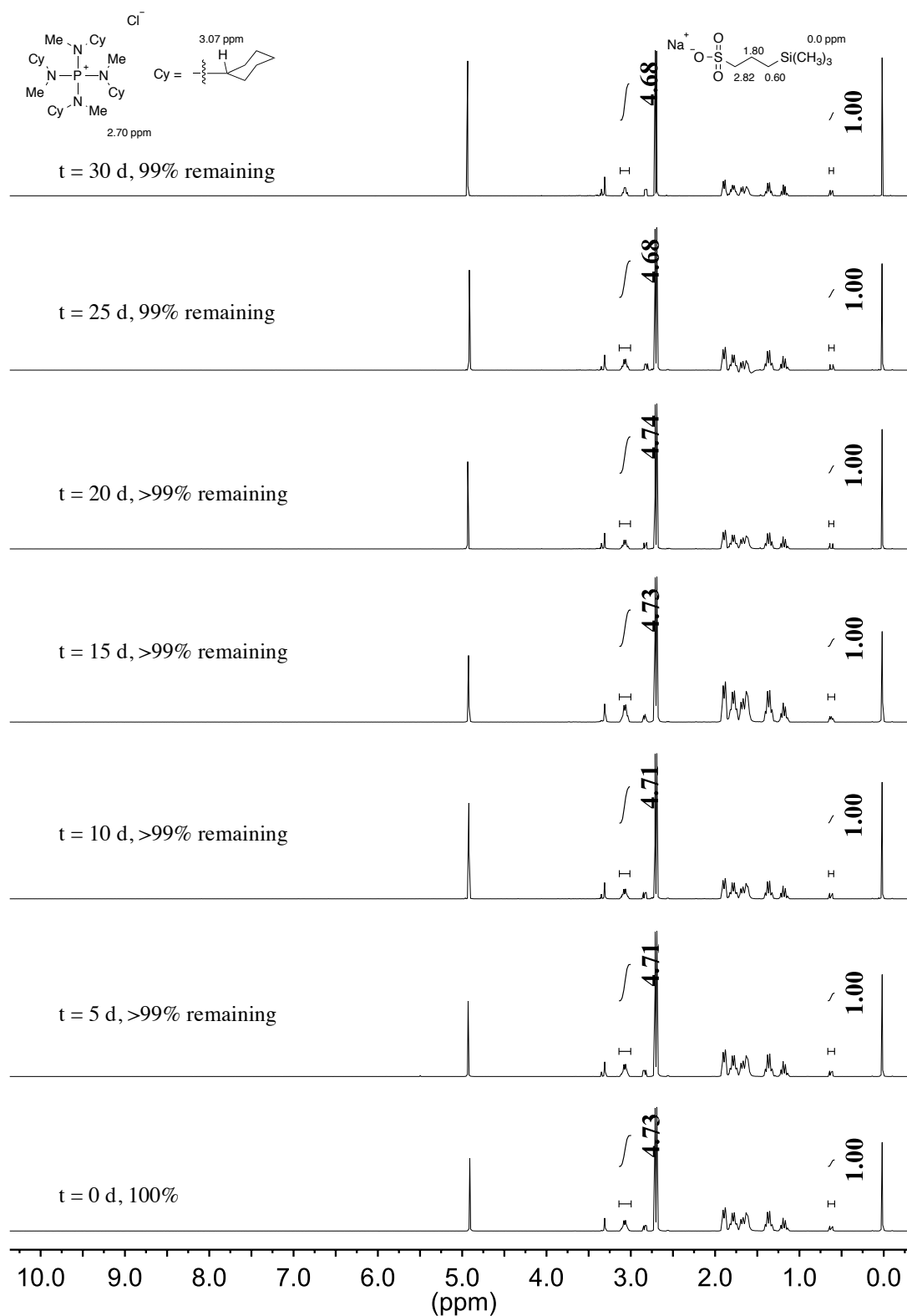


Figure 3.61 ^1H NMR spectra of **16** over 30 days dissolved in a basic CH_3OH solution at 80°C (1 M KOH, $[\text{KOH}]/[\text{16}] = 20$) with an internal standard ($\text{TMS}(\text{CH}_2)_3\text{SO}_3\text{Na}$).

3.5.8 Copies of HRMS (DART) Spectra for Model Compound Studies

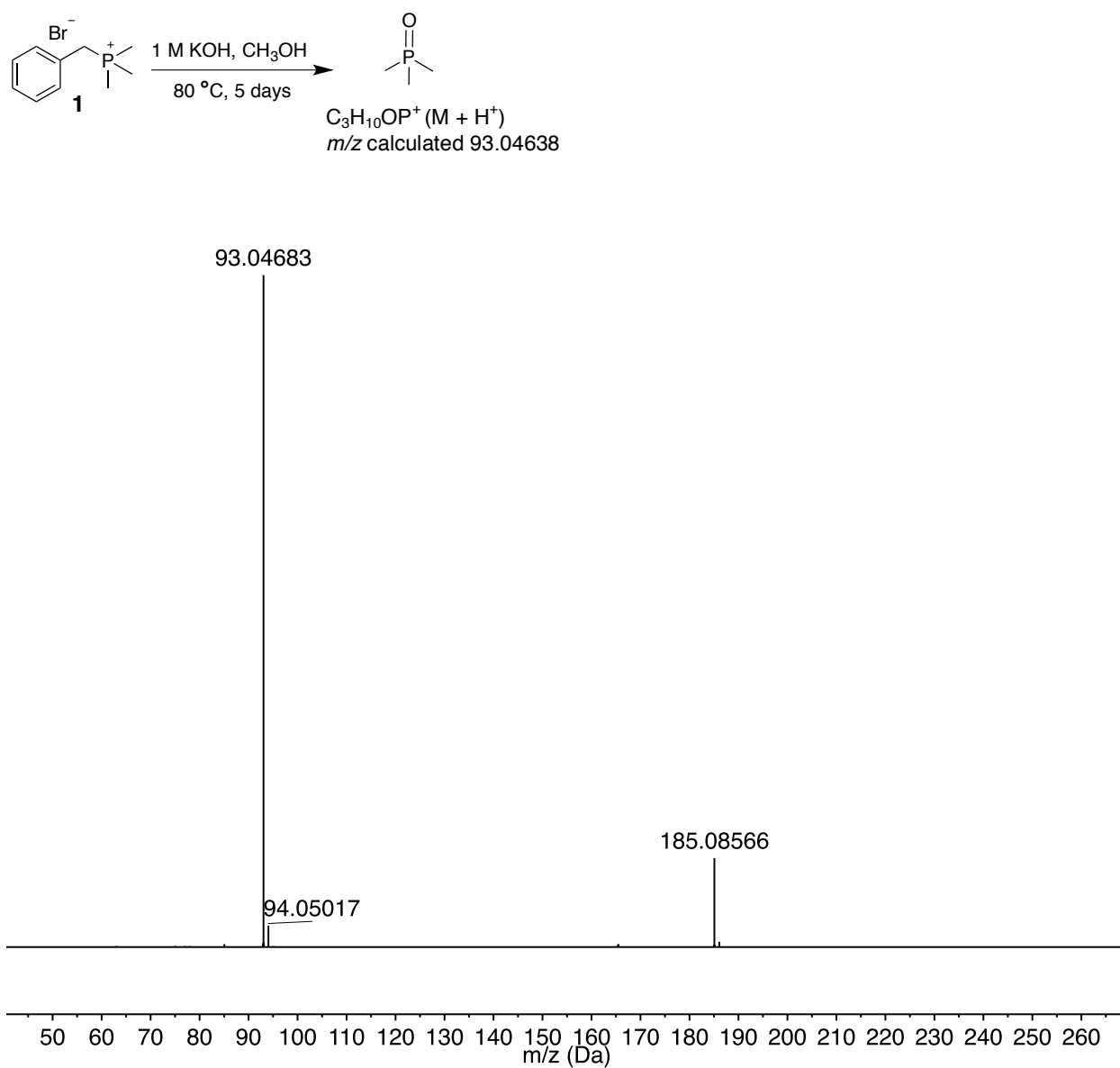


Figure 3.62 HRMS (DART) of **1** after 5 days dissolved in 1M KOH, CH₃OH solution at 80 °C.

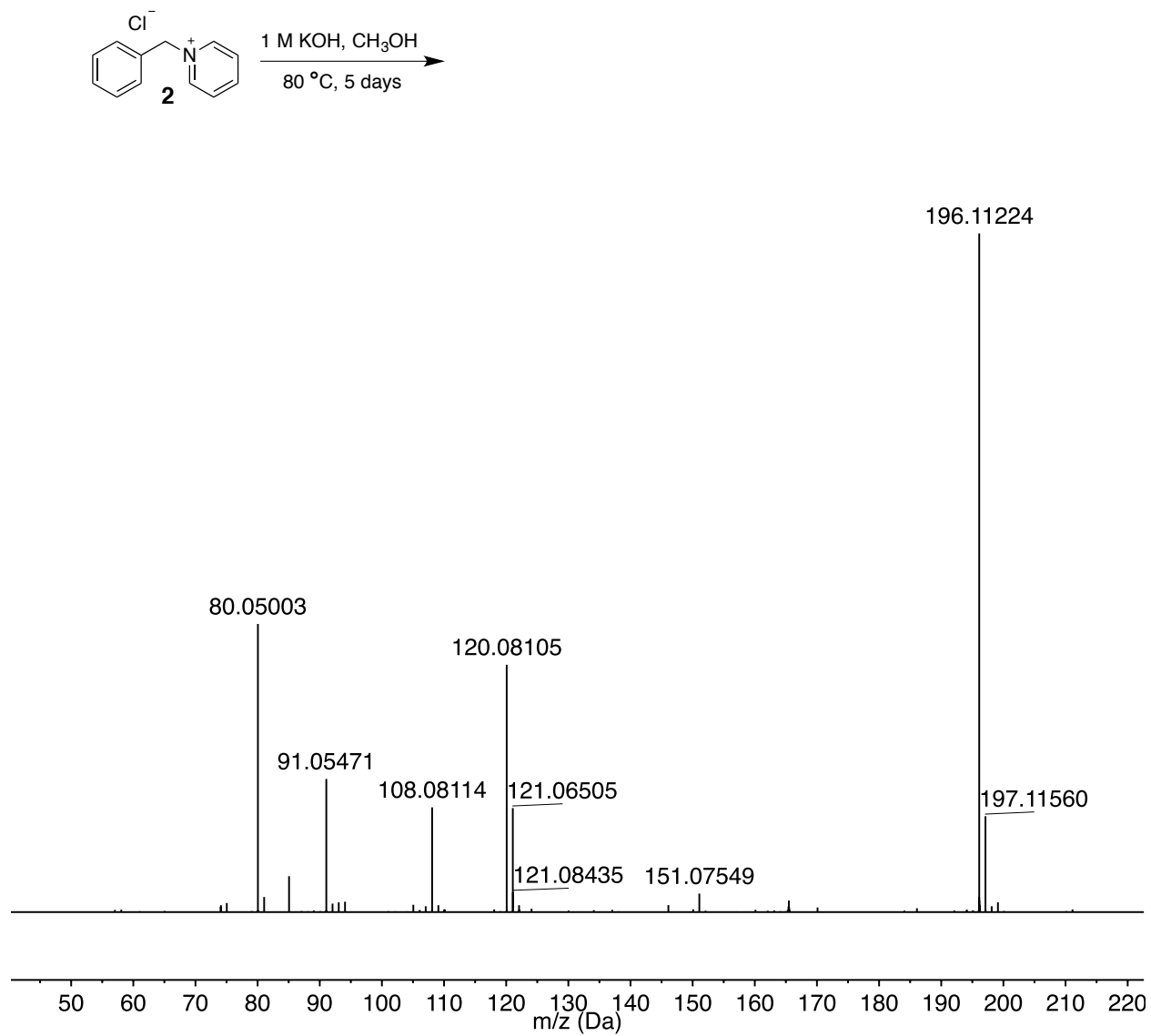


Figure 3.63 HRMS (DART) of **2** after 5 days dissolved in 1M KOH, CH₃OH solution at 80 °C.

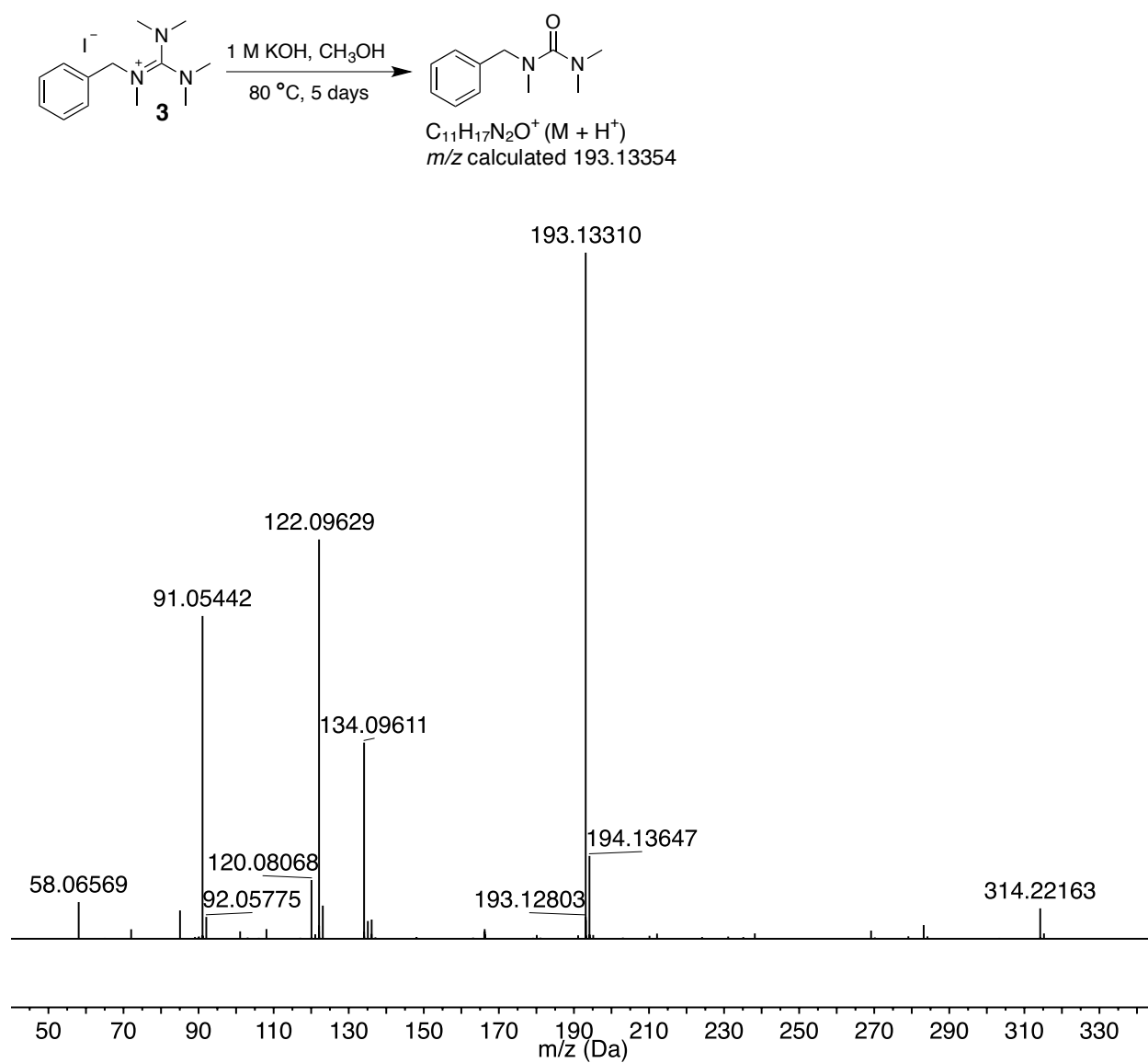


Figure 3.64 HRMS (DART) of **3** after 5 days dissolved in 1M KOH, CH₃OH solution at 80 °C.

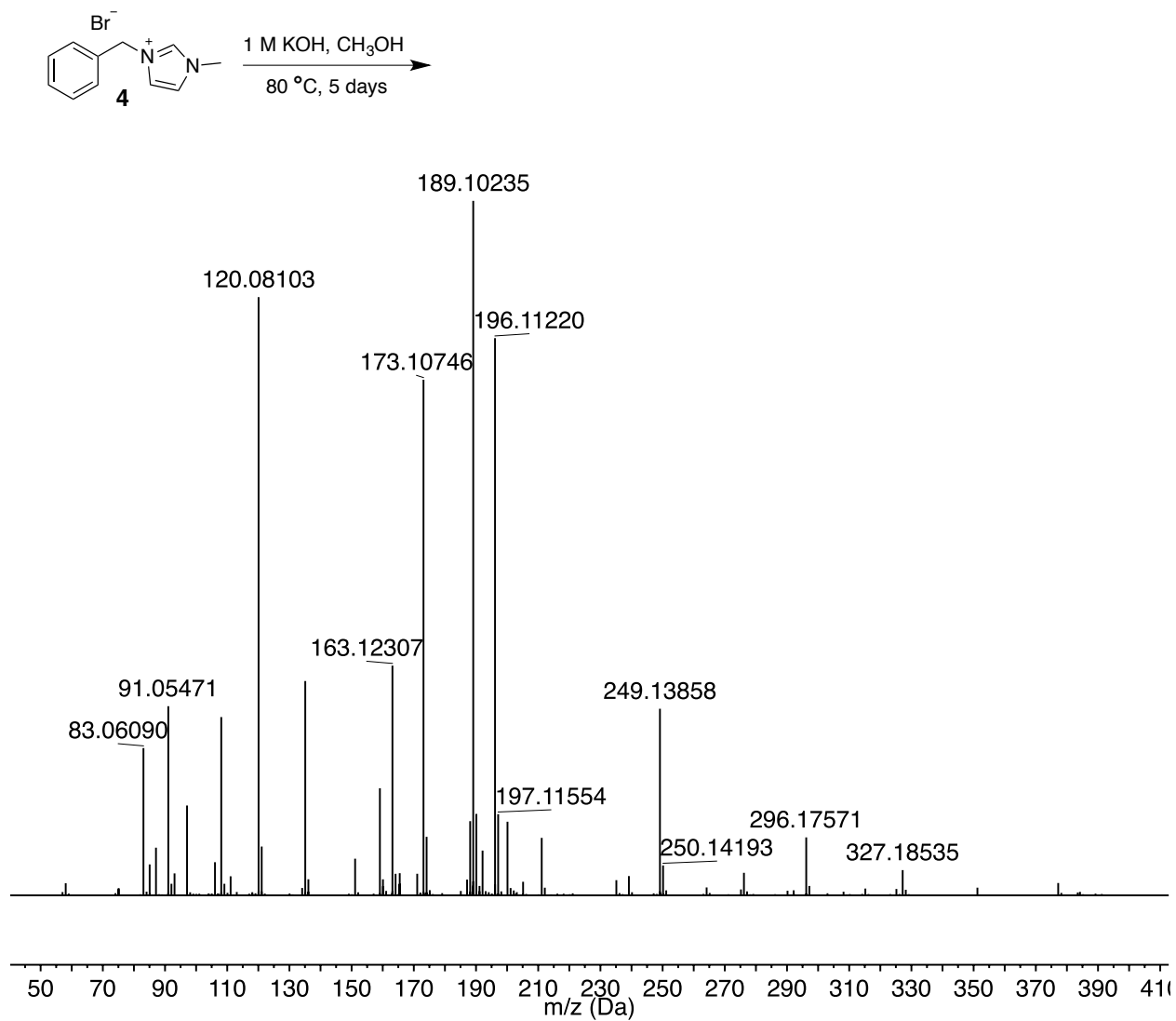


Figure 3.65 HRMS (DART) of **4** after 5 days dissolved in 1M KOH, CH₃OH solution at 80 °C.

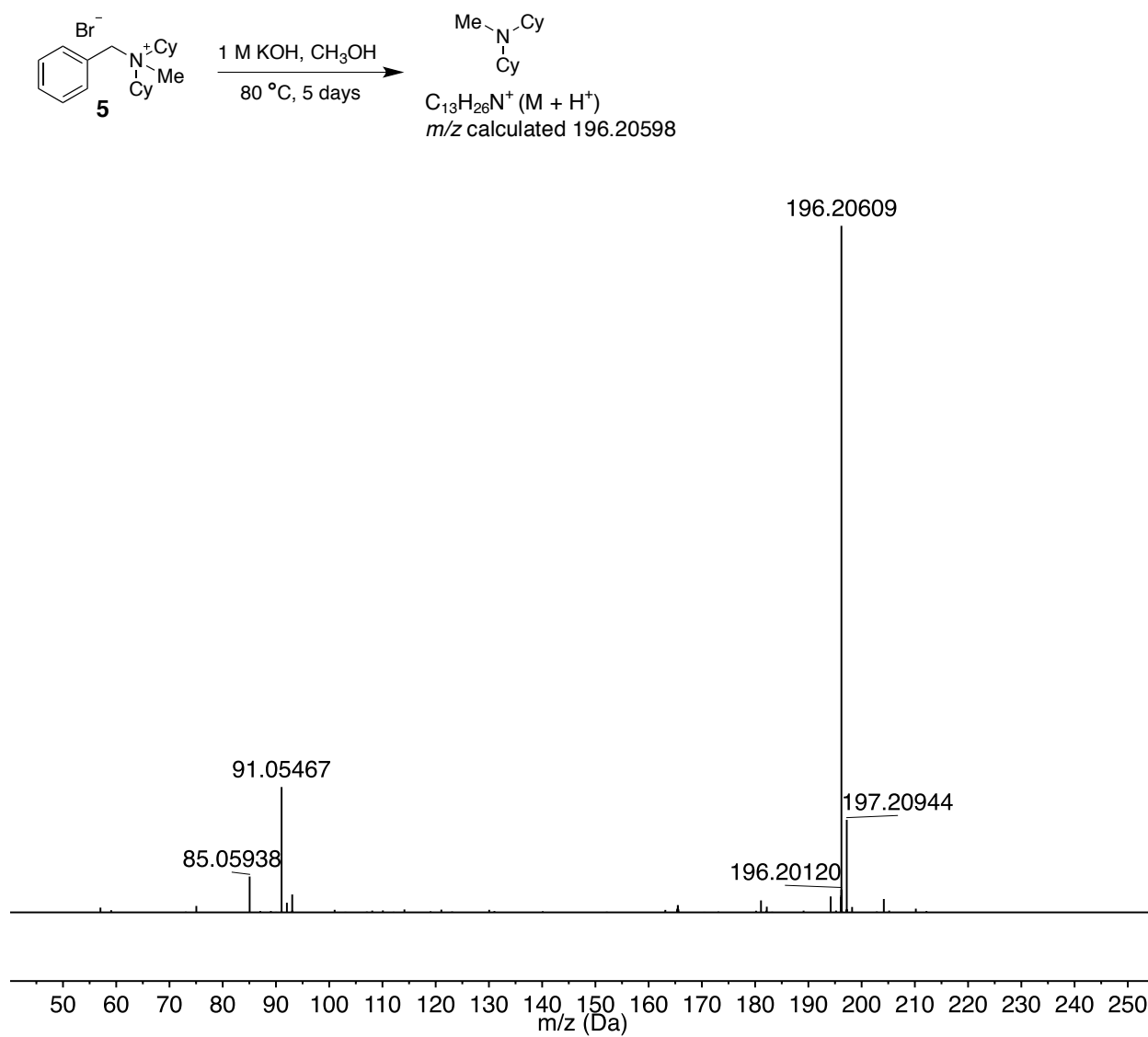


Figure 3.66 HRMS (DART) of **5** after 5 days dissolved in 1M KOH, CH₃OH solution at 80 °C.

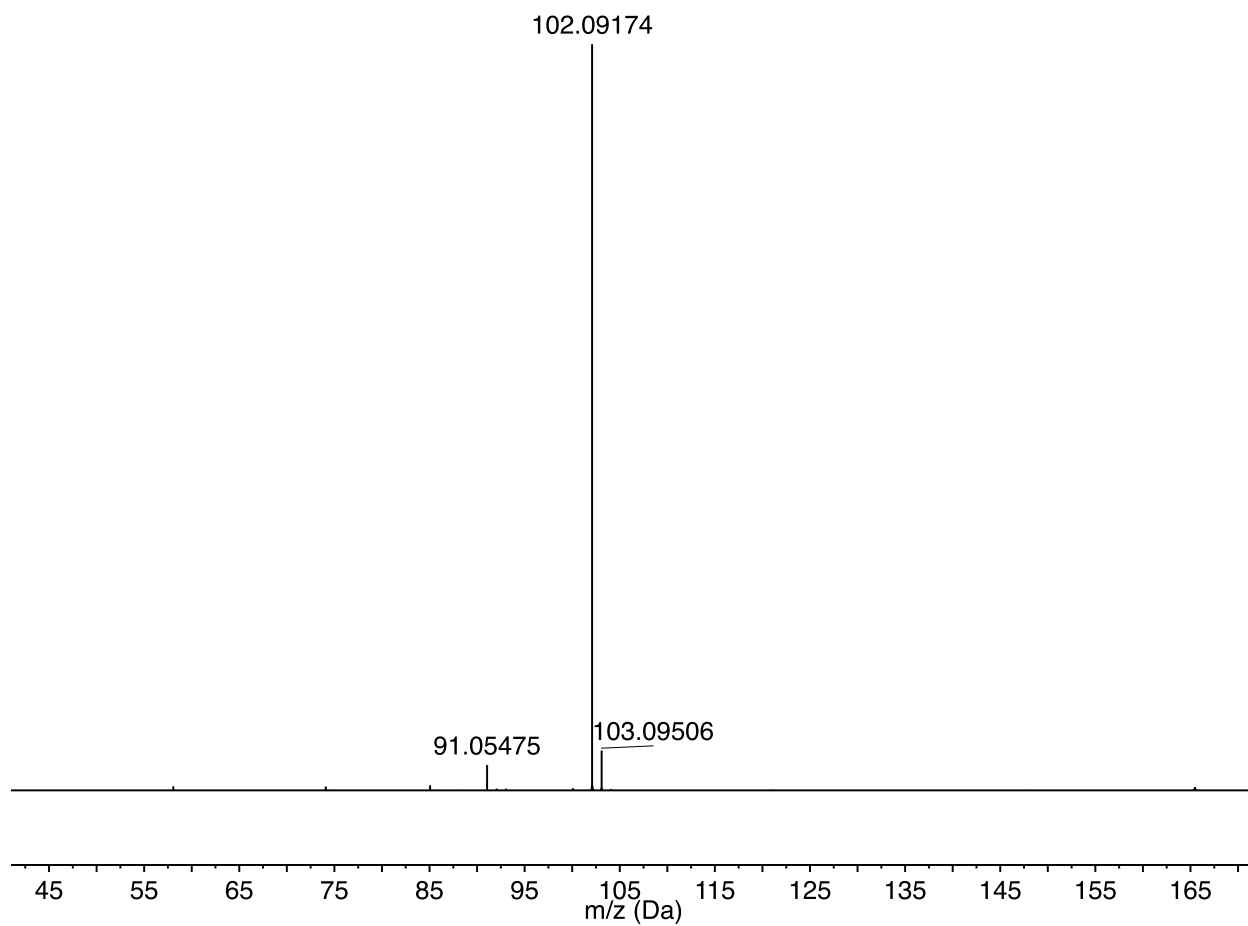
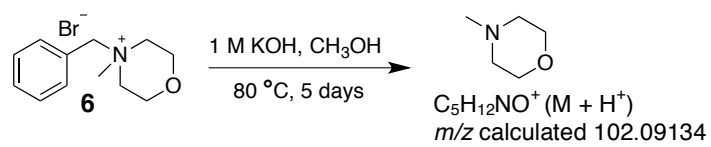


Figure 3.67 HRMS (DART) of **6** after 5 days dissolved in 1M KOH, CH₃OH solution at 80 °C.

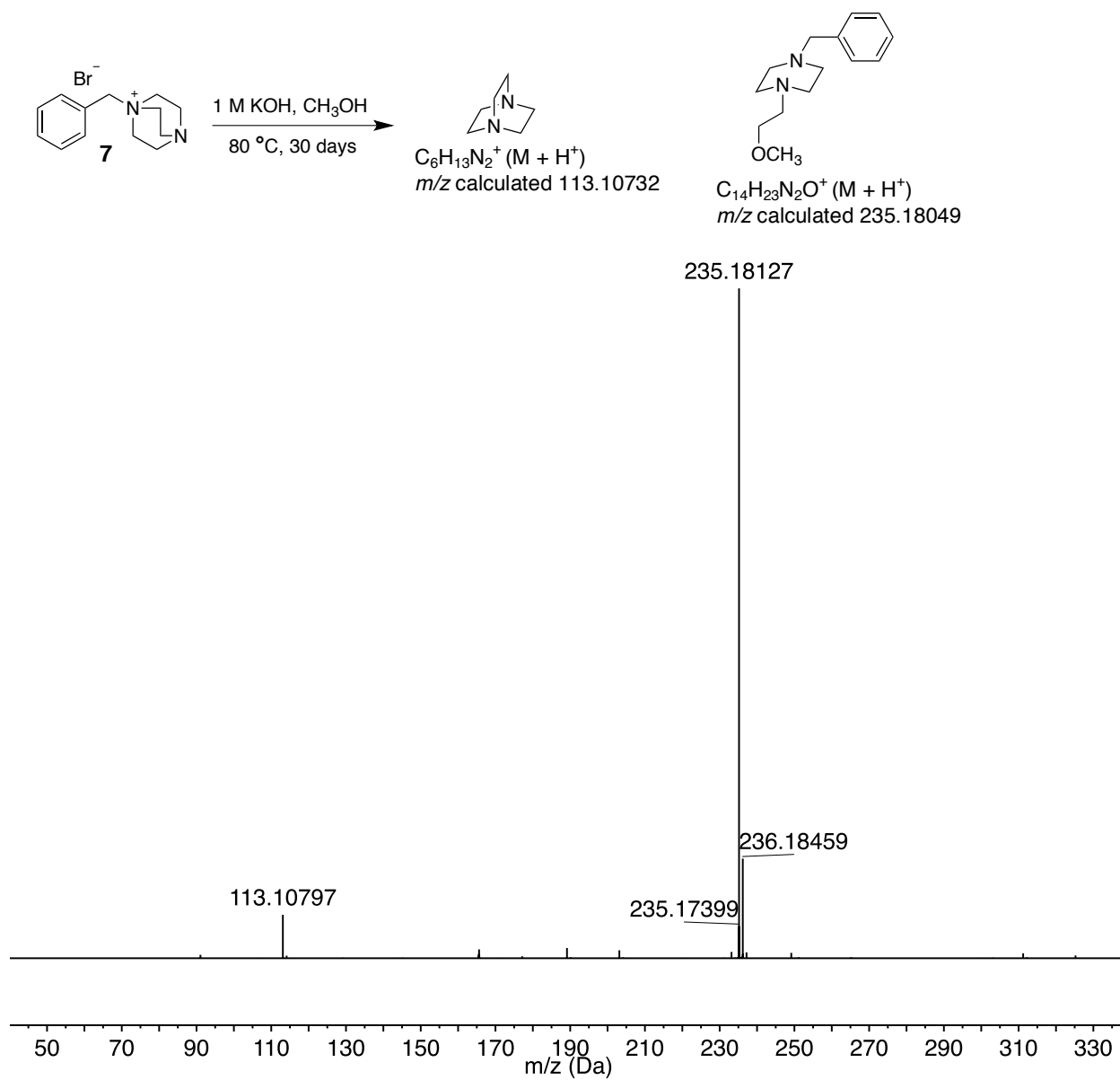


Figure 3.68 HRMS (DART) of **7** after 30 days dissolved in 1M KOH, CH₃OH solution at 80 °C.

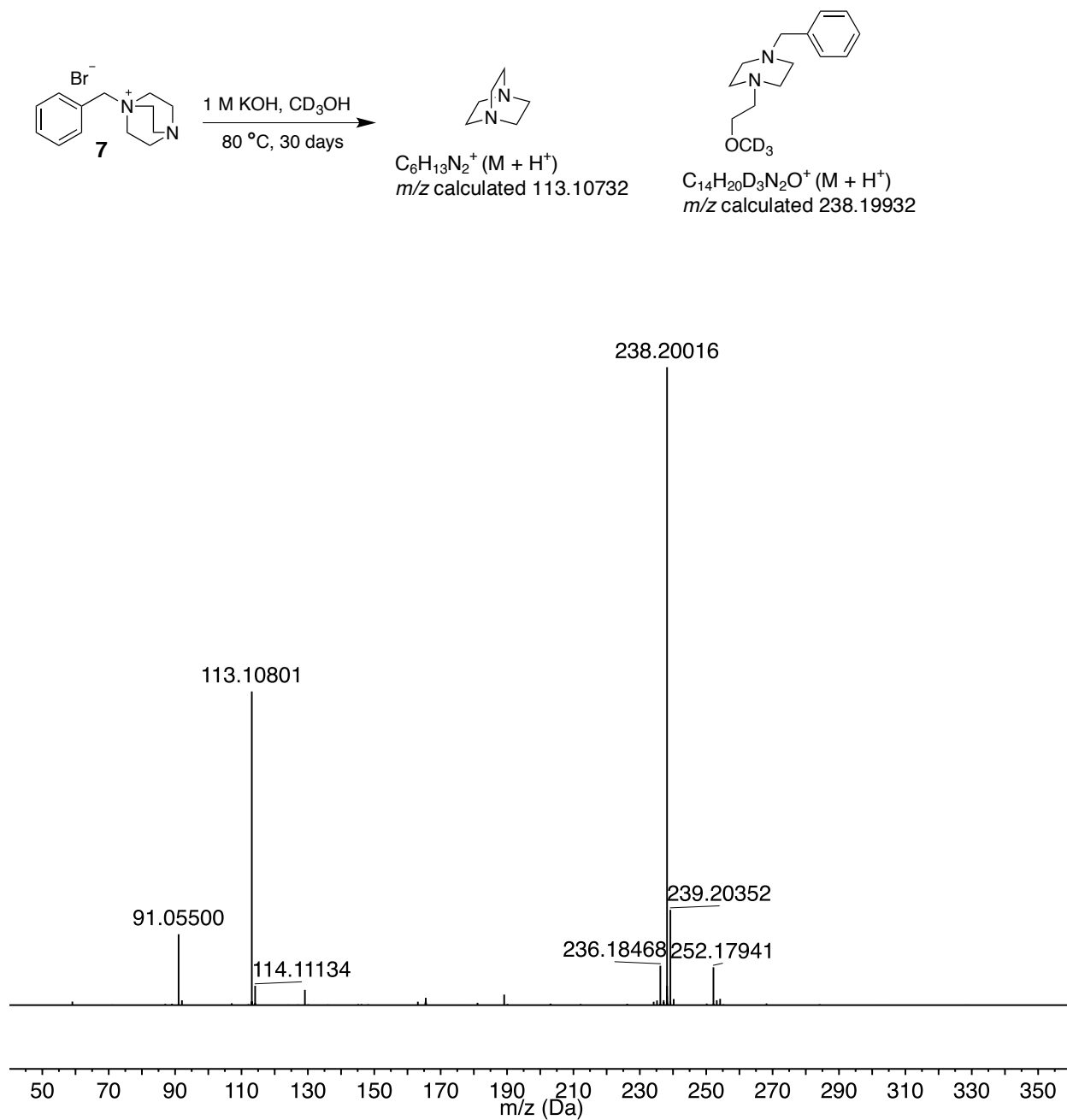


Figure 3.69 HRMS (DART) of **7** after 30 days dissolved in 1M KOH, CD₃OH solution at 80 °C.

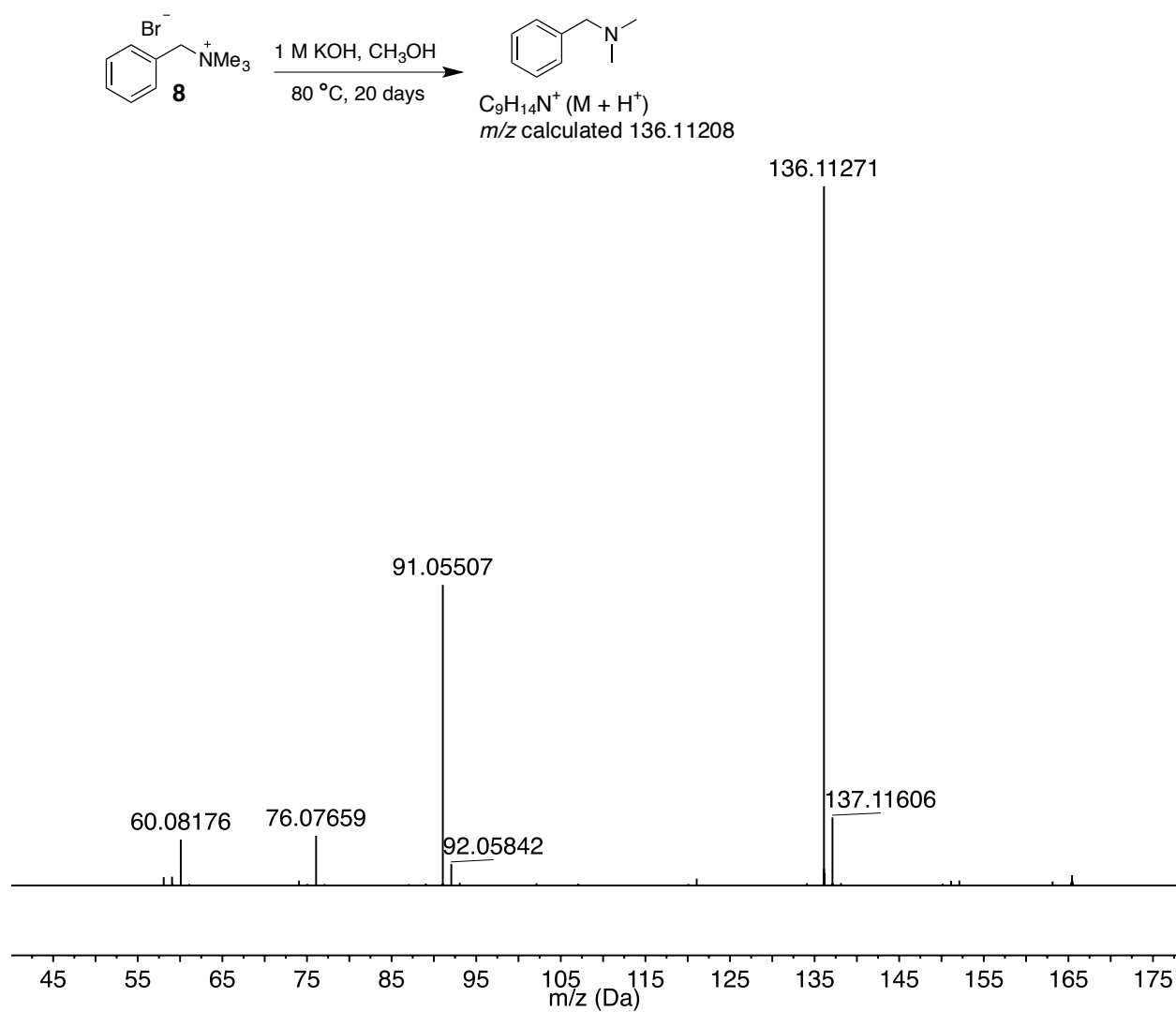


Figure 3.70 HRMS (DART) of **8** after 20 days dissolved in 1M KOH, CH_3OH solution at 80°C .

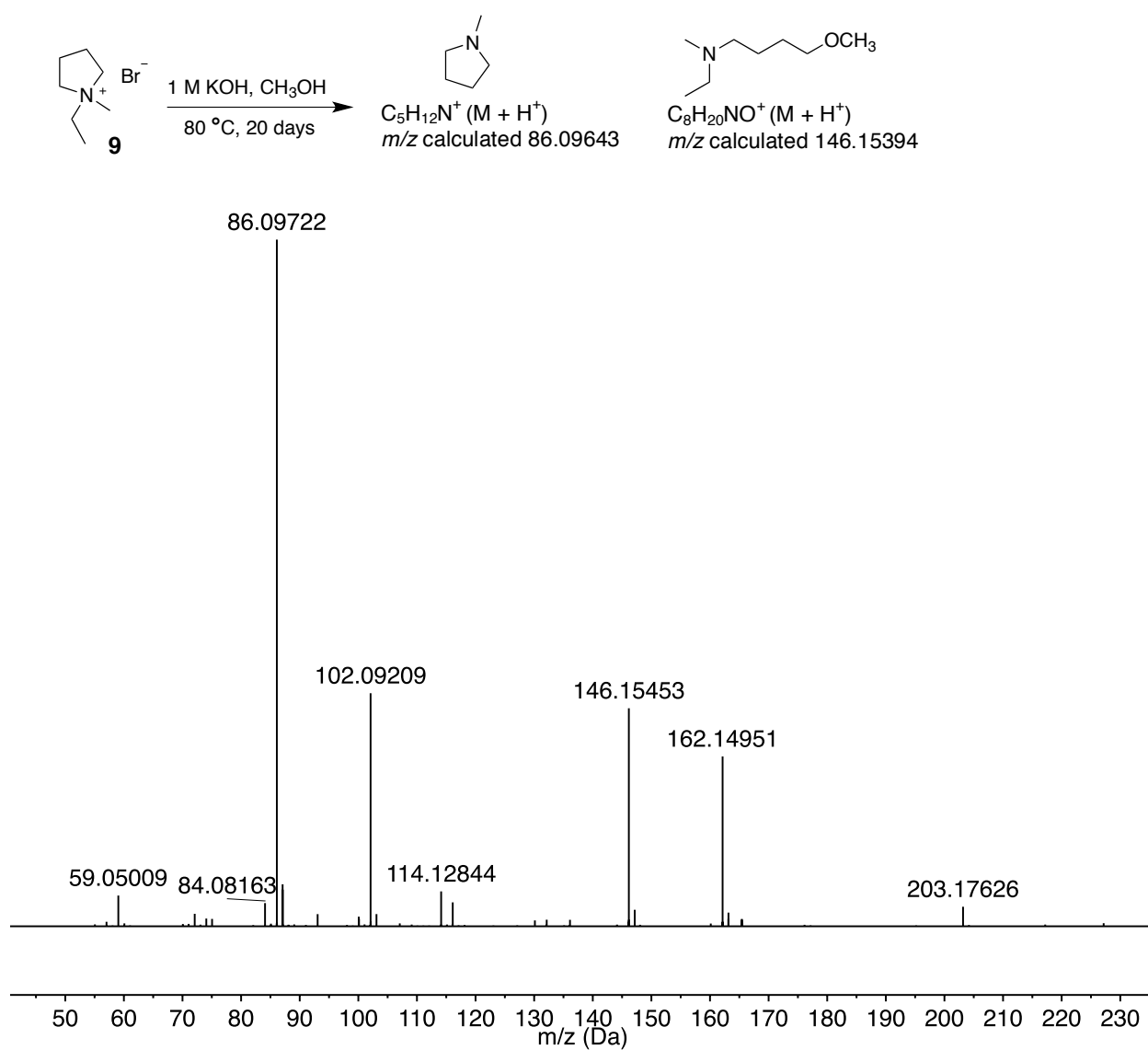


Figure 3.71 HRMS (DART) of **9** after 20 days dissolved in 1M KOH, CH₃OH solution at 80 °C.

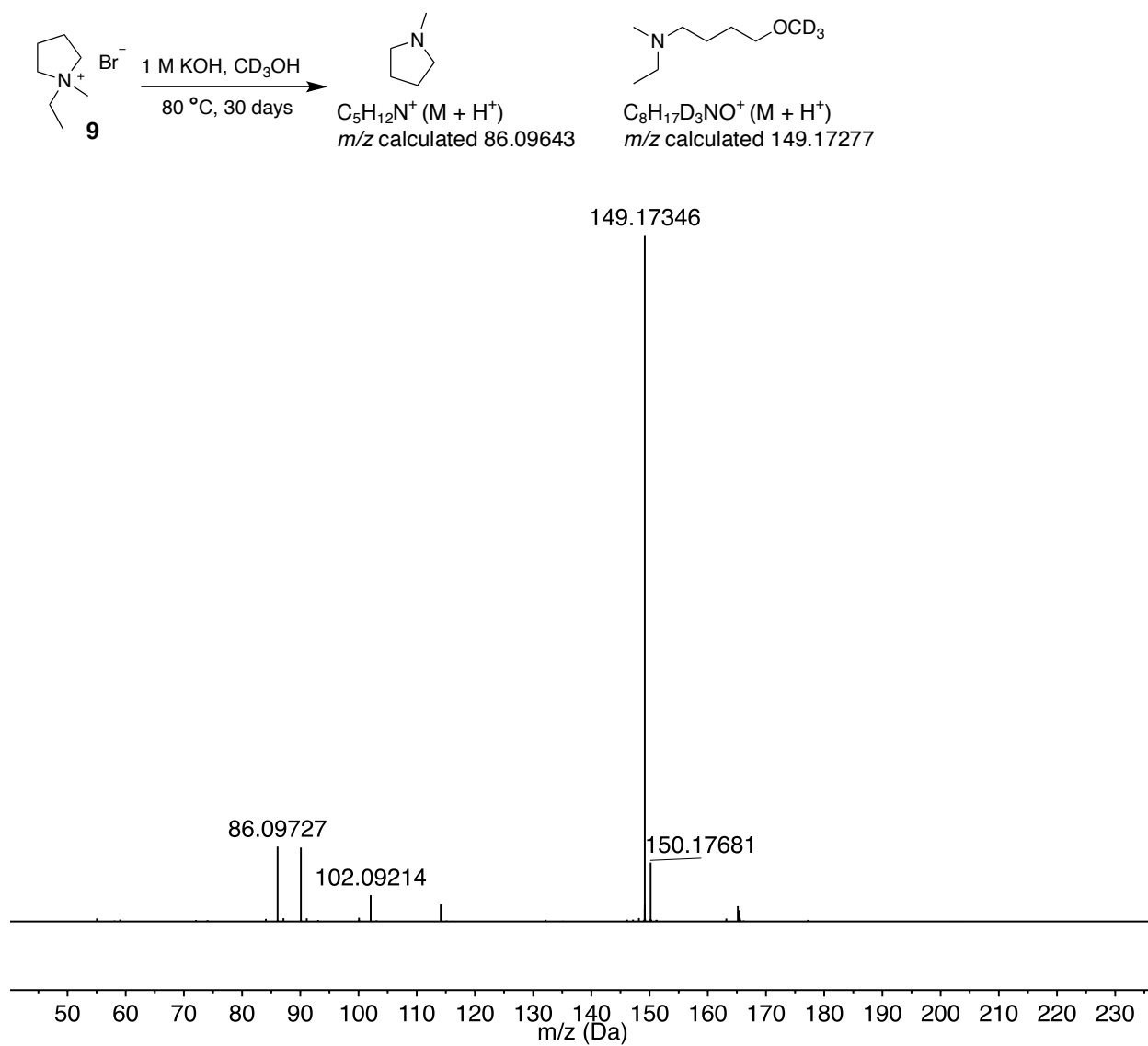


Figure 3.72 HRMS (DART) of **9** after 30 days dissolved in 1M KOH, CD₃OH solution at 80 °C.

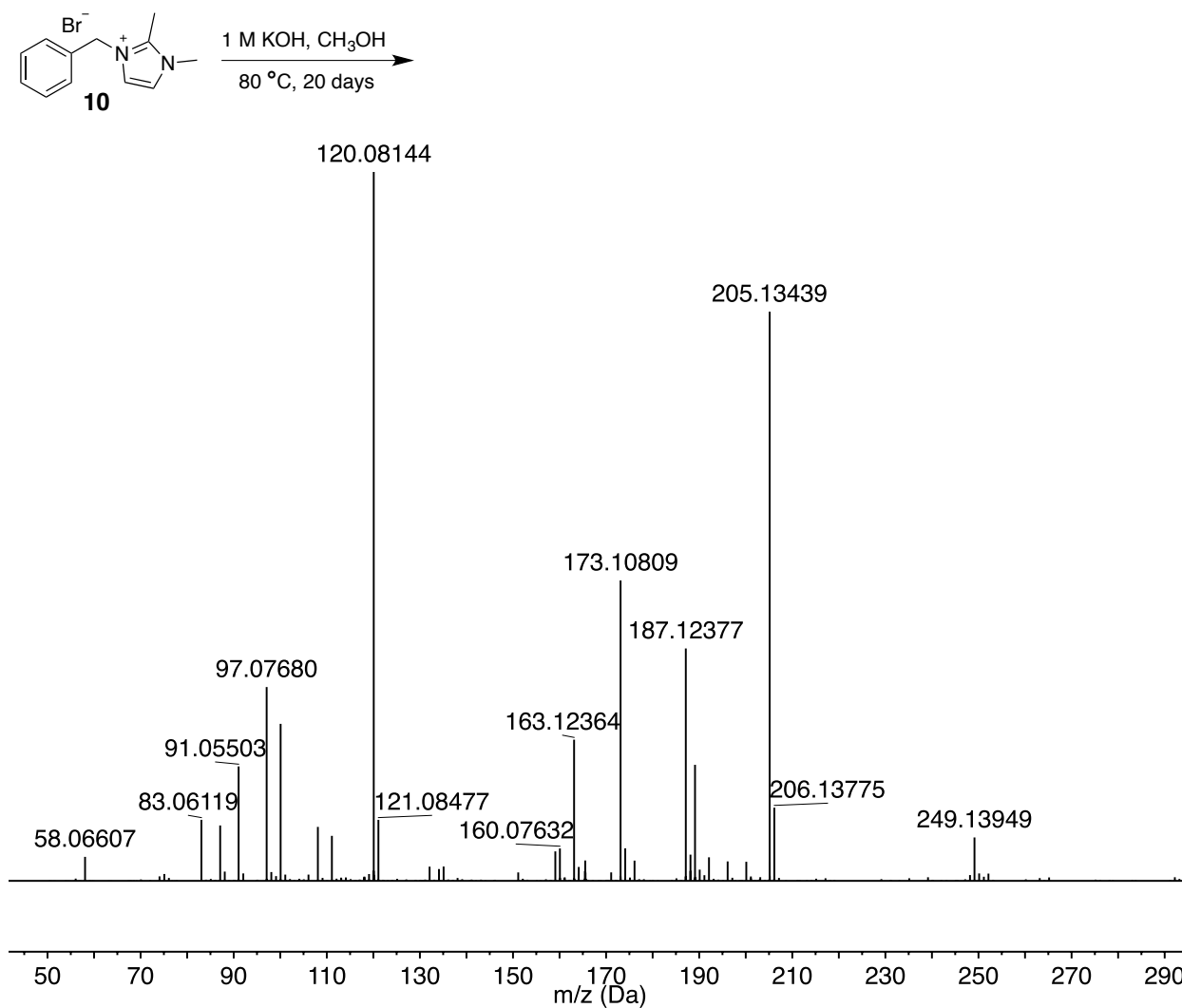


Figure 3.73 HRMS (DART) of **10** after 20 days dissolved in 1M KOH, CH₃OH solution at 80 °C.

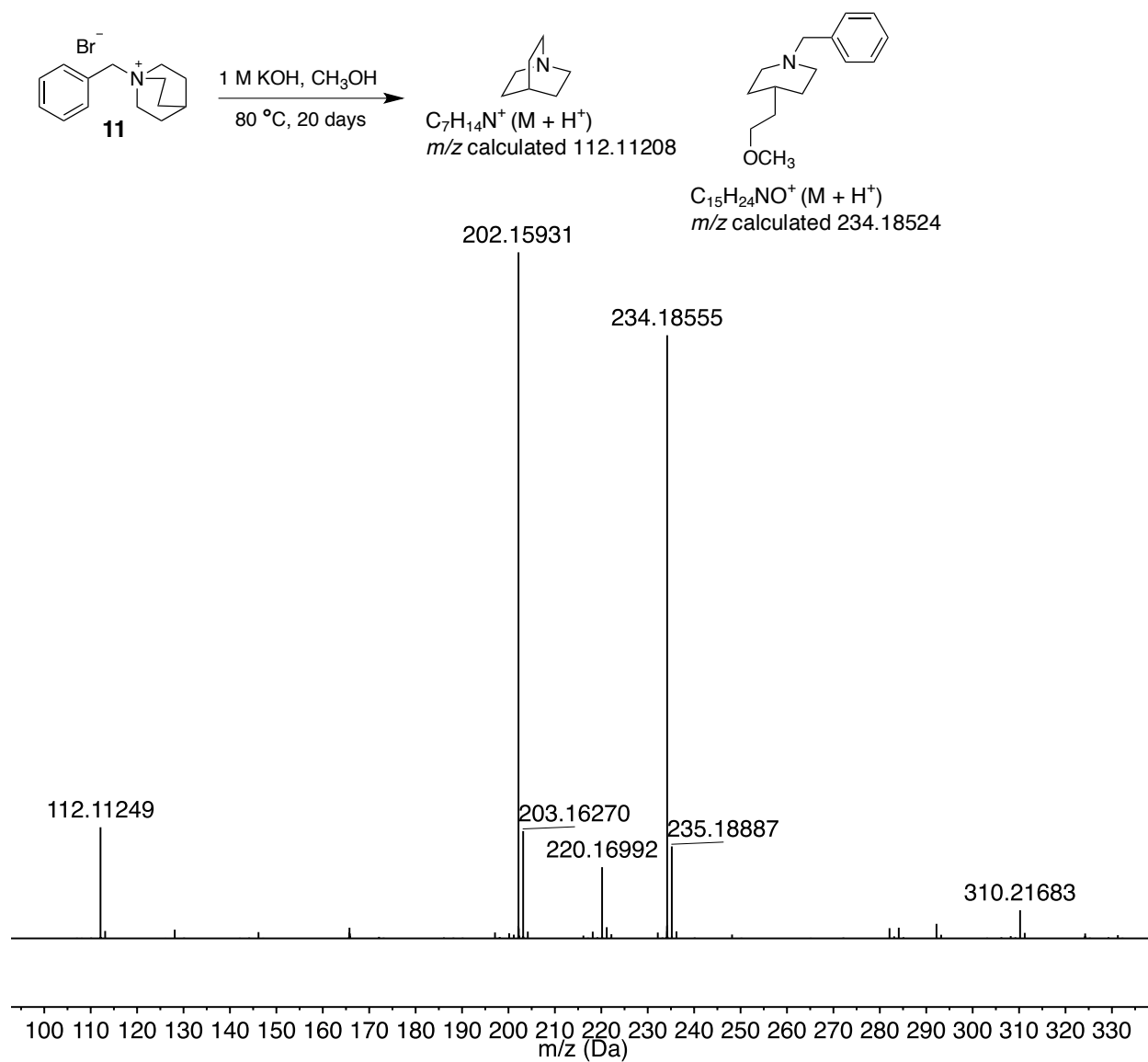


Figure 3.74 HRMS (DART) of **11** after 20 days dissolved in 1M KOH, CH₃OH solution at 80 °C.

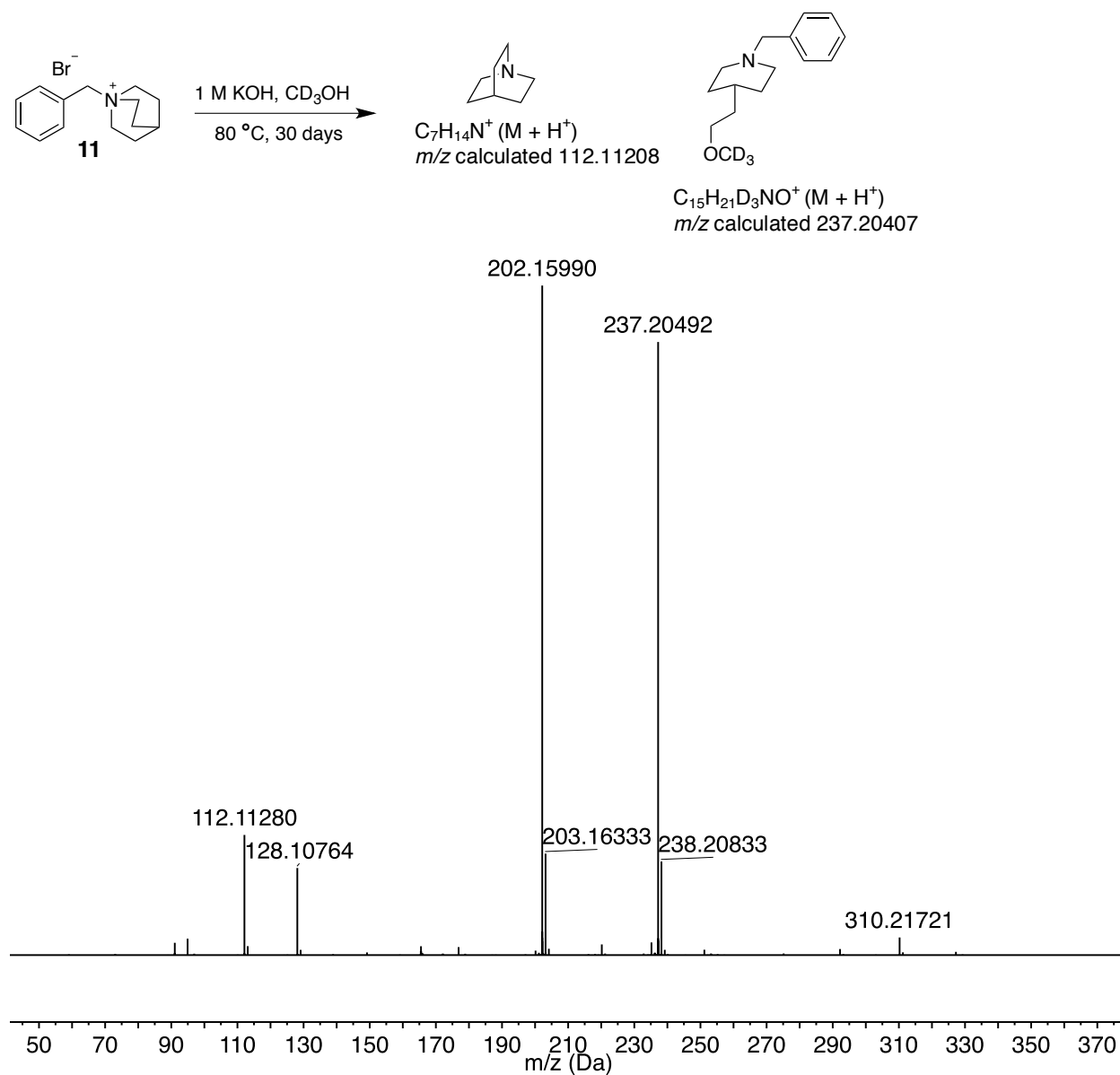


Figure 3.75 HRMS (DART) of **11** after 30 days dissolved in 1M KOH, CD₃OH solution at 80 °C.

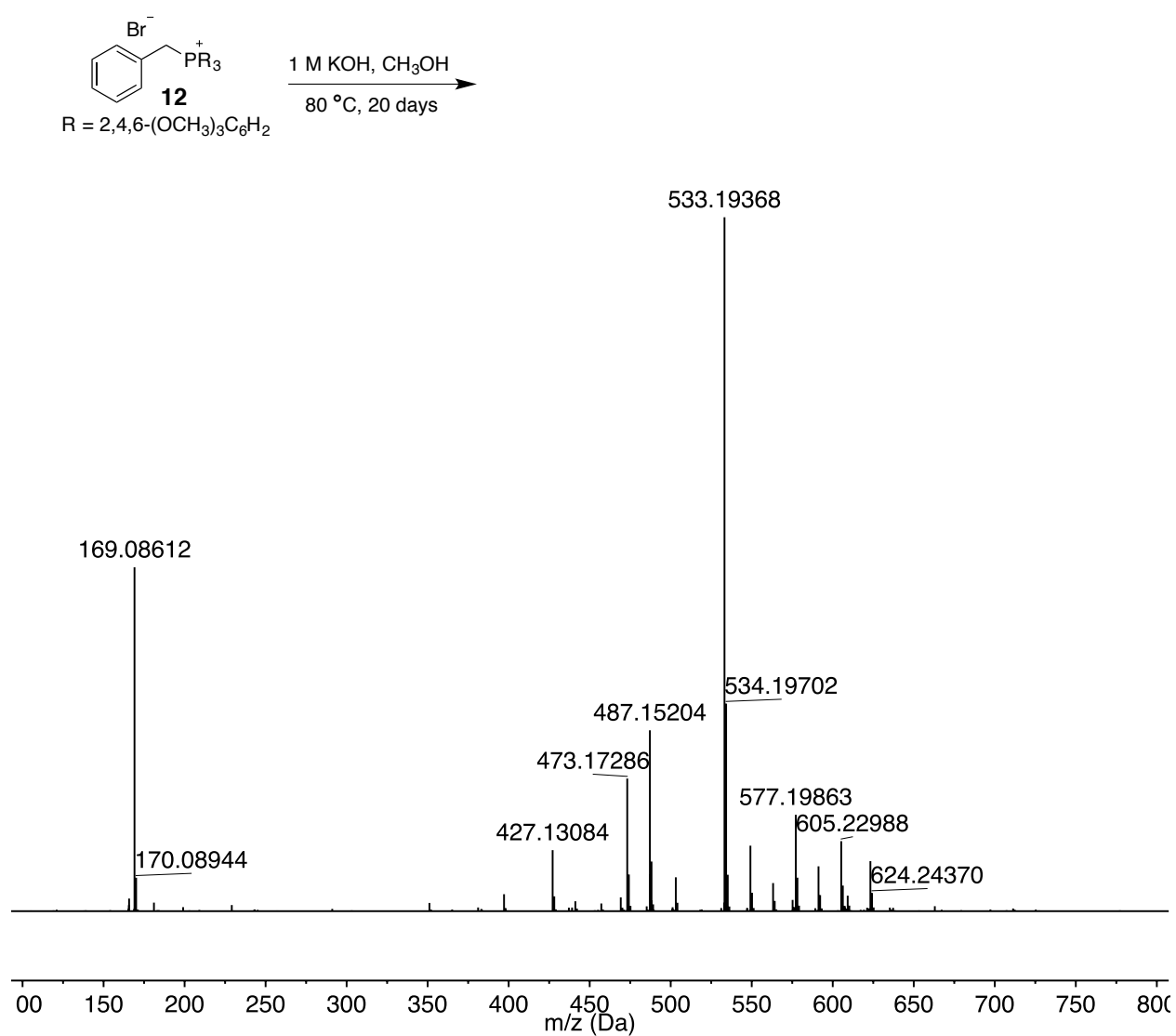


Figure 3.76 HRMS (DART) of **12** after 20 days dissolved in 1M KOH, CH₃OH solution at 80 °C.

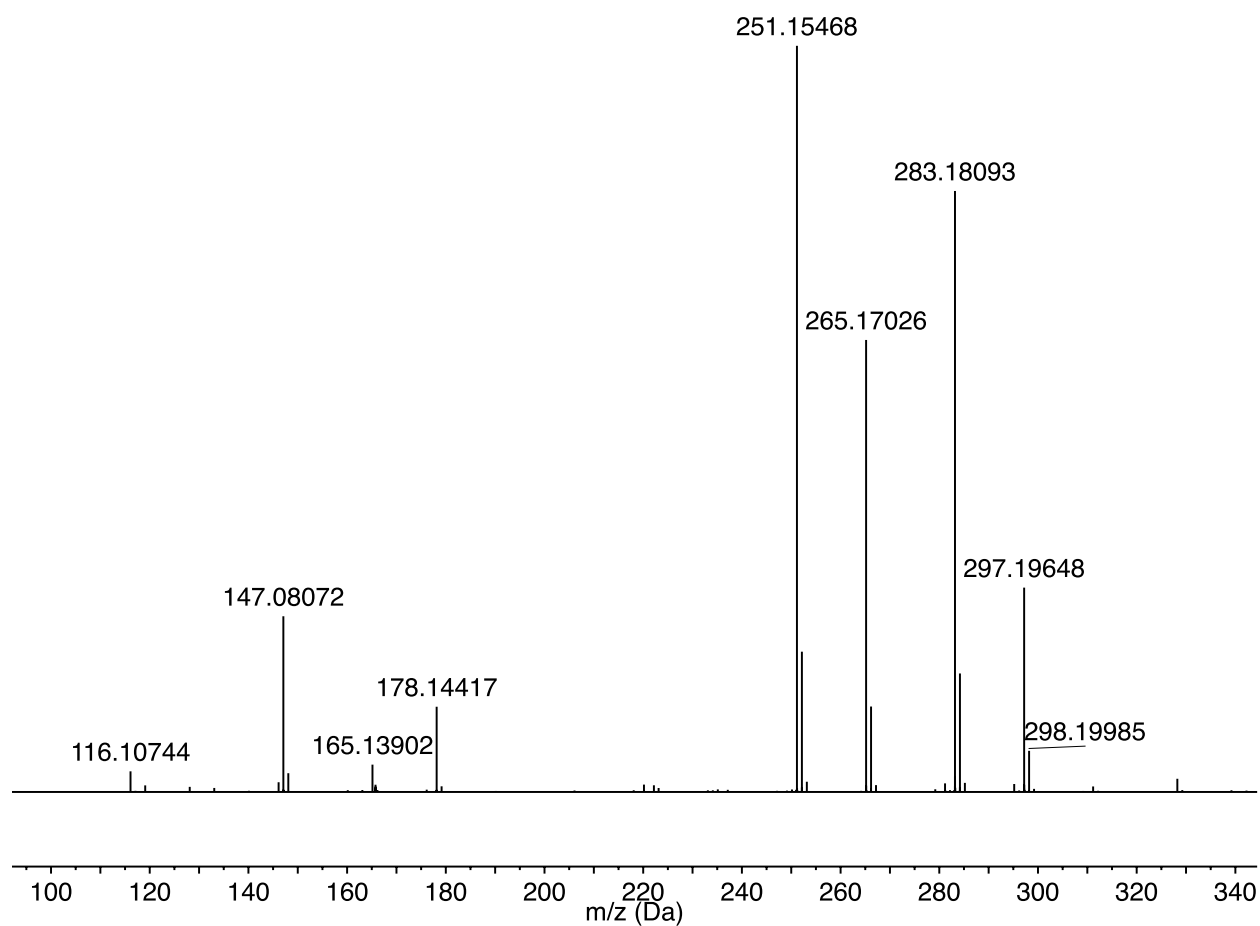
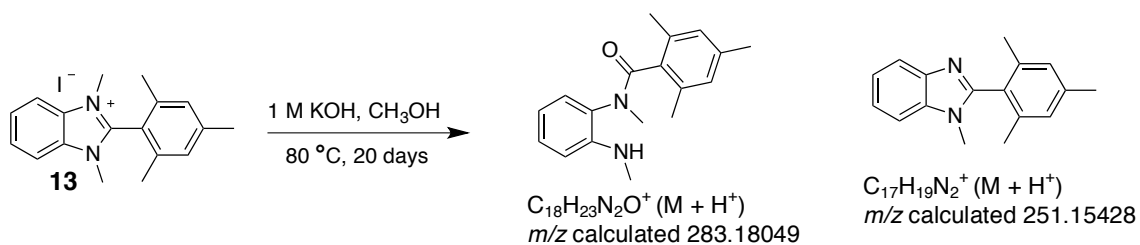


Figure 3.77 HRMS (DART) of **13** after 20 days dissolved in 1M KOH, CH₃OH solution at 80 °C.

REFERENCES

- (1) (a) Hickner, M. A. *Materials Today* **2010**, *13* (5), 34–41. (b) Tzanetakis, N.; Varcoe, J. R.; Slade, R. C. T.; Scott, K. *Desalination* **2005**, *174*, 257.
- (2) (a) Vidal, L.; Riekkola, M.-L.; Canals, A. *Anal. Chim. Acta* **2012**, *715*, 19–41. (b) Gu, Y.; Lodge, T. P. *Macromolecules* **2011**, *44*, 1732. (c) Karadas, F.; Atilhan, M.; Aparicio, S. *Energy Fuels* **2010**, *24* (11), 5817–5828.
- (3) (a) Kiaee, M.; Cruden, A.; Chladek, P.; Infield, D. *Energy Convers. Manage.* **2015**, *94*, 40–50. (b) Vengatesan, S.; Santhi, S.; Jeevanantham, S.; Sozhan, G. *J. Power Sources* **2015**, *284*, 361–368. (c) Parrondo, J.; Arges, C. G.; Niedzwiecki, M.; Anderson, E. B.; Ayers, K. E.; Ramani, V. *RSC Adv.* **2014**, *4*, 9875. (d) Leng, Y.; Chen, G.; Mendoza, A. J.; Tighe, T. B.; Hickner, M. A.; Wang, C.-Y. *J. Am. Chem. Soc.* **2012**, *134*, 9054.
- (4) (a) Maurya, S.; Shin, S.-H.; Kim, Y.; Moon, S.-H. *RSC Adv.* **2015**, *5* (47), 37206–37230. (b) Gu, S.; Gong, K.; Yan, E. Z.; Yan, Y. *Energy Environ. Sci.* **2014**, *7* (9), 2986.
- (5) (a) Zhou, T.; Shao, R.; Chen, S.; He, X.; Qiao, J.; Zhang, J. *J. Power Sources* **2015**, *293*, 946–975. (b) Wang, Y.-J.; Qiao, J.; Baker, R.; Zhang, J. *Chem. Soc. Rev.* **2013**, *42*, 3046–3070. (c) Merle, G.; Wessling, M.; Nijmeijer, K. *J. Membr. Sci.* **2011**, *377* (1-2), 1–35. (d) Couture, G.; Alaaeddine, A.; Boschet, F.; Ameduri, B. *Prog. Polym. Sci.* **2011**, *36* (11), 1521–1557.
- (6) Pellow, M. A.; Emmott, C. J. M.; Barnhart, C. J.; Benson, S. M. *Energy Environ. Sci.* **2015**, *8* (7), 1938–1952.
- (7) Cheng, J.; He, G.; Zhang, F. *Int. J. Hydrogen Energy* **2015**, *40* (23), 7348–7360.
- (8) (a) Scofield, M. E.; Liu, H.; Wong, S. S. *Chem. Soc. Rev.* **2015**, *44*, 5936–5956. (b) Kraytsberg, A.; Ein-Eli, Y. *Energy Fuels* **2014**, *28* (12), 7303–7330. (c) Zhang, H.; Shen, P. K. *Chem. Rev.* **2012**, *112*, 2780. (d) Hickner, M. A.; Ghassemi, H.; Kim, Y. S.; Einsla, B. R.; McGrath, J. E. *Chem. Rev.* **2004**, *104*, 4587.
- (9) (a) Banham, D.; Ye, S.; Pei, K.; Ozaki, J.; Kishimoto, T.; Imashiro, Y. *J. Power Sources* **2015**, *285*, 334–348 (and references therein). (b) Lu, S.; Pan, J.; Huang, A.; Zhuang, L.; Lu, J. *Proc. Natl. Acad. Sci.* **2008**, *105* (52), 20611–20614.

- (10) Lee, S.; Choun, M.; Ye, Y.; Lee, J.; Mun, Y.; Kang, E.; Hwang, J.; Lee, Y.-H.; Shin, C.-H.; Moon, S.-H.; Kim, S.-K.; Lee, E.; Lee, J. *Angew. Chem., Int. Ed.* **2015**, *54*, 9230–9234.
- (11) (a) Varcoe, J. R.; Slade, R. C. T.; Wright, G. L.; Chen, Y. *J. Phys. Chem. B* **2006**, *110*, 21041. (b) Varcoe, J. R.; Slade, R. C. T. *Fuel Cells* **2005**, *5*, 187.
- (12) (a) Varcoe, J. R.; Atanassov, P.; Dekel, D. R.; Herring, A. M.; Hickner, M. A.; Kohl, P. A.; Kucernak, A. R.; Mustain, W. E.; Nijmeijer, K.; Scott, K.; Xu, T.; Zhuang, L. *Energy Environ. Sci.* **2014**, *7*, 3135. (b) Hickner, M. A.; Herring, A. M.; Coughlin, E. B. *J. Polym. Sci., Part B: Polym. Phys.* **2013**, *51*, 1727.
- (13) DOE Fuel Cell Technical Team
http://energy.gov/sites/prod/files/2014/02/f8/fctt_roadmap_june2013.pdf (accessed July 28, 2015)
- (14) (a) Couture, G.; Ladmiral, V.; Améduri, B. *RSC Adv.* **2015**, *5* (14), 10243–10253. (b) Varcoe, J. R.; Slade, R. C. T.; Lam How Yee, E.; Poynton, S. D.; Driscoll, D. J.; Apperley, D. C. *Chem. Mater.* **2007**, *19*, 2686 (and references therein).
- (15) (a) Han, J.; Liu, Q.; Li, X.; Pan, J.; Wei, L.; Wu, Y.; Peng, H.; Wang, Y.; Li, G.; Chen, C.; Xiao, L.; Lu, J.; Zhuang, L. *ACS Appl. Mater. Interfaces* **2015**, *7* (4), 2809–2816. (b) Zhuo, Y. Z.; Nan Lai, A.; Zhang, Q. G.; Zhu, A. M.; Ye, M. L.; Liu, Q. L. *J. Membr. Sci.* **2015**, *491*, 138–148. (c) Nie, G.; Li, X.; Tao, J.; Wu, W.; Liao, S. J. *J. Membr. Sci.* **2015**, *474*, 187–195. (d) Park, A. M.; Turley, F. E.; Wycisk, R. J.; Pintauro, P. N. *Macromolecules* **2014**, *47*, 227. (e) Mohanty, A. D.; Lee, Y.-B.; Zhu, L.; Hickner, M. A.; Bae, C. *Macromolecules* **2014**, *47*, 1973. (f) Li, N.; Zhang, Q.; Wang, C.; Lee, Y. M.; Guiver, M. D. *Macromolecules* **2012**, *45*, 2411. (g) Ni, J.; Zhao, C.; Zhang, G.; Zhang, Y.; Wang, J.; Ma, W.; Liu, Z.; Na, H. *Chem. Commun.* **2011**, *47*, 8943. (h) Tanaka, M.; Fukasawa, K.; Nishino, E.; Yamaguchi, S.; Yamada, K.; Tanaka, H.; Bae, B.; Miyatake, K.; Watanabe, M. *J. Am. Chem. Soc.* **2011**, *133*, 10646. (i) Yan, J.; Hickner, M. A. *Macromolecules* **2010**, *43*, 2349. (j) Wang, J.; Zhao, Z.; Gong, F.; Li, S.; Zhang, S. *Macromolecules* **2009**, *42*, 8711. (k) Hibbs, M. R.; Hickner, M. A.; Alam, T. M.; McIntyre, S. K.; Fujimoto, C. H.; Cornelius, C. J. *Chem. Mater.* **2008**, *20*, 2566.
- (16) (a) Wu, L.; Pan, Q.; Varcoe, J. R.; Zhou, D.; Ran, J.; Yang, Z.; Xu, T. *J. Membr. Sci.* **2015**, *490*, 1–8. (b) Lai, A. N.; Wang, L. S.; Lin, C. X.; Zhuo, Y. Z.; Zhang, Q. G.; Zhu, A. M.; Liu, Q. L. *J. Membr. Sci.* **2015**, *481*, 9–18. (c) Arges, C. G.; Wang, L.; Jung, M.; Ramani, V. *J. Electrochem. Soc.* **2015**, *162* (7), F686–F693. (d) Li, Q.; Liu, L.; Miao, Q.; Jin, B.; Bai, R. *Chem. Commun.* **2014**, *50*, 2791. (e) Li, N.; Wang, L.; Hickner, M. *Chem. Commun.* **2014**, *50*, 4092. (f) Li, N.; Leng, Y.; Hickner, M. A.;

- Wang, C.-Y. *J. Am. Chem. Soc.* **2013**, *135*, 10124. (g) Li, X.; Yu, Y.; Liu, Q.; Meng, Y. *ACS Appl. Mater. Interfaces* **2012**, *4*, 3627. (h) Li, N.; Yan, T.; Li, Z.; Thurn-Albrecht, T.; Binder, W. H. *Energy Environ. Sci.* **2012**, *5*, 7888.
- (17) (a) Shen, K.; Zhang, Z.; Zhang, H.; Pang, J.; Jiang, Z. *J. Power Sources* **2015**, 287, 439–447. (b) Chen, D.; Hickner, M. A. *Macromolecules* **2013**, *46*, 9270. (c) Liu, Z.; Li, X.; Shen, K.; Feng, P.; Zhang, Y.; Xu, X.; Hu, W.; Jiang, Z.; Liu, B.; Guiver, M. D. *J. Mater. Chem. A* **2013**, *1*, 6481. (d) Zhang, Z.; Wu, L.; Varcoe, J.; Li, C.; Ong, A. L.; Poynton, S.; Xu, T. *J. Mater. Chem. A* **2013**, *1*, 2595.
- (18) (a) Zhang, X.; Higashihara, T.; Ueda, M.; Wang, L. *Polym. Chem.* **2014**, *5* (21), 6121–6141. (b) Li, Q.; Liu, L.; Miao, Q.; Jin, B.; Bai, R. *Chem. Commun.* **2014**, *50* (21), 2791. (c) Arges, C. G.; Wang, L.; Parrondo, J.; Ramani, V. *J. Electrochem. Soc.* **2013**, *160* (11), F1258–F1274. (d) Li, N.; Guiver, M. D.; Binder, W. H. *ChemSusChem* **2013**, *6*, 1376. (e) Hibbs, M. R.; Fujimoto, C. H.; Cornelius, C. J. *Macromolecules* **2009**, *42*, 8316.
- (19) (a) Vandiver, M. A.; Caire, B. R.; Ertem, S. P.; Tsai, T.-H.; Coughlin, E. B.; Herring, A. M.; Liberatore, M. W. *J. Electrochem. Soc.* **2015**, *162* (4), H206–H212. (b) Fang, J.; Lyu, M.; Wang, X.; Wu, Y.; Zhao, J. *J. Power Sources* **2015**, *284*, 517–523. (c) Tsai, T.-H.; Maes, A. M.; Vandiver, M. A.; Versek, C.; Seifert, S.; Tuominen, M.; Liberatore, M. W.; Herring, A. M.; Coughlin, E. B. *J. Polym. Sci., Part B: Polym. Phys.* **2013**, *51*, 1751. (d) Disabb-Miller, M. L.; Johnson, Z. D.; Hickner, M. A. *Macromolecules* **2013**, *46*, 949. (e) Varcoe, J. R.; Slade, R. C. T.; Lam How Yee, E. *Chem. Commun.* **2006**, 1428.
- (20) (a) Maes, A. M.; Pandey, T. P.; Vandiver, M. A.; Lundquist, L. K.; Yang, Y.; Horan, J. L.; Krosovsky, A.; Liberatore, M. W.; Seifert, S.; Herring, A. M. *Electrochim. Acta* **2013**, *110*, 260. (b) Zhang, M.; Kim, H. K.; Chalkova, E.; Mark, F.; Lvov, S. N.; Chung, T. C. M. *Macromolecules* **2011**, *44*, 5937. (c) Robertson, N. J.; Kostalik, H. A.; Clark, T. J.; Mutolo, P. F.; Abruña, H. D.; Coates, G. W. *J. Am. Chem. Soc.* **2010**, *132*, 3400. (d) Kostalik, H. A.; Clark, T. J.; Robertson, N. J.; Mutolo, P. F.; Longo, J. M.; Abruña, H. D.; Coates, G. W. *Macromolecules* **2010**, *43*, 7147. (e) Clark, T. J.; Robertson, N. J.; Kostalik IV, H. A.; Lobkovsky, E. B.; Mutolo, P. F.; Abruña, H. D.; Coates, G. W. *J. Am. Chem. Soc.* **2009**, *131*, 12888.
- (21) (a) Vijayakumar, E.; Sangeetha, D. *RSC Adv.* **2015**, *5* (53), 42828–42835. (b) Liu, L.; Tong, C.; He, Y.; Zhao, Y.; Hu, B.; Lü, C. *RSC Adv.* **2015**, *5* (54), 43381–43390. (c) Das, G.; Deka, B. K.; Lee, S. H.; Park, Y.-B.; Yoon, Y. S. *Macromol. Res.* **2015**, *23* (3), 256–264.

- (22) Lu, Y.; Armentrout, A. A.; Li, J.; Tekinalp, H. L.; Nanda, J.; Ozcan, S. *J. Mater. Chem. A* **2015**, 3 (25), 13350–13356.
- (23) (a) García-Cruz, L.; Casado-Coterillo, C.; Iniesta, J.; Montiel, V.; Irabien, Á. *J. Appl. Polym. Sci.* **2015**, 132 (29), DOI:10.1002/APP.42240. (b) Wang, J.-L.; Wang, L.-L.; Feng, R.; Zhang, Y. *Solid State Ionics* **2015**, 278, 144–151.
- (24) Liu, L.; Tong, C.; He, Y.; Zhao, Y.; Lü, C. *J. Membr. Sci.* **2015**, 487, 99–108.
- (25) Nuñez, S. A.; Hickner, M. A. *ACS Macro Lett.* **2013**, 2, 49.
- (26) (a) Long, H.; Kim, K.; Pivovar, B. S. *J. Phys. Chem. C* **2012**, 116, 9419. (b) Chempath, S.; Boncella, J. M.; Pratt, L. R.; Henson, N.; Pivovar, B. S. *J. Phys. Chem. C* **2010**, 114, 11977. (c) Chempath, S.; Einsla, B. R.; Pratt, L. R.; Macomber, C. S.; Boncella, J. M.; Rau, J. A.; Pivovar, B. S. *J. Phys. Chem. C* **2008**, 112, 3179.
- (27) (a) Edson, J. B.; Macomber, C. S.; Pivovar, B. S.; Boncella, J. M. *J. Membr. Sci.* **2012**, 399–400, 49. (b) Macomber, C. S.; Boncella, J. M.; Pivovar, B. S.; Rau, J. A. *Therm. Anal. Calorim.* **2008**, 93, 225. (c) Einsla, B. R.; Chempath, S.; Pratt, L.; Boncella, J.; Rau, J.; Macomber, C.; Pivovar, B. *ECS Trans.* **2007**, 11, 1173.
- (28) Mohanty, A. D.; Bae, C. *J. Mater. Chem. A* **2014**, 2 (41), 17314–17320.
- (29) (a) Morandi, C. G.; Peach, R.; Krieg, H. M.; Kerres, J. *J. Mater. Chem. A* **2015**, 3 (3), 1110–1120. (b) Gu, F.; Dong, H.; Li, Y.; Sun, Z.; Yan, F. *Macromolecules* **2014**, 47, 6740. (c) Hahn, S.-J.; Won, M.; Kim, T.-H. *Polymer Bull.* **2013**, 70, 3373.
- (30) Marino, M. G.; Kreuer, K. D. *ChemSusChem* **2015**, 8, 513.
- (31) (a) Katzfuß, A.; Poynton, S.; Varcoe, J.; Gogel, V.; Storr, U.; Kerres, J. *J. Membr. Sci.* **2014**, 465, 129. (b) Fang, J.; Yang, Y.; Lu, X.; Ye, M.; Li, W.; Zhang, Y. *Int. J. Hydrogen Energy* **2012**, 37, 594. (c) Wang, X.; Li, M.; Golding, B. T.; Sadeghi, M.; Cao, Y.; Yu, E. H.; Scott, K. *Int. J. Hydrogen Energy* **2011**, 36, 10022. (d) Faraj, M.; Elia, E.; Boccia, M.; Filpi, A.; Pucci, A.; Ciardelli, F. *J. Polym. Sci., Part A: Polym. Chem.* **2011**, 49, 3437.
- (32) (a) Miyake, J.; Fukasawa, K.; Watanabe, M.; Miyatake, K. *J. Poly. Sci. Part A: Polym. Chem.* **2014**, 52, 383. (b) Vöge, A.; Deimede, V.; Kallitsis, J. K. *RSC Adv.* **2014**, 4, 45040.

- (33) (a) Sherazi, T. A.; Zahoor, S.; Raza, R.; Shaikh, A. J.; Naqvi, S. A. R.; Abbas, G.; Khan, Y.; Li, S. *Int. J. Hydrogen Energy* **2015**, *40* (1), 786–796. (b) Liu, L.; Li, Q.; Dai, J.; Wang, H.; Jin, B.; Bai, R. *J. Membr. Sci.* **2014**, *453*, 52. (c) Sajjad, S. D.; Hong, Y.; Liu, F. *Polym. Adv. Technol.* **2014**, *25*, 108. (d) Li, W.; Wang, S.; Zhang, X.; Wang, W.; Xie, X.; Pei, P. *Int. J. Hydrogen Energy* **2014**, *39*, 13710. (e) Kim, D. S.; Fujimoto, C. H.; Hibbs, M. R.; Labouriau, A.; Choe, Y.-K.; Kim, Y. S. *Macromolecules* **2013**, *46*, 7826. (f) Lin, X.; Wu, L.; Liu, Y.; Ong, A. L.; Poynton, S. D.; Varcoe, J. R.; Xu, T. *J. Power Sources* **2012**, *217*, 373. (g) Qu, C.; Zhang, H.; Zhang, F.; Liu, B. *J. Mater. Chem.* **2012**, *22*, 8203. (h) Kim, D. S.; Labouriau, A.; Guiver, M. D.; Kim, Y. S. *Chem. Mater.* **2011**, *23*, 3795. (i) Wang, J.; Li, S.; Zhang, S. *Macromolecules* **2010**, *43*, 3890.
- (34) (a) Jangu, C.; Long, T. E. *Polymer* **2014**, *55*, 3298. (b) Ye, Y.; Stokes, K. K.; Beyer, F. L.; Elabd, Y. A. *J. Membr. Sci.* **2013**, *443*, 93. (c) Arges, C. G.; Parrondo, J.; Johnson, G.; Nadhan, A.; Ramani, V. *J. Mater. Chem.* **2012**, *22*, 3733. (d) Noonan, K. J. T.; Hugar, K. M.; Kostalik, H. A.; Lobkovsky, E. B.; Abruña, H. D.; Coates, G. W. *J. Am. Chem. Soc.* **2012**, *134*, 18161. (e) Gu, S.; Cai, R.; Yan, Y. *Chem. Commun.* **2011**, *47*, 2856. (f) Arges, C. G.; Kulkarni, S.; Baranek, A.; Pan, K.-J.; Jung, M.-S.; Patton, D.; Mauritz, K. A.; Ramani, V. *ECS Trans.* **2010**, *33*, 1903. (g) Kong, X.; Wadhwa, K.; Verkade, J. G.; Schmidt-Rohr, K. *Macromolecules* **2009**, *42*, 1659.
- (35) (a) Morandi, C. G.; Peach, R.; Krieg, H. M.; Kerres, J. *J. Membr. Sci.* **2015**, *476*, 256–263. (b) Li, Z.; Jiang, Z.; Tian, H.; Wang, S.; Zhang, B.; Cao, Y.; He, G.; Li, Z.; Wu, H. *J. Power Sources* **2015**, *288*, 384–392. (c) Lai, A. N.; Wang, L. S.; Lin, C. X.; Zhuo, Y. Z.; Zhang, Q. G.; Zhu, A. M.; Liu, Q. L. *ACS Appl. Mater. Interfaces* **2015**, *7* (15), 8284–8292. (d) Hossain, M. A.; Lim, Y.; Lee, S.; Jang, H.; Choi, S.; Jeon, Y.; Lee, S.; Ju, H.; Kim, W. G. *Solid State Ionics* **2014**, *262*, 754–760. (e) Ran, J.; Wu, L.; Varcoe, J. R.; Ong, A. L.; Poynton, S. D.; Xu, T. *J. Membr. Sci.* **2012**, *415–416*, 242–249. (f) Qiu, B.; Lin, B.; Qiu, L.; Yan, F. *J. Mater. Chem.* **2012**, *22* (3), 1040–1045. (g) Li, W.; Fang, J.; Lv, M.; Chen, C.; Chi, X.; Yang, Y.; Zhang, Y. *J. Mater. Chem.* **2011**, *21* (30), 11340. (h) Lin, B.; Qiu, L.; Lu, J.; Yan, F. *Chem. Mater.* **2010**, *22* (24), 6718–6725.
- (36) (a) Smith, T. W.; Zhao, M.; Yang, F.; Smith, D.; Cebe, P. *Macromolecules* **2013**, *46* (3), 1133–1143. (b) Rao, A. H. N.; Thankamony, R. L.; Kim, H.-J.; Nam, S.; Kim, T.-H. *Polymer* **2013**, *54* (1), 111–119. (c) Allen, M. H.; Wang, S.; Hemp, S. T.; Chen, Y.; Madsen, L. A.; Winey, K. I.; Long, T. E. *Macromolecules* **2013**, *46* (8), 3037–3045. (d) Ye, Y.; Elabd, Y. A. *Macromolecules* **2011**, *44* (21), 8494–8503. (e) Weber, R. L.; Ye, Y.; Schmitt, A. L.; Banik, S. M.; Elabd, Y. A.; Mahanthappa, M. K. *Macromolecules* **2011**, *44* (14), 5727–5735. (f) Weber, R. L.; Ye, Y.; Banik, S. M.; Elabd, Y. A.; Hickner, M. A.; Mahanthappa, M. K. *J. Polym. Sci., Part B: Polym. Phys.* **2011**, *49* (18), 1287–1296.

- (37) (a) Tsuchitani, R.; Nakanishi, H.; Shishitani, H.; Yamaguchi, S.; Tanaka, H.; Kasai, H. *Solid State Ionics* **2015**, 278, 5–10. (b) Yang, C.; Wang, S.; Ma, W.; Jiang, L.; Sun, G. *J. Mater. Chem. A* **2015**, 3 (16), 8559–8565. (c) Si, Z.; Sun, Z.; Gu, F.; Qiu, L.; Yan, F. *J. Mater. Chem. A* **2014**, 2, 4413. (d) Lin, X.; Varcoe, J. R.; Poynton, S. D.; Liang, X.; Ong, A. L.; Ran, J.; Li, Y.; Xu, T. *J. Mater. Chem. A* **2013**, 1, 7262. (e) Qiu, B.; Lin, B.; Si, Z.; Qiu, L.; Chu, F.; Zhao, J.; Yan, F. *J. Power Sources* **2012**, 217, 329. (f) Lin, B.; Qiu, L.; Qiu, B.; Peng, Y.; Yan, F. *Macromolecules* **2011**, 44, 9642.
- (38) (a) Wright, A. G.; Holdcroft, S. *ACS Macro Lett.* **2014**, 3, 444. (b) Zarrin, H.; Jiang, G.; Lam, G. Y.-Y.; Fowler, M.; Chen, Z. *Int. J. Hydrogen Energy* **2014**, 39, 18405. (c) Price, S. C.; Williams, K. S.; Beyer, F. L. *ACS Macro Lett.* **2014**, 3, 160. (d) Lin, X.; Liang, X.; Poynton, S. D.; Varcoe, J. R.; Ong, A. L.; Ran, J.; Li, Y.; Li, Q.; Xu, T. *J. Membr. Sci.* **2013**, 443, 193. (e) Thomas, O. D.; Soo, K. J. W. Y.; Peckham, T. J.; Kulkarni, M. P.; Holdcroft, S. *J. Am. Chem. Soc.* **2012**, 134, 10753. (f) Henkensmeier, D.; Cho, H.-R.; Kim, H.-J.; Nunes Kirchner, C.; Leppin, J.; Dyck, A.; Jang, J. H.; Cho, E.; Nam, S.-W.; Lim, T.-H. *Polym. Degrad. Stab.* **2012**, 97, 264. (g) Thomas, O. D.; Soo, K. J. W. Y.; Peckham, T. J.; Kulkarni, M. P.; Holdcroft, S. *Polym. Chem.* **2011**, 2, 1641. (h) Henkensmeier, D.; Kim, H.-J.; Lee, H.-J.; Lee, D. H.; Oh, I.-H.; Hong, S.-A.; Nam, S.-W.; Lim, T.-H. *Macromol. Mater. Eng.* **2011**, 296, 899.
- (39) (a) Yang, C.; Wang, S.; Ma, W.; Jiang, L.; Sun, G. *J. Membr. Sci.* **2015**, 487, 12–18. (b) Liu, Y.; Wang, J.; Yang, Y.; Brenner, T. M.; Seifert, S.; Yan, Y.; Liberatore, M. W.; Herring, A. M. *J. Phys. Chem. C* **2014**, 118 (28), 15136–15145. (c) Yang, Y.; Wang, J.; Zheng, J.; Li, S.; Zhang, S. *J. Membr. Sci.* **2014**, 467, 48–55. (d) Wang, W.; Wang, S.; Xie, X.; Lv, Y.; Ramani, V. K. *J. Membr. Sci.* **2014**, 462, 112–118. (e) Page, O. M. M.; Poynton, S. D.; Murphy, S.; Lien Ong, A.; Hillman, D. M.; Hancock, C. A.; Hale, M. G.; Apperley, D. C.; Varcoe, J. R. *RSC Adv.* **2013**, 3 (2), 579–587. (f) Lin, B.; Dong, H.; Li, Y.; Si, Z.; Gu, F.; Yan, F. *Chem. Mater.* **2013**, 25 (9), 1858–1867. (g) Lin, X.; Varcoe, J. R.; Poynton, S. D.; Liang, X.; Ong, A. L.; Ran, J.; Li, Y.; Xu, T. *J. Mater. Chem. A* **2013**, 1 (24), 7262.
- (40) (a) Choe, Y.-K.; Fujimoto, C.; Lee, K.-S.; Dalton, L. T.; Ayers, K.; Henson, N. J.; Kim, Y. S. *Chem. Mater.* **2014**, 26 (19), 5675–5682. (b) Parrondo, J.; Arges, C. G.; Niedzwiecki, M.; Anderson, E. B.; Ayers, K. E.; Ramani, V. *RSC Adv.* **2014**, 4 (19), 9875. (c) Arges, C. G.; Ramani, V. *Proc. Natl. Acad. Sci.* **2013**, 110 (7), 2490–2495. (d) Fujimoto, C.; Kim, D.-S.; Hibbs, M.; Wroblewski, D.; Kim, Y. S. *J. Membr. Sci.* **2012**, 423–424, 438–449. (e) Chen, D.; Hickner, M. A. *ACS Appl. Mater. Interfaces* **2012**, 4 (11), 5775–5781. (f) Wang, J.; Wang, J.; Li, S.; Zhang, S. *J. Membr. Sci.* **2011**, 368 (1–2), 246–253.

- (41) (a) Si, Z.; Sun, Z.; Gu, F.; Qiu, L.; Yan, F. *J. Mater. Chem. A* **2014**, 2 (12), 4413. (b) Amel, A.; Zhu, L.; Hickner, M.; Ein-Eli, Y. *J. Electrochem. Soc.* **2014**, 161 (5), F615–F621. (c) Fujimoto, C.; Kim, D.-S.; Hibbs, M.; Wroblewski, D.; Kim, Y. S. *J. Membr. Sci.* **2012**, 423–424, 438–449. (d) Deavin, O. I.; Murphy, S.; Ong, A. L.; Poynton, S. D.; Zeng, R.; Herman, H.; Varcoe, J. R. *Energy Environ. Sci.* **2012**, 5 (9), 8584.
- (42) (a) Ye, Y.; Elabd, Y. A. *Macromolecules* **2011**, 44 (21), 8494–8503. (b) Lee, W.-H.; Mohanty, A. D.; Bae, C. *ACS Macro Lett.* **2015**, 4 (4), 453–457.
- (43) (a) Arges, C. G.; Wang, L.; Parrondo, J.; Ramani, V. *J. Electrochem. Soc.* **2013**, 160 (11), F1258–F1274. (b) Arges, C. G.; Wang, L.; Parrondo, J.; Ramani, V. K. *ECS Trans.* **2013**, 58 (1), 1551–1561. (c) Arges, C. G.; Ramani, V. *Proc. Natl. Acad. Sci.* **2013**, 110 (7), 2490–2495.
- (44) (a) Si, Z.; Qiu, L.; Dong, H.; Gu, F.; Li, Y.; Yan, F. *ACS Appl. Mater. Interfaces* **2014**, 6, 4346. (b) Gu, F.; Dong, H.; Li, Y.; Si, Z.; Yan, F. *Macromolecules* **2014**, 47, 208. (c) Lin, B.; Dong, H.; Li, Y.; Si, Z.; Gu, F.; Yan, F. *Chem. Mater.* **2013**, 25, 1858. (e) Wang, J.; Gu, S.; Kaspar, R. B.; Zhang, B.; Yan, Y. *ChemSusChem* **2013**, 6, 2079.
- (45) Hugar, K. M.; Kostalik, H. A.; Coates, G. W. *J. Am. Chem. Soc.* **2015**, 137, 8730–8737.
- (46) Sturgeon, M. R.; Macomber, C. S.; Engtrakul, C.; Long, H.; Pivovar, B. S. *J. Electrochem. Soc.* **2015**, 162 (4), F366–F372.
- (47) Section 3.5 – Experimental.
- (48) Varshneya, Arun K. *Fundamentals of Inorganic Glasses Book*
- (49) Jia, Z.; Yuan, W.; Sheng, C.; Zhao, H.; Hu, H.; Baker, G. L. *J. Polym. Sci., Part A: Polym. Chem.* **2015**, 53 (11), 1339–1350.
- (50) For additional references on solvent suppression theory and applications: (a) Hore, P. *J. Methods Enzymol.* **1989**, 176, 64. (b) Guéron, M.; Plateau, P.; Decorps, M. *Prog. Nucl. Magn. Reson. Spectrosc.* **1991**, 23, 135. (c) Braun, S.; Kalinowski, H.-O.; Berger, S. *150 and More Basic NMR Experiments: A Practical Course*; Wiley-VCH: Weinheim, Germany, 1999.

- (51) Chapter 4 – Imidazolium Cations with Exceptional Alkaline Stability: A Systematic Study of Structure-Stability Relationships
- (52) Schwesinger, R.; Link, R.; Wenzl, P.; Kossek, S.; Keller, M. *Chemistry - A European Journal* **2006**, *12* (2), 429.
- (53) Mugridge, J. S.; Bergman, R. G.; Raymond, K. N. *J. Am. Chem. Soc.* **2012**, *134* (4), 2057.
- (54) Shkrob, I. A.; Marin, T. W.; Hatcher, J. L.; Cook, A. R.; Szreder, T.; Wishart, J. F. *J. Phys. Chem. B* **2013**, *117* (46), 14385.
- (55) Robiette, R.; Conza, M.; Aggarwal, V. K. *Org. Biomol. Chem.* **2006**, *4* (4), 621.
- (56) Kim, Y.-S.; Yang, C.-T.; Wang, J.; Wang, L.; Li, Z.-B.; Chen, X.; Liu, S. *J. Med. Chem.* **2008**, *51* (10), 2971.

CHAPTER 4

Imidazolium Cations with Exceptional Alkaline Stability: A Systematic Study of Structure-Stability Relationships

Reprinted with Permission from

Journal of the American Chemical Society **2015**, *137*, 8730—8737

Copyright © 2015 by the American Chemical Society

CHAPTER 4

Imidazolium Cations with Exceptional Alkaline Stability: A Systematic Study of Structure-Stability Relationships

4.1 Abstract

Highly base-stable cationic moieties are a critical component of anion exchange membranes (AEMs) in alkaline fuel cells (AFCs) however; the commonly employed organic cations have limited alkaline stability. To address this problem, we synthesized and characterized the stability of a series of imidazolium cations in 1 M, 2 M, or 5 M KOH/CD₃OH at 80 °C, systematically evaluating the impact of substitution on chemical stability. The substituent identity at each position of the imidazolium ring has a dramatic effect on the overall cation stability. We report imidazolium cations that have the highest alkaline stabilities reported to date, >99% cation remaining after 30 days in 5M KOH/CD₃OH at 80 °C.

4.2 Introduction

The environmental and financial implications of our near exclusive dependence on fossil fuels have expedited research efforts to develop more effective methods of extracting the energy stored in chemical bonds.¹ Fuel cells have emerged as attractive electrochemical conversion devices due to their high energy density and their ability to produce energy more cleanly and efficiently compared to conventional systems, such as internal combustion engines.² In particular, proton exchange membrane fuel cells (PEMFCs) have been useful in many commercial applications.³ However, widespread production is limited by the cost and durability of the materials, specifically the platinum electrodes and electrolyte membrane.⁴ To address these challenges, alkaline fuel cells (AFCs) have been investigated, which operate by transporting hydroxide ions through the electrolyte under basic conditions.⁵ At elevated pH, oxygen reduction is more facile and lower overpotentials are required, enabling the use of non-noble metal catalysts in AFCs.⁶ Indeed, the earliest examples of commercial fuel cells used aqueous potassium hydroxide solutions as the electrolyte medium to facilitate anion conduction.

Unfortunately, the performance of these early fuel cells was compromised by exposure to carbon dioxide, a common component of feedstock gases, which reacts with hydroxide to produce carbonate salts.⁷ To overcome this issue, alkaline anion exchange membranes (AAEMs), which are generally comprised of organic cations covalently linked to a polymer backbone, are employed to prevent the formation of mobile salts and retain the conductive organic cation/hydroxide species.⁸

Tetraalkylammonium cations have been appended to various polymer architectures to prepare AAEMs, including perfluorinated membranes,⁹ aromatic polysulfones,¹⁰ poly(arylene ethers),¹¹ poly(arylene ether ketones),¹² polyphenylenes,¹³ polystyrenes,¹⁴ and various aliphatic backbones.¹⁵ Despite exhibiting high initial conductivity, numerous studies, such as those by Boncella and coworkers,^{16e} have demonstrated that ammonium cations degrade rapidly under fuel cell operating conditions, limiting their utility and making the improvement of AAEM stability a critical priority.¹⁶ Of note, the alkaline stability of membranes composed of a variety of polymer backbones was followed using ¹H NMR spectroscopy by Nuñez and Hickner.^{16a} The disadvantages of using ammonium cations, particularly the ubiquitous benzyl trimethylammonium (BTMA) cation, have spurred investigations into the stability of other positively-charged moieties in the presence of hydroxide, such as guanadinium,¹⁷ phosphonium,¹⁸ diazabicyclooctane-based (DABCO),¹⁹ benzimidazolium,²⁰ morpholinium,²¹ pyridinium,²² pyrrolidinium,²³ metal organic frameworks (MOFs)²⁴ and ruthenium²⁵ cations (Figure 4.1). Marino and Kreuer recently described a class of quaternary spiro-ammonium compounds that exhibited improved alkaline stability compared to the acyclic counterparts.^{19a} Polymers containing base-stable cationic groups are also useful in other applications, including: electrolysis,²⁶ gas separation,²⁷ desalination²⁸ and as stimuli-responsive materials.²⁹ Our group reported a polyethylene membrane containing a tetrakis(dialkylamino)phosphonium cation that exhibited excellent stability;³⁰ however, the synthesis of this cation requires several difficult multistep reactions. Ideally, the best candidates for practical fuel cell devices are cations that are

easy to make and incorporate into polymers, while maintaining optimal conductivity and stability.

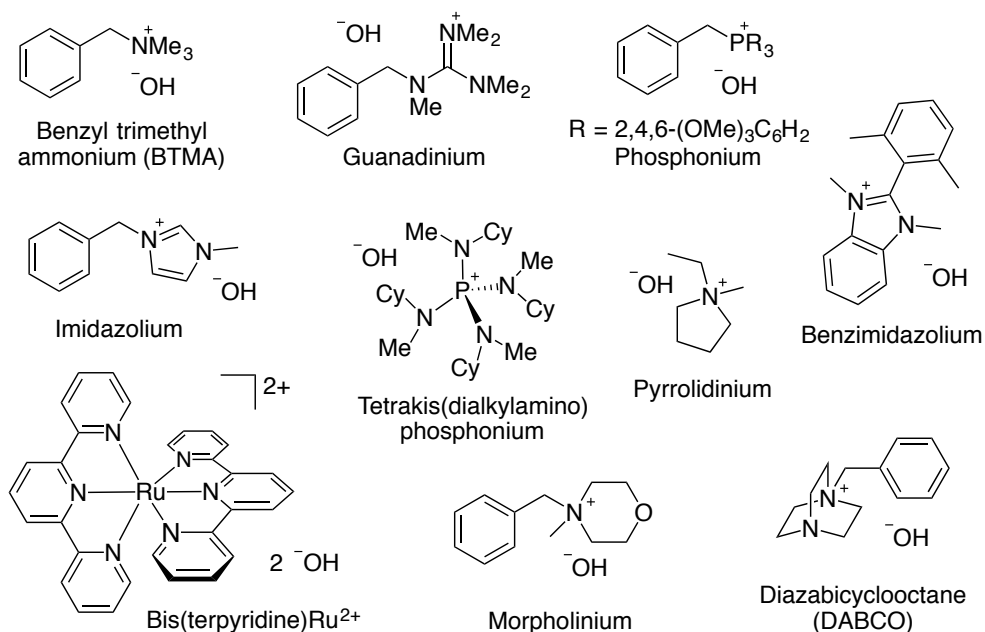


Figure 4.1 Selected cations investigated for use in alkaline anion exchange membranes (AAEMs).

Imidazoles are a class of organic compounds that are amenable to synthesis because they are prepared by a modular route, with easily modified substituents, and are readily converted to the cationic form via alkylation. Additionally, they are stabilized by charge delocalization like the virtually inert tetrakis(dialkylamino)phosphonium cations. Researchers have attached *N*-methyl³¹ or *N*-alkyl³² benzyl imidazoliums to polymers and investigated them as alternatives to ammonium cations, and while these cations transport hydroxide sufficiently, the chemical stabilities of unsubstituted imidazoliums are generally much too low for fuel cell applications.³³ In fact, imidazolium cations with higher stability would be beneficial in many applications, such as organocatalysis,³⁴ solar cell electrolytes,³⁵ phase transfer catalysis³⁶ and as carbon material precursors,³⁷ in addition to AAEMs. Imidazoliums degrade under alkaline conditions via four distinct mechanisms, and the identities of the substituents direct the degradation pathways

(Figure 4.2).³⁸ By selecting the appropriate substituents several degradation routes are inhibited, thus deterring reactions between the organic cation and reactive counteranions. Accordingly, recent studies on polymers containing imidazoliums with methyl groups in the C2 position suggested that this substitution improved alkaline stability compared to unsubstituted imidazoliums.³⁹ The numbering system of the imidazolium cation is described in Figure 4.2. The attenuation in reactivity is attributed to steric factors, where nucleophilic addition and subsequent ring-opening of the heterocycle are hindered by the C2-methyl group (Figure 4.2a).

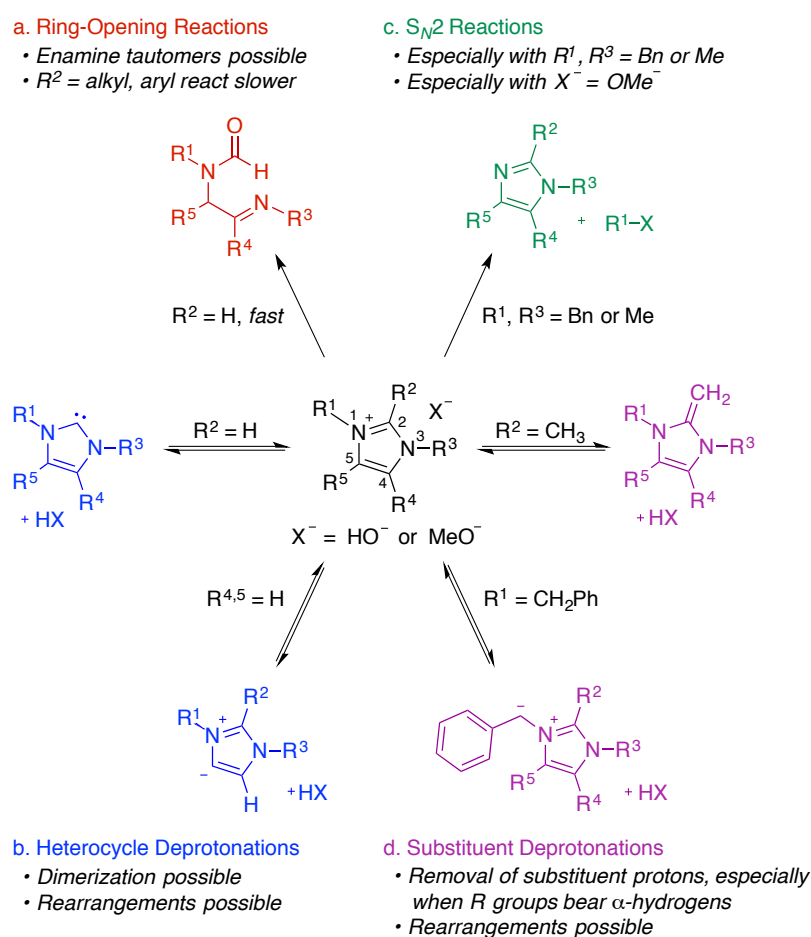


Figure 4.2 Degradation pathways of imidazolium cations under alkaline conditions.

Several researchers have explored the effect of C2 substitution on alkaline stability.⁴⁰ Specifically, studies on a related class of compounds, benzimidazolium cations, by

Beyer,^{20c} Holdcroft^{20e} and coworkers highlight the importance of bulky substituents at the C2 position. Density functional theory (DFT) calculations by Pivovar,^{41a} Ramani,^{41b} and others^{41c,d} predict that substitution at the C4 and C5 positions will improve stability. These claims are supported experimentally in original work conducted by Wang *et al.*,^{40e} which investigated imidazoliums with C4,5 methyl groups. Presumably, C4,5 substitution improves imidazolium stability by preventing deprotonation reactions (Figure 4.2b). The degradation pathways discussed thus far only involve reactions directly at the ring positions (Figure 4.2a and 4.2b); however, reactions with the peripheral substituents are also predicted (Figure 4.2c and 4.2d). In fact, deprotonation of the peripheral substituents containing α -hydrogens is readily observed in basic solutions that contain protic deuterated solvents, as evidenced by hydrogen/deuterium exchange. Imidazolium reactivity is easily regulated by substituent variation and eliminating the sites of vulnerability prevents degradation. The synthetic convenience, simplistic modification and resonance stabilization of imidazoliums make them attractive targets, and we hypothesized that these features would enable the creation of cations with exceptional base stability.

Model compound studies, wherein the degradation rates of small molecules are assessed under alkaline conditions, are effective at determining the relative stabilities of a series of compounds. Once promising cations are identified, they must be incorporated into polymers where the collective stability of the AAEM can be determined under real-world operating conditions. In a recent report from Mohanty *et al.*,⁴² a variety of quaternary ammonium hydroxide complexes were prepared and studied under relevant fuel cell operating temperatures. Several other protocols have been reported for determining model compound stabilities; however, the conditions vary widely making productive comparisons between individual accounts difficult.⁴⁰ In order to rigorously assess the performance of new cations, we have developed an NMR spectroscopy method that unambiguously ranks the stability of cations.⁴³ Solutions of the cation are prepared in basified methanol-*d*₃ (KOH/CD₃OH) and stored in flame-sealed NMR tubes at 80 °C. At uniform time intervals, the solutions are analyzed by ¹H NMR spectroscopy for amount of cation remaining relative to an internal standard.⁴⁴ The use of CD₃OH precludes a

hydrogen/deuterium exchange process that causes a reduction in the cation signals (not related to degradation) and obscures new product signals. Methanol is a more universal solvent and conveniently dissolves organic cations and potential degradation products, a consideration of paramount importance for NMR spectroscopy studies. Key aspects of the degradation routes were revealed with this new protocol, which facilitates the design of new imidazoliums with strategically placed substituents to prevent decomposition.

To date, investigations of imidazolium substitution patterns have been typically restricted to commercially available imidazoles. Fortunately, tetrasubstituted imidazoles, the neutral precursors to imidazoliums, can be prepared using simple multi-component reactions.⁴⁵ Herein, we report the synthesis of a variety of imidazoliums (Figure 4.3), systematically altering the structures to examine the precise influence of substitution patterns on the alkaline stability.

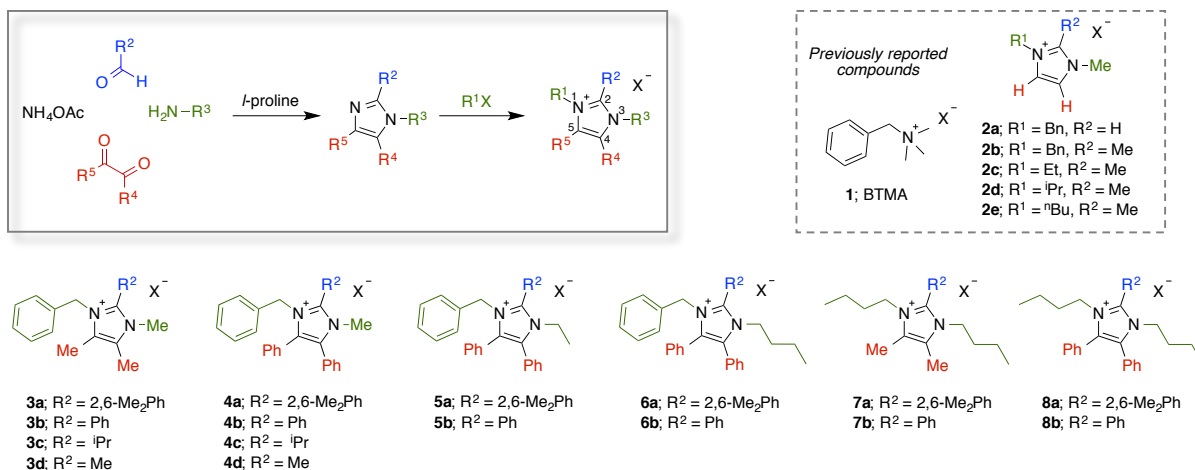


Figure 4.3 Summary of model compounds investigated, including the synthesis of imidazoliums with varied substitution patterns.

Ultimately, these experiments led to the synthesis of imidazolium cations with higher resistance to reaction with bases and nucleophiles than any previously reported model compound studies. Furthermore, the synthetic accessibility of imidazoliums simplifies their incorporation into polymer architectures to achieve AAEMs with high conductivities and stabilities.

4.3 Results and Discussion

Initially, we explored the impact of C4,5 substitution on cation stability by evaluating imidazoliums with hydrogen, methyl, or phenyl groups in the C4,5 positions (Figure 4.4). Methyl groups were installed at the C2 position because these substituents produce cations that are more stable than their C2-unsubstituted counterparts. To start, we investigated imidazoliums with N1-benzyl and N3-methyl groups, as the majority of imidazolium-based AAEMs reported in the literature have these functionalities. This series of cations was compared to benzyl trimethylammonium (1) (BTMA) and the C2 unsubstituted imidazolium, 1-benzyl-3-methylimidazolium bromide (**2a**) (Figure 4.3).

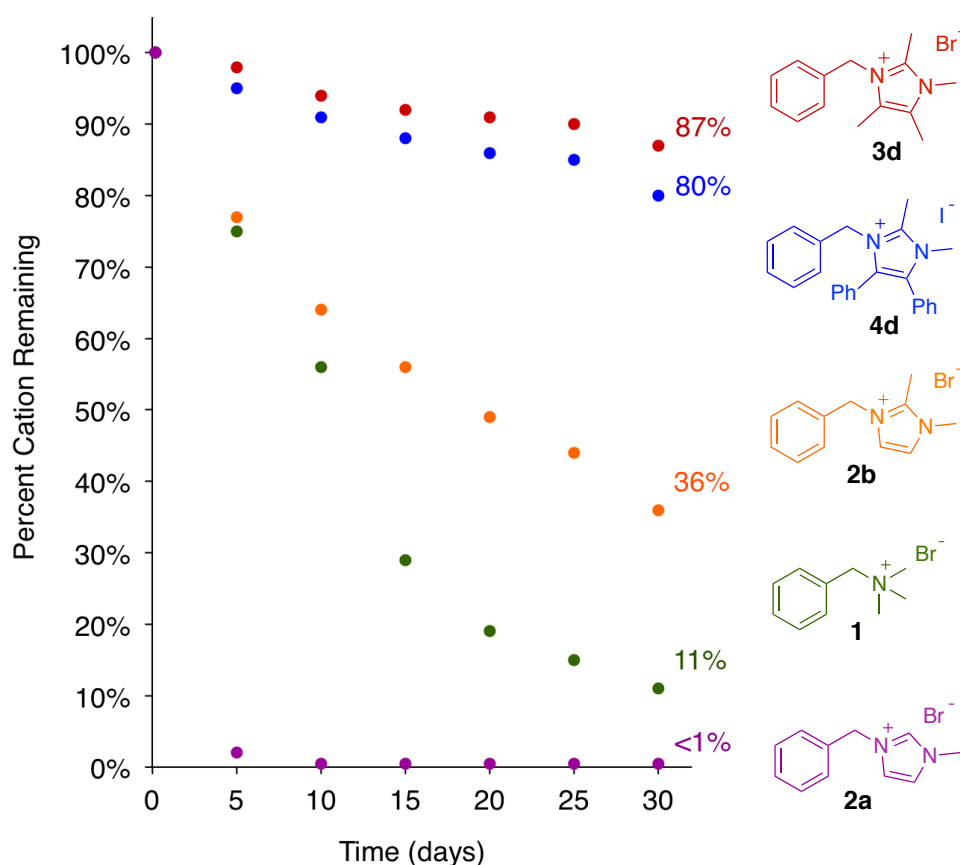


Figure 4.4 Stability of C4,5 substituted imidazolium cations (0.05 M) in 1 M KOH/CD₃OH at 80 °C.

As previously reported, **2a** degrades rapidly under mildly basic conditions, with less than 2% cation remaining after five days.⁴³ In contrast, the imidazolium with a C2-methyl substituent (**2b**) reacts more slowly, leaving 36% remaining after 30 days. This simple imidazolium **2b** is already an improvement over BTMA (**1**), which degraded to 11% remaining in the same time. BTMA degrades by nucleophilic attack at the benzylic and methyl positions, producing *N,N*-dimethylbenzylamine and benzyl methyl ether, as evident by ¹H NMR spectroscopy.³⁰ The resonances for similar nucleophilic displacement products (benzyl methyl ether, dimethyl ether, and the corresponding N1-benzyl or N3-methyl imidazoles) are not observed for **2a** or **2b** indicating that S_N2 reactions did not occur (Figure 4.2c). Nucleophilic addition of hydroxide to the C2 position and concomitant ring-opening is reported for imidazolium degradation (Figure 4.2a); however, the amide and imine signals corresponding to this degradation pathway are not observed for either compound. In fact, analysis by ¹H NMR spectroscopy indicates that imidazolium decomposition is more complicated than suggested in Figure 4.2. We propose that the initial product(s) formed are not stable under the protocol conditions and undergo further degradation or rearrangement reactions. Additional work is needed to confirm the identity of the products and elucidate the secondary degradation mechanism(s). Introducing substituents to the C4,5 positions results in a substantial increase in stability. The imidazolium with C4,5-phenyl substituents (**4d**) degrades moderately faster than the C4,5-methyl version (**3d**), yielding 80% and 87% cation after 30 days, respectively. The degradation products for **3d** are not yet identified, although **3d** does not appear to degrade by an S_N2 mechanism. A small amount of nucleophilic displacement is observed for **4d**; however, other degradation pathways are more prominent. Deprotonation of substituent hydrogens (i.e. C2-methyl or benzylic protons) followed by rearrangement is a plausible mode of degradation for both **3d** and **4d** (Figure 4.2d). These examples strongly indicate that imidazolium stability is enhanced by C4,5 substitution, which agrees with the results obtained by Yan,^{40e} Zhang^{38a} and coworkers. Therefore, this work focuses on compounds with C4,5-methyl or phenyl substituents, but other alkyl and aryl substituents should behave similarly.

Next, we investigated the effects of C2 substitution on imidazolium stability (Figure 4.5). Imidazoliums generated from commercially available imidazoles (C2-methyl, isopropyl or phenyl groups and C4,5-hydrogens) were previously studied by Lin *et al.*^{40d} Holdcroft and coworkers investigated bulky C2-aryl groups and found that 2,6-dimethylphenyl substituents improved the stability of benzimidazoliums, compared to phenyl groups alone.^{20e} For comparison, we combined these four C2 substituents with our substitution patterns and evaluated their impact on imidazolium stability by reporting the percent cation remaining after 30 days (approximately 720 hours).

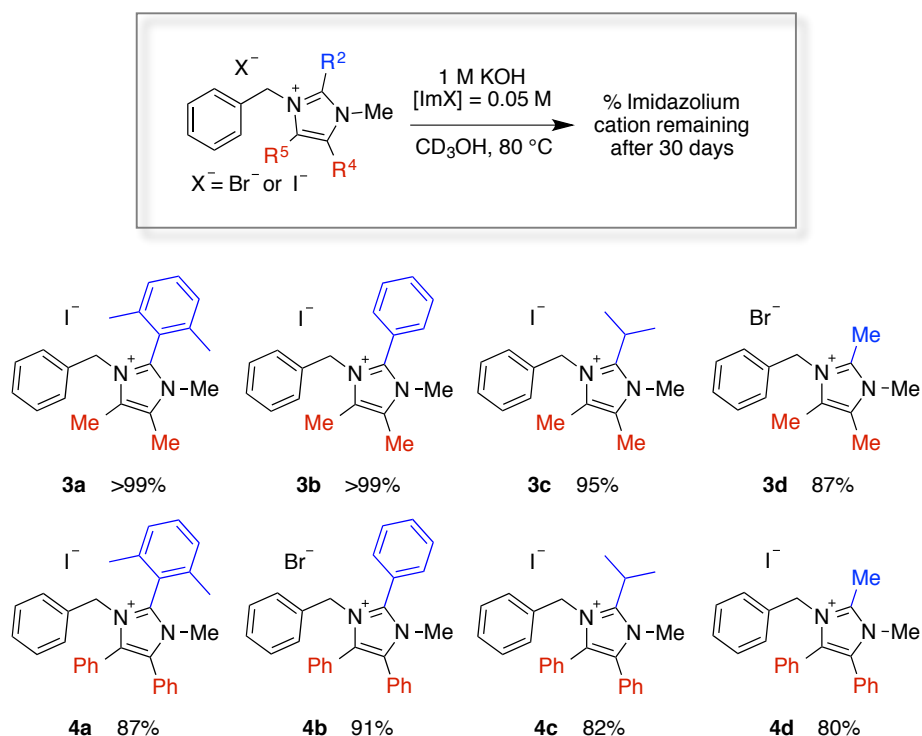


Figure 4.5 Percent cation remaining after 30 days at 80 °C – Influence of C2 substituents on imidazolium stability. Determined by 1H NMR spectroscopy.

Imidazoliums with C4,5-methyl substituents (Figure 4.5, **3a – 3d**) are more stable than the analogous compounds with phenyl groups (Figure 4.5, **4a – 4d**). In fact, little decomposition is observed over 30 days for the C4,5-methyl substituted compounds, with the exception of **3d**,

as discussed previously. For this reason, the C4,5-phenyl substituted series, which experienced moderate degradation, is used to analyze trends in the impact of C2 substitution (*vide infra*).

Imidazoliums with aryl groups at the C2 position (Figure 4.5, **4a** and **4b**) are more base-stable than those with alkyl groups (Figure 4.5, **4c** and **4d**). This observation contrasts with C2 trends observed by Yan and coworkers where alkyl substituents improved stability compared to phenyl groups.^{40d} The degradation rates for C2-aryl substituted compounds (Figure 4.5, **4a** and **4b**) are very similar (87% and 91% cation remaining, respectively). Likewise, varying the steric bulk of the C2-alkyl substituent does not strongly influence the base stability (Figure 4.5, **4c** and **4d**). These results indicate that nucleophilic addition to the C2 position is not a major degradation pathway for **4a** – **4d**. Amide and enamine resonances are not observed by ¹H NMR spectroscopy, suggesting that ring-opening decomposition is not occurring (Figure 4.2a). The lack of ether and imidazole degradation products suggests that imidazoliums with C2-alkyls (**4c** and **4d**) do not degrade by S_N2 attack, leaving substituent deprotonation and subsequent rearrangement reactions as potential decomposition routes (Figure 4.2d). In contrast, the imidazoliums with C2-aryls (**4a** and **4b**) clearly degrade by S_N2 attack at the nitrogen substituents and the resonances for benzyl methyl ether, dimethyl ether and both imidazole products are observed (Figure 4.6, diagnostic signals are highlighted for **4a**). Imidazoliums **4a** and **4b** react via S_N2 pathways primarily at the benzylic position followed by the N3-methyl position as evidenced by the distribution of products in the ¹H NMR spectra. Overall, C2-aryl groups improve the resistance of the imidazolium cation to base and were selected for continued examination.

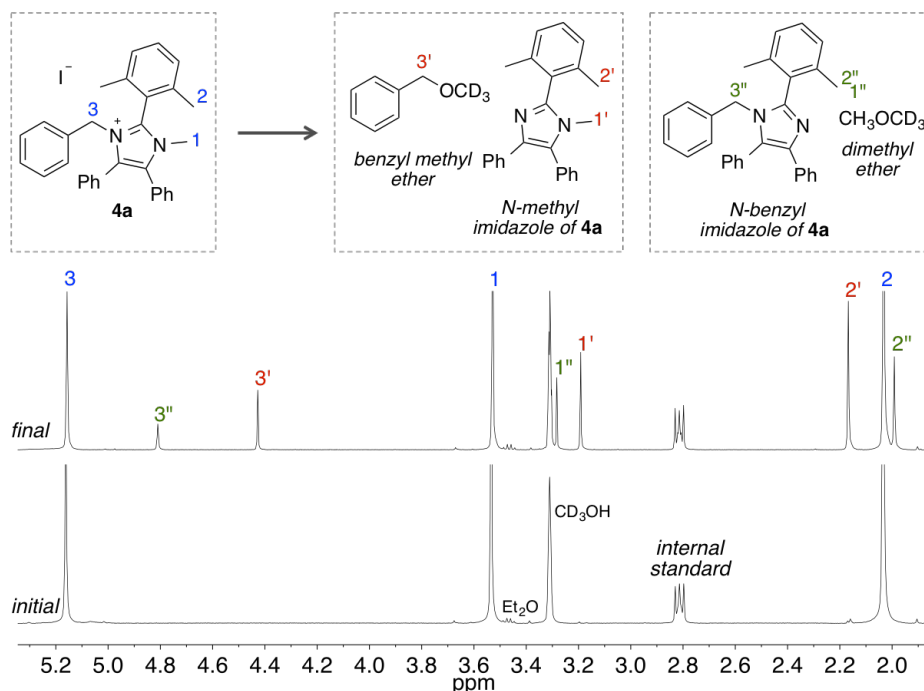


Figure 4.6 Degradation of **4a** after 3 months in 1 M KOH/CD₃OH at 80 °C.

We evaluated the impact of changing the nitrogen substituents by increasing the steric bulk of the N3-alkyl group from an N3-methyl to an N3-ethyl or N3-butyl. Synthesizing imidazoliums with both N1- and N3-butyl groups eliminated the reactive benzylic position altogether. We assessed imidazoliums with C4,5-phenyl groups because stability trends were more apparent with faster degradation rates (Figure 4.7); although, after determining the best N1 and N3 substituents, we reinvestigated imidazoliums with C4,5-methyl groups. To delineate trends in stability in a more convenient time frame, we raised the base concentration from 1 M to 2 M or 5 M KOH, increasing the rate of the degradation reactions.

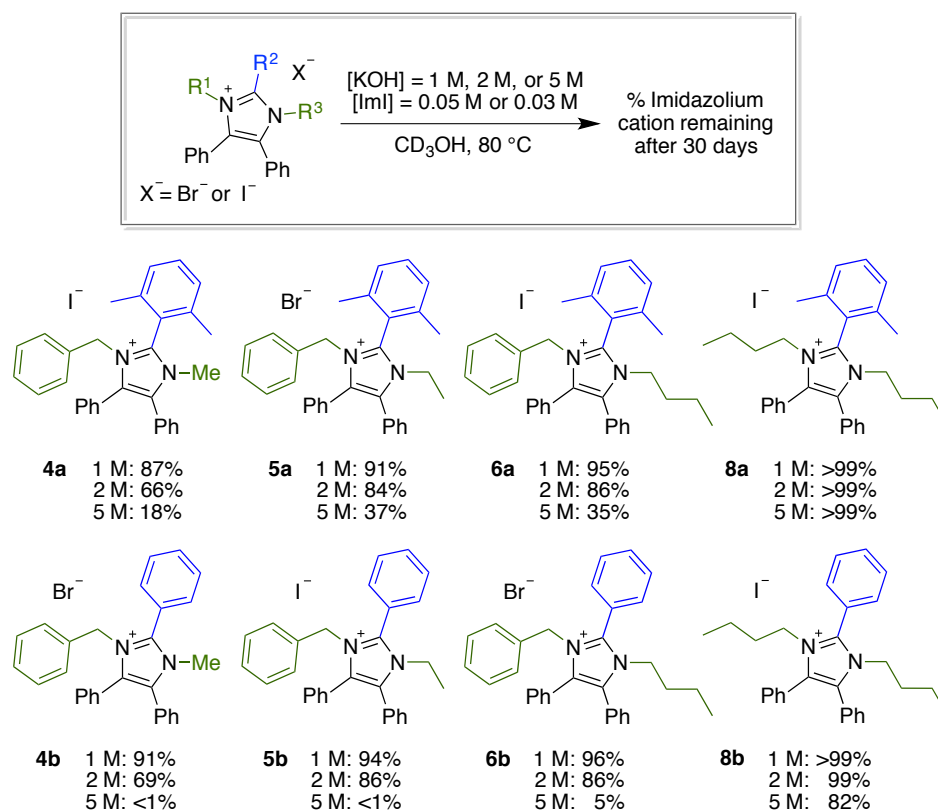


Figure 4.7 Percent cation remaining after 30 days at 80 °C – Influence of N1 and N3 substituents on imidazolium stability. Determined by ^1H NMR spectroscopy.

In a series of benzyl imidazoliums with either C2-phenyls (Figure 4.7, **4b**, **5b** and **6b**) or C2-aryls (Figure 4.7, **4a**, **5a**, and **6a**), the stability improved by switching from N3-methyl to N3-ethyl or N3-butyl substituents. A similar result was reported by Gu *et al.*,^{40b} which showed that *n*-butyl groups improved imidazolium stability compared to methyl groups. For example, in 1 M KOH, 87% of **4a** remains after 30 days, whereas 91% and 95% of **5a** and **6a** remain, respectively. The differences became larger as the concentration of base increases to 2 M KOH; 66% of **4a** remains, while 84% and 86% of **5a** and **6a** remain, respectively. When comparing 1 M to 2 M KOH conditions (Figure 4.7, **4a** – **6a** and **4b** – **6b**), the reaction rates increase consistently with the increase in base concentration and degradation continues to occur by an $\text{S}_{\text{N}}2$ mechanism. A decrease in nucleophilic attack at the α -carbon of the N3-substituent is observed as the length of the N3-alkyl group increases, which explains the prior observation that longer

alkyl chains improve cation stability. ^1H NMR signals corresponding to ethylene or 1-butene are not readily detected, suggesting that Hofmann elimination (deprotonation and elimination of alkyl groups that contain β -hydrogens) is not a major degradation pathway for alkyl imidazoliums. An increase in degradation rate larger than predicted is observed for **4b**, **5b** and **6b** in 5 M KOH and ^1H NMR signals related to new degradation products are observed. At very high concentrations of base these imidazoliums degrade by a mechanism other than $\text{S}_{\text{N}}2$ attack at the substituents bound to the nitrogens. The trend is only observed for the C2-phenyl imidazoliums (Figure 4.7, **4b**, **5b** and **6b**), which suggests that the new degradation pathway involves addition of base to the C2 position. One possible explanation involves the participation of multiple species of base (^-OH or ^-OMe) in the rate-determining step of the reaction, resulting in a higher order dependence of base under very high concentrations of base. It is important to emphasize that the goal of increasing the base concentration is to accelerate reactions that occur at 1 M KOH, not to introduce new degradation pathways. Stability studies that are conducted in excess base are not necessarily representative of fuel cell operation and extrapolating degradation rates must be judiciously considered. Nevertheless, a cation that is stable under such caustic conditions will likely demonstrate excellent stability at lower base concentrations. Importantly, this facilitates membrane electrode assembly (MEA) fabrication due to the improved cation stability at elevated temperatures in the absence of water.

Replacing the N1-benzyl with an N1-butyl group and retaining the N3-butyl group led to the most stable imidazoliums in the series (**8a** and **8b**) for which signal integrations are essentially unchanged at 2 M KOH after 30 days and very little degradation is observed even at 5 M KOH (Figure 4.7, **8a** and **8b**). Interestingly, the stability of **8b** with a C2-phenyl group is only slightly altered at 5 M KOH, unlike **4b**, **5b**, and **6b**, which appear to react with methoxide at the C2 position at high base concentrations. This may indicate that an N1-butyl group is more effective than an N1-benzyl group at blocking nucleophilic addition to the C2 position of the imidazolium ring. Alternatively, a more soluble organic cation with aliphatic groups may remain better solvated, which can reduce the effective strength of the base, shielding the cation from

interaction with the neighboring nucleophile. The results in Figure 4.7 establish that imidazoliums with N1-butyl groups are less prone to nucleophilic attack compared to the N1-benzyl counterparts and addition reactions at the C2 position are least likely with 2,6-dimethylphenyl substituents. We prepared optimized imidazoliums, which incorporated the best substituents at each of the ring positions and assessed their alkaline stability (Figure 4.8).

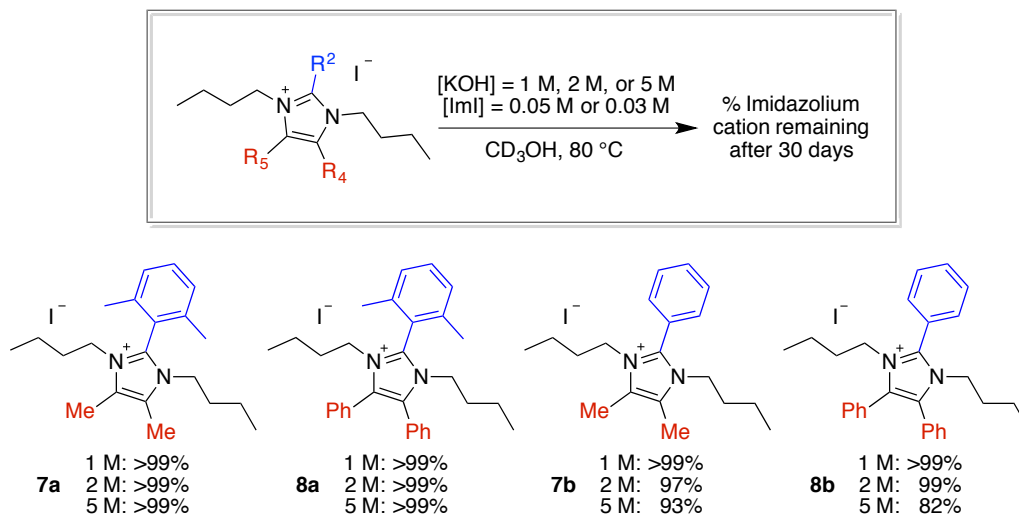


Figure 4.8 Percent cation remaining after 30 days at 80 °C – Optimization of base stable imidazoliums. Determined by ^1H NMR spectroscopy.

As predicted, imidazoliums with methyl groups at the C4,5 positions (Figure 4.8, **7a** and **7b**) are quite stable at 2 M KOH concentrations. At 5 M KOH concentrations, the stability of **7b** drops off; however, the stability remains higher than the analogous cation **8b** with C4,5 phenyl groups. Significant changes in the signal integrations for **7a** are not observed over 30 days, even at 5 M KOH and 80 °C (Figure 4.9). By systematically screening substituent effects on the overall imidazolium stability, we developed cations with exceptionally high resistance to reaction with base.

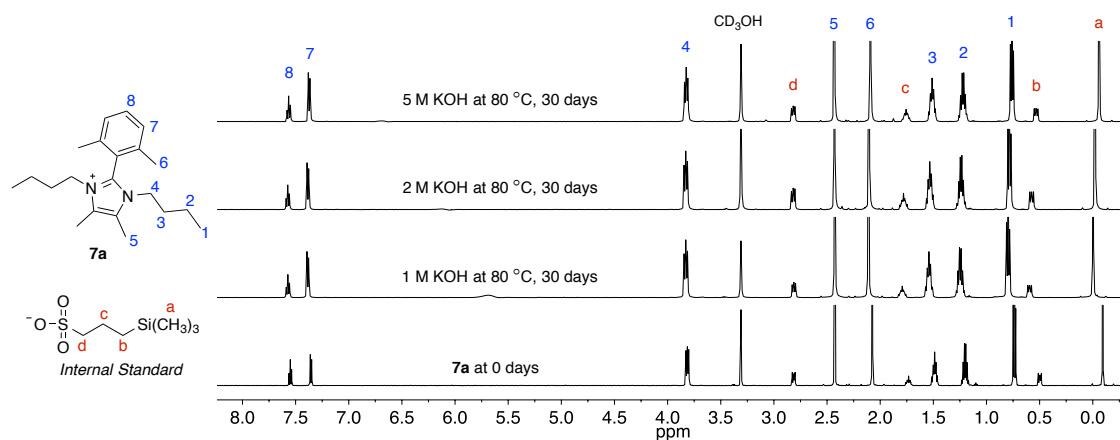


Figure 4.9 Analysis of **7a** under alkaline conditions using ^1H NMR spectroscopy in CD_3OH . Residual signals between 5.5 – 7.0 ppm are due to solvent; see Section 4.5 for discussion on solvent suppression.⁴⁴

We compared the stability of **7a** and **8a** to imidazoliums that have been previously reported and some important trends are highlighted (Figure 4.10). Imidazoliums with substitution at the C2 position demonstrate greatly improved stability over the unsubstituted version and better resistance to degradation than BTMA. Introducing alkyl substituents to the nitrogens consistently enhances the stability compared to the benzylic counterparts. The best stability is observed when both N1- and N3-alkyls are larger than methyls and substituents are present at the C4,5 positions. The use of 2 M and 5 M test conditions permits quantitative comparison between highly stable systems.

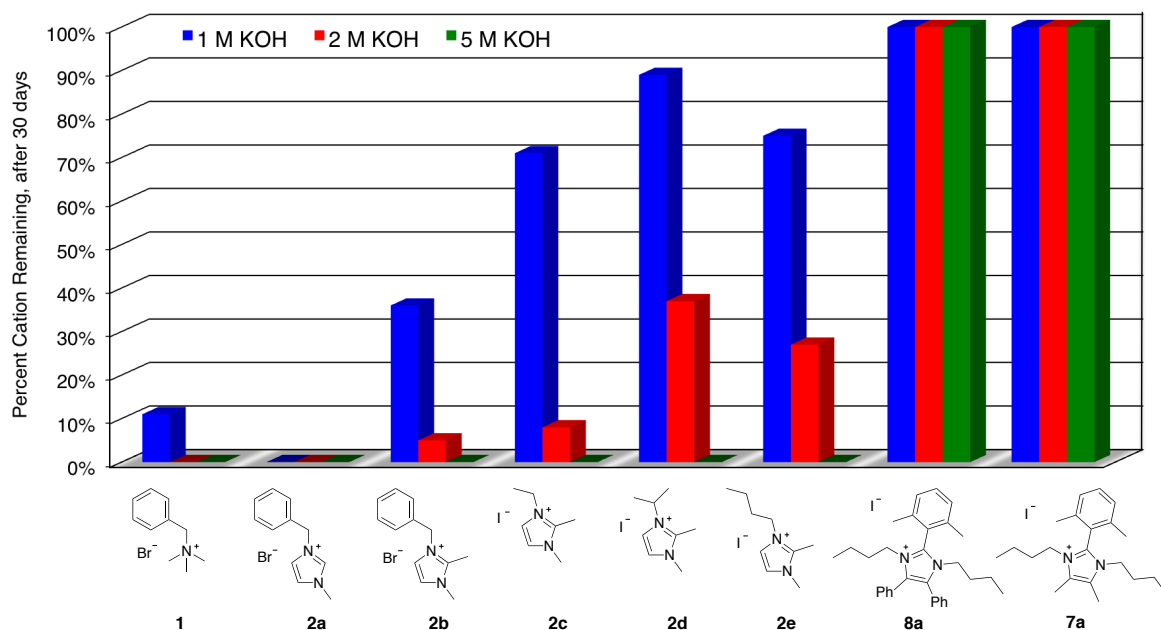


Figure 4.10 Comparison of model compound stabilities, percent remaining after 30 days at 80 °C (determined by ^1H NMR spectroscopy relative to an internal standard).⁴⁴

4.4 Conclusions

The effect of imidazolium substituents on base stability was systematically studied. The model compounds were assessed for stability under alkaline conditions by ^1H NMR spectroscopy and the degradation modes were analyzed. Based on these structural trends, we rationally modified the imidazolium ring to install substituents that would impede reaction with anions. Ultimately, we arrived at cations that were stable under the harsh alkaline conditions we assessed, in excess of operating fuel cell hydroxide concentrations. We found that C4 and C5 substitution was very important to the alkaline stability of the imidazolium cations, with methyl groups slightly improving the stability relative to phenyl groups. Moreover, methyl groups offer an advantage over phenyl groups when used in AAEMs because they increase the ion exchange capacity (IEC) of the membrane. Substitution at the C2 position inhibited degradation and 2,6-dimethylphenyl substituents were the most effective. The use of alkyl substituents on the nitrogens, particularly *n*-butyl groups, prevented degradation better than benzyl or methyl groups. Since the majority of polymerization techniques applied to synthesize AAEMs append

cations to benzylic positions, it will be necessary to develop new synthetic routes to attach the base-stable imidazoliums to polymers. Furthermore, several of the commonly employed polymer architectures have been discovered to be unstable under fuel cell operating conditions.⁴⁶ Developing AAEMs based on inert polymer backbones, such as the recent work by Coughlin and coworkers,⁴⁷ which describes the synthesis of a copolymer of isoprene and ammonium-functionalized styrene, may bypass these issues. Future work will focus on appending these cations to highly stable polymer architectures and characterizing the membranes for hydroxide conductivity and alkaline stability.

4.5 Experimental

4.5.1 General considerations

Methods and instruments

Flash chromatography was performed with silica gel (particle size 40-64 μm , 230-400 mesh) using either mixtures of ethyl acetate and hexanes, diethylether and hexanes or mixtures of dichloromethane and methanol as the eluent. ^1H and ^{13}C NMR spectra were recorded on a Varian INOVA 500 or 600 MHz instrument at 22 $^{\circ}\text{C}$ with shifts reported relative to the residual solvent peak (CD_3OD or CD_3OH ; 3.31 ppm (^1H) and 49.00 ppm (^{13}C) or CDCl_3 ; 7.26 ppm (^1H) and 77.16 ppm (^{13}C)). High resolution mass spectrometry (DART-HRMS) analyses were performed on a Thermo Scientific Exactive Orbitrap MS system equipped with an Ion Sense DART ion source.

Solvent suppression procedure^{48,49}

Quantitative ^1H NMR spectra for model compound stability studies were acquired in CD_3OH to 1) prevent unwanted hydrogen/deuterium exchange in model compounds and degradation products and 2) improve the solubility of model compounds and degradation products. The $-\text{OH}$ signal in CD_3OH was suppressed by prestauration with a 2 second presaturation delay and continuous wave irradiation with decoupler field strength (γB_1) of 113 Hz (equivalent to a presaturation power of 9). Spectra were acquired over a spectral width of -1 to 14 ppm with 60 second relaxation delay and nominal 90° excitation pulse. 16 scans were averaged for each analysis. NMR spectra were processed using MestReNova Version 9.0.1-13254 (Mestrelab Research S.L). Residual $-\text{OH}$ signal was further suppressed with the signal suppression feature in the software. Spectra were zero-filled to 256k complex points and an exponential window function of 0.2 Hz was applied prior to manual phase correction. Whittaker smoother baseline correction was applied and linear correction was used for all integrals. Note: Residual signals between 5.5 – 7.0 ppm often derive from solvent suppression.

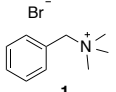
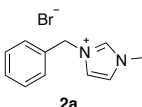
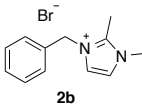
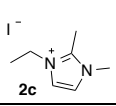
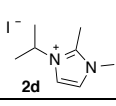
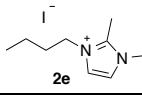
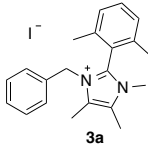
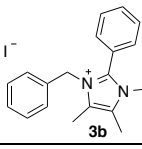
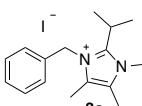
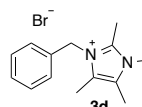
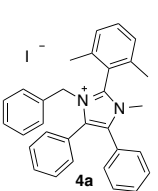
Chemicals

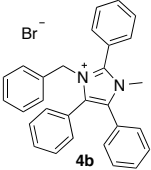
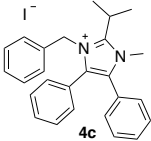
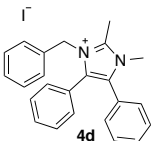
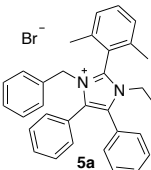
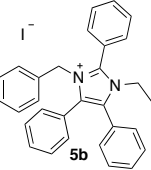
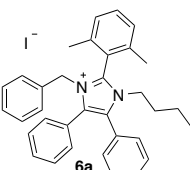
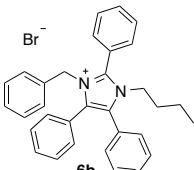
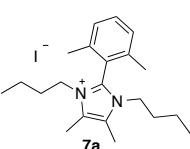
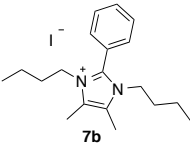
Benzaldehyde, 2,6-dimethylbenzaldehyde, 2-methylproprionaldehyde, ethanal, 2,3-butanedione, diphenylethanedione, *n*-butylamine, 2M methyl amine in methanol, 2M ethyl amine in methanol, L-proline, benzyl bromide, ethyl iodide, *n*-butyl iodide, 2-iodopropane, 1-methyl imidazole and 1,2-dimethyl imidazole were purchased from Aldrich and used as received. Benzyl amine and methyl iodide were purchased from Alfa Aesar and used as received. Ammonium acetate, dichloromethane, ethyl acetate and chloroform were purchased from Fischer and used as received. Trimethyl amine (31-35% in ethanol) was purchased from Fluka and used and received. 3-(Trimethylsilyl)-1-propanesulfonic acid sodium salt and 1,2,4,5-tetramethylimidazole were purchased from TCI Chemicals and used as received. Methanol-*d*3 was purchased from Acros and used as received. Methanol-*d*4 and chloroform-*d* were purchased from Cambridge Isotope Laboratories. Methanol, hexanes and acetonitrile were purchased from Macron and used as received. Tetrahydrofuran magnesium sulfate and diethyl ether were purchased from J.T. Baker and used as received. Potassium hydroxide was purchased from Mallinckrodt and used as received.

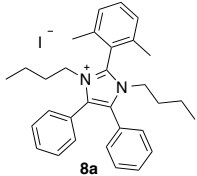
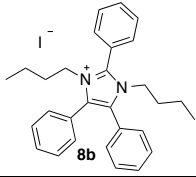
The following compounds were prepared previously according to literature procedures: Benzyl trimethylammonium (**1**),³⁰ 1-Benzyl-3-methylimidazolium bromide (**2a**),^{40b} 1-Benzyl-2,3-dimethylimidazolium bromide (**2b**),⁵⁰ 1-Ethyl-2,3-dimethylimidazolium iodide (**2c**),^{40d} 1-Isopropyl-2,3-dimethylimidazolium iodide (**2d**),^{40b} 1-*n*-Butyl-2,3-dimethylimidazolium iodide (**2e**),^{40b} 1-Benzyl-2-isopropyl-4,5-dimethyl-1*H*-imidazole (**IM-3c**),⁵¹ 1-Benzyl-2,3,4,5-tetramethylimidazolium bromide (**3d**),⁵² 1-Methyl-2,4,5-triphenyl-1*H*-imidazole (**IM-4b**),⁴⁵ 1-Benzyl-2,4,5-triphenyl-1*H*-imidazole (**IM2-4b**),⁵¹ 1-Benzyl-2-isopropyl-4,5-diphenyl-1*H*-imidazole (**IM-4c**),⁵¹ and 1-*n*-Butyl-2,4,5-triphenyl-1*H*-imidazole (**IM-6b**).⁵³

Expanded data tables

Table 4.1 Summary of model compound studies.^a

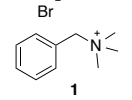
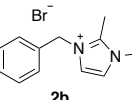
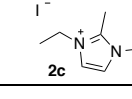
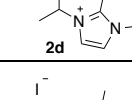
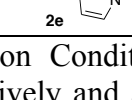
Model Compound	[KOH]	Cation remaining (%) ^b					
		5d	10d	15d	20d	25d	30d
 1	1M	75	56	29	19	15	11
	2M ^c	45	28	n.d. ^d	8	n.d.	<1
	5M ^{c,e}	5	n.d.	n.d.	<1	n.d.	n.d.
 2a	1M	2	<1	n.d.	n.d.	n.d.	n.d.
	2M ^c	<1	n.d.	n.d.	n.d.	n.d.	n.d.
	5M ^c	<1	n.d.	n.d.	n.d.	n.d.	n.d.
 2b	1M	77	64	56	49	44	36
	2M ^{c,e}	28	5	n.d.	n.d.	n.d.	n.d.
	5M ^{c,e}	<1	n.d.	n.d.	n.d.	n.d.	n.d.
 2c	1M	95	91	86	n.d.	72	71
	2M ^c	43	29	20	13	11	8
	5M ^{c,e}	<1	n.d.	n.d.	n.d.	n.d.	n.d.
 2d	1M	98	96	94	n.d.	92	89
	2M ^c	72	63	56	46	41	37
	5M ^{c,e}	1	n.d.	n.d.	n.d.	n.d.	n.d.
 2e	1M	95	87	85	80	77	75
	2M ^c	68	56	45	34	29	27
	5M ^{c,e}	<1	n.d.	n.d.	n.d.	n.d.	n.d.
 3a	1M	n.d.	>99	>99	n.d.	>99	>99
	2M ^c	>99	99	98	99	n.d.	99
	5M ^c	99	99	98	99	97	96
 3b	1M	>99	>99	>99	99	>99	>99
	2M ^c	99	98	97	96	97	95
	5M ^c	81	71	61	54	49	43
 3c	1M	99	97	97	96	96	95
 3d	1M	98	94	92	91	90	87
 4a	1M	97	95	92	91	90	87
	2M ^c	93	87	77	n.d.	70 ^f	66
	5M ^c	70	52	39	31	21	18

Model Compound	[KOH]	Cation remaining (%) ^b					
		5d	10d	15d	20d	25d	30d
 4b	1M	97	95	94	93	92	91
	2M ^c	98	94	89	82	76	69
	5M ^c	1	n.d.	n.d.	n.d.	n.d.	n.d.
 4c	1M	98	94	91	89	86	82
 4d	1M	95	91	88	86	85	80
 5a	1M	97	97	95	94	93	91
	2M ^c	97	93	91	88	85	84
	5M ^c	80	70	55	46	42	37
 5b	1M	99	98	98	97	95	94
	2M ^c	96	94	92	91	89	86
	5M ^c	29	9	4	2	n.d.	n.d.
 6a	1M	98	98	n.d.	96	95	95
	2M ^c	98	95	92	89	87	86
	5M ^c	80	69	61	46	39	35
 6b	1M	n.d.	99	98	97	97	96
	2M ^c	96	94	92	90	88	86
	5M ^c	44	30	19	11	8	5
 7a	1M	>99	>99	99	>99	99	>99
	2M ^c	>99	99	98	99	>99	>99
	5M ^c	>99	>99	>99	>99	>99	>99
 7b	1M	>99	>99	>99	>99	99	>99
	2M ^c	99	96	97	96	97	97
	5M ^c	>99	>99	96	96	96	93

Model Compound	[KOH]	Cation remaining (%) ^b					
		5d	10d	15d	20d	25d	30d
 8a	1M	>99	>99	99	>99	>99	>99
	2M ^c	99	>99	>99	99	>99	>99
	5M ^c	>99	>99	>99	>99	>99	>99
 8b	1M	>99	>99	>99	>99	>99	>99
	2M ^c	99	>99	>99	>99	>99	99
	5M ^c	96	92	90	86	85	82

^aReaction Conditions: [ImX]:[KOH] = 1:20, 1:67, 1:167 for 1M, 2M, and 5M KOH experiments, respectively and at 80 °C. ^bPercent of cation remaining, determined by ¹H NMR spectroscopy relative to an internal standard, 3-(trimethylsilyl)-1-propanesulfonic acid sodium salt. ^cThe imidazolium concentration was reduced from 0.05M to 0.03M at higher base concentrations due to reduced solubility of the organic salt. ^dNot determined. ^eAnalyses were performed at time intervals less than 5 days for samples that were anticipated to have low stability. ^fAnalysis performed after 17 days.

Table 4.2 Model compound studies, selected compounds analyzed at 1-5 days.^a

Model Compound	[KOH]	Cation remaining (%) ^b				
		1d	2d	3d	4d	5d ^e
 1	5M ^c	83	44	28	n.d. ^d	5
 2b	2M ^c	77	67	50	37	28
	5M ^c	<1	n.d.	n.d.	n.d.	n.d.
 2c	5M ^c	12	1	n.d.	n.d.	n.d.
 2d	5M ^c	53	24	8	3	1
 2e	5M ^c	32	9	1	n.d.	n.d.

^aReaction Conditions: [ImX]:[KOH] = 1:67 or 1:167 for 2M and 5M KOH experiments, respectively and at 80 °C. ^bPercent of cation remaining, determined by ¹H NMR spectroscopy relative to an internal standard, 3-(trimethylsilyl)-1-propanesulfonic acid sodium salt. ^cThe imidazolium concentration was reduced from 0.05M to 0.03M at higher base concentrations due to reduced solubility of the organic salt. ^dNot determined.

4.5.2 Synthetic Procedures

General Procedure A – Multicomponent Synthesis of Substituted Imidazoles

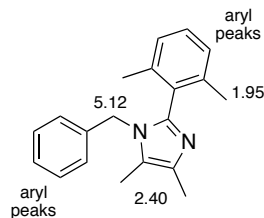
The appropriate aldehyde, dione and primary amine were combined with ammonium acetate and L-proline in methanol and stirred at 60 °C for 12 hours. After cooling to 22 °C, the solvent was removed under reduced pressure. The residue was dissolved in chloroform, washed with H₂O, dried with magnesium sulfate, filtered and concentrated under reduced pressure. The crude product was further purified via recrystallization, flash column chromatography or a combination of both.

General Procedure B – Quaternization of Imidazoles with Alkyl or Benzyl Halides

The appropriate imidazole precursor was dissolved in acetonitrile and halide reagent was added while stirring. The mixture was stirred at 80 °C for 12 hours. After cooling to room temperature, the solvent was removed under reduced pressure. The residue was dissolved in chloroform and purified by precipitation into ether, ethyl acetate, methanol or tetrahydrofuran. Precipitation was repeated to obtain pristine products. Note: To obtain salts without residual solvent, the powders were mixed with a small portion of dichloromethane and solvent was removed under reduced pressure.

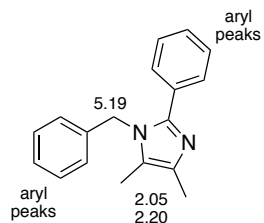
Synthesis of starting materials

1-Benzyl-2-(2,6-dimethylphenyl)-4,5-dimethyl-1*H*-imidazole (**IM-3a**)



Following general procedure A, 2,6-dimethylbenzaldehyde (1.00 g, 7.45 mmol), 2,3-butanedione (0.65 ml, 7.5 mmol), benzylamine (0.81 ml, 7.5 mmol) and ammonium acetate (0.574 g, 7.45 mmol) were combined with L-proline (0.136 g, 1.18 mmol) in methanol (30 ml). The residue was purified via flash column chromatography (2% methanol/dichloromethane) to give **IM-3a** (0.359 g, 17 %) as an orange oil. **¹H NMR** (600 MHz, CD₃OD): δ 7.46 (t, *J* = 7.7 Hz, 1H), 7.34 – 7.27 (m, 3H), 7.23 (d, *J* = 7.7 Hz, 2H), 6.94 (d, *J* = 7.6 Hz, 2H), 5.12 (s, 2H), 2.40 (s, 3H), 2.40 (s, 3H), 1.95 (s, 6H). **¹³C NMR** (126 MHz, CD₃OD): δ 143.80, 140.52, 134.95, 133.52, 130.12, 129.74, 129.42, 128.50, 128.47, 127.29, 123.78, 50.05, 19.67, 9.31, 9.01. **HRMS** (DART) *m/z* calculated for C₁₅H₂₁N₂⁺ (*M* + H⁺) 291.18558, found 291.18515.

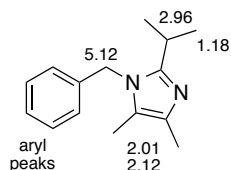
1-Benzyl-4,5-dimethyl-2-phenyl-1*H*-imidazole (**IM-3b**)



Following general procedure A, benzaldehyde (5.0 ml, 49 mmol), 2,3-butanedione (4.3 ml, 49 mmol), benzylamine (5.9 ml, 54 mmol) and ammonium acetate (3.78 g, 49.0 mmol) were combined with L-proline (0.846 g, 7.35 mmol) in methanol (100 ml). The residue was purified via flash column chromatography (50% ethyl acetate/hexanes). The product was recrystallized from acetonitrile to give **IM-3b** (2.54 g, 20 %) as a pale yellow powder. **¹H NMR** (500 MHz, CD₃OD): δ 7.45 (m, 2H), 7.38 (m, 3H), 7.32 (t, *J* = 7.4 Hz, 2H), 7.30 – 7.24 (t, *J* = 7.4 Hz, 1H),

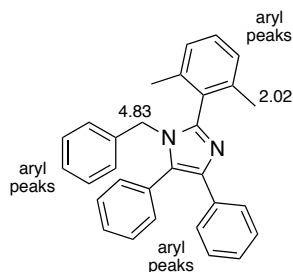
6.98 – 6.94 (d, $J = 7.6$ Hz, 2H), 5.19 (s, 2H), 2.20 (s, 3H), 2.05 (s, 3H). ^{13}C NMR (126 MHz, CD_3OD): δ 147.56, 138.54, 133.91, 131.73, 130.00, 129.96, 129.69, 129.66, 128.57, 126.65, 125.57, 48.71, 12.38, 8.98. HRMS (DART) m/z calculated for $\text{C}_{18}\text{H}_{19}\text{N}_2^+$ ($\text{M} + \text{H}^+$) 263.15428, found 263.15349.

1-Benzyl-2-isopropyl-4,5-dimethyl-1H-imidazole (IM-3c)



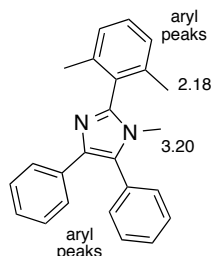
Following general procedure A, 2-methylpropionaldehyde (5.2 ml, 57 mmol), 2,3-butanedione (5.0 ml, 57 mmol), benzylamine (6.2 ml, 57 mmol) and ammonium acetate (4.40 g, 57.0 mmol) were combined with L-proline (0.984 g, 8.55 mmol) in methanol (100 ml). The residue was purified via flash column chromatography (1:10:90 triethylamine/methanol/dichloromethane). The product was recrystallized from acetonitrile at -20 °C and sublimed to give **IM-3c** (0.841 g, 6.5 %) as a white powder. ^1H NMR (600 MHz, CD_3OD): δ 7.31 (t, $J = 7.6$ Hz, 2H), 7.25 (t, $J = 7.4$ Hz, 1H), 6.93 (d, $J = 7.8$ Hz, 2H), 5.12 (s, 2H), 2.96 (hept, $J = 6.9$ Hz, 1H), 2.12 (s, 3H), 2.01 (s, 3H), 1.18 (d, $J = 6.9$ Hz, 6H). ^{13}C NMR (126 MHz, CD_3OD): δ 152.94, 138.84, 132.04, 129.88, 128.49, 126.74, 123.08, 47.22, 27.17, 22.27, 12.14, 8.67. HRMS (DART) m/z calculated for $\text{C}_{15}\text{H}_{21}\text{N}_2^+$ ($\text{M} + \text{H}^+$) 229.16993, found 229.1705.

1-Benzyl-2-(2,6-dimethylphenyl)-4,5-diphenyl-1H-imidazole (IM-4a)



Following general procedure A, 2,6-dimethylbenzaldehyde (1.00 g, 7.45 mmol), diphenylethanedione (1.57 g, 7.45 mmol), benzylamine (0.80 ml, 7.5 mmol) and ammonium acetate (0.574 g, 7.45 mmol) were combined with L-proline (0.129 g, 1.12 mmol) in methanol (30 ml). The residue was purified via flash column chromatography (10% ethyl acetate/hexanes). The product was recrystallized from acetonitrile to give **IM-4a** (0.787 g, 25 %) as a white powder. **¹H NMR** (600 MHz, CD₃OD): δ 7.50 – 7.43 (m, 3H), 7.41 (m, 4H), 7.30 (t, *J* = 7.6 Hz, 1H), 7.18 (tm, *J* = 7.4 Hz, 2H), 7.16 – 7.10 (m, 4H), 7.06 (t, *J* = 7.7 Hz, 2H), 6.59 (d, *J* = 7.7 Hz, 2H), 4.83 (s, 2H), 2.02 (s, 6H). **¹³C NMR** (126 MHz, CDCl₃): δ 146.54, 138.83, 137.41, 136.34, 134.78, 131.47, 131.31, 130.54, 129.27, 129.04, 128.57, 128.52, 128.12, 128.03, 127.49, 127.41, 127.38, 126.64, 126.15, 47.76, 19.93. **HRMS** (DART) *m/z* calculated for C₁₉H₃₁N₂⁺ (M⁺) 415.21688, found 415.21722.

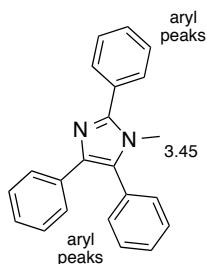
2-(2,6-Dimethylphenyl)-1-methyl-4,5-diphenyl-1H-imidazole (IM2-4a)



Following general procedure A, 2,6-dimethylbenzaldehyde (2.08 g, 15.5 mmol), diphenylethanedione (3.26 mg, 15.5 mmol), 2M methylamine in methanol (7.8 ml, 16 mmol) and ammonium acetate (1.19 g, 15.5 mmol) were combined with L-proline (0.892 g, 7.75 mmol) in methanol (60 ml). The residue was purified via flash column chromatography (15% ethyl acetate/hexanes). The product was recrystallized from acetonitrile to give **IM2-4a** (1.30 g, 25 %)

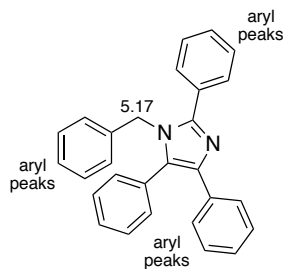
as a white powder. **¹H NMR** (600 MHz, CD₃OD): δ 7.53 – 7.45 (m, 3H), 7.41 (m, 4H), 7.33 (t, *J* = 7.6 Hz, 1H), 7.24 – 7.16 (m, 4H), 7.16 – 7.12 (t, *J* = 7.3 Hz, 1H), 3.20 (s, 3H), 2.18 (s, 6H). **¹³C NMR** (126 MHz, CD₃OD): δ 148.14, 140.11, 138.21, 135.51, 132.05, 132.04, 131.28, 130.98, 130.52, 130.21, 129.89, 129.13, 128.58, 128.19, 127.60, 31.73, 19.96. **HRMS** (DART) *m/z* calculated for C₂₄H₂₃N₂⁺ (*M* + H⁺) 339.18558, found 339.18505.

1-Methyl-2,4,5-triphenyl-1*H*-imidazole (**IM-4b**)



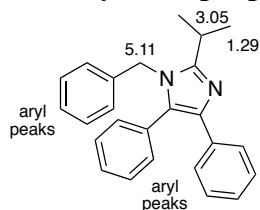
Following general procedure A, benzaldehyde (2.5 ml, 25 mmol), diphenylethanedione (5.20 g, 24.7 mmol), 2M methylamine in methanol (12 ml, 25 mmol) and ammonium acetate (1.90 g, 24.7 mmol) were combined with L-proline (0.427 g, 3.70 mmol) in methanol (100 ml). The residue was recrystallized in methanol from give **IM-4b** (2.88 g, 38 %) as a white powder. **¹H NMR** (600 MHz, CD₃OD): δ 7.69 (dm, *J* = 7.7 Hz, 2H), 7.51 (m, 2H), 7.49 – 7.40 (m, 4H), 7.37 (m, 4H), 7.20 – 7.14 (m, 2H), 7.14 – 7.07 (tm, *J* = 7.6 Hz, 1H), 3.45 (s, 3H). **¹³C NMR** (126 MHz, CDCl₃): δ 147.93, 137.78, 134.72, 131.26, 131.01, 130.92, 130.52, 129.11, 129.09, 128.79, 128.62*, 128.13, 127.00, 126.35, 33.21. **HRMS** (DART) *m/z* calculated for C₂₂H₁₉N₂⁺ (*M* + H⁺) 311.15428, found 311.15334. *The resonances for two carbon nuclei are found at this chemical shift, which is supported by line width and peak intensity analysis.

1-Benzyl-2,4,5-triphenyl-1*H*-imidazole (IM2-4b)



Following general procedure A, benzaldehyde (2.0 ml, 20 mmol), diphenylethanedione (4.10 g, 19.6 mmol), benzylamine (2.1 ml, 20 mmol) and ammonium acetate (1.50 g, 19.6 mmol) were combined with L-proline (0.338 g, 2.94 mmol) in methanol (80 ml). The residue was purified via flash column chromatography (10% ethyl acetate/hexanes to 50% ethyl acetate/hexanes). The product was recrystallized in methanol at -20 °C from give **IM2-4b** (1.84 g, 24 %) as a white powder. **¹H NMR** (600 MHz, CD₃OD): δ 7.66 – 7.61 (m, 2H), 7.48 – 7.45 (m, 3H), 7.45 – 7.41 (m, 2H), 7.41 – 7.31 (m, 3H), 7.26 – 7.23 (dm, *J* = 7.8 Hz, 2H), 7.22 – 7.11 (m, 6H), 6.73 (dm, *J* = 7.9 Hz, 2H), 5.17 (s, 2H). **¹³C NMR** (126 MHz, CDCl₃): δ 148.11, 138.12, 137.58, 134.55, 131.10, 131.08, 131.02, 130.11, 129.09, 128.93, 128.83, 128.66, 128.63, 128.61, 128.13, 127.39, 126.82, 126.40, 126.04, 48.31. **HRMS** (DART) *m/z* calculated for C₂₈H₂₃N₂⁺ (*M* + H⁺) 387.18558, found 387.18430.

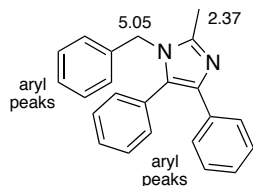
1-Benzyl-2-isopropyl-4,5-diphenyl-1*H*-imidazole (IM-4c)



Following general procedure A, 2-methylpropionaldehyde (2.5 ml, 28 mmol), diphenylethanedione (5.76 g, 27.4 mmol), benzylamine (3.0 ml, 27 mmol) and ammonium acetate (2.17 g, 27.4 mmol) were combined with L-proline (0.473 g, 4.11 mmol) in methanol (100 ml). The residue was purified via flash column chromatography (1:10:90 triethylamine/ethyl acetate/hexanes) to give **IM-4c** (2.41 g, 25 %) as a white powder. **¹H NMR** (600 MHz, CD₃OD): δ 7.39 – 7.31 (m, 5H), 7.28 (t, *J* = 7.4 Hz, 2H), 7.25 – 7.20 (m, 3H), 7.20 –

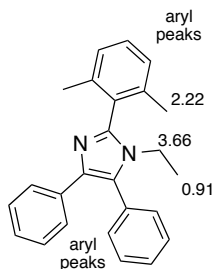
7.16 (tm, $J = 7.7$ Hz, 2H), 7.16 – 7.11 (tm, $J = 7.4$ Hz, 1H), 6.92 (d, $J = 7.6$ Hz, 2H), 5.11 (s, 2H), 3.05 (hept, $J = 6.9$ Hz, 1H), 1.29 (d, $J = 6.9$ Hz, 6H). ^{13}C NMR (126 MHz, CD_3OD): δ 155.14, 138.82, 138.21, 135.76, 132.27, 132.02, 129.90*, 129.80, 129.71, 128.99, 128.64, 128.55, 127.51, 126.89, 47.76, 27.69, 22.09. HRMS (DART) m/z calculated for $\text{C}_{25}\text{H}_{25}\text{N}_2^+$ ($\text{M} + \text{H}^+$) 353.20123, found 353.20105. *The resonances for two carbon nuclei are found at this chemical shift, which is supported by line width and peak intensity analysis.

1-Benzyl-2-methyl-4,5-diphenyl-1H-imidazole (IM-4d)



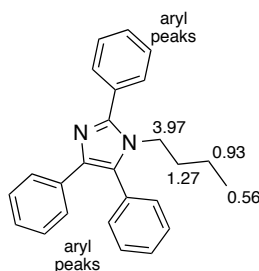
Following general procedure A, ethanal (2.0 ml, 36 mmol), diphenylethanedione (7.48 mg, 35.6 mmol), benzylamine (4.3 ml, 36 mmol) and ammonium acetate (2.74 g, 35.6 mmol) were combined with L-proline (0.615 g, 5.34 mmol) in methanol (30 ml). The residue was purified via flash column chromatography (1:20:80 triethylamine/ethyl acetate/hexanes). The product was recrystallized from acetonitrile at -20 °C to give **IM-4d** (0.652 g, 5.6 %) as a white powder. ^1H NMR (600 MHz, CD_3OD): δ 7.41 – 7.33 (m, 5H), 7.28 (tm, $J = 7.6$ Hz, 2H), 7.25 – 7.19 (m, 3H), 7.17 (tm, $J = 7.4$ Hz, 2H), 7.14 – 7.09 (tm, $J = 7.3$ Hz, 1H), 6.92 – 6.89 (m, 2H), 5.05 (s, 2H), 2.37 (s, 3H). ^{13}C NMR (126 MHz, CD_3OD): δ 146.63, 138.22, 137.45, 135.49, 132.19, 132.01, 130.61, 130.01, 129.89*, 129.09, 128.60, 128.06, 127.50, 127.00, 48.10, 13.16. HRMS (DART) m/z calculated for $\text{C}_{23}\text{H}_{21}\text{N}_2^+$ ($\text{M} + \text{H}^+$) 325.16993, found 325.1705. *The resonances for two carbon nuclei are found at this chemical shift, which is supported by line width and peak intensity analysis.

2-(2,6-Dimethylphenyl)-1-ethyl-4,5-diphenyl-1H-imidazole (IM-5a)



Following general procedure A, 2,6-dimethylbenzaldehyde (1.00 g, 7.45 mmol), diphenylethanedione (1.57 g, 7.45 mmol), 2M ethylamine in methanol (7.5 ml, 15 mmol) and ammonium acetate (0.570 g, 7.45 mmol) were combined with L-proline (0.128 g, 1.12 mmol) in methanol (30 ml). The residue was purified via flash column chromatography (10% ethyl acetate/hexanes). The product was recrystallized from acetonitrile at -20 °C to give **IM-5a** (0.411 g, 16 %) as a white powder. ¹H NMR (600 MHz, CD₃OD): δ 7.52 (m, 3H), 7.44 (d, *J* = 7.4 Hz, 2H), 7.38 (d, *J* = 7.4 Hz, 2H), 7.34 (t, *J* = 7.7 Hz, 1H), 7.22 (d, *J* = 7.6 Hz, 2H), 7.18 (t, *J* = 7.3 Hz, 2H), 7.15 – 7.11 (m, 1H), 3.66 (q, *J* = 7.1 Hz, 2H), 2.22 (s, 6H), 0.91 (t, *J* = 7.1 Hz, 3H). ¹³C NMR (126 MHz, CD₃OD): δ 147.37, 139.99, 138.57, 135.47, 132.33, 132.22, 131.45, 130.97, 130.30, 130.00, 129.86, 129.10, 128.73, 128.11, 127.54, 40.47, 20.19, 15.92. HRMS (DART) *m/z* calculated for C₂₅H₂₅N₂⁺ (*M* + *H*⁺) 353.20123, found 353.20028.

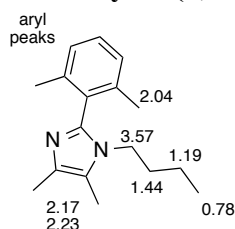
1-*n*-Butyl-2,4,5-triphenyl-1H-imidazole (IM-6b)



Following general procedure A, benzaldehyde (2.0 ml, 20 mmol), diphenylethanedione (4.54 g, 21.6 mmol), *n*-butylamine (2.1 ml, 22 mmol) and ammonium acetate (1.51 g, 19.6 mmol) were combined with L-proline (0.260 g, 2.26 mmol) in methanol (80 ml). The residue was purified via flash column chromatography (10% ethyl acetate/hexanes to 100% ethyl acetate). The product was recrystallized from acetonitrile to give **IM-6b** (6.39 g, 93 %) as a white powder. ¹H NMR

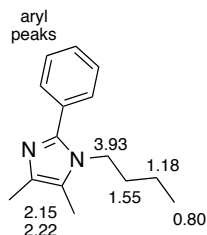
(600 MHz, CD₃OD): δ 7.71 – 7.66 (d, J = 7.4 Hz, 2H), 7.58 – 7.45 (m, 6H), 7.44 – 7.36 (m, 4H), 7.21 – 7.16 (t, J = 7.4 Hz, 2H), 7.16 – 7.11 (m, 1H), 4.00 – 3.93 (m, 2H), 1.27 (p, J = 7.4 Hz, 2H), 0.93 (sext, J = 7.4 Hz, 2H), 0.56 (t, J = 7.4 Hz, 3H). ¹³C NMR (126 MHz, CDCl₃): δ 147.71, 137.73, 134.71, 131.66, 131.63, 131.08, 129.70, 129.24, 129.08, 128.82, 128.64*, 128.07, 126.85, 126.22, 44.55, 32.58, 19.49, 13.33. HRMS (DART) m/z calculated for C₂₅H₂₅N₂⁺ (M + H⁺) 353.20123, found 353.20124. * The resonances for two carbon nuclei are found at this chemical shift, which is supported by line width and peak intensity analysis.

1-*n*-Butyl-2-(2,6-dimethylphenyl)-4,5-dimethyl-1*H*-imidazole (IM-7a)



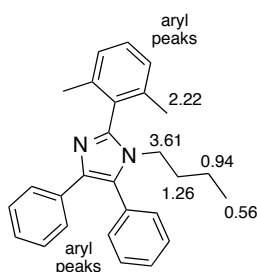
Following general procedure A, 2,6-dimethylbenzaldehyde (2.00 g, 14.9 mmol), 2,3-butanedione (1.3 ml, 15 mmol), *n*-butylamine (1.5 ml, 15 mmol) and ammonium acetate (1.15 g, 14.9 mmol) were combined with L-proline (0.251 g, 2.24 mmol) in methanol (60 ml). The crude mixture was initially purified via flash column chromatography (5% methanol/dichloromethane to 50% methanol/dichloromethane) to afford a brown oil. The residue was further purified via flash column chromatography (5% ethyl acetate/hexanes to 100% ethyl acetate) to give **IM-7a** (0.554 g, 15 %) as a pale brown oil. ¹H NMR (600 MHz, CD₃OD): δ 7.27 (t, J = 7.6 Hz, 1H), 7.14 (d, J = 7.6 Hz, 2H), 3.63 – 3.48 (m, 2H), 2.23 (s, 3H), 2.17 (s, 3H), 2.04 (s, 6H), 1.49 – 1.40 (p, J = 7.4 Hz, 2H), 1.19 (sext, J = 7.4 Hz, 2H), 0.78 (t, J = 7.4 Hz, 3H). ¹³C NMR (126 MHz, CD₃OD): δ 145.11, 139.87, 132.93, 131.97, 130.51, 128.50, 123.49, 44.78, 33.50, 20.78, 20.05, 13.79, 12.29, 8.95. HRMS (DART) m/z calculated for C₁₇H₂₅N₂⁺ (M + H⁺) 257.20123, found 257.20141.

1-*n*-Butyl-4,5-dimethyl-2-phenyl-1*H*-imidazole (IM-7b)



Following general procedure A, benzaldehyde (2.0 ml, 20 mmol), 2,3-butanedione (1.9 ml, 22 mmol), *n*-butylamine (1.9 ml, 20 mmol) and ammonium acetate (1.51 g, 19.6 mmol) were combined with L-proline (0.260 g, 2.26 mmol) in methanol (80 ml). The residue was initially purified via flash column chromatography (50% ethyl acetate/hexanes) to give **IM-7b** (3.44 g, 77 %) as a dark brown oil. Distillation under vacuum with a Hickman apparatus produced a pale yellow oil. ¹H NMR (600 MHz, CD₃OD): δ 7.54 – 7.36 (m, 5H), 3.96 – 3.91 (m, 2H), 2.22 (s, 3H), 2.15 (s, 3H), 1.59 – 1.49 (p, *J* = 7.4 Hz, 2H), 1.18 (sext, *J* = 7.4 Hz, 2H), 0.80 (t, *J* = 7.4 Hz, 3H). ¹³C NMR (126 MHz, CD₃OD): δ 147.03, 133.39, 132.53, 130.11, 129.88, 129.68, 124.91, 45.07, 33.76, 20.63, 13.78, 12.16, 8.97. HRMS (DART) *m/z* calculated for C₁₅H₂₁N₂⁺ (*M* + H⁺) 229.16993, found 229.16942.

1-*n*-Butyl-2-(2,6-dimethylphenyl)-4,5-diphenyl-1*H*-imidazole (IM-8a)

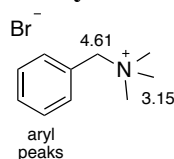


Following general procedure A, 2,6-dimethylbenzaldehyde (2.00 g, 14.9 mmol), diphenylethanedione (3.13 g, 14.9 mmol), *n*-butylamine (1.5 ml, 15 mmol) and ammonium acetate (1.15 g, 14.9 mmol) were combined with L-proline (0.257 g, 2.26 mmol) in methanol (60 ml). The residue was purified via flash column chromatography (10% ethyl acetate/hexanes). The product was recrystallized in acetonitrile to give **IM-8a** (0.975 g, 17 %) as a white powder. ¹H NMR (600 MHz, CD₃OD): δ 7.55 – 7.46 (m, 3H), 7.44 – 7.41 (dm, *J* = 7.4 Hz, 2H), 7.40 –

7.38 (dm, $J = 7.9$ Hz, 2H), 7.34 (t, $J = 7.7$ Hz, 1H), 7.22 (d, $J = 7.7$ Hz, 2H), 7.19 – 7.15 (tm, $J = 7.6$ Hz, 2H), 7.15 – 7.11 (tm, $J = 7.3$ Hz, 1H), 3.63 – 3.59 (m, 2H), 2.22 (s, 6H), 1.26 (p, $J = 7.4$ Hz, 2H), 0.94 (sext, $J = 7.4$ Hz, 2H), 0.56 (t, $J = 7.4$ Hz, 3H). ^{13}C NMR (126 MHz, CD_3OD): δ 147.49, 139.87, 138.34, 135.44, 132.30, 132.21, 131.38, 130.90, 130.26, 130.06, 129.94, 129.10, 128.73, 128.08, 127.52, 45.10, 33.14, 20.48, 20.31, 13.52. HRMS (DART) m/z calculated for $\text{C}_{27}\text{H}_{29}\text{N}_2^+$ ($\text{M} + \text{H}^+$) 381.23253, found 381.23138.

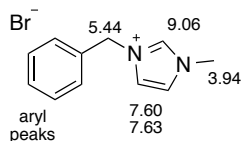
Synthesis of model compounds

Benzyl trimethylammonium bromide (1)



Trimethylamine, 30% in ethanol, (0.76 ml, 3.1 mmol) was treated with benzyl bromide (0.40 ml, 3.4 mmol) in acetonitrile (5 ml). The residue was dissolved in chloroform and purified via precipitation into ether to give **1** (0.693 g, 90 %) as a white powder. ^1H NMR (600 MHz, CD_3OD): δ 7.63 – 7.60 (dm, $J = 7.7$ Hz, 2H), 7.59 – 7.52 (m, 3H), 4.61 (s, 2H), 3.15 (s, 9H). ^{13}C NMR (126 MHz, CD_3OD): δ 134.10, 131.87, 130.26, 129.19, 70.15, 53.19, 53.16, 53.13. HRMS (DART) m/z calculated for $\text{C}_{10}\text{H}_{16}\text{N}^+$ (M^+) 150.12773, found 150.12750.

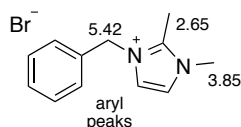
1-Benzyl-3-methylimidazolium bromide (2a)



Following general procedure B, 1-methylimidazole (1.0 ml, 13 mmol) was treated with benzyl bromide (1.5 ml, 12 mmol) in acetonitrile (10 ml). The residue was dissolved in chloroform and purified via precipitation into ether to give **2a** (3.03 g, 98 %) as a brown oil. ^1H NMR (600 MHz, CD_3OD): δ 9.06 (s, 1H), 7.64 – 7.62 (m, 1H), 7.61 – 7.58 (m, 1H), 7.47 – 7.40 (m, 4H), 5.44 (s, 2H), 3.94 (s, 3H). ^{13}C NMR (151 MHz, CD_3OD): δ 137.97, 135.25, 130.39, 130.33, 129.71,

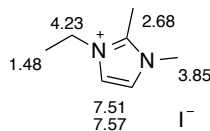
125.26, 123.66, 54.11, 36.69. **HRMS** (DART) m/z calculated for $C_{11}H_{13}N_2^+$ (M^+) 173.10732, found 173.10709.

1-Benzyl-2,3-dimethylimidazolium bromide (**2b**)



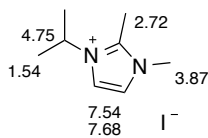
Following general procedure B, 1,2-dimethyl imidazole (2.00 g, 20.8 mmol) was treated with benzyl bromide (3.0 ml, 25 mmol) in acetonitrile (100 ml). The product was recrystallized from chloroform to give **2b** (3.05 g, 55 %) as a white powder. **1H NMR** (600 MHz, CD_3OD): δ 7.53 (m, 2H), 7.45 – 7.41 (m, 2H), 7.41 – 7.37 (m, $J = 7.3$ Hz, 1H), 7.36 – 7.33 (d, $J = 7.6$ Hz, 2H), 5.42 (s, 2H), 3.85 (s, 3H), 2.65 (s, 3H). **^{13}C NMR** (126 MHz, CD_3OD): δ 146.06, 135.18, 130.25, 129.84, 129.11, 123.77, 122.43, 52.66, 35.96, 10.58. **HRMS** (DART) m/z calculated for $C_{12}H_{15}N_2^+$ (M^+) 187.12298, found 187.12293.

1-Ethyl-2,3-dimethylimidazolium iodide (**2c**)



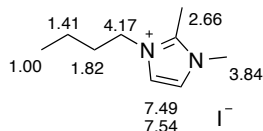
Following general procedure B, 1,2-dimethyl imidazole (2.00 g, 20.8 mmol) was treated with ethyl iodide (2.0 ml, 25 mmol) in acetonitrile (100 ml). The product was dissolved in chloroform and purified via precipitation into tetrahydrofuran to give **2c** (5.01 g, 96 %) as a white powder. **1H NMR** (600 MHz, CD_3OD): δ 7.57 (d, $J = 2.1$ Hz, 1H), 7.51 (d, $J = 2.1$ Hz, 1H), 4.23 (q, $J = 7.3$ Hz, 2H), 3.85 (s, 3H), 2.68 (s, 3H), 1.48 (t, $J = 7.3$ Hz, 3H). **^{13}C NMR** (126 MHz, CD_3OD): δ 145.46, 123.53, 121.45, 44.73, 36.23, 15.61, 10.89. **HRMS** (DART) m/z calculated for $C_7H_{13}N_2^+$ (M^+) 125.10732, found 125.10757.

1-Isopropyl-2,3-dimethylimidazolium iodide (2d)



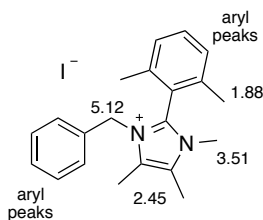
Following general procedure B, 1,2-dimethyl imidazole (2.00 g, 20.8 mmol) was treated with 2-iodopropane (2.3 ml, 23 mmol) in acetonitrile (20 ml). The product was dissolved in chloroform and purified via precipitation into ethyl acetate to give **2d** (2.36 g, 50 %) as a light beige powder. **¹H NMR** (600 MHz, CD₃OD): δ 7.68 (d, *J* = 2.2 Hz, 1H), 7.54 (d, *J* = 2.2 Hz, 1H), 4.75 (hept, *J* = 6.8 Hz, 1H), 3.87 (s, 3H), 2.72 (s, 3H), 1.54 (d, *J* = 6.8 Hz, 6H). **¹³C NMR** (126 MHz, CD₃OD): δ 144.98, 124.02, 118.46, 52.08, 35.91, 22.74, 10.67. **HRMS** (DART) *m/z* calculated for C₈H₁₅N₂⁺ (*M*⁺) 139.12298, found 139.12305.

1-*n*-Butyl-2,3-dimethylimidazolium iodide (2e)



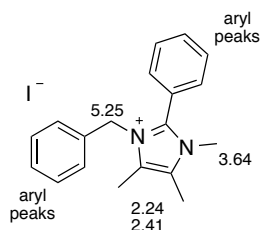
Following general procedure B, 1,2-dimethyl imidazole (2.00 g, 20.8 mmol) was treated with *n*-butyl iodide (2.6 ml, 23 mmol) in acetonitrile (20 ml). The product was dissolved in chloroform and purified via precipitation into ethyl acetate to give **2e** (4.57 g, 78 %) as a white powder. **¹H NMR** (600 MHz, CD₃OD): δ 7.54 (d, *J* = 2.1 Hz, 1H), 7.49 (d, *J* = 2.1 Hz, 1H), 4.17 (m, 2H), 3.84 (s, 3H), 2.66 (s, 3H), 1.82 (p, *J* = 7.4 Hz, 2H), 1.41 (sext, *J* = 7.4 Hz, 2H), 1.00 (t, *J* = 7.4 Hz, 3H). **¹³C NMR** (126 MHz, CD₃OD): δ 145.65, 123.50, 122.12, 49.35, 36.15, 32.74, 20.48, 13.95, 10.77. **HRMS** (DART) *m/z* calculated for C₉H₁₇N₂⁺ (*M*⁺) 153.13863, found 153.13876.

1-Benzyl-2-(2,6-dimethylphenyl)-3,4,5-trimethylimidazolium iodide (3a)



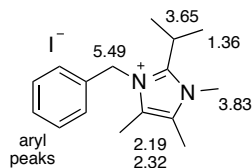
Following general procedure B, **IM-3a** (0.400 g, 1.38 mmol) was treated with methyl iodide (0.90 ml, 1.5 mmol) in acetonitrile (1.5 ml). The product was dissolved in chloroform and purified via precipitation into ethyl acetate to give **3a** (0.382 g, 72 %) as a off-white powder. **¹H NMR** (600 MHz, CD₃OD): δ 7.52 (t, *J* = 7.7 Hz, 1H), 7.34 – 7.21 (m, 5H), 6.93 (d, *J* = 7.4 Hz, 2H), 5.12 (s, 2H), 3.51 (s, 3H), 2.47 – 2.44 (m, 6H), 1.88 (s, 6H). **¹³C NMR** (126 MHz, CD₃OD): δ 144.55, 140.88, 134.83, 133.96, 130.09, 129.70*, 129.50, 128.50, 128.45, 122.52, 50.54, 32.93, 19.69, 9.56, 9.14. **HRMS** (DART) *m/z* calculated for C₂₁H₂₅N₂⁺ (M⁺) 305.20123, found 305.20134. *The resonances for two carbon nuclei are found at this chemical shift, which is supported by line width and peak intensity analysis.

1-Benzyl-3,4,5-trimethyl-2-phenylimidazolium iodide (**3b**)



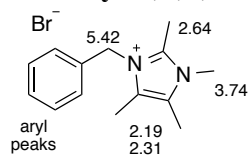
Following general procedure B, **IM-3b** (2.54 g, 9.68 mmol) was treated with methyl iodide (0.70 ml, 12 mmol) in acetonitrile (7 ml). The product was dissolved in chloroform and purified via precipitation into ether to give **3b** (1.74 g, 50 %) as an off-white powder. **¹H NMR** (600 MHz, CD₃OD): δ 7.74 – 7.69 (t, *J* = 7.6 Hz, 1H), 7.63 (t, *J* = 7.6 Hz, 2H), 7.61 – 7.57 (d, *J* = 7.6 Hz, 2H), 7.37 – 7.28 (m, 3H), 7.07 – 7.02 (d, *J* = 7.6 Hz, 2H), 5.25 (s, 2H), 3.64 (s, 3H), 2.41 (s, 3H), 2.24 (s, 3H). **¹³C NMR** (126 MHz, CD₃OD): δ 145.24, 135.44, 133.65, 131.76, 130.78, 130.21, 129.33, 129.30, 127.95, 127.33, 123.41, 50.35, 34.00, 9.14, 9.08. **HRMS** (DART) *m/z* calculated for C₁₉H₂₁N₂⁺ (M⁺) 277.16993, found 277.17009.

1-Benzyl-2-isopropyl-3,4,5-trimethylimidazolium iodide (**3c**)



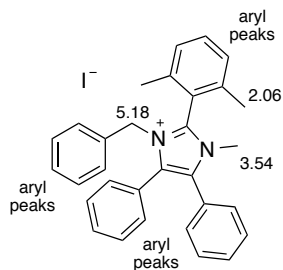
Following general procedure B, **IM-3c** (1.07 g, 4.69 mmol) was treated with methyl iodide (0.32 ml, 5.2 mmol) in acetonitrile (5 ml). The product was dissolved in chloroform and purified via precipitation into ether to give **3c** (1.58 g, 91 %) as an orange solid. **¹H NMR** (600 MHz, CD₃OD): δ 7.41 (t, *J* = 7.6 Hz, 2H), 7.37 – 7.32 (t, *J* = 7.6 Hz, 1H), 7.13 – 7.08 (d, *J* = 7.6 Hz, 2H), 5.49 (s, 2H), 3.83 (s, 3H), 3.65 (hept, *J* = 7.3 Hz, 1H), 2.32 (s, 3H), 2.19 (s, 3H), 1.36 (d, *J* = 7.3 Hz, 6H). **¹³C NMR** (126 MHz, CD₃OD): δ 149.98, 135.89, 130.33, 129.35, 128.79, 127.23, 126.97, 49.49, 33.60, 26.62, 19.13, 8.91, 8.90. **HRMS** (DART) *m/z* calculated for C₁₆H₂₃N₂⁺ (*M*⁺) 243.18558, found 243.18580.

1-Benzyl-2,3,4,5-tetramethylimidazolium bromide (**3d**)



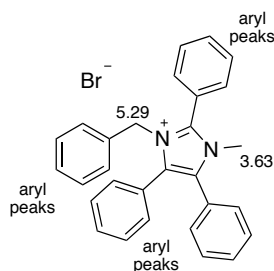
Following general procedure B, 1,2,4,5-tetramethylimidazole (2.00 g, 16.1 mmol) was treated with benzyl bromide (1.9 ml, 16 mmol) in acetonitrile (10 ml). The product was dissolved in chloroform and purified via precipitation into ether to give **3d** (3.60 g, 76 %) as an off-white powder. **¹H NMR** (600 MHz, CD₃OD): δ 7.40 (t, *J* = 7.7 Hz, 2H), 7.37 – 7.33 (t, *J* = 7.6 Hz, 1H), 7.19 – 7.14 (d, *J* = 7.6 Hz, 2H), 5.42 (s, 2H), 3.74 (s, 3H), 2.64 (s, 3H), 2.31 (s, 3H), 2.19 (s, 3H). **¹³C NMR** (126 MHz, CD₃OD): δ 144.40, 135.40, 130.23, 129.27, 127.79, 127.49, 126.60, 49.42, 33.02, 10.98, 8.97, 8.91. **HRMS** (DART) *m/z* calculated for C₁₄H₁₉N₂⁺ (*M*⁺) 215.15428, found 215.1548.

1-Benzyl-2-(2,6-dimethylphenyl)-3-methyl-4,5-diphenylimidazolium bromide (**4a**)



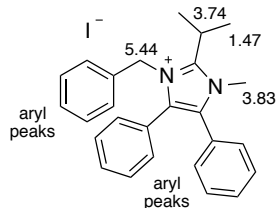
Following general procedure B, **IM-4a** (0.350 g, 0.844 mmol) was treated with methyl iodide (0.06 ml, 0.9 mmol) in acetonitrile (1.2 ml). The product was dissolved in chloroform and purified via precipitation into ether to give **4a** (0.096 g, 22 %) as a white powder. **¹H NMR** (500 MHz, CD₃OD): δ 7.64 – 7.44 (m, 11H), 7.35 (d, *J* = 7.7 Hz, 2H), 7.24 (t, *J* = 7.6 Hz, 1H), 7.15 (t, *J* = 7.6 Hz, 2H), 6.66 (d, *J* = 7.7 Hz, 2H), 5.18 (s, 2H), 3.54 (s, 3H), 2.06 (s, 6H). **¹³C NMR** (126 MHz, CD₃OD): δ 146.19, 140.90, 134.58, 134.37, 134.35, 133.87, 132.68, 132.15, 131.76, 131.57, 130.47, 130.19, 129.94*, 129.89, 129.23, 126.75, 126.43, 122.38, 51.29, 34.14, 19.66. **HRMS** (DART) *m/z* calculated for C₂₃H₂₁N₂⁺ (M⁺) 325.16993, found 325.16996. *The resonances for two carbon nuclei are found at this chemical shift, which is supported by line width and peak intensity analysis.

1-Benzyl-3-methyl-2,4,5-triphenylimidazolium bromide (**4b**)



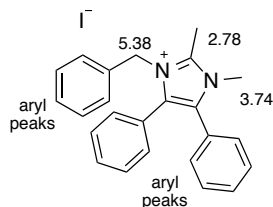
Following general procedure B, **IM-4b** (0.880 g, 2.84 mmol) was treated with benzyl bromide (0.40 ml, 3.1 mmol) in acetonitrile (10 ml). The product was dissolved in chloroform and purified via precipitation into ether to give **4b** (0.567 g, 41 %) as an off-white powder. **¹H NMR** (600 MHz, CD₃OD): δ 7.83 (d, *J* = 7.6 Hz, 2H), 7.78 – 7.74 (t, *J* = 7.6 Hz, 1H), 7.70 (t, *J* = 7.6 Hz, 2H), 7.53 (dm, *J* = 7.6 Hz, 2H), 7.50 – 7.40 (m, 4H), 7.37 (m, 4H), 7.23 – 7.12 (m, 3H), 6.81 – 6.75 (m, 2H), 5.29 (s, 2H), 3.63 (s, 3H). **¹³C NMR** (126 MHz, CD₃OD): δ 146.40, 135.36, 134.32, 133.88, 133.33, 132.31, 132.18, 131.92, 131.32*, 130.87, 130.02, 129.98, 129.79, 129.25, 127.95, 127.00, 126.84, 123.49, 51.25, 35.24. **HRMS** (DART) *m/z* calculated for C₂₉H₂₅N₂⁺ (M⁺) 401.20123, found 401.20079. *The resonances for two carbon nuclei are found at this chemical shift, which is supported by line width and peak intensity analysis.

1-Benzyl-2-isopropyl-3-methyl-4,5-diphenylimidazolium iodide (4c)



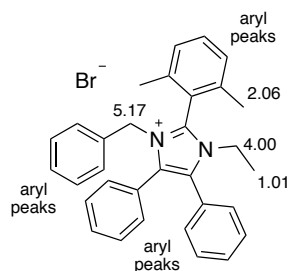
Following general procedure B, **IM-4c** (1.00 g, 2.89 mmol) was treated with methyl iodide (0.19 ml, 3.1 mmol) in acetonitrile (5 ml). The product was dissolved in chloroform and purified via precipitation into ether to give **4c** (1.06 g, 84 %) as a pale yellow powder. **¹H NMR** (600 MHz, CD₃OD): δ 7.54 – 7.49 (d, *J* = 7.4 Hz, 2H), 7.44 (m, 3H), 7.37 (m, 5H), 7.33 – 7.28 (m, 3H), 7.12 (d, *J* = 7.4 Hz, 2H), 5.44 (s, 2H), 3.83 (s, 3H), 3.74 (hept, *J* = 7.3 Hz, 1H), 1.47 (d, *J* = 7.3 Hz, 6H). **¹³C NMR** (126 MHz, CD₃OD): δ 150.82, 135.93, 134.29, 133.00, 132.60, 132.44, 131.27, 131.22, 130.17, 129.88, 129.84, 129.30, 127.41, 127.02, 126.83, 50.43, 35.05, 27.34, 19.18. **HRMS** (DART) *m/z* calculated for C₂₆H₂₇N₂⁺ (M⁺) 367.21688, found 367.21702.

1-Benzyl-2,3-dimethyl-4,5-diphenylimidazolium iodide (4d)



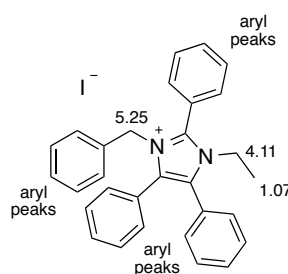
Following general procedure B, **IM-4d** (0.405 g, 1.25 mmol) was treated with methyl iodide (0.09 ml, 1 mmol) in acetonitrile (1.5 ml). The product was dissolved in chloroform and purified via precipitation into ether to give **4d** (0.190 g, 36 %) as a white powder. **¹H NMR** (600 MHz, CD₃OD): δ 7.50 – 7.39 (m, 6H), 7.37 – 7.29 (m, 5H), 7.29 – 7.25 (dm, *J* = 7.8 Hz, 2H), 7.08 (dm, *J* = 7.5 Hz, 2H), 5.38 (s, 2H), 3.74 (s, 3H), 2.78 (s, 3H). **¹³C NMR** (126 MHz, CD₃OD): δ 146.00, 135.36, 133.48, 132.71, 132.31, 132.22, 131.34, 131.26, 130.22, 130.02, 129.98, 129.43, 127.65, 126.96, 126.95, 50.28, 34.06, 11.54. **HRMS** (DART) *m/z* calculated for C₂₄H₂₃N₂⁺ (M⁺) 339.18558, found 339.18559.

1-Benzyl-2-(2,6-dimethylphenyl)-3-ethyl-4,5-diphenylimidazolium bromide (**5a**)



Following general procedure B, **IM-5a** (0.110 g, 0.312 mmol) was treated with benzyl bromide (0.05 ml, 0.4 mmol) in acetonitrile (1 ml). The product was dissolved in chloroform and purified via precipitation into ether to give **5a** (0.080 g, 49 %) as a white powder. **¹H NMR** (600 MHz, CD₃OD): δ 7.65 – 7.45 (m, 11H), 7.36 (d, *J* = 7.7 Hz, 2H), 7.24 (t, *J* = 7.5 Hz, 1H), 7.15 (tm *J* = 7.7 Hz, 2H), 6.64 (d, *J* = 7.7 Hz, 2H), 5.17 (s, 2H), 4.00 (q, *J* = 7.3 Hz, 2H), 2.06 (s, 6H), 1.01 (t, *J* = 7.3 Hz, 3H). **¹³C NMR** (126 MHz, CD₃OD): δ 145.59, 140.73, 134.58, 134.37, 134.31, 133.87, 132.65, 132.16, 131.74, 131.70, 130.43, 130.37, 130.12, 129.96, 129.89, 129.26, 126.63, 126.61, 122.40, 51.22, 43.49, 19.92, 14.96. **HRMS** (DART) *m/z* calculated for C₃₂H₃₁N₂⁺ (*M*⁺) 443.24818, found 443.24856.

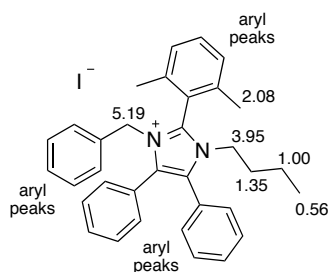
1-Benzyl-3-ethyl-2,4,5-triphenylimidazolium iodide (**5b**)



Following general procedure B, **IM2-4b** (0.825 g, 2.14 mmol) was treated with ethyl iodide (0.19 ml, 2.4 mmol) in acetonitrile (3 ml). The product was dissolved in chloroform and purified via precipitation into ether to give **5b** (0.805 g, 76 %) as an off-white powder. **¹H NMR** (600 MHz, CD₃OD): δ 7.82 – 7.74 (m, 3H), 7.70 (m, 2H), 7.58 – 7.45 (m, 5H), 7.43 (m, 1H), 7.36 (m, 4H), 7.18 (m, 3H), 6.75 (d, *J* = 7.6 Hz, 2H), 5.25 (s, 2H), 4.11 (q, *J* = 7.3 Hz, 2H), 1.07 (t, *J* = 7.3 Hz, 3H). **¹³C NMR** (126 MHz, CD₃OD): δ 145.84, 135.25, 133.95*, 133.49, 132.41, 132.34,

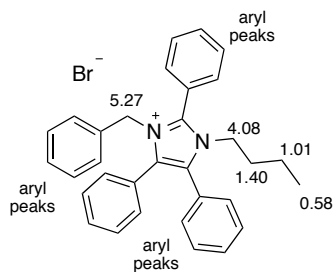
132.00, 131.51, 131.36, 130.93, 130.14, 129.92, 129.84, 129.30, 128.08, 126.96, 126.87, 123.51, 51.23, 43.73, 15.46. *The resonances for two carbon nuclei are found at this chemical shift, which is supported by line width and peak intensity analysis. **HRMS** (DART) m/z calculated for $C_{30}H_{27}N_2^+$ (M^+) 415.21688, found 415.21657.

1-Benzyl-3-*n*-butyl-2-(2,6-dimethylphenyl)-4,5-diphenylimidazolium iodide (6a)

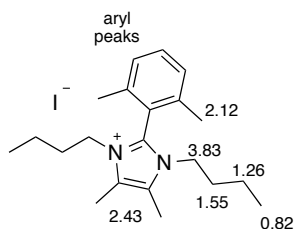


Following general procedure B, **IM-4a** (0.500 g, 1.21 mmol) was treated with *n*-butyl iodide (0.15 ml, 1.3 mmol) in acetonitrile (1 ml). The product was dissolved in chloroform and purified via precipitation into ether to give **6a** (0.397 g, 60 %) as a pale yellow powder. **¹H NMR** (600 MHz, CD_3OD): δ 7.63 – 7.54 (m, 5H), 7.50 (m, 6H), 7.36 (dm, $J = 7.5$ Hz, 2H), 7.23 (tm, $J = 7.5$ Hz, 1H), 7.14 (tm, $J = 7.6$ Hz, 2H), 6.63 (dm, $J = 7.6$ Hz, 2H), 5.19 (s, 2H), 3.97 – 3.92 (m, 2H), 2.08 (s, 6H), 1.35 (p, $J = 7.4$ Hz, 2H), 1.00 (sext, $J = 7.4$ Hz, 2H), 0.56 (t, $J = 7.4$ Hz, 3H). **¹³C NMR** (126 MHz, CD_3OD): δ 145.70, 140.72, 134.42, 134.35, 134.28, 134.06, 132.69, 132.27, 131.69, 131.66, 130.41, 130.33, 130.13, 129.92, 129.88, 129.25, 126.70, 126.60, 122.40, 51.32, 47.70, 32.17, 20.30, 20.12, 13.22. **HRMS** (DART) m/z calculated for $C_{34}H_{35}N_2^+$ (M^+) 471.27948, found 471.27828.

1-Benzyl-3-*n*-butyl-2,4,5-triphenylimidazolium bromide (6b)

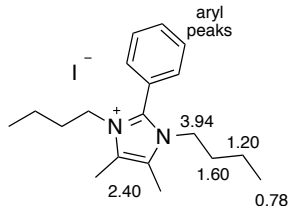


Following general procedure B, **IM-6b** (1.10 g, 3.12 mmol) was treated with benzyl bromide (0.40 ml, 3.4 mmol) in acetonitrile (3 ml). The product was dissolved in chloroform and purified via precipitation into ether to give **6b** (0.527 g, 32 %) as a white powder. ¹H NMR (600 MHz, CD₃OD): δ 7.84 – 7.74 (m, 3H), 7.71 (d, *J* = 6.8 Hz, 2H), 7.55 (dm, *J* = 7.6 Hz, 2H), 7.53 – 7.46 (m, 3H), 7.42 (m, 1H), 7.40 – 7.33 (m, 4H), 7.17 (m, 3H), 6.79 – 6.67 (d, *J* = 7.5 Hz, 2H), 5.27 (s, 2H), 4.08 (m, 2H), 1.40 (p, *J* = 7.4 Hz, 2H), 1.01 (sext, *J* = 7.4 Hz, 2H), 0.58 (t, *J* = 7.4 Hz, 3H). ¹³C NMR (126 MHz, CD₃OD): δ 146.14, 135.26, 134.01, 133.96, 133.69, 132.29, 132.20, 131.90, 131.54, 131.42, 131.03, 130.23, 130.03, 129.85, 129.37, 128.02, 126.98, 126.82, 123.54, 51.23, 47.90, 32.39, 20.21, 13.29. HRMS (DART) *m/z* calculated for C₃₂H₃₁N₂⁺ (M⁺) 443.24818, found 443.24683.



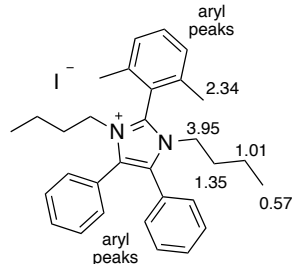
Following general procedure B, **IM-7a** (0.240 g, 0.937 mmol) was treated with *n*-butyl iodide (0.13 ml, 1.1 mmol) in acetonitrile (1.5 ml). The product was dissolved in chloroform and purified via precipitation into ether to give **7a** (0.366 g, 89 %) as a light beige powder. **¹H NMR** (600 MHz, CD₃OD): δ 7.57 (t, *J* = 7.7 Hz, 1H), 7.39 (d, *J* = 7.7 Hz, 2H), 3.89 – 3.75 (m, 4H), 2.43 (s, 6H), 2.12 (s, 6H), 1.59 – 1.52 (p, *J* = 7.4 Hz, 4H), 1.26 (sext, *J* = 7.4 Hz, 4H), 0.82 (t, *J* = 7.4 Hz, 6H). **¹³C NMR** (126 MHz, CD₃OD): δ 143.30, 140.40, 133.97, 130.02, 128.66, 122.75, 46.91, 32.43, 20.61, 20.09, 13.57, 9.06. **HRMS** (DART) *m/z* calculated for C₂₁H₃₃N₂⁺ (M⁺) 313.26383, found 313.26388.

1,3-Di-*n*-butyl-4,5-dimethyl-2-phenylimidazolium iodide (7b)



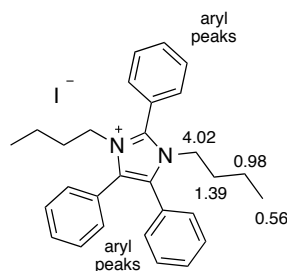
Following general procedure B, **IM-7b** (0.262 g, 1.15 mmol) was treated with *n*-butyl iodide (0.15 ml, 1.4 mmol) in acetonitrile (1 ml). The product was dissolved in chloroform and purified via precipitation into ether to give **7b** (0.298 g, 63 %) as a orange waxy solid. **¹H NMR** (600 MHz, CD₃OD): δ 7.80 – 7.75 (t, *J* = 7.4 Hz 1H), 7.73 (t, *J* = 7.6 Hz, 2H), 7.68 – 7.65 (d, *J* = 7.6 Hz, 2H), 3.99 – 3.85 (m, 4H), 2.40 (s, 6H), 1.65 – 1.56 (p, *J* = 7.4 Hz, 4H), 1.20 (sext, *J* = 7.4 Hz, 4H), 0.78 (t, *J* = 7.4 Hz, 6H). **¹³C NMR** (126 MHz, CD₃OD): δ 144.16, 133.61, 131.93, 130.89, 128.00, 123.85, 79.60, 46.95, 32.70, 20.50, 13.59, 9.04. **HRMS** (DART) *m/z* calculated for C₁₉H₂₉N₂⁺ (M⁺) 285.23253, found 285.23174.

1,3-Di-*n*-butyl-2-(2,6-dimethylphenyl)-4,5-diphenylimidazolium iodide (8a)



Following general procedure B, **IM-8a** (1.86 g, 4.89 mmol) was treated with *n*-butyl iodide (0.61 ml, 5.4 mmol) in acetonitrile (5 ml). The product was dissolved in chloroform and purified via precipitation into ether to give **8a** (1.27 g, 46 %) as an pale beige powder. **¹H NMR** (600 MHz, CD₃OD): δ 7.63 (t, *J* = 7.7 Hz, 1H), 7.57 – 7.54 (m, 4H), 7.54 – 7.44 (m, 8H), 3.99 – 3.89 (m, 4H), 2.34 (s, 6H), 1.40 – 1.29 (p, *J* = 7.4 Hz, 4H), 1.01 (sext, *J* = 7.4 Hz, 4H), 0.57 (t, *J* = 7.4 Hz, 6H). **¹³C NMR** (126 MHz, CD₃OD): δ 144.95, 140.54, 134.31, 134.06, 132.26, 131.61, 130.29, 130.23, 126.76, 122.42, 47.65, 32.22, 20.39, 20.32, 13.24. **HRMS** (DART) *m/z* calculated for C₃₁H₃₇N₂⁺ (M⁺) 437.29513, found 437.29517.

1,3-Di-*n*-butyl-2,4,5-triphenylimidazolium iodide (**8b**)



Following general procedure B, **IM-6b** (3.74 g, 10.6 mmol) was treated with *n*-butyl iodide (1.8 ml, 16 mmol) in acetonitrile (10 ml). The product was dissolved in chloroform and purified via precipitation into ether to give **8b** (3.50 g, 61 %) as a white powder. ^1H NMR (500 MHz, CD_3OD): δ 8.02 (d, $J = 7.6$ Hz, 2H), 7.79 (m, 3H), 7.63 – 7.56 (d, $J = 7.3$ Hz, 4H), 7.50 – 7.40 (m, 6H), 4.02 (m, 4H), 1.39 (p, $J = 7.4$ Hz, 4H), 0.98 (sext, $J = 7.4$ Hz, 4H), 0.56 (t, $J = 7.4$ Hz, 6H). ^{13}C NMR (126 MHz, CD_3OD): δ 145.32, 133.93, 133.36, 132.36, 132.18, 131.39, 131.00, 130.08, 127.19, 123.79, 47.73, 32.47, 20.27, 13.30. HRMS (DART) m/z calculated for $\text{C}_{29}\text{H}_{33}\text{N}_2^+$ (M^+) 409.26383, found 409.26371.

4.5.3 Model Compound Studies

General procedure C: Model compound study procedure

Stock solution of the basic methanol were prepared by dissolving KOH (1M, 2M, or 5M) and 3-(Trimethylsilyl)-1-propanesulfonic acid sodium salt (0.025M) in CD_3OH . The model compound (0.05M for 1M KOH and 0.03M for 2M and 5M KOH) was dissolved in the methanol solution (0.5 mL) and passed through a glass wool plug into an NMR tube. The NMR tube was flame sealed and analyzed by ^1H NMR spectroscopy for the initial time point. Integration of a selected signal in the model compound relative to a signal related to 3-(Trimethylsilyl)-1-propanesulfonic acid sodium salt provided the initial quantity of model compound. The tube was heated in an oil bath at 80 $^\circ\text{C}$. At specified time points, every 5 days, the tubes were removed,

cooled to room temperature and analyzed by ^1H NMR spectroscopy in order to determine the quantity of model compound remaining (^1H NMR spectra are provided in Figures 4.11 – 4.68).

Examples of stock solution preparation:

1. A 1M KOH stock solution was prepared by dissolving KOH (617 mg, 11.0 mmol) and 3-(Trimethylsilyl)-1-propanesulfonic acid sodium salt (60.0 mg, 0.275 mmol) in 11 mL of CD_3OH .
2. A 2M KOH stock solution was prepared by dissolving KOH (337 mg, 6.00 mmol) and 3-(Trimethylsilyl)-1-propanesulfonic acid sodium salt (16.4 mg, 0.0750 mmol) in 3 mL of CD_3OH .
3. A 5M KOH stock solution was prepared by dissolving KOH (842 mg, 15.0 mmol) and 3-(Trimethylsilyl)-1-propanesulfonic acid sodium salt (16.4 mg, 0.0750 mmol) in 3 mL of CD_3OH .

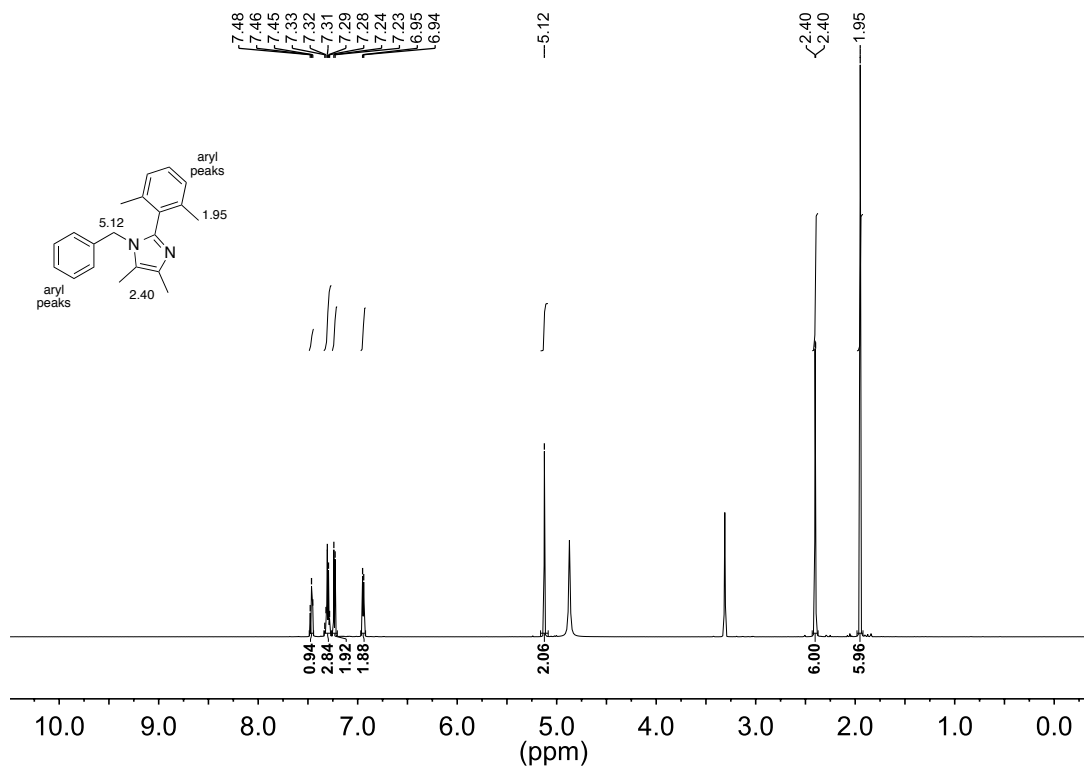
Examples of model compound study solution preparation:

1. Following General Procedure C, model compound **2b** (6.7 mg, 0.025 mmol) was dissolved in 0.5 ml of 1M KOH stock solution.
2. Following General Procedure C, model compound **3c** (4.4 mg, 0.015 mmol) was dissolved in 0.5 ml of 2M KOH stock solution.
3. Following General Procedure C, model compound **4b** (7.2 mg, 0.015 mmol) was dissolved in 0.5 ml of 5M KOH stock solution.

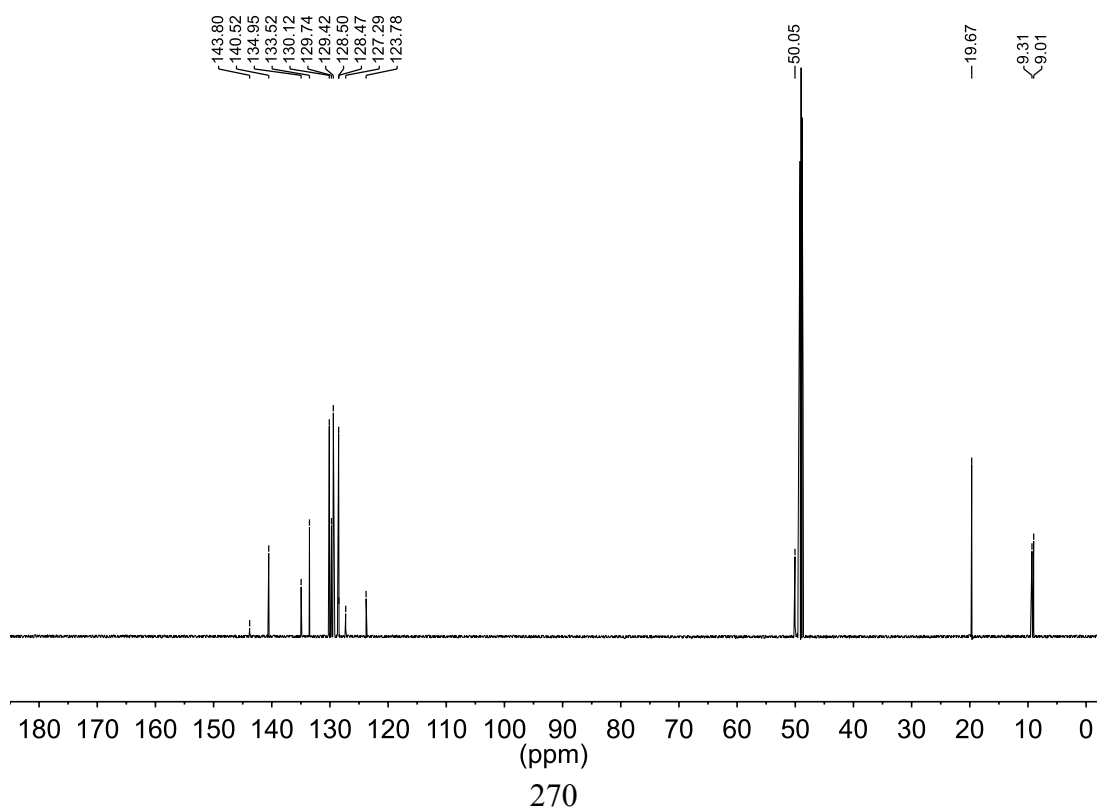
4.5.4 Copies of ^1H and ^{13}C NMR Spectra

1-Benzyl-2-(2,6-dimethylphenyl)-4,5-dimethyl-1*H*-imidazole (IM-3a)

^1H NMR spectrum (600 MHz, CD_3OD)

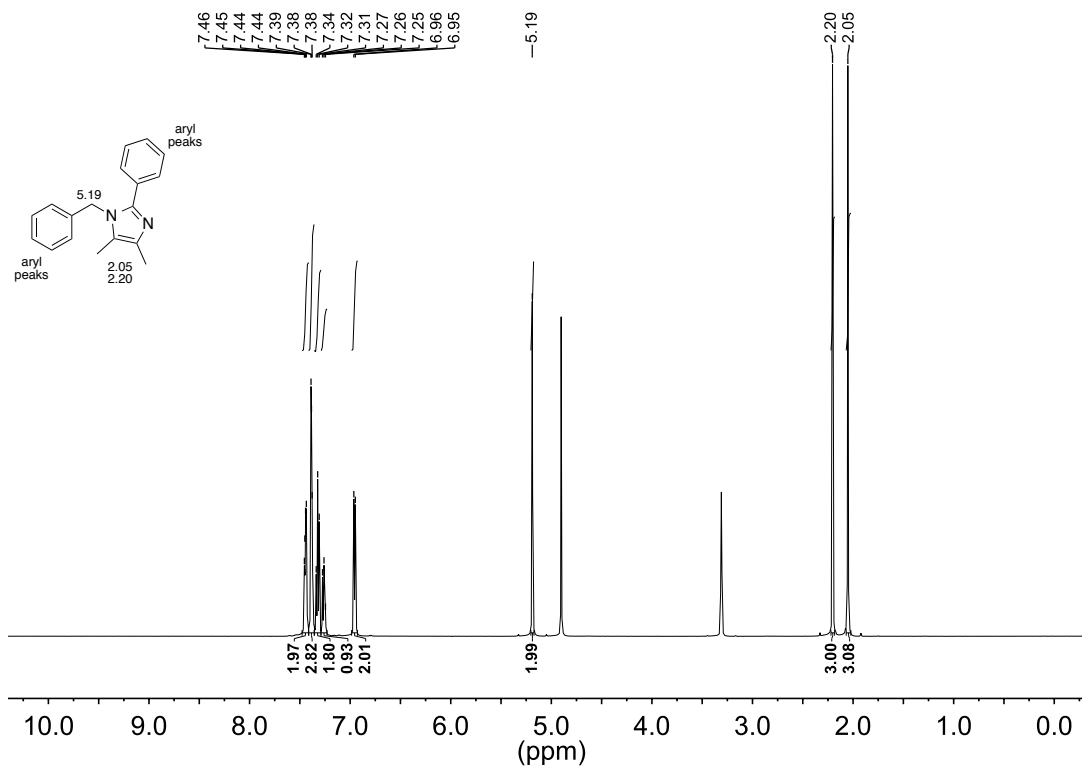


^{13}C NMR spectrum (126 MHz, CD_3OD)

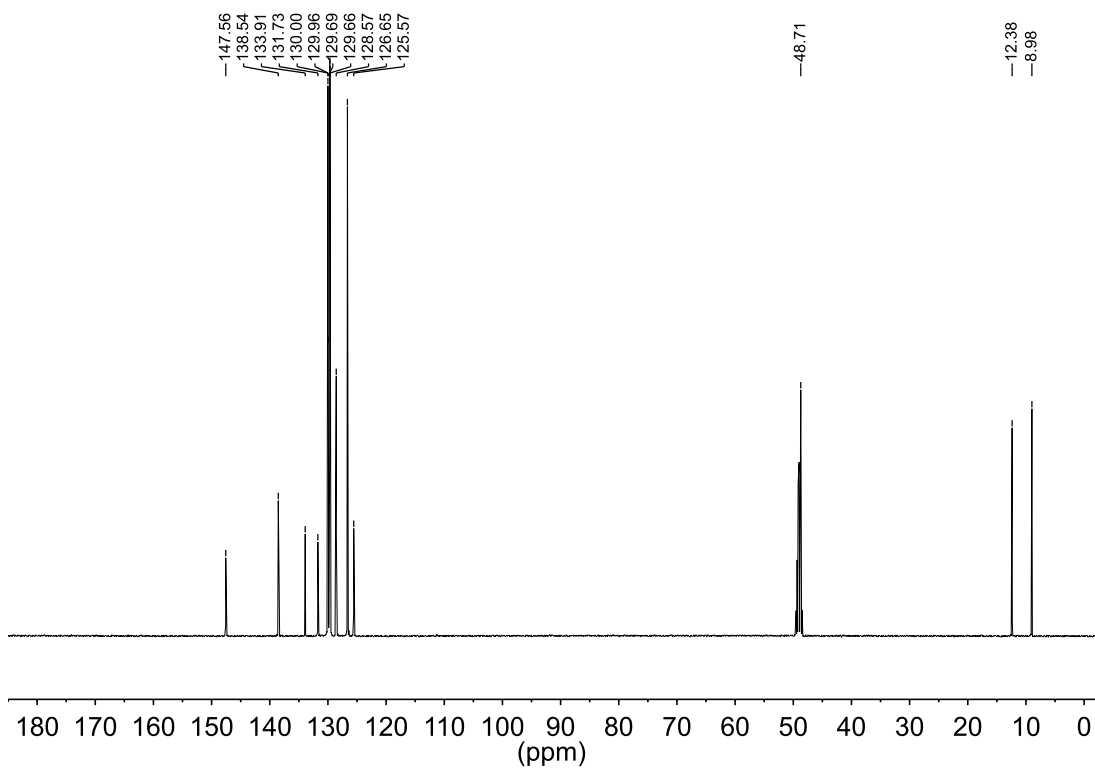


1-Benzyl-4,5-dimethyl-2-phenyl-1*H*-imidazole (IM-3b)

¹H NMR spectrum (500 MHz, CD₃OD)

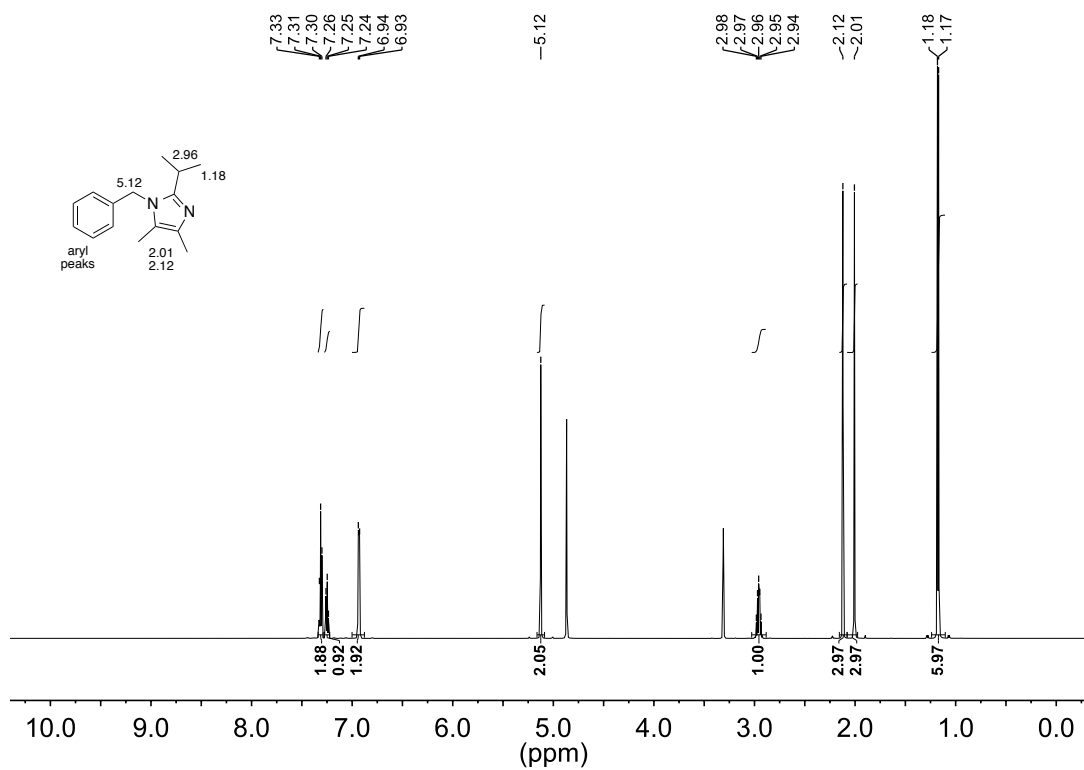


¹³C NMR spectrum (126 MHz, CD₃OD)

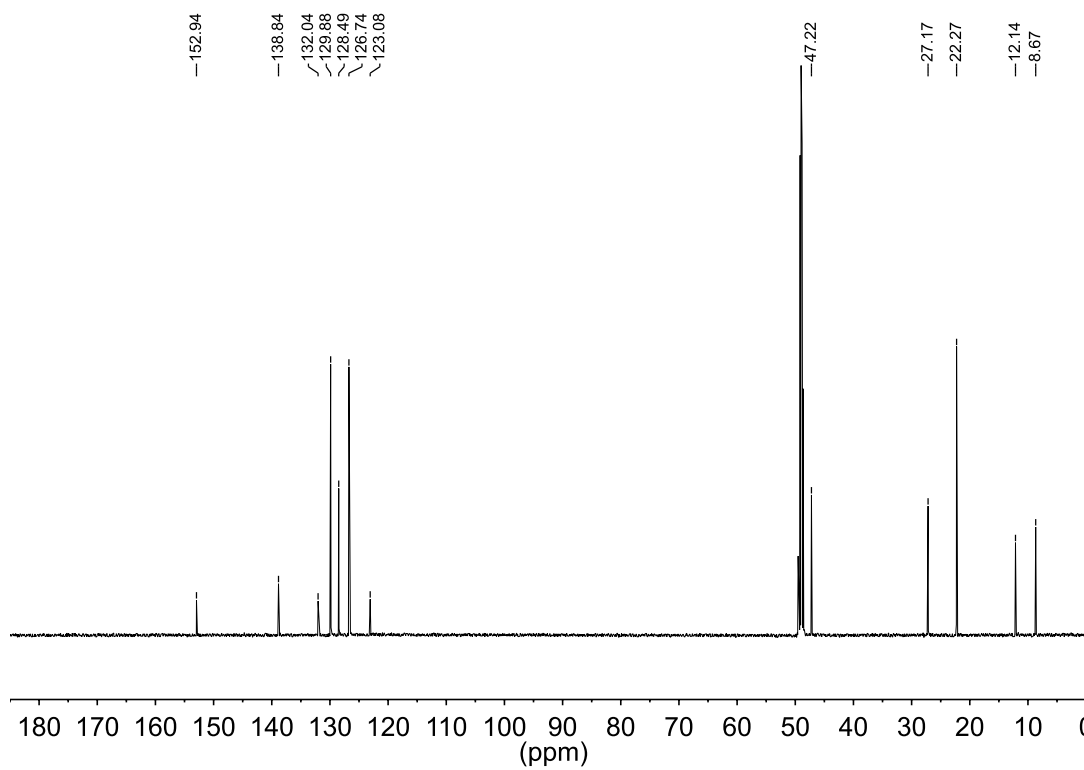


1-Benzyl-2-isopropyl-4,5-dimethyl-1*H*-imidazole (IM-3c)

¹H NMR spectrum (600 MHz, CD₃OD)

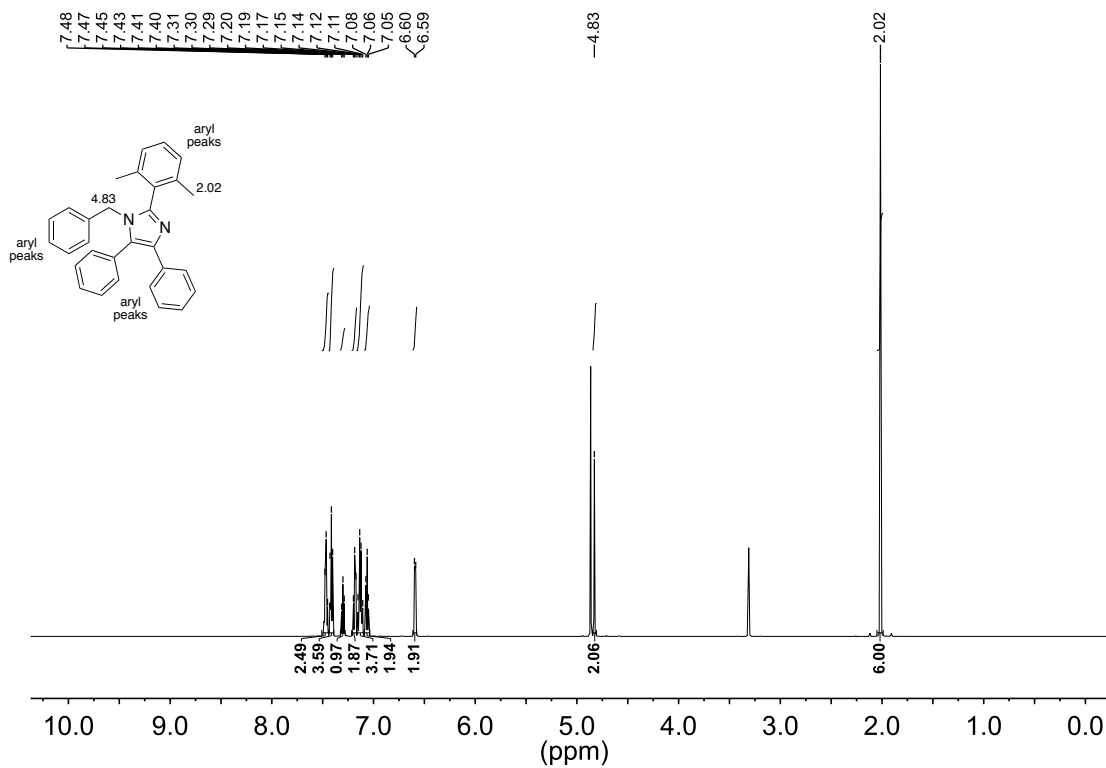


¹³C NMR spectrum (126 MHz, CD₃OD)

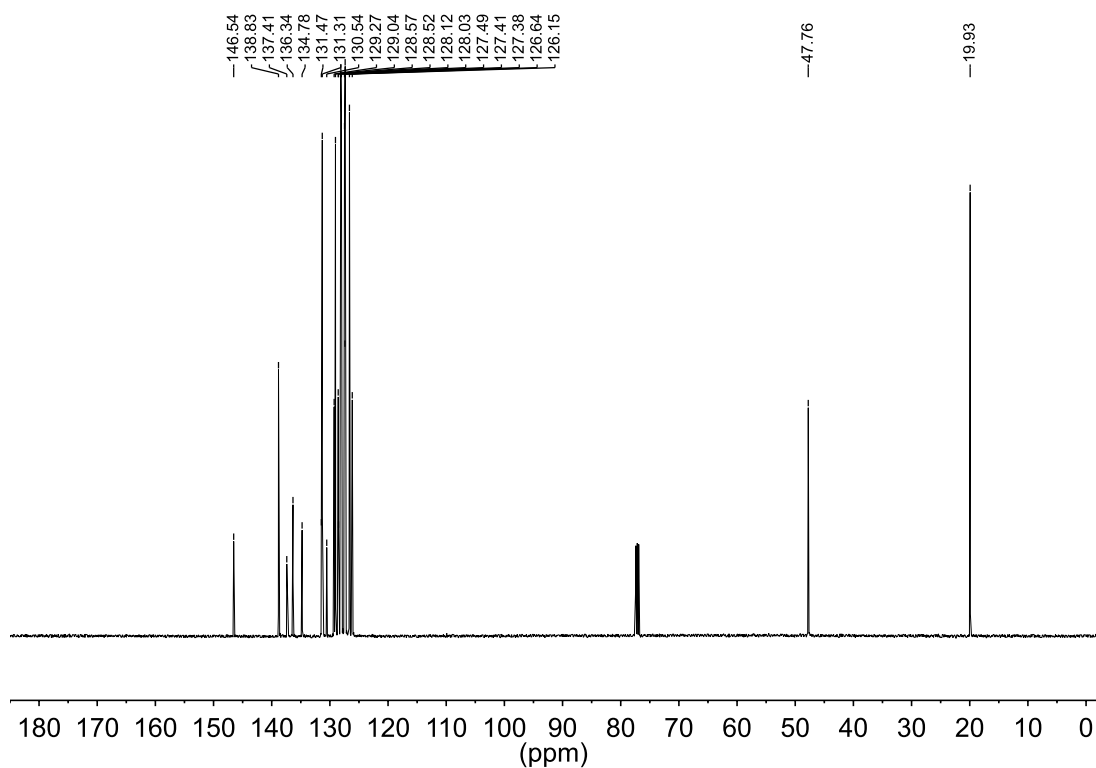


1-Benzyl-2-(2,6-dimethylphenyl)-4,5-diphenyl-1*H*-imidazole (IM-4a)

¹H NMR spectrum (600 MHz, CD₃OD)

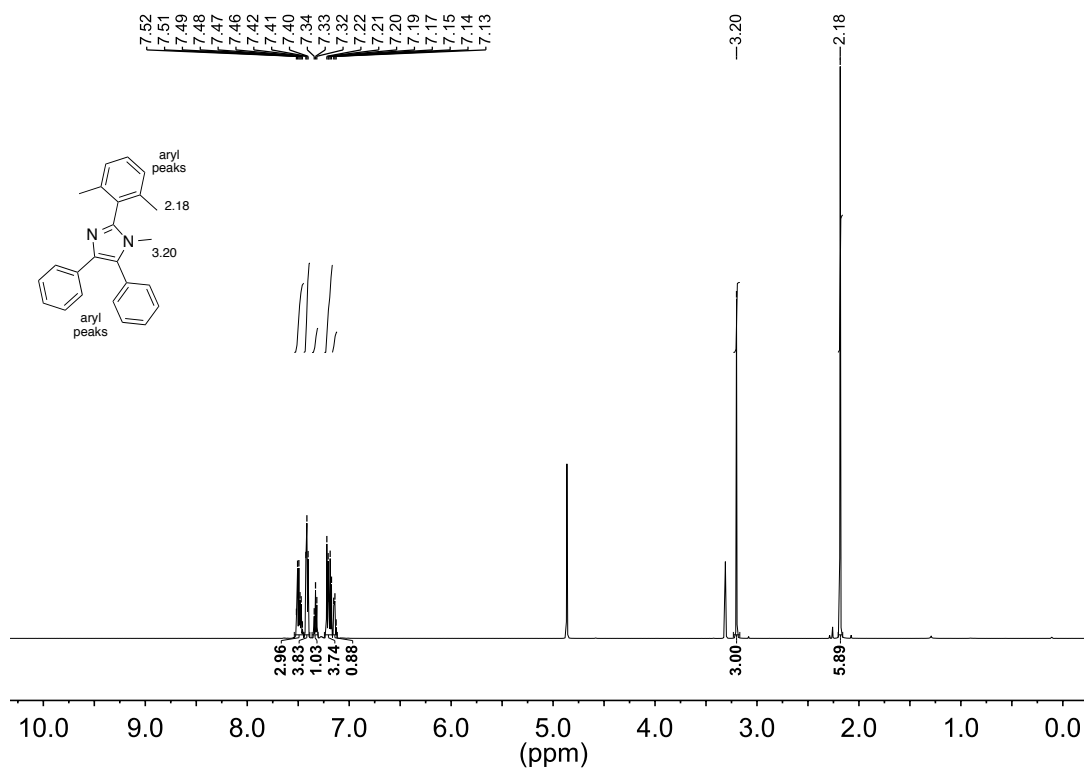


¹³C NMR spectrum (126 MHz, CDCl₃)

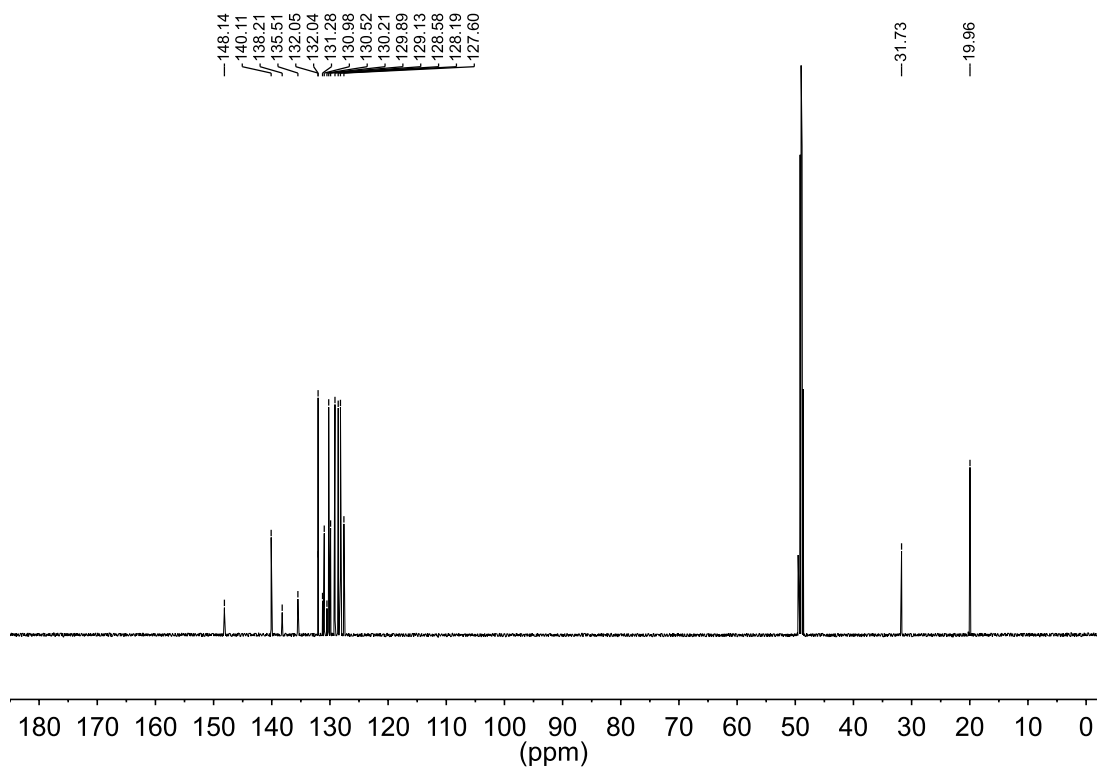


2-(2,6-Dimethylphenyl)-1-methyl-4,5-diphenyl-1*H*-imidazole (IM2-4a)

¹H NMR spectrum (600 MHz, CD₃OD)

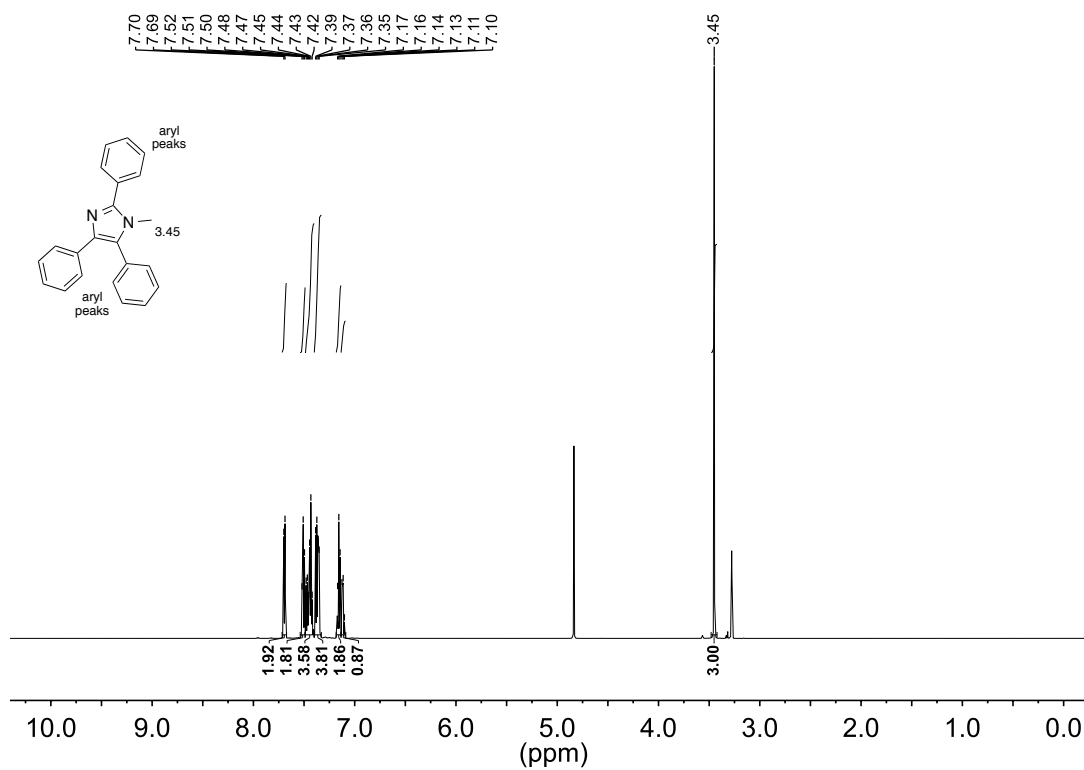


¹³C NMR spectrum (126 MHz, CD₃OD)

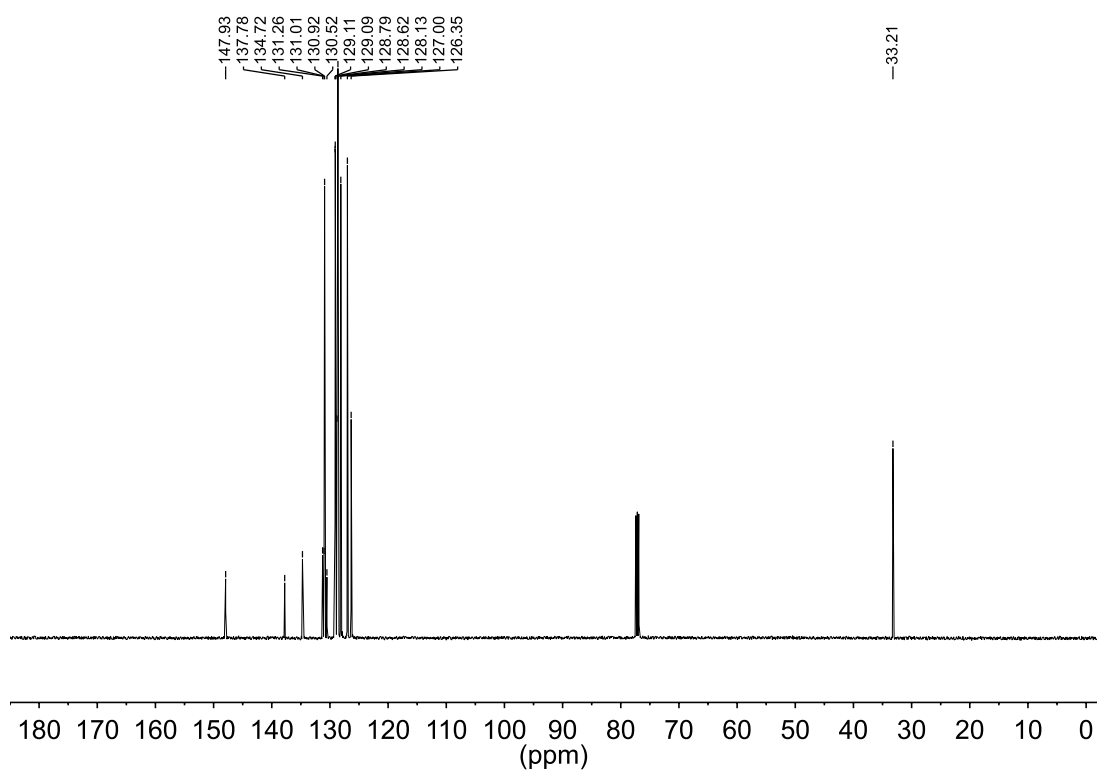


1-Methyl-2,4,5-triphenyl-1*H*-imidazole (IM-4b)

¹H NMR spectrum (600 MHz, CD₃OD)

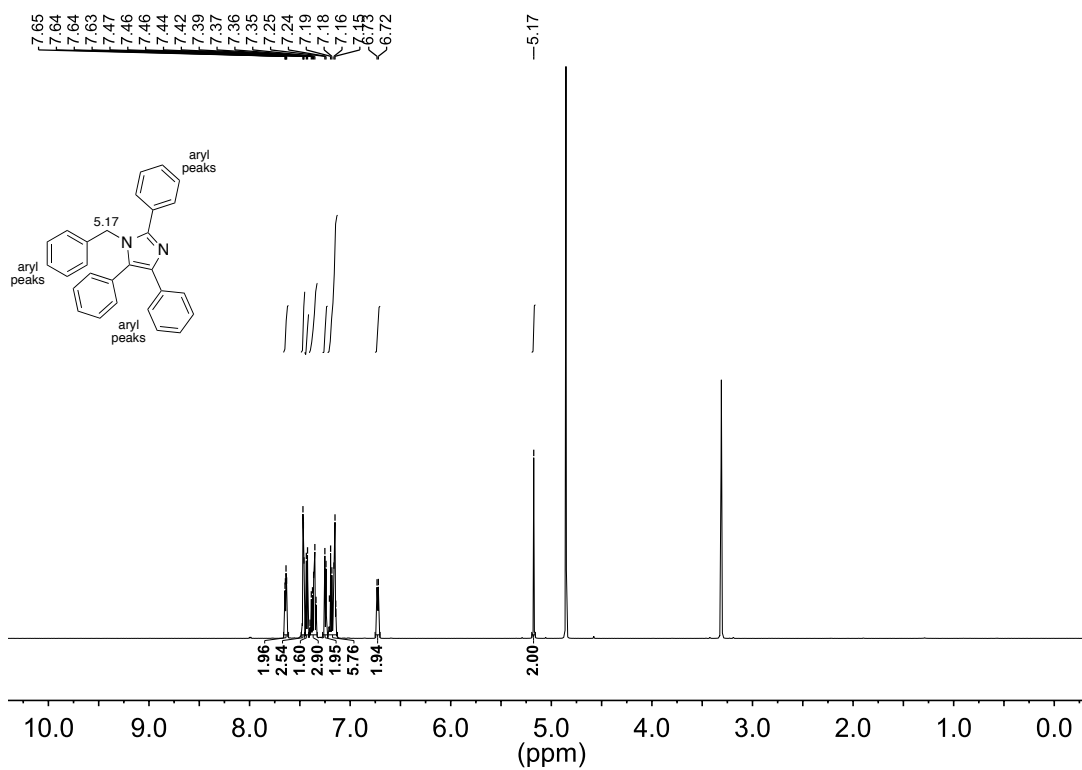


¹³C NMR spectrum (126 MHz, CDCl₃)

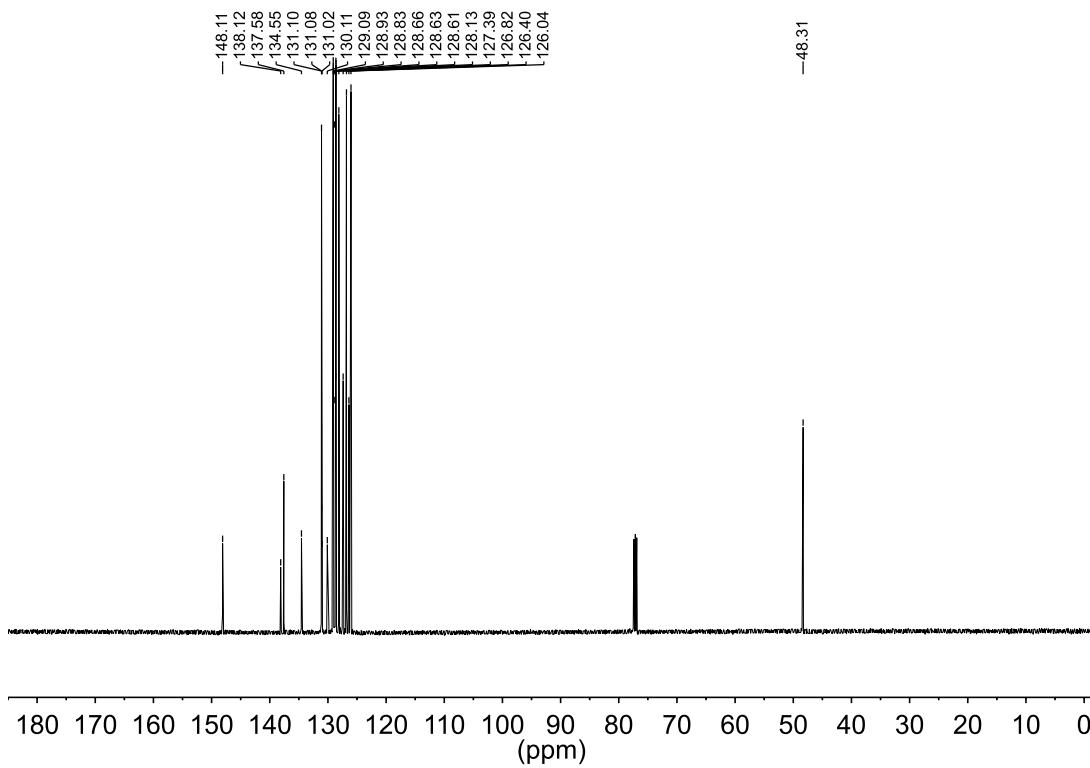


1-Benzyl-2,4,5-triphenyl-1*H*-imidazolium bromide (IM2-4b)

¹H NMR spectrum (600 MHz, CD₃OD)

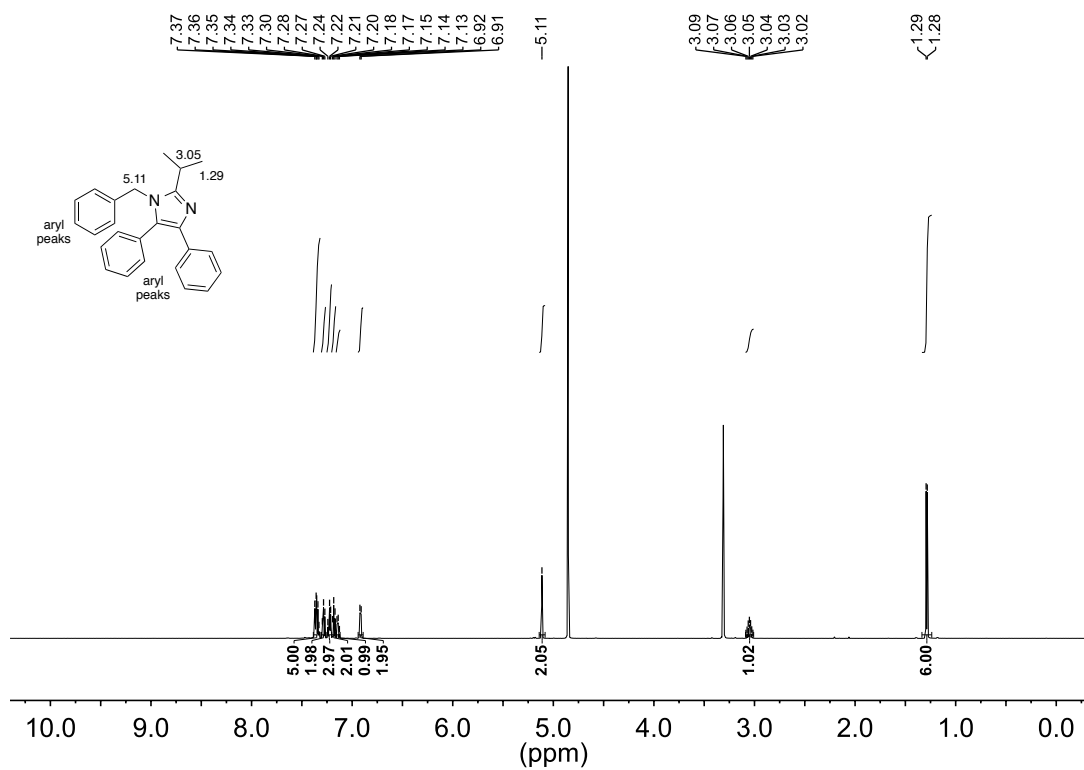


¹³C NMR spectrum (126 MHz, CDCl₃)

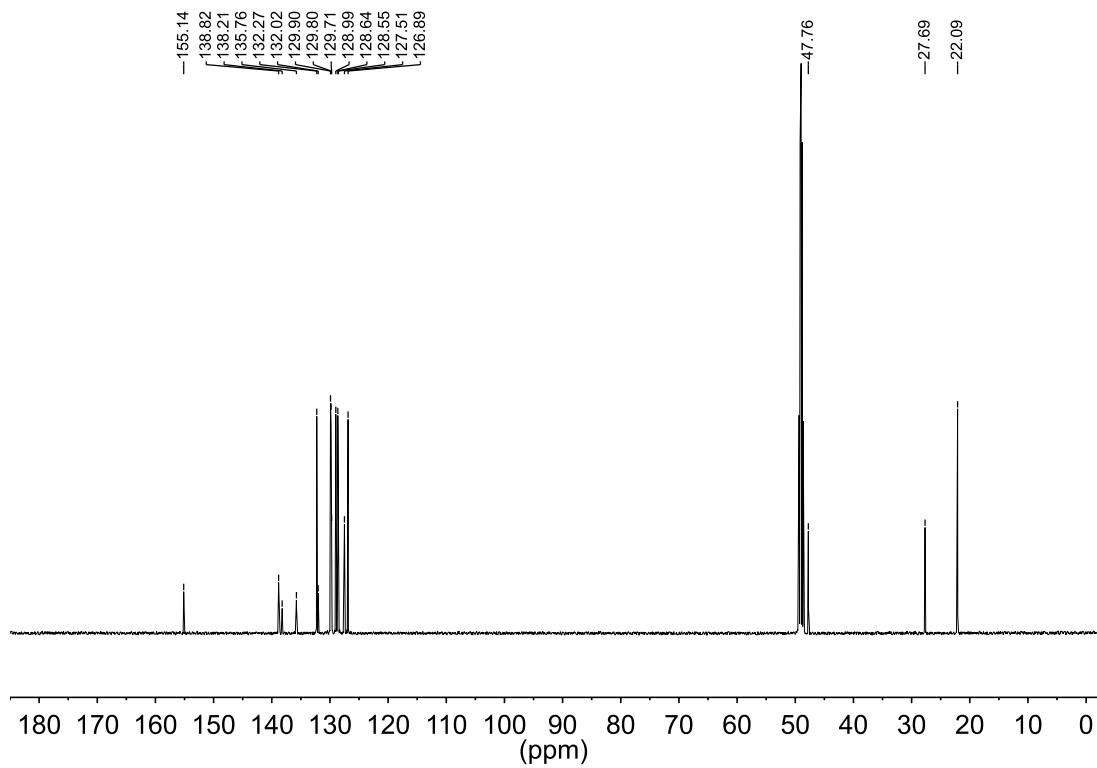


1-Benzyl-2-isopropyl-4,5-diphenyl-1*H*-imidazole (IM-4c)

¹H NMR spectrum (600 MHz, CD₃OD)

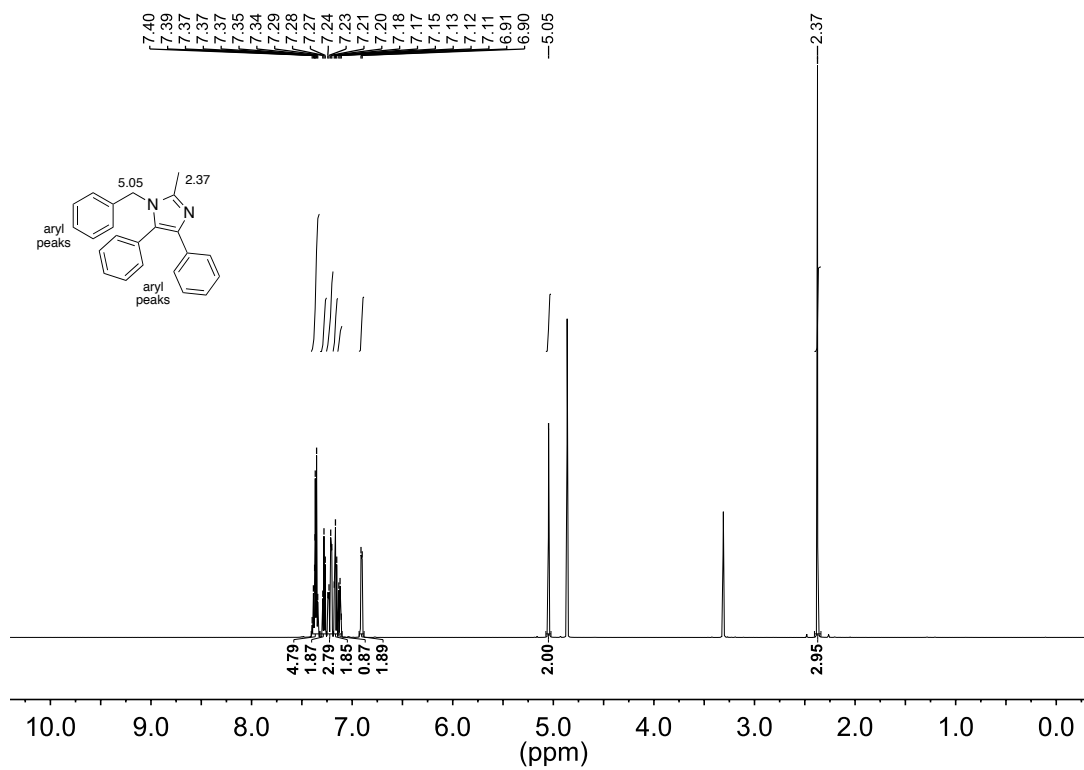


¹³C NMR spectrum (126 MHz, CD₃OD)

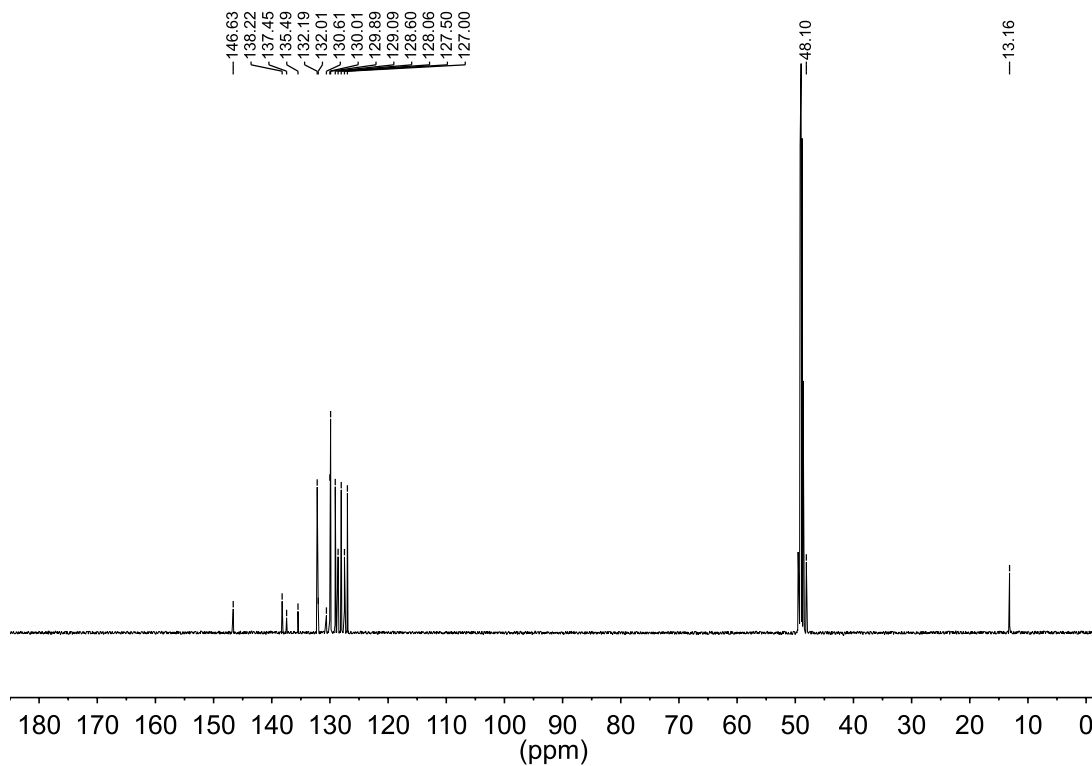


1-Benzyl-2-methyl-4,5-diphenyl-1*H*-imidazole (IM-4d)

¹H NMR spectrum (600 MHz, CD₃OD)

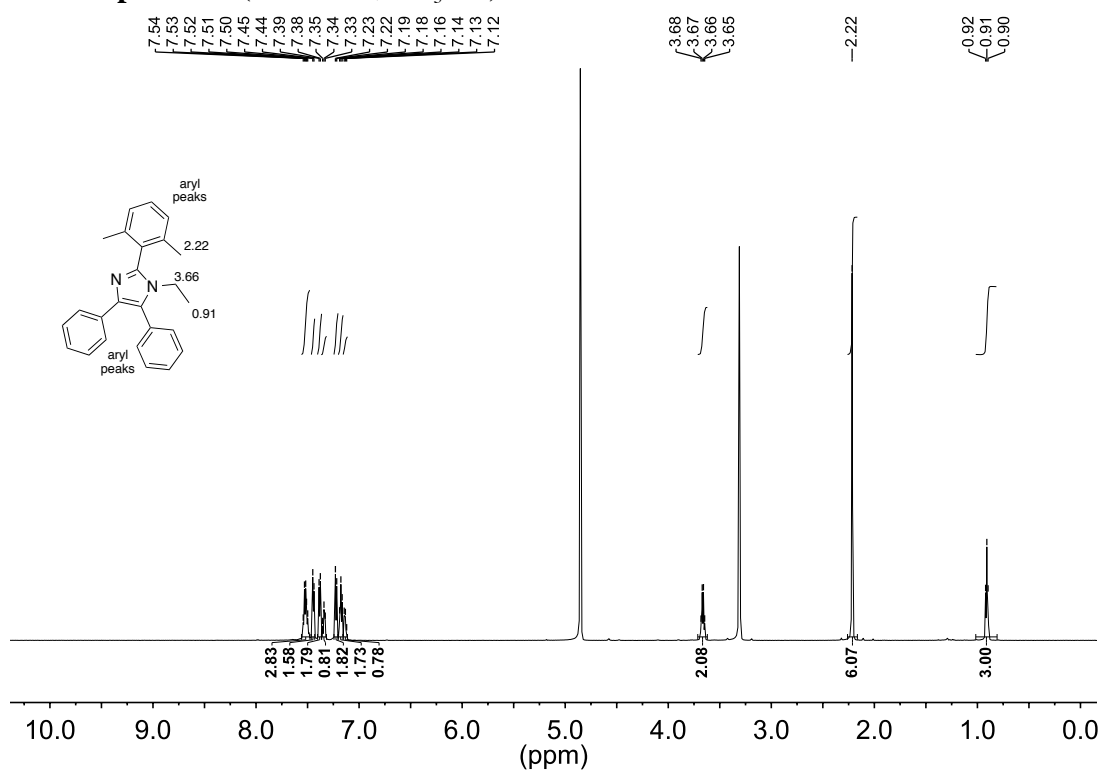


¹³C NMR spectrum (126 MHz, CD₃OD)

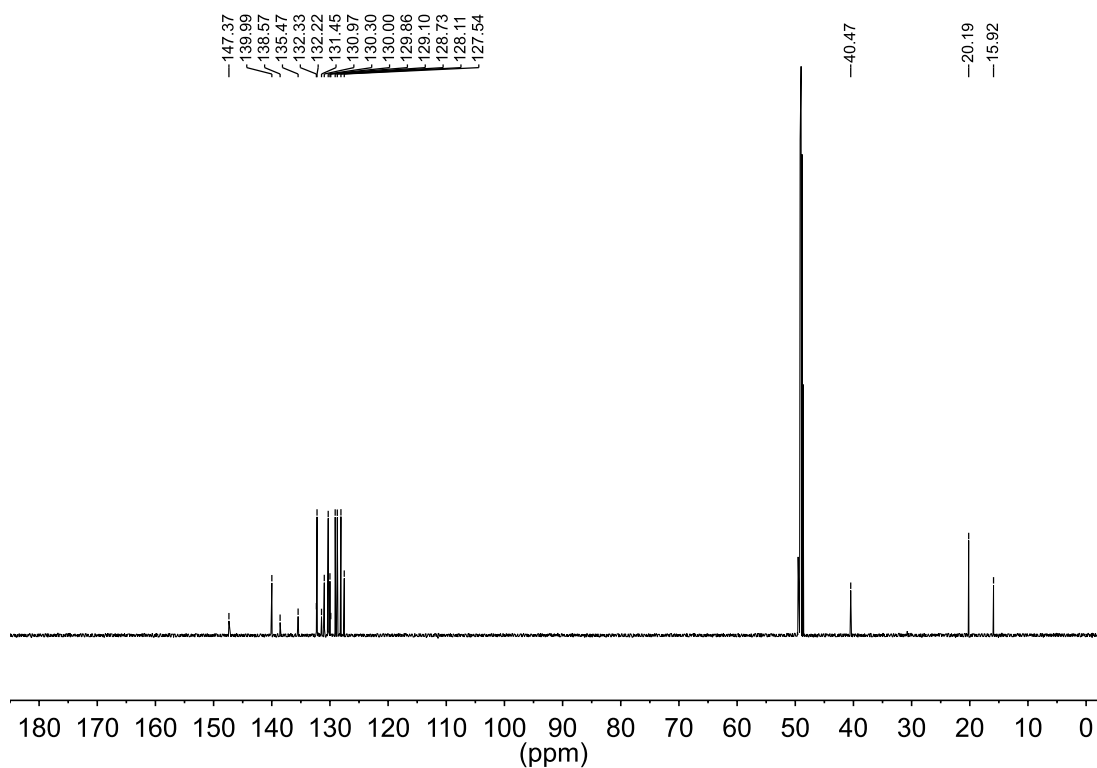


2-(2,6-Dimethylphenyl)-1-ethyl-4,5-diphenyl-1*H*-imidazole (IM-5a)

¹H NMR spectrum (600 MHz, CD₃OD)

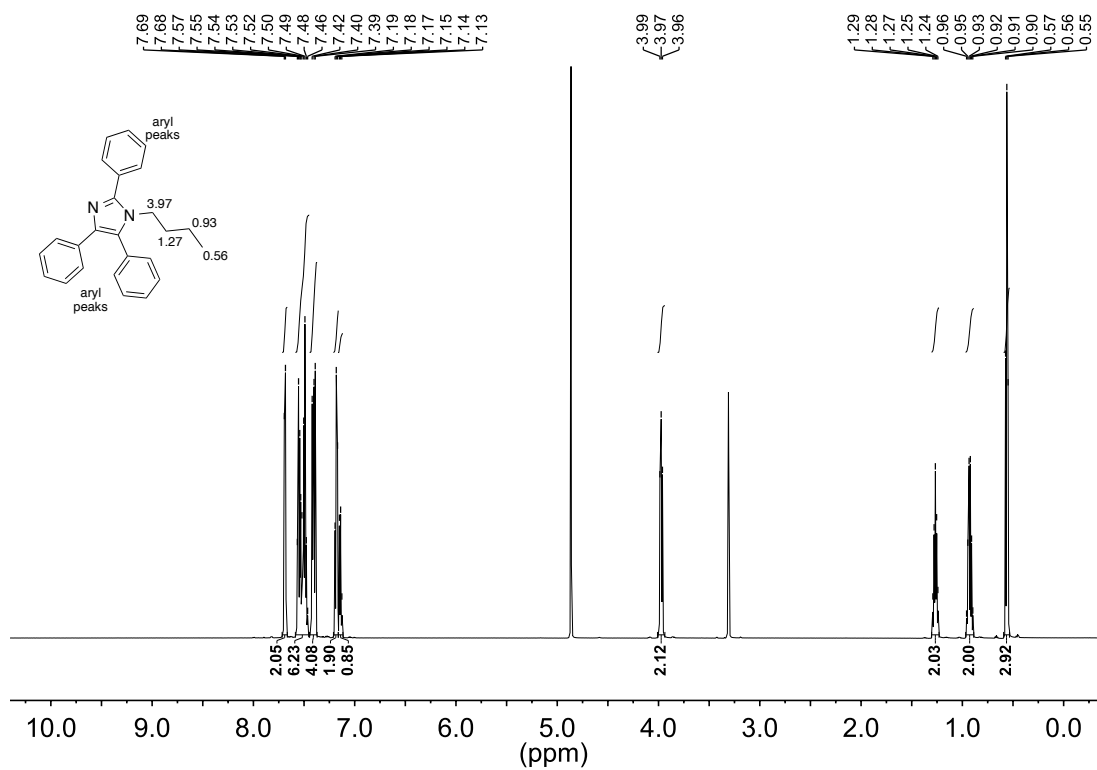


¹³C NMR spectrum (126 MHz, CD₃OD)

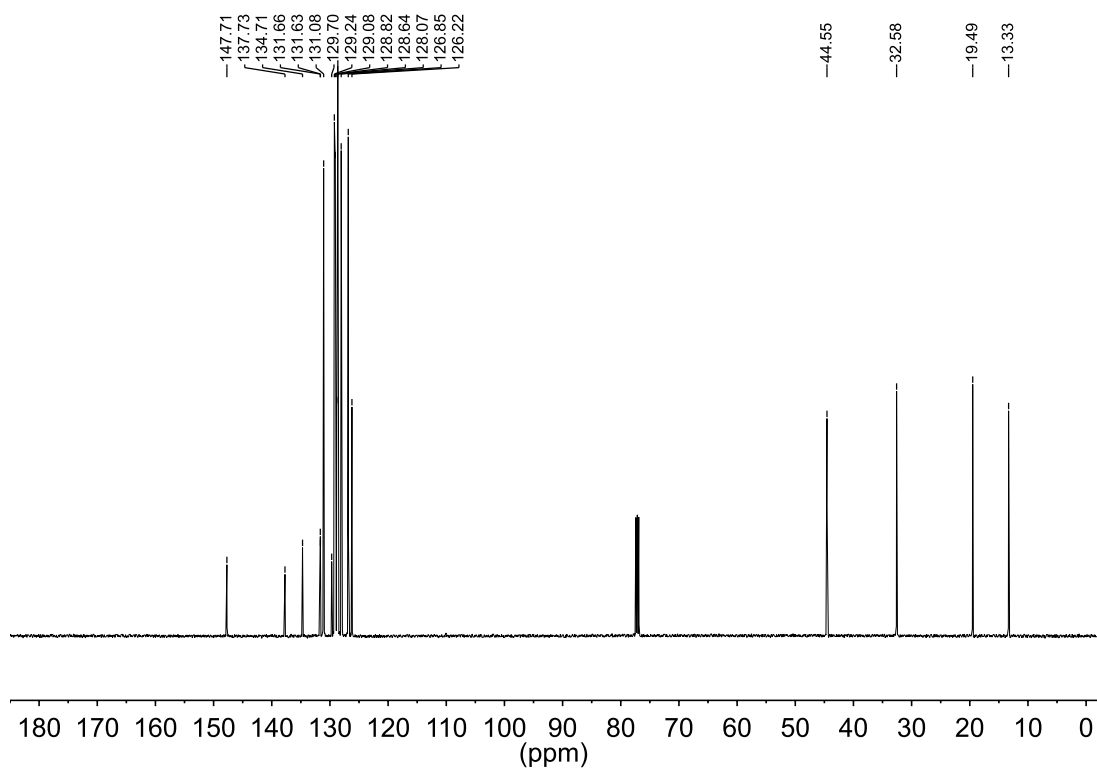


1-*n*-Butyl-2,4,5-triphenyl-1*H*-imidazole (IM-6b)

¹H NMR spectrum (600 MHz, CD₃OD)

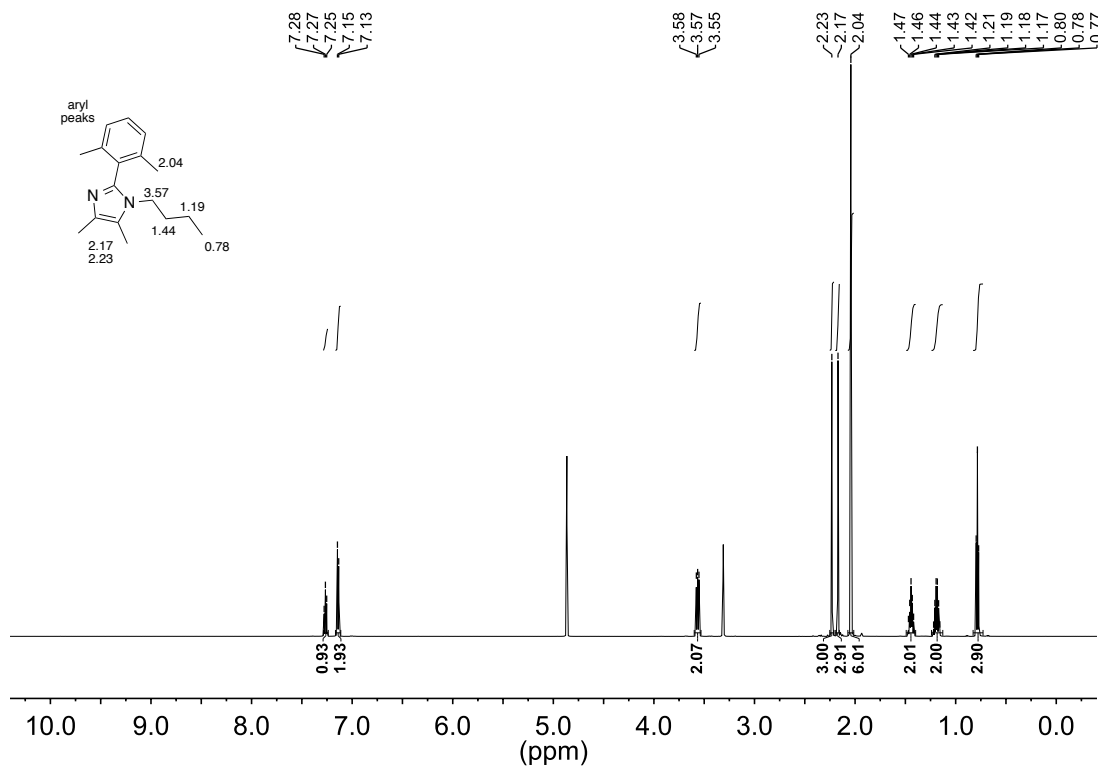


¹³C NMR spectrum (126 MHz, CDCl₃)

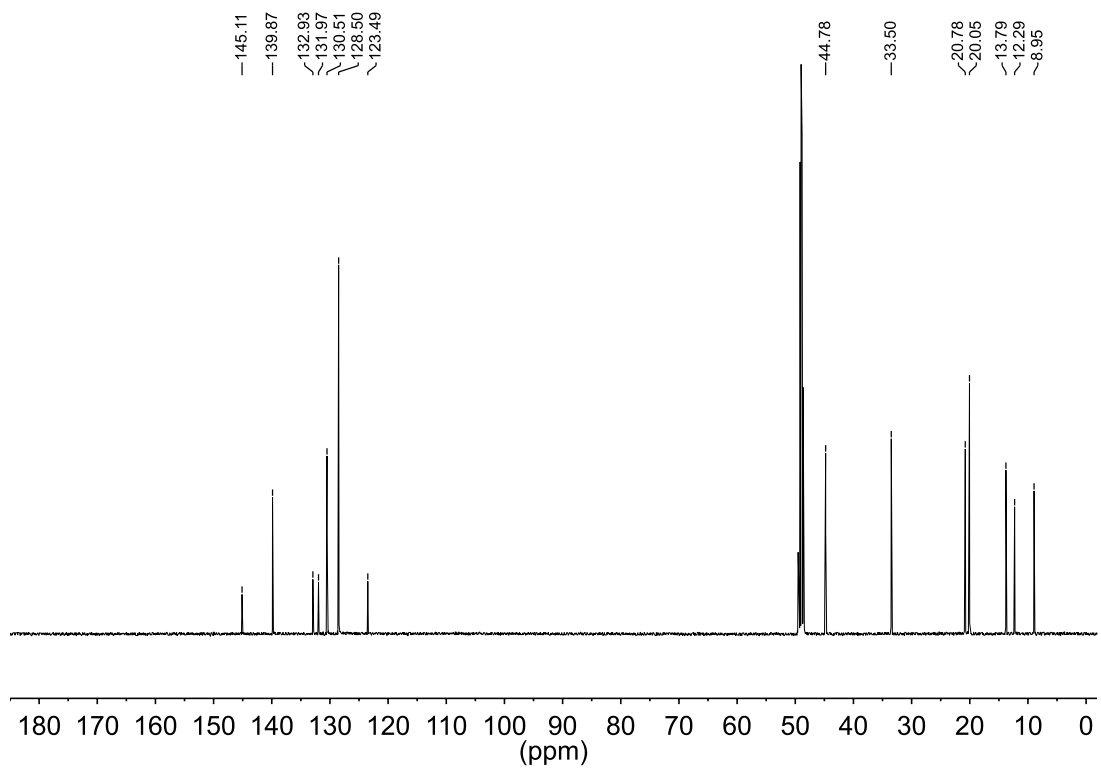


1-*n*-Butyl-2-(2,6-dimethylphenyl)-4,5-dimethyl-1*H*-imidazole (IM-7a)

¹H NMR spectrum (600 MHz, CD₃OD)

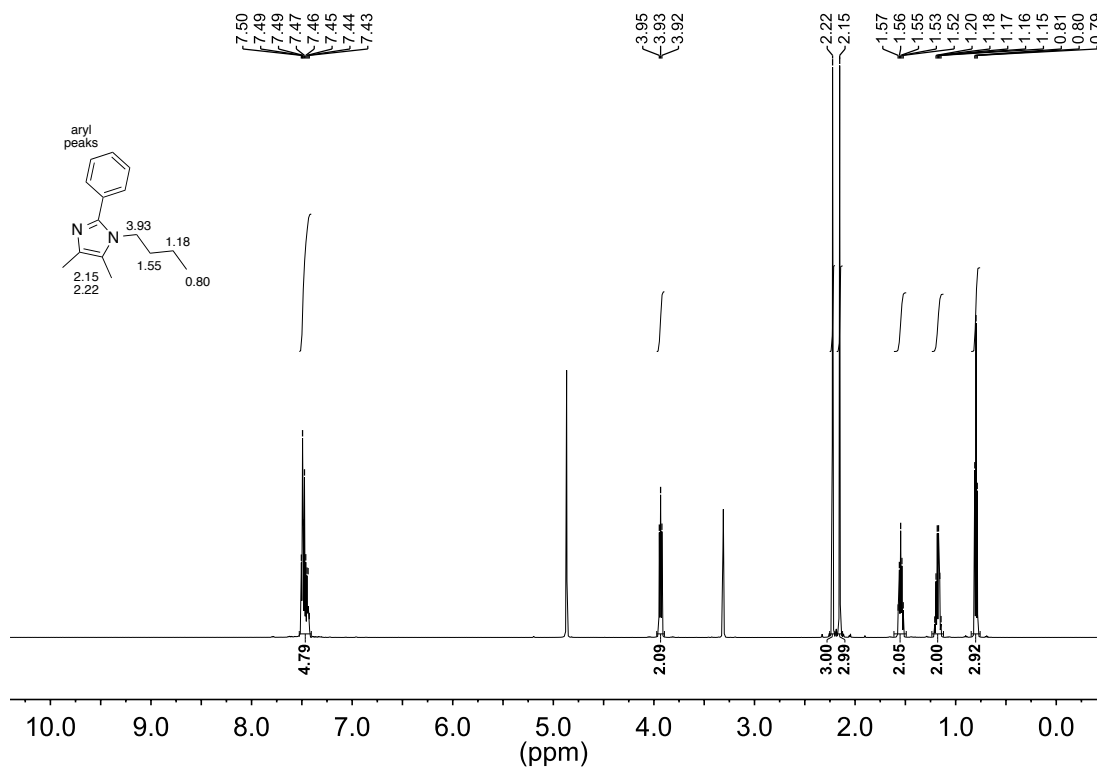


¹³C NMR spectrum (126 MHz, CD₃OD)

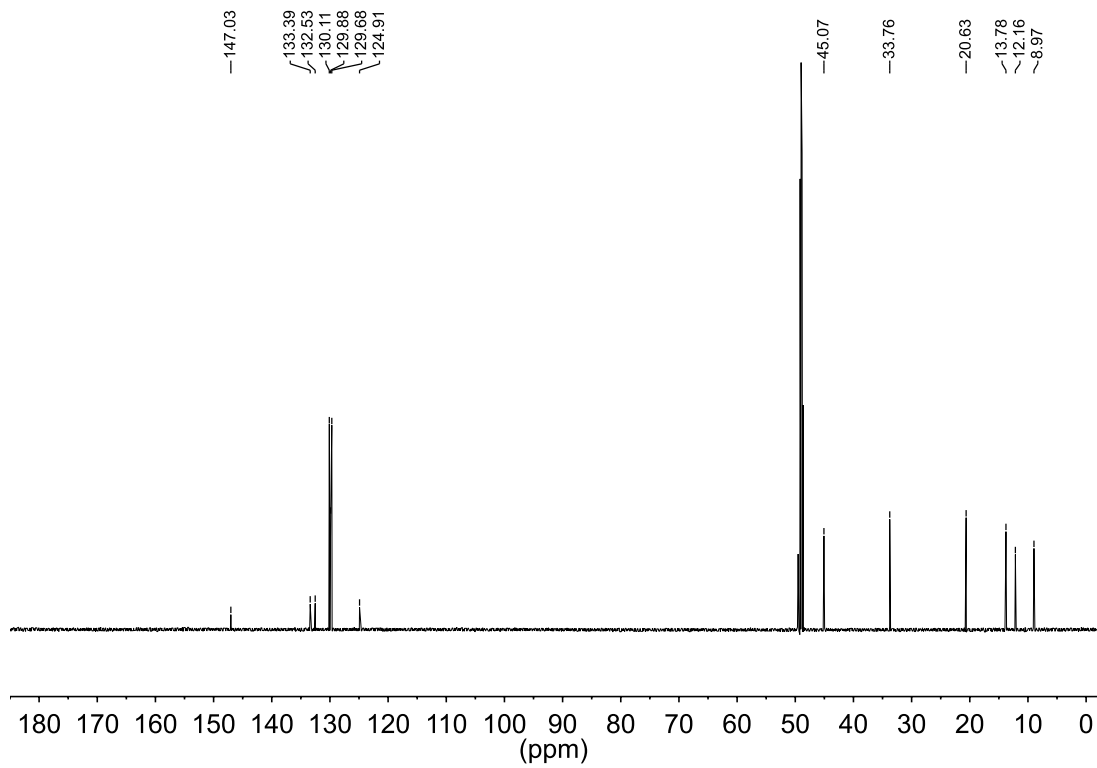


1-*n*-Butyl-4,5-dimethyl-2-phenyl-1*H*-imidazole (IM-7b)

¹H NMR spectrum (600 MHz, CD₃OD)

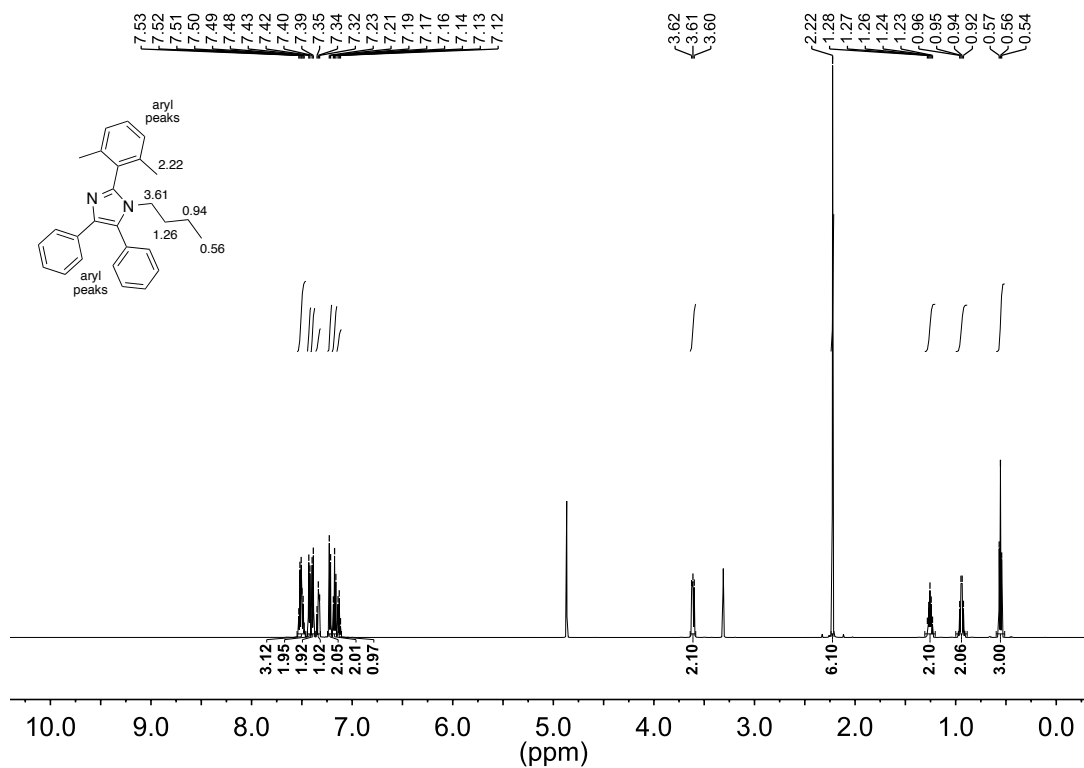


¹³C NMR spectrum (126 MHz, CD₃OD)

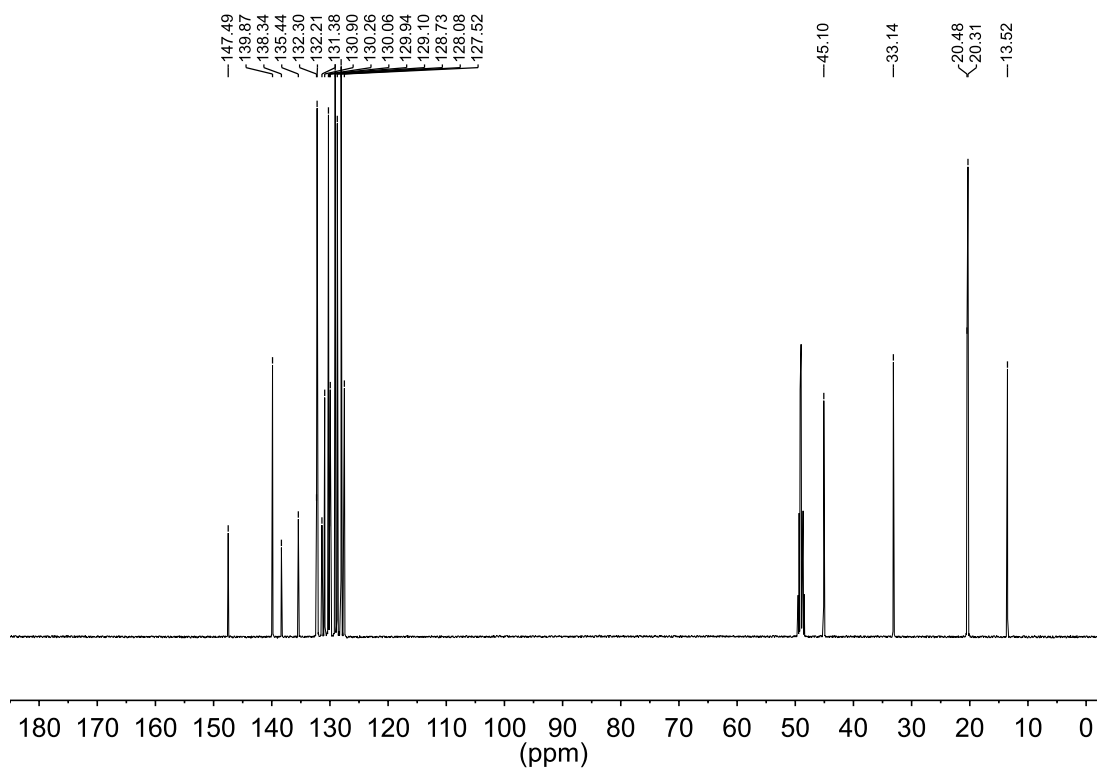


1-*n*-Butyl-2-(2,6-dimethylphenyl)-4,5-diphenyl-1*H*-imidazole (IM-8a)

¹H NMR spectrum (600 MHz, CD₃OD)

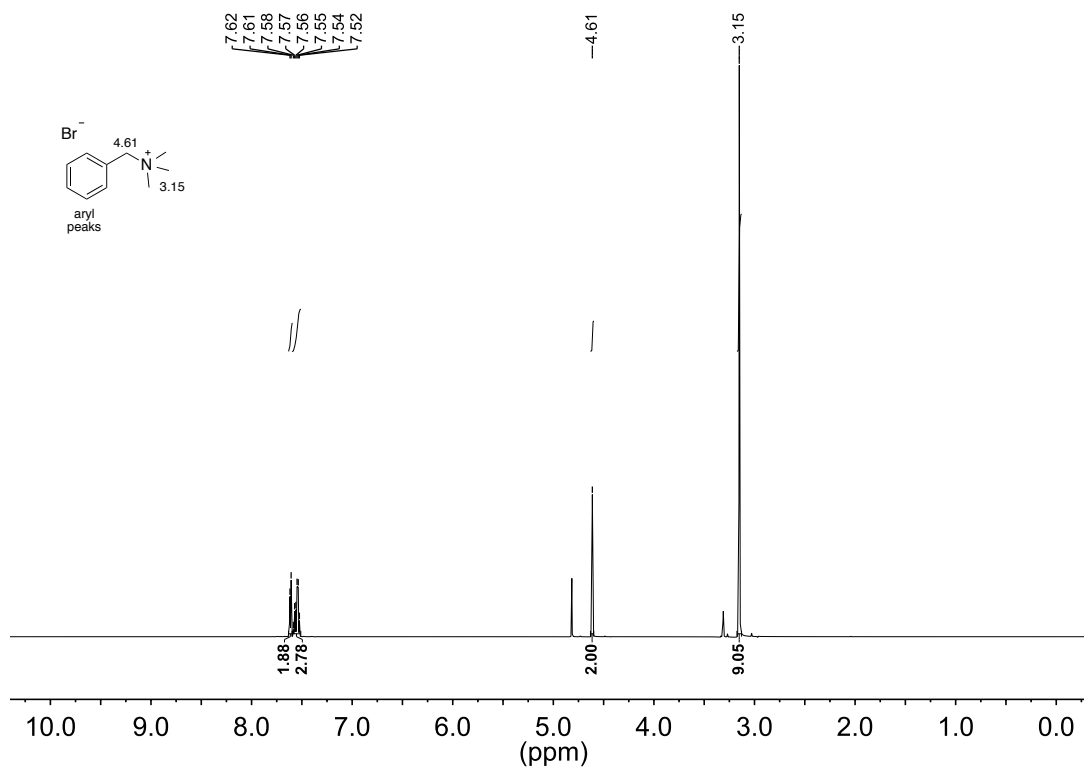


¹³C NMR spectrum (126 MHz, CD₃OD)

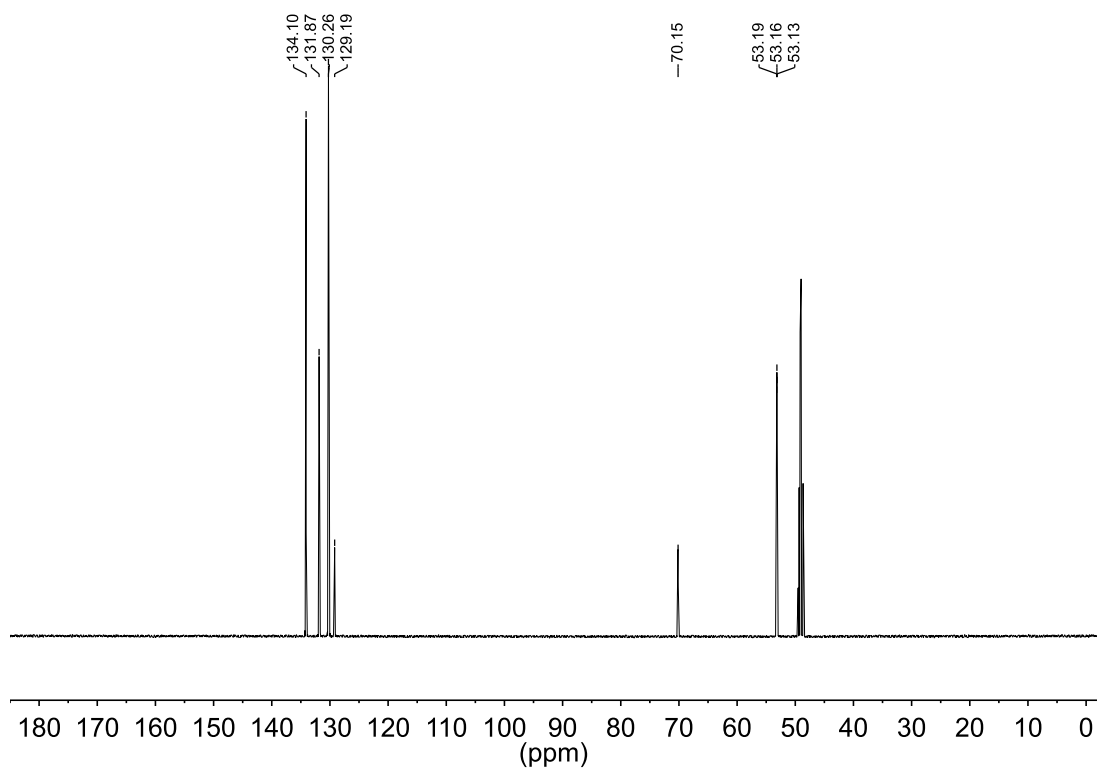


Benzyl trimethylammonium bromide (1)

^1H NMR spectrum (600 MHz, CD_3OD)

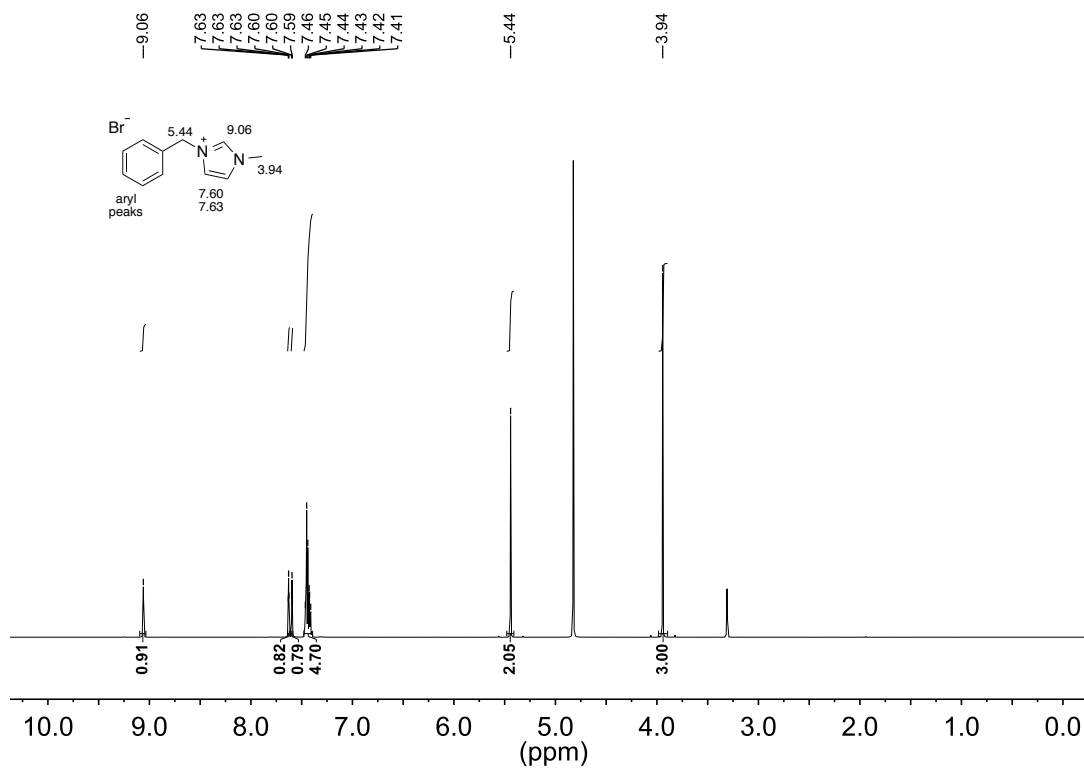


^{13}C NMR spectrum (126 MHz, CD_3OD)

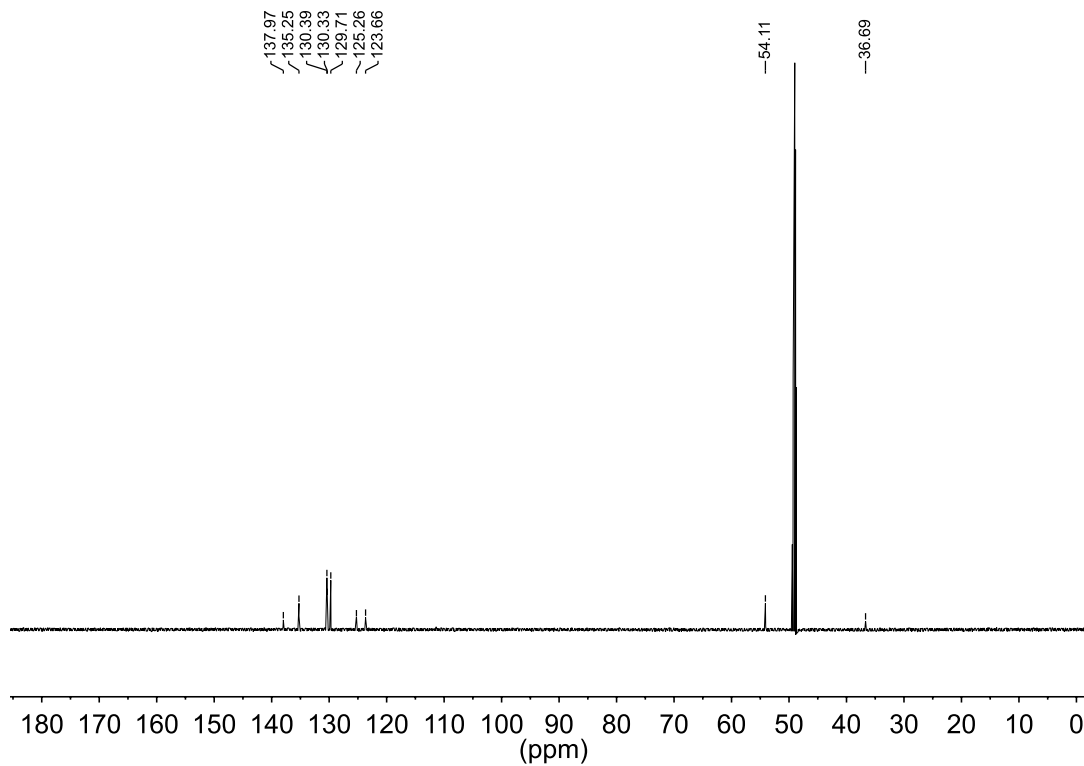


1-Benzyl-3-methylimidazolium bromide (2a)

^1H NMR spectrum (600 MHz, CD_3OD)

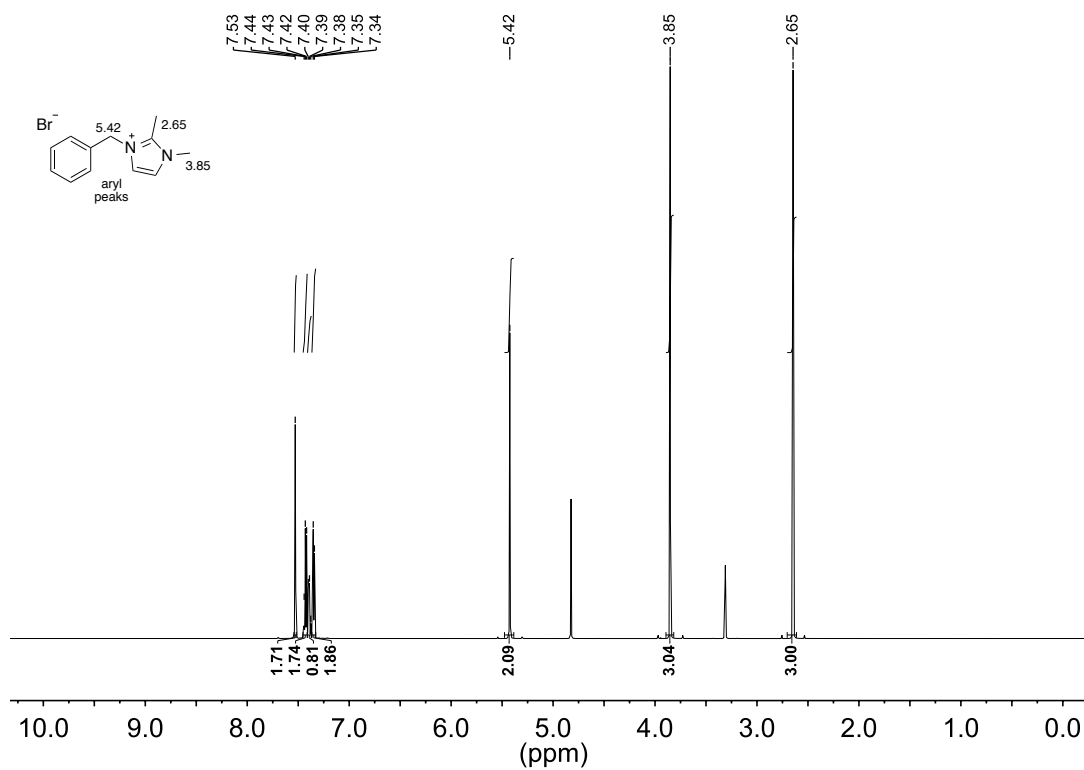


^{13}C NMR spectrum (151 MHz, CD_3OD)

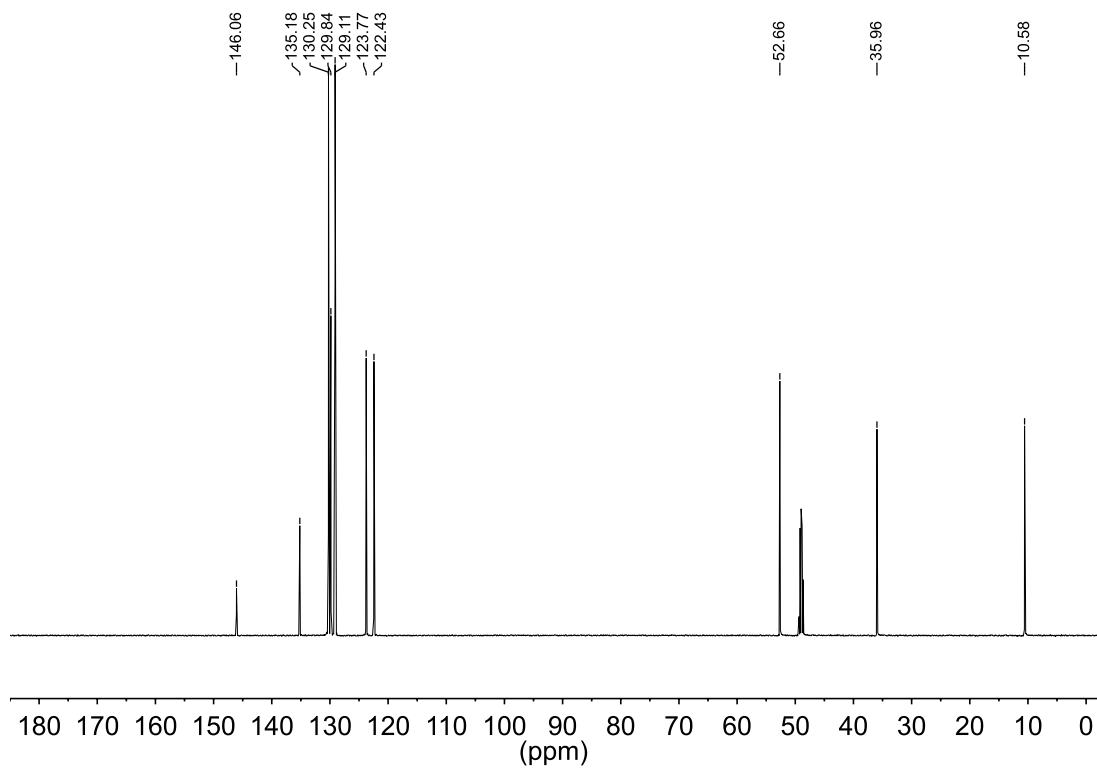


1-Benzyl-2,3-dimethylimidazolium bromide (2b)

^1H NMR spectrum (600 MHz, CD_3OD)

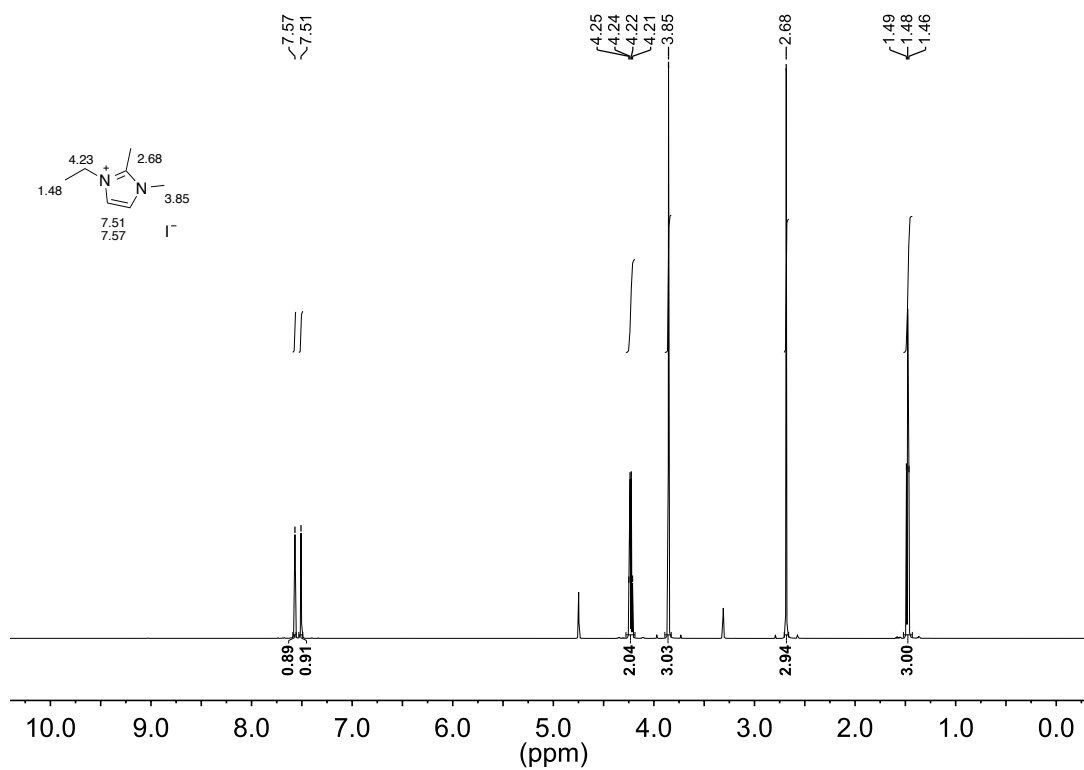


^{13}C NMR spectrum (126 MHz, CD_3OD)

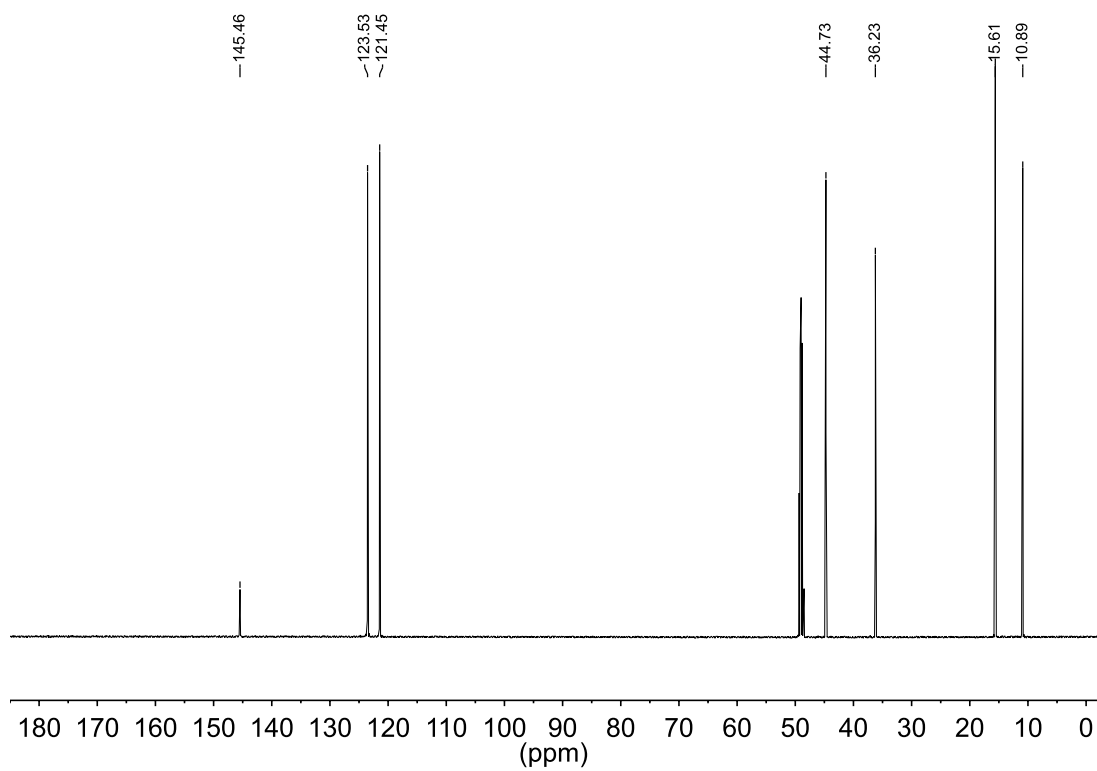


1-Ethyl-2,3-dimethylimidazolium iodide (2c)

^1H NMR spectrum (600 MHz, CD_3OD)

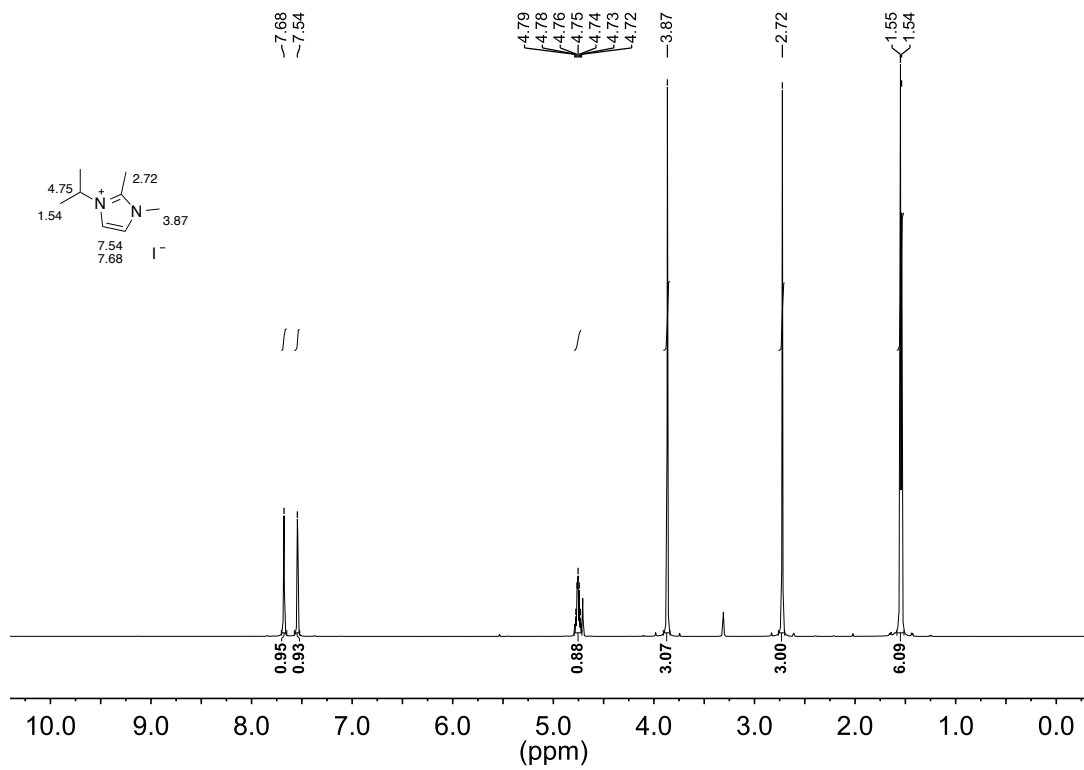


^{13}C NMR spectrum (126 MHz, CD_3OD)

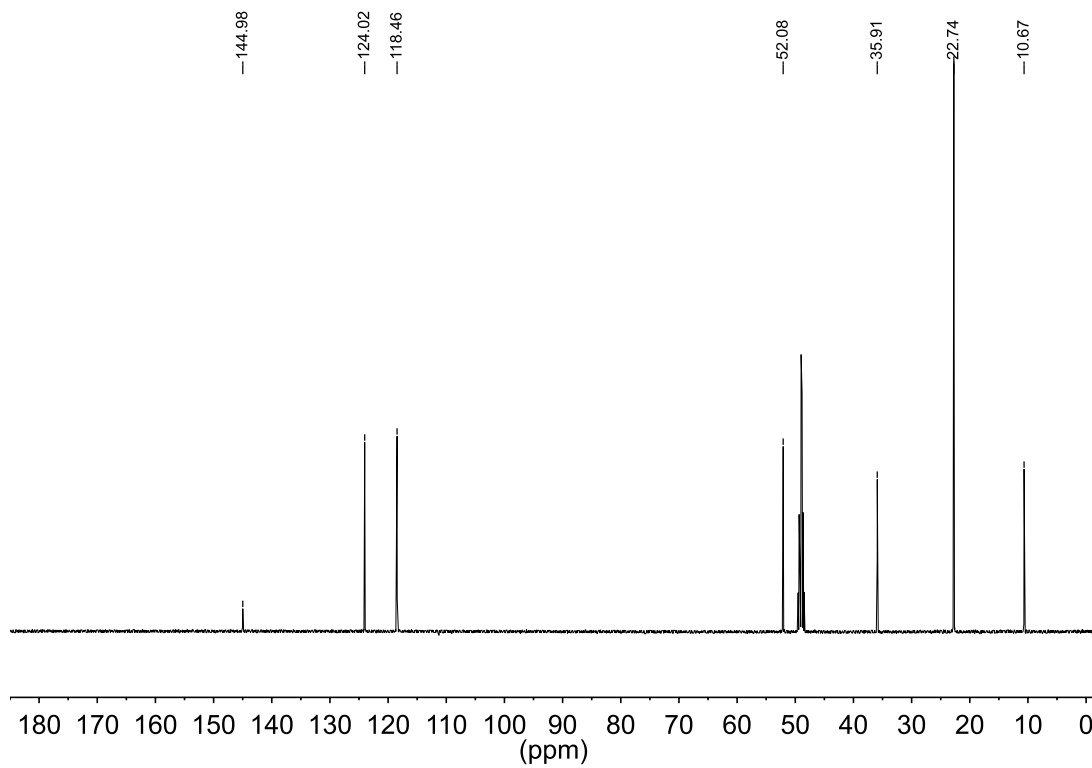


1-Isopropyl-2,3-dimethylimidazolium iodide (2d)

^1H NMR spectrum (600 MHz, CD_3OD)

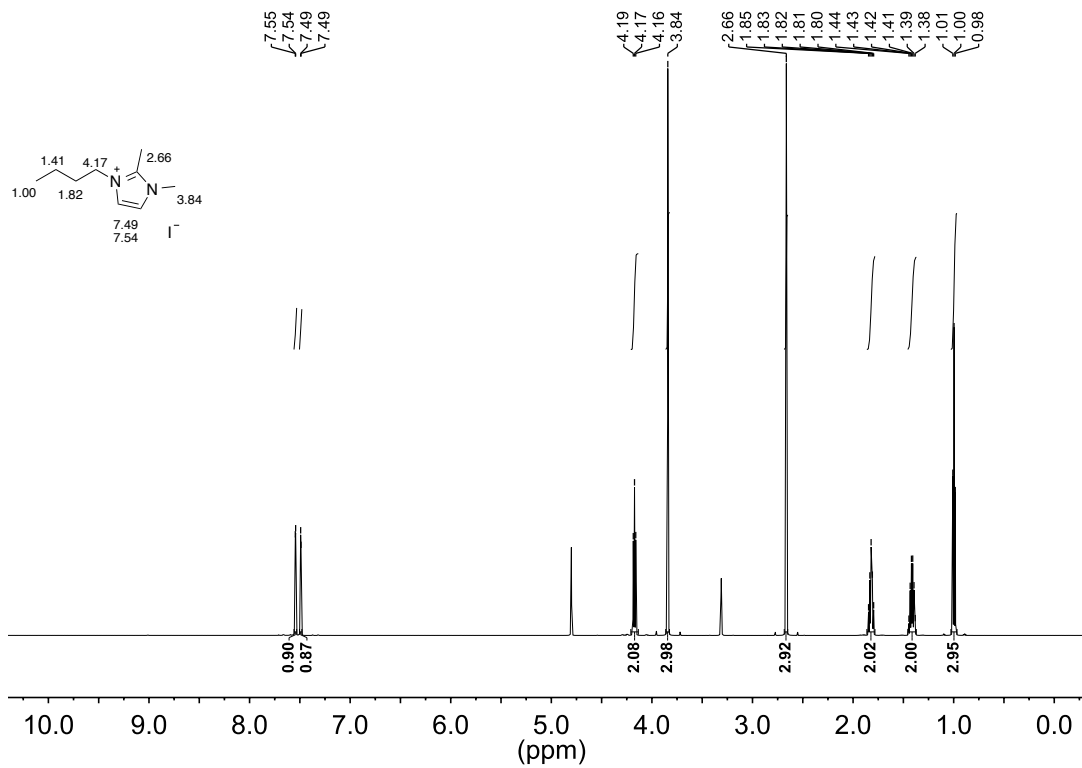


^{13}C NMR spectrum (126 MHz, CD_3OD)

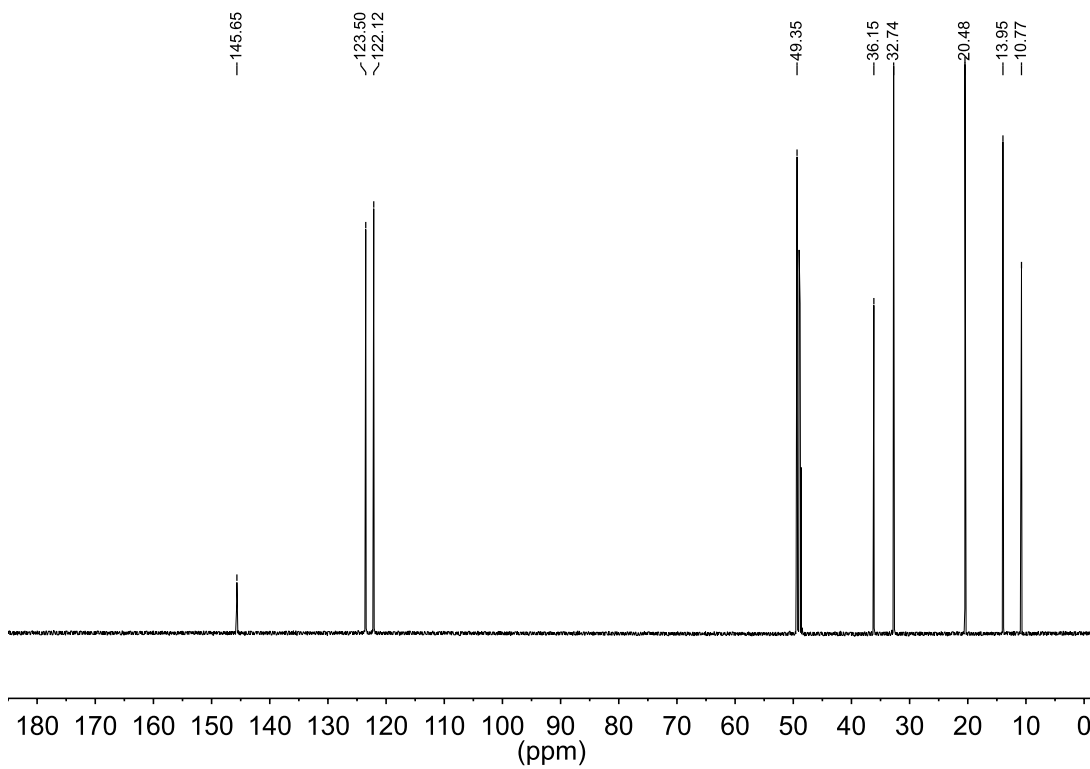


1-*n*-Butyl-2,3-dimethylimidazolium iodide (2e)

¹H NMR spectrum (600 MHz, CD₃OD)

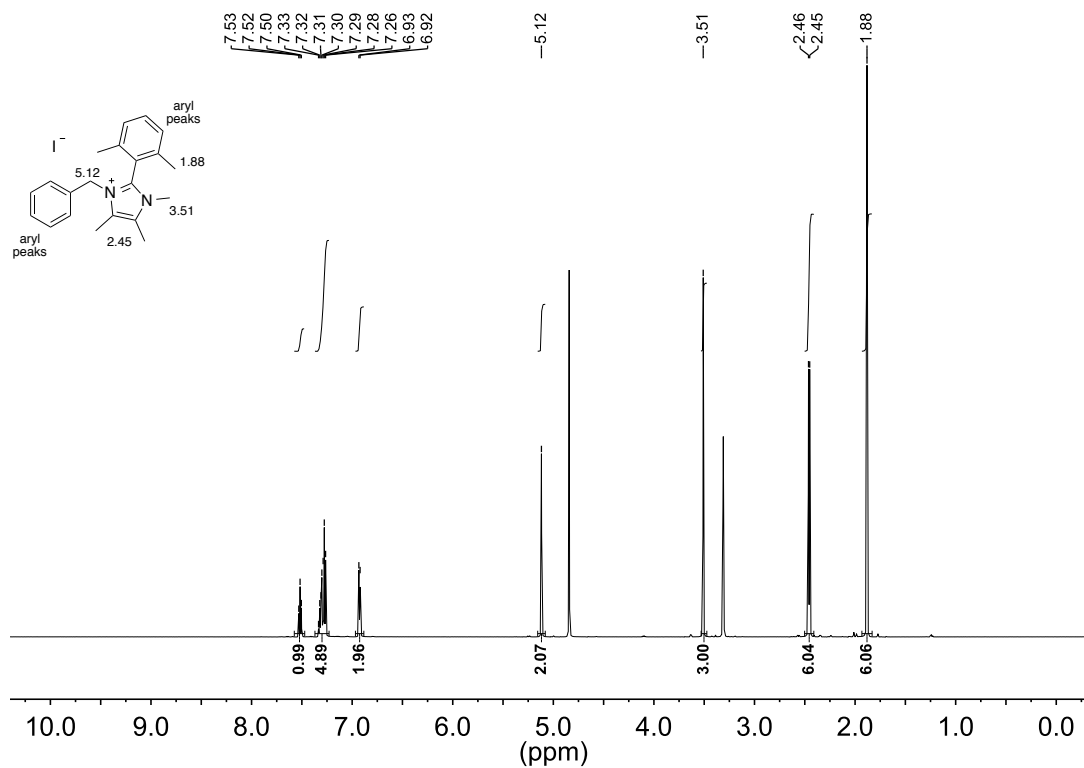


¹³C NMR spectrum (126 MHz, CD₃OD)

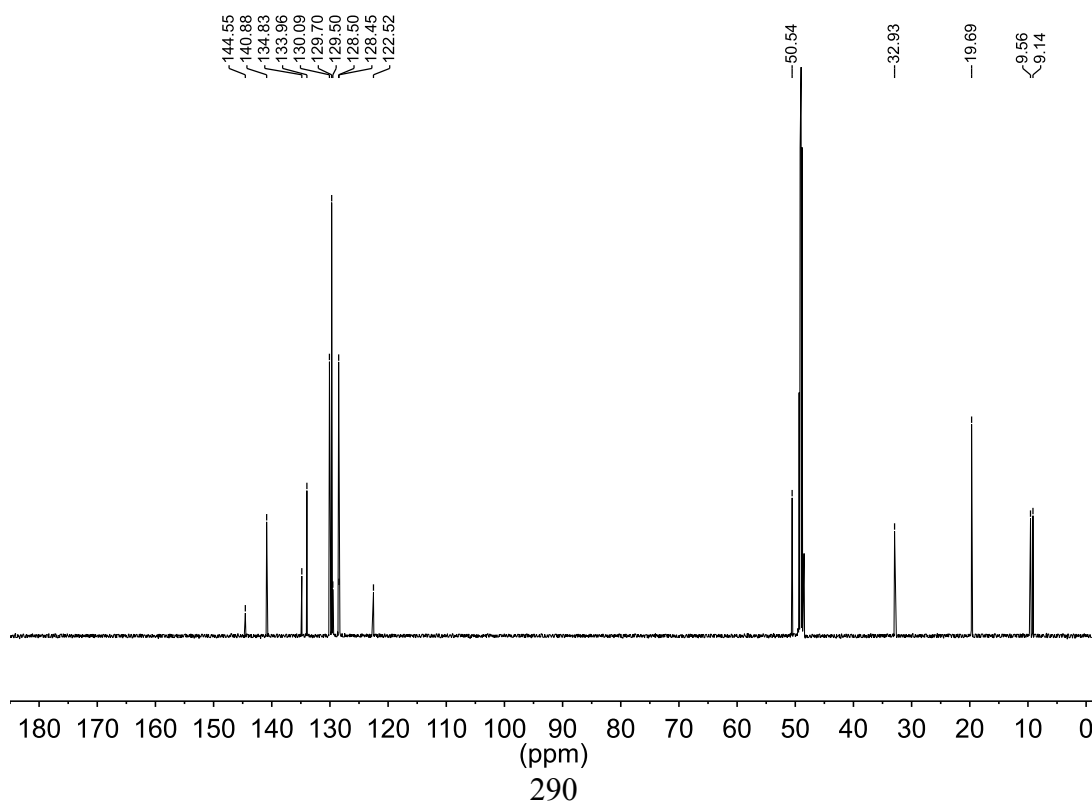


1-Benzyl-2-(2,6-dimethylphenyl)-3,4,5-trimethylimidazolium iodide (3a)

^1H NMR spectrum (600 MHz, CD_3OD)

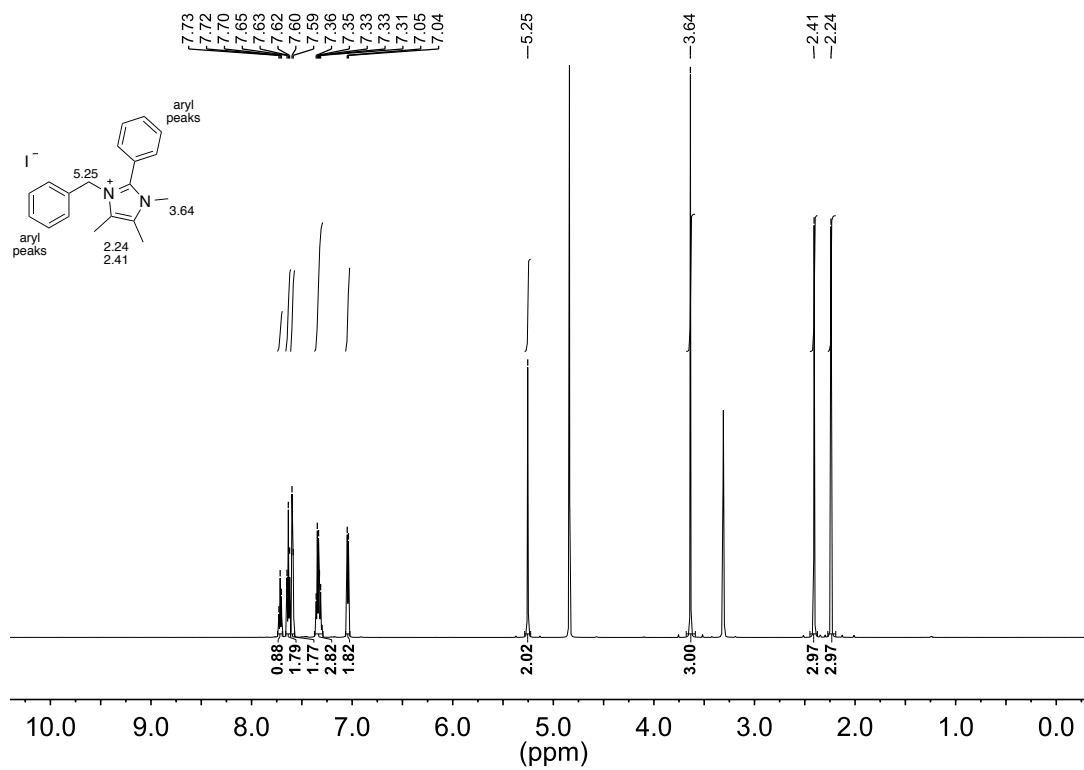


^{13}C NMR spectrum (126 MHz, CD_3OD)

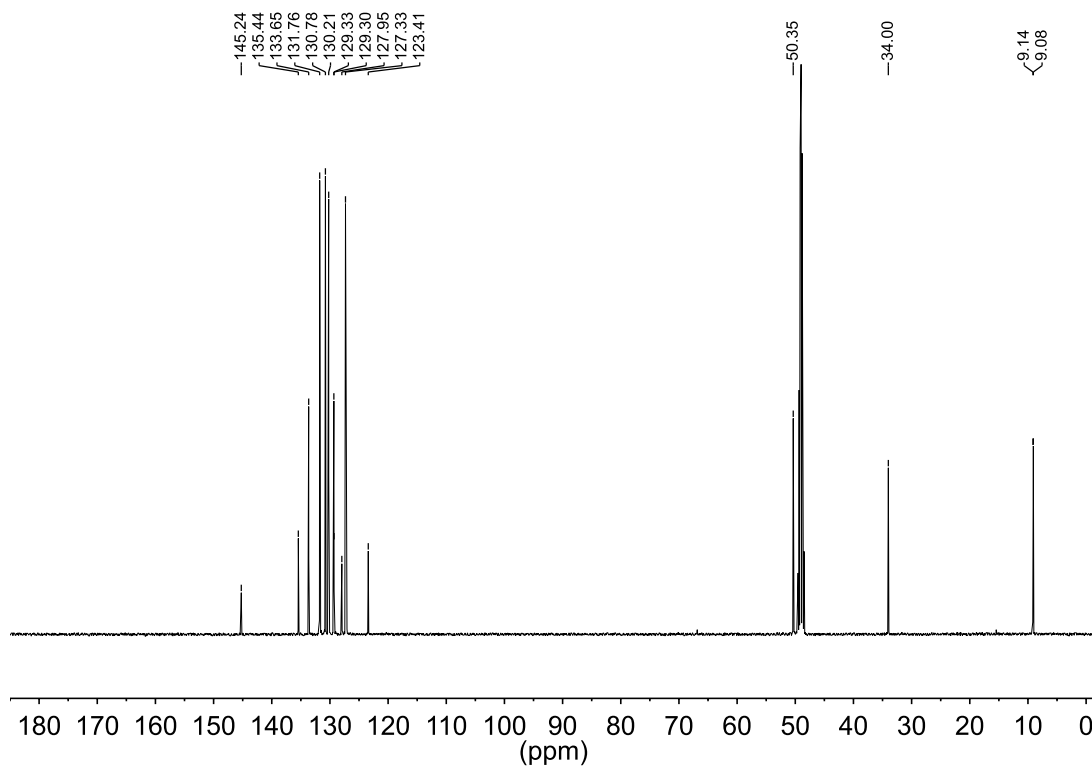


1-Benzyl-3,4,5-trimethyl-2-phenylimidazolium iodide (3b)

^1H NMR spectrum (600 MHz, CD_3OD)

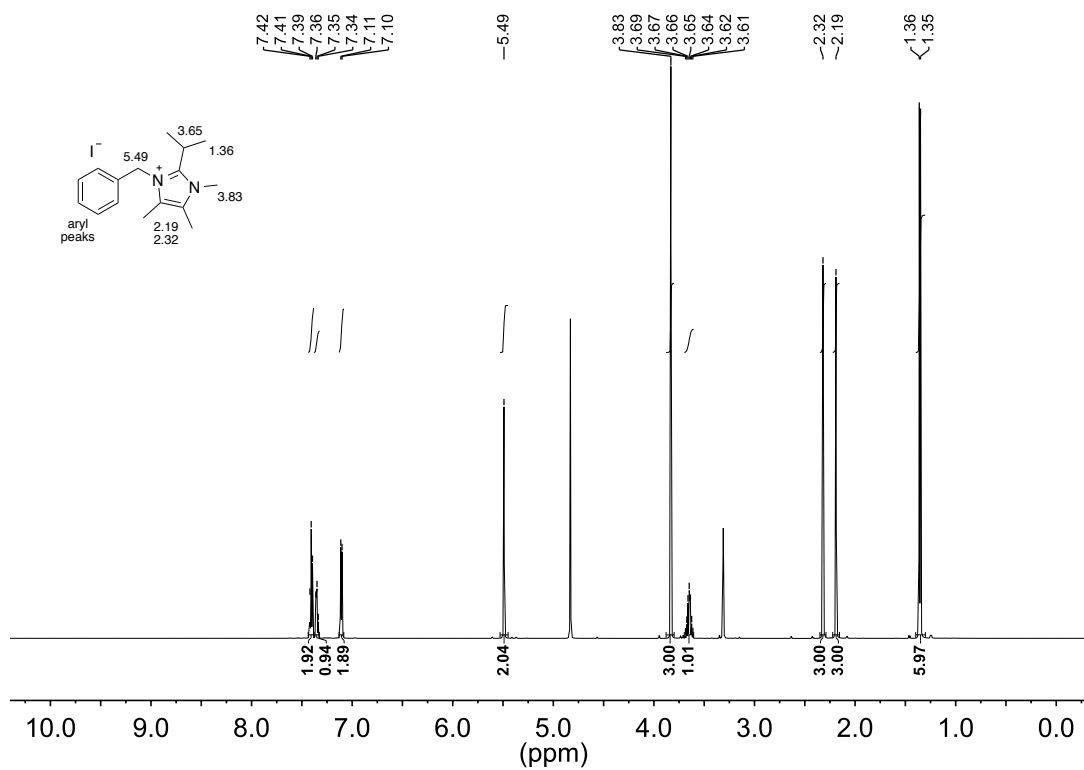


^{13}C NMR spectrum (126 MHz, CD_3OD)

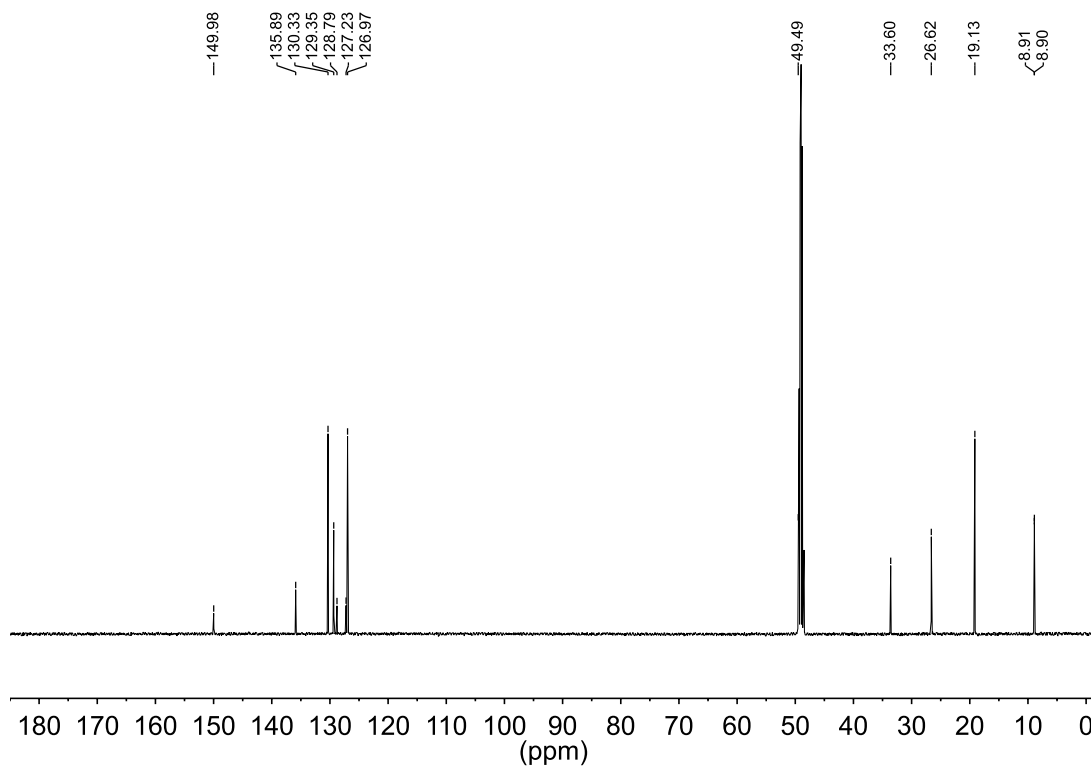


1-Benzyl-2-isopropyl-3,4,5-trimethylimidazolium iodide (3c)

^1H NMR spectrum (600 MHz, CD_3OD)

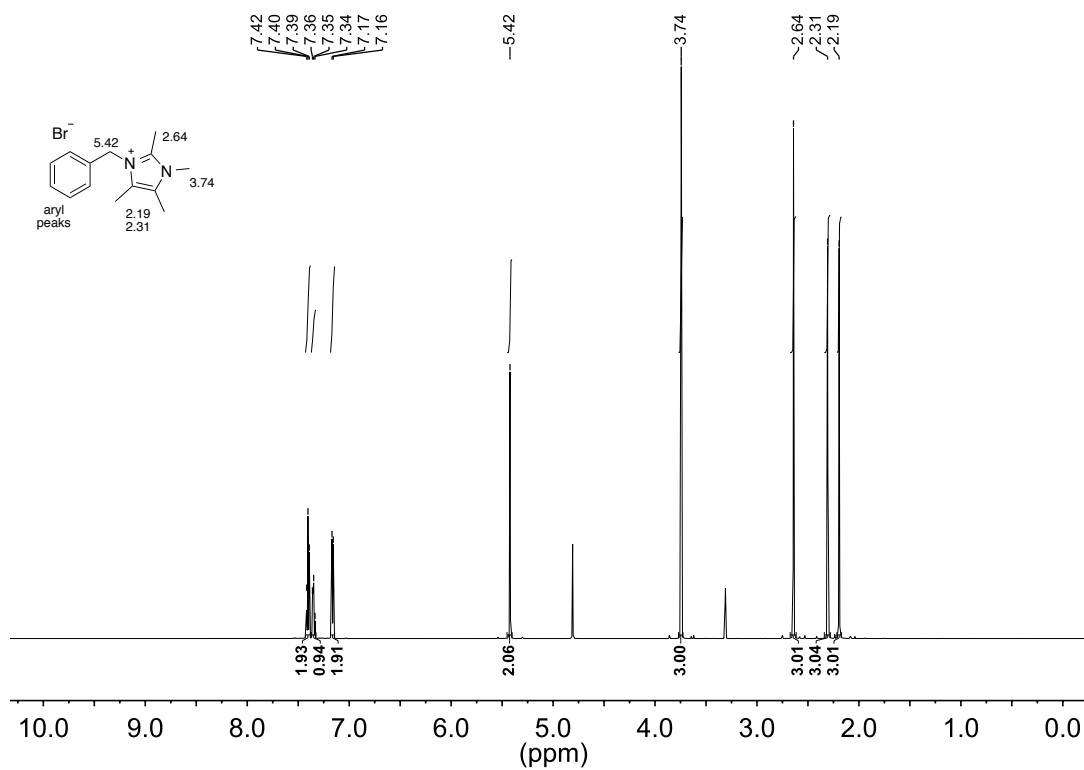


^{13}C NMR spectrum (126 MHz, CD_3OD)

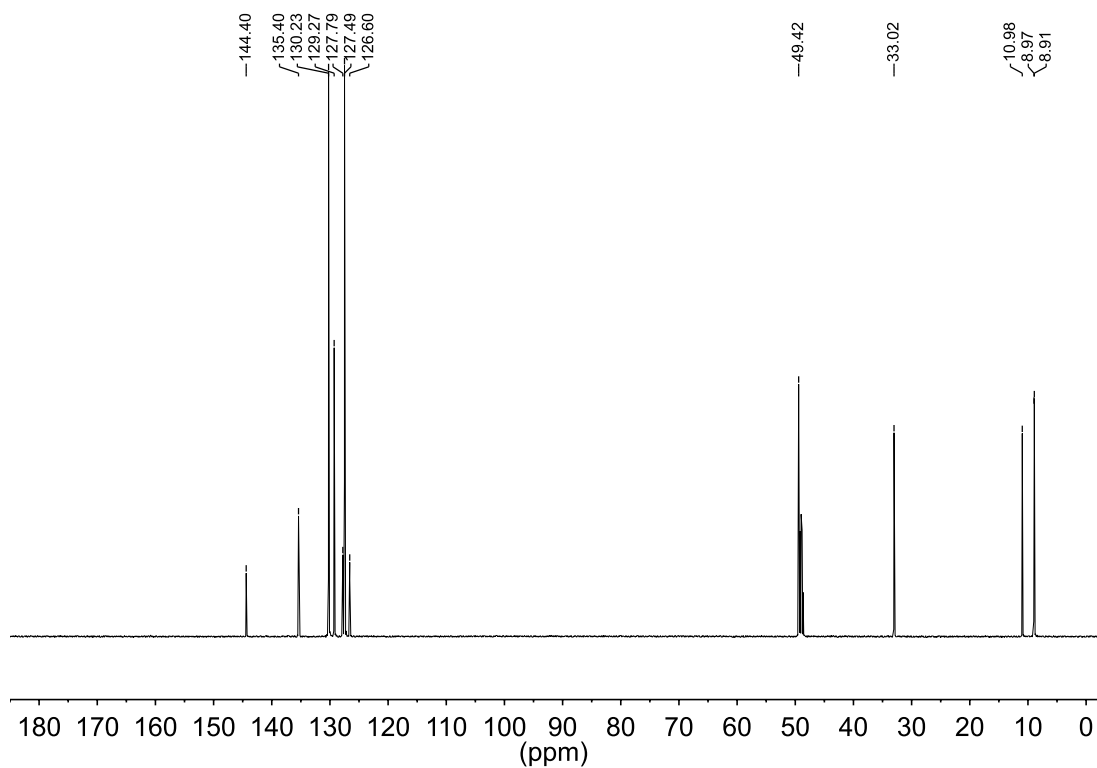


1-Benzyl-2,3,4,5-tetramethylimidazolium bromide (3d)

^1H NMR spectrum (600 MHz, CD_3OD)

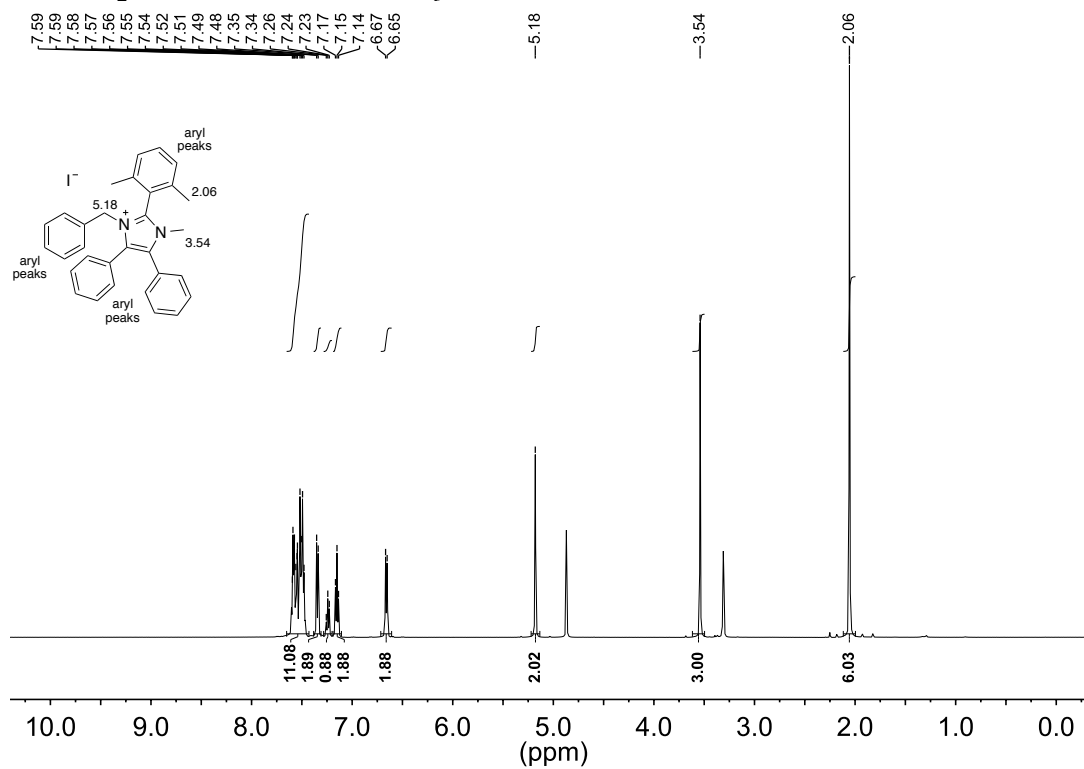


^{13}C NMR spectrum (126 MHz, CD_3OD)

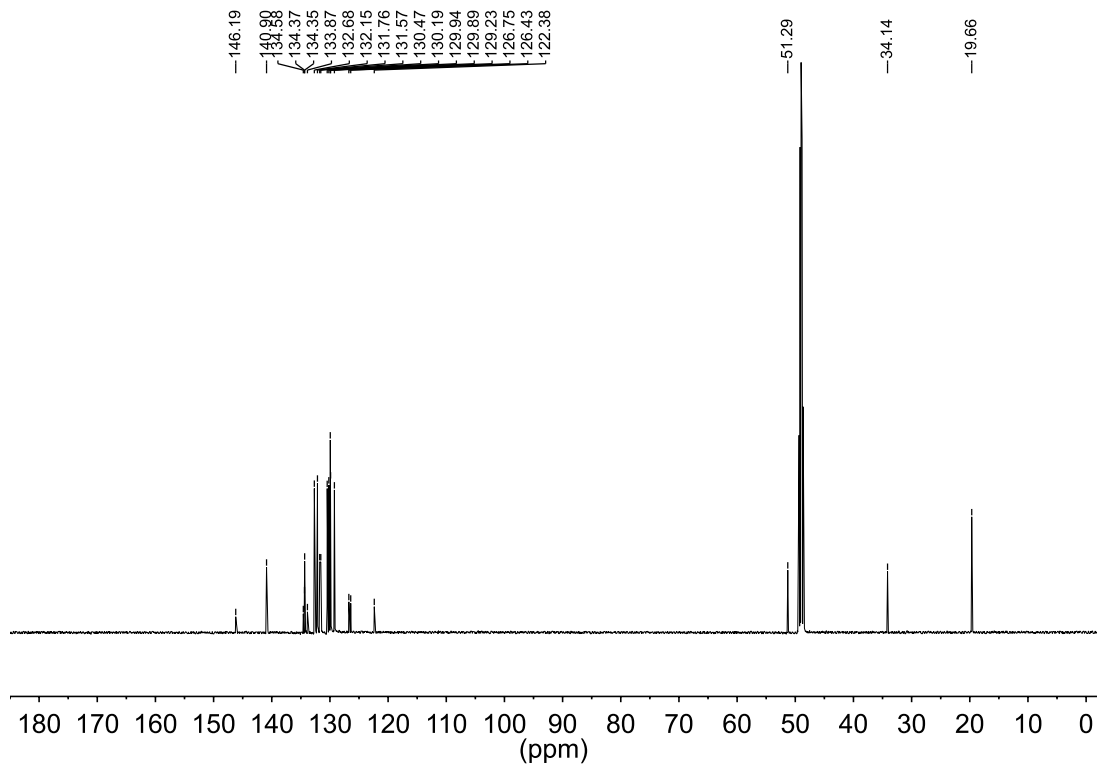


1-Benzyl-2-(2,6-dimethylphenyl)-3-methyl-4,5-diphenylimidazolium iodide (4a)

¹H NMR spectrum (500 MHz, CD₃OD)

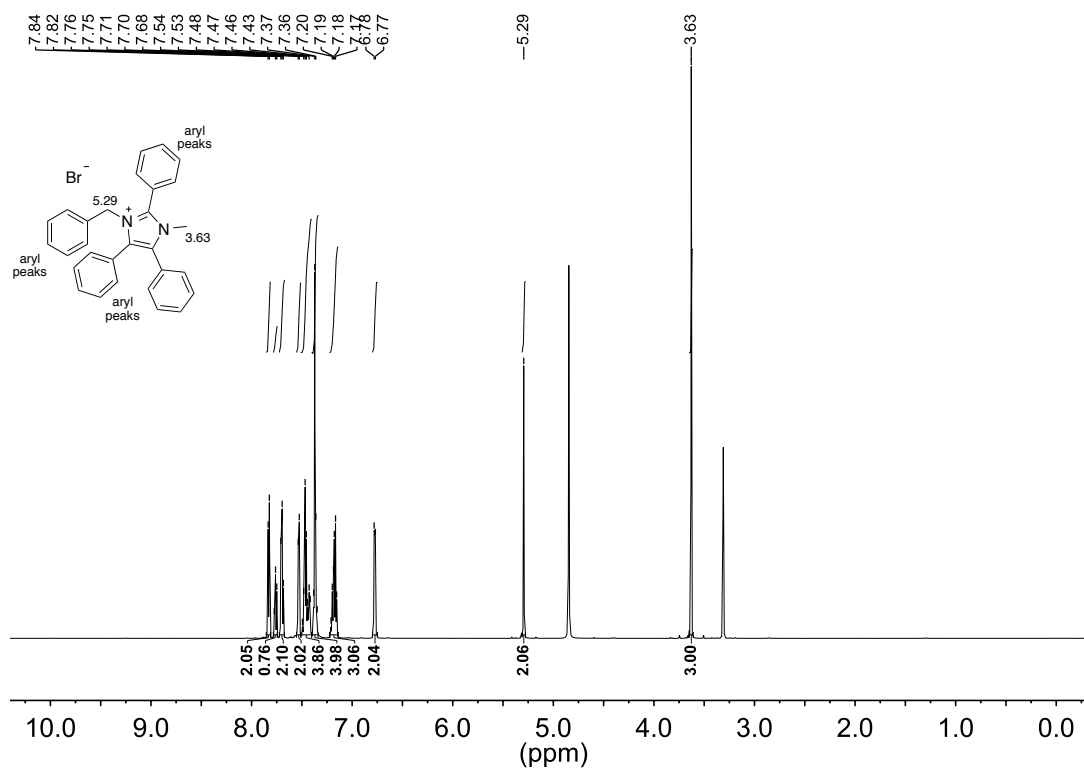


¹³C NMR spectrum (126 MHz, CD₃OD)

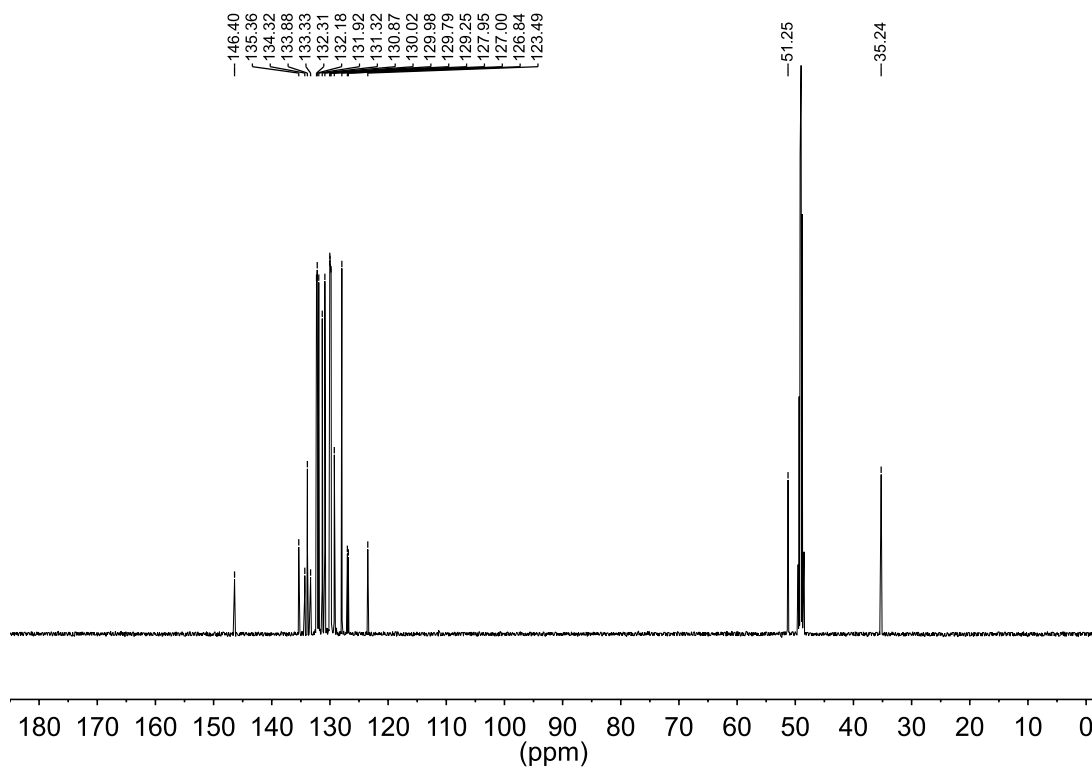


1-Benzyl-3-methyl-2,4,5-triphenylimidazolium bromide (4b)

^1H NMR spectrum (600 MHz, CD_3OD)

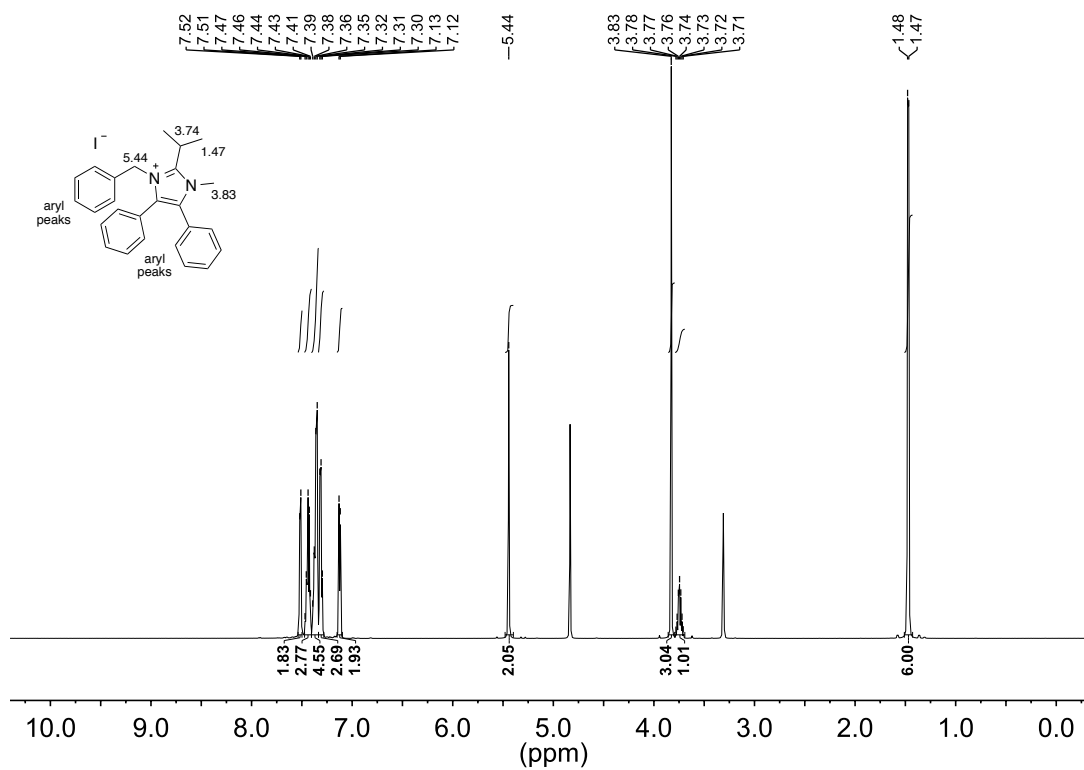


^{13}C NMR spectrum (126 MHz, CD_3OD)

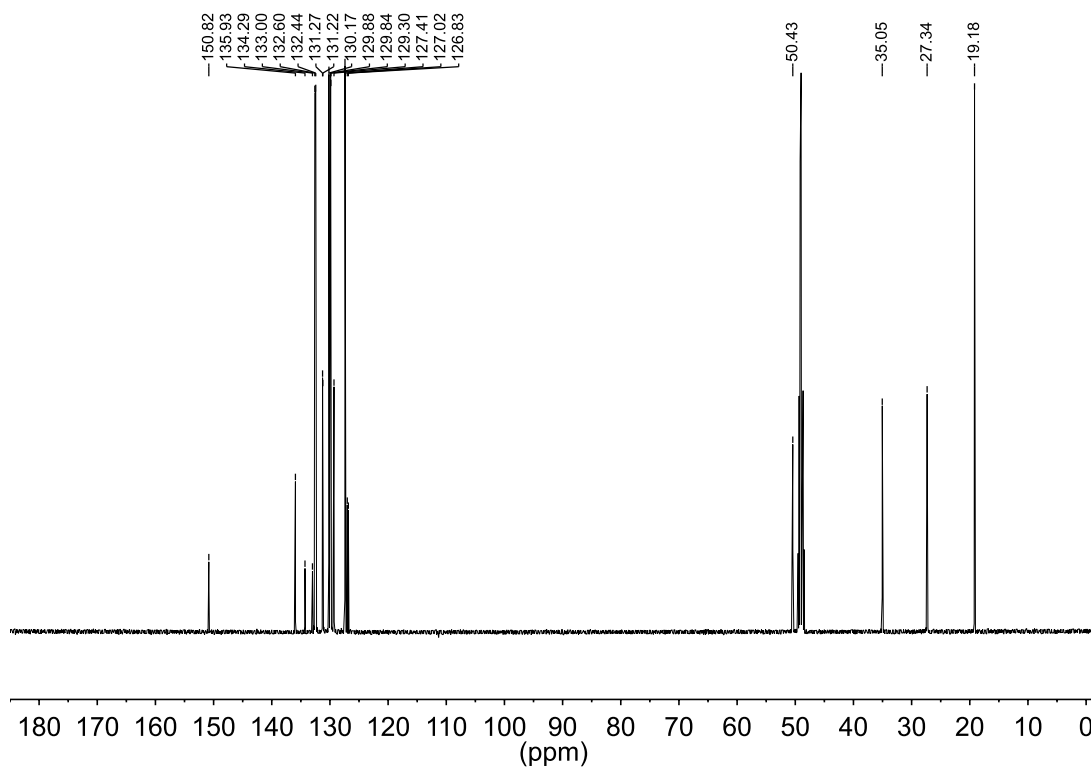


1-Benzyl-2-isopropyl-3-methyl-4,5-diphenylimidazolium iodide (4c)

^1H NMR spectrum (600 MHz, CD_3OD)

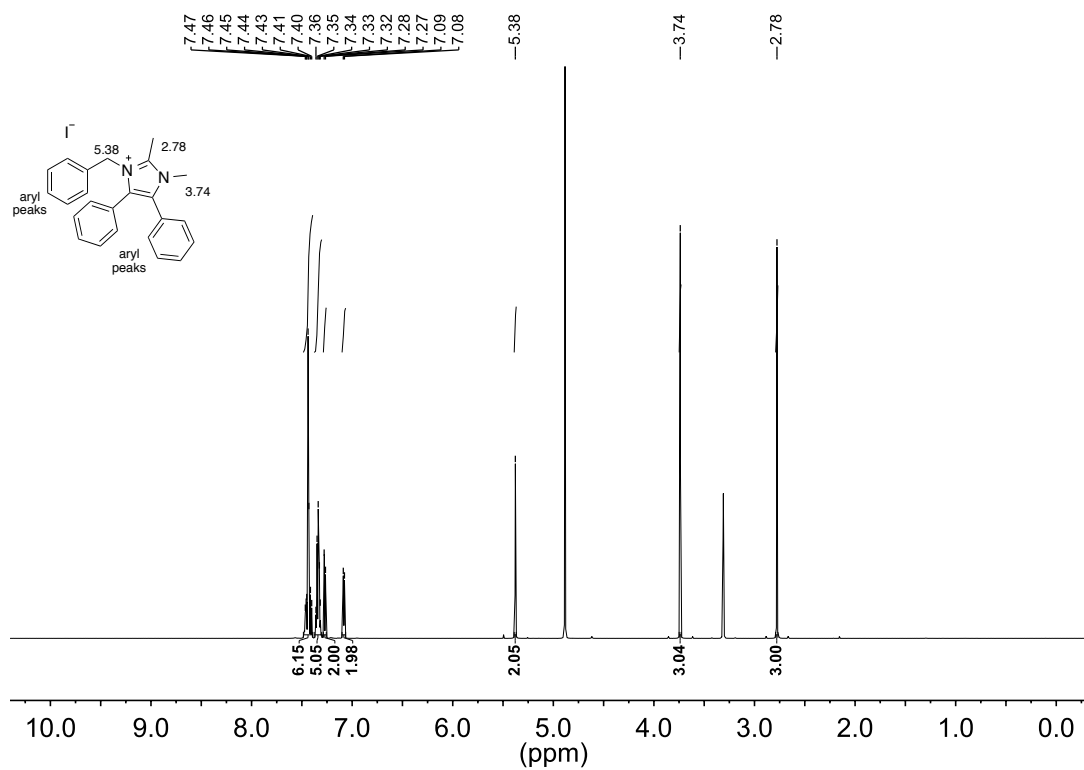


^{13}C NMR spectrum (126 MHz, CD_3OD)

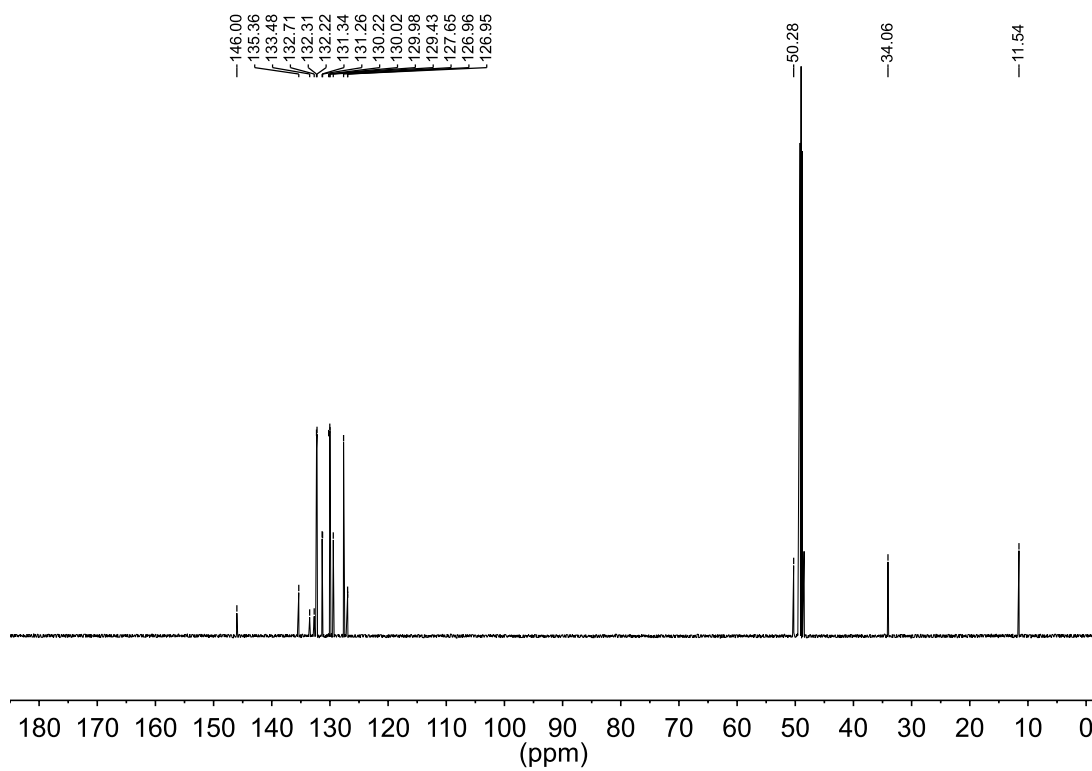


1-Benzyl-2,3-dimethyl-4,5-diphenylimidazolium iodide (4d)

^1H NMR spectrum (600 MHz, CD_3OD)

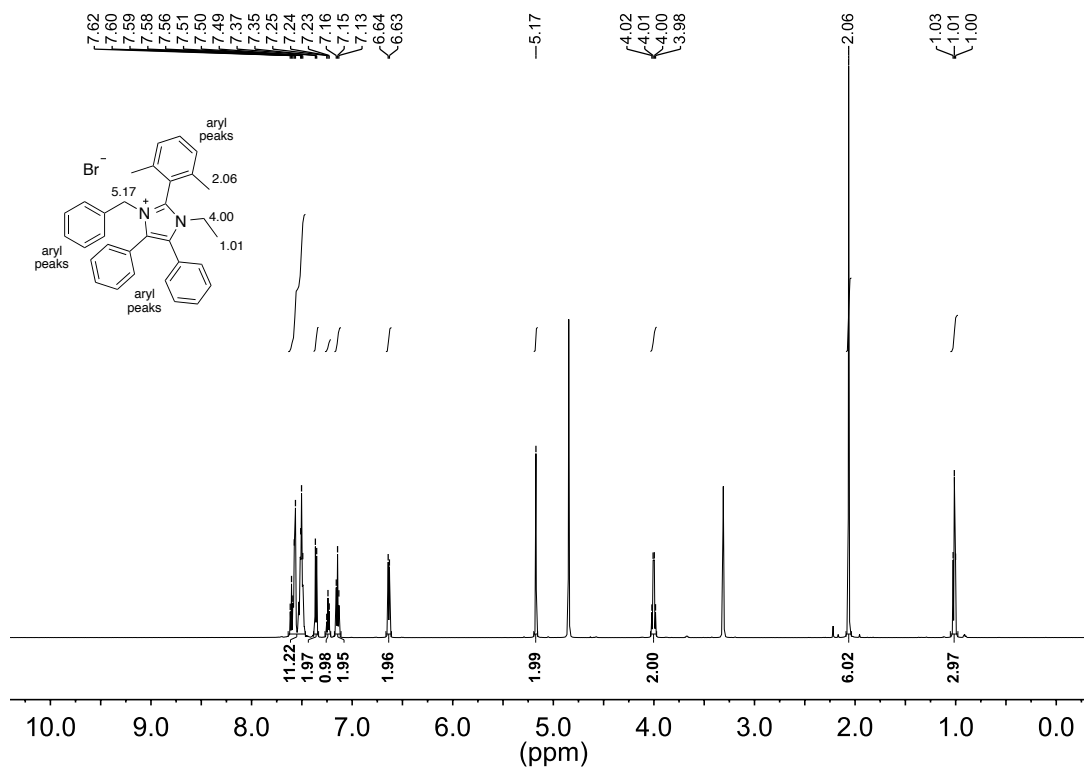


^{13}C NMR spectrum (126 MHz, CD_3OD)

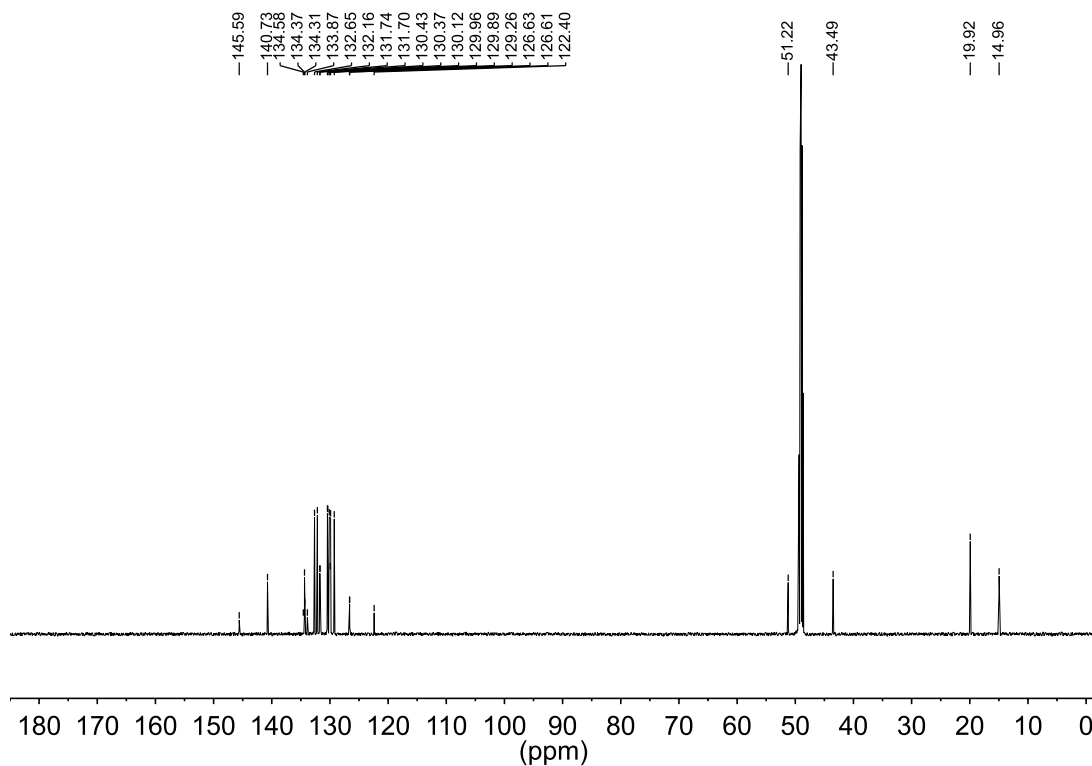


1-Benzyl-2-(2,6-dimethylphenyl)-3-ethyl-4,5-diphenylimidazolium bromide (5a)

^1H NMR spectrum (600 MHz, CD_3OD)

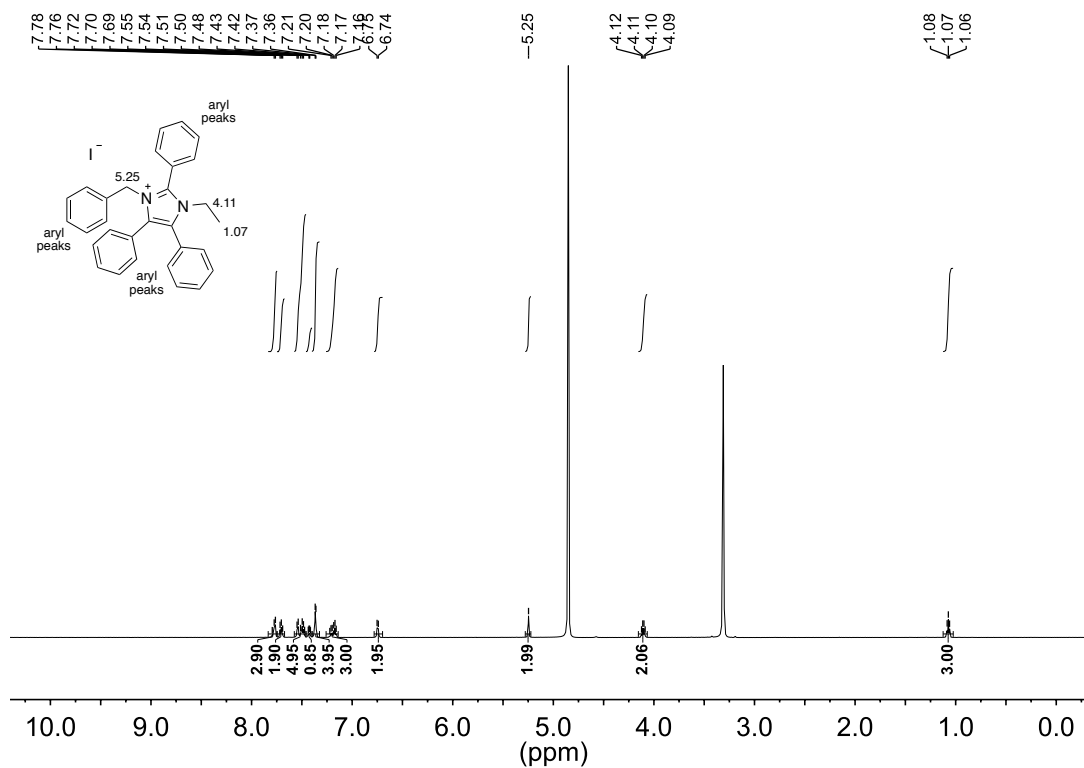


^{13}C NMR spectrum (126 MHz, CD_3OD)

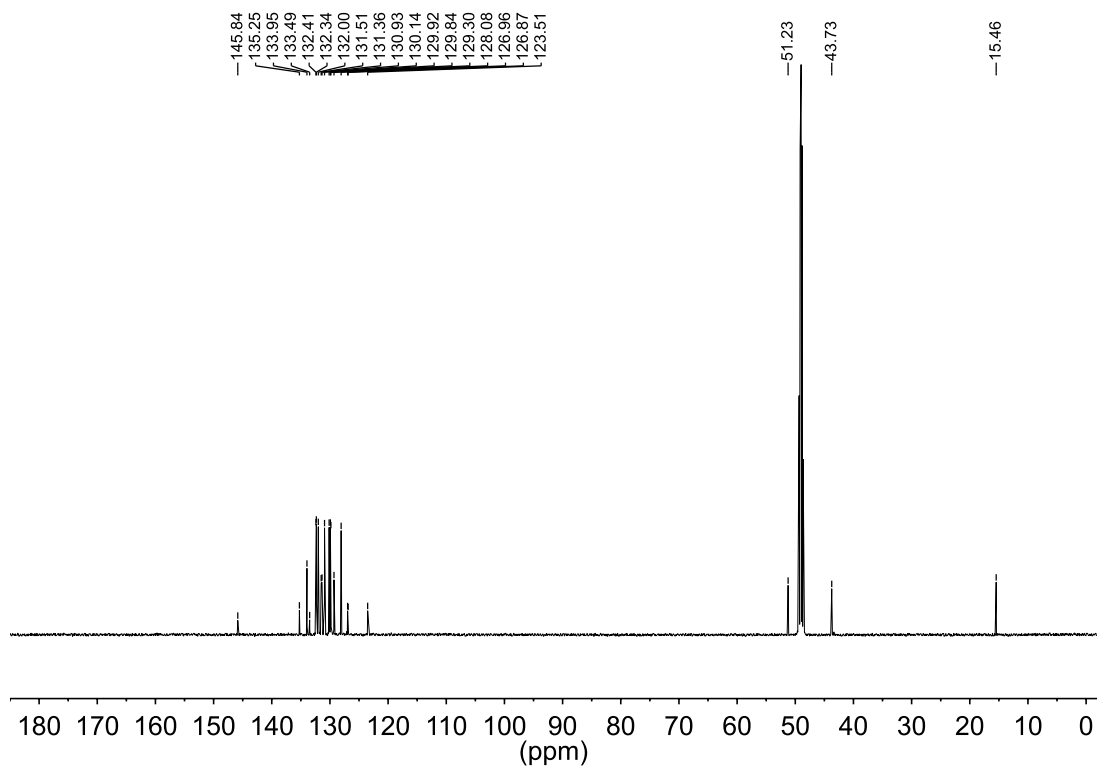


1-Benzyl-3-ethyl-2,4,5-triphenylimidazolium iodide (5b)

^1H NMR spectrum (600 MHz, CD_3OD)

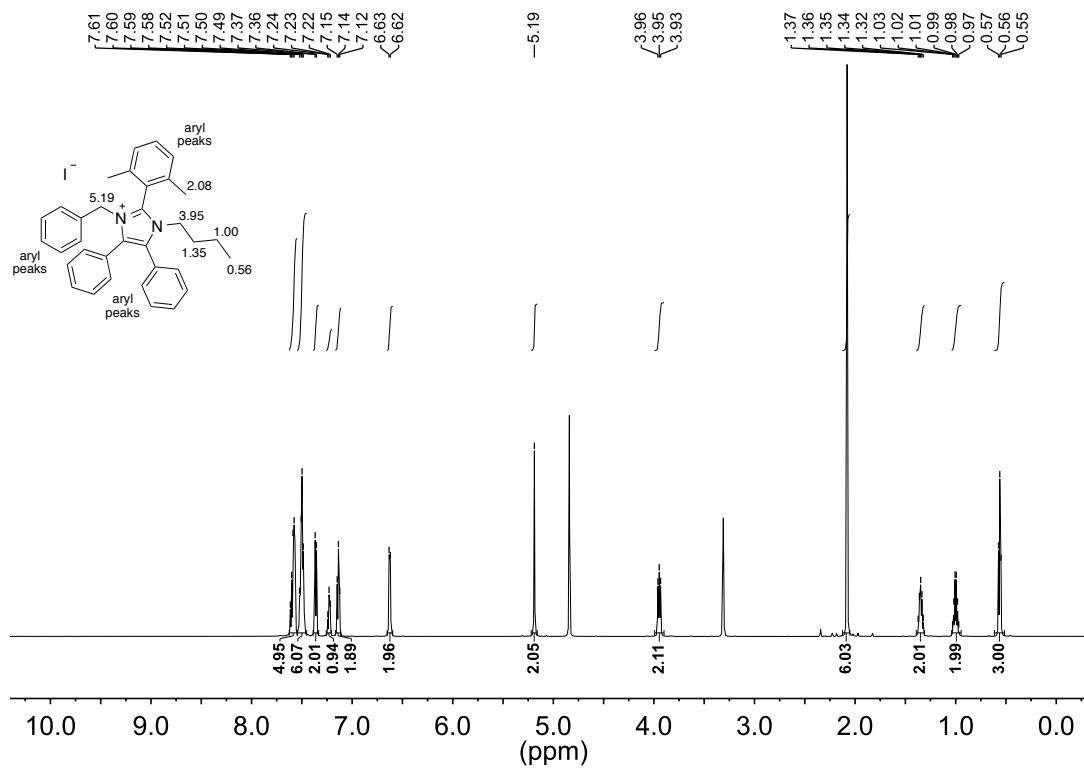


^{13}C NMR spectrum (126 MHz, CD_3OD)

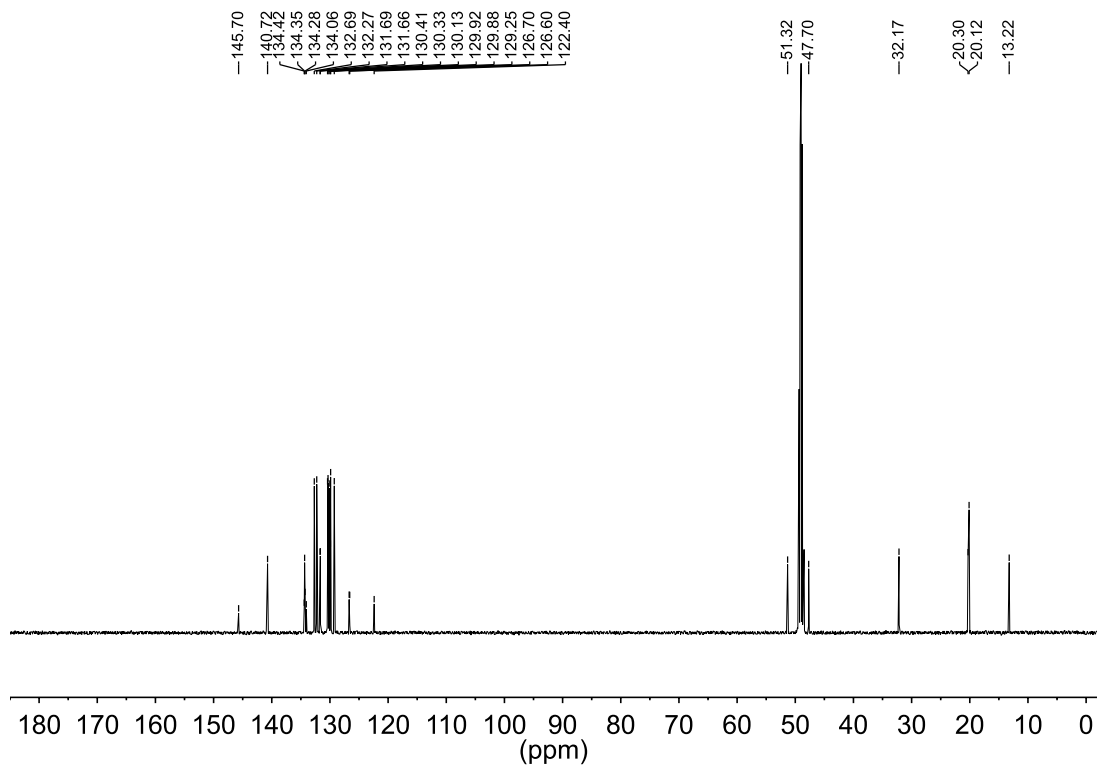


1-Benzyl-3-*n*-butyl-2-(2,6-dimethylphenyl)-4,5-diphenylimidazolium iodide (6a)

¹H NMR spectrum (600 MHz, CD₃OD)

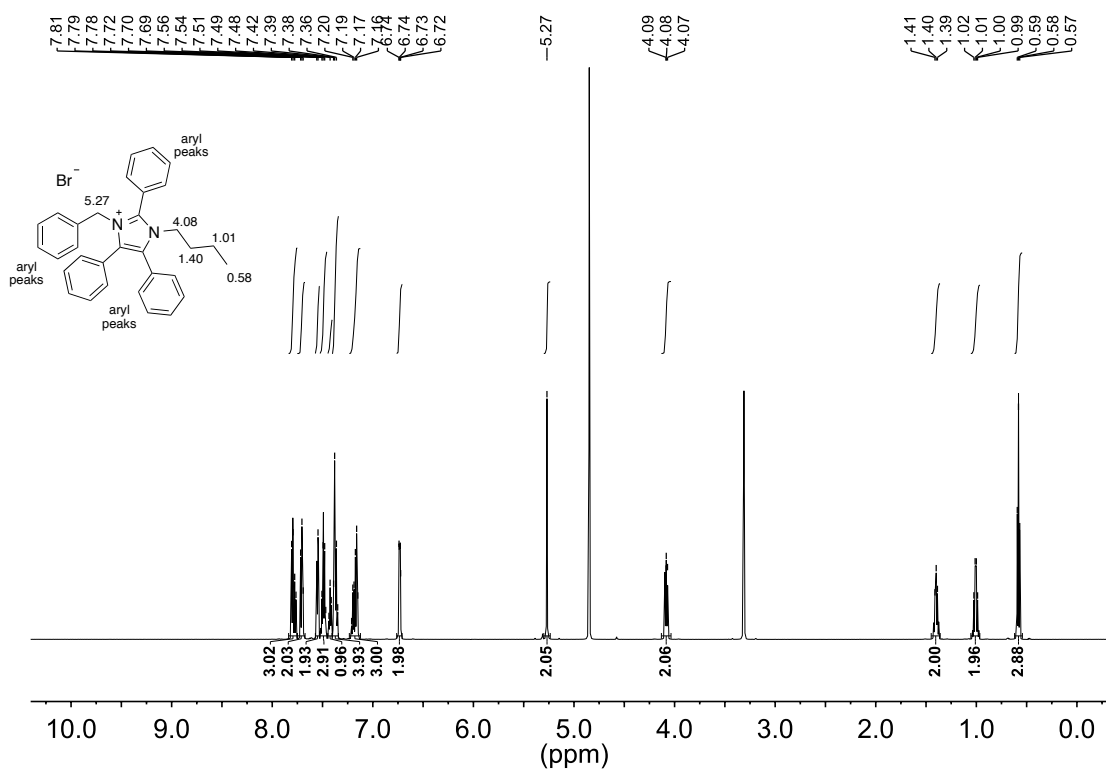


¹³C NMR spectrum (126 MHz, CD₃OD)

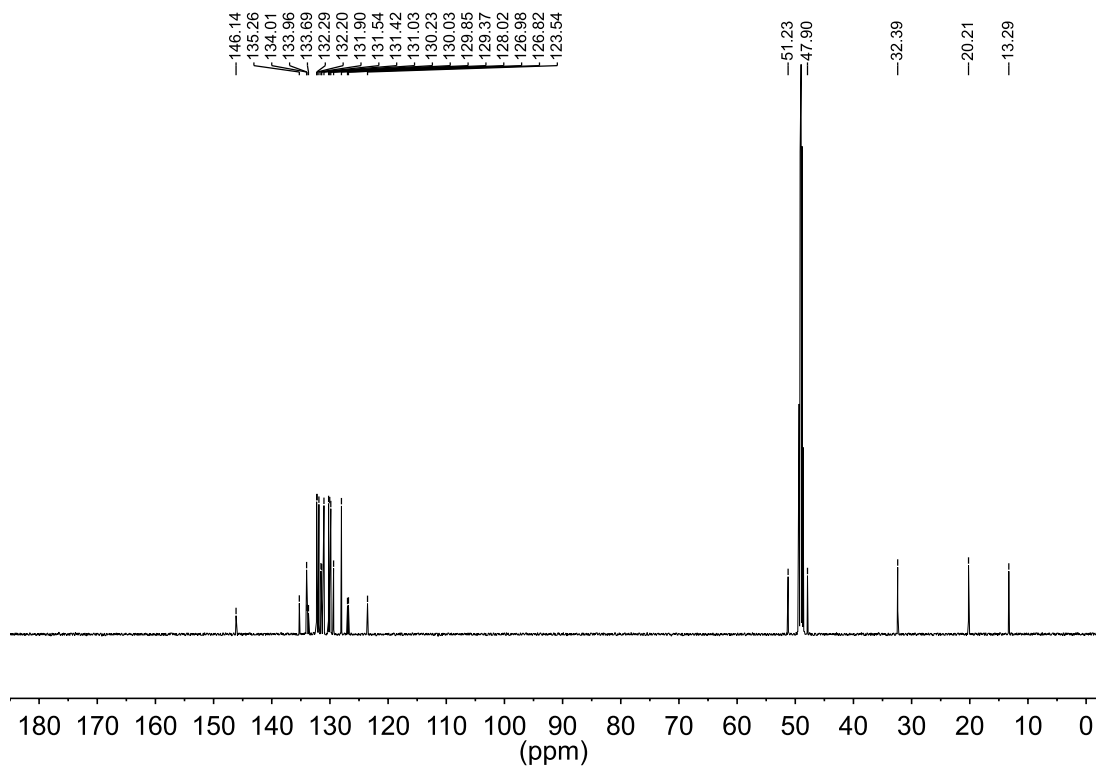


1-Benzyl-3-*n*-butyl-2,4,5-triphenylimidazolium bromide (6b)

^1H NMR spectrum (600 MHz, CD_3OD)

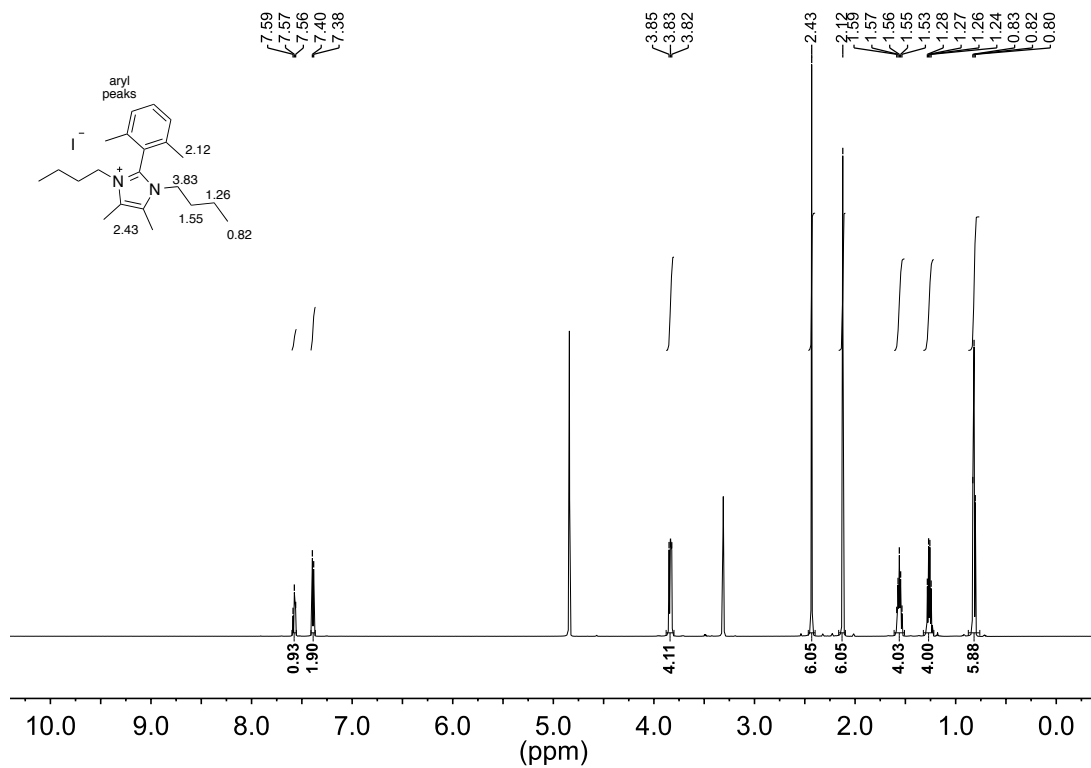


^{13}C NMR spectrum (126 MHz, CD_3OD)

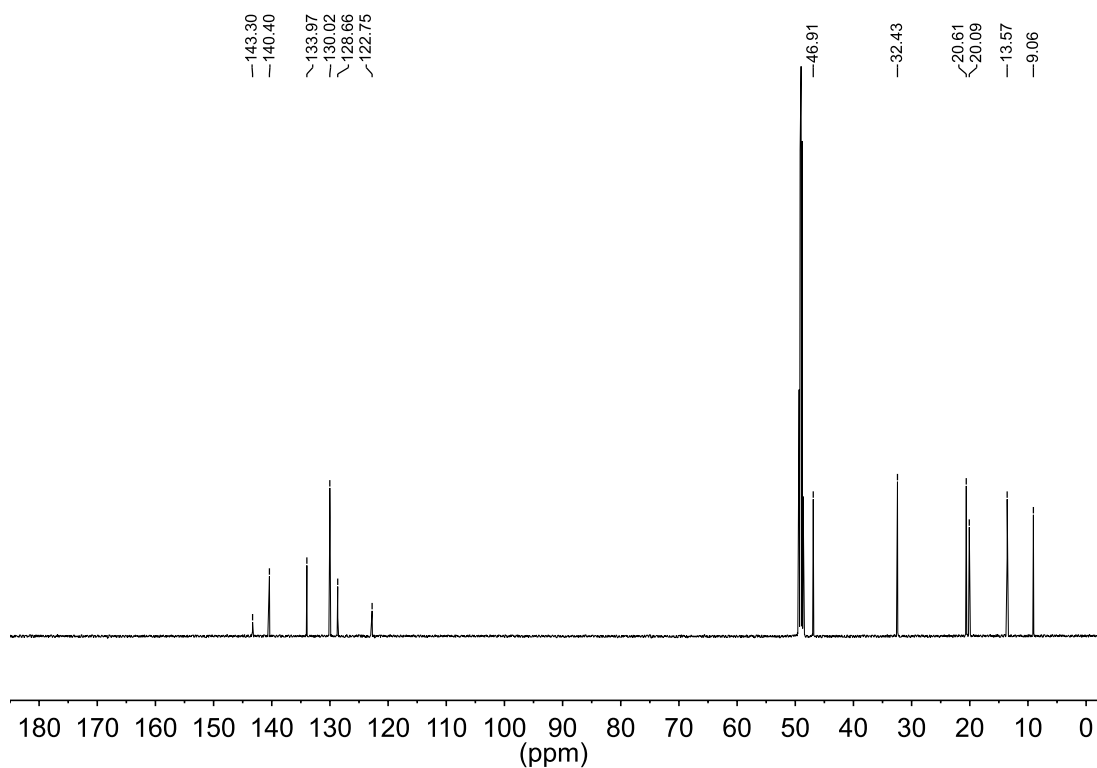


1,3-Di-*n*-butyl-2-(2,6-dimethylphenyl)-4,5-dimethylimidazolium iodide (7a)

^1H NMR spectrum (600 MHz, CD_3OD)

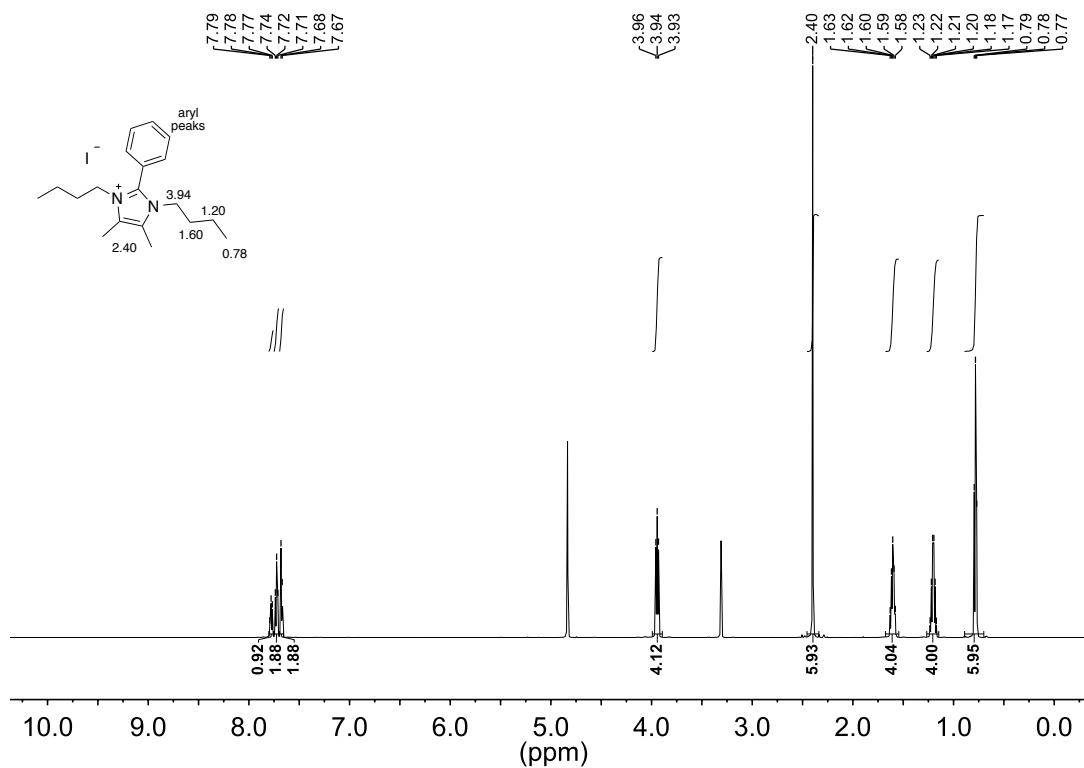


^{13}C NMR spectrum (126 MHz, CD_3OD)

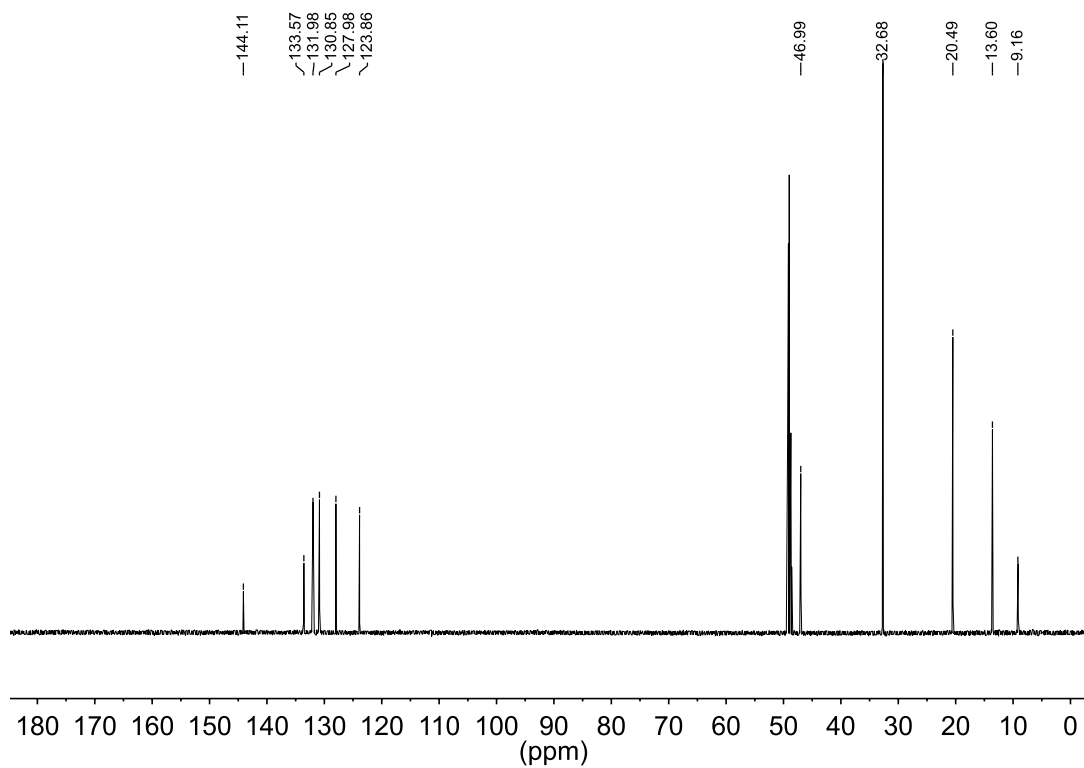


1,3-Di-*n*-butyl-4,5-dimethyl-2-phenylimidazolium iodide (7b)

¹H NMR spectrum (600 MHz, CD₃OD)

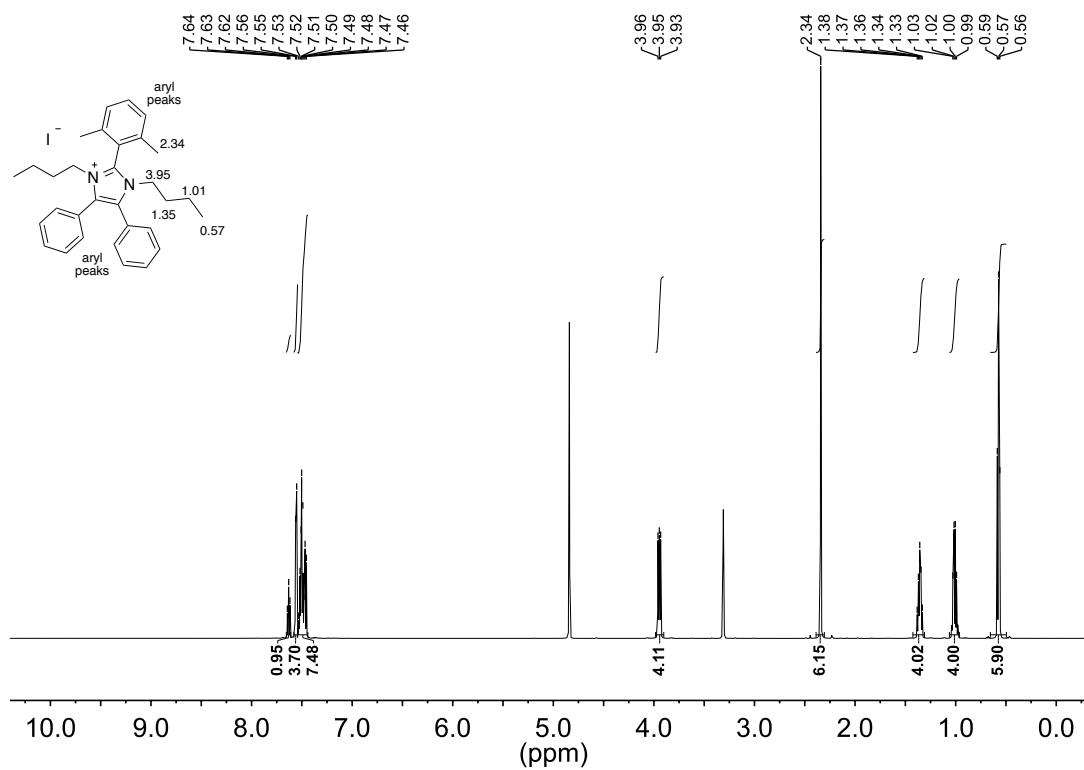


¹³C NMR spectrum (126 MHz, CD₃OD)

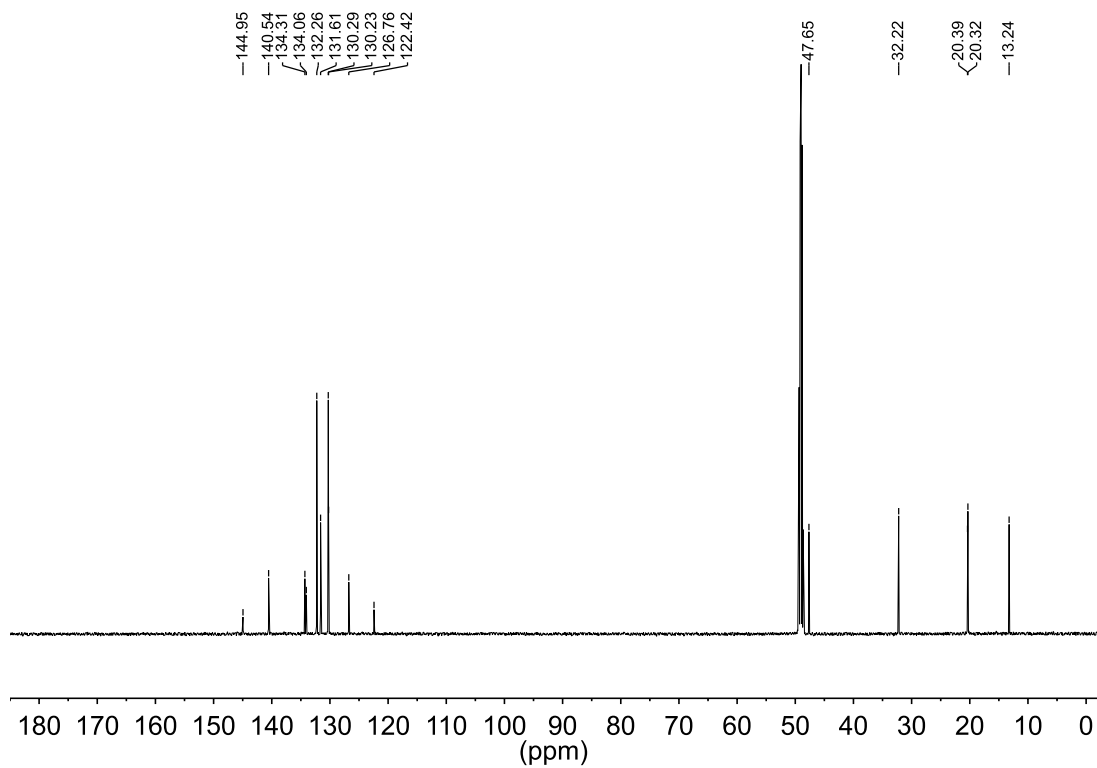


1,3-Di-*n*-butyl-2-(2,6-dimethylphenyl)-4,5-diphenylimidazolium iodide (8a)

¹H NMR spectrum (600 MHz, CD₃OD)

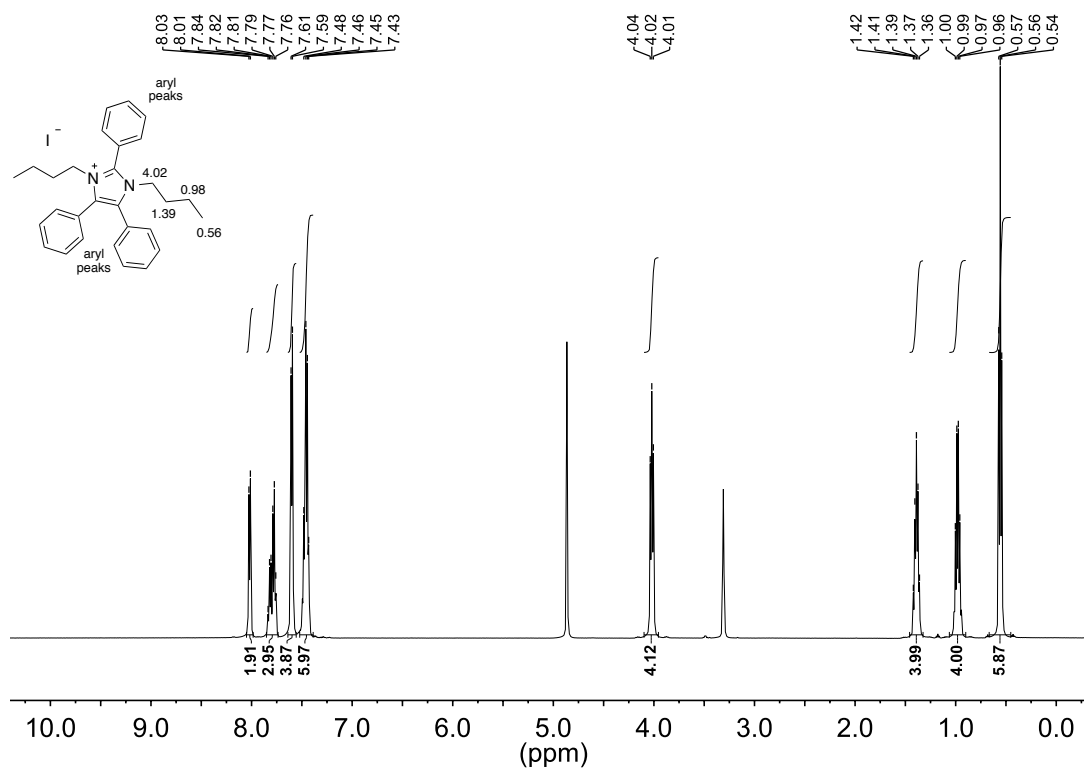


¹³C NMR spectrum (126 MHz, CD₃OD)

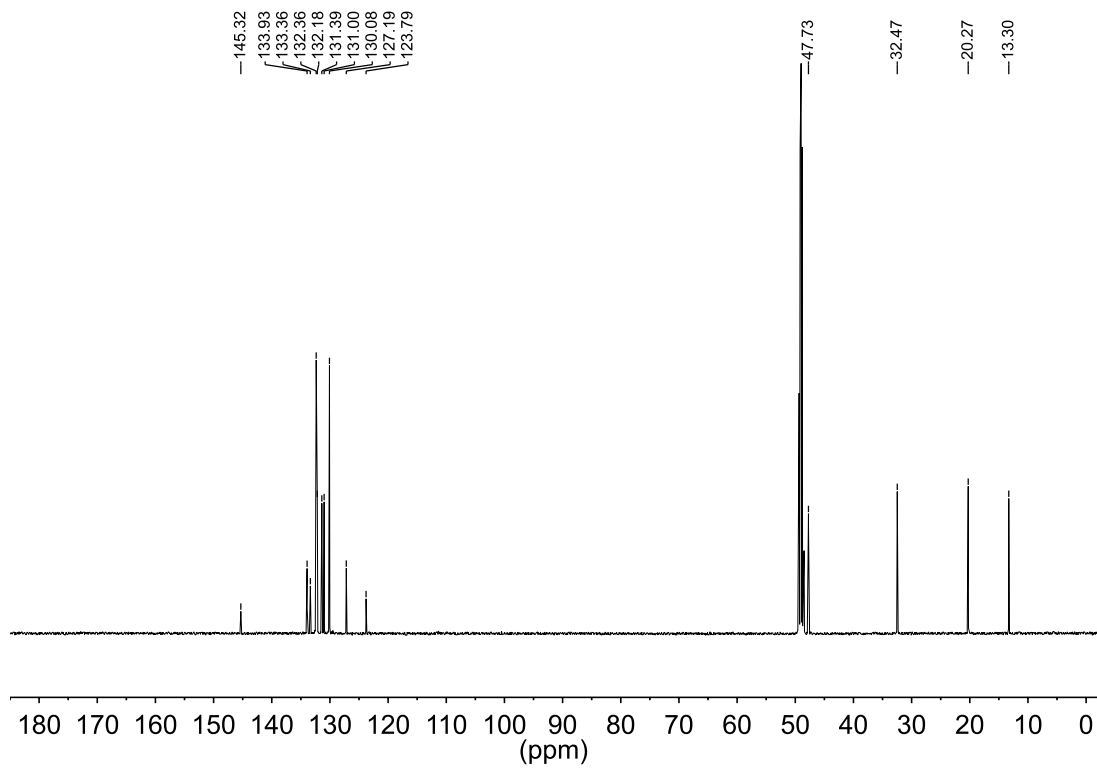


1,3-Di-*n*-butyl-2,4,5-triphenylimidazolium iodide (8b)

^1H NMR spectrum (500 MHz, CD_3OD)



^{13}C NMR spectrum (126 MHz, CD_3OD)



4.5.5 Copies of ¹H NMR Spectra for Model Compound Studies

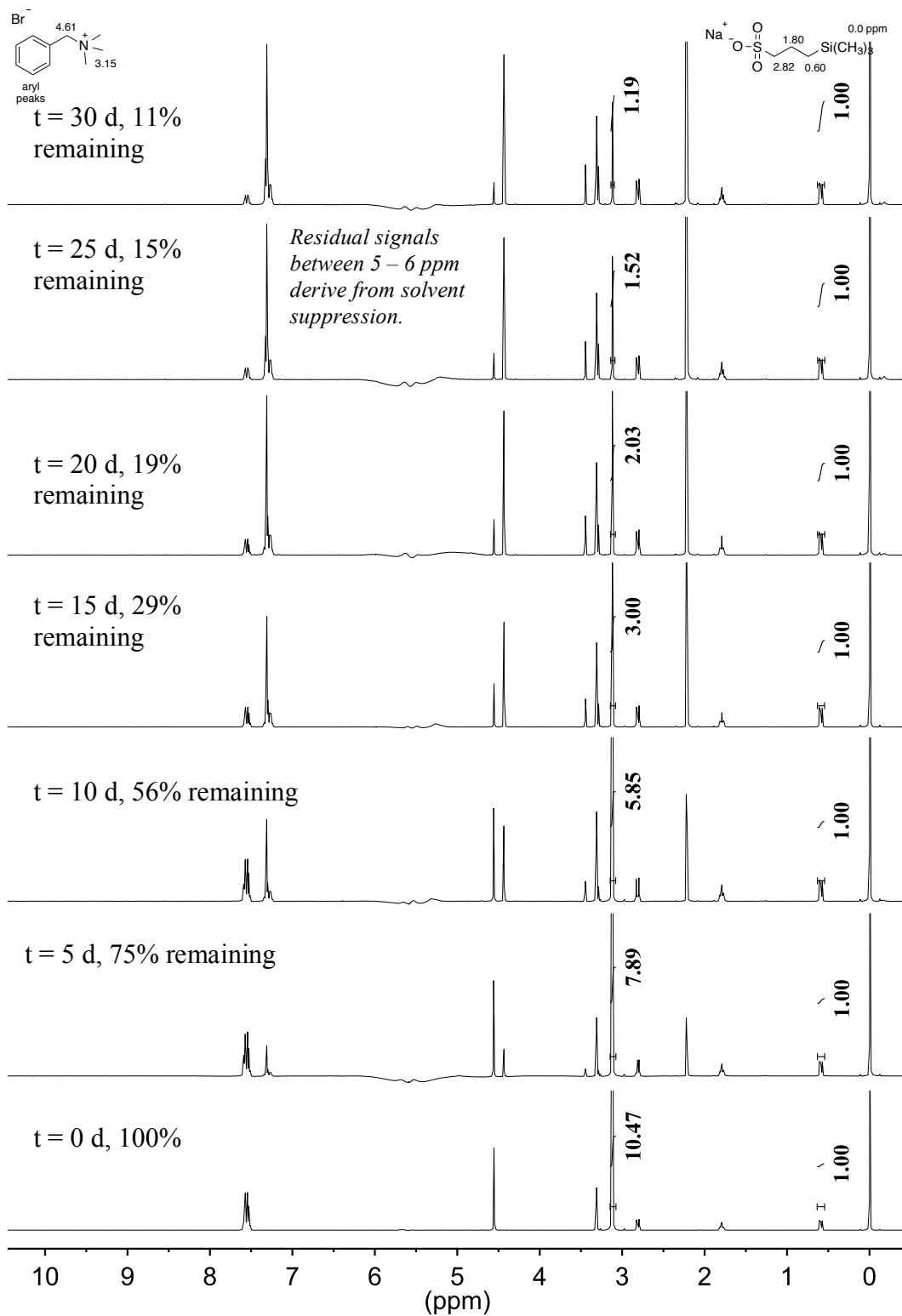


Figure 4.11 ^1H NMR spectra of **1** over 30 days dissolved in a basic CD_3OH solution at 80°C (1 M KOH, $[\text{KOH}]/[\mathbf{1}] = 20$ with an internal standard ($\text{TMS}(\text{CH}_2)_3\text{SO}_3\text{Na}$).

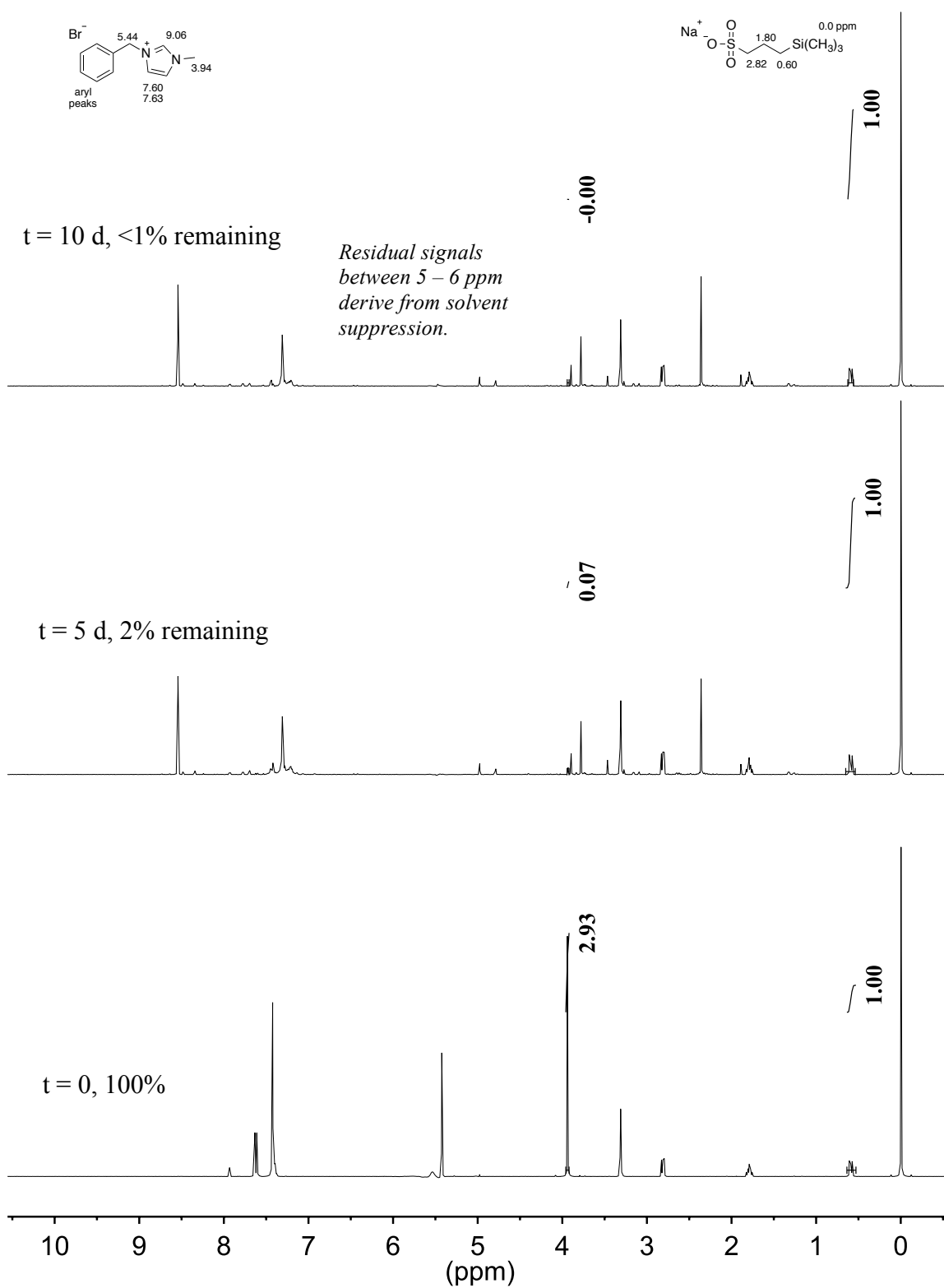


Figure 4.12. ^1H NMR spectra of **2a** over 10 days dissolved in a basic CD_3OH solution at $80\text{ }^\circ\text{C}$ (1 M KOH, $[\text{KOH}]/[\text{2a}] = 20$) with an internal standard ($\text{TMS}(\text{CH}_2)_3\text{SO}_3\text{Na}$).

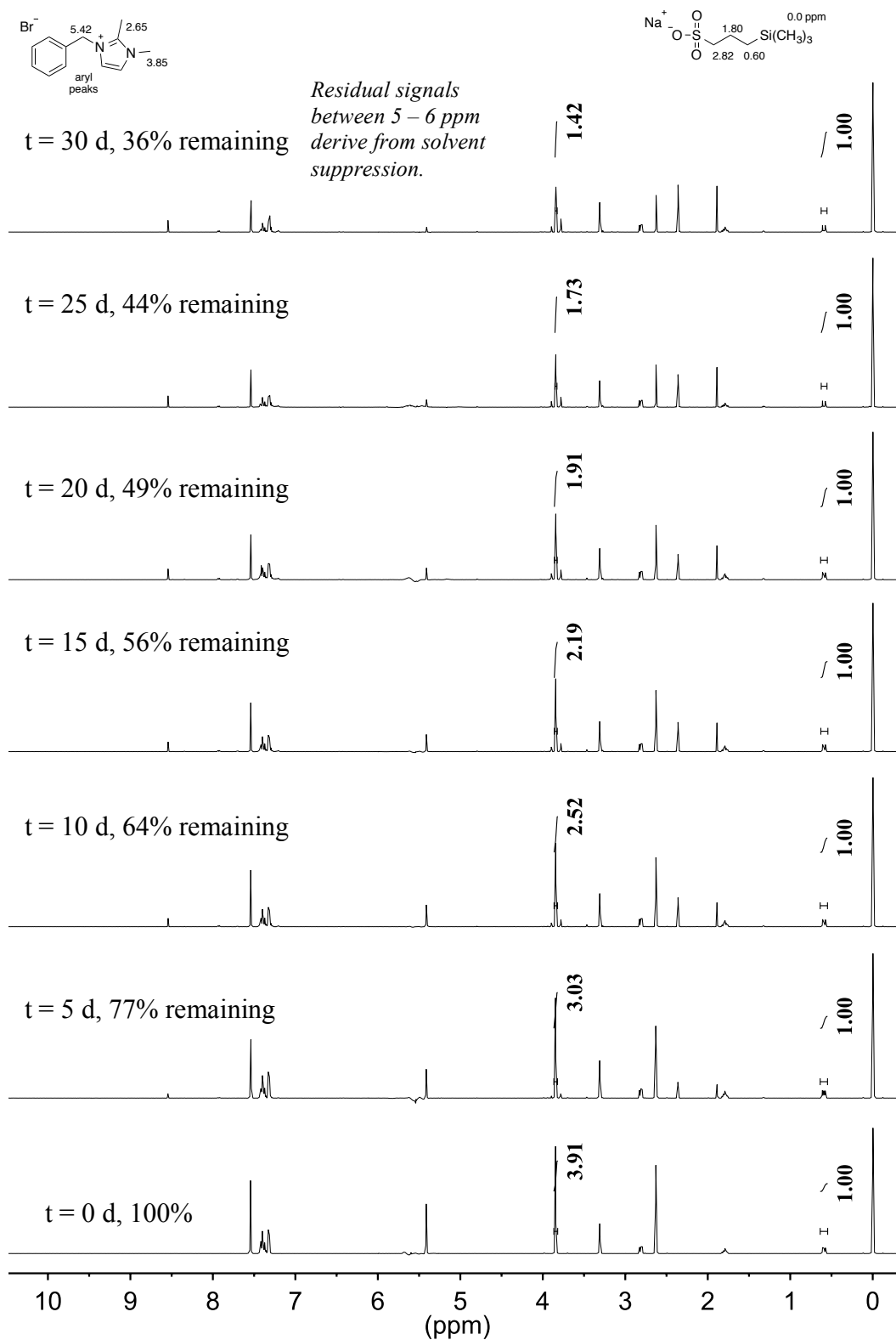


Figure 4.13 ¹H NMR spectra of **2b** over 30 days dissolved in a basic CD₃OH solution at 80 °C (1 M KOH, [KOH]/[**2b**] = 20) with an internal standard (TMS(CH₂)₃SO₃Na).

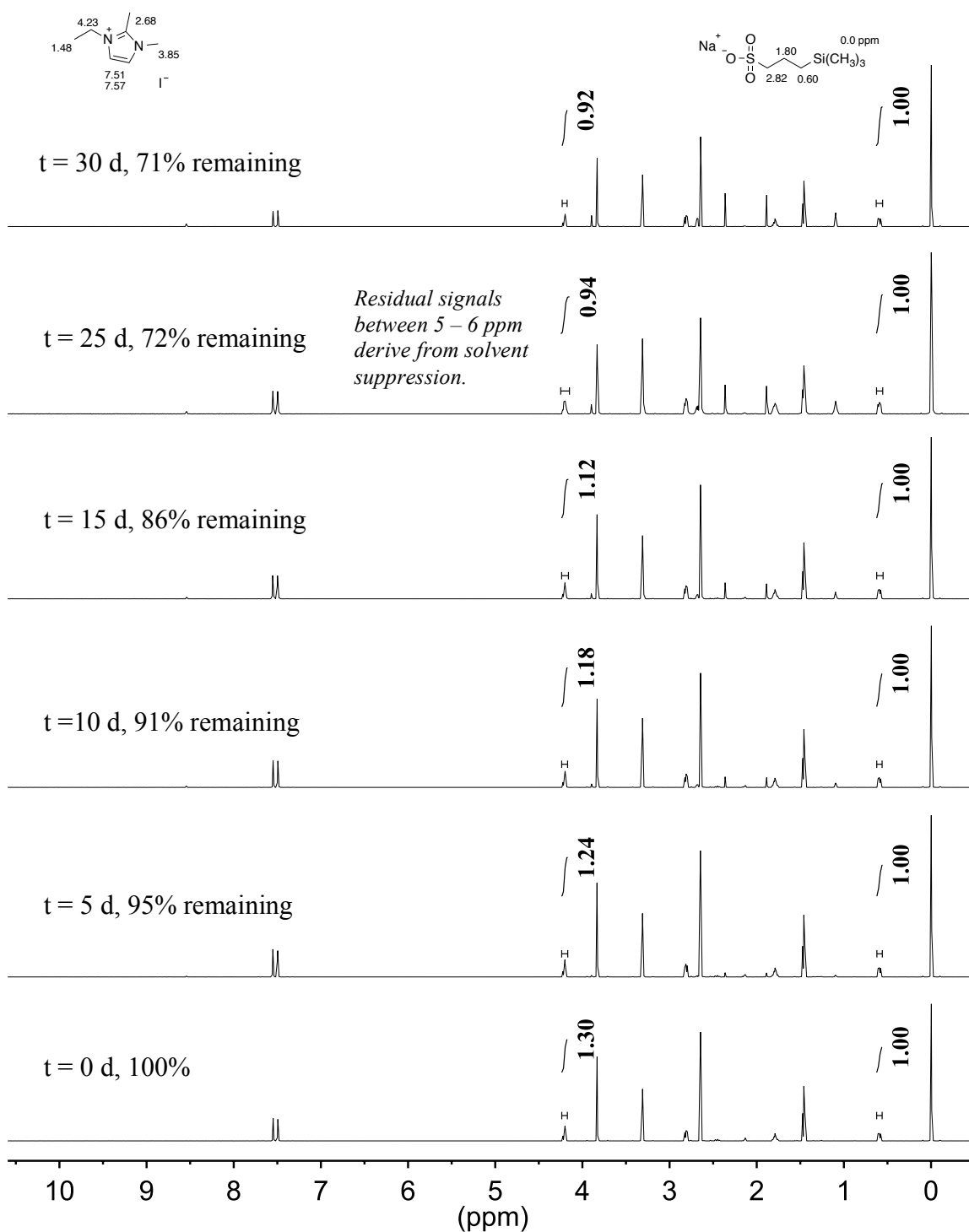


Figure 4.14 ^1H NMR spectra of **2c** over 30 days dissolved in a basic CD_3OH solution at $80\text{ }^\circ\text{C}$ (1 M KOH, $[\text{KOH}]/[\text{2c}] = 20$) with an internal standard ($\text{TMS}(\text{CH}_2)_3\text{SO}_3\text{Na}$).

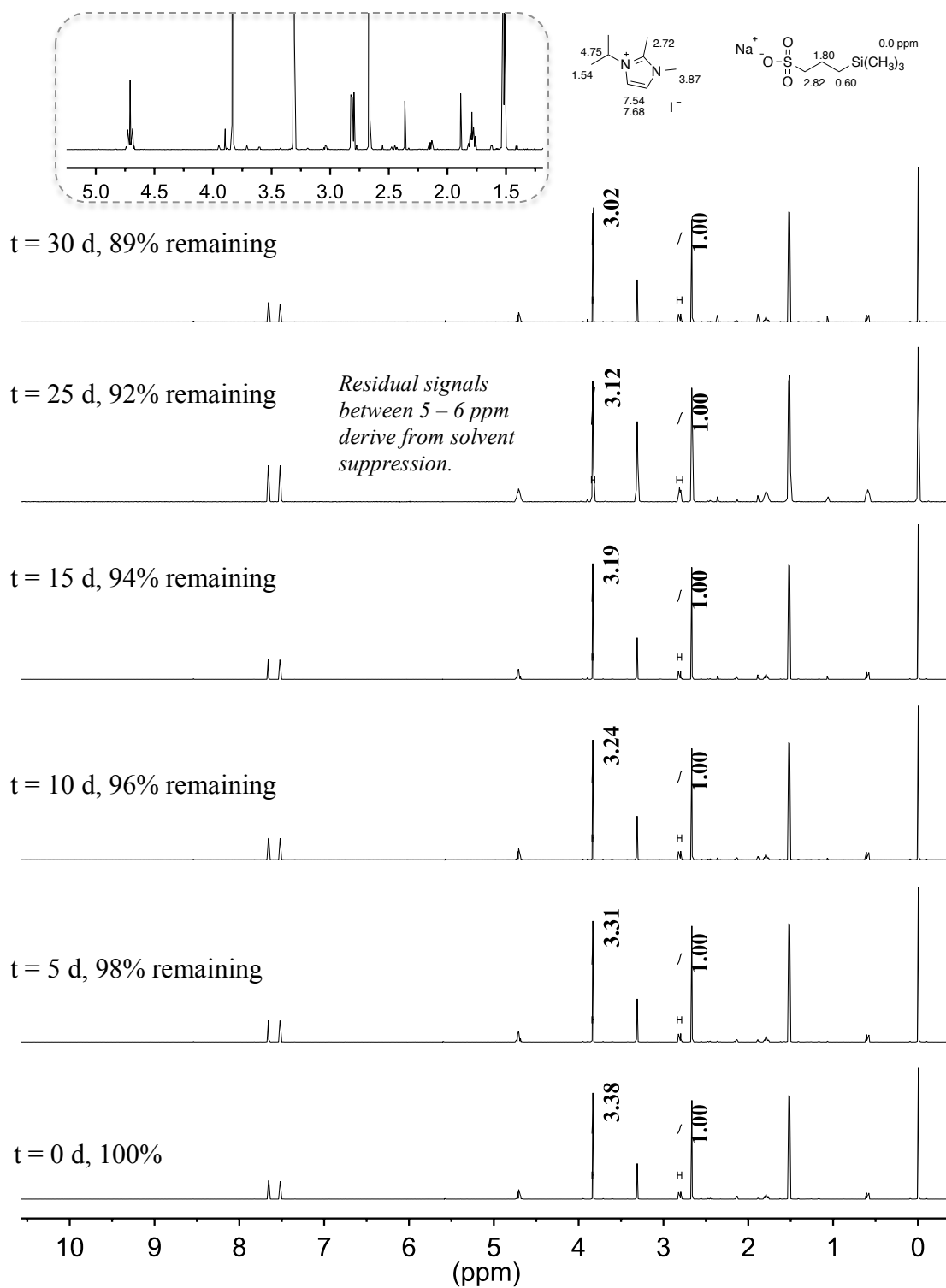


Figure 4.15 ^1H NMR spectra of **2d** over 30 days dissolved in a basic CD_3OH solution at 80°C (1 M KOH, $[\text{KOH}]/[\text{2d}] = 20$) with an internal standard (TMS(CH_2) $_3\text{SO}_3\text{Na}$). Inset is extracted from $t = 30$ d.

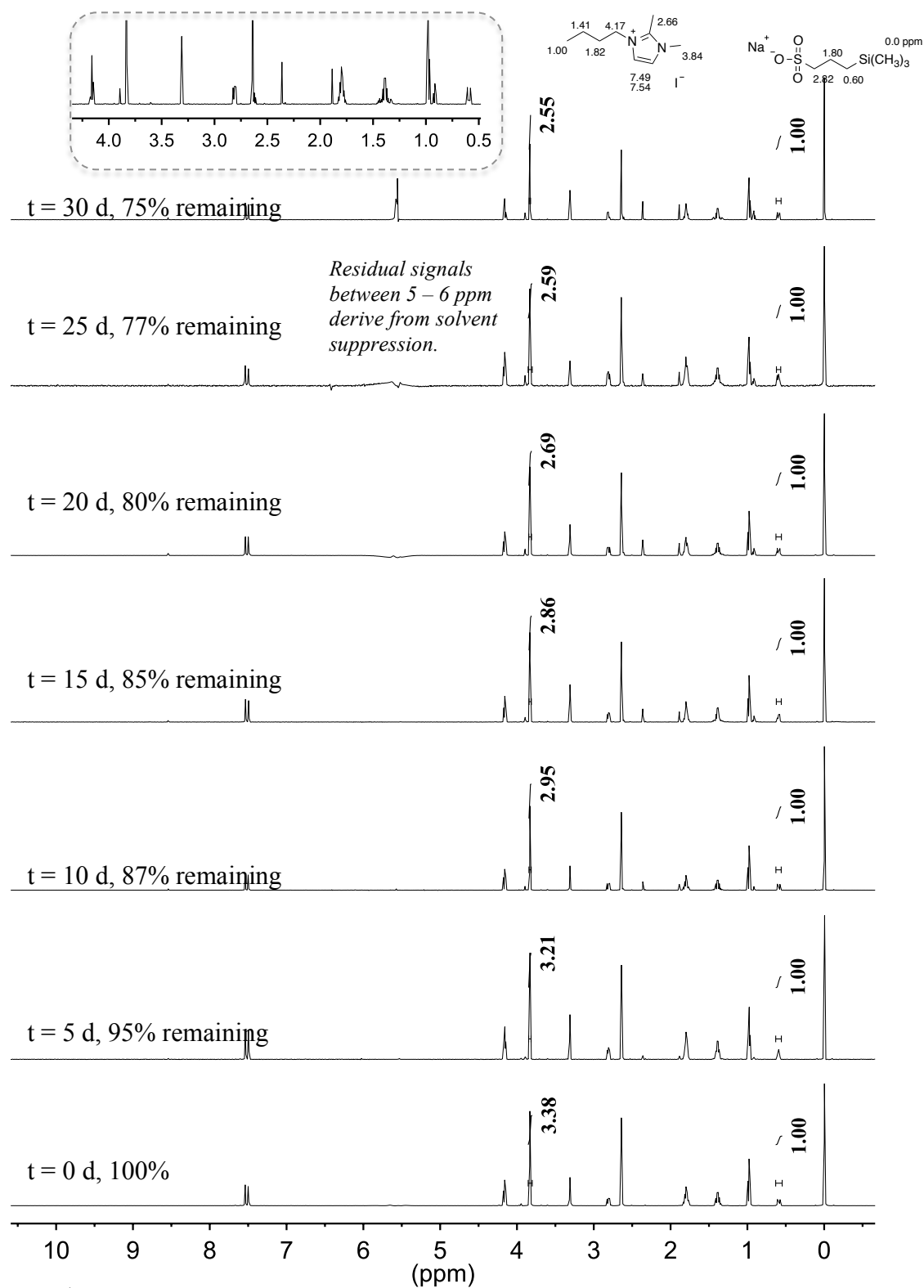


Figure 4.16 ^1H NMR spectra of **2e** over 30 days dissolved in a basic CD_3OH solution at 80°C (1 M KOH, $[\text{KOH}]/[\text{2e}] = 20$) with an internal standard (TMS(CH_2) $_3$ SO $_3$ Na). Inset is extracted from t = 30 d.

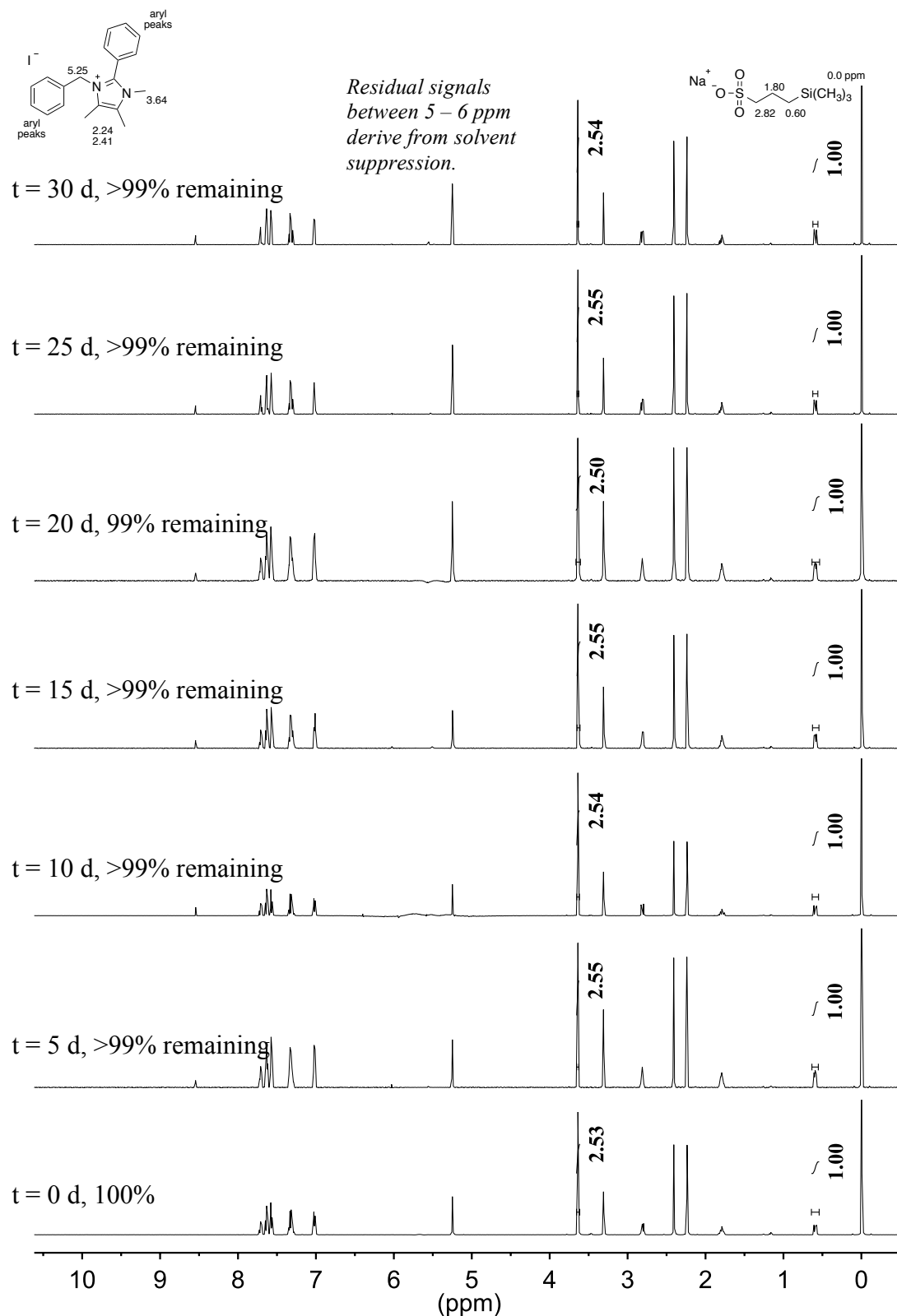


Figure 4.17 ¹H NMR spectra of **3a** over 30 days dissolved in a basic CD₃OH solution at 80 °C (1 M KOH, [KOH]/[**3a**] = 20) with an internal standard (TMS(CH₂)₃SO₃Na).

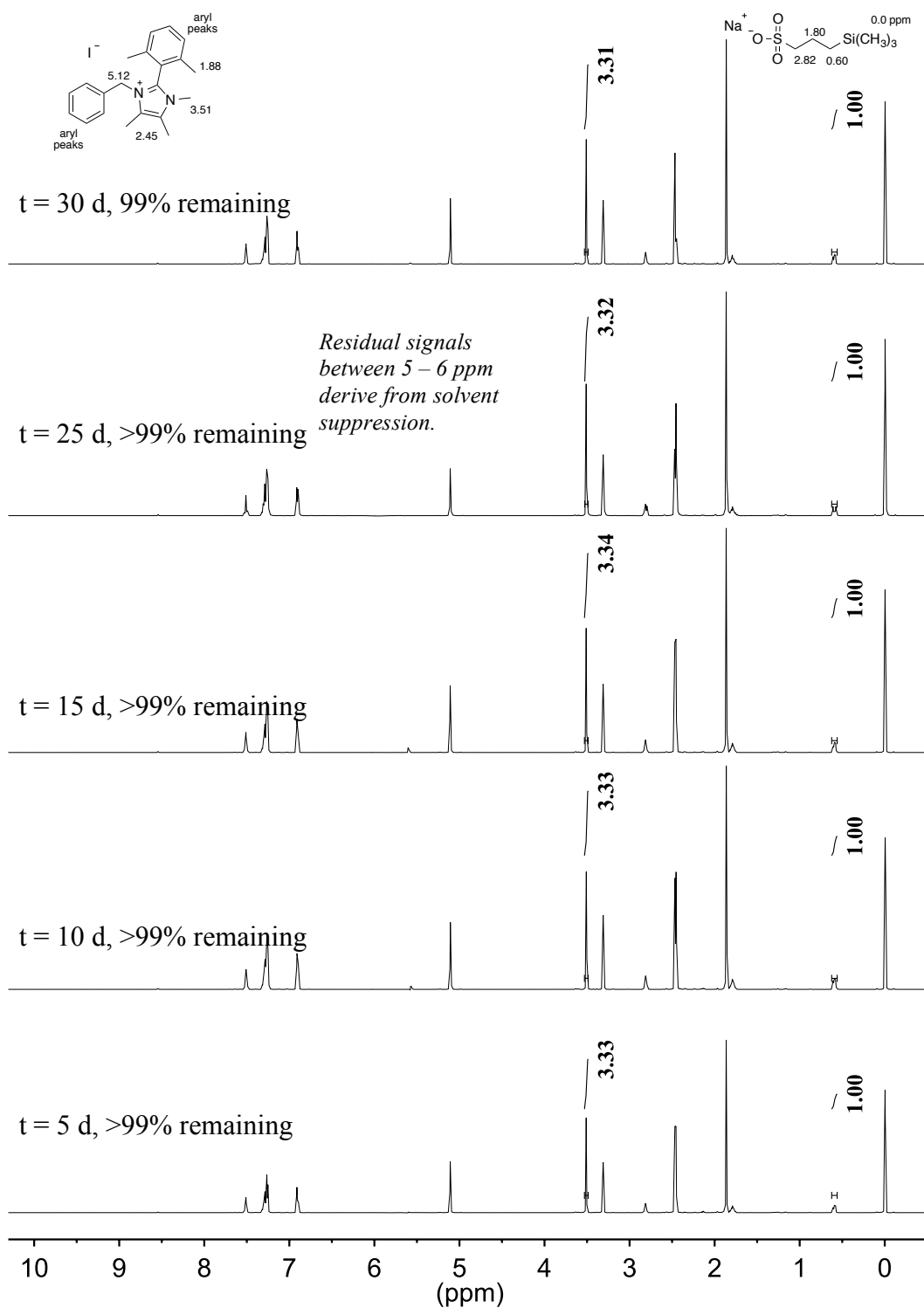


Figure 4.18 ^1H NMR spectra of **3b** over 30 days dissolved in a basic CD_3OH solution at 80°C (1 M KOH, $[\text{KOH}]/[\text{3b}] = 20$) with an internal standard ($\text{TMS}(\text{CH}_2)_3\text{SO}_3\text{Na}$).

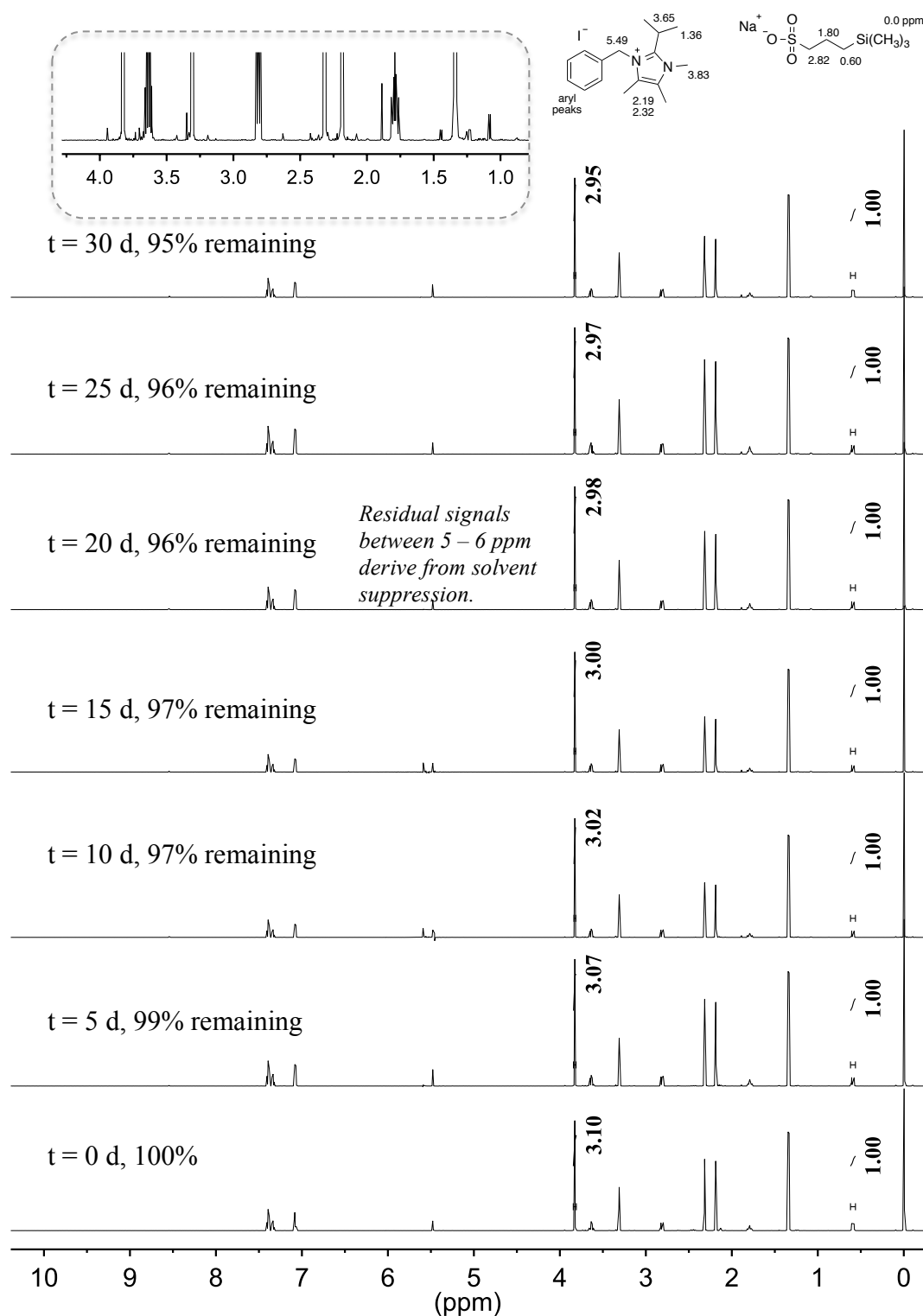


Figure 4.19 ¹H NMR spectra of **3c** over 30 days dissolved in a basic CD₃OH solution at 80 °C (1 M KOH, [KOH]/[**3c**] = 20) with an internal standard (TMS(CH₂)₃SO₃Na). Inset is extracted from t = 30 d.

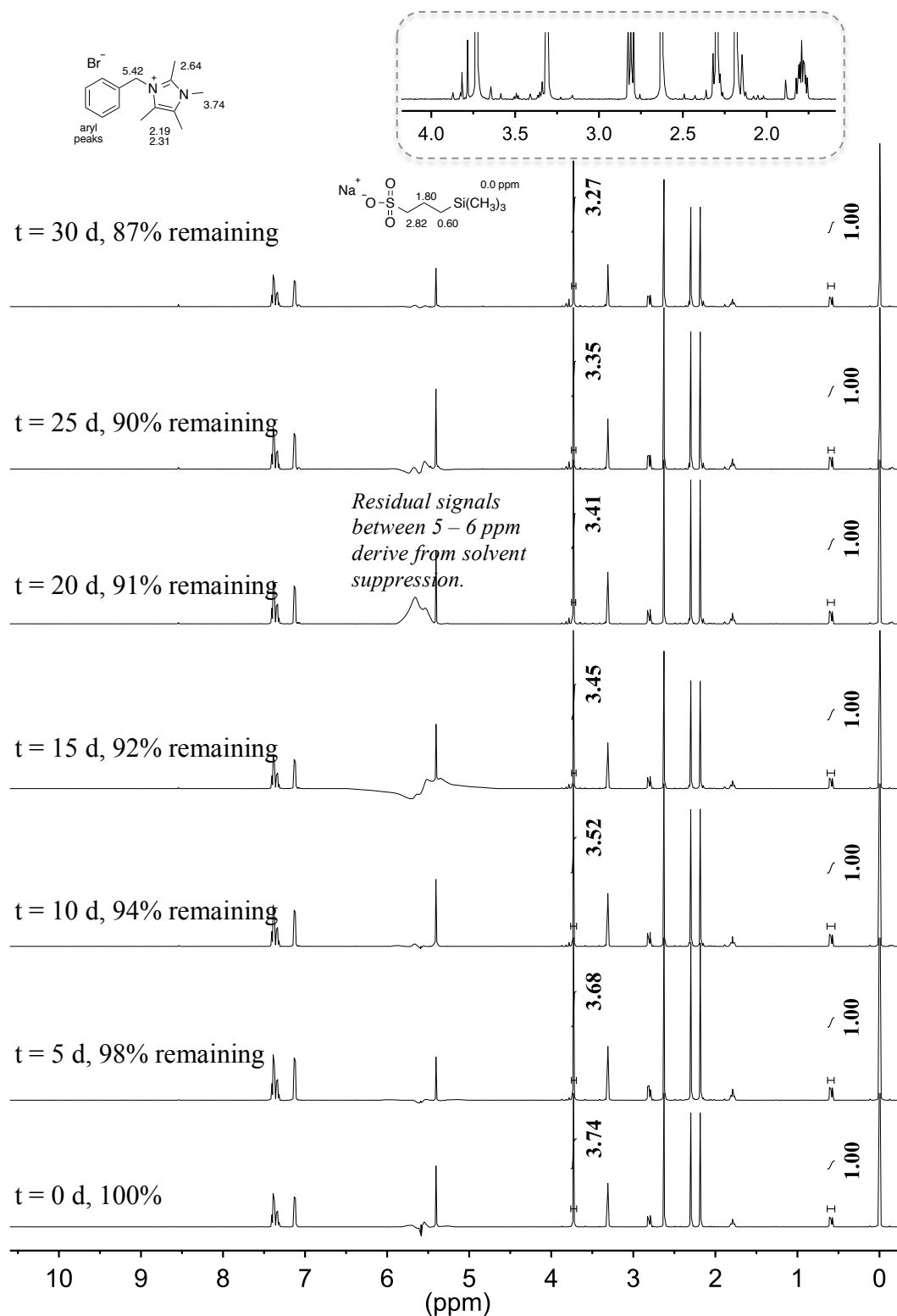


Figure 4.20 ^1H NMR spectra of **3d** over 30 days dissolved in a basic CD_3OH solution at $80\text{ }^\circ\text{C}$ (1 M KOH, $[\text{KOH}]/[\text{3d}] = 20$) with an internal standard ($\text{TMS}(\text{CH}_2)_3\text{SO}_3\text{Na}$). Inset is extracted from $t = 30$ d.

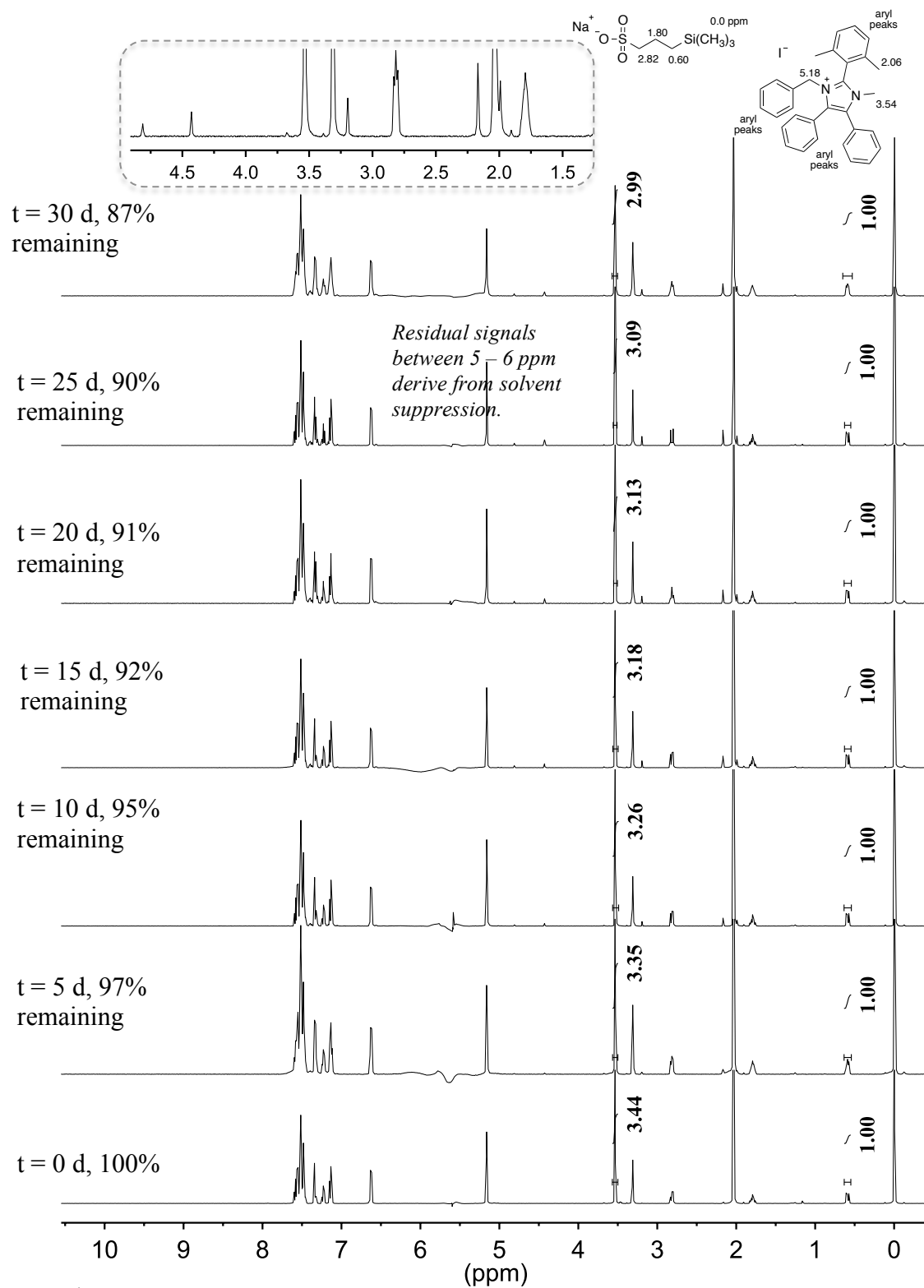


Figure 4.21 ^1H NMR spectra of **4a** over 30 days dissolved in a basic CD_3OH solution at 80°C (1 M KOH, $[\text{KOH}]/[\text{4a}] = 20$) with an internal standard ($\text{TMS}(\text{CH}_2)_3\text{SO}_3\text{Na}$). Inset is extracted from $t = 30$ d.

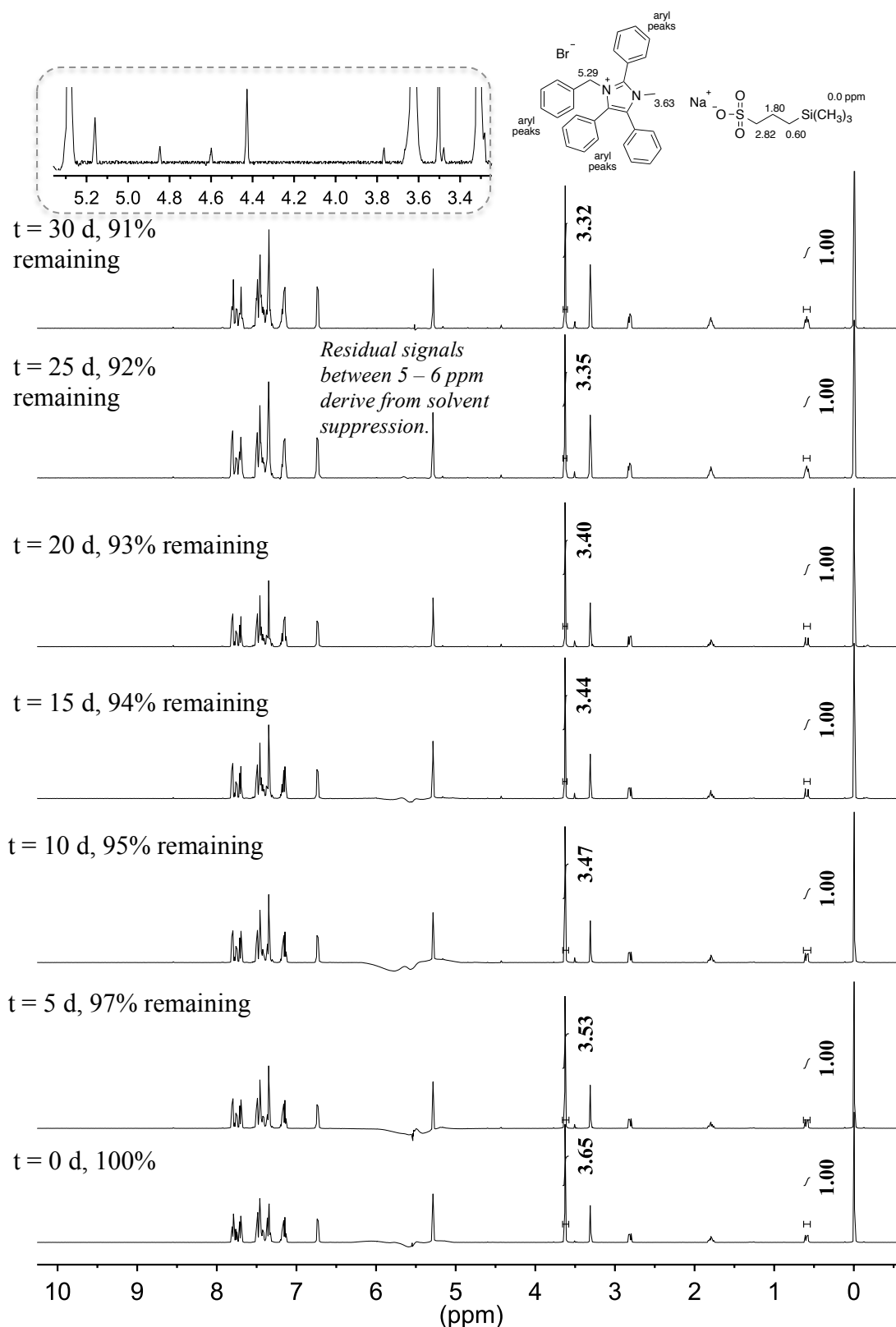


Figure 4.22 ¹H NMR spectra of **4b** over 30 days dissolved in a basic CD₃OH solution at 80 °C (1 M KOH, [KOH]/[**4b**] = 20) with an internal standard (TMS(CH₂)₃SO₃Na). Inset is extracted from t = 30 d.

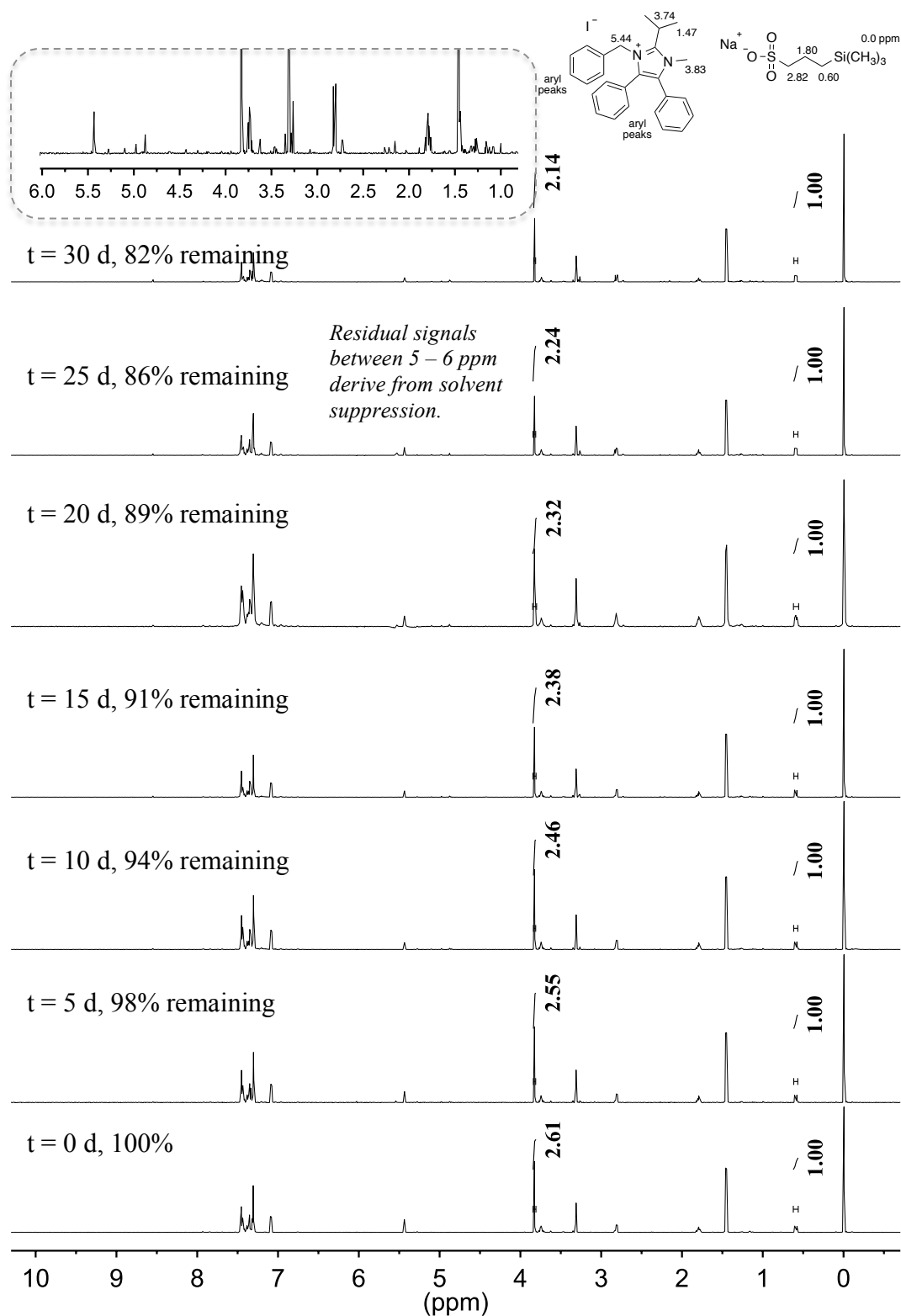


Figure 4.23 ^1H NMR spectra of **4c** over 30 days dissolved in a basic CD_3OH solution at 80°C (1 M KOH, $[\text{KOH}]/[\text{4c}] = 20$) with an internal standard ($\text{TMS}(\text{CH}_2)_3\text{SO}_3\text{Na}$). Inset is extracted from $t = 30$ d.

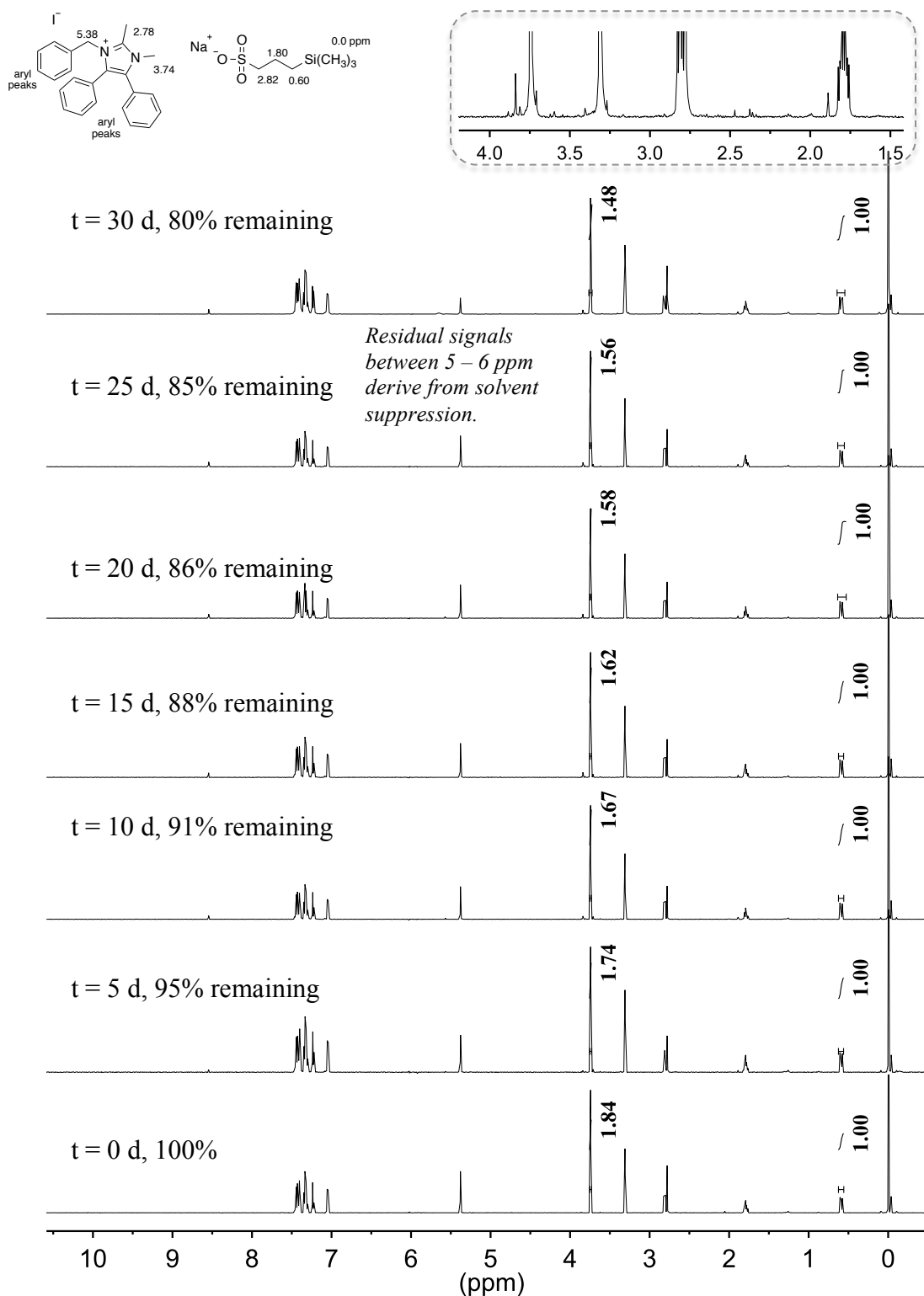


Figure 4.24 ^1H NMR spectra of **4d** over 30 days dissolved in a basic CD_3OH solution at $80\text{ }^\circ\text{C}$ (1 M KOH, $[\text{KOH}]/[\text{4d}] = 20$) with an internal standard ($\text{TMS}(\text{CH}_2)_3\text{SO}_3\text{Na}$). Inset is extracted from $t = 30$ d.

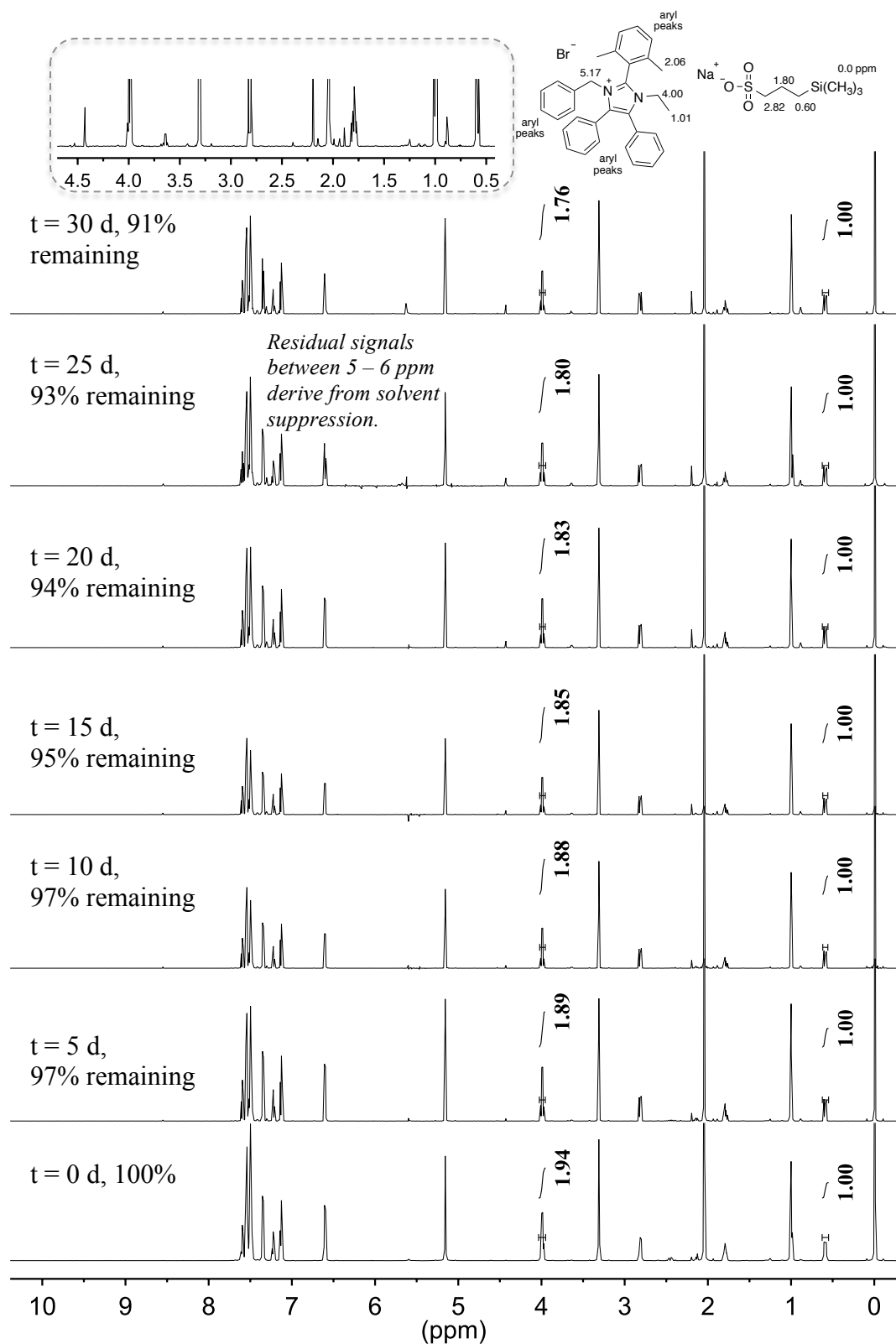


Figure 4.25 ¹H NMR spectra of **5a** over 30 days dissolved in a basic CD₃OH solution at 80 °C (1 M KOH, [KOH]/[**5a**] = 20) with an internal standard (TMS(CH₂)₃SO₃Na). Inset is extracted from t = 30 d.

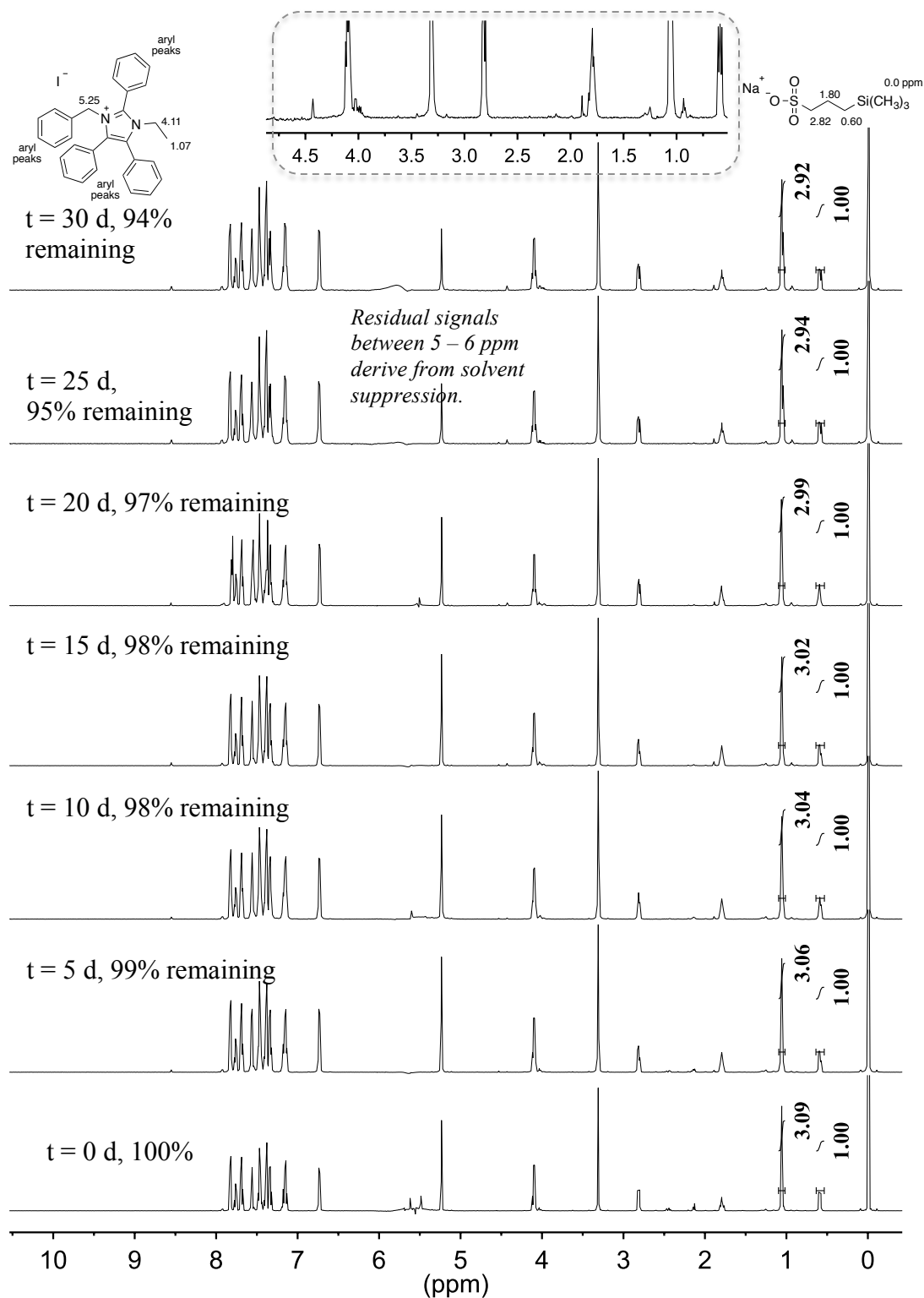


Figure 4.26 ¹H NMR spectra of **5b** over 30 days dissolved in a basic CD₃OH solution at 80 °C (1 M KOH, [KOH]/[**5b**] = 20) with an internal standard (TMS(CH₂)₃SO₃Na). Inset is extracted from t = 30 d.

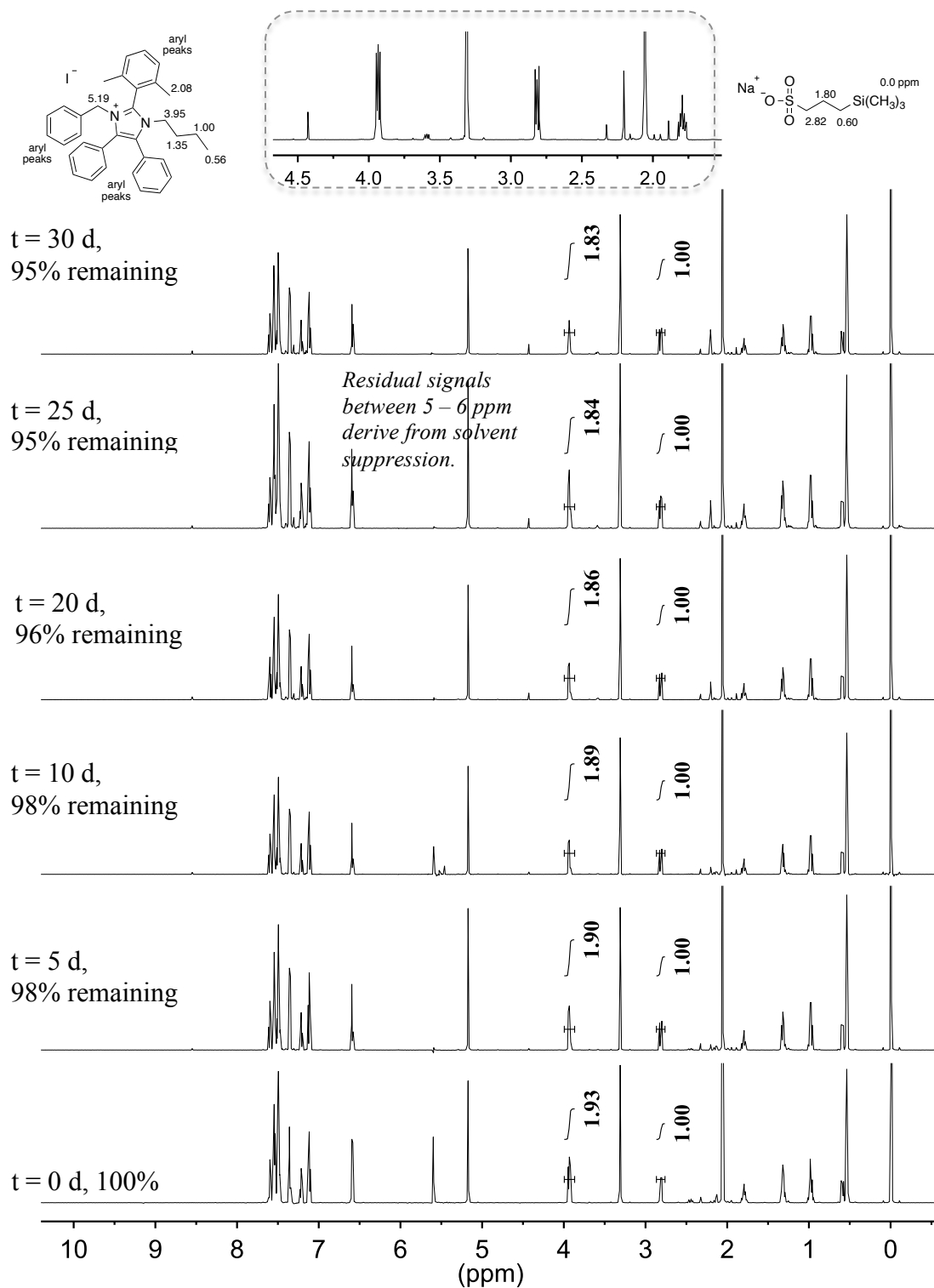


Figure 4.27 ^1H NMR spectra of **6a** over 30 days dissolved in a basic CD_3OH solution at $80\text{ }^\circ\text{C}$ (1 M KOH, $[\text{KOH}]/[\text{6a}] = 20$) with an internal standard ($\text{TMS}(\text{CH}_2)_3\text{SO}_3\text{Na}$). Inset is extracted from $t = 30\text{ d}$

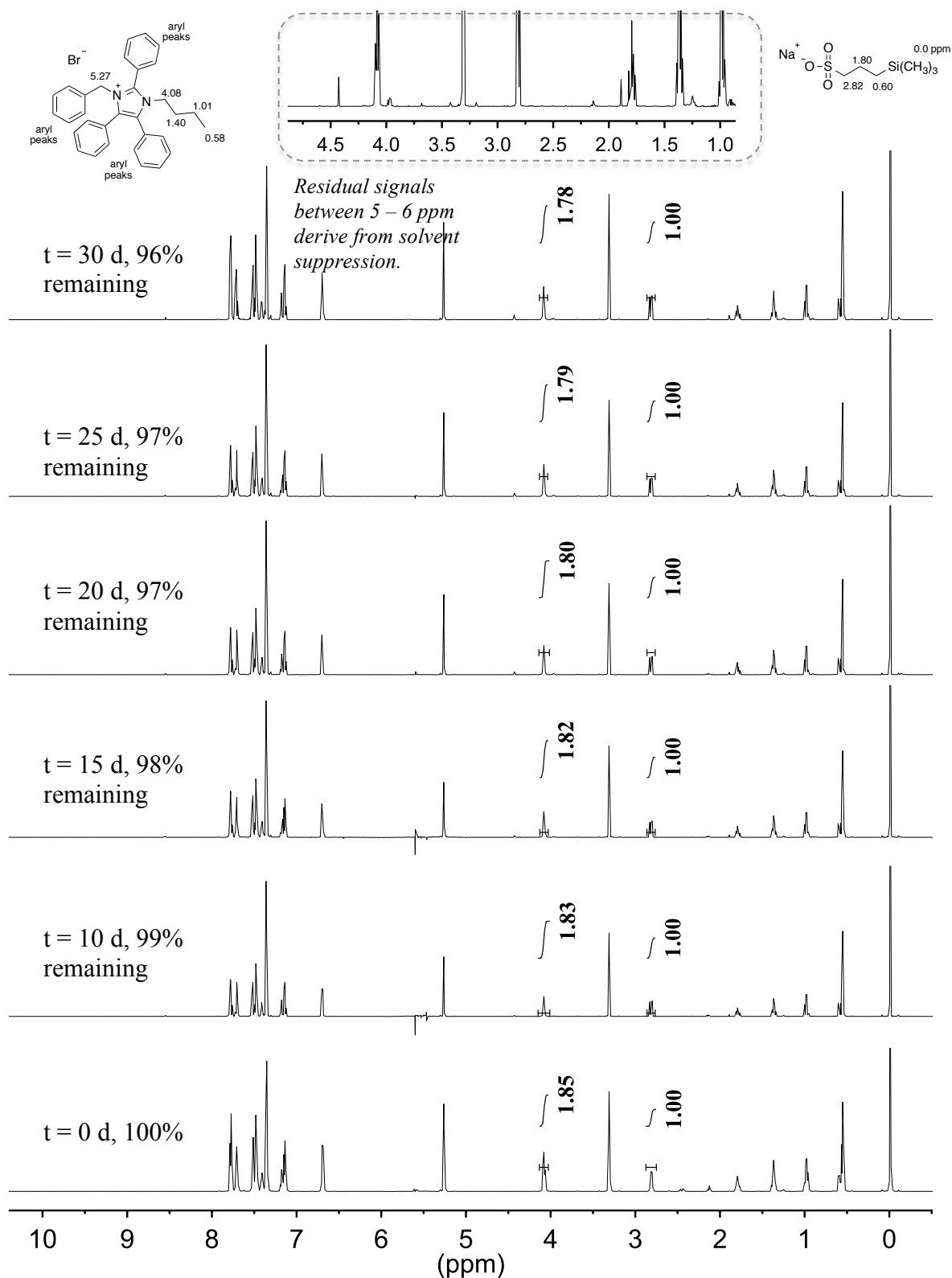


Figure 4.28 ¹H NMR spectra of **6b** over 30 days dissolved in a basic CD₃OH solution at 80 °C (1 M KOH, [KOH]/[**6b**] = 20) with an internal standard (TMS(CH₂)₃SO₃Na). Inset is extracted from t = 30 d.

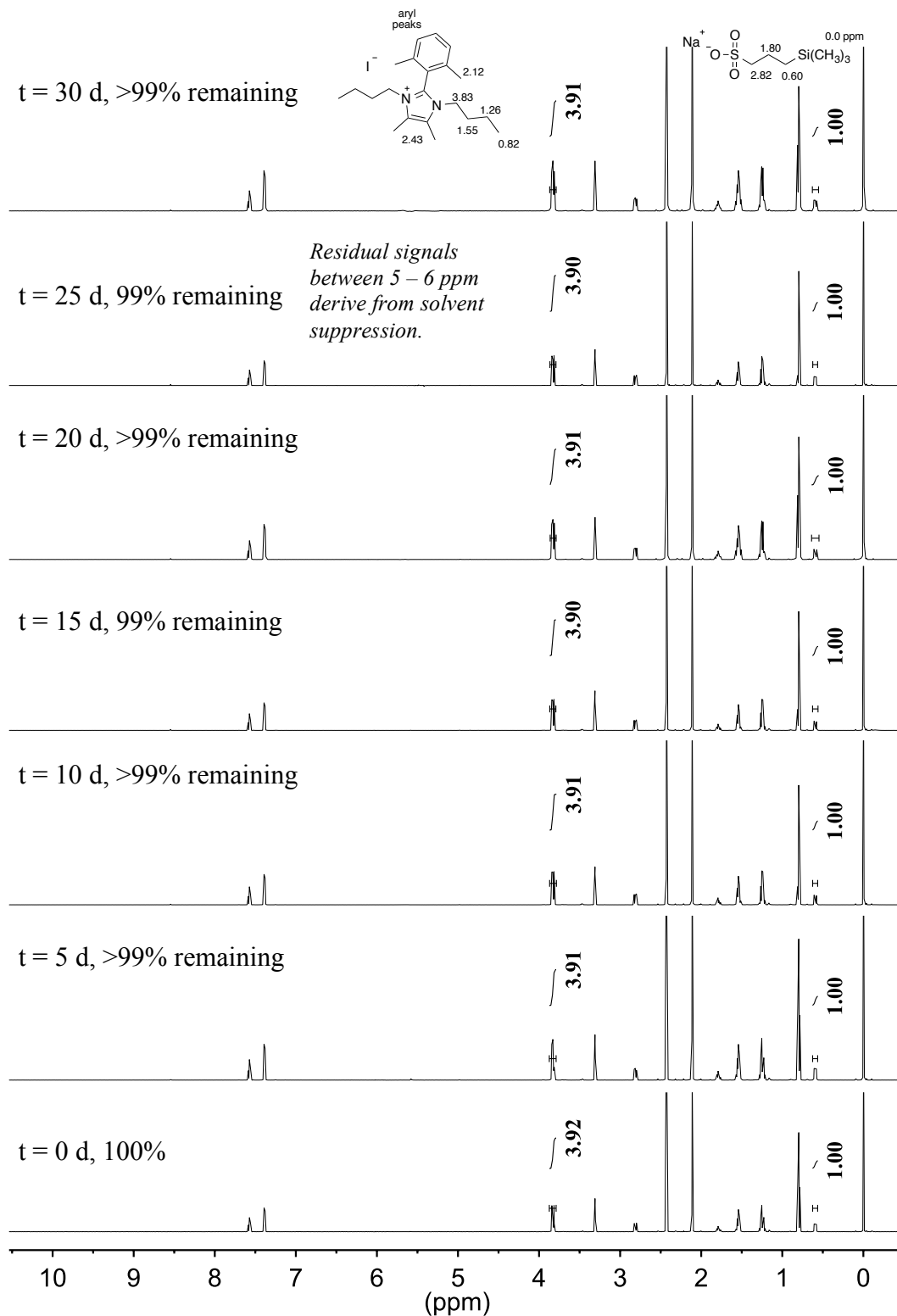


Figure 4.29 ^1H NMR spectra of **7a** over 30 days dissolved in a basic CD_3OH solution at 80°C (1 M KOH, $[\text{KOH}]/[\text{7a}] = 20$) with an internal standard ($\text{TMS}(\text{CH}_2)_3\text{SO}_3\text{Na}$).

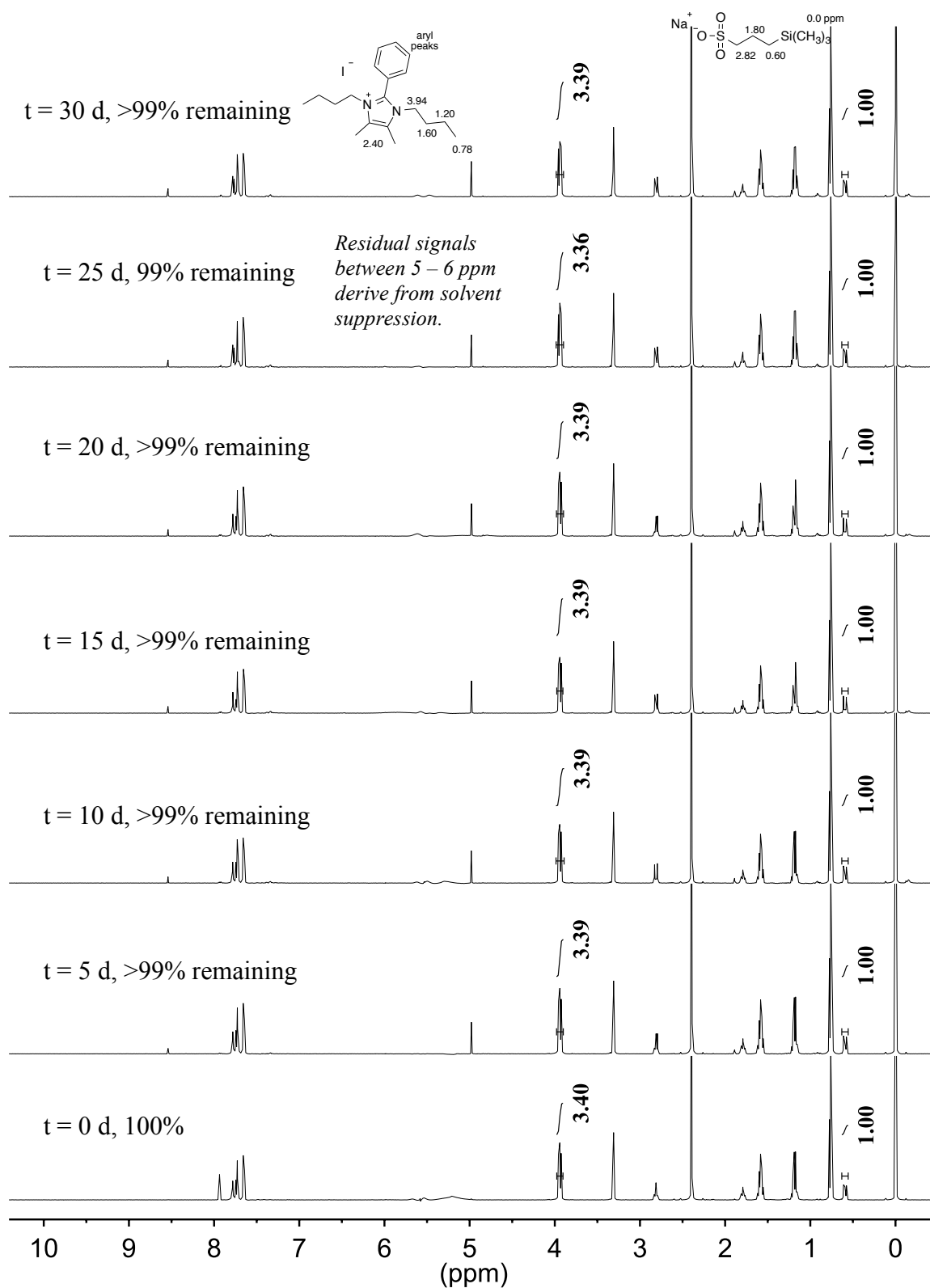


Figure 4.30 ¹H NMR spectra of **7b** over 30 days dissolved in a basic CD₃OH solution at 80 °C (1 M KOH, [KOH]/[**7b**] = 20) with an internal standard (TMS(CH₂)₃SO₃Na).

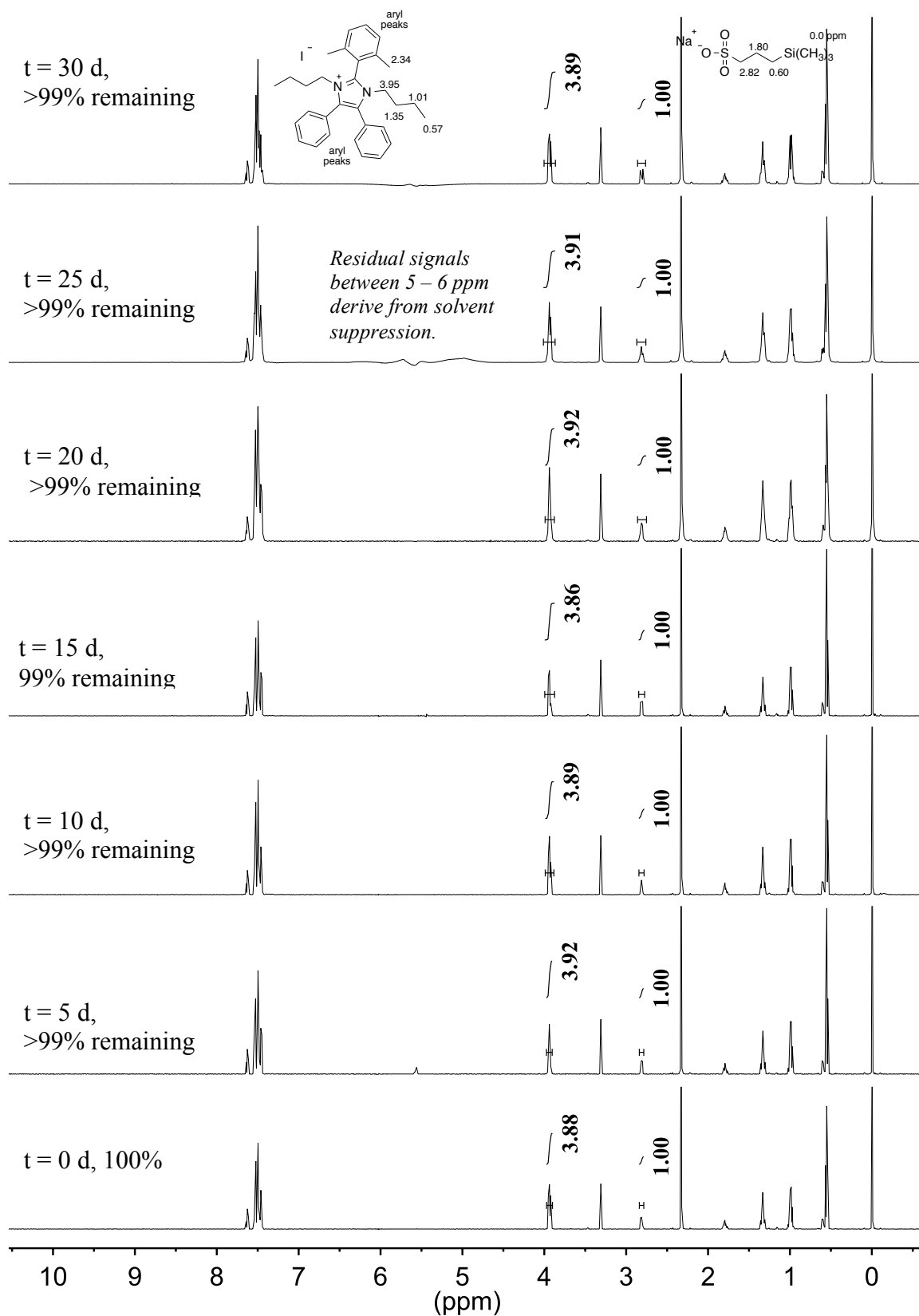


Figure 4.31 ^1H NMR spectra of **8a** over 30 days dissolved in a basic CD_3OH solution at 80°C (1 M KOH, $[\text{KOH}]/[\text{8a}] = 20$) with an internal standard (TMS(CH_2) $_3\text{SO}_3\text{Na}$).

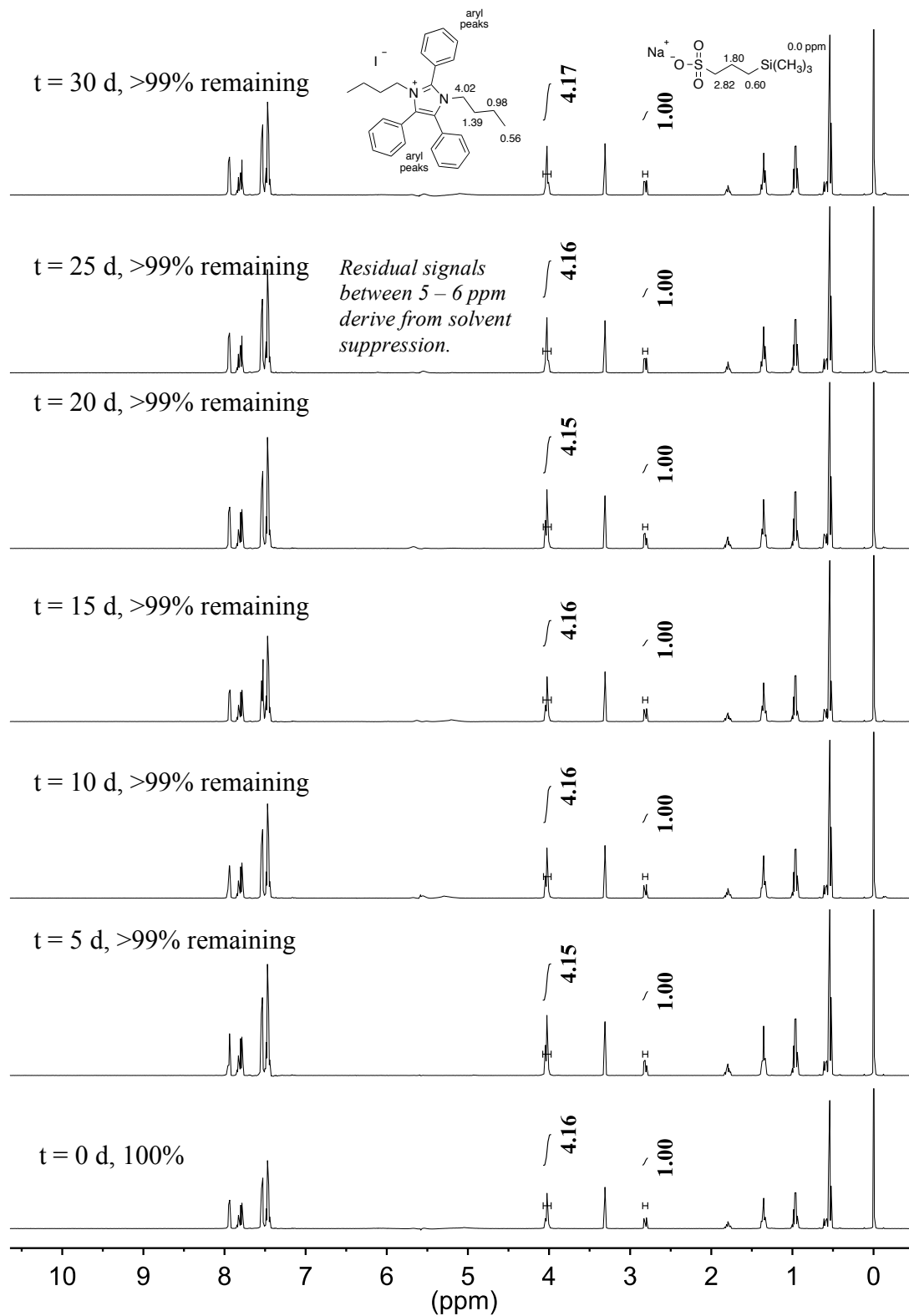


Figure 4.32 ¹H NMR spectra of **8b** over 30 days dissolved in a basic CD₃OH solution at 80 °C (1 M KOH, [KOH]/[**8b**] = 20) with an internal standard (TMS(CH₂)₃SO₃Na).

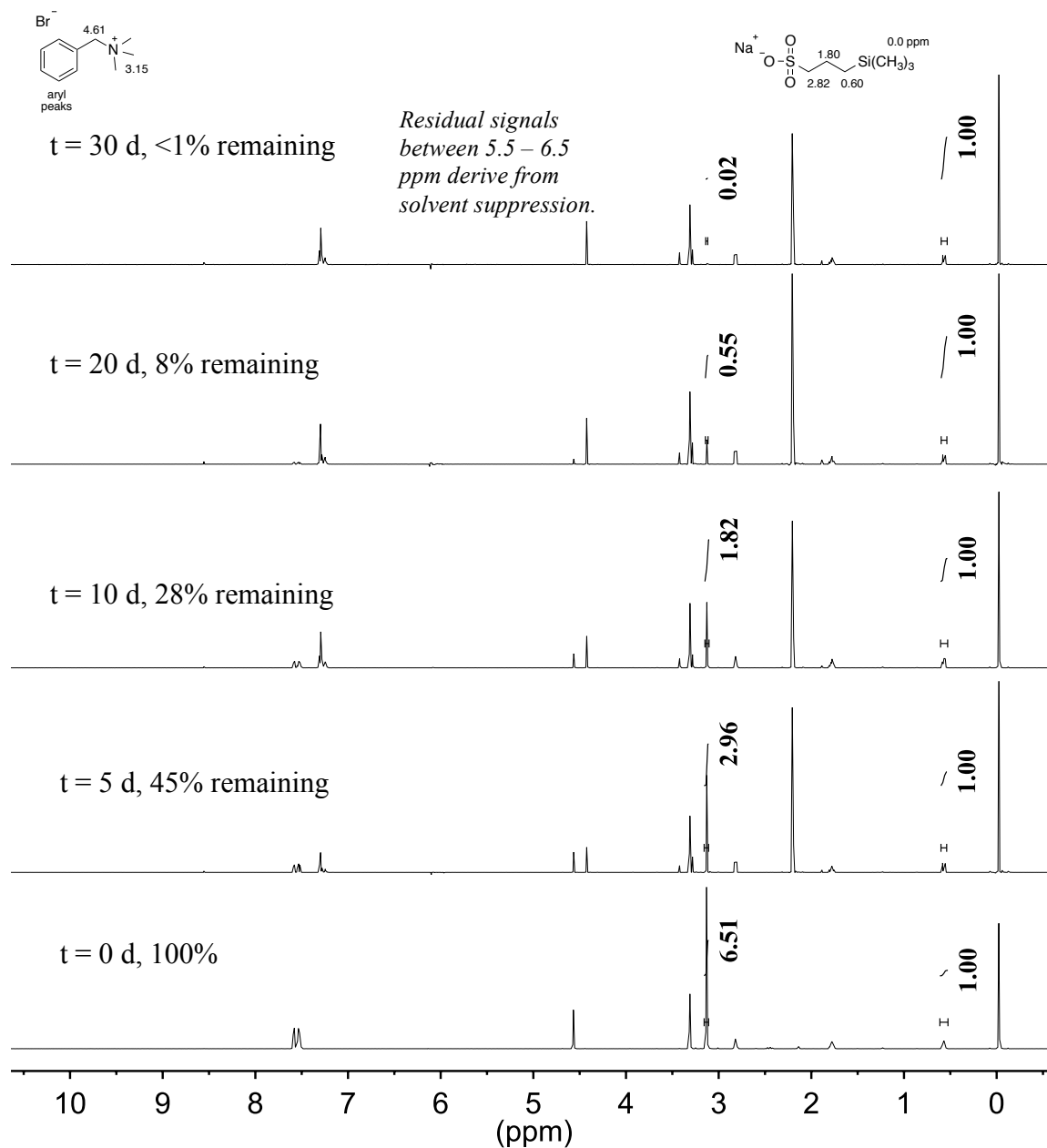


Figure 4.33 ¹H NMR spectra of **1** over 30 days dissolved in a basic CD₃OH solution at 80 °C (2 M KOH, [KOH]/[**1**] = 67 with an internal standard (TMS(CH₂)₃SO₃Na).

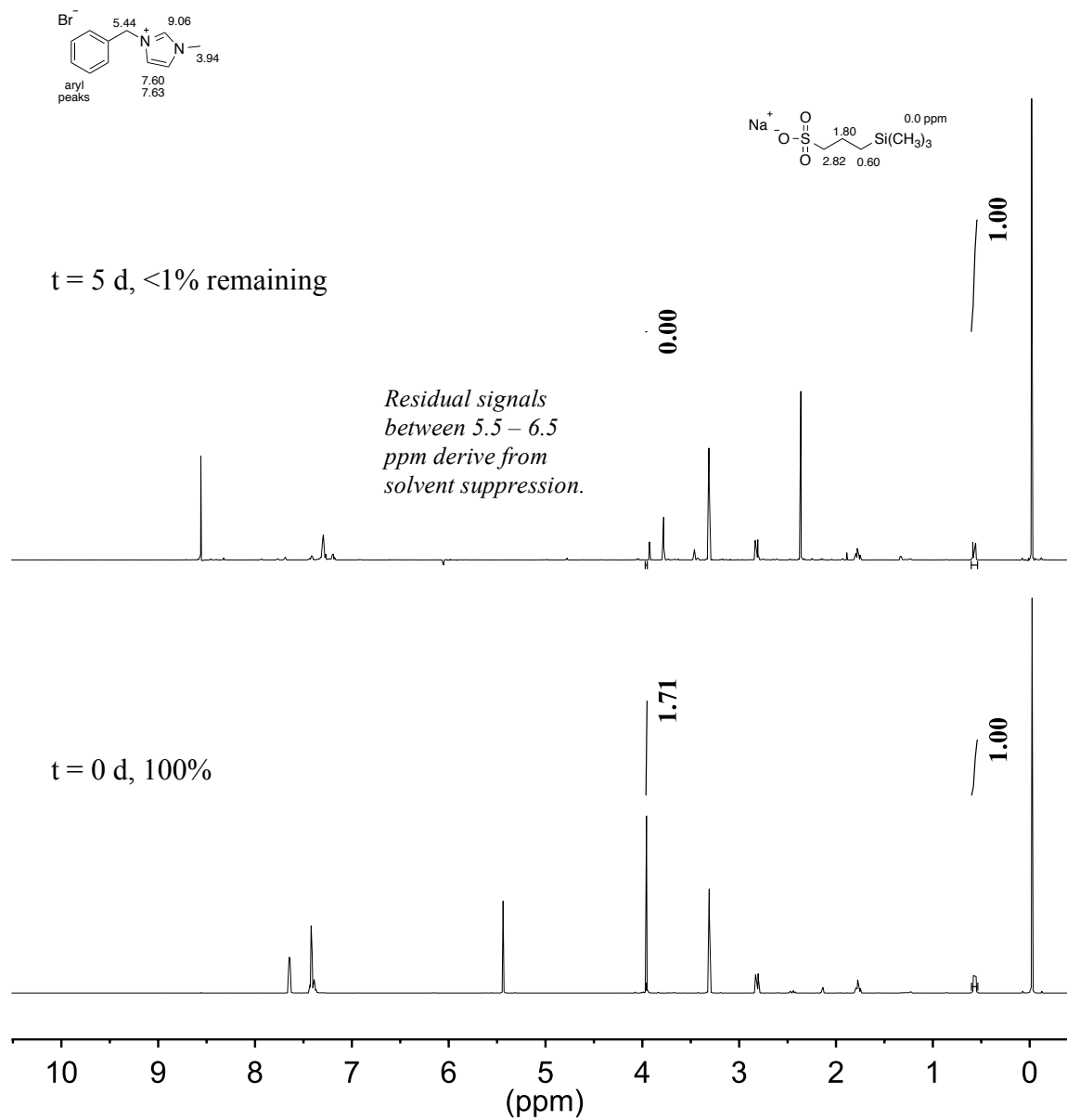


Figure 3.34 ^1H NMR spectra of **2a** over 5 days dissolved in a basic CD_3OH solution at 80°C (2 M KOH, $[\text{KOH}]/[\text{2a}] = 67$ with an internal standard ($\text{TMS}(\text{CH}_2)_3\text{SO}_3\text{Na}$).

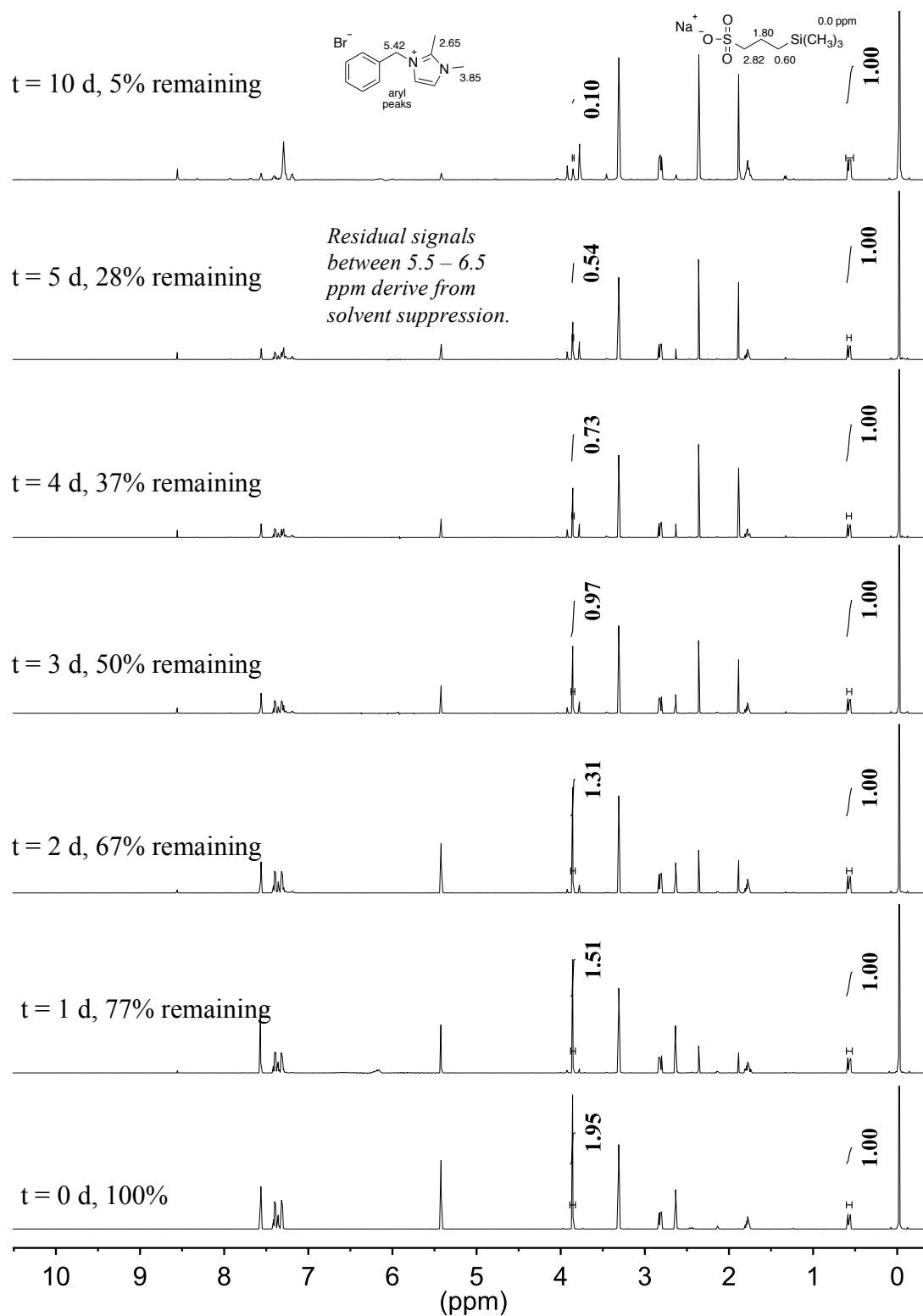


Figure 3.35 ¹H NMR spectra of **2b** over 10 days dissolved in a basic CD₃OH solution at 80 °C (2 M KOH, [KOH]/[**2b**] = 67) with an internal standard (TMS(CH₂)₃SO₃Na).

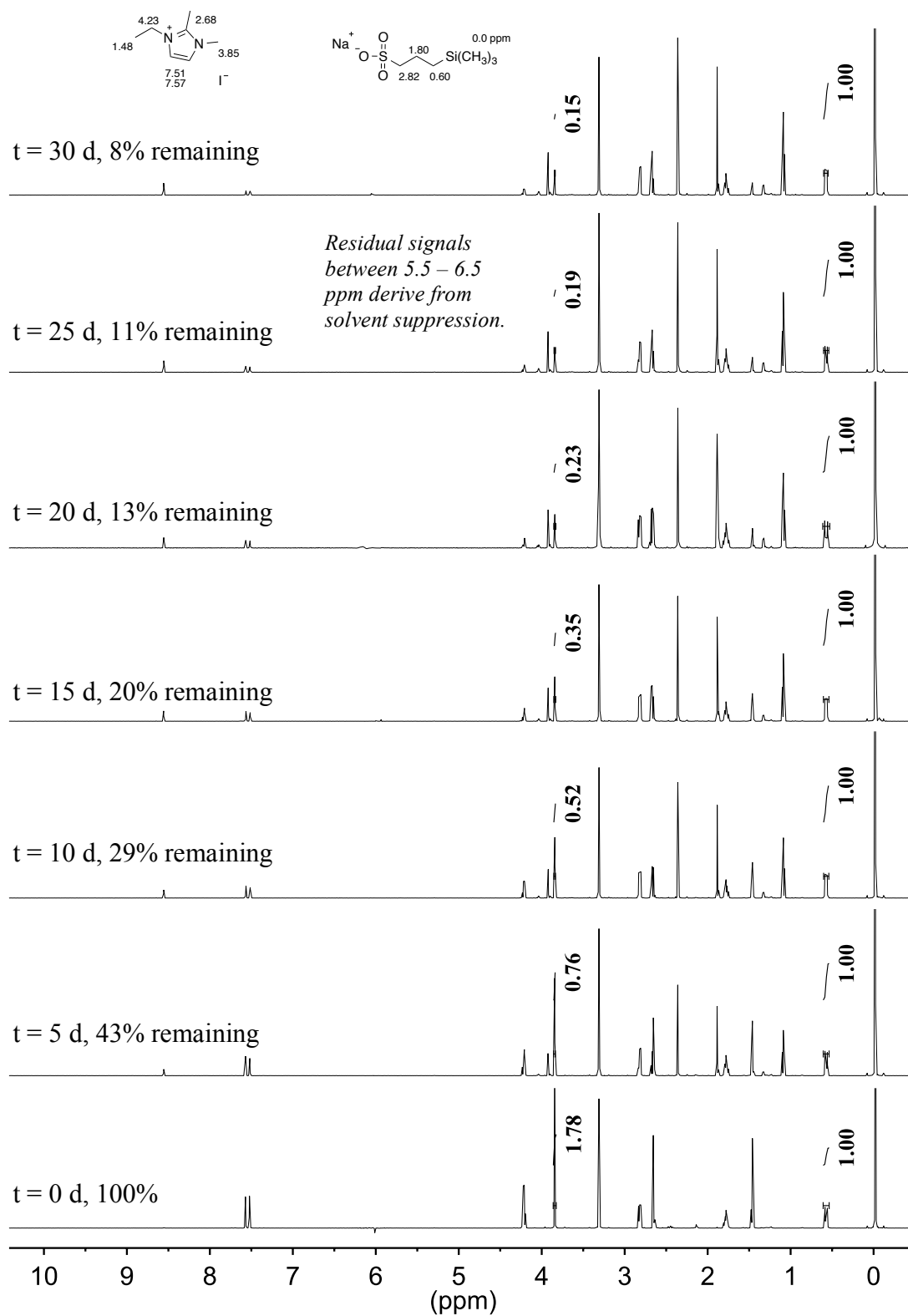


Figure 4.36 ¹H NMR spectra of **2c** over 30 days dissolved in a basic CD₃OH solution at 80 °C (2 M KOH, [KOH]/[**2c**] = 67) with an internal standard (TMS(CH₂)₃SO₃Na).

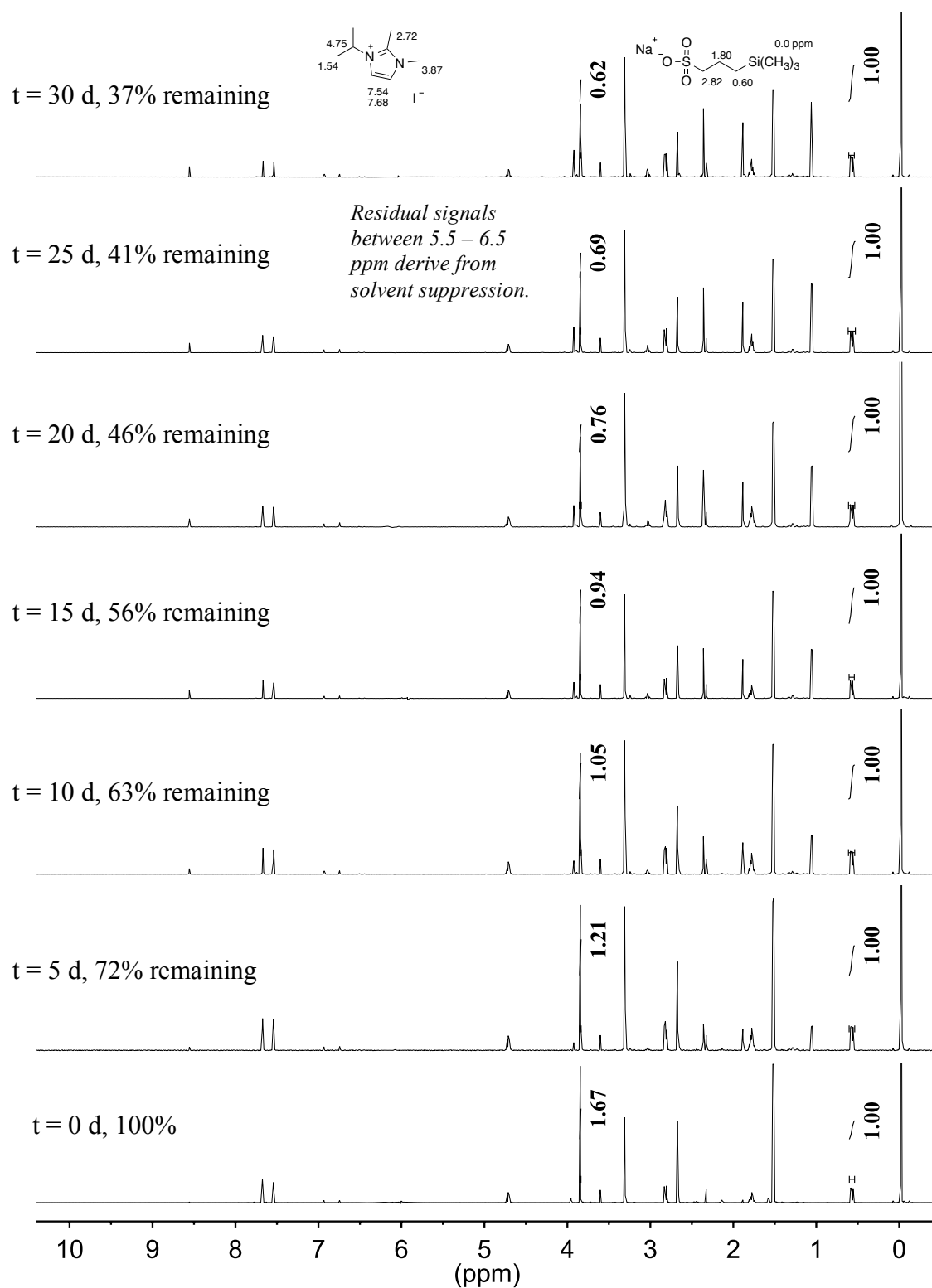


Figure 4.37 ^1H NMR spectra of **2d** over 30 days dissolved in a basic CD_3OH solution at $80\text{ }^\circ\text{C}$ (2 M KOH, $[\text{KOH}]/[\text{2d}] = 67$) with an internal standard ($\text{TMS}(\text{CH}_2)_3\text{SO}_3\text{Na}$).

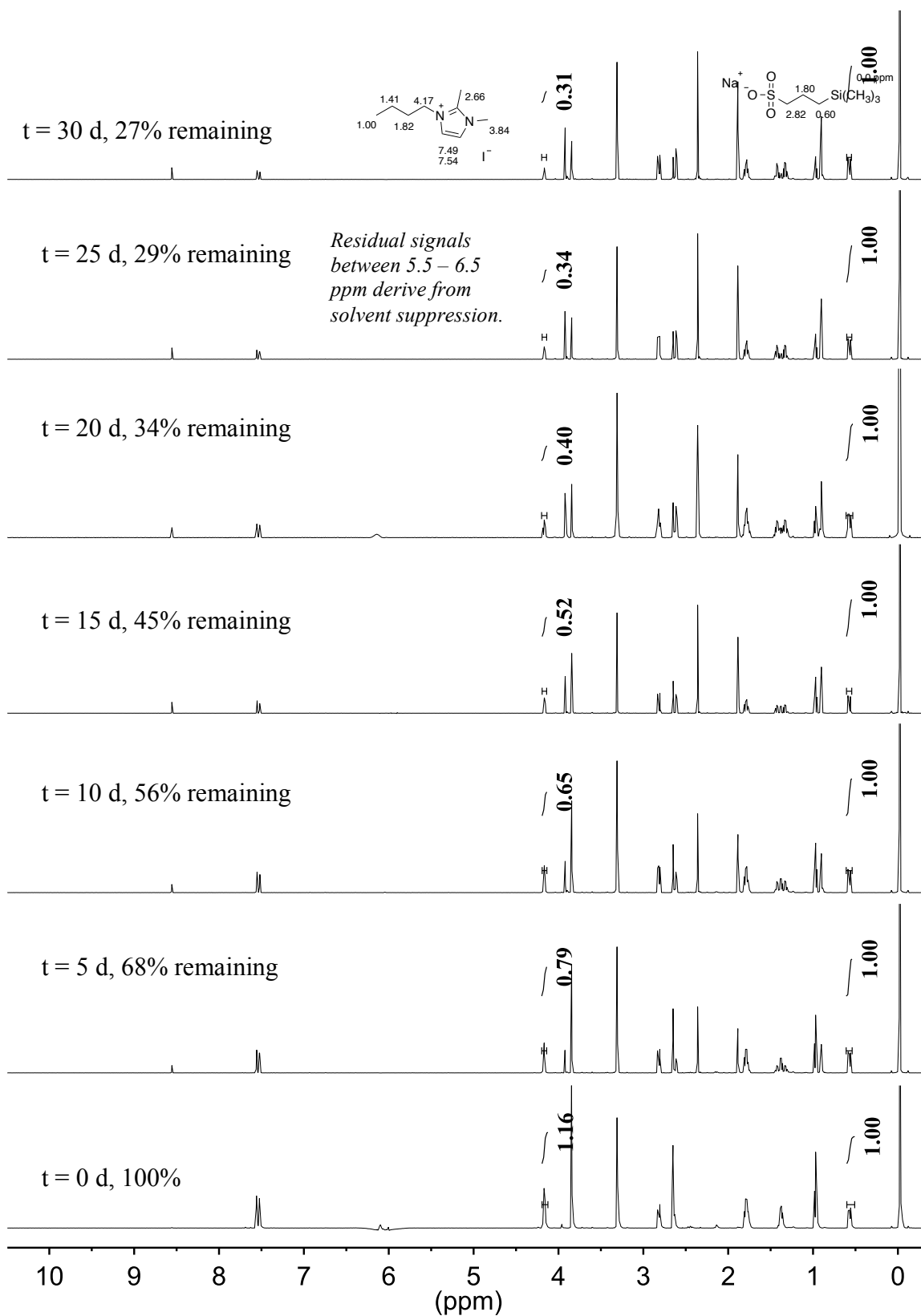


Figure 4.38 ^1H NMR spectra of **2e** over 30 days dissolved in a basic CD_3OH solution at $80\text{ }^\circ\text{C}$ (2 M KOH, $[\text{KOH}]/[\text{2e}] = 67$) with an internal standard ($\text{TMS}(\text{CH}_2)_3\text{SO}_3\text{Na}$).

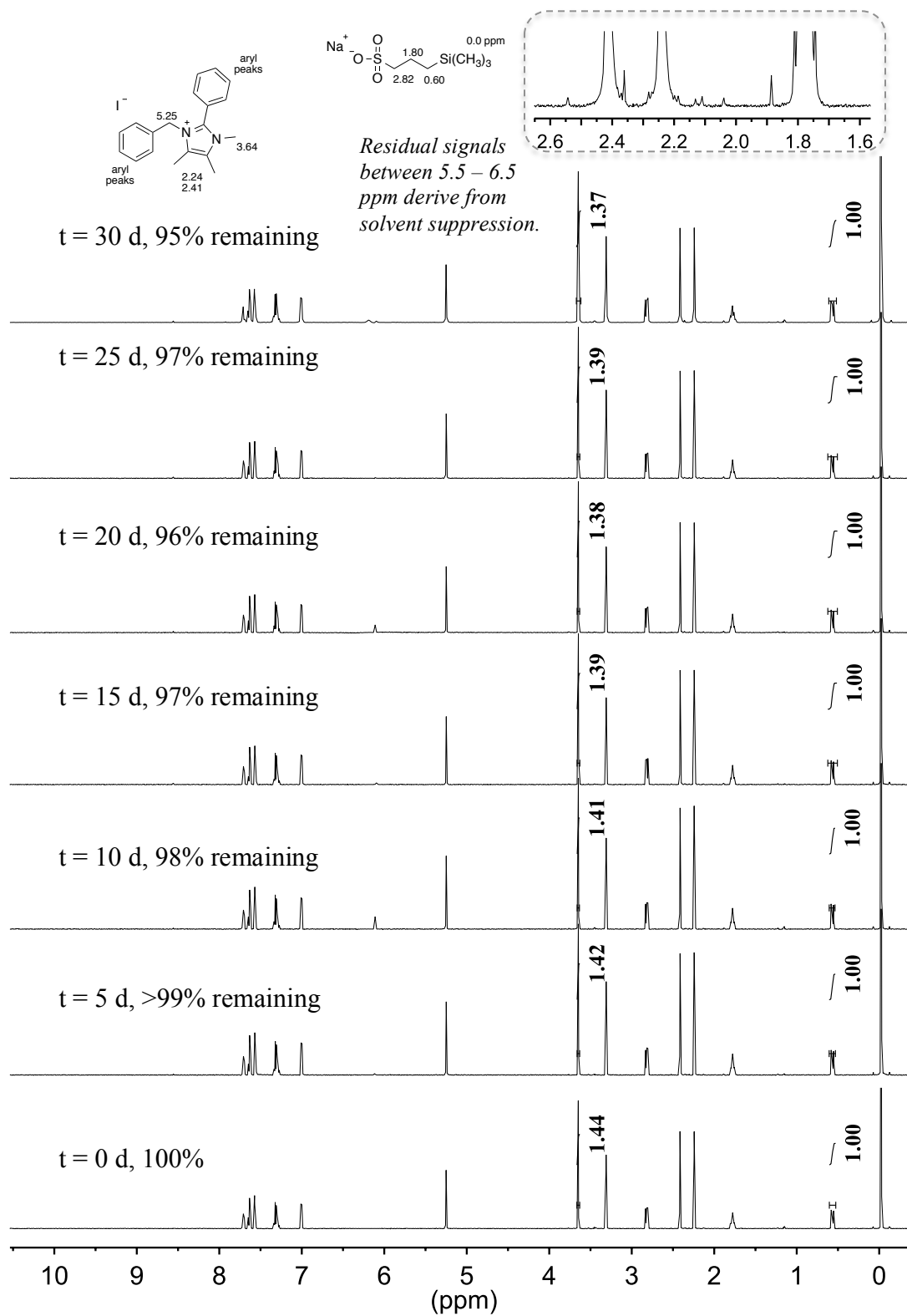


Figure 4.39 ^1H NMR spectra of **3a** over 30 days dissolved in a basic CD_3OH solution at 80°C (2 M KOH, $[\text{KOH}]/[\text{3a}] = 67$) with an internal standard (TMS(CH_2) $_3\text{SO}_3\text{Na}$).

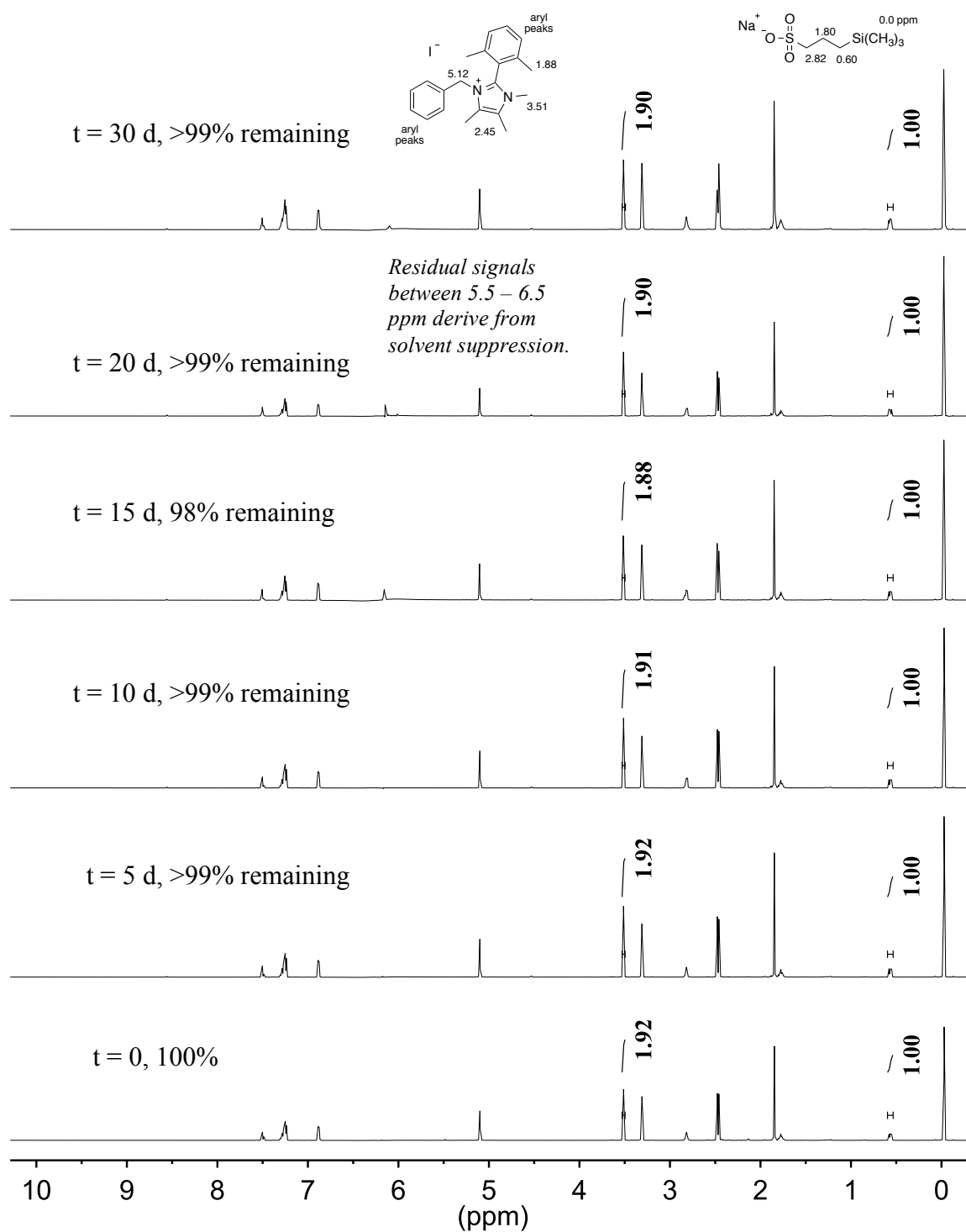


Figure 4.40 ¹H NMR spectra of **3b** over 30 days dissolved in a basic CD₃OH solution at 80 °C (2 M KOH, [KOH]/[**3b**] = 67) with an internal standard (TMS(CH₂)₃SO₃Na). Inset is extracted from t = 30 d.

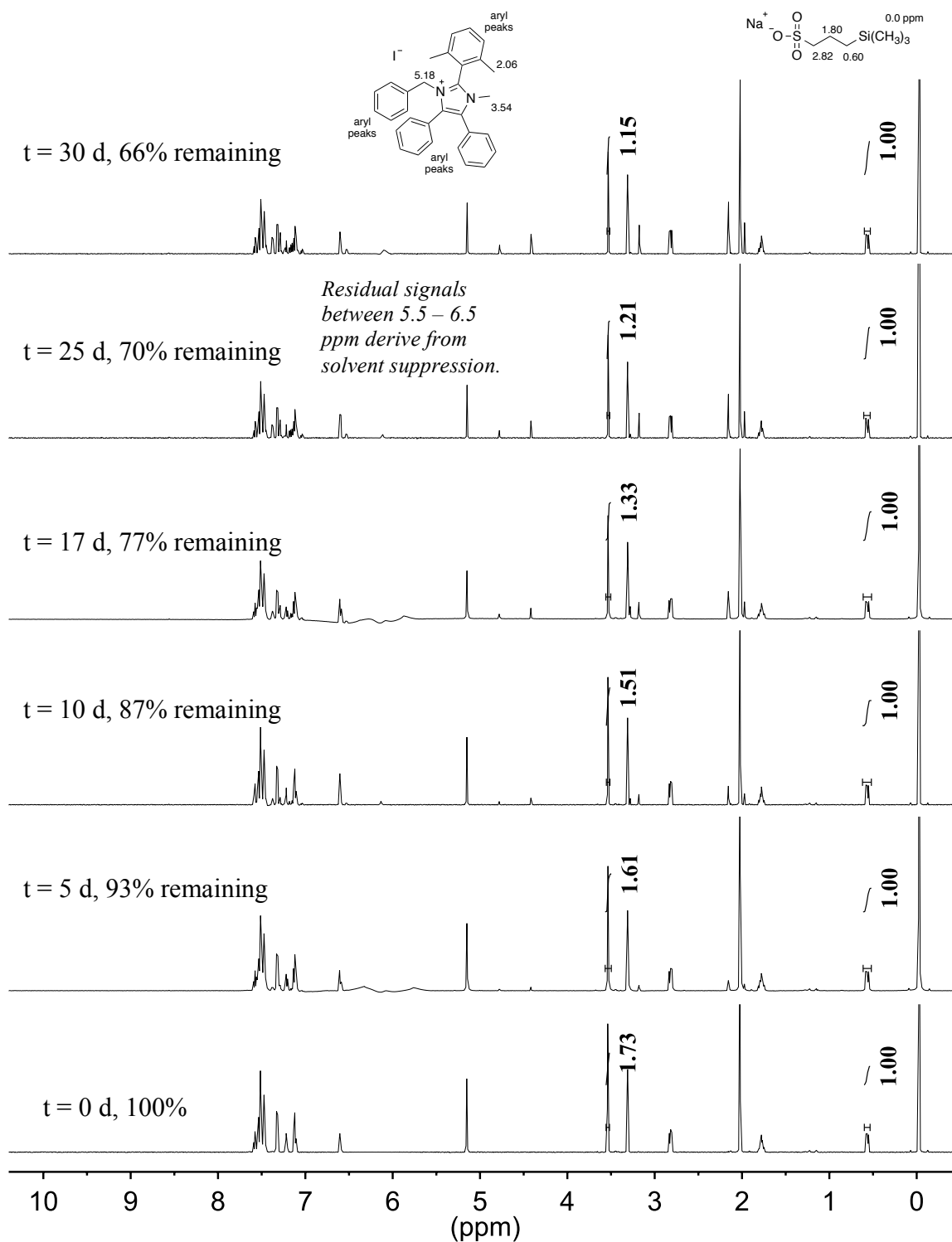


Figure 4.41 ^1H NMR spectra of **4a** over 30 days dissolved in a basic CD_3OH solution at 80°C (2 M KOH, $[\text{KOH}]/[\text{4a}] = 67$) with an internal standard ($\text{TMS}(\text{CH}_2)_3\text{SO}_3\text{Na}$).

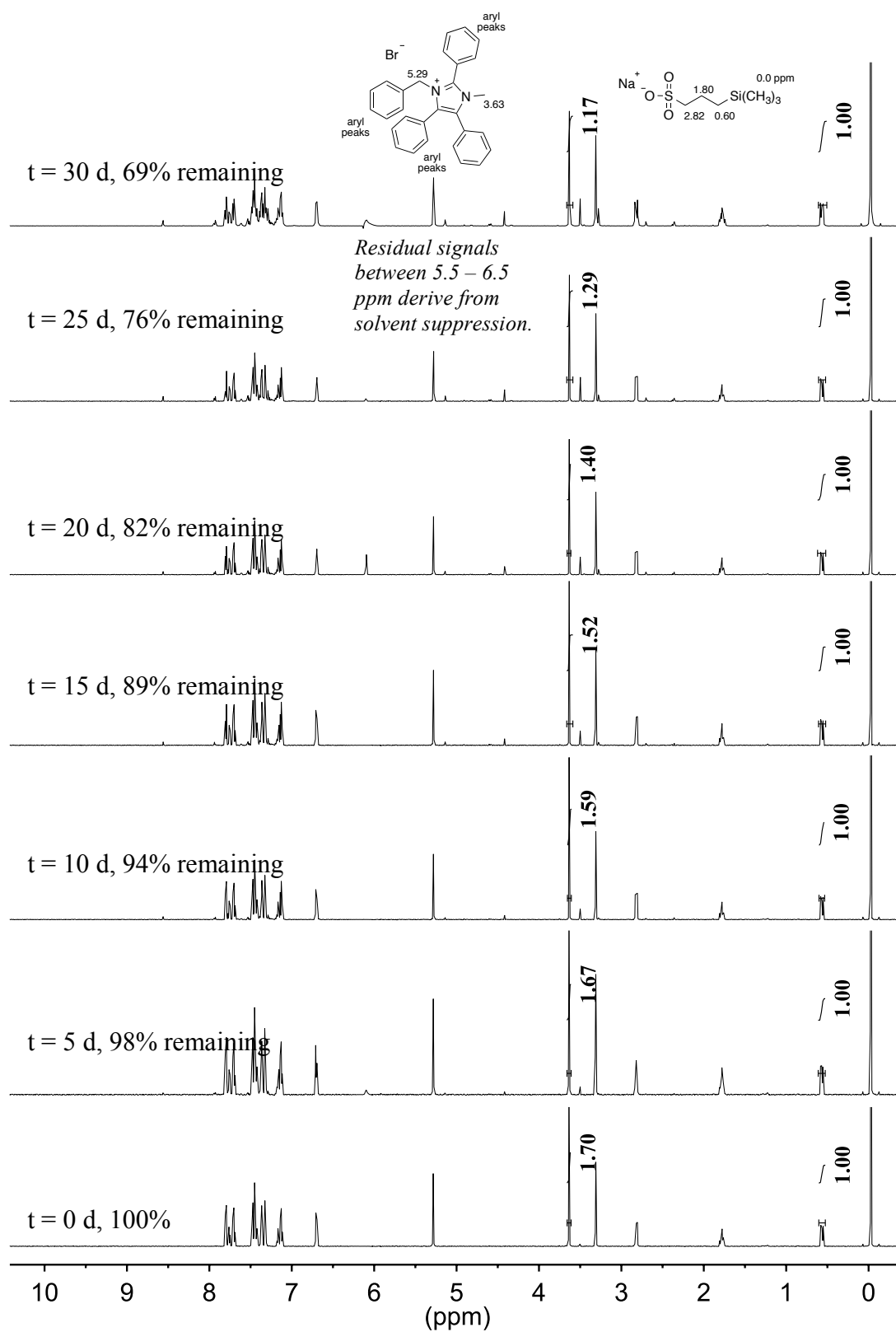


Figure 4.42 ^1H NMR spectra of **4b** over 30 days dissolved in a basic CD_3OH solution at 80°C (2 M KOH, $[\text{KOH}]/[\text{4b}] = 67$) with an internal standard ($\text{TMS}(\text{CH}_2)_3\text{SO}_3\text{Na}$).

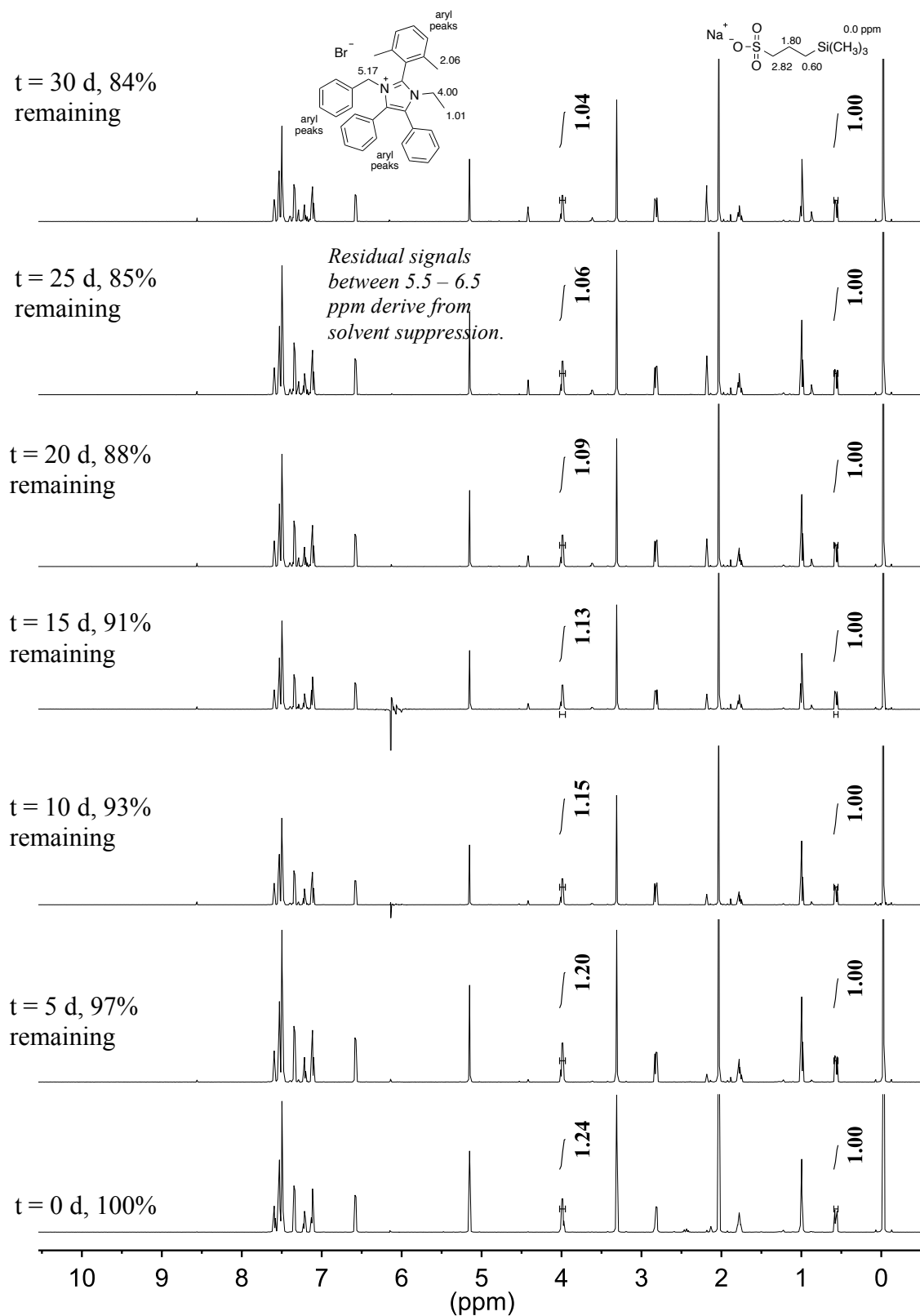


Figure 4.43 ^1H NMR spectra of **5a** over 30 days dissolved in a basic CD_3OH solution at 80°C (2 M KOH, $[\text{KOH}]/[\text{5a}] = 67$) with an internal standard ($\text{TMS}(\text{CH}_2)_3\text{SO}_3\text{Na}$).

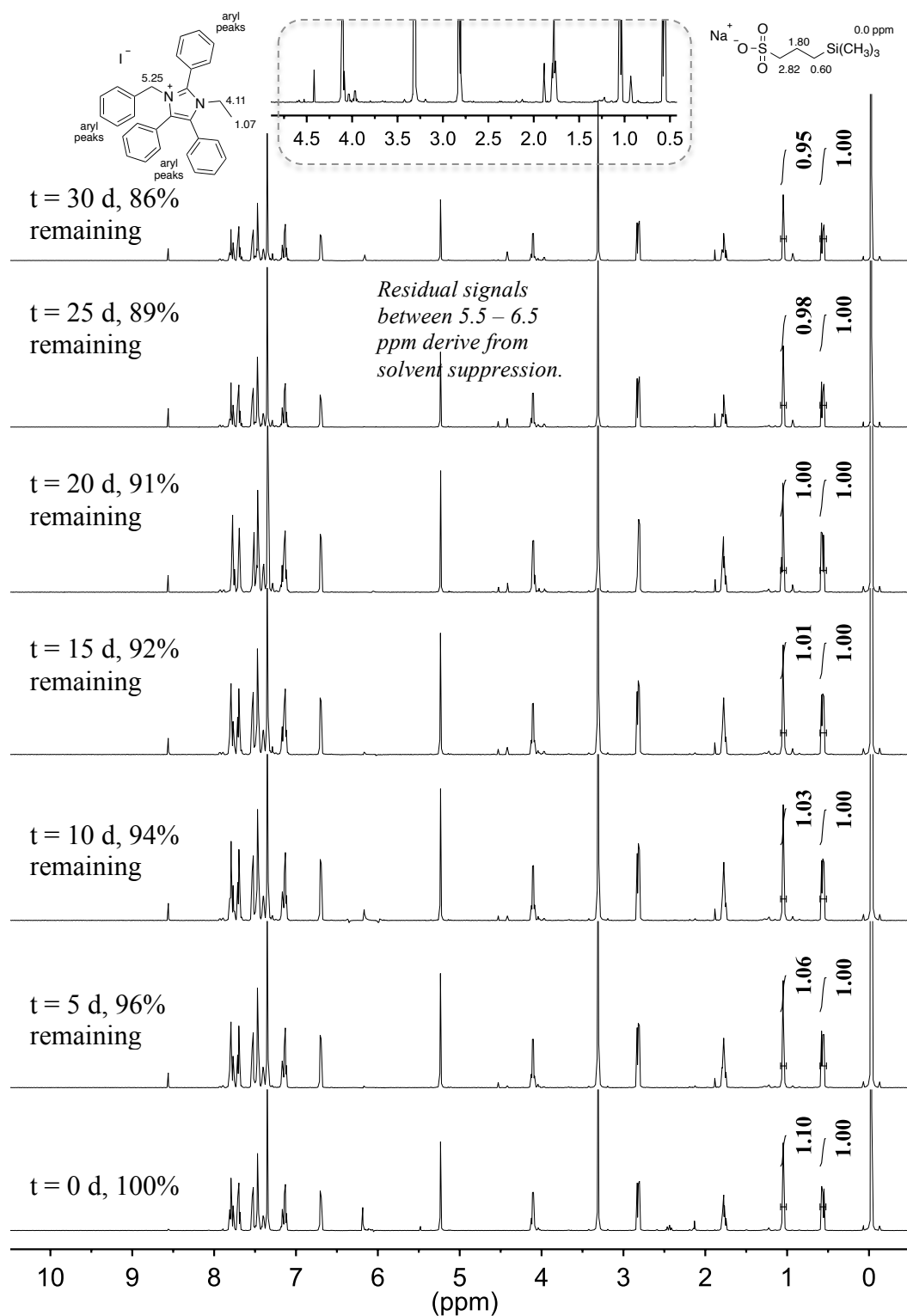


Figure 4.44 ^1H NMR spectra of **5b** over 30 days dissolved in a basic CD_3OH solution at 80°C (2 M KOH, $[\text{KOH}]/[\mathbf{5b}] = 67$) with an internal standard ($\text{TMS}(\text{CH}_2)_3\text{SO}_3\text{Na}$). Inset is extracted from $t = 30$ d.

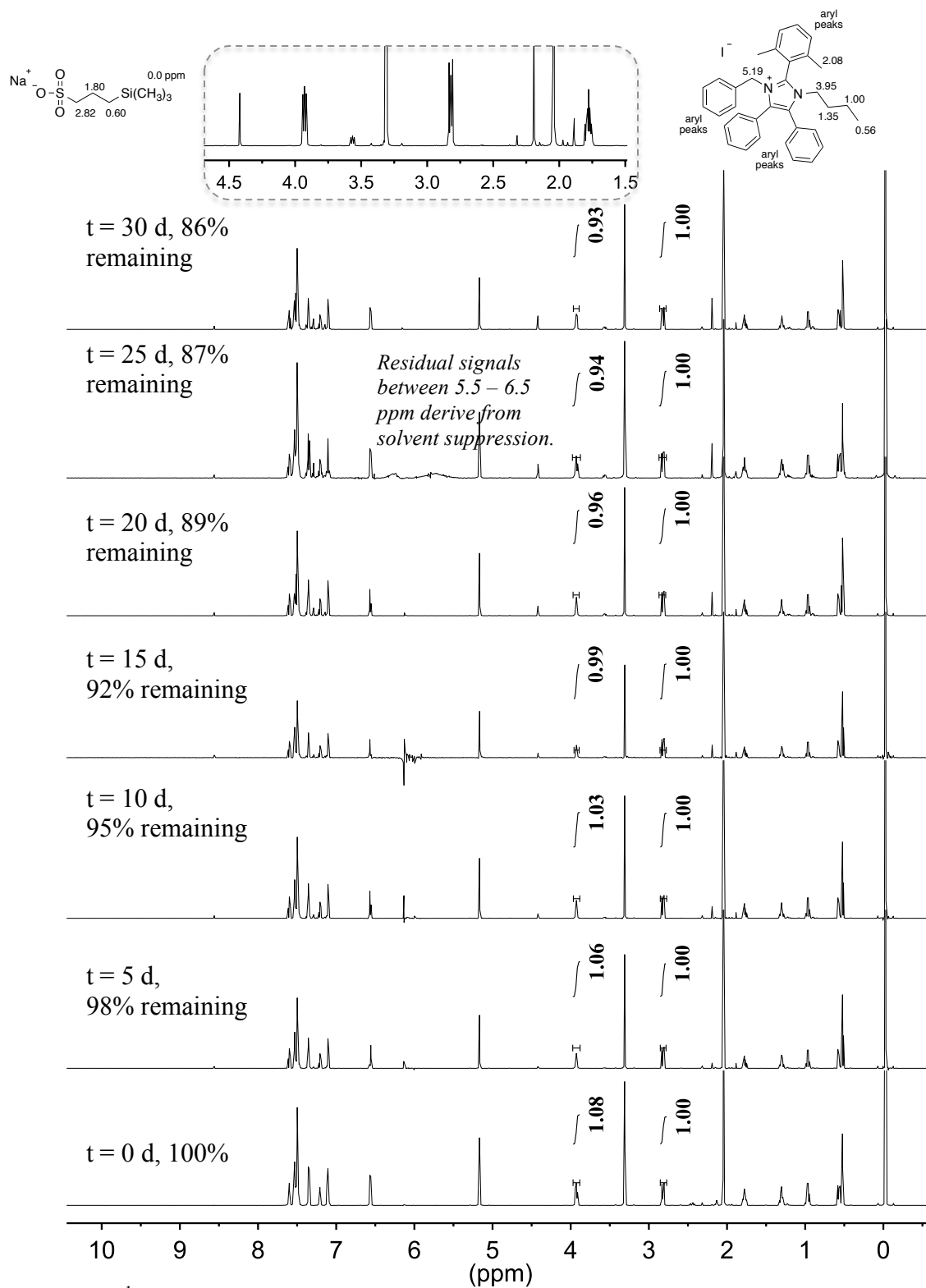


Figure 4.45 ^1H NMR spectra of **6a** over 30 days dissolved in a basic CD_3OH solution at 80°C (2 M KOH, $[\text{KOH}]/[\text{6a}] = 67$) with an internal standard (TMS(CH_2) $_3$ SO $_3$ Na). Inset is extracted from t = 30 d.

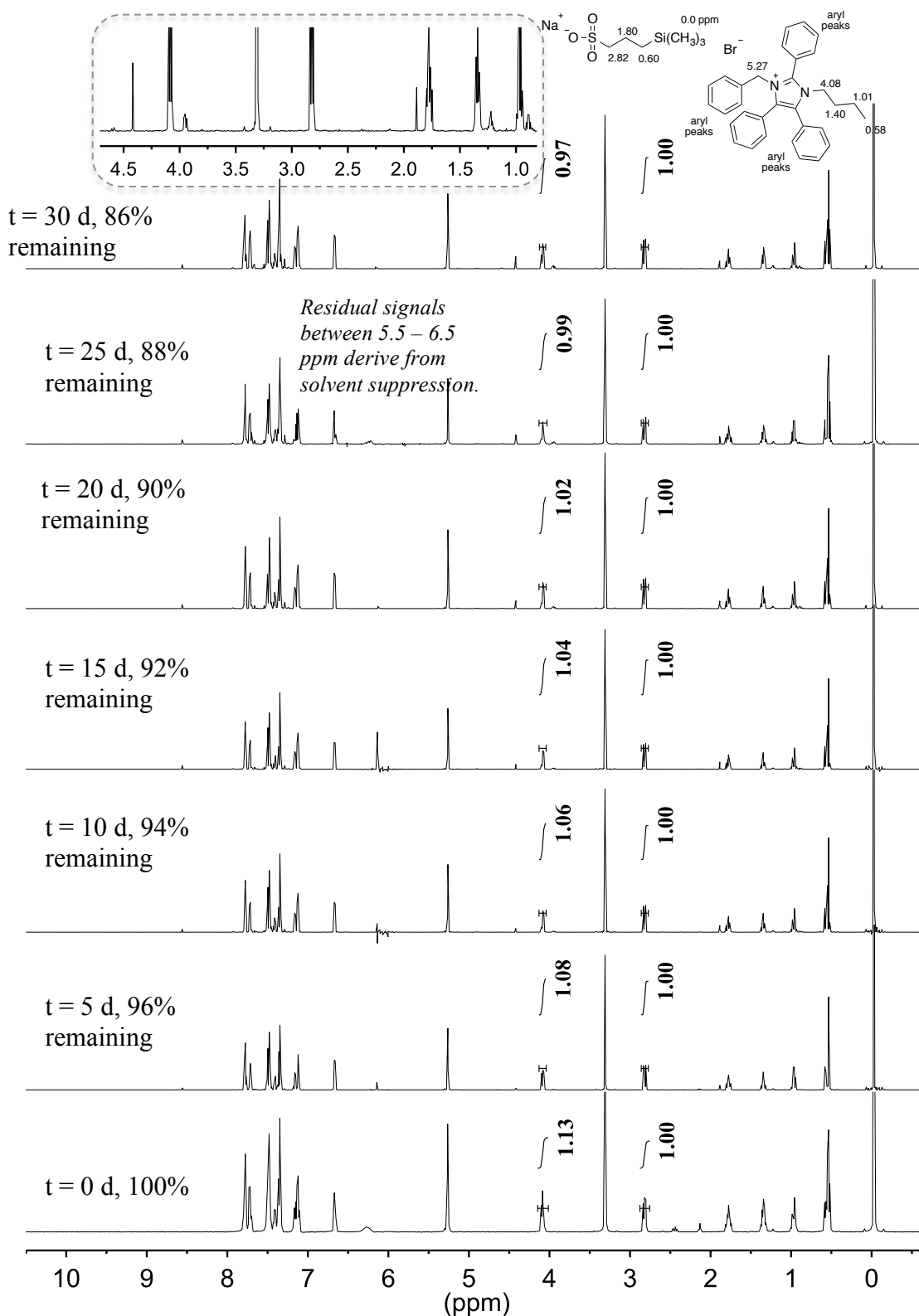


Figure 4.46 ^1H NMR spectra of **6b** over 30 days dissolved in a basic CD_3OH solution at 80°C (2 M KOH, $[\text{KOH}]/[\text{6b}] = 67$) with an internal standard (TMS(CH_2) $_3$ SO $_3$ Na). Inset is extracted from $t = 30$ d.

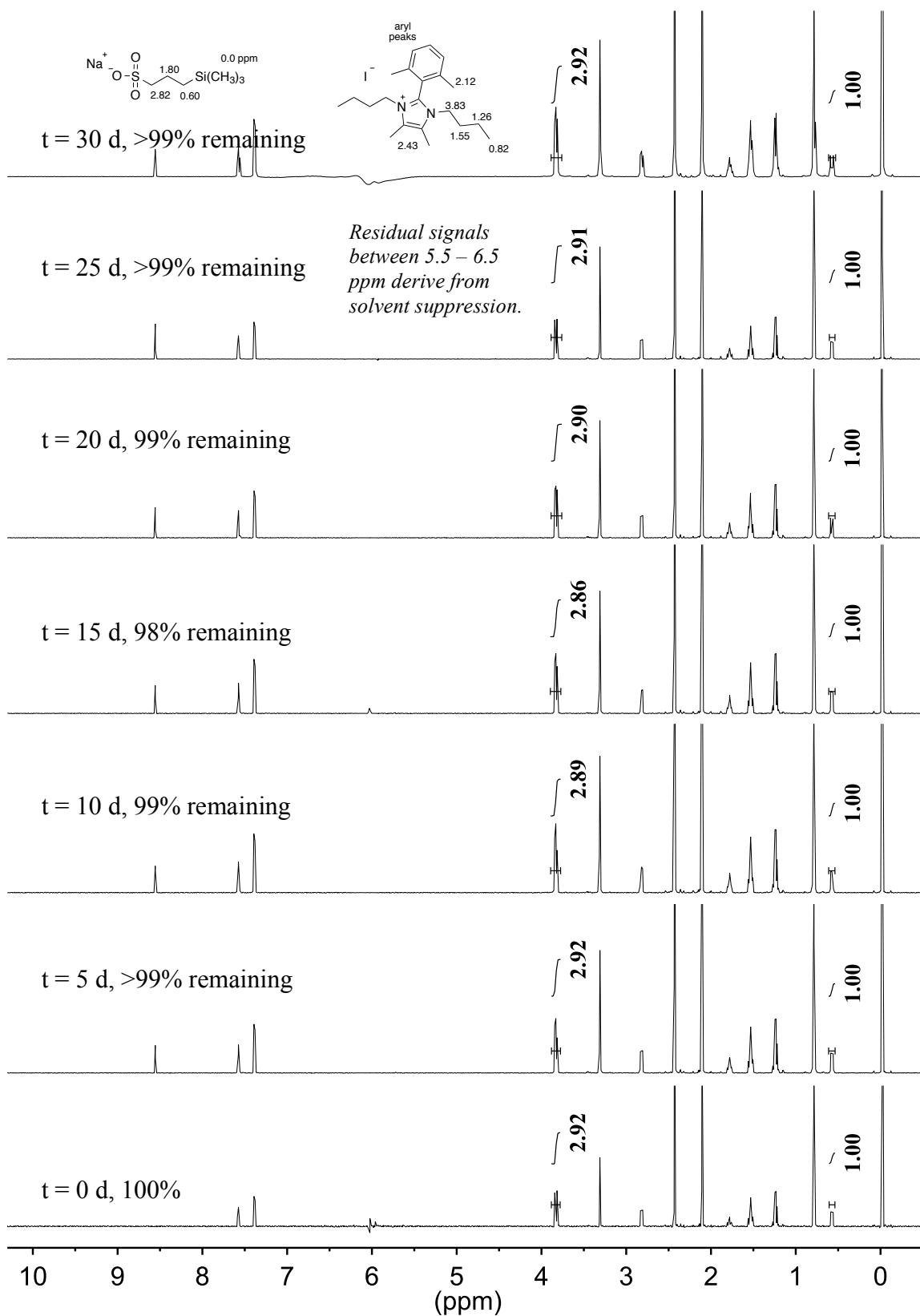


Figure 4.47 ¹H NMR spectra of **7a** over 30 days dissolved in a basic CD₃OH solution at 80 °C (2 M KOH, [KOH]/[**7a**] = 67 with an internal standard (TMS(CH₂)₃SO₃Na).

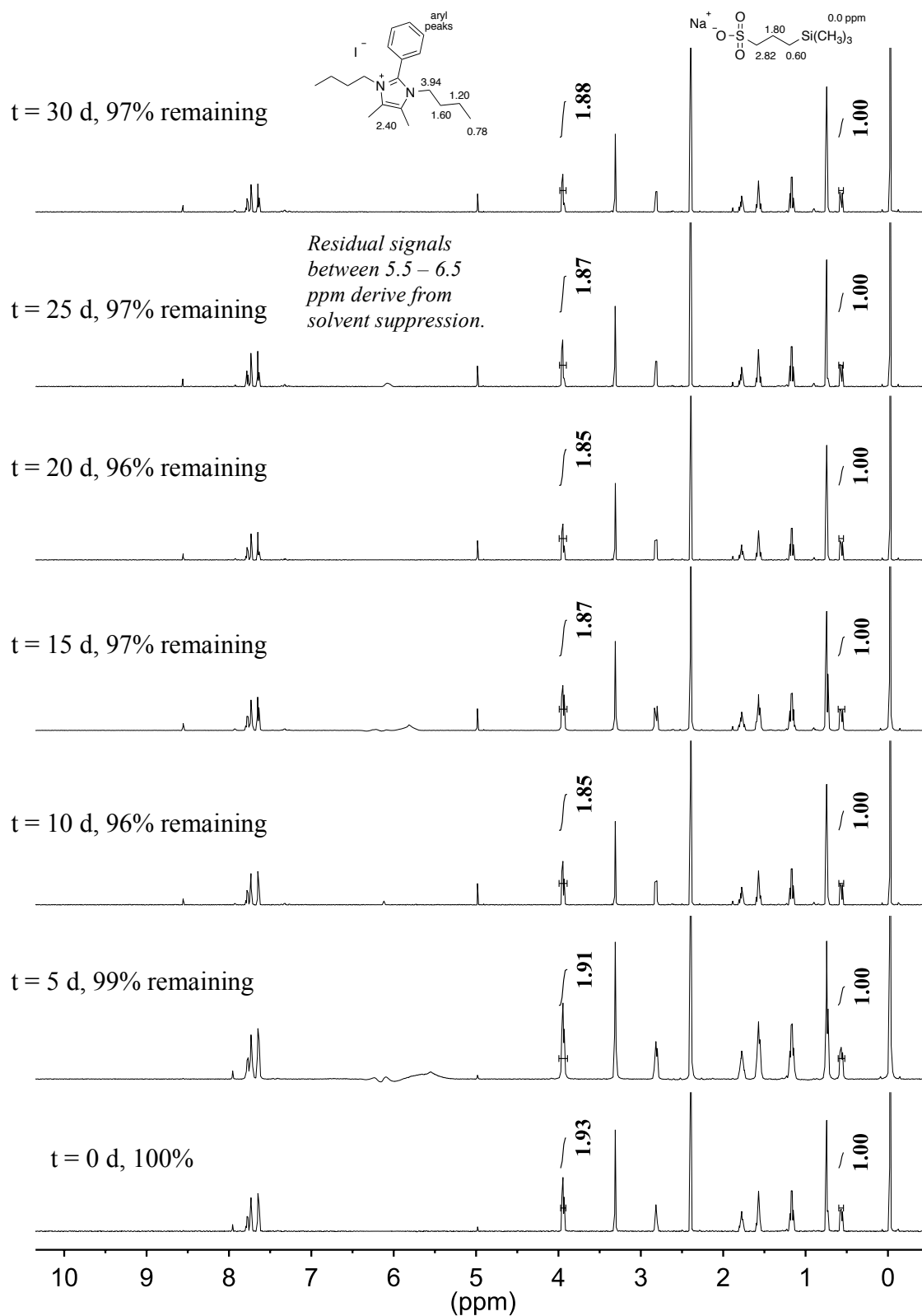


Figure 4.48 ¹H NMR spectra of **7b** over 30 days dissolved in a basic CD₃OH solution at 80 °C (2 M KOH, [KOH]/[**7b**] = 67) with an internal standard (TMS(CH₂)₃SO₃Na).

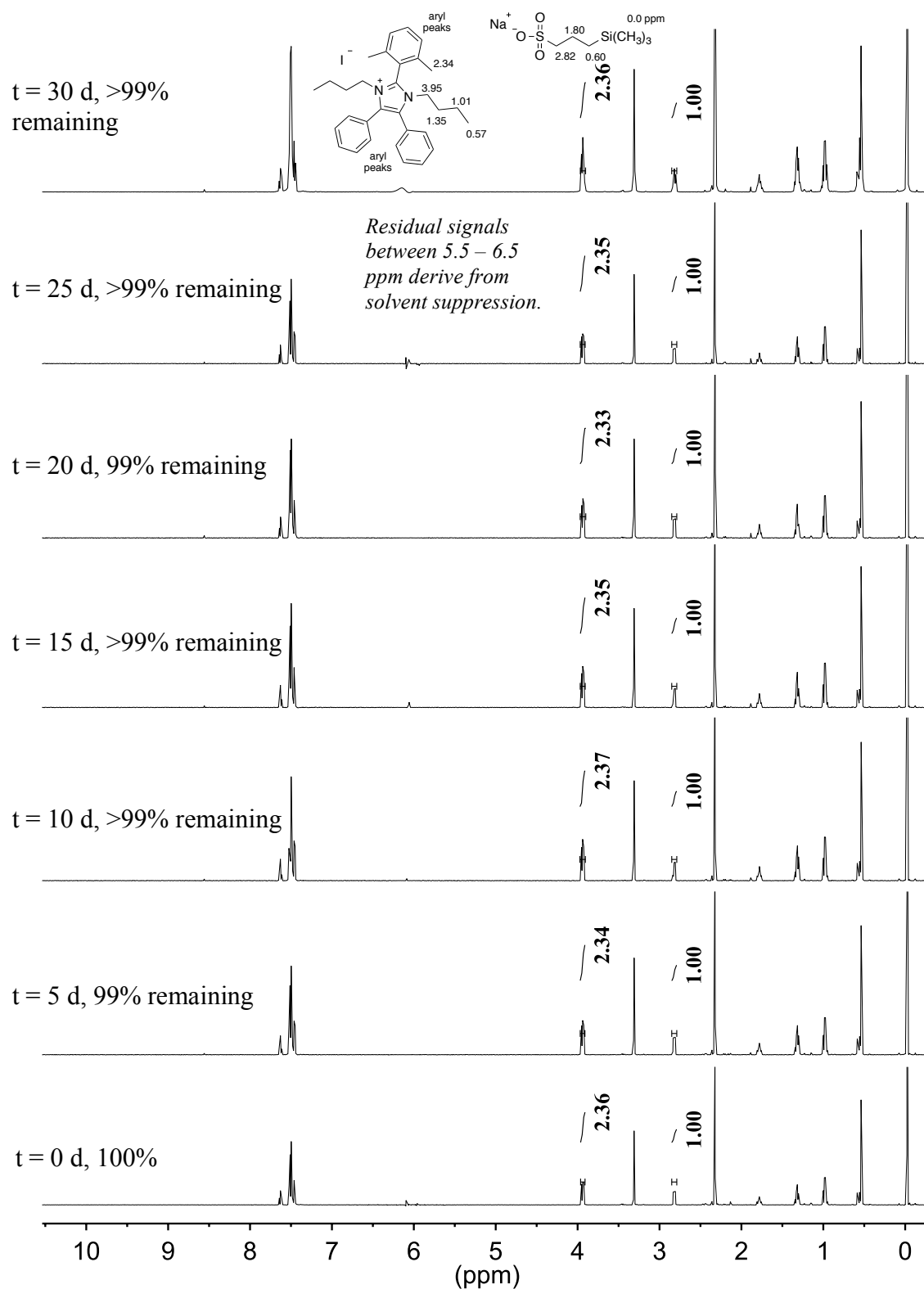


Figure 4.49 ¹H NMR spectra of **8a** over 30 days dissolved in a basic CD₃OH solution at 80 °C (2 M KOH, [KOH]/[**8a**] = 67) with an internal standard (TMS(CH₂)₃SO₃Na).

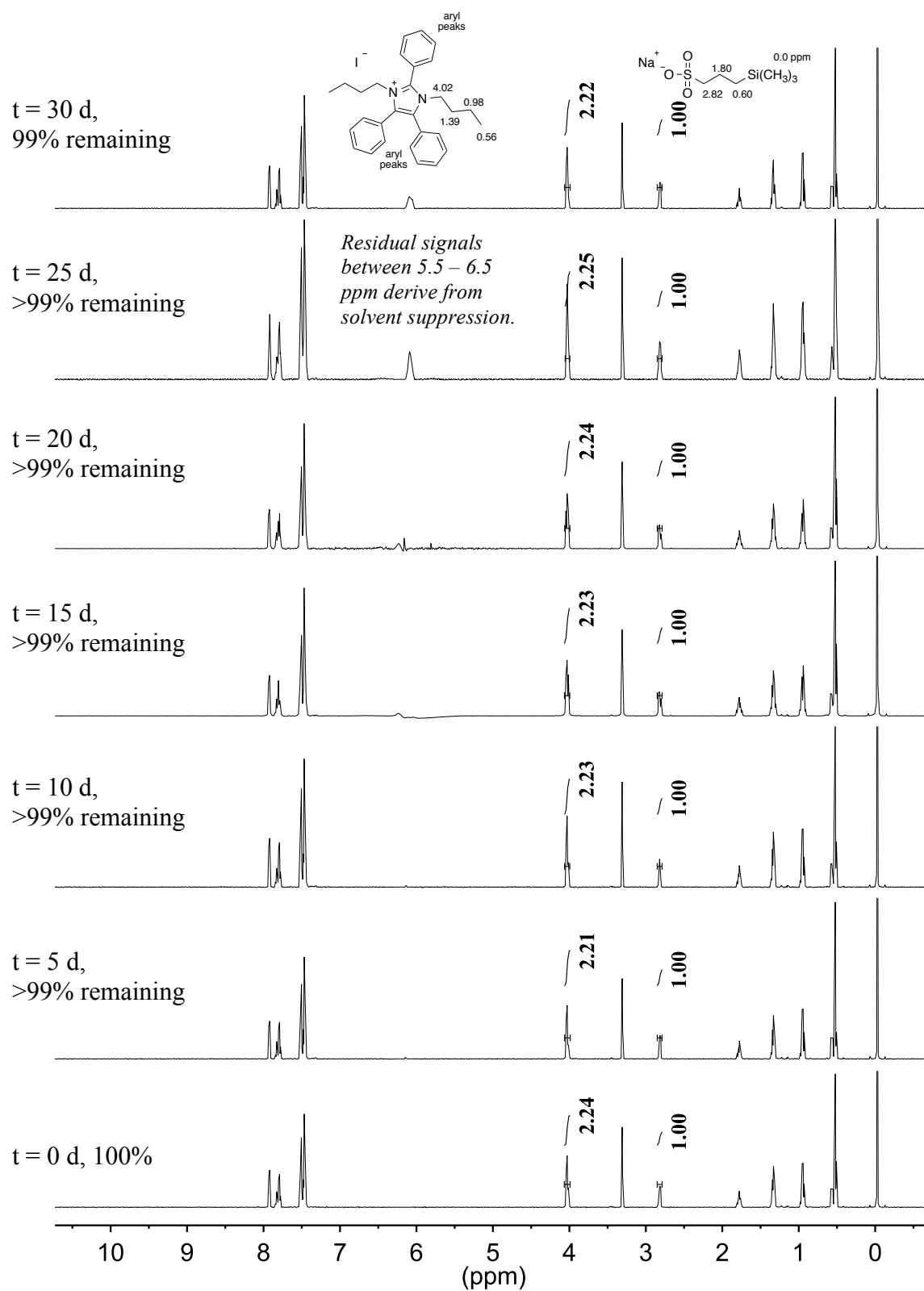


Figure 4.50 1H NMR spectra of **8b** over 30 days dissolved in a basic CD_3OH solution at $80\text{ }^\circ C$ (2 M KOH, $[KOH]/[8b] = 67$) with an internal standard (TMS(CH_2) $_3$ SO $_3$ Na).

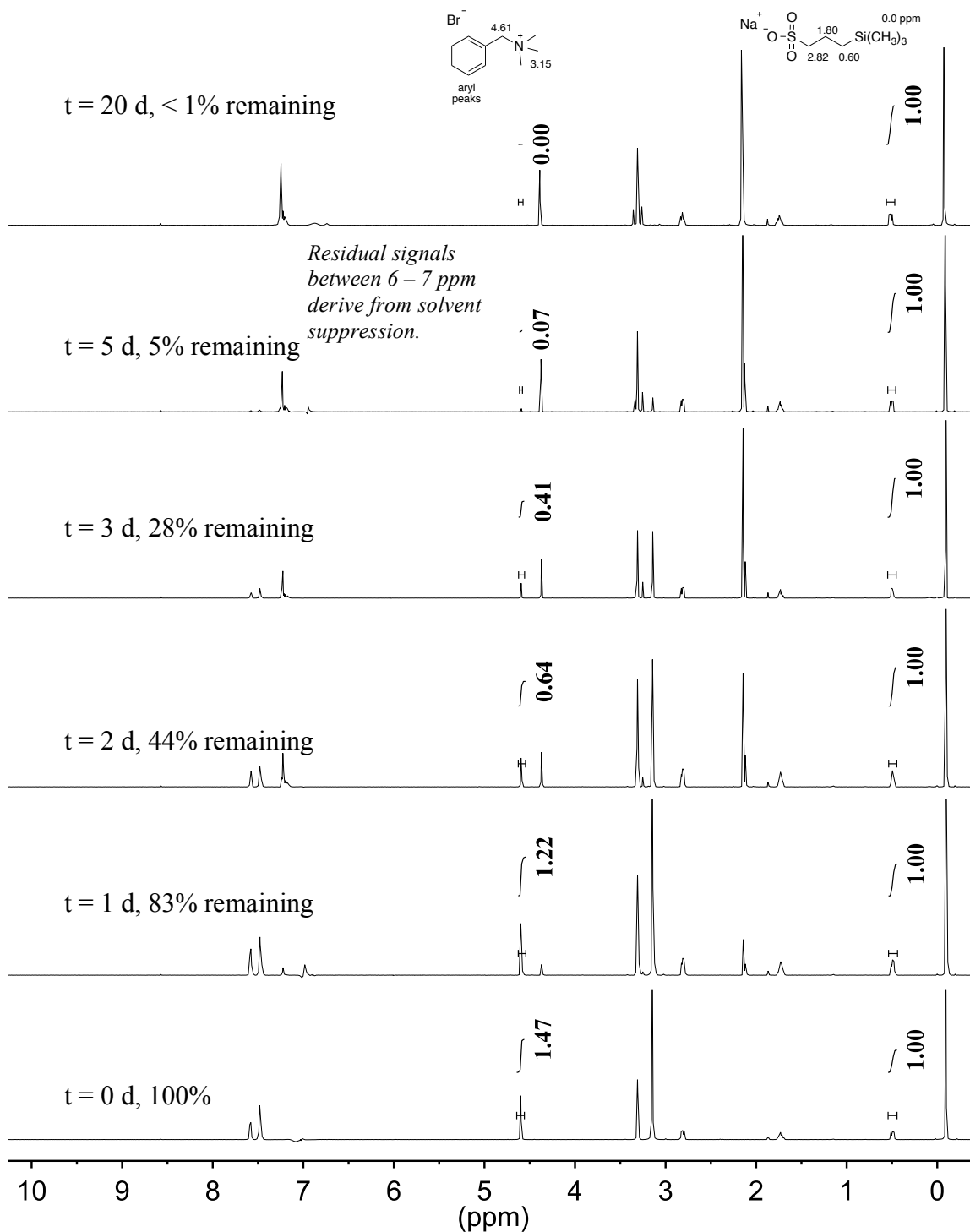


Figure 4.51 ¹H NMR spectra of **1** over 20 days dissolved in a basic CD₃OH solution at 80 °C (5 M KOH, [KOH]/[**1**] = 167 with an internal standard (TMS(CH₂)₃SO₃Na).

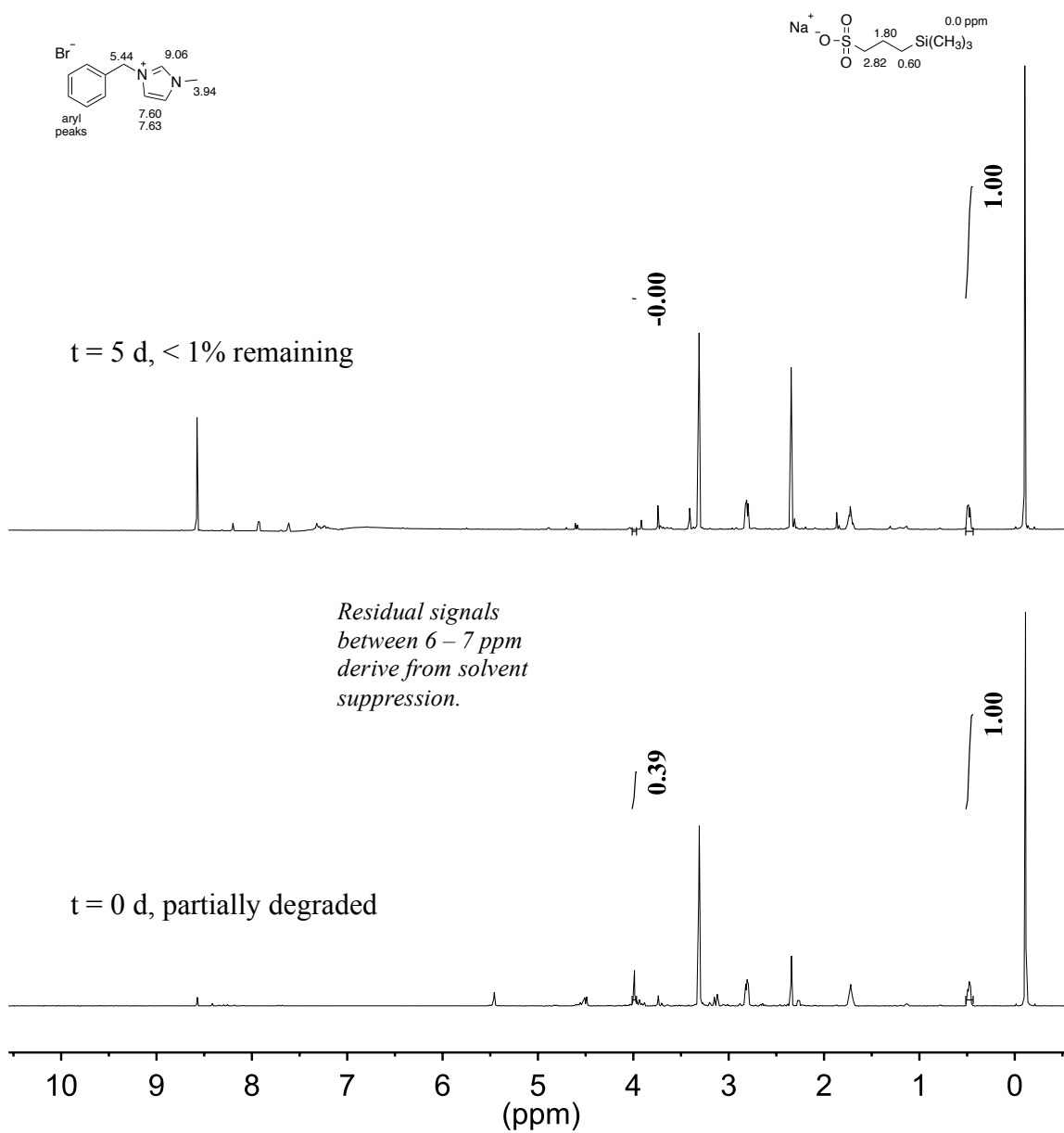


Figure 4.52 ^1H NMR spectra of **2a** over 5 days dissolved in a basic CD_3OH solution at $80\text{ }^\circ\text{C}$ (5 M KOH, $[\text{KOH}]/[\mathbf{2a}] = 167$ with an internal standard ($\text{TMS}(\text{CH}_2)_3\text{SO}_3\text{Na}$).

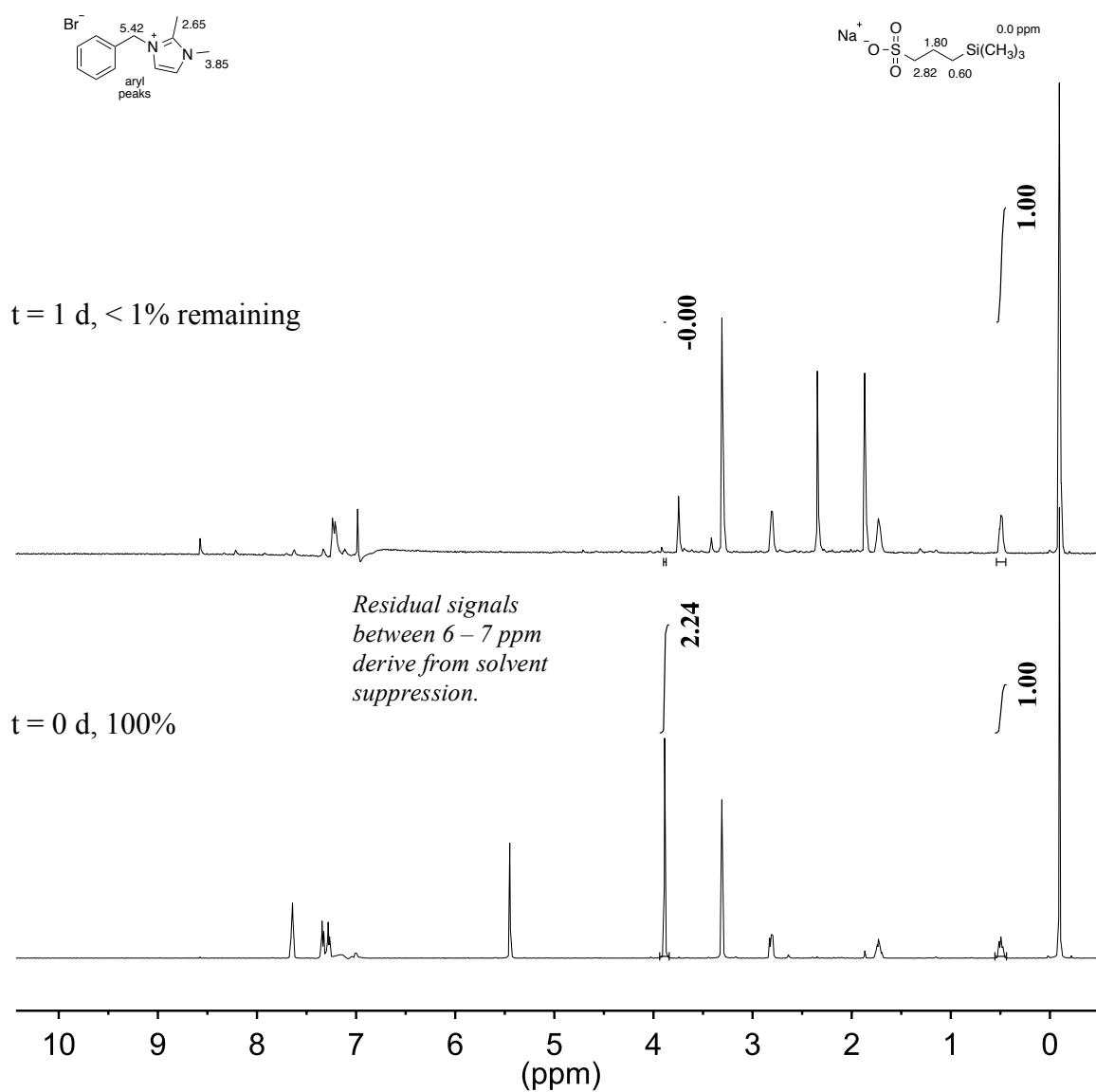


Figure 4.53 ¹H NMR spectra of **2b** over 1 day dissolved in a basic CD₃OH solution at 80 °C (5 M KOH, [KOH]/[**2b**] = 167) with an internal standard (TMS(CH₂)₃SO₃Na).

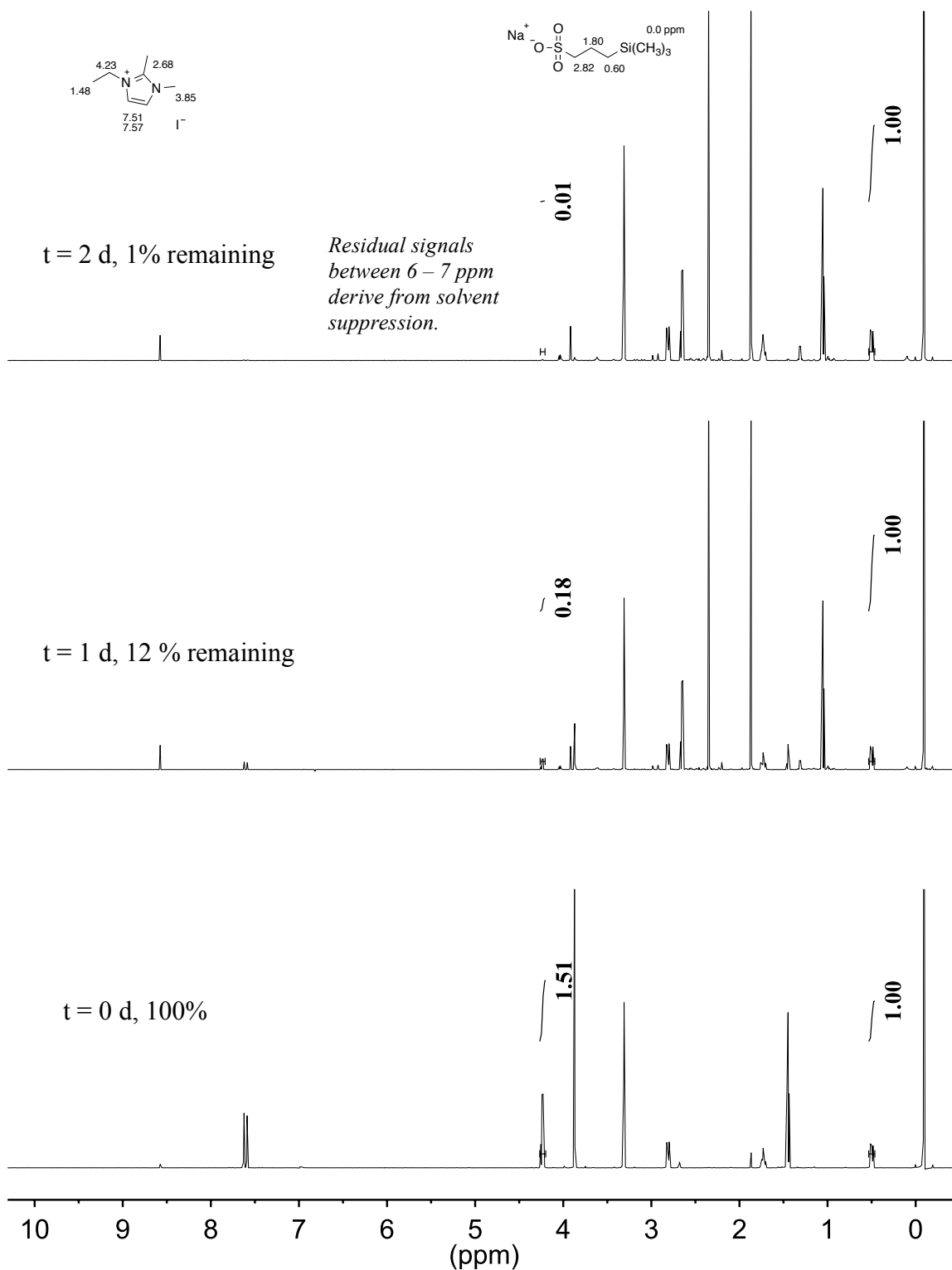


Figure 4.54 ¹H NMR spectra of **2c** over 2 days dissolved in a basic CD₃OH solution at 80 °C (5 M KOH, [KOH]/[**2c**] = 167) with an internal standard (TMS(CH₂)₃SO₃Na).

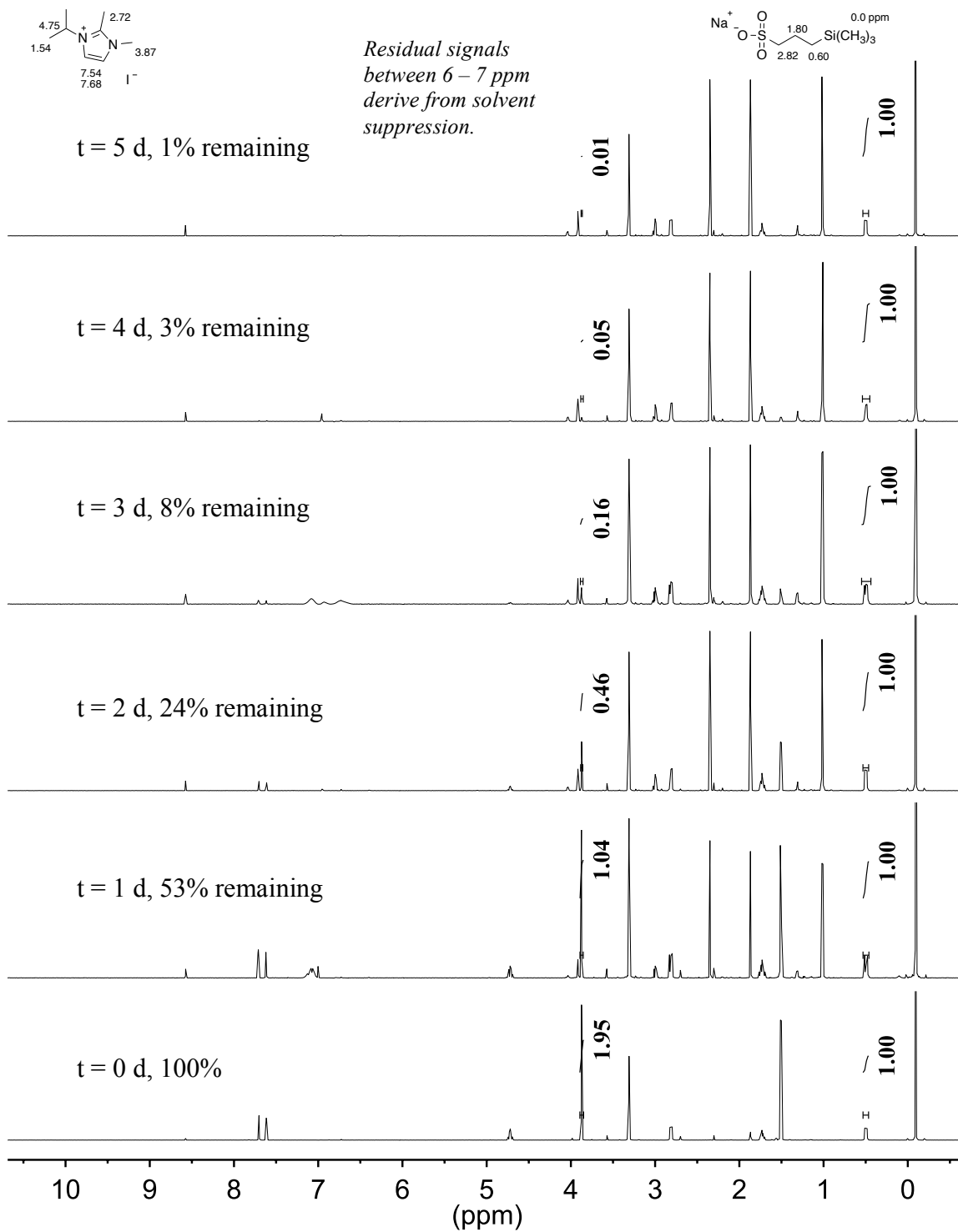


Figure 4.55 ¹H NMR spectra of **2d** over 5 days dissolved in a basic CD₃OH solution at 80 °C (5 M KOH, [KOH]/[**2d**] = 167) with an internal standard (TMS(CH₂)₃SO₃Na).

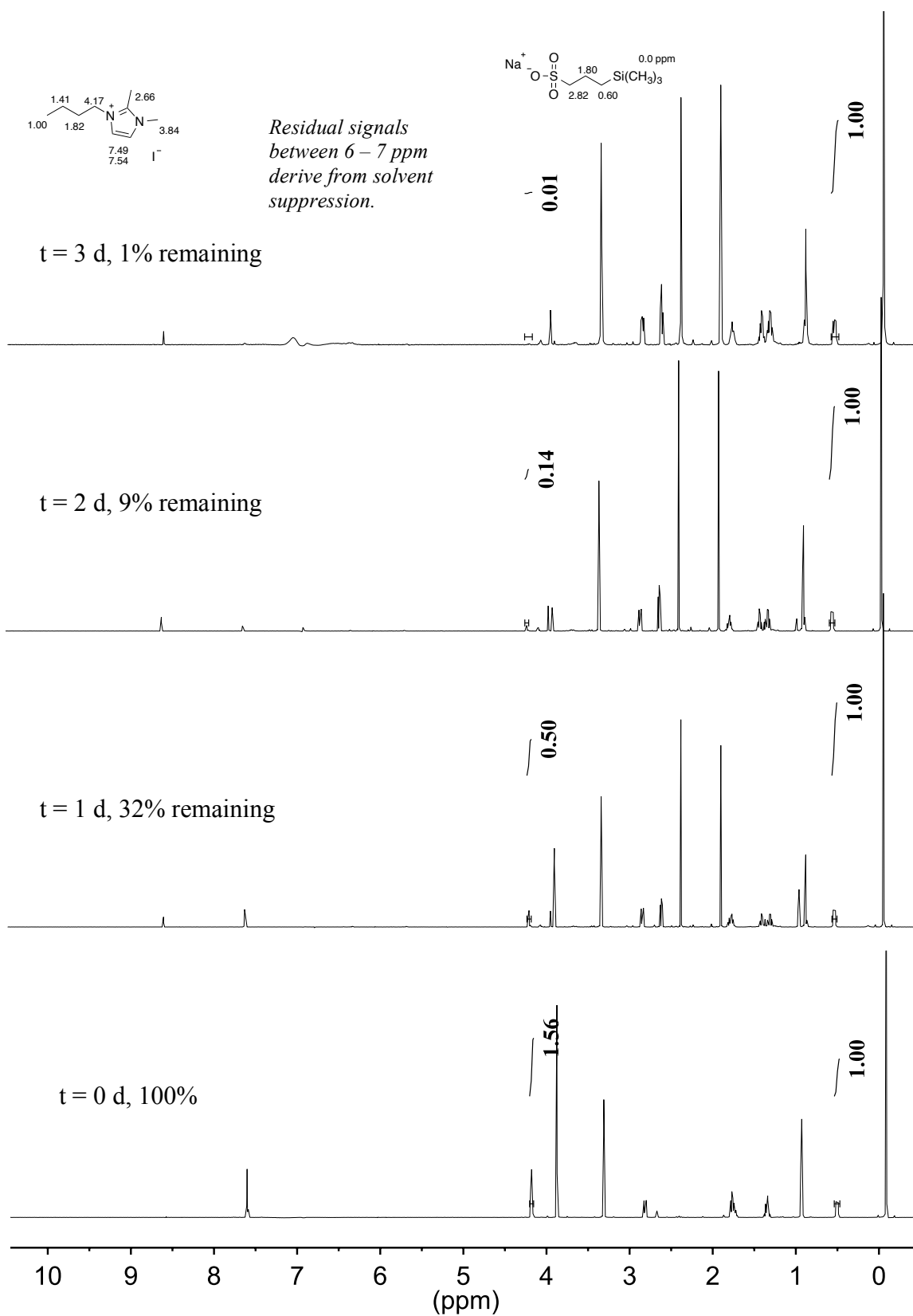


Figure 4.56 ^1H NMR spectra of **2e** over 3 days dissolved in a basic CD_3OH solution at 80°C (5 M KOH, $[\text{KOH}]/[\mathbf{2e}] = 167$) with an internal standard ($\text{TMS}(\text{CH}_2)_3\text{SO}_3\text{Na}$).

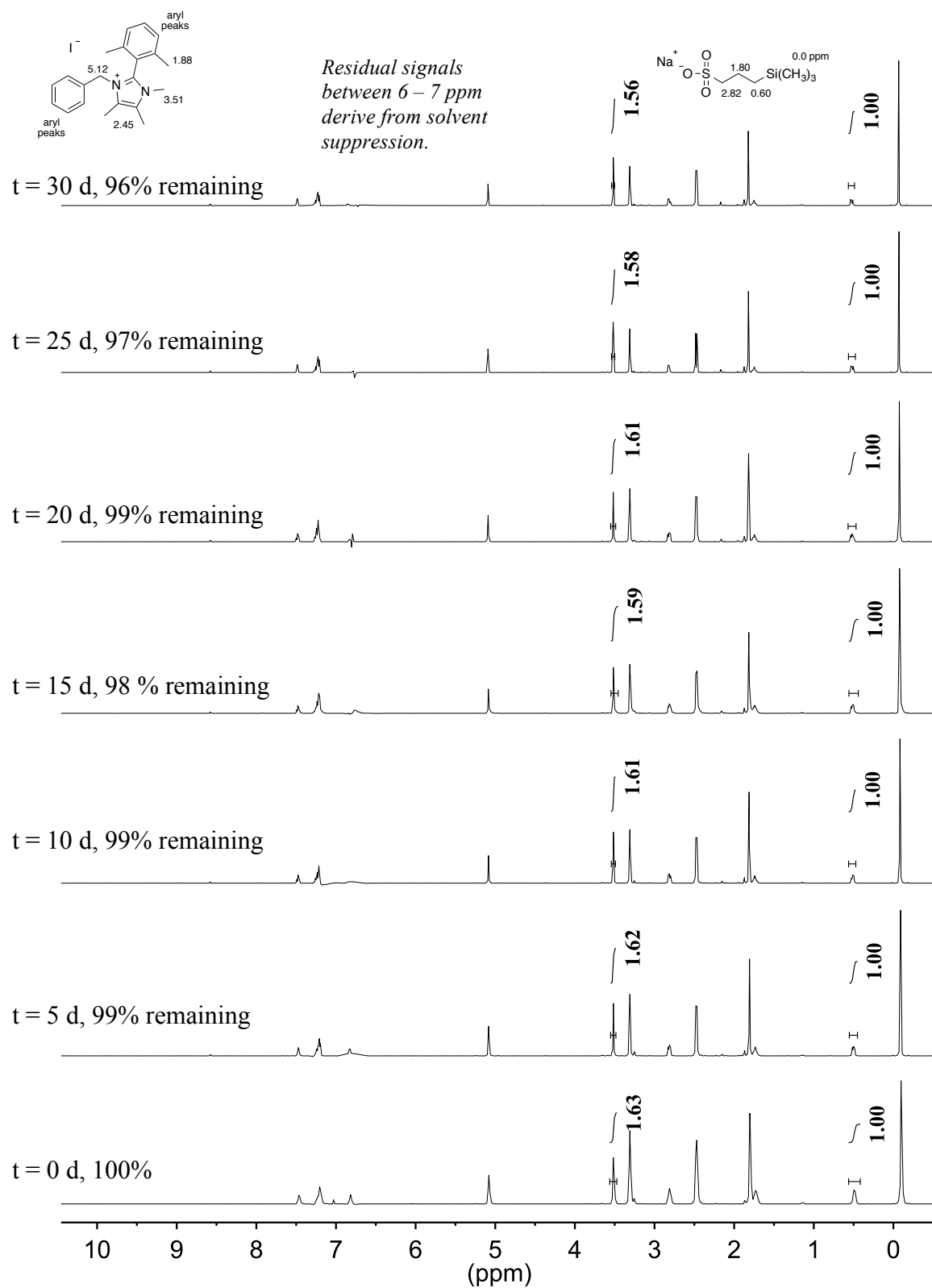


Figure 4.57 1H NMR spectra of **3a** over 30 days dissolved in a basic CD_3OH solution at 80 °C (5 M KOH, $[KOH]/[3a] = 167$) with an internal standard (TMS(CH_2) $_3$ SO $_3$ Na).

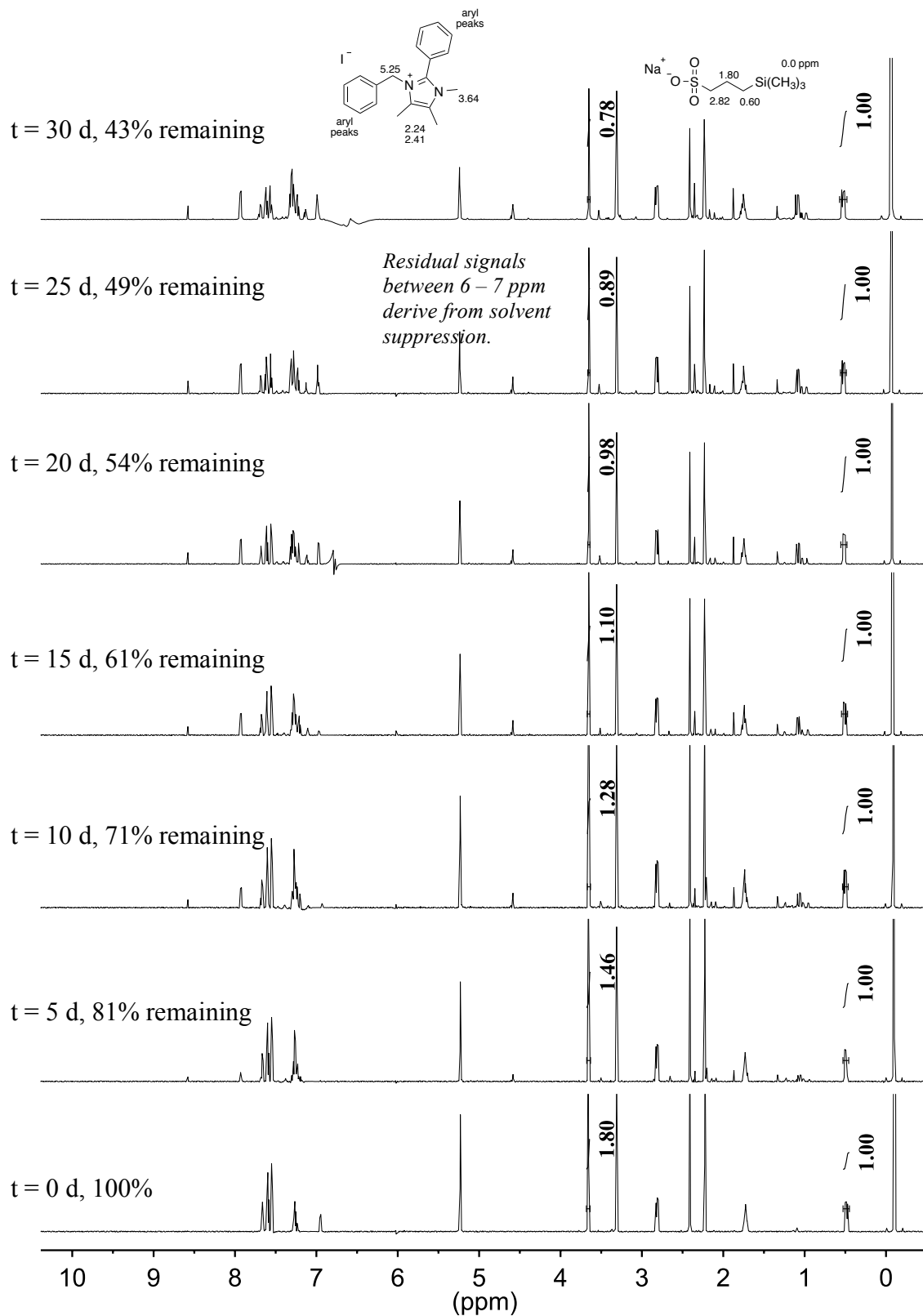


Figure 4.58 ^1H NMR spectra of **3b** over 30 days dissolved in a basic CD_3OH solution at 80°C (5 M KOH, $[\text{KOH}]/[\text{3b}] = 167$) with an internal standard ($\text{TMS}(\text{CH}_2)_3\text{SO}_3\text{Na}$).

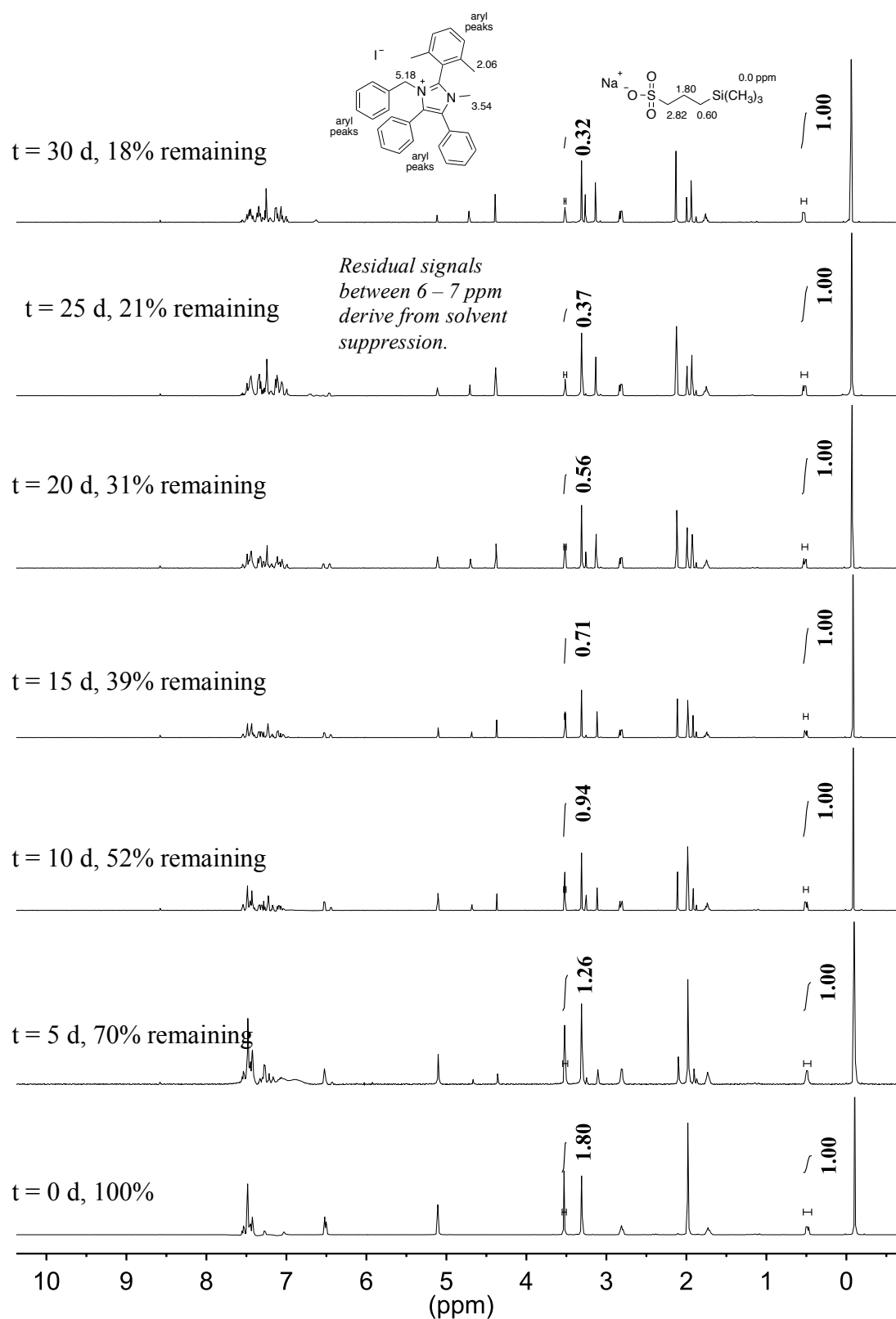


Figure 4.59 ^1H NMR spectra of **4a** over 30 days dissolved in a basic CD_3OH solution at 80°C (5 M KOH, $[\text{KOH}]/[\text{4a}] = 167$) with an internal standard ($\text{TMS}(\text{CH}_2)_3\text{SO}_3\text{Na}$).

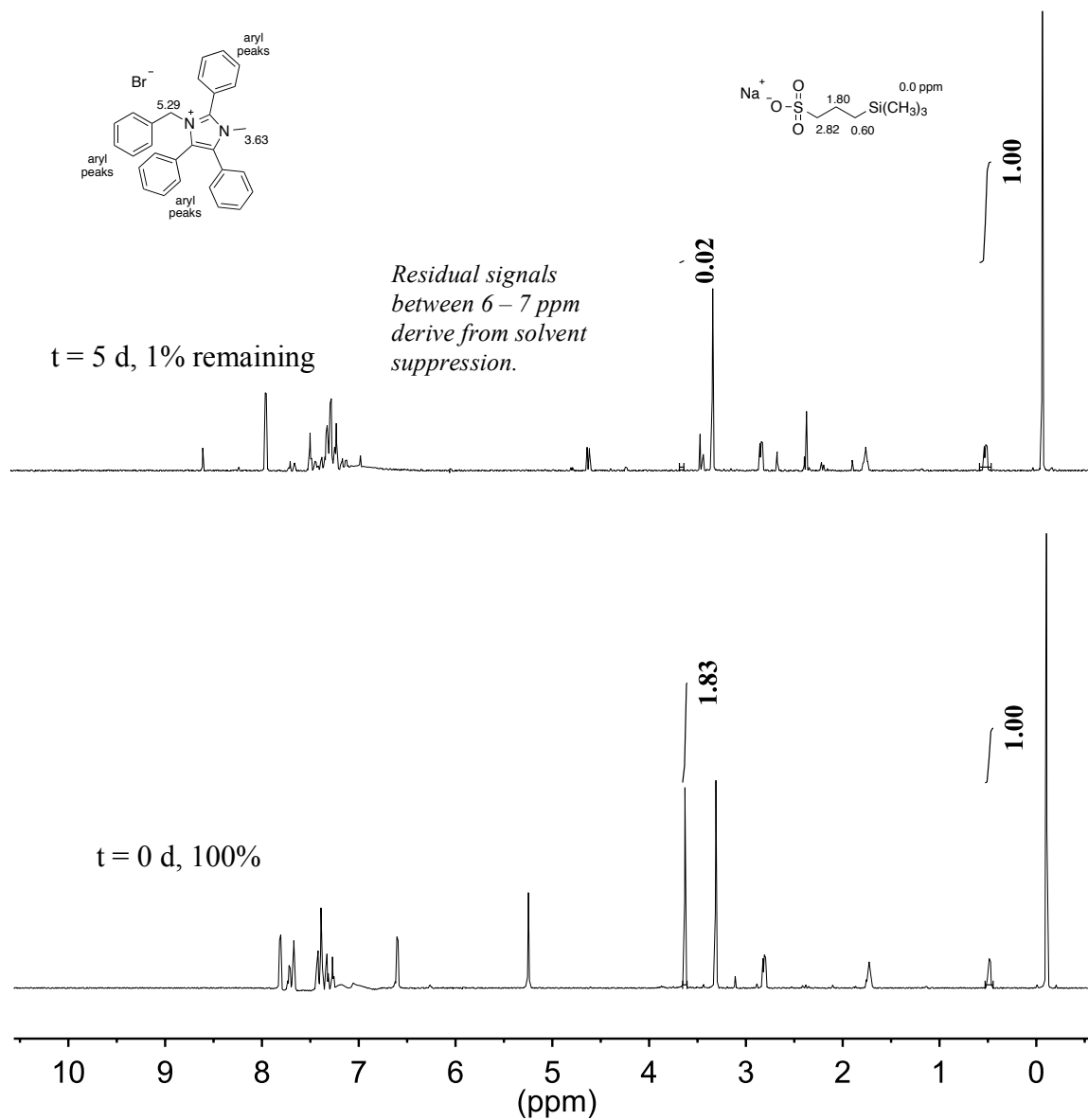


Figure 4.60 ^1H NMR spectra of **4b** over 5 days dissolved in a basic CD_3OH solution at 80°C (5 M KOH, $[\text{KOH}]/[\text{4b}] = 167$) with an internal standard ($\text{TMS}(\text{CH}_2)_3\text{SO}_3\text{Na}$).

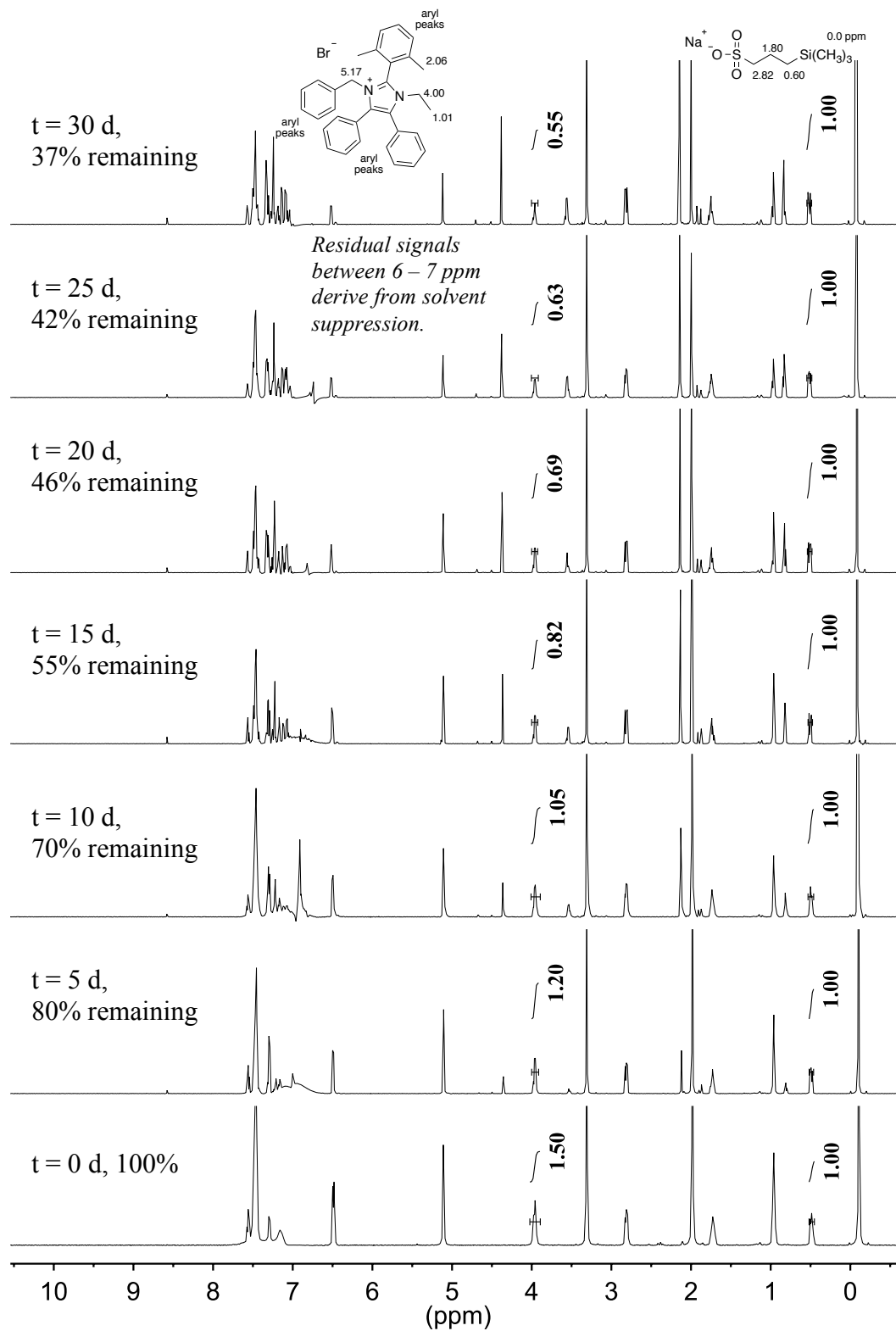


Figure 4.61 ¹H NMR spectra of 5a over 30 days dissolved in a basic CD₃OH solution at 80 °C (5 M KOH, [KOH]/[5a] = 167) with an internal standard (TMS(CH₂)₃SO₃Na).

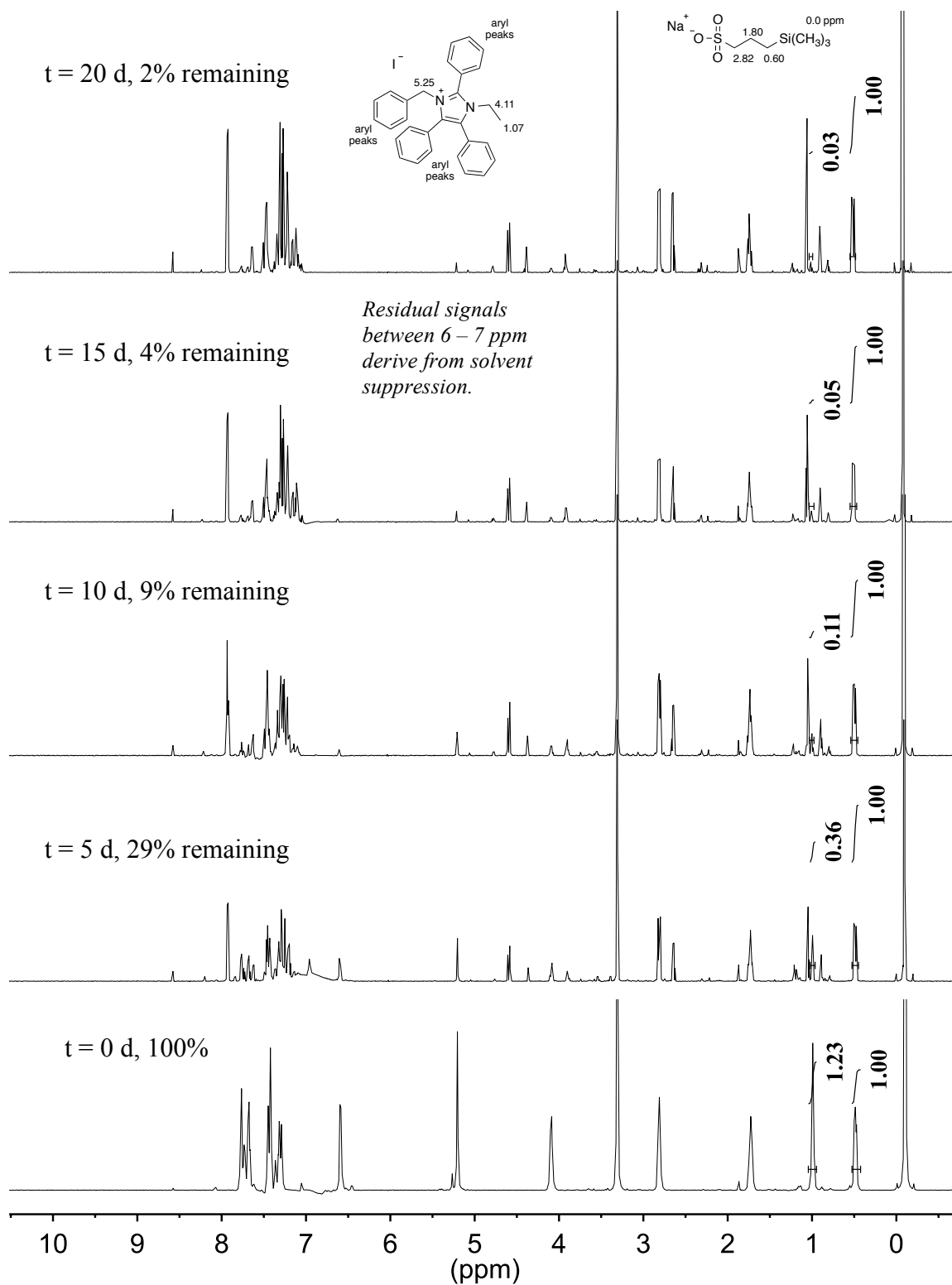


Figure 4.62 ^1H NMR spectra of **5b** over 30 days dissolved in a basic CD_3OH solution at 80°C (5 M KOH, $[\text{KOH}]/[\text{5b}] = 167$) with an internal standard ($\text{TMS}(\text{CH}_2)_3\text{SO}_3\text{Na}$).

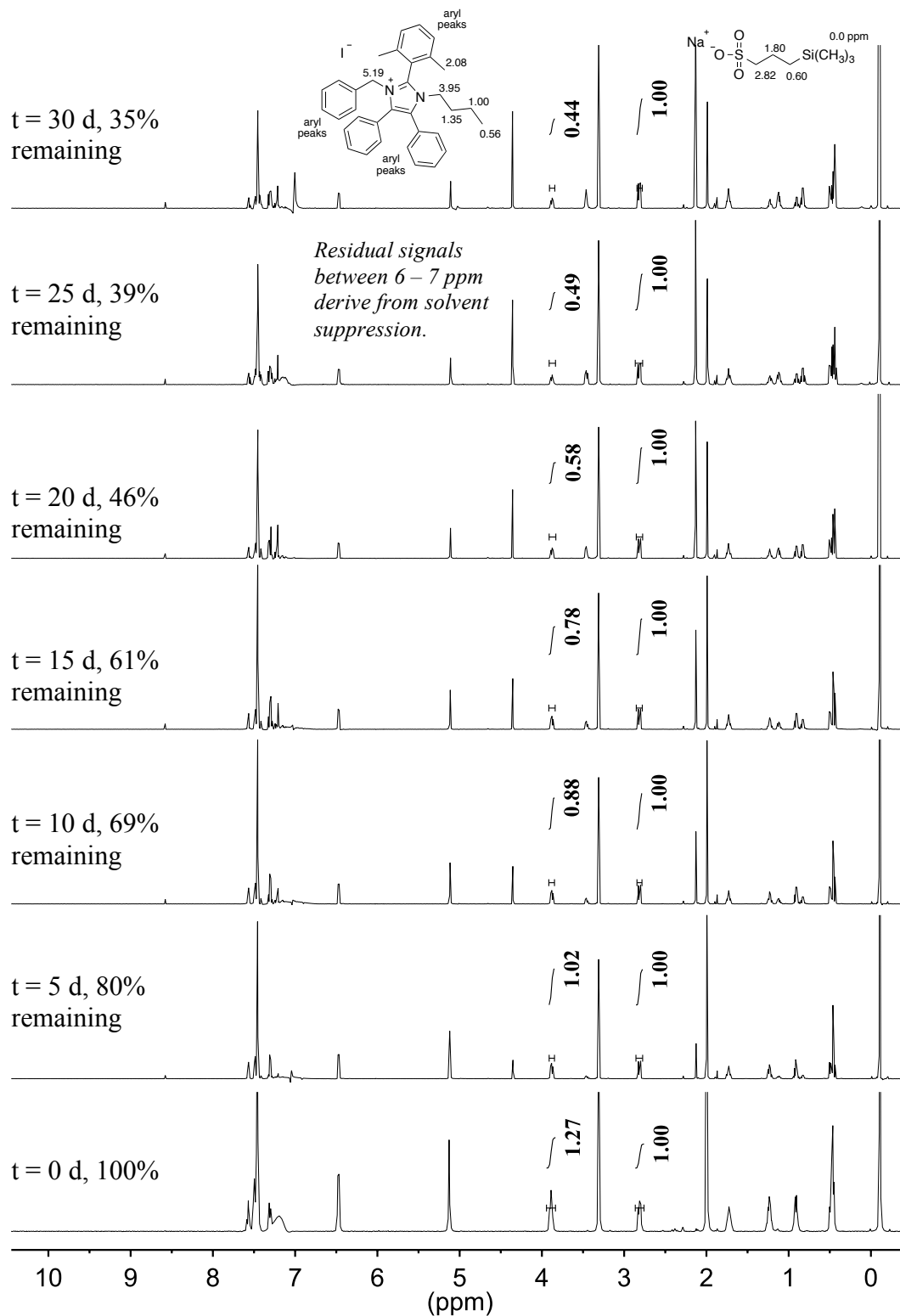


Figure 4.63 ¹H NMR spectra of **6a** over 30 days dissolved in a basic CD₃OH solution at 80 °C (5 M KOH, [KOH]/[**6a**] = 167) with an internal standard (TMS(CH₂)₃SO₃Na).

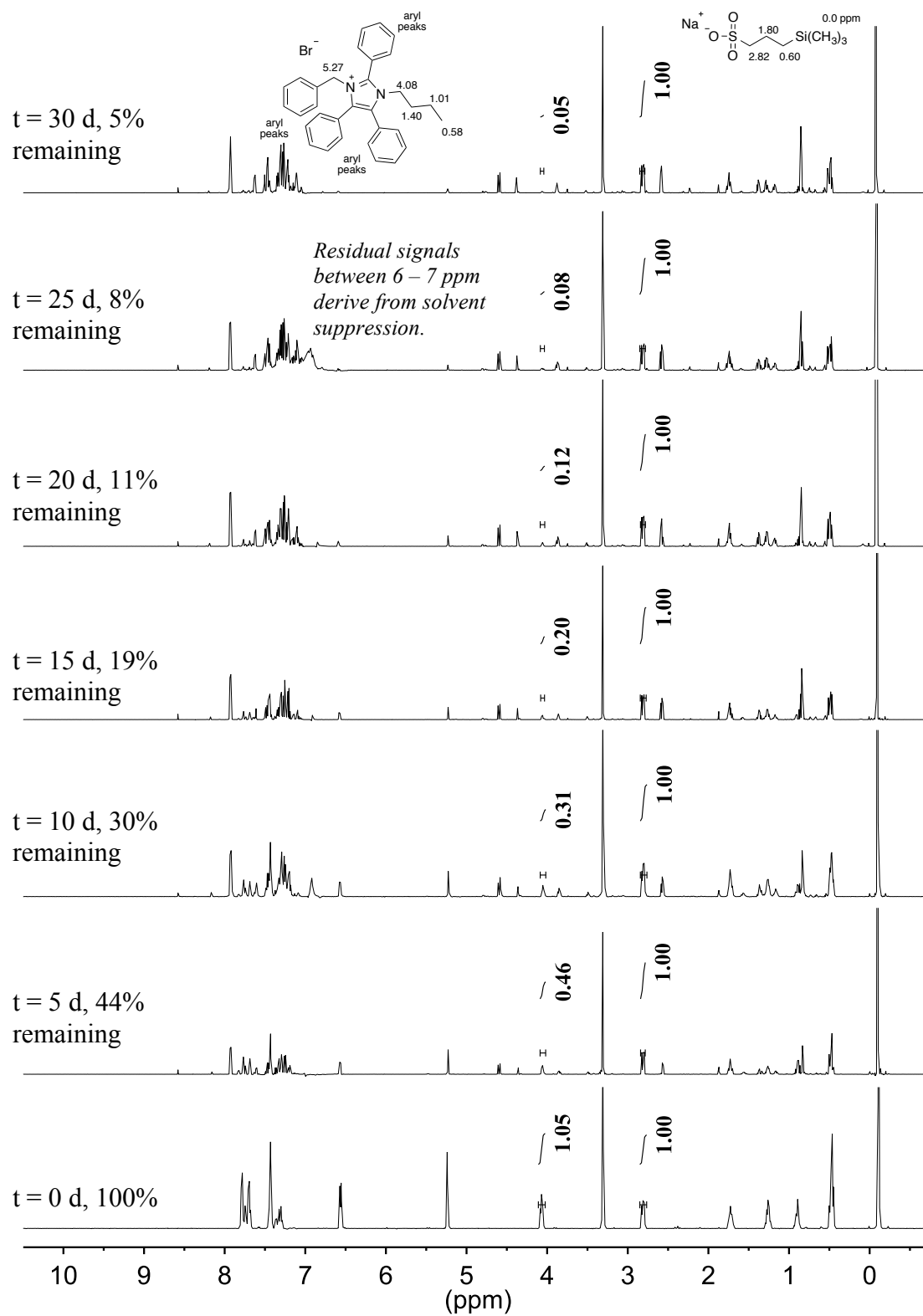


Figure 4.64 ^1H NMR spectra of **6b** over 30 days dissolved in a basic CD_3OH solution at 80°C (5 M KOH, $[\text{KOH}]/[\text{6b}] = 167$) with an internal standard ($\text{TMS}(\text{CH}_2)_3\text{SO}_3\text{Na}$).

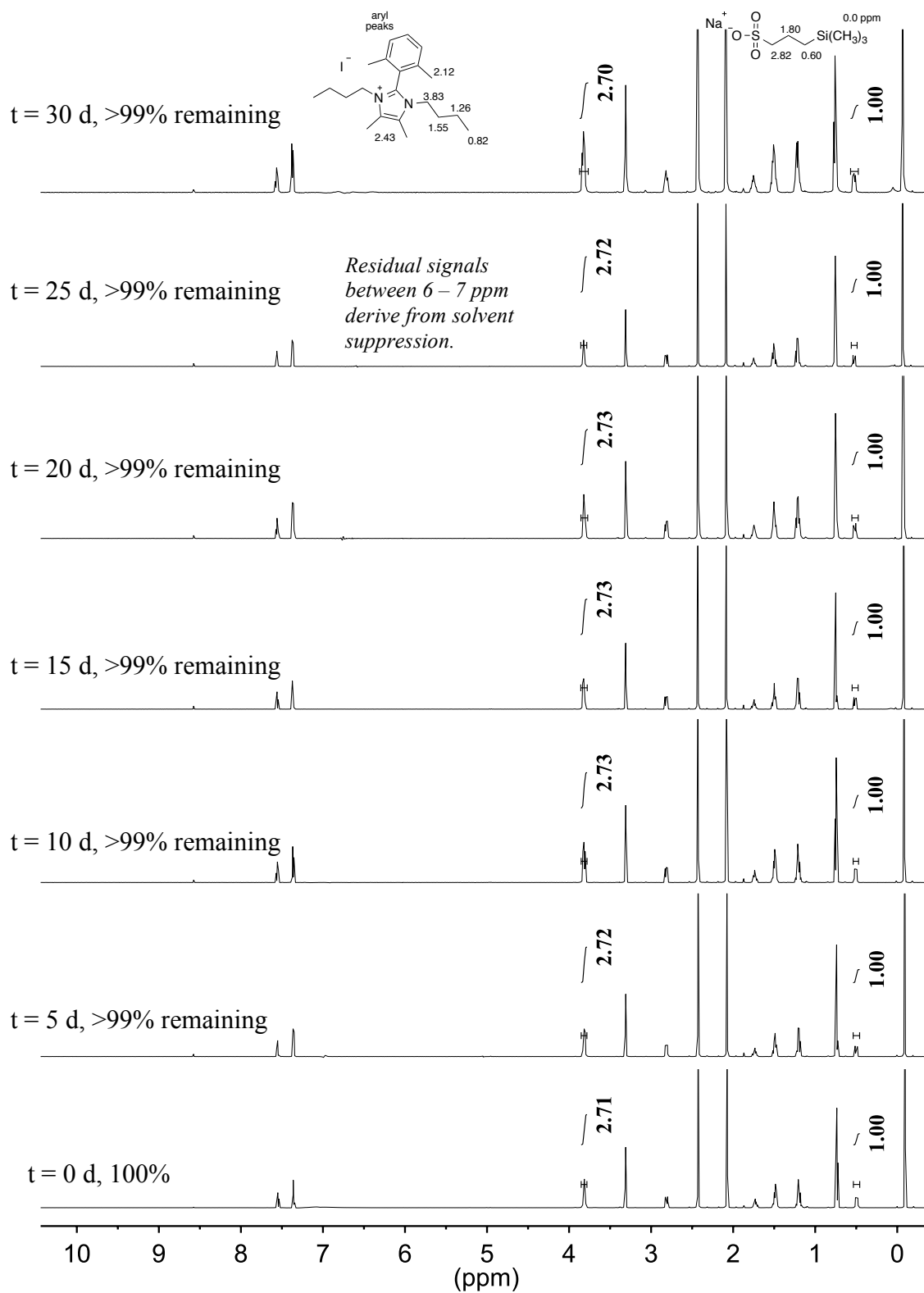


Figure 4.65 ^1H NMR spectra of **7a** over 30 days dissolved in a basic CD_3OH solution at 80°C (5 M KOH, $[\text{KOH}]/[\text{7a}] = 167$ with an internal standard ($\text{TMS}(\text{CH}_2)_3\text{SO}_3\text{Na}$).

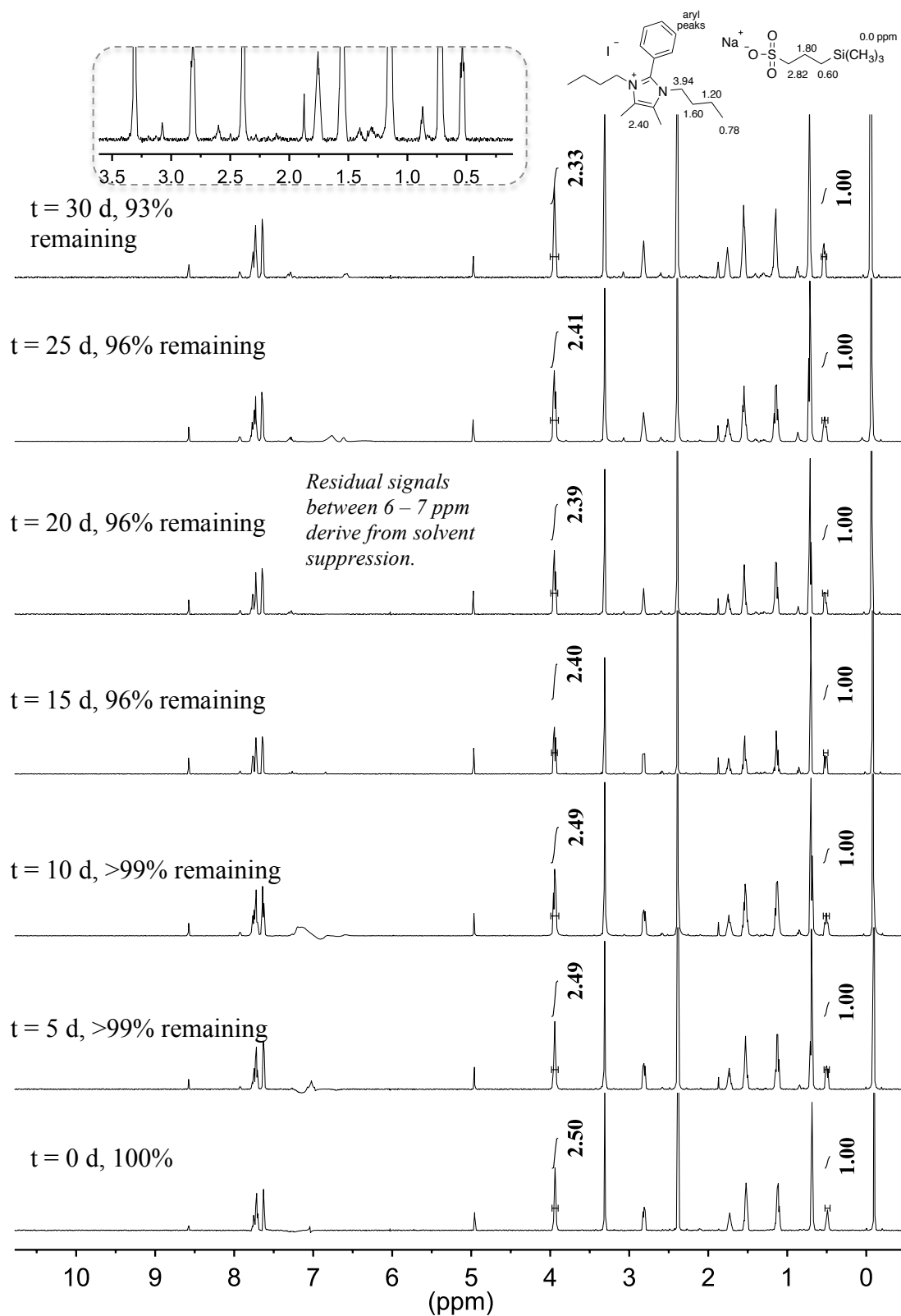


Figure 4.66 ^1H NMR spectra of **7b** over 30 days dissolved in a basic CD_3OH solution at 80°C (5 M KOH, $[\text{KOH}]/[\text{7b}] = 167$) with an internal standard (TMS(CH_2) $_3$ SO $_3$ Na). Inset is extracted from $t = 30$ d.

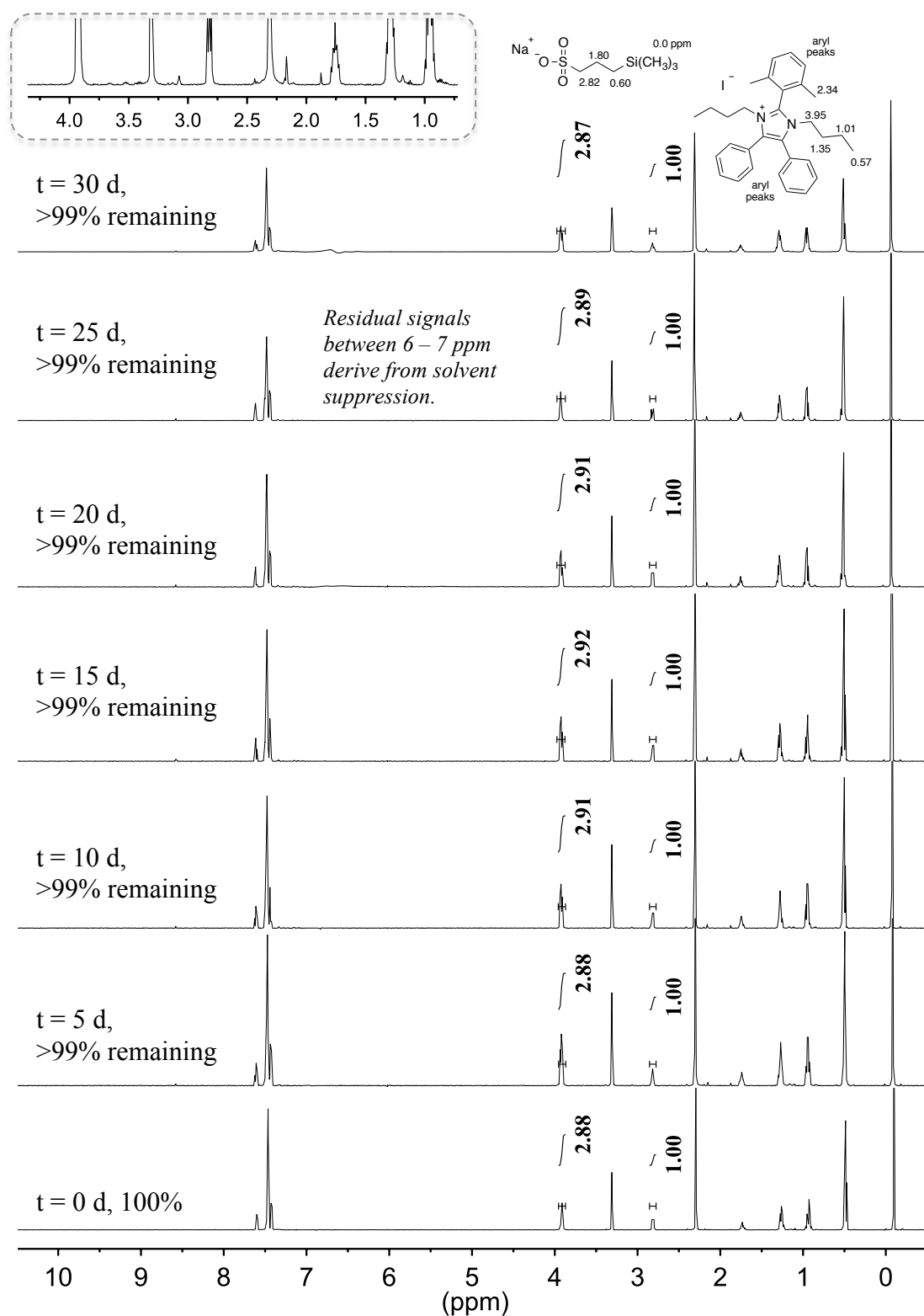


Figure 4.67 ^1H NMR spectra of **8a** over 30 days dissolved in a basic CD_3OH solution at 80°C (5 M KOH, $[\text{KOH}]/[\textbf{8a}] = 167$) with an internal standard ($\text{TMS}(\text{CH}_2)_3\text{SO}_3\text{Na}$). Inset is extracted from $t = 30$ d.

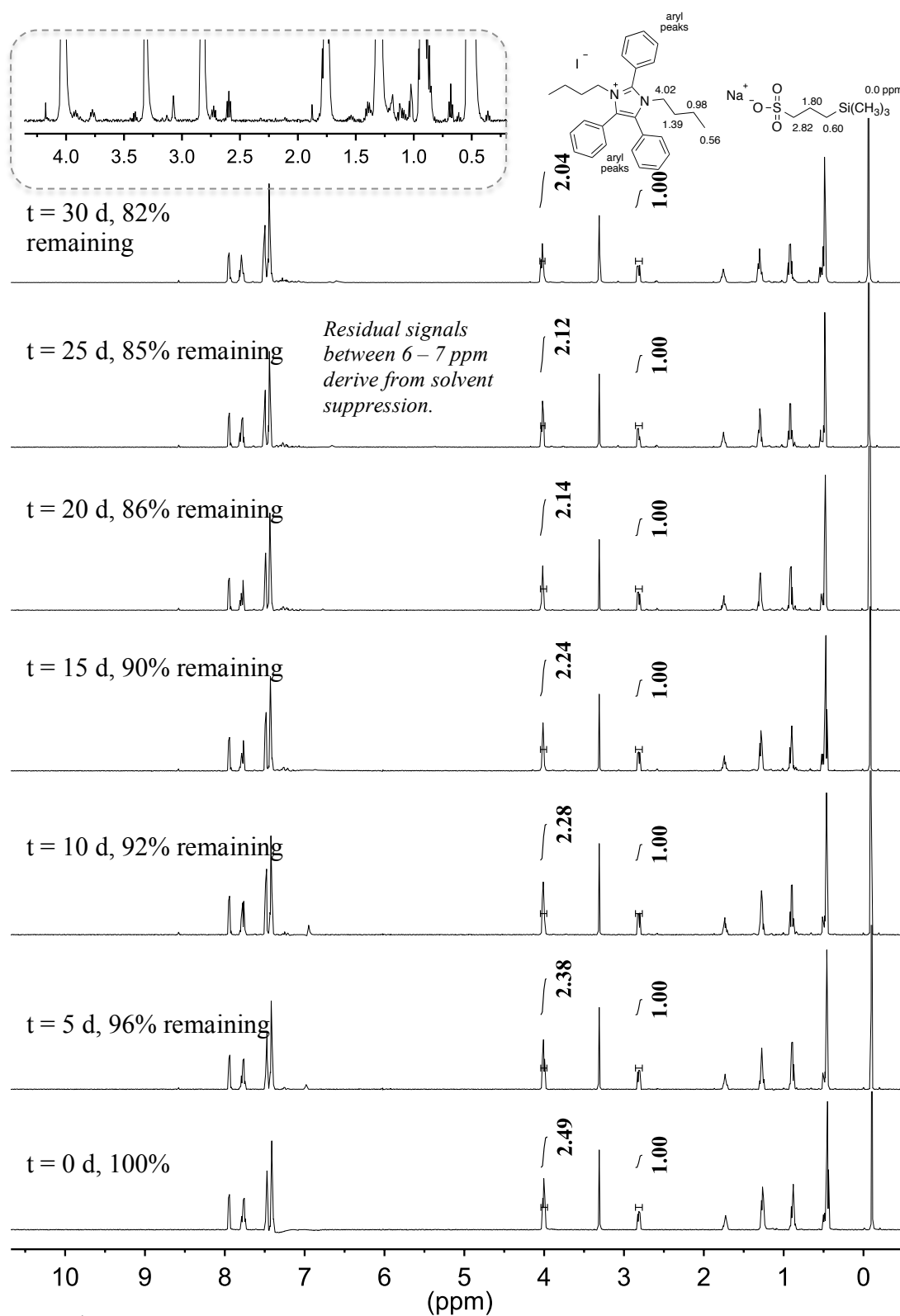


Figure 4.68 ^1H NMR spectra of **8b** over 30 days dissolved in a basic CD_3OH solution at 80°C (5 M KOH, $[\text{KOH}]/[\text{8b}] = 167$) with an internal standard (TMS(CH_2) $_3$ SO $_3$ Na). Inset is extracted from $t = 30$ d.

REFERENCES

- (1) (a) Jacobson, M. Z. *Science* **2005**, *308*, 1901. (b) Dunn, S. *Int. J. Hydrogen Energy* **2002**, *27*, 235.

- (2) For recent reviews: (a) Lucia, U. *Renewable Sustainable Energy Rev.* **2014**, *30*, 164. (b) O'Hayre, R. P. *Fuel Cell Fundamentals*; Wiley: Hoboken, NJ, 2006. (c) Whittingham, M. S.; Zawodzinski, T. *Chem. Rev.* **2004**, *104*, 4243.

- (3) (a) Zhang, H.; Shen, P. K. *Chem. Rev.* **2012**, *112*, 2780. (b) Hickner, M. A. *Mater. Today* **2010**, *13*, 34. (c) Hickner, M. A.; Ghassemi, H.; Kim, Y. S.; Einsla, B. R.; McGrath, J. E. *Chem. Rev.* **2004**, *104*, 4587. (d) Stone, C. *Solid State Ionics* **2002**, *152-153*, 1.

- (4) Borup, R.; Meyers, J.; Pivovar, B.; Kim, Y. S.; Mukundan, R.; Garland, N.; Myers, D.; Wilson, M.; Garzon, F.; Wood, D.; Zelenay, P.; More, K.; Stroh, K.; Zawodzinski, T.; Boncella, J.; McGrath, J. E.; Inaba, M.; Miyatake, K.; Hori, M.; Ota, K.; Ogumi, Z.; Miyata, S.; Nishikata, A.; Siroma, Z.; Uchimoto, Y.; Yasuda, K.; Kimijima, K.; Iwashita, N. *Chem. Rev.* **2007**, *107*, 3904.

- (5) (a) Poynton, S. D.; Kizewski, J. P.; Slade, R. C. T.; Varcoe, J. R. *Solid State Ionics* **2010**, *181*, 219. (b) Lu, S.; Pan, J.; Huang, A.; Zhuang, L.; Lu, J. *Proc. Natl. Acad. Sci.* **2008**, *105*, 20611. (c) Wagner, N.; Schulze, M.; Gülzow, E. *J. Power Sources* **2004**, *127*, 264. (d) McLean, G. *Int. J. Hydrogen Energy* **2002**, *27*, 507.

- (6) (a) Sleightholme, A. E. S.; Varcoe, J. R.; Kucernak, A. R. *Electrochem. Commun.* **2008**, *10*, 151. (b) Varcoe, J. R.; Slade, R. C. T.; Wright, G. L.; Chen, Y. *J. Phys. Chem. B* **2006**, *110*, 21041. (c) Spendelow, J. S.; Goodpaster, J. D.; Kenis, P. J. A.; Wieckowski, A. *J. Phys. Chem. B* **2006**, *110*, 9545. (d) Varcoe, J. R.; Slade, R. C. T. *Fuel Cells* **2005**, *5*, 187.

- (7) Merle, G.; Wessling, M.; Nijmeijer, K. *J. Membr. Sci.* **2011**, *377*, 1 (and references therein).

- (8) (a) Varcoe, J. R.; Atanassov, P.; Dekel, D. R.; Herring, A. M.; Hickner, M. A.; Kohl, P. A.; Kucernak, A. R.; Mustain, W. E.; Nijmeijer, K.; Scott, K.; Xu, T.; Zhuang, L. *Energy Environ. Sci.* **2014**, *7*, 3135. (b) Hickner, M. A.; Herring, A. M.; Coughlin, E. B. *J. Polym. Sci., Part B: Polym. Phys.* **2013**, *51*, 1727. (c) Couture, G.; Alaaeddine, A.; Boschet, F.; Ameduri, B. *Prog. Polym. Sci.* **2011**, *36*, 1521. (d) Varcoe, J. R.; Poynton, S. D.; Slade, R. C. T.; Vielstich, W.; Lamm, A.; Gasteiger, H. A.;

Yokokawa, H., Eds. *Handbook of Fuel Cells*; John Wiley & Sons, Ltd: Chichester, UK, 2010.

- (9) Varcoe, J. R.; Slade, R. C. T.; Lam How Yee, E.; Poynton, S. D.; Driscoll, D. J.; Apperley, D. C. *Chem. Mater.* **2007**, *19*, 2686 (and references therein).
- (10) (a) Park, A. M.; Turley, F. E.; Wycisk, R. J.; Pintauro, P. N. *Macromolecules* **2014**, *47*, 227. (b) Mohanty, A. D.; Lee, Y.-B.; Zhu, L.; Hickner, M. A.; Bae, C. *Macromolecules* **2014**, *47*, 1973. (c) Li, N.; Zhang, Q.; Wang, C.; Lee, Y. M.; Guiver, M. D. *Macromolecules* **2012**, *45*, 2411. (d) Ni, J.; Zhao, C.; Zhang, G.; Zhang, Y.; Wang, J.; Ma, W.; Liu, Z.; Na, H. *Chem. Commun.* **2011**, *47*, 8943. (e) Tanaka, M.; Fukasawa, K.; Nishino, E.; Yamaguchi, S.; Yamada, K.; Tanaka, H.; Bae, B.; Miyatake, K.; Watanabe, M. *J. Am. Chem. Soc.* **2011**, *133*, 10646. (f) Yan, J.; Hickner, M. A. *Macromolecules* **2010**, *43*, 2349. (g) Wang, J.; Zhao, Z.; Gong, F.; Li, S.; Zhang, S. *Macromolecules* **2009**, *42*, 8711. (h) Hibbs, M. R.; Hickner, M. A.; Alam, T. M.; McIntyre, S. K.; Fujimoto, C. H.; Cornelius, C. J. *Chem. Mater.* **2008**, *20*, 2566.
- (11) (a) Li, Q.; Liu, L.; Miao, Q.; Jin, B.; Bai, R. *Chem. Commun.* **2014**, *50*, 2791. (b) Li, N.; Wang, L.; Hickner, M. *Chem. Commun.* **2014**, *50*, 4092. (c) Li, N.; Leng, Y.; Hickner, M. A.; Wang, C.-Y. *J. Am. Chem. Soc.* **2013**, *135*, 10124. (d) Li, X.; Yu, Y.; Liu, Q.; Meng, Y. *ACS Appl. Mater. Interfaces* **2012**, *4*, 3627. (e) Li, N.; Yan, T.; Li, Z.; Thurn-Albrecht, T.; Binder, W. H. *Energy Environ. Sci.* **2012**, *5*, 7888. (f) Wang, G.; Weng, Y.; Chu, D.; Xie, D.; Chen, R. *J. Membr. Sci.* **2009**, *326*, 4. (g) Wu, L.; Xu, T.; Yang, W. *J. Membr. Sci.* **2006**, *286*, 185.
- (12) (a) Chen, D.; Hickner, M. A. *Macromolecules* **2013**, *46*, 9270. (b) Han, J.; Peng, H.; Pan, J.; Wei, L.; Li, G.; Chen, C.; Xiao, L.; Lu, J.; Zhuang, L. *ACS Appl. Mater. Interfaces* **2013**, *5*, 13405. (c) Liu, Z.; Li, X.; Shen, K.; Feng, P.; Zhang, Y.; Xu, X.; Hu, W.; Jiang, Z.; Liu, B.; Guiver, M. D. *J. Mater. Chem. A* **2013**, *1*, 6481. (d) Zhang, Z.; Wu, L.; Varcoe, J.; Li, C.; Ong, A. L.; Poynton, S.; Xu, T. *J. Mater. Chem. A* **2013**, *1*, 2595.
- (13) (a) Li, N.; Guiver, M. D.; Binder, W. H. *ChemSusChem* **2013**, *6*, 1376. (b) Hibbs, M. R.; Fujimoto, C. H.; Cornelius, C. J. *Macromolecules* **2009**, *42*, 8316.
- (14) (a) Tsai, T.-H.; Maes, A. M.; Vandiver, M. A.; Versek, C.; Seifert, S.; Tuominen, M.; Liberatore, M. W.; Herring, A. M.; Coughlin, E. B. *J. Polym. Sci., Part B: Polym. Phys.* **2013**, *51*, 1751. (b) Disabb-Miller, M. L.; Johnson, Z. D.; Hickner, M. A. *Macromolecules* **2013**, *46*, 949. (c) Zeng, Q. H.; Liu, Q. L.; Broadwell, I.; Zhu, A. M.; Xiong, Y.; Tu, X. P. *J. Membr. Sci.* **2010**, *349*, 237. (d) Varcoe, J. R.; Slade, R. C. T.; Lam How Yee, E. *Chem. Commun.* **2006**, 1428.

- (15) (a) Maes, A. M.; Pandey, T. P.; Vandiver, M. A.; Lundquist, L. K.; Yang, Y.; Horan, J. L.; Krosovsky, A.; Liberatore, M. W.; Seifert, S.; Herring, A. M. *Electrochim. Acta* **2013**, *110*, 260. (b) Zhang, M.; Kim, H. K.; Chalkova, E.; Mark, F.; Lvov, S. N.; Chung, T. C. M. *Macromolecules* **2011**, *44*, 5937. (c) Robertson, N. J.; Kostalik, H. A.; Clark, T. J.; Mutolo, P. F.; Abruña, H. D.; Coates, G. W. *J. Am. Chem. Soc.* **2010**, *132*, 3400. (d) Kostalik, H. A.; Clark, T. J.; Robertson, N. J.; Mutolo, P. F.; Longo, J. M.; Abruña, H. D.; Coates, G. W. *Macromolecules* **2010**, *43*, 7147. (e) Clark, T. J.; Robertson, N. J.; Kostalik IV, H. A.; Lobkovsky, E. B.; Mutolo, P. F.; Abruña, H. D.; Coates, G. W. *J. Am. Chem. Soc.* **2009**, *131*, 12888.
- (16) (a) Nuñez, S. A.; Hickner, M. A. *ACS Macro Lett.* **2013**, *2*, 49. (b) Arges, C. G.; Ramani, V. *Proc. Natl. Acad. Sci.* **2013**, *110*, 2490. (c) Fujimoto, C.; Kim, D.-S.; Hibbs, M.; Wroblewski, D.; Kim, Y. S. *J. Membr. Sci.* **2012**, *423-424*, 438. (d) Long, H.; Kim, K.; Pivovar, B. S. *J. Phys. Chem. C* **2012**, *116*, 9419. (e) Edson, J. B.; Macomber, C. S.; Pivovar, B. S.; Boncella, J. M. *J. Membr. Sci.* **2012**, *399-400*, 49. (f) Wang, J.; Wang, J.; Li, S.; Zhang, S. *J. Membr. Sci.* **2011**, *368*, 246. (g) Chempath, S.; Boncella, J. M.; Pratt, L. R.; Henson, N.; Pivovar, B. S. *J. Phys. Chem. C* **2010**, *114*, 11977. (h) Macomber, C. S.; Boncella, J. M.; Pivovar, B. S.; Rau, J. A. *Therm. Anal. Calorim.* **2008**, *93*, 225. (i) Chempath, S.; Einsla, B. R.; Pratt, L. R.; Macomber, C. S.; Boncella, J. M.; Rau, J. A.; Pivovar, B. S. *J. Phys. Chem. C* **2008**, *112*, 3179. (j) Einsla, B. R.; Chempath, S.; Pratt, L.; Boncella, J.; Rau, J.; Macomber, C.; Pivovar, B. *ECS Trans.* **2007**, *11*, 1173. (k) Komkova, E.; Stamatialis, D.; Strathmann, H.; Wessling, M. *J. Membr. Sci.* **2004**, *244*, 25.
- (17) (a) Liu, L.; Li, Q.; Dai, J.; Wang, H.; Jin, B.; Bai, R. *J. Membr. Sci.* **2014**, *453*, 52. (b) Sajjad, S. D.; Hong, Y.; Liu, F. *Polym. Adv. Technol.* **2014**, *25*, 108. (c) Li, W.; Wang, S.; Zhang, X.; Wang, W.; Xie, X.; Pei, P. *Int. J. Hydrogen Energy* **2014**, *39*, 13710. (d) Kim, D. S.; Fujimoto, C. H.; Hibbs, M. R.; Labouriau, A.; Choe, Y.-K.; Kim, Y. S. *Macromolecules* **2013**, *46*, 7826. (e) Lin, X.; Wu, L.; Liu, Y.; Ong, A. L.; Poynton, S. D.; Varcoe, J. R.; Xu, T. *J. Power Sources* **2012**, *217*, 373. (f) Qu, C.; Zhang, H.; Zhang, F.; Liu, B. *J. Mater. Chem.* **2012**, *22*, 8203. (g) Kim, D. S.; Labouriau, A.; Guiver, M. D.; Kim, Y. S. *Chem. Mater.* **2011**, *23*, 3795. (h) Wang, J.; Li, S.; Zhang, S. *Macromolecules* **2010**, *43*, 3890. (i) Zhang, Q.; Li, S.; Zhang, S. *Chem. Commun.* **2010**, *46*, 7495.
- (18) (a) Jangu, C.; Long, T. E. *Polymer* **2014**, *55*, 3298. (b) Ye, Y.; Stokes, K. K.; Beyer, F. L.; Elabd, Y. A. *J. Membr. Sci.* **2013**, *443*, 93. (c) Arges, C. G.; Parrondo, J.; Johnson, G.; Nadhan, A.; Ramani, V. *J. Mater. Chem.* **2012**, *22*, 3733. (d) Stokes, K. K.; Orlicki, J. A.; Beyer, F. L. *Polym. Chem.* **2011**, *2*, 80. (e) Gu, S.; Cai, R.; Yan, Y. *Chem. Commun.* **2011**, *47*, 2856. (f) Gu, S.; Cai, R.; Luo, T.; Jensen, K.; Contreras, C.; Yan, Y. *ChemSusChem* **2010**, *3*, 555. (g) Arges, C. G.; Kulkarni, S.; Baranek, A.; Pan, K.-J.; Jung, M.-S.; Patton, D.; Mauritz, K. A.; Ramani, V. *ECS Trans.* **2010**, *33*, 1903. (h) Kong, X.; Wadhwa, K.; Verkade, J. G.; Schmidt-Rohr, K. *Macromolecules*

- 2009**, 42, 1659. (i) Gu, S.; Cai, R.; Luo, T.; Chen, Z.; Sun, M.; Liu, Y.; He, G.; Yan, Y. *Angew. Chem., Int. Ed.* **2009**, 48, 6499.
- (19) (a) Marino, M. G.; Kreuer, K. D. *ChemSusChem* **2015**, 8, 513. (b) Katzfuß, A.; Poynton, S.; Varcoe, J.; Gogel, V.; Storr, U.; Kerres, J. *J. Membr. Sci.* **2014**, 465, 129. (c) Katzfuß, A.; Gogel, V.; Jörissen, L.; Kerres, J. *J. Membr. Sci.* **2013**, 425-426, 131. (d) Fang, J.; Yang, Y.; Lu, X.; Ye, M.; Li, W.; Zhang, Y. *Int. J. Hydrogen Energy* **2012**, 37, 594. (e) Wang, X.; Li, M.; Golding, B. T.; Sadeghi, M.; Cao, Y.; Yu, E. H.; Scott, K. *Int. J. Hydrogen Energy* **2011**, 36, 10022. (f) Faraj, M.; Elia, E.; Boccia, M.; Filpi, A.; Pucci, A.; Ciardelli, F. *J. Polym. Sci., Part A: Polym. Chem.* **2011**, 49, 3437.
- (20) (a) Wright, A. G.; Holdcroft, S. *ACS Macro Lett.* **2014**, 3, 444. (b) Zarrin, H.; Jiang, G.; Lam, G. Y.-Y.; Fowler, M.; Chen, Z. *Int. J. Hydrogen Energy* **2014**, 39, 18405. (c) Price, S. C.; Williams, K. S.; Beyer, F. L. *ACS Macro Lett.* **2014**, 3, 160. (d) Lin, X.; Liang, X.; Poynton, S. D.; Varcoe, J. R.; Ong, A. L.; Ran, J.; Li, Y.; Li, Q.; Xu, T. *J. Membr. Sci.* **2013**, 443, 193. (e) Thomas, O. D.; Soo, K. J. W. Y.; Peckham, T. J.; Kulkarni, M. P.; Holdcroft, S. *J. Am. Chem. Soc.* **2012**, 134, 10753. (f) Henkensmeier, D.; Cho, H.-R.; Kim, H.-J.; Nunes Kirchner, C.; Leppin, J.; Dyck, A.; Jang, J. H.; Cho, E.; Nam, S.-W.; Lim, T.-H. *Polym. Degrad. Stab.* **2012**, 97, 264. (g) Thomas, O. D.; Soo, K. J. W. Y.; Peckham, T. J.; Kulkarni, M. P.; Holdcroft, S. *Polym. Chem.* **2011**, 2, 1641. (h) Henkensmeier, D.; Kim, H.-J.; Lee, H.-J.; Lee, D. H.; Oh, I.-H.; Hong, S.-A.; Nam, S.-W.; Lim, T.-H. *Macromol. Mater. Eng.* **2011**, 296, 899.
- (21) (a) Morandi, C. G.; Peach, R.; Krieg, H. M.; Kerres, J. *J. Mater. Chem. A* **2014**, 3, 1110. (b) Hahn, S.-J.; Won, M.; Kim, T.-H. *Polymer Bull.* **2013**, 70, 3373.
- (22) (a) Miyake, J.; Fukasawa, K.; Watanabe, M.; Miyatake, K. *J. Poly. Sci. Part A: Polym. Chem.* **2014**, 52, 383. (b) Vöge, A.; Deimede, V.; Kallitsis, J. K. *RSC Adv.* **2014**, 4, 45040.
- (23) Gu, F.; Dong, H.; Li, Y.; Sun, Z.; Yan, F. *Macromolecules* **2014**, 47, 6740.
- (24) (a) Mao, C.; Kudla, R. A.; Zuo, F.; Zhao, X.; Mueller, L. J.; Bu, X.; Feng, P. *J. Am. Chem. Soc.* **2014**, 136, 7579. (b) Sadakiyo, M.; Kasai, H.; Kato, K.; Takata, M.; Yamauchi, M. *J. Am. Chem. Soc.* **2014**, 136, 1702.
- (25) Disabb-Miller, M. L.; Zha, Y.; DeCarlo, A. J.; Pawar, M.; Tew, G. N.; Hickner, M. A. *Macromolecules* **2013**, 46, 9279.

- (26) (a) Parrondo, J.; Arges, C. G.; Niedzwiecki, M.; Anderson, E. B.; Ayers, K. E.; Ramani, V. *RSC Adv.* **2014**, *4*, 9875. (b) Leng, Y.; Chen, G.; Mendoza, A. J.; Tighe, T. B.; Hickner, M. A.; Wang, C.-Y. *J. Am. Chem. Soc.* **2012**, *134*, 9054.
- (27) Gu, Y.; Lodge, T. P. *Macromolecules* **2011**, *44*, 1732.
- (28) (a) Tzanetakis, N.; Varcoe, J. R.; Slade, R. C. T.; Scott, K. *Desalination* **2005**, *174*, 257. (b) Tzanetakis, N.; Taama, W. M.; Scott, K.; Varcoe, J.; Slade, R. S. *Desalination* **2003**, *151*, 275.
- (29) (a) Irie, Y.; Naka, K. *J. Polym. Sci., Part A: Polym. Chem.* **2013**, *51*, 2695. (b) Richter, T. V.; Bühler, C.; Ludwigs, S. *J. Am. Chem. Soc.* **2012**, *134*, 43.
- (30) Noonan, K. J. T.; Hugar, K. M.; Kostalik, H. A.; Lobkovsky, E. B.; Abruña, H. D.; Coates, G. W. *J. Am. Chem. Soc.* **2012**, *134*, 18161.
- (31) (a) Hossain, M. A.; Lim, Y.; Lee, S.; Jang, H.; Choi, S.; Jeon, Y.; Lee, S.; Ju, H.; Kim, W. G. *Solid State Ionics* **2014**, *262*, 754. (b) Yan, X.; He, G.; Gu, S.; Wu, X.; Du, L.; Wang, Y. *Int. J. Hydrogen Energy* **2012**, *37*, 5216. (c) Ran, J.; Wu, L.; Varcoe, J. R.; Ong, A. L.; Poynton, S. D.; Xu, T. *J. Membr. Sci.* **2012**, *415-416*, 242. (d) Qiu, B.; Lin, B.; Qiu, L.; Yan, F. *J. Mater. Chem.* **2012**, *22*, 1040. (e) Chen, D.; Hickner, M. A. *ACS Appl. Mater. Interfaces* **2012**, *4*, 5775. (f) Zhang, F.; Zhang, H.; Qu, C. *J. Mater. Chem.* **2011**, *21*, 12744. (g) Li, W.; Fang, J.; Lv, M.; Chen, C.; Chi, X.; Yang, Y.; Zhang, Y. *J. Mater. Chem.* **2011**, *21*, 11340. (h) Lin, B.; Qiu, L.; Lu, J.; Yan, F. *Chem. Mater.* **2010**, *22*, 6718. (i) Guo, M.; Fang, J.; Xu, H.; Li, W.; Lu, X.; Lan, C.; Li, K. *J. Membr. Sci.* **2010**, *362*, 97.
- (32) (a) Smith, T. W.; Zhao, M.; Yang, F.; Smith, D.; Cebe, P. *Macromolecules* **2013**, *46*, 1133. (b) Rao, A. H. N.; Thankamony, R. L.; Kim, H.-J.; Nam, S.; Kim, T.-H. *Polymer* **2013**, *54*, 111. (c) Allen, M. H.; Wang, S.; Hemp, S. T.; Chen, Y.; Madsen, L. A.; Winey, K. I.; Long, T. E. *Macromolecules* **2013**, *46*, 3037. (d) Weber, R. L.; Ye, Y.; Schmitt, A. L.; Banik, S. M.; Elabd, Y. A.; Mahanthappa, M. K. *Macromolecules* **2011**, *44*, 5727. (e) Weber, R. L.; Ye, Y.; Banik, S. M.; Elabd, Y. A.; Hickner, M. A.; Mahanthappa, M. K. *J. Polym. Sci Part B: Polym. Phys.* **2011**, *49*, 1287.
- (33) (a) Wang, W.; Wang, S.; Xie, X.; lv, Y.; Ramani, V. K. *J. Membr. Sci.* **2014**, *462*, 112. (b) Chen, D.; Hickner, M. A. *ACS Appl. Mater. Interfaces* **2012**, *4*, 5775. (c) Deavin, O. I.; Murphy, S.; Ong, A. L.; Poynton, S. D.; Zeng, R.; Herman, H.; Varcoe, J. R. *Energ. Environ. Sci.* **2012**, *5*, 8584. (d) Ye, Y.; Elabd, Y. A. *Macromolecules* **2011**, *44*, 8494.

- (34) (a) Alsarraf, J.; Ammar, Y. A.; Robert, F.; Cloutet, E.; Cramail, H.; Landais, Y. *Macromolecules* **2012**, *45*, 2249. (b) Jahnke, M. C.; Hussain, M.; Hupka, F.; Pape, T.; Ali, S.; Hahn, F. E.; Cavell, K. J. *Tetrahedron* **2009**, *65*, 909.
- (35) (a) Jin, H. M.; Seo, D. W.; Lee, S. H.; Lim, Y. D.; Islam, M. M.; Kim, W. G. *J. Ind. Eng. Chem.* **2012**, *18*, 1499. (b) Seo, D. W.; Parvez, M. K.; Lee, S. H.; Kim, J. H.; Kim, S. R.; Lim, Y. D.; Kim, W. G. *Electrochim. Acta* **2011**, *57*, 285.
- (36) Schwesinger, R.; Link, R.; Wenzl, P.; Kossek, S.; Keller, M. *Chem. – Eur. J.* **2006**, *12*, 429.
- (37) Zhang, S.; Miran, M. S.; Ikoma, A.; Dokko, K.; Watanabe, M. *J. Am. Chem. Soc.* **2014**, *136*, 1690.
- (38) (a) Yang, Y.; Wang, J.; Zheng, J.; Li, S.; Zhang, S. *J. Membr. Sci.* **2014**, *467*, 48. (b) Kelemen, Z.; Péter-Szabó, B.; Székely, E.; Hollóczki, O.; Firaha, D. S.; Kirchner, B.; Nagy, J.; Nyulászi, L. *Chem. – Eur. J.* **2014**, *20*, 13002. (c) Wang, Y.-B.; Wang, Y.-M.; Zhang, W.-Z.; Lu, X.-B. *J. Am. Chem. Soc.* **2013**, *135*, 11996. (d) Hollóczki, O.; Terleczy, P.; Szieberth, D.; Mourgas, G.; Gudat, D.; Nyulászi, L. *J. Am. Chem. Soc.* **2011**, *133*, 780. (e) Aggarwal, V. K.; Emme, I.; Mereu, A. *Chem. Commun.* **2002**, 1612. (f) Denk, M. K.; Rodezno, J. M.; Gupta, S.; Lough, A. J. *J. Org. Chem.* **2001**, *617-618*, 242.
- (39) (a) Lin, B.; Chu, F.; Ren, Y.; Jia, B.; Yuan, N.; Shang, H.; Feng, T.; Zhu, Y.; Ding, J. *J. Power Sources* **2014**, *266*, 186. (b) Si, Z.; Sun, Z.; Gu, F.; Qiu, L.; Yan, F. *J. Mater. Chem. A* **2014**, *2*, 4413. (c) Page, O. M. M.; Poynton, S. D.; Murphy, S.; Lien Ong, A.; Hillman, D. M.; Hancock, C. A.; Hale, M. G.; Apperley, D. C.; Varcoe, J. R. *RSC Adv.* **2013**, *3*, 579. (d) Lin, X.; Varcoe, J. R.; Poynton, S. D.; Liang, X.; Ong, A. L.; Ran, J.; Li, Y.; Xu, T. *J. Mater. Chem. A* **2013**, *1*, 7262. (e) Qiu, B.; Lin, B.; Si, Z.; Qiu, L.; Chu, F.; Zhao, J.; Yan, F. *J. Power Sources* **2012**, *217*, 329. (f) Lin, B.; Qiu, L.; Qiu, B.; Peng, Y.; Yan, F. *Macromolecules* **2011**, *44*, 9642.
- (40) (a) Si, Z.; Qiu, L.; Dong, H.; Gu, F.; Li, Y.; Yan, F. *ACS Appl. Mater. Interfaces* **2014**, *6*, 4346. (b) Gu, F.; Dong, H.; Li, Y.; Si, Z.; Yan, F. *Macromolecules* **2014**, *47*, 208. (c) Liu, Y.; Wang, J.; Yang, Y.; Brenner, T. M.; Seifert, S.; Yan, Y.; Liberatore, M. W.; Herring, A. M. *J. Phys. Chem. C* **2014**, *118*, 15136. (d) Lin, B.; Dong, H.; Li, Y.; Si, Z.; Gu, F.; Yan, F. *Chem. Mater.* **2013**, *25*, 1858. (e) Wang, J.; Gu, S.; Kaspar, R. B.; Zhang, B.; Yan, Y. *ChemSusChem* **2013**, *6*, 2079. (f) Sarode, H.; Vandiver, M.; Caire, B.; Liu, Y.; Horan, J. L.; Yang, Y.; Li, Y.; Herbst, D.; Lindberg, G. E.; Tse, Y.-L. S.; Seifert, S.; Coughlin, E. B.; Knauss, D. M.; Yan, Y.; Voth, G.; Witten, T.; Liberatorre, M.; Herring, A. M. *ECS Trans.* **2013**, *58*, 393.

- (41) (a) Long, H.; Pivovar, B. *J. Phys. Chem. C* **2014**, *118*, 9880. (b) Wang, W.; Wang, S.; Xie, X.; Lv, Y.; Ramani, V. *Int. J. Hydrogen Energy* **2014**, *39*, 14355. (c) Dong, H.; Gu, F.; Li, M.; Lin, B.; Si, Z.; Hou, T.; Yan, F.; Lee, S.-T.; Li, Y. *ChemPhysChem* **2014**, *15*, 3006. (d) Tsuchitani, R.; Nakanishi, H.; Kasai, H. *e-J Surf. Sci. Nanotechnol.* **2013**, *11*, 138.
- (42) Mohanty, A. D.; Bae, C. *J. Mater. Chem. A* **2014**, *2*, 17314.
- (43) Chapter 3 – A Universal Protocol for the Quantitative Assessment of Pendant Cation Stability in Polymer Electrolytes.
- (44) Section 4.5 – Experimental.
- (45) Samai, S.; Nandi, G. C.; Singh, P.; Singh, M. S. *Tetrahedron* **2009**, *65*, 10155.
- (46) (a) Choe, Y.-K.; Fujimoto, C.; Lee, K.-S.; Dalton, L. T.; Ayers, K.; Henson, N. J.; Kim, Y. S. *Chem. Mater.* **2014**, *26*, 5675. (b) Amel, A.; Zhu, L.; Hickner, M.; Ein-Eli, Y. *J. Electrochem. Soc.* **2014**, *161*, F615. (c) Arges, C. G.; Wang, L.; Parrondo, J.; Ramani, V. K. *ECS Trans.* **2013**, *58*, 1551. (d) Arges, C. G.; Wang, L.; Parrondo, J.; Ramani, V. *J. Electrochem. Soc.* **2013**, *160*, F1258. (e) Arges, C. G.; Ramani, V. *Proc. Natl. Acad. Sci.* **2013**, *110*, 2490. (f) Fujimoto, C.; Kim, D.-S.; Hibbs, M.; Wroblewski, D.; Kim, Y. S. *J. Membr. Sci.* **2012**, *423-424*, 438. (g) Hübner, G.; Roduner, E. *J. Mater. Chem.* **1999**, *9*, 409.
- (47) Tsai, T.-H.; Ertem, S. P.; Maes, A. M.; Seifert, S.; Herring, A. M.; Coughlin, E. B. *Macromolecules* **2015**, *48*, 665.
- (48) Chapter 3 – A Universal Protocol for the Quantitative Assessment of Pendant Cation Stability in Polymer Electrolytes
- (49) For additional references on solvent suppression theory and applications: (a) Hore, P. *J. Methods Enzymol.* **1989**, *176*, 64. (b) Guéron, M.; Plateau, P.; Decors, M. *Prog. Nucl. Magn. Reson. Spectrosc.* **1991**, *23*, 135. (c) Braun, S.; Kalinowski, H.-O.; Berger, S. *150 and More Basic NMR Experiments: A Practical Course*; Wiley-VCH: Weinheim, Germany, 1999.
- (50) Gao, G.; Xiao, R.; Yuan, Y.; Zhou, C.-H.; You, J.; Xie, R.-G. *J. Chem. Res.* **2002**, *2002*, 262.

- (51) Kantevari, S.; Vuppalapati, S. V. N.; Biradar, D. O.; Nagarapu, L. *J. Mol. Catal. A: Chem.* **2007**, *266*, 109.
- (52) Wilhelm, M. E.; Anthofer, M. H.; Reich, R. M.; D'Elia, V.; Basset, J.-M.; Herrmann, W. A.; Cokoja, M.; Kühn, F. E. *Catal. Sci. Technol.* **2014**, *4*, 1638.
- (53) Keivanloo, A.; Bakherad, M.; Imanifar, E.; Mirzaee, M. *Appl. Catal., A* **2013**, *467*, 291.